Electrochemical detection of antibiotics and antibiotic susceptibility

Perrine Lasserre

Department of Biomedical Engineering

University of Strathclyde

Thesis submitted in partial fulfilment for the degree of Doctor of Philosophy

2024

ABSTRACT

Antibiotic resistance is a global health threat that affects individuals differently. Mitigation strategies, such as improved antibiotic stewardship, depend on timely antibiotic susceptibility testing. However, current methods face limitations, including slow turnaround times and labour-intensive protocols conducted in centralised laboratories, highlighting the need for better solutions. Electrochemical sensors, offering sensitive, selective detection with user-friendly, low-cost solutions, can overcome many obstacles associated with current susceptibility testing methods, enabling closer-to-point-of-need applications. Three main case studies were explored.

First, electrochemical characterization of actinorhodin, a pigmented antibiotic from *Streptomyces coelicolor*, was studied as a proxy for bacterial growth and antibiotic production monitoring. While a complex mixture was observed, further fundamental characterization is needed for direct electrochemical identification from bacterial cultures. Next, an aptasensor for moxifloxacin, a widely used antibiotic, was developed. Initially, a support oligonucleotide hybridized to the aptamer did not produce a detectable signal via electrochemical impedance spectroscopy. However, using a methylene blue label and stabilizing the aptamer with a molecularly imprinted structure improved the binding event and signal detection. Lastly, a dual characterization strategy for bacterial biofilms was designed. *Pseudomonas aeruginosa* biofilms, characterized by the biomarker pyocyanin, and less electroactive biofilms like *Acinetobacter baumannii*, were studied using voltammetry and impedance spectroscopy. The response to antibiotics was monitored at 24 and 48 hours using resazurin as a metabolic indicator.

These studies demonstrate the potential of electrochemical sensors for antibiotic and susceptibility detection closer to the point of need, providing promising solutions for rapid diagnostics and improved antibiotic stewardship.

ACKNOWLEDGMENTS

PUBLICATIONS

The paper below was produced in the context of this thesis. As part of a collaborative funding, this was a joint first co-authorship between R. D. Dunphy and P. Lasserre. P. Lasserre was involved in the experimental work pertaining to hyperspectral camera set-up and use, hyperspectral imaging data acquisition and interpretation. Data acquired for Figure 6.6 was performed by L. Riordan.

Dunphy, R. D.; **Lasserre, P.**; Riordan, L.; Duncan, K. R.; McCormick, C.; Murray, P.; Corrigan, D. K. Combining Hyperspectral Imaging and Electrochemical Sensing for Detection of *Pseudomonas aeruginosa* through Pyocyanin Production. Sensors & Diagnostics 2022, 1 (4), 841–850. https://doi.org/10.1039/d2sd00044j.

The following papers were published in addition to the work presented:

Domingo-Roca, R.; **Lasserre, P.**; Riordan, L.; Macdonald, A. R.; A. Dobrea; Duncan, K. R.; Hannah, S.; Murphy, M.; Hoskisson, P. A.; Corrigan, D. K. Rapid Assessment of Antibiotic Susceptibility Using a Fully 3D-Printed Impedance-Based Biosensor. *Biosensors and bioelectronics. X* **2023**, *13*, 100308–100308. https://doi.org/10.1016/j.biosx.2023.100308.

Lasserre, P.; Balansethupathy, B.; Vezza, V. J.; Butterworth, A.; Macdonald, A.; Blair, E. O.; McAteer, L.; Hannah, S.; Ward, A. C.; Hoskisson, P. A.; Longmuir, A.; Setford, S.; Farmer, E. C. W.; Murphy, M. E.; Flynn, H.; Corrigan, D. K. SARS-CoV-2 Aptasensors Based on Electrochemical Impedance Spectroscopy and Low-Cost Gold Electrode Substrates. *Analytical Chemistry* **2022**, *94* (4), 2126–2133. https://doi.org/10.1021/acs.analchem.1c04456.

Vezza, V. J.; Butterworth, A.; **Lasserre, P.**; Blair, E. O.; MacDonald, A.; Hannah, S.; Rinaldi, C.; Hoskisson, P. A.; Ward, A. C.; Longmuir, A.; Setford, S.; Farmer, E. C. W.; Murphy, M. E.; Corrigan, D. K. An Electrochemical SARS-CoV-2 Biosensor Inspired by Glucose Test Strip Manufacturing Processes. *Chemical Communications* **2021**, *57* (30), 3704–3707. https://doi.org/10.1039/d1cc00936b.

Hannah, S.; Dobrea, A.; **Lasserre, P**.; Blair, E. O.; Alcorn, D.; Hoskisson, P. A.; Corrigan, D. K. Development of a Rapid, Antimicrobial Susceptibility Test for *E. coli* Based on Low-Cost, Screen-Printed Electrodes. Biosensors 2020, 10 (11), 153. https://doi.org/10.3390/bios10110153.

CONTENTS

LIST OF FIGURES

LIST OF TABLES

ABBREVIATIONS

[moxi.]	Moxifloxacin concentration
α-act.	α-actinorhodin
AA	Ammonium acetate
ABC	ATP-Binding cassette
AC	Alternating current
Act.	Actinorhodin
Act. acid	Actinorhodinic acid
AFM	Atomic force microscopy
AI	Artificial intelligence
AMR	Antimicrobial resistance
AMS	Antimicrobial stewardship
Apt.	Aptamer
AST	Antibiotic susceptibility testing
ATP	Adenosine triphosphate
β-act.	β-actinorhodin
BGC	Biosynthetic gene cluster
BSA	Bovine Serum Albumin
BSAC	British Society for Antimicrobial Chemotherapy
bwd	backward
CARB-X	Combatting Antibiotic-Resistant Bacteria Biopharmaceutical Accelerator
C$_{DL}$	Double layer capacitance
CE	Counter electrode
CFU	Colony-forming unit
CIP	Cell-imprinted polymer
CLSI	Clinical and Laboratory Standard Institute
CLSM	Confocal laser scanning microscopy
CNT	Carbon nanotubes

CPE	Constant phase element
CTC	5-cyano-2,3-di-(tolyl)-tetrazolium chloride
CV	Cyclic voltammetry
DC	Direct current
DHK	Dihydrokalafungin
DNA	Deoxyribonucleic acid
DPV	Differential Pulse Voltammetry
DTT	Dithiothreitol
EIS	Electrochemical impedance spectroscopy
ELISA	Enzyme-linked immunosorbent assay
EMV	Electron multiplier voltage
EPS	Exopolysaccharide
ESI	Electrospray ionisation
ESKAPE	*Enterococcus faecium*, *Staphylococcus aureus*, *Klebsiella pneumoniae*, *Acinetobacter baumannii*, *Pseudomonas aeruginosa*, *Enterobacter* spp.
ESKAPEEc	ESKAPE from above and less often added *Escherichia coli*
EtOAc	Ethyl acetate
EUCAST	European Committee on Antibiotic Susceptibility Testing
FA	Formic acid
FDA	Food and Drug Administration
FET	Field-effect transistor
FISH	Fluorescence *in situ* hybridisation
FLLS	Forward laser light scattering
FTIR	Fourier transform infrared
FRA	Frequency response analyser
fwd	forward
GARDP	Global Antibiotic Research & Development Partnership
GC	Gas chromatography

GCE	Glassy carbon electrode
GLASS	Global Antimicrobial Resistance and Use Surveillance System
GO	Graphene oxide
GP	General practitioner
HAI	Hospital-acquired infections/Healthcare-associated infections
HPLC	High performance liquid chromatography
HRP	Horseradish peroxidase
HSI	Hyperspectral imaging
HTA	Health technology assessment
IDE	Interdigitated electrode
IoT	Internet of things
IP	Intellectual property
ISO	International Organisation for Standardization
IR	Infrared (spectroscopy)
IUPAC	International Union of Pure and Applied Chemistry
IVD	*In vitro* diagnostics
LAMP	Loop-mediated isothermal amplification
LB	Luria Bertani
LESB58	*Pseudomonas aeruginosa* Liverpool Epidemic Strain B58
LLE	Liquid-liquid extraction
LoD	Limit of detection
LSV	Linear sweep voltammetry
MALDI	Matrix assisted laser desorption ionisation
MATE	Multidrug and toxic compound extrusion
MB	Methylene blue
MB-Apt.	5' Methylene blue-tagged aptamer
MB-Scr.	5' Methylene blue-tagged scrambled aptamer
MBC	Minimum bactericidal concentration
MBEC	Minimum biofilm eradication concentration

MCH	6-Mercapto-1-hexanol
MCP	2-Mercaptopropan-1-ol
MDR	Multi-drug resistance
MFC	Minimum fungicidal concentration
MFS	Major superfacilitator
ML	Machine learning
MI	first compartmentalised mycelium
MII	second multinucleated mycelium
MIC	Minimum inhibitory concentration
MIP	Molecularly imprinted polymer
moxi.	moxifloxacin
mRNA	messenger ribonucleic acid
MS	Mass spectrometry
MSI	Multispectral imaging
MTT	3-(4,5-dimethyl-2-thiazolyl)-2,5-diphenyl-2H-tetrazolium bromide
MWCNT	Multi-walled carbon nanotubes
Mx SPE	Multiplexed Screen-printed electrodes
NAP	Nucleic acid purification
NFC	Near-field communication
NGS	Next-generation sequencing
NHS	National Health Service (UK)
NMR	Nuclear magnetic resonance
NP	Nanoparticles
o/n	overnight
OCP	Open circuit potential
OD	Optical density
OSMAC	One strain many compounds
PA14	*Pseudomonas aeruginosa* PA14

PACE	Proteobacterial antimicrobial compound efflux
PAINS	Pan assay interference substance
PBS	Phosphate-buffered saline
PCD	Programmed cell death
PCR	Polymerase chain reaction
PES	Polyethersulfone
PFDT	1H,1H,2H,2H-Perfluorodecanethiol
PGE	Polycrystalline gold electrodes
PK/PD	Pharmacokinetic/Pharmacodynamic
PKS	Polyketide synthase
PNA	Peptide nucleic acid
PQS	Pseudomonas quinolone signal
PTFE	Polytetrafluorethylene
QCM	Quartz crystal microbalance
QD	Quantum dots
QMAC	Quantamatrix
qPCR	Quantitative PCR
QS	Quorum sensing
R&D	Research and development
rAST	rapid Antibiotic susceptibility testing
R_{ct}	Charge-transfer resistance
RE	Reference electrode
RNA	Ribonucleic acid
RND	Resistance nodulation cell division
RPA	Recombinant polymerase amplification
R_S	Resistance of the solution
Rt	Retention time
RT-PCR	Reverse transcriptase – polymerase chain reaction

(S)-DNPA	4-dihydro-9-hydroxy-1-methyl-10-oxo-3-H-naptho-[2,3-c]-pyran-3-(S)-acetic acid
SAM	Self-assembled monolayer
SARS-CoV-2	Severe acute respiratory syndrome coronavirus 2
SCP1	Super core promoter-1
SELEX	Systematic evolution of ligands by exponential enrichment
SH-Apt.	5'-thiolated aptamer
SMR	Small multidrug resistance
SNV	Standard normal variate
SPE	Screen-printed electrodes
SPR	Surface plasmon resonance
SRS	Spontaneous raman scattering
STXM	Scanning transmission X-ray microscopy
Supp.	Support
SWIR	Shortwave-infrared
SWV	Square wave voltammetry
TB	Tuberculosis
TCA	Tricarboxylic acid cycle
TCEP	Tris (2-carboxyethyl) phosphine
TEM	Transmission electron microscopy
TFGE	Thin film gold electrodes
TIC	Total ion count
TOF	Time-of-flight
UV	Ultraviolet
v/v	Volume/volume
VBNC	Viable but non culturable
VNIR	Visible and near infrared
W	Warburg element
WE	Working electrode

WGS	Whole genome sequencing
WHO	World Health Organisation
XDR	Extensively drug-resistant
YEME	Yeast extract-malt extract

Chapter 1 Introduction

Antibiotics were the world's first blockbuster drugs and have built the foundation of pharmaceutical industry success.[1] It all started with Alexander Fleming, who discovered penicillin in 1928 and Ernst Chain and Howard Florey, ten years later, who further led investigations to chemically characterise the antibiotic.[2] World War II proved an opportune economic environment to introduce a new treatment, test it, ramp up large scale production and encourage wide use in reduced timeframes. In these unique times, general willingness to invest and try something new to save lives was welcomed as a large proportion of the world was constantly endangered by the war.[2] Antibiotics improved general life expectancy through treatment of various illnesses, have become foundations for other cures, surgeries and medical progress to take place[1] added to wealth and job creation in difficult economic times. At the time, the discovery and production of penicillin was qualified by Time magazine in 1944 of being much more significant on the scale of time in terms of lives saved than the actual end of World War II.[3] As Fleming was awarded the Nobel prize in physiology or medicine in 1945 alongside Chain and Florey, he delivered an early warning against observations of antibiotic resistance.[2]

Antibiotics are small molecules, often between 150 and 5000 Daltons, of natural (bacterial, plant or fungal), semi-synthetic or fully synthetic origin. They either possess a bacteriostatic or bactericidal mode of action, respectively inhibiting bacterial growth or killing them. Antibiotic resistance is defined as the ability of bacteria to withstand the activity of drugs whose action previously prevented their growth or survival.[4] Antibiotic resistance is often encompassed in the term antimicrobial resistance (AMR), including parasites, fungi and viruses. Often referred to as the "silent pandemic"[5–9], AMR is a global public health issue threatening the foundations of modern medicine, where many infectious diseases might not be treated anymore[10] and lifesaving medical procedures would become a risky undertaking.[11] Longer hospital stays, poor health outcomes, for instance postoperative complications or emerging drug resistant tuberculosis in diabetic

patients, and increased patient morbidity and mortality would become more common with less effective antibiotic treatments.[12]

AMR does not follow national borders.[5] Regardless of the country or income level, increasing resistance rates have been and are being reported.[11] The current global estimate of 1.27 million deaths directly attributed to and 4.95 million related to AMR in 2019[13] is predicted to reach 10 million victims annually by 2050, should the current situation remain unchanged.[14] Moreover, the ESKAPEEc group of pathogens, composed of *Enterococcus faecium*, *Staphylococcus aureus*, *Klebsiella pneumoniae*, *Acinetobacter baumannii*, *Pseudomonas aeruginosa*, *Enterobacter* spp. and less often added *Escherichia coli*, cause most of the antibiotic-resistant hospital-acquired or healthcare-associated infections (HAI).[15–17] Using a published prediction model, without intervention, these pathogens will have acquired pandrug resistance in the next 8-15 years.[16,17]

With over 6000 mechanisms known, antibiotic resistance is inevitable.[18] This comes from the evolutionary ability of bacteria to rapidly respond to external stresses. The most common mechanisms at a cellular level include efflux pumps, changes in membrane permeability, enzymatic degradation of antibiotics, alteration of antibiotic targets or emergence of new metabolic pathways. Resistance mechanisms can be innate, intrinsically part of the bacteria, acquired through genetic mutations (vertical transfer) or uptake from other strains through transformation, transduction or conjugation (horizontal transfer).[10] Another successful strategy at the collective level is the formation of biofilms,[19] causing at least over half of the bacterial infections.[19,20] As biofilm individuals are phenotypically different from planktonic bacteria for which antibiotics and antibiotic susceptibility tests have been developed, biofilm-related infections lack specific and appropriate treatment[21,22] and diagnosis.[23,24]

Bacterial infections tend to often be either incorrectly treated or with delay. Healthcare practitioners hold the challenging responsibility of treating the patient's condition, preventing complications[30] while at the same time, minimising antibiotic

use to avoid resistance.[17] Between 2000 and 2015, the worldwide use of critically important antimicrobials listed by World Health Organisation (WHO) has increased by 91%.[26] Often cited as main drivers of AMR are the misuse and overuse of antibiotics; not only in humans but also in animals and plants.[11] A recent example of antibiotic misuse is illustrated by almost 75% of Covid-19 patients in the USA receiving antibiotics.[27] As antibiotic production was taken over by the private sector, other antibiotic uses were investigated for bigger volumes to be sold, and eventually more profits to be made.[1] Indeed, 73% of all antimicrobials sold are used for animals, as an essential component of intensive farming to treat, prevent infections and promote growth.[28] Moreover, antibiotic consumption is not systematically reported, and therefore, antimicrobials sold are used as proxy to estimate antibiotic use.[28] With 20 countries allowing antibiotic use to tackle plant diseases, bacteria on plants are more and more likely to become resistant, and impact humans and/or animals through food and feed. The Global Antimicrobial resistance and use Surveillance System (GLASS) initiative led by the WHO intends to encourage and harmonise AMR official reporting and antimicrobial consumption at national levels.[29] Even if, national surveillance systems are not yet at a uniform implementation stage,[29] GLASS motivates an integrated One Health approach to estimate AMR and mitigate negative consequences at the animal-human interface.[29]

Despite AMR being one of the most important global threats, public funds do not counterbalance the little political action and private sector disinvestment.[27] With major reporting gaps, mostly from lower income countries, it is impossible to reliably estimate AMR global impact.[27] As the cost and threat of increased resistance is uncertain, exact investments needed to mitigate AMR are also difficult to assess.[1] The economic cost of AMR was estimated by the Review on Antimicrobial Resistance through additional healthcare costs of disease and treatment, lost productivity and the value of a statistical life, social cost of illness or death. The total cost of AMR on world health systems has been estimated at USD 57 billion and would cost a decrease in productivity of USD 174 billion per year.[1] AMR requires long-term investments on several fronts.[27] To overcome the short-term bias of current politics, benefits

generated need to be witnessed on the short-term, which is not the case for this global issue.[1]

Promoting prudent and responsible use of antimicrobials through effective antimicrobial stewardship and limiting agriculture use has not been sufficient to control the spread of AMR so far, as appropriate surveillance and monitoring programmes are also necessary.[30] Low and middle income countries, in addition, might not have the diagnostic capacity, antibiotic availability or the financial means to meet standards for infection prevention and control through surveillance systems.[27,31] Striking a balance by lowering use without hindering access is a key problematic limit which contradictorily encourages the use of broad rather than narrow spectrum antibiotics. In many cases, antimicrobial use appears to be a substitute for imperfect infrastructures and failing systems. Bridging knowledge and action is necessary to counter the current low level of action implementation.[5]

The traditional approach to counteract AMR has manifested as inventing and producing new antibiotics.[5] This has been successful during the golden age of discovery, but the pace has slowed down since then. No new class of antibiotics has been marketed since the 1970-80s[10] and all the more, none active against Gram-negative bacteria since the 1960s. Antibiotic classes group molecules with similar chemical structures. Resistance against one antibiotic is often accompanied to resistance against most antibiotics of the same class.[32] As resistance to antibiotics arises much faster than their discovery and commercialisation,[33] a strong and sustainable pipeline of antibiotics with new mode of actions is urgently needed to keep working antibiotics at hand using this approach.[5,32,34]

Early stage discovery/development is well promoted by public funds, however later stages lack financial support.[12] New drugs are costly and time-consuming to develop, likely to fail and have intrinsically a limited scope and lifespan.[31] For an antibiotic to reach the market, an average of USD 1-2.5 billion investment over 10 years is required, with only a 10% success rate from candidates entering clinical

trials.[10] Knowing that it takes 22 months to produce a marketed drug, a self-sustaining revenue is only achieved in the seventh year post launch, without accounting for pre-launch R&D investments.[35] Market entry rewards for the commercialisation of new antibiotics could provide a solution for faster profit.[14] For a new antibiotic entering the market, its use would be restricted to ensure its safe-guarding with resistance inevitably increasing while its clinical utility would decrease. Innovation in antibiotic discovery, however, possess high translational risks and is mostly pioneered by small and medium enterprises, which do not have the same financial leverage as big pharmaceutical companies, that have gradually left this market space.[1,12,36] The global market for antibiotics is worth a yearly US$40 billion, with only 12% or US$4.7 billion for patented antibiotics,[14] while generics are not profitable enough to support R&D costs.[1] In 2015, one top-selling cancer drug and fifteen pharmaceutical drugs each generated more revenue than all antibiotics combined.[1,14] Limited by the volume of sales and therefore profits, the antibiotic market has become unattractive and needing better incentives to lower the R&D costs.[31] A focus on non-profit antibiotic development with a public health vision, such as the Innovative Medicines Initiative,[37] the RoadMap by Pew Trust,[38] GARDP[39] and CARB-X[40] could set the norm for new funding strategies while populating the antibiotic pipeline.[30]

In practice, when antibiotics do not work, synergistic combinations are prescribed in many cases as the sole efficient treatment choice, requiring in reality, more in-depth official pharmacokinetic/pharmacodynamics (PK/PD) studies and outcome assessments. Increased exposure regimens have also shown some success in urgent cases when very little treatment options are available. Both gather under "salvage treatments" owing to the scarcity of studies published.[15] Vaccines are available but vaccination rates remain low and do not make up for unsafe water and sanitation, often catalysers for increased resistance and spread of pathogens. Investments in these areas are key to mitigate AMR and promote antibiotic stewardship.

Antibiotic Susceptibility Testing (AST) allows to assess the efficacy of antibiotics and their appropriate treatment dose.[25] Phenotypic assays constitute the gold standard practice since treatments are not only based on the existence of resistance - the main focus of genotypic methods - but also bacteria susceptibility, determined by the minimum inhibitory concentration (MIC).[41] However, routine AST protocols are time-consuming, costly and require specialist equipment and trained users.[25,42] For instance, susceptibility testing for the complete panel of antimicrobial candidates has been reported in less than 10% of pandrug-resistant Gram-negative bacteria studies.[15] Antibiotic susceptibility standard testing methods and procedures are neither adequate nor fast enough to run in urgent situations, where empirical prescriptions prevail. Depending on the ability and conditions to culture pathogens, appropriate antibiotic treatments are often delayed, leading to longer hospital stays, higher costs and death rates.

Point-of-care systems are diagnostic instruments providing rapid results in non-laboratory environments and possibly handled by untrained users,[43] for instance at home, in GP practices or hospitals.[44] Increasingly sensitive solutions are being developed, integrating additional functions for better sensing capabilities such as preconcentration of samples, signal amplification, microfluidics and electrochemical detection.[44] The development of electrochemical biosensing platforms for AST can bring highly sensitive, specific, repeatable, rapid, label-free, compact, robust and low-cost solutions "from bench to bedside"[25,42,45] with minimal to no sample preparation.[46]

The International Union of Pure and Applied Chemistry (IUPAC) defined a biosensor as "a self-contained integrated device which is capable of providing specific quantitative or semi-quantitative analytical instrumentation using a biological recognition element (biochemical receptor) which is in direct spatial contact with a transducer element."[47] Transducers can be of various natures, for instance mechanical, optical or electrochemical.[46] Electrochemical transducers take the form

of electrodes, with extensive applications towards pathogen detection.[46] Electrodes and electrolyte solutions enable the conversion of chemical energy associated with a specific target binding the biorecognition element into an electrical signal.[46] Biorecognition elements can induce a reaction catalysed by macromolecules (catalytic-based) or an interaction of the analyte with macromolecules or organised molecular assemblies (affinity-based).[46] Antibodies are the most common biorecognition elements but their disadvantages triggered synthetic alternatives such as cell or molecularly-imprinted polymers (CIPs and MIPs)[46] or oligonucleotides such as single-stranded DNA and aptamers.[46]

The large scale epidemics over the past 40 years have shown a lack of rapid, accessible, accurate diagnostic response that hampered the public health response.[48] Two recent examples illustrate the impact of point-of-care biosensors. One is the optimal access to diagnostics in the 1990s to control HIV/AIDS in Uganda, with a prevalence reduced by 67% reduction.[49] Most recently, the SARS-CoV-2 pandemic emphasised issues occurring from relying only on laboratory-based techniques such as RT-PCR, with supply shortages of kits, asymptomatic patients and diagnostics being major bottlenecks.[50] As a safe and effective vaccine was the most powerful strategy but needed time to be developed and deployed,[50] and so did treatments, mass testing had a key role to identify and isolate clusters, made possible by point-of-care affordable tests.[51] *In vitro* diagnostics also played a primary role to determine therapeutic pathways and inform the clinical decision.[49] Antibiotic resistant infections however, have a slower impact despite an accelerated spread through international travel and migration.[27] Availability of medical countermeasures such as diagnostics, improved surveillance and equitable access,[27] an area tackled by the Longitude prize initiative, have been deemed essential to detect and prevent antibiotic resistance.[52]

Electrochemical biosensors can deliver faster results by minimising time from sample collection to AST results[53] with improved clinical outcomes; potentially reducing antimicrobial use and associated mortality, along with hospital stays and duration.[46] They enable low sample volumes, miniaturised components for actuation, data acquisition and readout.[42,46] Moreover, they also facilitate multiparametric

sensing by combining existing and emerging technologies such as data mining and machine learning for more robust systems[25] and take advantage of connectivity, consumer electronics and data analytics[44] for a smoother integration in the clinical workflow.[25,44] Electrochemical sensing has been reported to monitor bacterial growth over time through perturbations in current or voltage.[25] Identification and quantification of pathogens can be undertaken directly from body fluids, with diagnostically relevant concentrations varying in each type of matrix.[46]

To establish clear rationales behind the design and optimisation of point-of-care antibiotic detection and susceptibility assays using electrochemical biosensors, an account of current understanding behind antibiotic resistance mechanisms ensues. An account and discussion of current and innovative antibiotic susceptibility methods follows to clearly define some of the technological and practical challenges to be addressed. Finally, further insights into electrochemical biosensing, through measurement techniques, instrumentation and functionalisation strategies specifically motivate the conception of rapid, sensitive, reliable and low-cost antibiotic sensing and susceptibility solutions for this thesis:

- Electrochemical characterisation of actinorhodin, a non-commercialised antibiotic from *Streptomyces* spp., as an indicator of antibiotic production,
- Detection of moxifloxacin, one of the most used antibiotics, using aptamers and,
- Dual detection of monospecies biofilms using *P. aeruginosa* with hyperspectral imaging and *A. baumannii*.

Chapter 2 Detecting antibiotic susceptibility via electrochemical solutions: state of the art and considerations to develop and bring solutions to the point of need

This review focuses on antibiotic resistance, and therefore on infectious bacteria by definition when antimicrobial resistance also includes infectious diseases caused by fungi, virus or parasites. By any means, this does not underestimate the challenges brought by antimicrobial resistance in other microorganisms such as the extremely limited therapeutic options from the three classes of commercialised antifungal agents.[54]

The nature of what is to be detected is described first, from antibiotics as such to the mechanisms of resistance as well as existing and envisaged counter strategies against antibiotic resistance. Antibiotic Susceptibility Testing (AST) principles and existing techniques available in clinical and community environments are then examined alongside additional techniques with improvement potential. Challenges to be answered by the development and adoption of more mainstream point-of-care diagnostics are discussed to support better antibiotic stewardship. Taking advantage of electrochemical detection as an existing and widely available solution for glucose sensing, an understanding of system composition and possible measurements is provided. Following is an account of biosensors to carefully consider fit-for-purpose designs and optimisations. Finally, reported point of care approaches based on electrochemical sensing, targeting antibiotics, bacteria and their susceptibility to antibiotics directly through growth or via a proxy for growth (active metabolism) are reviewed.

2.1 Antibiotics

2.1.1 Definitions

An **antimicrobial agent** is defined as a biological, semi-synthetic or synthetic compound capable of inhibiting microorganism growth or killing them in the perspective of being used as treatment for infections. Antimicrobials include

antibiotic, antiviral, antifungal, antiparasitic, antiseptic agents and disinfectants.[55] An **antibiotic** is defined as any small molecule produced by a microorganism to hinder the growth or kill other bacteria.[56] Antibiotics have specific modes of action with a sufficiently potent activity to eradicate the infection without being toxic to the host.[56] Contrarily to antibiotics, **biocides** affect microorganisms growth non-selectively. **Antiseptics** prevent the growth of any infectious microorganism on tissues or skin and **disinfectants** have a similar action on non-living surfaces.[57]

2.1.2 Fast forward from dyes to antibiotic classes of today

Before antibiotics were industrially produced and sold en masse, dyes were common practice to kill microbes in wounds without harming the patient and, from a later perspective, without risking resistance development.[58] Unsurprisingly, the pharmaceutical branch of the 160-year old chemical industry has derived from the dye production occurring before World War II.[58] This proved to be the right time for penicillin, discovered by Alexander Fleming in 1928 and ten years later, characterised by the teams of Ernst Chain and Howard Florey. Due to its efficacy, convenient administration and large-scale production, treatments with penicillin and other antibiotics quickly supplanted dyes to treat infectious diseases.[59] Nowadays, over 15 classes of antibiotics[60,61] are commercialised based on their chemical structure and diverse mechanisms of actions (Table 2.1).

Table 2.1. Overview of antibiotic classes currently commercialised, comparing their mode of action and spectrum of activity.

Class	Bacteriostatic	Bactericidal	Active against Gram-negative bacteria?	Ref.
β-Lactams		√	√	62
Glycopeptides		√		60,63,64
Aminoglycosides		√	Some	65
Tetracyclines	√		√	66
Macrolides	√			67
Quinolones		√	√	68

Class	Bacteriostatic	Bactericidal	Active against Gram-negative bacteria?	Ref.
Oxazolidinones	√			[69]
Sulfonamides	√		√	[70]
Phenicols	√		√	[71]
Ansamycins		√	Some	[72]
Streptogramins		√		[72]
Lipopeptides		√		[72,73]
Polymyxins		√	√	[73,74]
Fosfomycins		√	√	[75,76]
Lincosamides	√	√	√	[77,78]
Defensins		√	√	[79]

2.1.3 Screening for novelty and diversity

Most of the antibiotic classes known today (Table 2.1) were discovered in the Golden Age, spanning from the 1940s to the 1960s (Figure 2.1).

From 1939, Waksman, who realised the potential of actinomycetes, developed a platform with systematic agar overlay of more than 10 000 microbial species. With lawyers from Merck, Waksman enabled the possibility to patent natural products for their activity, providing a strong foundation for the pharmaceutical industry with most antibiotics used today coming from actinomycetes.[56]
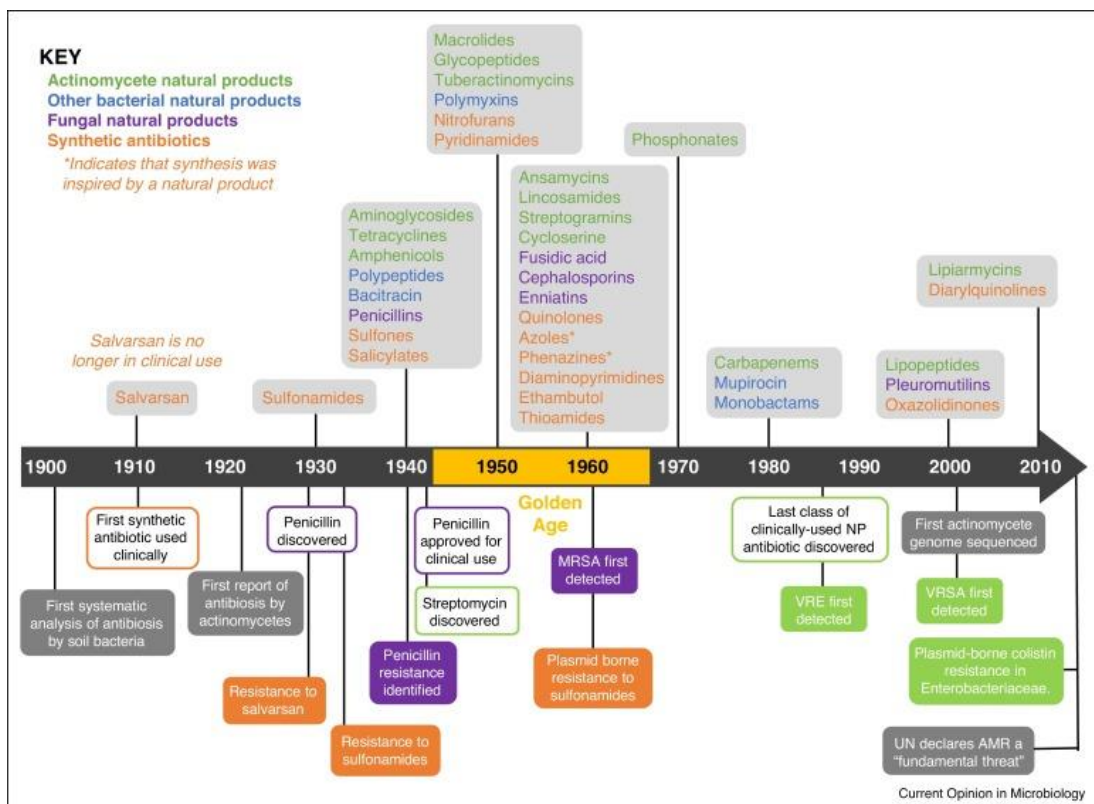
Figure 2.1. Chronology of antibiotic classes reaching the clinic in parallel with antibiotic resistance detection and coloured by source, namely Actinomycetes in green, other bacteria in blue, fungi in purple, synthetic compounds in orange and the Golden Age in yellow on the arrow. Key dates below the timeline are linked to antibiotic discovery and antimicrobial resistance, including the first reports of methicillin-resistant *S. aureus* (MRSA), vancomycin-resistant enterococci (VRE), vancomycin-resistant *S. aureus* (VRSA) and plasmid-borne colistin resistance in Enterobacteriaceae.[80] Adapted from Hutchings, M. I.; Truman, A. W.; Wilkinson, B. Antibiotics: Past, Present and Future. *Current Opinion in Microbiology* **2019**, *51* (1), 72–80. under CC BY 4.0 with yellow highlight on the arrow of the Golden Age period.

Antibiotic discovery is crucial in outpacing arising and spreading resistance. To the systematic procedures of the antibiotic golden age based on **natural products** have been added **semi-synthetic** – modification of existing scaffolds through fermentation to improve effectiveness, chemical stability or diminish side effects - and fully **synthetic** strategies to discover new drug leads. An exhaustion of antibiotic discovery platforms, through redundant discoveries or limited translation to the clinic, has fed the need for new antibiotic discovery platforms.[56] Target-based platforms have emerged in the genomics era (1995-2004), with new modes of action awaited.[56] Hit-to-lead assessment showed difficult to be pursued[38,81] without crystal structure or purified target. No new drug emerged from the genomic era as a more phenotypic-based strategy was needed, prompting the return of cell-based screening under the reverse genomics movement.[38,56] This led to five marketed products, three of which

derived from natural products and the remaining from chemical synthesis. Except one, these new molecules all target Gram-positive bacteria, leaving the more challenging Gram-negative bacteria space still short of solutions.[63]

Developing new antibiotics and even antimicrobials in general, is an expensive, risky and long process (Figure 2.2). For instance, considering more than 21 000 drug candidates over 15 years,[82] only 13.8% of drug development initiatives resulted in market approval. Only 20 % of Phase I drugs with possible antibacterial roles are likely to obtain final FDA approval.[60] Disinterest from large pharmaceutical industries is also fuelled by the availability of effective generic antibiotics, expensive antibiotics being put on the backburner by public health systems, and efforts to reduce use through stewardship initiatives and safeguarding new antibiotics.[83] Most of the recently developed leads are either refurbished or rely on combinations of known molecules with only a small amount reaching commercialisation, very limited potential with narrow scope and short life span.[83]

A robust pipeline of antibiotics targeting novel mechanisms of action is lacking,[83] especially to treat MDR Gram-negative bacteria.[38] Looking for structural features involved in uptake and related mechanisms has been ongoing for over three decades.[60] Even for known antibiotics, knowledge about drivers of accumulation or permeation rate remains scarce.[38] The limited understanding of compound entry and efflux mechanisms out of Gram-negative bacteria is a key bottleneck in the discovery of new antibiotics, lacking support from molecular tools.[38] Traditionally, large-scale screening initiatives without specific targets have not proved fruitful in the search for novel mechanisms of action, such as the ones conducted by AstraZeneca or GlaxoSmithKline.[38] Predictive cellular assays, tools or models for structure-activity relationship and better compound accumulation knowledge are also lacking.[38] Divergences between compounds in high-throughput screening collections and available antibacterial drugs decrease the likelihood of hit-to-lead transfer,[38] but also limits hits to what is already known. Permeating the Gram-negative membrane calls for a diversity in chemical structures,[38] when, for instance, the outer membrane permeability in *P. aeruginosa* is ~12 to 100-fold lower compared to that of *E. coli.*[83]

Developing antibiotics is expensive and risky, making it hard to attract investment

	Minimum duration (years)	Minimum cost per launch (USDmn)
EARLY DRUG DISCOVERY	3	Up to $110
PRECLINICAL	0.5	Up to $70
CLINICAL TRIALS		
Phase 1	1	Up to $150
Phase 2	1	Up to $130
Phase 3	2	Up to $230
Registration	1	At least $22
POST-APPROVAL		
Expansion of indications[1]	3+	Up to $250
DEVELOPING A NEW ANTIBIOTIC	takes at least **9 years**	costs at least **$1 billion**

1 Additional studies run to test antibiotic on different bacteria and in different patient groups.

wellcome

Source: WHO, bit.ly/WHO-doc, p2

Figure 2.2. Costs and durations involved in the development of an antibiotic from early discovery to post-market approval. Wellcome Trust infographic[84] based on data from Pulling together to beat superbugs by the World Bank (2019).[85]

The current post-genomics era focuses on accumulating new information on microbial metabolism, using omics technologies that are not at their full potential

yet.[56] For now, their throughput and simultaneous complementarity limits screening possibilities of antibiotic discovery platforms as connections between phenotypic events and high-information omics approaches are not strongly established yet. PROSPECT, which stands for primary screening of strains to prioritise expanded chemistry and targets, is one recent example in drug development platforms using omics.[38] As clinically available antibiotics only target a portion of essential genes, PROSPECT intends to focus on essential but non-targeted gene products.[38] Increased access to unexploited targets allows to assess more combined antibiotic treatments.[38] Antibiotic discovery platforms are now starting to benefit from the expansion of artificial intelligence and machine learning. Based on deep learning of antibiotic activity and human cell cytotoxicity of over 12 million compounds, Wong *et al.* (2023) selected 283 compounds to be screened for antibiotic activity against *S. aureus*, with one candidate pursued for further *in vitro* and *in vivo* antibiotic activity characterisation.[86]

Decisions made about which compounds to investigate are crucial in influencing future discovery.[38] Simplifying to minimal requirement has not always been successful to drive compound permeation or accumulation.[38] Broader datasets to explore structure-activity relationships emphasising on uptake and efflux are needed - not only for antibacterial compounds - in order to explore structure and physicochemical diversity.[38] Teelucksingh *et al.* (2022) reported the development of an efflux pump platform using an *E. coli* knock-out strain, devoid of 35 efflux pumps.[87] Different combinations of pumps and pores using different strains enabled the investigation of inhibition and interplay between efflux entities with little understanding of the individual fitness advantage throughout bacteria lifecycle, leading to the necessity to consider all pumps.[88] The published efflux pump platform allowed to profile efflux pumps of interest, assess their physiological function and substrate specificity.[87] This platform has the potential to inform the design of new antimicrobial and efflux pump inhibitors and apply it to more species.[87]

Researchers tend to move away from unique overarching rules solely relying on structural or physicochemical properties towards guidelines adaptable by bacterial

species and antibiotic chemical class with broad ranges of physicochemical properties.[38] A better understanding of structure-activity relationship concerning intake and efflux of antibiotics is likely to benefit innovative accumulation strategies, porin permeation and prevention of efflux[38] as new modes of action are needed to counter antibiotic resistance. An account of the current ones from marketed antibiotics is undertaken next (Figure 2.3) along with known resistance strategies challenging their activity.

2.2 Antibiotic targets & resistance mechanisms from a single cell viewpoint

The fate and efficacy of antibiotics is determined by their ability to reach their target. [89] Mutations can therefore impact the interaction between antibiotic and bacterial target via changes in the target, inactivation of the antibiotic through enzymatic activity or alteration of influx or efflux entities.[90] DNA replication, including both bacterial chromosome and plasmid, is an error-prone process, with random base substitutions at 10^{-9} per gene, insertions or deletions.[90] Mutations leading to target modification generally impact a restricted number of antibiotic classes whereas restrictions in passive diffusion or increased efflux affect a greater number of classes depending on their recognition.[90]
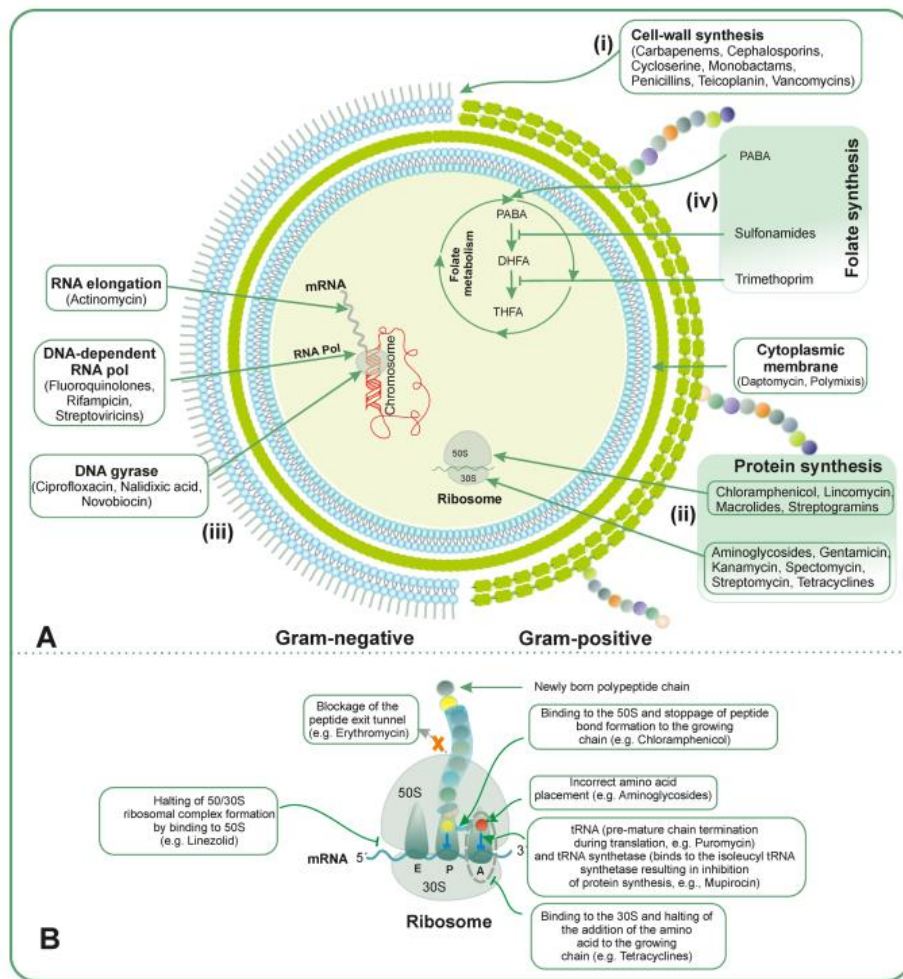
Figure 2.3. Antibiotic targets for both Gram-negative and Gram-positive bacteria. Overall view (A) with more precise effects on ribosome subunits (B). Reprinted with permission from Baral, B. and Mozafari, M.R., 2020. Strategic moves of "superbugs" against available chemical scaffolds: signalling, regulation, and challenges. ACS Pharmacology & Translational Science, 3(3), pp.373-400. Copyright 2020 American Chemical Society.

2.2.1 Bacterial membrane composition

Antibiotics first need to cross the cell membrane to access intracellular targets.[89] As anionic lipids are exposed on the bacterial surface, most antibacterial agents are therefore developed as cations, enabling a greater selectivity for the bacterial membrane[60] and against eukaryotic membranes. Bacterial membranes present a complex multilayered structure allowing to modulate permeability for entry and exit of extracellular compounds, dividing them between Gram-positive and Gram-negative categories.[60] Gram-positive bacteria possess a thicker peptidoglycan but no outer layer and Gram-negative bacteria, an asymmetric phospholipid layer, an outer membrane with inner phospholipids, a thin peptidoglycan and outer lipopolysaccharides (Figure 2.4).[60] The complexity of the membrane restricts the flow of hydrophobic and hydrophilic molecules across the membrane and shields Gram-negative bacteria from harsh environmental conditions enabling them to easily form biofilms, and making it more difficult to cross than the Gram-positive peptidoglycan (Figure 2.4).[60]

Disrupting the integrity of the bacterial cell membrane is a mode of action shared among several antibiotic classes such as β-lactams, carbapenems, cephalosporins, defensins and polymyxin B.[60] One of the most successful resistance strategies involving the bacterial membrane consists in the alteration of passive and active transport to modify overall antibiotic intake and efflux.
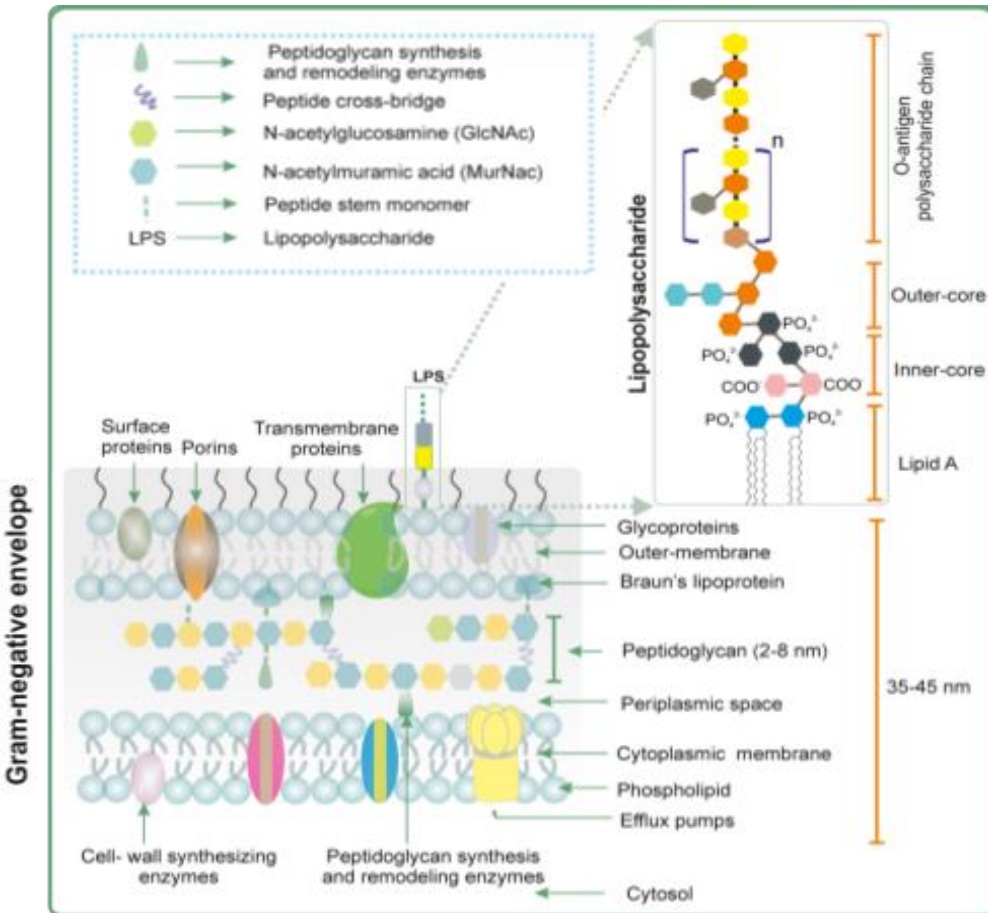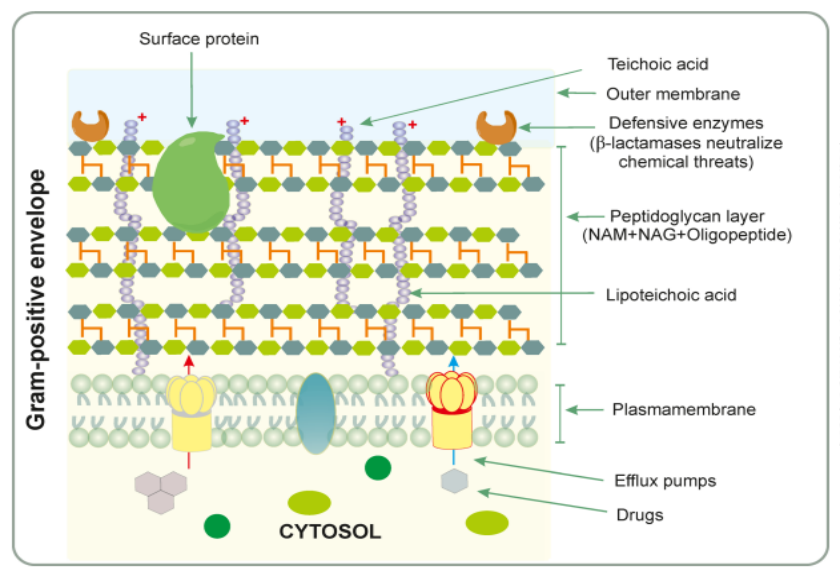
Figure 2.4. Bacterial membrane composition of Gram-positive and Gram-negative species (respectively left and right). Reprinted with permission from Baral, B. and Mozafari, M.R., 2020. Strategic moves of "superbugs" against available chemical scaffolds: signalling, regulation, and challenges. ACS Pharmacology & Translational Science, 3(3), pp.373-400. Copyright 2020 American Chemical Society.

2.2.2 Bacterial membrane permeability

Conserved through evolution, multidrug efflux pumps are ubiquitous and able to recognise and transport a wide range of antibacterial substrates.[60,89] Contrarily to passive diffusion, active transport using pumps requires energy.[91] Efflux can be one of the fastest and most effective coping strategies for bacteria under antibiotic selective pressure.[89] Aminoglycosides, fluoroquinolones, tetracyclines, β-lactams and macrolides are prone to immediate efflux.[60] Six major families of efflux systems are reported, grouped by sequence and function similarities (Figure 2.5).[60]

ATP-binding cassettes (ABC) are primary transporters of antibiotics but also vitamins, xenobiotics, amino acids and sugars using energy from ATP hydrolysis.[60] All other transporters are secondary since they rely on proton motive force.[60]

Small Multidrug resistance (SMR) pumps are the smallest drug efflux proteins and mainly target lipophilic cationic drugs.[60] **The Major Superfacilitator Superfamily (MFS)** are substrate specific porters for a multiplicity of molecules including cationic drugs.[60] These make them the largest group of secondary transporters.[60] Their conformational change determines their transport mechanism as antiporters (ion and substrate moved in opposite directions), symporters (ion and substrate transported in the same direction) or uniporters (substrate transported without coupled ion) that include alternate binding and releasing of substrates.[60,89] **Resistance Nodulation cell Division (RND)** are efflux pumps capable of translocating drugs and toxic cations thanks to proton motive force.[60] They are ideal targets for antibiotic adjuvants through the development of chemical entities that the pump fails to recognise, shuttle out or only partially or even using an antibiotic that inhibits the pump.[60] They are vital in pathogenic clinical bacteria as they efflux out most antibiotics.[60] **Multidrug And Toxic compound Extrusion (MATE)** take advantage of the electrochemical potential of sodium ions as a driving force across the membrane compared to the proton gradient used by RND and MFS families and are therefore characterised as Na^+/drug antiporters (with some H^+/drug antiporters).[60] They enable resistance towards a multiplicity of drugs.[60]
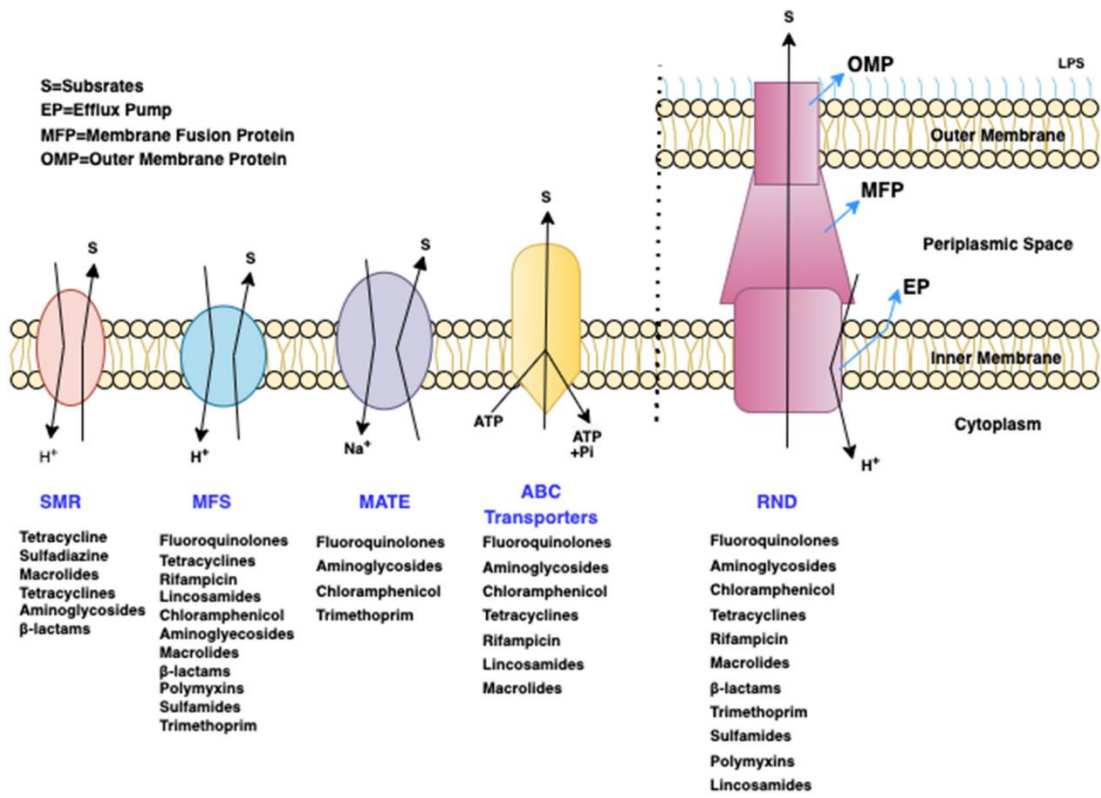
Figure 2.5. Antibiotic transport by multidrug resistant efflux pumps.[92] Reproduced with permission from Başaran, S. N., Öksüz, L. The Role of Efflux Pumps in Antibiotic Resistance of Gram-Negative Rods. *Archives of microbiology* 2023, *205* (5).

Proteobacterial Antimicrobial Compound Efflux (PACE) constitute a new class of transporters contributing to antibiotic resistance in Gram-negative pathogens.[60] They enable the efflux of cationic biocides, mainly antiseptic and disinfectants. Likely to be powered by proton gradient, they are either conserved or acquired through lateral transfer.[60]

Overexpression of efflux pumps is a major indicator to test the efficacy of different antibiotic classes.[60] Peptidomimetics and pyridopyrimidines are well known efflux pump inhibitors.[60] However, their toxicity to human cells at high doses prevents their progression through clinical trials.[60] Disruption of the pump assembly, altering the drug structure, blocking the efflux energy, using competitive/non-competitive drug inhibitor to block inner/outer membrane proteins are established strategies to prevent drug efflux.[60] Efflux pump inhibitors can also prevent biofilm formation.[60]

Multidrug efflux pumps constitute a complex regulatory network, strategy even amplified in biofilms, and targeting their concerted actions to promote

accumulation could improve antibiotic susceptibility. Combined with their various multidrug efflux transporters, the bacterial membrane is a major determinant for antimicrobial resistance, especially with the low permeability of Gram-negative outer membranes.[89]

2.2.3 Syntheis of cell building blocks: nucleic acids and DNA, amino acids and proteins, and folates

Once the bacterial membrane is crossed, two classes of antibiotics exist to disrupt DNA replication: aminocoumarins competitively inhibiting a DNA gyrase or topoisomerase II, and quinolones to stop decatenation of replicating DNA.[60] Resistance to quinolones has been observed as mutated topoisomerases.[60]

Another mode of action consists in hindering the synthesis of ribosomal proteins (aminoglycosides, tetracyclines, chloramphenicol, macrolides, oxazolidinones).[60] A variety of resistance strategies to cope with these antibiotics has arisen such as alterations in ribosome units to prevent binding to the target site. Concerning tetracyclines, more than 60 genes have been identified, responsible for efflux mechanisms, target protection and antibiotic inactivation.[93] For macrolides, lincosamides and streptogramins, antibiotic enzymatic modification, target alteration and efflux mechanisms all work in concert and also involve phenicol coresistance.[93]

The folate pathway, present in certain microorganisms - but not in humans as they are auxotrophic -, constitutes a specific target for antibacterial activity.[60] Folates are cofactors involved in the biosynthesis of vital cellular components.[60] Sulfonamides and trimethoprim impact the production of thymidine, purines and methionine, exerting a control over the biosynthesis of nucleotides and amino acids.[60] Resistance is observed as competing proteins to colistin, quinolones, sulfonamides, trimethoprim or fusidic acid to protect the antibiotic target.[93]

Despite the diversity in antibiotic modes of action, bacterial evolution and survival strategies enable the emergence of resistance. This is the case for single specimens but also by establishing local communities, better known as biofilms.

2.3 Resistance mechanisms from a bacterial community viewpoint

2.3.1 Transmission between individual bacteria

Frequent successful mutations enabling survival and replication provide a key advantage over other bacterial populations.[90] New mutations are more likely to be transmitted with a low cost-to-fitness and increase in virulence.[90] Resistance to an antibiotic can be temporary, hereditary or common to whole species, arising from genetic mutations or acquired by organisms previously susceptible from genetic mutation or intake of foreign DNA containing resistance genes (Figure 2.6).[90]

Adaptive resistance is a temporary, non-inheritable trait allowing bacteria to prosper in presence of antibiotics by changes in gene or protein expression levels and disappears once the environmental trigger is removed.[38] Weak selection pressures enable a gradually higher tolerance of microorganisms to antibiotics. **Innate resistance** might select for species able to survive antibiotic pressure in a given environment and shift the balance between microorganisms present, which is the case in hospital environments with nosocomial pathogens more resistant to any antibiotic compared to the same species found in the community.[90]

Genetic material transfer between bacteria can be inherited and occur vertically, from mother to daughter cells or horizontally, between two individuals[90] and mostly takes place via plasmids and mobile genetic elements (insertion sequences, integrons and transposons). Possible **pathways of horizontal transmission** are described in Figure 2.6. ESKAPE pathogens are currently responsible for hospital infections with lateral acquisition of genes from the environment.[60]
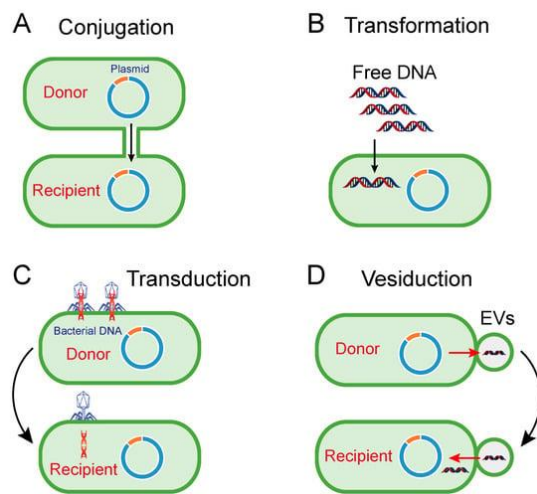
Figure 2.6. Horizontal gene transfer routes.[94] External genetic material can be transferred by conjugation involving physical contact between donor and recipient (A), transformation or the incorporation of DNA free from a membrane - specific bacterial genera such as *Streptococcus spp.*, *Neisseria spp.*, and *Haemophilus spp.* can naturally integrate DNA fragments from lysed organisms in their proximity[90] - (B), transduction occurring through a bacteriophage (C) or extracellular vesicles (D)[38]. Reuse under a CC-BY license from Liu *et al*. Correlation between Exogenous Compounds and the Horizontal Transfer of Plasmid-Borne Antibiotic Resistance Genes. *Microorganisms* 2020, *8* (8), 1211.

From a few to over 500 kilobases, plasmids can exist in single to multiple copies within a cell, depending on their size. They hold a variety of functions, from maintenance and replication, to partitioning in cell division and mobility but also metabolic pathways or colonisation.[93] Provenance of these genes might come from chromosomes of other bacterial species. Antibiotic-producing organisms often possess a specific resistance gene against the synthesised natural product, that can be transmitted.[90] Multiple resistance genes can be carried by a plasmid, implying that selection for one of the resistance determinants can also include additional resistance genes.[90] Plasmid acquisition is not always beneficial as it could be a metabolic burden in absence of selective pressure, although reduced with time.[38] High risk clones are successful epidemic lineages often bearing MDR, XDR or pandrug resistance that have followed pandemic spread patterns.[38]

2.3.2 Biofilms

Biofilms are sessile microbial communities surrounded by extracellular polymeric substance (EPS) established on a biotic or abiotic surface.[88,95] This bacterial organisation and cooperation constitutes a defence strategy against external stressors (altered pH, osmolarity, nutrient scarcity, mechanical and shear forces among

others).[88,95] Biofilms protect their constituents against host immune defences and antimicrobials, providing a higher tolerance compared to planktonic counter parts.[60,95] Constituted mostly of water, polysaccharides, lipids and proteins, extracellular DNA and insoluble components can also be found in the matrix.[88,95] Production of the EPS is initiated depending on nutrient availability or microbial competition, and secreted by bacteria.[95] Well-known bacterial resistance mechanisms, namely efflux pumps, enzymatic inactivation or target alteration are not responsible for the formation and protection of biofilms.[60] The exact EPS composition varies depending on bacterial species, environmental conditions and stage of biofilm maturation.[95]

Biofilms can be beneficial, as for instance the human gut microbiota, but also a major virulence and infectious strategy,[95] responsible for an estimated 80% of chronic and recurrent microbial infections in the human body.[88] Microbial cells located in a biofilm can require up to four times the MIC to be killed,[95] which is why a Minimum Biofilm Eradication Concentration (MBEC) is referred to for this phenotype.[88] Slower penetration of drugs, presence of persister cells characterised by a dormant state and altered chemical microenvironments,[95] are contributing mechanisms to lower antibiotic susceptibility.[88] Clinical difficulties to treat biofilms stem from their variability in terms of composition and dynamics, as well as tolerance to growth-dependent antimicrobials due to the anaerobic conditions of the biofilm and nutrient depletion conditions slowing down bacterial growth that reach stationary phase.[60,95] Since susceptibility is restored to a certain level upon dispersion and resistance is genetic-based, tolerance can be described as phenotypic resistance.[95]

The most effective treatment, when possible, is the removal of the biofilm.[88] Early antibiotic treatment has shown more effective at disrupting biofilms,[88] dependent on the time of formation[60] and rarely occurs due to their poor detection. Combination therapies to target a variety of components bears more hope[95] to restore antibiotic efficacy and host defence functions.[88]

Biofilm inhibition and eradication can be undertaken by targeting the EPS or dormant cells, quorum sensing and surface modification.[95] Natural products are a common approach to attempt biofilm control.[95] Forming pores is efficient at affecting both dormant and metabolically-active cells. Quorum sensing allows constant chemical communication via small molecule intermediates between bacteria located in close proximity to regulate cell density and biofilm formation[95] in order to adapt in a varying environment.[60] Regardless of the stress, bacteria can be willing to sacrifice their lives to save the community.[60] Indeed, they are able to sequestrate toxic compounds until a certain threshold and undergo programmed cell death or apoptosis before toxic compounds are expelled.[60] Effect of new antibiotics on biofilms or human microbiota is rarely evaluated which could be very informative upon selective toxicity.[95] A more detailed review of biofilms is undertaken in Chapter 6.

2.4 Counteroffensive on the bacterial resistance strategies

2.4.1 Overview of resistance mechanisms to antibiotics

Six overall mechanisms participate in multidrug resistance through biochemical strategies, receptor inactivation, decrease of membrane permeability or increased expression of genes encoding efflux pumps:[60]

- Target alteration or overproduction of target proteins for streptomycin, sulfonamides, trimethoprim or glycopeptides;
- Inactivation of the drug through enzymes, comprising hydrolysis, group transfer or redox reactions (aminoglycosidases, β-lactamases, carbapenemases, cephalosporinases and esterases to hydrolyse macrolides);
- Preventing drugs to access their targets either through modulated influx by porins, specific protein channels or lipid bilayer or immediate efflux of antibiotics by specific transporters (oxazolidinones, rifamycins, chloramphenicol);
- Target bypassing through resistance genes and target alteration;
- Acquisition of resistant genes through lateral transfer of mobile genetic elements;

- Biofilms as a key virulence factor for a wide range of microbial communities.

sTo combat or prevent the growth of opportunistic pathogens, sensing and invading strategies need more in-depth elucidation.

2.4.2 What is considered/used to counteract antibiotic resistance

Tremendous efforts are undertaken in the search of new hit molecules to slow the spread of multidrug resistant bacteria.[60] High-throughput strategies to search for bacteria's Achilles heel through novel chemical scaffolds from alternative sources are needed.[60] With natural products being so far the best source of therapeutic leads,[60] hopes are placed in poorly studied places or virgin habitats to discover new compounds and novel synthetic pathways.[60] New chemical scaffolds are also explored through genomics and the activation of cryptic, silent or orphan biosynthetic routes.[60] Unveiling the actual targets and mode of action of new natural products could be also highly beneficial[60] along with predictions of possible bacterial evolution and identification of key targets.[60] As known and newly developed antibiotic discovery platforms have yet to unlock novelty at a higher speed, novel approaches to discover candidates with enhanced bioactivity and new delivery of drugs to counteract resistance are also critically needed, even more for the 12 bacterial families on the WHO priority pathogen list lacking available efficient antimicrobial treatment.[38,60] New antibiotics only constitute a part of the whole scenario to mitigate rising antimicrobial resistance.[96,97]

2.4.2.1 Using knowledge and compounds already available

Previously discovered antibiotics had a fast mode of action and an easy administration route.[60] Out of the 30+ new antibiotics developed in the past two decades, half of them were synthetically-derived, 40 % derived from natural products and the rest resulting from new combinations.[60]

Synergistic combinations often occur as the sole efficient treatment choice, requiring deeper pharmacokinetic/pharmacodynamics and outcome assessments. A cocktail of antibiotics with other adjuvants can allow permeation of the cell membrane to reach targets.[60] Increased exposure regimens have also proved

successful in urgent cases with very limited treatment options. Both gather under "salvage treatments" owing to the scarcity of studies published. Higher doses however, favour the emergence of a gradual resistance and longer exposure to antibiotics has negative consequences on the host system.[60]

Repurposing old drugs has a lower cost, faster development time and enables the use of de-risked compounds.[60] It has the potential of uncovering new targets and pathways while also bearing the possibility of antibiotics being less effective.[60] Repurposing also involves shifting from a single to multiple target approach.[60] Candidate identification precedes a mechanistic assessment of the drug effect and the evaluation of its efficacy, that can each be tackled computationally and experimentally.[60] Identification can last close to two years, and so does the acquisition of a compound involving licensing.[60] Going through the different phases of clinical trials can then total a minimum of 12 years before a drug can reach the market.[60] Examples of repurposed drugs include auranofin,[98] bithionol,[99] celecoxib,[100] cotrimazole,[101] duloxetine,[102] ketoconazole,[103] minoxidil,[88] raloxifene,[104] sildenafil and thalidomide[105].

2.4.2.2 Alternative approaches to antibiotics

As focusing solely on antibiotics has not proved successful to counter antibiotic resistance, other strategies have emerged.

Bacteriophages are viruses able to infect bacteria, already used as anti-infectious agents two decades before antibiotics started in the clinic. Their abundance and diversity make them suitable for various purposes such as decontamination, detection or even diagnosis. Advantageously, they are highly specific and do not affect either eukaryotic cells or the normal bacterial flora, present low immunogenicity, can be easily isolated and combined in cocktails.[106] Several points are yet to be uncovered such as their pharmacokinetics, ability to develop resistance or transfer virulence.[107]

Probiotics can be defined as an adequate amount of live microorganisms administered to a host for health benefits.[108] Administration can take the form of engraftment from a healthy donor, oral administration or food supplements.[60]

Probiotics lead to an alteration of metabolic and immunological activity of the microbiota through specific adhesion to the surface of the gut epithelium.[60] Lee, Kim and Kang (2019) demonstrated that bacteriocin synthesised by *Pediococcus acidilactici* prevented *P. aeruginosa* to form biofilm and produce virulence factors.[109] Mageswary *et al.* (2021) reported the use of *Bacillus lactis* Probio-M8 as a non-drug treatment of respiratory tract infections for hospitalised young children.[110] Gut mucosal barriers are the first line of defence for the host and an efficient colonisation of the mucus by probiotics can prevent infections.[60] Piewngam *et al.* (2020) showed that *Bacillus subtilis* probiotics could eliminate *S. aureus* colonisation in mice and humans and most importantly without adverse effects and alteration of the microbiota.[111]

Using **essential oils** as a replacement of or combined to antibiotics also circumvents resistance.[60] Essential oils are concentrated volatile and aromatic natural products from plants composed of primary terpenoids (monoterpenes and sesquiterpenes) and other molecules such as acids, alcohols, aldehydes, aliphatic hydrocarbons, acyclic esters or lactones.[60] Wang, Mandell and Bohrer (2020) studied the effects on substituting antibiotics by essential oils in cattle feed and concluded that the final quality of the meat was unchanged.[112] Andrés *et al.* (2024) tested the effects of supplementing milk replacement for calves with oregano oil, which revealed that growth performance was improved only for a defined suckling period and microbiota and plasma metabolome were altered.[113] Certain pathogens display resistance to essential oils as passage through the Gram-negative membrane is difficult for instance.[60] Using essential oils with antibiotics and nanoparticles has been reported with lower emergence of resistant variants and stopping MDR pathogens bearing plasmids to grow.[60]

Nanomaterials at low concentrations can be considered as antibiotic replacements. Physicochemical properties are easy to adjust and can also be used as nanocarriers. However, ensuring their safety and production scale-up are necessary to achieve first.[114]

As an alternative to antibiotics, **photoantimicrobials** could offer local disinfection properties as well as patient decolonisation.[58] However, toxicity risks are too concerning to allow large patient trials. Furthermore, GP intervention and supervision would be required whereas antibiotics are mostly self-administered and alleviate the pressure on healthcare providers. Active participation of healthcare and the pharmaceutical industry is required to promote a come-back, which still requires design and implementation of specific protocols.[58]

Vaccines have allowed the control of 16 diseases so far and could also contribute to slow down resistance.[115] As vaccination allows the host to build an immune response prior pathogen exposure, a reduced number of bacteria develops compared to a normal infection.[115] This is favourable to minimise resistance arising by using antibiotics only when necessary, lowering probabilities of resistant phenotypes emerging, reducing the possibilities of resistance transmission between close bacteria and having close control on targeting antibiotic-resistant pathogens.[115] Nevertheless, no vaccine candidate has made it to phase III yet, explained by the multiplicity of antibiotic resistance mechanisms to be targeted and the lack of animal models.[115] Moreover, cost and benefits to vaccines assessments do not encompass the long-term benefits of this solution, which might explain why more funding has not been directed towards their development yet.[115]

Considering how bacteria become resistant along with its spread between organisms and human hosts can inform infection control strategies and therapy development.[90] The knowledge of resistance mechanisms informs the development of antibiotics or inhibitors able to counter them.[93] Targeting plasmids as a strategy to overcome resistance has not been successfully undertaken yet.[93] Reducing the selecting pressure is another strategy called antibiotic stewardship. This includes reducing uses for agriculture and veterinary purposes but also more appropriate uses in the case of human health, especially considering that a majority of antibiotics used in hospitals are not necessary, given inappropriately or with the wrong dosage.[93] The case of colistin, desperately needed as a last-resort treatment of multidrug-resistant

infections caused by Gram-negative bacteria, is still employed for prophylaxis, treatment and growth promotion in animals destined for human consumption.[116]

Faster diagnostics are likely to improve antibiotic stewardship and extend current antibiotic lifespan, waiting for new antibiotics and strategies.[93] Antibiotic stewardship is supported by antibiotic susceptibility testing, which is in need of solutions at the point of care to drive improvements for better antibiotic uses. Principles and techniques currently in use and available in the clinic and community followed by additional techniques with improvement potential are reviewed next.

2.5 Antibiotic susceptibility testing methods

2.5.1 Detecting AMR vs AST

Antibiotic susceptibility tests provide guidance for the choice of antibiotics to use against a pathogen and are able to detect potential resistance.[117] Phenotypic AST can be defined as the culture on solid or liquid medium of a single organism with or without an antimicrobial agent (Figure 2.7).[117] Results inform on the susceptibility of the tested microorganism at the set concentrations, with a quantitative aspect given by the MIC.[117] AMR detection, on the contrary, reports on pre-existing proteomic or genomic markers indicative of known antibiotic resistance (Figure 2.7).[117] Based on amplification techniques such as polymerase chain reaction (PCR) and next-generation sequencing (NGS) or whole genome sequencing (WGS) approaches, pathogens can be identified within hours of sample collection. Predictions of resistance phenotypes are based on well-described and known genetic markers and only correct if the phenotype is the exact expression of the genotype, which is not always the case.[36] Despite time-consuming protocols and high starting bacterial load required, phenotypic methods remain dominant among gold standard routine procedures.[117,118]
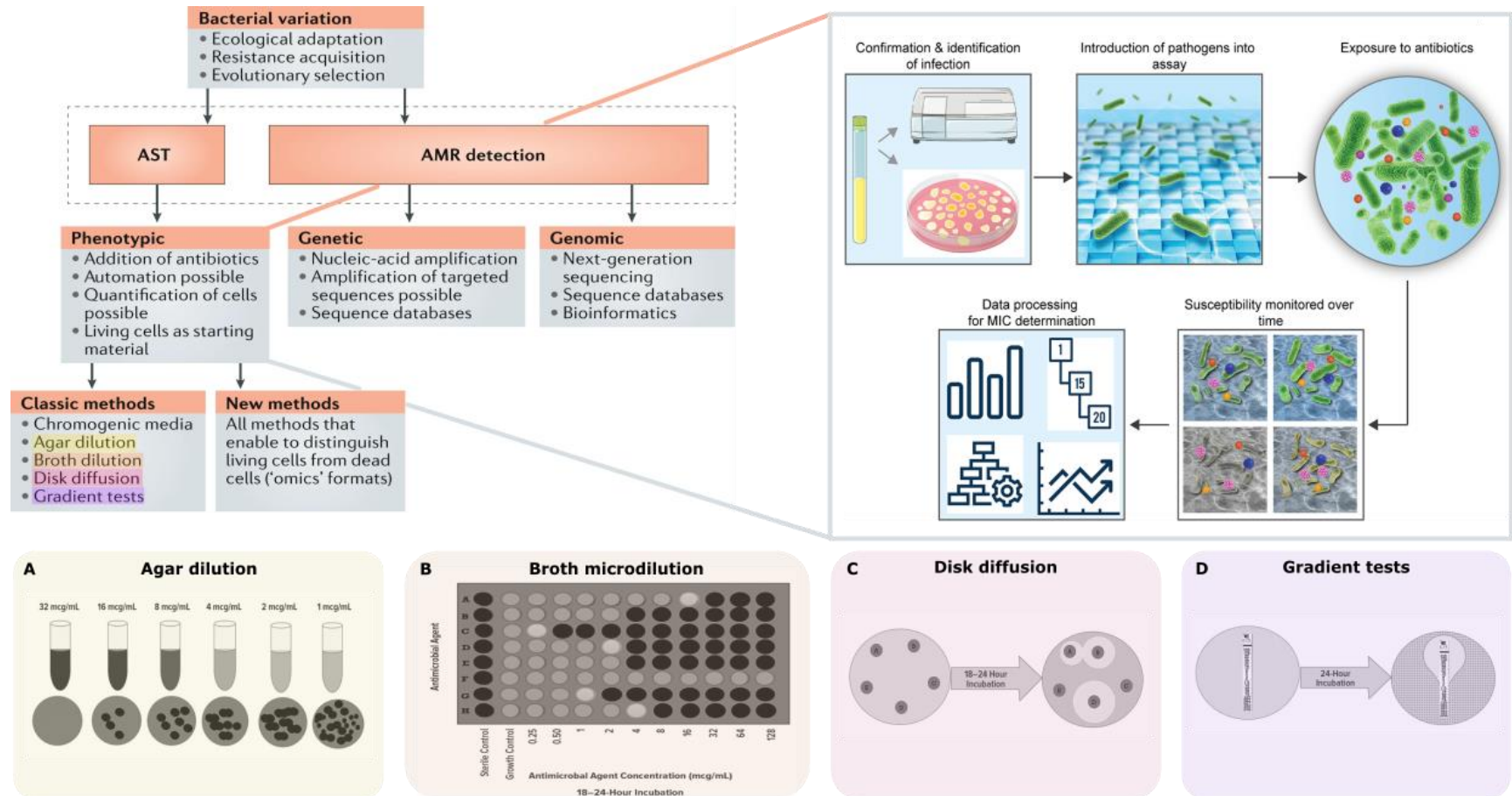
Figure 2.7. Detecting antibiotic susceptibility.[117] Phenotypic method workflow (top right grey rectangle)[119] and most common AST techniques (A-D)[120]. Reprinted and adapted with permission from van Belkum, A. *et al.* Innovative and Rapid Antimicrobial Susceptibility Testing Systems. Nature Reviews Microbiology 2020, 18 (5), 299–311; Leonard, H., Colodner, R., Halachmi, S. and Segal, E., 2018. Recent advances in the race to design a rapid diagnostic test for antimicrobial resistance. ACS sensors, 3(11), pp.2202-2217. Copyright 2018 American Chemical Society; Giuliano, C.; Patel, C. R.; Kale-Pradhan, P. B. A Guide to Bacterial Culture Identification and Results Interpretation. Pharmacy and Therapeutics 2019, 44 (4), 192–200.

2.5.2 Gold standard culture-dependent AST methods

AST is carried out for surveillance tests on antimicrobial resistance, epidemiological studies to assess susceptibility and the comparison between new and known antimicrobial agents. Gold standard techniques for AST involve solid or liquid culturing of microorganisms isolated from patient samples. These robust protocols fundamentally changed very little since their first descriptions, which require adaptations to meet the fast pace of emerging antibiotic resistance. After the presence of a pathogen within a sample is confirmed and identified, it is introduced in the appropriate measurement device.[119] Exposure to preloaded antibiotics and monitoring occurs to differentiate growth or death patterns with a chosen sensing modality.[119] The main limitation arises from the time bacteria take to grow and divide.[119] Assessing the MIC of an antibiotic against a specific bacterial species is the most widespread measure of antibiotic potency. Furthermore, variations in MIC over time and geographically reflect the emergence of antibiotic resistance. This quantitative indicator can be complemented by qualitative parameters such as breakpoints established by authoritative entities worldwide. Intra- and inter-laboratory reproducibility are ensured by well-established standard procedures, with EUCAST and CLSI being the most widespread standards.[118] Standard operating procedures and indicators are not necessarily identical across the main organisations.

Phenotypic resistance detection by evaluating the bacterial growth in the presence of antibiotics, can be classified in two categories, manual and automated. Manual tests include agar dilution, gradient test, disk diffusion, and broth microdilution antimicrobial susceptibility testing methods, all detailed below. Broth macro-, micro- and agar dilution methods represent quantitative reference AST methods.[118] The automated commercial platforms (VITEK®2 COMPACT, Sensititre™ ARIS™ 2X, and Alfred 60AST system) use some of the aforementioned methods.[121]

2.5.2.1 Broth dilution

Broth macrodilution consists in two-fold dilutions of antimicrobial agents in liquid medium inoculated for a minimal volume of 2 mL per repeat.[118] After an overnight or 4-10 days incubation for either bacterial or fungal strains respectively,

microbial growth is evidenced by turbidity.[118] Detecting bacterial growth by absorbance is the most basic strategy.[119] The minimum bactericidal concentration (MBC) or minimum fungicidal concentration represent the lowest concentration of antimicrobial inhibiting at least 99.9% of bacterial or fungal growth and can be determined by further culture of microtitration plate samples for 24 or 48 h.[118] The broth macrodilution was later miniaturised to broth microdilution, based on a similar principle with a total volume of 0.1-0.2 mL in 96-well plates instead of test tubes (Figure 2.7B). Down-sizing has improved efficiency and practicality of the method, raising its popularity for AST purposes.[118] The description of the ISO 20776-1 broth microdilution technique is based on reports from Ericsson & Sherris (1971)[122] and is fairly identical to EUCAST and CLSI procedures. The MIC is equivalent to the lowest concentration without turbidity within a two-fold dilution range for precision.[118]

The final microbial concentration in each well reaches $1*10^5$ CFU/mL and following a suitable incubation period, the MIC is assessed visually or by reading absorbance at 620 nm.[118] International guidelines state a final inoculum at $5*10^5$ CFU /mL for broth microdilution, with a tolerance range between 2 and 8.[123] Accurate comparison is only possible as close to the exact value as possible since minor differences can influence the MIC value.[123]

2.5.2.2 Agar diffusion

Moving on to solid methods, two-fold concentrations of antimicrobial drug are infused into molten agar, which, upon hardening, are inoculated and incubated for the specified time after which the MIC is assessed visually.[118] Agar dilutions are mostly preferred for fastidious microorganisms, compound colouring affecting detection or simultaneous test of a compound against a wide range of strains (Figure 2.7A).[118] Chromogenic culture media can selectively identify resistance with enhanced sensitivity from fluorescent substrates.[117] This has recently been reported for the differentiation of *Candida* species,[124] to facilitate faster identification of urogenic pathogens,[125] and support culturomics studies.[126]

2.5.2.2.1 Disk diffusion

Agar disk diffusion belongs among the oldest AST methods. It is also one of the most commonly used procedures thanks to its simplicity, reproducibility, versatility and low cost. Agar disk diffusion consists in inoculated agar plates where paper disks infused with various concentrations of antimicrobial agents are laid on the surface. After a 16-24 hour incubation, growth-inhibition diameter zones provide a qualitative estimation of microorganisms tested as susceptible, intermediate or resistant (Figure 2.7C).[118] The larger the inhibition zone obtained, the more susceptible the microorganism tested. Inhibition zones can be manually measured with a sliding caliper or ruler or automatically with ADAGIO Automated System or SIR scan automatic zone reader. While agar disk diffusion is not used for MIC determination, MIC estimations can be calculated from inhibition zones nonetheless considering the diffusion ability of a drug into agar.[118] The most efficient assay for polymicrobial samples appears to be disk diffusion.[123]

2.5.2.3 Antimicrobial gradient

Diffusion and dilution techniques meet in the antimicrobial gradient method.[118] The strip contains a gradient of defined antimicrobial and can be directly applied to inoculated agar medium.[118,127] Following overnight incubation, the intersection of the growth inhibition zone with the strip indicates MIC values (Figure 2.7D).[118,121,127] Different commercial versions of the antimicrobial gradient strip are available from bioMérieux (Etest), Liofilchem (MIC Test Strip), Oxoid (M.I.C. Evaluator) or HiMedia Laboratories Pvt. Ltd. (Ezy MIC Strip).[118] The rapidity and ease of use of this method are counterbalanced by high costs when ran for high volumes of samples.[118,123] The gradient strip is the least affected method by inoculum variations.[123]

Quick, robust, sensitive and cost-effective results providing AST and bacterial identification are more and more needed and sought for, hence the pressure to automate these techniques.[118,121] This modernisation brings the opportunity to maximise throughput in terms of sample numbers, time and costs while facilitating

reporting through connected interfaces and therefore monitoring as well as supporting diagnostics and treatments of infectious diseases (Figure 2.8).[118]
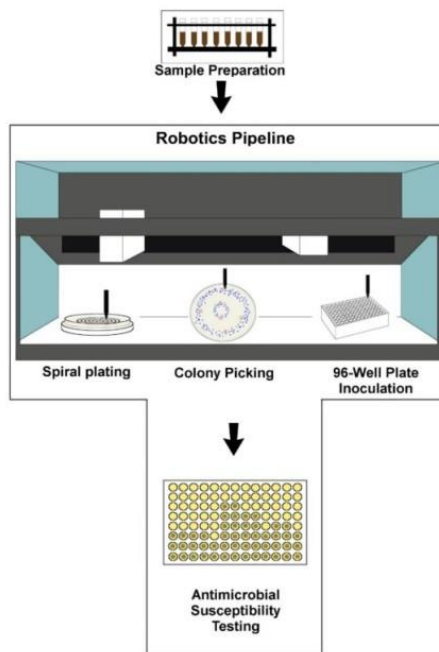
Figure 2.8. Robotic antibiotic susceptibility platform.[128] Adapted with permission from Truswell, A. *et al*. Robotic Antimicrobial Susceptibility Platform (RASP): A Next-Generation Approach to One Health Surveillance of Antimicrobial Resistance. *Journal of Antimicrobial Chemotherapy* 2021, *76* (7), 1800–1807.

2.5.2.4 Automated higher-throughput equipment

A by-product of US space exploration, VITEK (bioMérieux) entered the market in 1973.[118] After manual preparation of bacterial isolates, its later iteration **VITEK-2** automated identification and AST through an optical read of bacterial growth every 15 minutes assessing fluorescence, turbidity and colorimetry.[118] Competition in the automated AST space grew fast with Autobac IDX, MS-2 and AutoSCAN-3 out within the following decade.[118] The **MicroScan WalkAway System** (Siemens Healthcare Diagnostics) evolved from a semi-automated AutoSCAN-3 with frozen substrates in microdilution plates to dry panels and updated database and then an automated version with incubator-reader through to fluorogenic and pH probes to now detect bacterial enzymatic activity.[118] Trek Diagnostic Systems capitalised on the Sensititre Autoreader coupled with the AutoInoculator from the same series and the **Sensititre ARIS 2X.**[118] The first system relies on fluorometric readings of fluorogenic substrates hydrolysed following bacterial growth while the second integrates both incubation

and reading technologies.[118] **BD Phoenix 100** (BD Diagnostics) aims at automating pathogen isolation and AST preparation complemented to growth monitoring three times per hour for identification and AST, which halved AST preparation time compared to manual labour via colorimetry, fluorescence, redox parameters and turbidimetry.[118] Accelerate Diagnostics and Quantamatrix have designed new automated AST systems based on real-time microscopy to further reduce handling and turnaround time. However, test completeness, offering diversity and low costs emerge as limitations.[117]

Bacterial morphology can be an indicator of antibiotic activity. BacterioScan uses a Forward Laser Light Scatter System for a sensitive optical density measurement taking into account cell shape and size.[119] Due to bacterial size most often above 500 nm, imaging methods do not require costly equipment.[119] Time-lapse microscopy is the principle behind the **PhenoBC** kit by Accelerate Diagnostics.[119] Bacteria are identified and concentrated by fluorescence *in situ* hybridisation (FISH) within 90 minutes and analysed by dark-field microscopy with computer algorithms and machine learning to yield a phenotypic MIC in 7 hours. Using the **oCelloScope**, bacteria are first identified then grown to a specific density.[119] Cells are isolated then mixed with microspheres for better focus during time-lapse microscopy.[119] Images are taken under a microscope with additional data on morphology and analysed via an algorithm for segmentation and surface area estimation.[119] **QMAC-dRAST** uses microfluidics to monitor single bacterial cell changes treated with antibiotics.[119,129] Additional deep learning techniques as well as more in-depth cell morphology studies have been undertaken using those systems.[119] For instance, the use of resazurin as a fluorescent dye and reflecting metabolic activity has successfully differentiated using time-lapse microscopy susceptible and resistant bacterial phenotypes.[119] Resazurin combined to a fluorescence read-out has also been used in an AST millifluidic-based system, outperforming VITEK-2 and broth microdilution.[130] Indeed, Avesar *et al.* (2017) developed a rapid and scalable AST with resazurin and droplet arrays at the nanolitre level and able to provide results in half the time compared to conventional AST.[131]

Automated AST solutions provide more control and stability over culture environment or temperature, which facilitates a more rapid growth. By automating disk diffusion, faster generation of results is possible within 4 to 8 hours from positive blood cultures combined with specialised softwares, such as AntibiogramJ, more reproducibility, reliability in interpretations and increased reporting of antibiotic susceptibility determination from inhibition zones can facilitate epidemiological surveillance and monitoring of the efficacy of stewardship interventions.[117] The need for concentrated bacterial inocula remains a prerequisite and limiting factor of all automated AST.[117]

A final comparison between the commercially available antibiotic susceptibility methods is undertaken in Table 2.2 and provides a simplified overview on compromises required for faster results in terms of costs or skilled labour.

Table 2.2. Main commercially available AST methods. Adapted with permission from Leonard, H., Colodner, R., Halachmi, S. and Segal, E., 2018. Recent advances in the race to design a rapid diagnostic test for antimicrobial resistance. ACS sensors, 3(11), pp.2202-2217. Copyright 2018 American Chemical Society.

Method	Test time	Ref.
Agar dilution	>16 h	132,133
Broth microdilution	>16 h	132–134
Disk diffusion	>16 h	132,133,135
Etest	16-20 h	133,136
BD Phoenix	8-10 h	137–140
Vitek-2	>7.5 h	139,141
Microscan walkaway	4-7 h 5-18 h	139,141,142
Phenotest BC kit	<7 h	143
QMAC	6 h	129,144
Sensititre	>16 h	117,118
oCelloscope	6h30	118
Live/dead staining	2-4 h	132,145

Method	Test time	Cost	Ref.
MALDI-TOF MS	1-3 h	low cost per test (after purchase of the instrument)	146–149
Real-time microscopy	2-3 h		150,151

2.5.3 Standards around culture-dependent AST

Culture-dependent AST has been increasingly standardised over time to allow for more comparison and reproducibility intra- and inter-laboratories, between methods and monitoring of drug resistance across regions.

2.5.3.1 MIC & breakpoints

A widely used AST indicator is the MIC. First mentioned in 1929 by Alexander Fleming,[134] it represents the lowest concentration in mg/L of antimicrobial agent hindering visible growth of microorganisms assumed to be infectious, under specific *in vitro* conditions and for a defined duration.[118,121] This time depends on the possibility to culture the species *in vitro* and the replicating cycle of the microorganism.[118] For instance, anaerobic bacteria are much less likely to be culture positive.[118,152] MICs are established by serial dilutions of the antimicrobial agent tested in broth or agar. In practice, MICs are usually a dominant central value comprised in an interval of 2 to 3 doubling dilutions. For lower density of bacteria, the obtained MIC is attributed to single cells while higher density inoculum (above 10^6 CFU/mL) is believed to reflect antibiotic susceptibility of bacterial communities.[119] This reference indicator enables the comparison between AST techniques to generate robust and reliable results.

The MIC reflects the activity of the antimicrobial agent tested considering pharmacology, pharmacokinetics and bacterial resistance to guide clinicians to select the best treatment. It contrasts as a quantitative strategy compared to qualitative breakpoints.[118] Breakpoints differentiate susceptible against resistant behaviours to inform the treatability or resistance of the infectious microorganisms using chosen

drugs.[118] Breakpoints also vary depending on the antimicrobial agent and species combination tested along with local standard organisations thresholds.[118]

2.5.3.2 Complying with adequate regulation and norms

Interpretation of MIC values is mostly guided by standards issued by the European Committee on Antimicrobial Susceptibility Testing (EUCAST)[153] in Europe and the Clinical Laboratory Standards Institutes (CLSI) in the United States.[118,153] Another important body framing and normalising industrial practices into International Standards is the International Standardization Organisation (ISO) with a technical committee responsible for "Clinical laboratory testing and *in vitro* diagnostic test systems" (ISO/TC 212), which exists since 1994. There are two complementary ISO 20776 norms regulating antimicrobial susceptibility testing for intra- and inter-laboratory reproducibility: ISO 20776-1:2019 on broth microdilution followed by ISO 20776-2:2007.

Additional regulations for AST to comply with belong to the *in vitro* diagnostic medical devices (IVD) category. They are defined as « any reagent, reagent product, calibrator, control material, kit, instrument, apparatus, equipment, or system used for the *in vitro* examination of human specimens".[154] For an IVD device to be marketed around Europe, the manufacturers issue a compliance declaration themselves. For CE (Conformité Européenne) marking, the statement encompasses relevant European laws of thirty countries as of 2013.[154] No performance data is needed, solely the disclosure that such data exist and is robust.[154] An annual audit of the manufacturer's quality assurance is required but not by a specific body.[154] Performance data is only reviewed for a handful of tests, targeting HIV, Hepatitis B, C and D.[154] CE marking does not require for the device to have good clinical utility.[154] The US FDA has a more stringent approval process, notably concerning clinical testing, making it longer and more expensive. It is however, not mandatory.[154]

2.6 What is not working and where to go next

Despite a few regulated and standardised AST methods, current needs to inform timely on antibiotic treatment are not met. Moreover, initiatives to

standardise methods and impacts of generated outcomes fall behind when sustaining antibiotic resistance emergence.

2.6.1 Considering current limitations to feed improved AST

Species-level pathogen identification is also a time-limiting step in AST protocols, considering the 24 hours required for routine AST to grow pathogens from a clinical sample and an additional 24 hours to characterise the isolate (Figure 2.9).[118] As using culture-independent methods relying on PCR, genome sequencing or MALDI-TOF MS facilitated and fast-tracked bacterial identification, susceptibility testing improvements appear to be next.[127]

The main drawbacks of current AST platforms are lack of automation and long time-to-result (Figure 2.9), since covering as many drug-pathogen combinations as possible is vital to identify the best treatment and sample handling using microbiological culture methods without automation is labour intensive.[117,128] High-throughput equipment requiring little maintenance and occupying little laboratory space are preferred but the approval of new AST technology is faced with long timeframes, costly procedures, challenging regulations and difficult logistics to comply with.[117]

The ability and conditions to culture infectious agents, with increased time for difficult pathogens, delay appropriate antibiotic treatments, eventually leading to longer hospital stays and higher death rates.[118] Antibiotic resistance reported from anaerobic bacteria is on the rise and facilities and equipment to grow anaerobes are not common for most laboratories.[117] Certain strains also show delayed phenotypic resistance.[154] Antibiotics display greater action on rapid compared to slower growing cells, potentially hindered by a long initial lag phase.[154] As culture-dependent parameters mostly result from intrinsic biology (lag and growth phases), little improvements of these aspects is possible.[117] Even with results from automated systems available within 18 hours, staff working hours and shifts restrict the actual time-to-result to the next day, a major constraint already warned against 30 years ago.[123] Optimisation of sample collection to AST results, via steps prior testing such

as sample collection and handling or clinical decision and patient management follow-up, are more likely to reduce turnaround times in new AST solutions.[117]
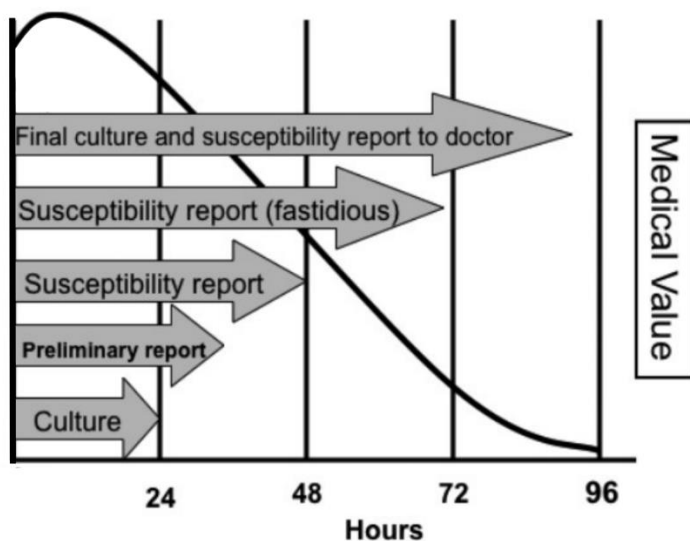
Figure 2.9. Evolution of medical value from culture-dependent AST methods.[155] Reproduced with permission from Goff, D. A.; Jankowski, C.; Tenover, F. C. Using Rapid Diagnostic Tests to Optimize Antimicrobial Selection in Antimicrobial Stewardship Programs. *Pharmacotherapy: The Journal of Human Pharmacology and Drug Therapy* 2012, *32* (8), 677–687.

Among other challenges to be overcome by new AST techniques are the high bacterial load needed for analysis and overcoming market competition.[117] Reducing the time-to-result with a lower amount of material has also not been achieved reliably yet.[117] Despite propositions of novel platforms, market penetration of new solutions is very modest, slowing down innovation.[117] The development and implementation of new AST methods is also faced with cost issues.[117] Getting to the proof-of-principle stage is feasible but the full validation with all bacterial species and antibiotics is much more challenging on technical and financial levels for start-ups.[117] The diversity of approaches, bacteria and antibiotics direct the spotlight onto comparable parameters such as time-to-result or comparisons in the commercial landscape.[117] Disadvantages of techniques tend to be highlighted against minimised strengths as well as a magnification of commercialised solutions over novel technologies.[117] Devoid of a guaranteed success, leveraging enough funds to develop and implement the technology can fail and prevent new AST technologies to reach the market.[117]

2.6.2 The gears of standardisation are sticky

Susceptibility testing of antibiotics provides crucial information to treat patients and monitor antibiotic resistance to mitigate infection spread.[127] Conventional methods to assess antibiotic susceptibility include broth microdilution, disk diffusion assay, E-test strip or the automated Vitek-2 or Phoenix BD, whose result interpretations rely on international guidelines.[83] These tests should normally be run prior treatment decision.[83] Ideally, de-escalation, once AST results are known, should be conducted with adjustment of PK/PD parameters depending on class of compound used, patient and infection location.[83] In a majority of cases, the long time-to-results are exacerbated by limits of culture-based methods. Delaying treatment is not always an option, especially in cases of bacteraemia or sepsis. This reinforces motives behind empirical prescriptions[83] with the healthcare industry only relying on a small handful of *in vitro* bioassays to assess antibiotic susceptibility.[156]

Phenotypic AST such as agar and broth dilution have resisted advances in clinical microbiology diagnostics.[118] Broth and agar serial dilution methods were used prior the 1950s and became more mainstream in the following two decades but have remained quasi unchanged since then.[127] Labour-intensive and time-consuming aspects triggered the development of replacement techniques, in the form of breakpoints and disc diffusion.[127]

In 1960, a WHO expert committee was asked for more clarity around standard AST, with the intent of reaching a consensus around a main method.[127] Ten years later, published recommendations advised on national reference laboratories to report their preferred methods and interpretations.[127]

Four different disc diffusion methods were originally developed[127] (same overarching principle with slight differences in culture medium and preparation).[157] The growing adoption of disc diffusion throughout the 1970s correlated with an increased need of test standardisation for better reproducibility and surveillance.[127] In 1972, the then CLSI attempted a standard publication on a disc diffusion method.[127] Common use of the Stokes (control and tested organisms placed on the same plate)

method in the UK and Kirby-Bauer (size of the test zone correlated to MIC) method recommended by the FDA and CLSI spread more during the 1980s with suggestions of inoculum standardised via spectrophotometer readings.[127] More standardisation of the disc diffusion technique, the most utilised AST method was requested in the 1990s. This reduced variability and increased reproducibility, especially following its 2001 first publication by the British Society for Antimicrobial Chemotherapy (BSAC), annually updated along a EUCAST version.[127] The available standardisation attracted laboratories in the USA as well.[127]

Advantages of the truncated MIC or breakpoint approach (Susceptible, Intermediate, Resistant) was potential for automation, correlation with disc diffusion and possibility to be performed using either broth or agar dilutions.[127] Incorporation with breakpoints, of the treatment outcome in the 1980s and inclusion of pharmacological attributes of the antimicrobial improved breakpoint determination.[127] Establishment of pharmacodynamics and pharmacokinetics in the 1990s from new and marketed compounds refined established and novel breakpoints, despite variability in geographical locations.[127] Additional knowledge about resistance mechanisms has also benefitted better detection.[127] EUCAST MIC breakpoints became increasingly adopted in the 2000s. Harmonisation of breakpoints occurred via EUCAST, differing from CLSI established ones.[127] Breakpoints have been extended to antifungals and antimicrobials in use in the veterinary field.[127]

The antimicrobial gradient strip test provided a new alternative throughout the 1980s to obtain a MIC value.[127] The multiplicity of publications applying it to a variety of microorganisms built a strong basis to refer to for laboratories wanting to adopt the method.[127]

Even if regulatory requirements to submit AST data and proposed breakpoints for new antibiotics are in place,[158] the actual number of colonies to be tested constitutes a range or threshold rather than an exact value whether for genotypic or phenotypic testing.[117] As current guidelines restrict the number of patient isolates, extrapolation of resistance profiles is limited.[158] Including specimen type and species

could provide key information for better empiric treatment as differences are well-known between hospital stay duration, patient age, institutions, etc.[158] Clinical metadata is crucial to interpret genomic epidemiology as significant variability is often noticed.[38] Standardisation plays a key role in minimising inherent error rates,[127] but needs to keep up with current needs. ISO mentions a reviews of standards every five years. Despite the awareness around AMR, it took 13 years to update standards. The main modifications between the earliest and latest versions are the focus solely on broth microdilution performance, the removal of S, I and R breakpoint definitions - respectively for Susceptible, Intermediate and Resistant -, and the update of reagents and method efficiency.

Overall, there is little awareness of healthcare authorities in the need for rapid and new AST.[117] For instance, the institutional antibiogram is a guide to select the appropriate treatment when the infectious agent has been identified.[158] Due to its yearly reporting frequency, on top of complex guidelines, the institutional antibiogram is not sufficient to effectively reflect AMS interventions.[158] Even if the initiative is powerful, fast and rapid AST is still needed to support more frequent updates.[158] The possibility to run disk diffusion using reduced incubation times has taken almost 40 years for EUCAST to update guidelines.[123,159–162] A smart antibiogram could embody a more refined solution with real-time access to cumulative antibiotic profiling.[158]

Due to the absence of safety net to systematically differentiate good and bad performance, gaps in control testing for IVD allow deficiencies to go undetected.[154] The existing centre for evidence-based purchasing informing the UK NHS spending was decommissioned in 2010.[154] Changes phased during the 2015 to 2019 period are not to be applied retrospectively and new tests now need formal reviewing for clinical utility before implementation.[154]

Novel and rapid AST is expected to be versatile and adaptable to the possible present and future ways of prescription.[158] Because of antibiotic resistance, guidelines are reconsidered and antibiotics against which resistance rises, could be

shifted to different prescribing schemes rather than being deemed obsolete.[158] Simultaneous development of new antibiotic and specific AST could be beneficial in positioning the drug in the clinic.[158] Moreover, demands from the different resourced settings might not make all techniques suitable.[163,164] Finally, a single method overtaking completely current high-throughput AST is not foreseeable in the near future, but several solutions complementing each other.[117]

2.7 Laboratory-based non-standard AST

While gold- standard methods rely on differential bacterial growth, they are often too slow at delivering results. This is only partly improved by automated systems that still require an overnight culture step.[165] The infrequent use of susceptibility testing for the complete panel of antimicrobial candidates has been underlined, reported in less than 10% of pandrug-resistant Gram-negative bacteria studies despite being standardised and cheap on a routine protocol basis. Ideally, susceptibility of the pathogen would be available at the start of treatment. Early treatment has been linked to lower mortality rates by enabling a personalised treatment on localised rather than systemic infections.[165]

A large portfolio of alternative AST is being developed in the scientific literature. The methods, their capabilities, strengths and weaknesses are reviewed below and divided between molecular biology-based approaches, spectroscopic, optical and mechanical detection.

2.7.1 Molecular biology

As the cost per bacterial genome has reduced consequently,[121] the more routine adoption of Next-Generation Sequencing (NGS) in microbiology facilities depends on manpower, laboratory and computational infrastructure, bioinformatic needs, quality control and costs[38] and pre-enrichment can be necessary.[38] Whole Genome Sequencing (WGS) is foreseen as the gold standard for epidemiology of infectious diseases.[83] However, WGS still requires a minimum 18-hour culture step as well as costly investments for most microbiological laboratories.[83]

Correct analyses of bacterial genome have the power to identify species, antibiotic susceptibility patterns and virulence features.[38] As genotypic methods are not self-sufficient to conclude on AST, extrapolation of obtained parameters or combined approaches provide a more robust antibiotic susceptibility profile. Taking advantage of the digital PCR time-to-result performances, the monitoring of 16S rDNA copies by real-time PCR has been used for rapid AST. Quantification of the number of nucleic acid copies post drug exposure can be considered as phenotypic AST, overall contents depending on the antibiotic tested.[165] Bhattacharyya *et al.* used antibiotic-induced transcriptional changes at an early-stage from positive blood cultures to detect antibiotic susceptibility by combining RNA detection and machine learning.[166] Taking the example of *Streptococcus pneumoniae*, Leschchiner *et al.* (2022) built an atlas of its genome and how it responds to 20 different antibiotics.[167]

Isothermal amplification constitute a PCR alternative technique without thermocycler that can be utilised closer to the patient.[121] Among possible techniques, loop-mediated isothermal amplification (LAMP) and recombinant polymerase amplification (RPA) are amenable to the point of need with their lower power requirements, increased sensitivity and faster results.

Current protocols encounter genotypic-to-phenotypic inconsistencies and unknown antibiotic resistance mechanisms are not taken into account.[83] Nevertheless, new resistance factors can be easily and quickly implemented into existing workflows.[121] More reliable predictions coming from genotypic-to-phenotypic methods were expected with specific attribution of genetic determinants to resistance patterns. These are now projected onto machine learning algorithms and potential behind multi-omics.[83] Genomic approaches will pursue their development and supplement but not necessarily fully supplant phenotypic testing.[38]

2.7.2 Spectroscopy

Detection of AST using spectroscopic methods including mass spectrometry, infrared, Raman, fluorescence spectroscopy and nuclear magnetic resonance has

been recently reviewed by Ramzan *et al.* (2024).[168] A short account of Raman spectroscopy and MALDI-TOF MS is provided here given their popularity.

2.7.2.1 MALDI-TOF MS: Making the lowest resolution MS work not only for bacterial identification and AST profiling

Progress in the mass spectrometry area has enabled the analysis of various biomolecules including proteins, lipids and carbohydrates in the omics sphere.[169] From an AST viewpoint, mass spectrometry-based methods are more likely to be used for routine quantification of intracellular antibiotic concentrations. Illustrating this, reports of tracking target metabolites instead of the inhibitor have proven 100-fold more sensitive than comparative MIC using LC-MS and automated solid phase extraction MS.[38,170] The combination of MS with stable isotope labelling is another strategy that can yield mass shifts from ^{13}C or ^{15}N incorporated from the growth medium with or without antibiotics to determine antibiotic susceptibility. This rapid and universal method enables a differentiation between susceptible and resistant phenotypes via active metabolism but no MIC estimation.[165] Additional whole metabolome approaches have been more reflective of antibiotic effects.[38,171]. However, a one-size-fits-all assay does not seem relevant as optimal incubation times vary, non-specific binding of compounds or strains to plates differ among other parameters.[38]

Matrix Assisted Laser Desorption Ionisation (MALDI) and ElectroSpray Ionisation (ESI) represent the most commonly used ionisation methods as they preserve the integrity of the analyte - hence qualified of "soft".[169] ESI facilitates ionisation via spraying the sample solution while MALDI involves co-crystallisation with a large excess of matrix, absorbing laser energy and vaporising the analyte to generate almost only single-charge ions.[169] The time of flight (TOF) analyser is the fastest available for MS and is based on the time taken by ions of different masses to travel from the ion source to the detector.[169]

MALDI-TOF MS is therefore the simplest and lowest resolution mass spectrometer and can **identify bacteria at the species level** through a molecular

fingerprint of whole-cell protein extracts via a mass spectrum,[119] compared to reference spectra through database correlation and scoring algorithms.[169] With lower turnaround time and smaller sample volumes, MALDI-TOF MS can achieve higher selectivity than the gold standard routine 16S rRNA sequencing in terms of bacterial identification and is used for epidemiological surveillance.[169] Two major instruments for microbial identification are commercially available, the VITEK MS Plus from Biomérieux and the Biotyper from Bruker Daltonics at high upfront costs of USD 200,000,[169] meaning not accessible to all,[172] even if later compensated by low costs per analyses.[169] Incompatibility between systems from the different vendors is limiting possibilities as databases for reference spectra as well as scoring algorithms differ. Low bacterial concentrations are preventing accurate identification as well as non-indexed microorganisms, which would benefit from reference database expansion and synchronisation. Additionally, only bacterial colonies grown on agar or from a blood culture pellet can be analysed with MALDI-TOF MS. Optimising sample preparation can be tedious but benefits the low resolution from the instrument. The presence of multiple organisms within a single sample still yields correct differentiation and identification.[169]

MALDI-TOF MS has been developed as a fast method not only for pathogen identification but also **antibiotic susceptibility testing,**[119] through rapid, accurate and simple detection of known resistant mechanisms.[165] Proteomic analysis of pathogens incubated with different antibiotics at breakpoint concentrations for 60-150 minutes, without any need for calibration, can also provide relative growth variations.[119] A method developed by Maelegheer and Nulens (2017) using minimal sample preparation via centrifugation and washing, minimising analysis costs, provided an identification and AST profile of *E. coli* and *S. aureus* in blood cultures within 24 hours thanks to MALDI-TOF MS.[172] Changes in the bacterial metabolome following drug treatment can be applied to more bacterial species, antibiotics and resistance mechanisms,[165] such as modified antibiotic target or biomarkers.[173] Mass shifts from specific enzymatic activity such as β-lactamases and carbapenemases allow the detection of antibiotic resistance mechanisms activity after 30 to 180 minutes of

incubation.[119] The detection of specific patterns and complex workflow requiring protocol optimisations and experienced operation[165] do not make it a fully universal method yet.[119]

Having an integrated solution for bacterial identification and AST all in one is the power of MALDI-TOF MS,[117,165] digital PCR still being unbeaten on the time-to-result aspect.[165] A more detailed account of MALDI detection of resistance is available by Yoon and Jeong (2021).[153]

2.7.2.2 Raman

Raman techniques are based on vibrational spectroscopy, that require no sample extraction, are non-invasive and label-free.[165] Raman spectroscopy provides a fingerprint of metabolites,[165] similar to infrared spectroscopy (IR),[119] with intensity proportional to concentration.[165]

Changes of shape and intensity therefore reflects metabolic shifts[165] that can be correlated to antibiotic resistance or susceptibility. Additionally, this can also provide information for species identification.[119] Another Raman approach for AST can be via the quantification of carbon-deuterium peak intensity change from deuterium labelling of bacteria.[165]

Spontaneous Raman Scattering (SRS) with microscopy benefits from high speed imaging and resolution below micron level to detect bacteria.[165] D_2O-SRS has proved able to detect bacteria, within 10 min and their metabolic response to antibiotics SRS AST methods are universal and can measure clinical samples directly.[165] Spectral differences can be hindered by background noise and long integration times are often required to reach high accuracy.[165] The throughput of the method remains low with single measurements and a necessary sample drying.[121,165] A case-by-case basis is necessary to analyse antibiotics and bacteria, preventing Raman of being a universal method.[165] A full review on AST using SERS is available from Novikov *et al.* (2022)[174] and Dina *et al.* (2023)[175].

The development of programs to enable the translation of phenotypic data into actionable information for clinicians is ongoing but not yet available.[117] The

integration of deep learning could lower assay time, reported as time-consuming and low-throughput,[165] as identification of spectral motifs and patterns has improved but not yet been integrated into databases.[121] Despite an expensive and bulky piece of equipment, it is tunable, highly sensitive[119] and can offer higher-throughput processing capabilities[165] – depending on authors.[38]

Combinations of detection methods are also possible for confirmation or added information. Most techniques mentioned in this part are available in centralised laboratory facilities but efforts to bring them to the point of care are increasingly seen. The following methods are found in central laboratories but can be adapted and simplified for on-field detection.

2.7.3 Optical methods

Optical methods to assess antibiotic susceptibility can be based on either the detection of whole cells or metabolic changes linked to antibiotic susceptibility or response. They are usually non-invasive, non-destructive and not disturbing for the culture with the highest potential for adaptation into higher throughput solutions.[176] Culture-independent methods constitute an alternative approach to reduce AST time-to-result but also provide a possibility to test for antibiotic susceptibility for non-culturable microorganisms. As the correlation between bacterial metabolism and antibiotic resistance is well-established and changes resulting from microbial metabolism are much faster than obtaining multiple generations in a culture,[165] comparisons of bacterial behaviour in presence and absence of antibiotics provides an alternative for more rapid AST.[165] Outcome of both methods might differ depending on the microorganisms and antibiotic combinations tested. As a result, indicators of viability compared to direct phenotypic cell viability might be assessed.[117]

2.7.3.1 Imaging

Optical detection based on imaging can be heavily based on microscopy or cameras.[176] A direct alternative method to colony counting includes a wide field-of-view real-time microscopy on-chip detection called ePetri. This compact solution

allows automated colony dynamics monitoring.[177] As traditional microscopy techniques suffer from the difficulty of analysing multiple samples at once,[119] multiplexed automated digital microscopy has been proposed. Both identification and antibiotic susceptibility are obtained from clinical samples within 6 hours via FISH for identification and digital microscopy for AST.[178] Single cell analysis enables lower amounts of starting material.[119] Single-cell morphological analysis can also determine antibiotic susceptibility based on cell shape variations induced by antibiotic treatment.[179] The commercial oCelloscope monitors a cell population based on digital imaging of cell autofluorescence in liquid with real-time growth monitoring at high throughput by image stack processing.[176]

2.7.3.2 Non-imaging

Optical density (OD) measurements are based on the amount of scattered or absorbed light and can be directly correlated to microbial population count.[176] They provide a less time-consuming and labour- intensive alternative to colony counting by sampling at set time points and are readily adaptable to different conditions but can be disturbing for growth.[176] Light diffraction can provide a monitoring of variations occurring in a culture, that is possibly applicable to single cells.[176] No labelling, staining or tracking is necessary for this low-cost method.[176] The refractive index captured by photodiodes or induced by lasers is a possible way to assess AST.[176] Using forward laser light scattering (FLLS) allows the simultaneous assessment of multiple samples for microbial growth and is the technique behind the BacterioScan.[176] It determines bacterial cell count and size based on angular changes in scattered light intensity.[180,181]

Surface Plasmon Resonance (SPR), as well as its imaging associated version SPRi detects a surface plasmon wave generated by the oscillation of charge density located at the interface between two media with dielectric constants of opposite signs.[182] Identification of bacterial cells and their susceptibility to antibiotics using SPR has been reported by a multiplicity of authors.[183] For wider adoption, better accessibility and affordability of this method would be required.

With flow cytometry, single cell characteristics (morphology, number) are analysed, which requires long sample preparation and can include fluorescent labelling for viability, identification.[119] Based on light scattering, flow cytometry for AST is not widely adopted, possibly because of non-optimal staining and cell autofluorescence, no possible differentiation between bacteriostatic and bactericidal effects or scarcity of available databases for clinical validation.[180]

Non-imaging methods can suffer from low sensitivity and specificity while imaging relies on operator skills for accuracy and throughput. Both categories require bulky and sophisticated instrumentation and can be reliant on bacterial culture, meaning also plagued by its drawbacks.[176]

2.7.3.3 Colorimetry

Belonging to optical assessments are colorimetric methods via chromogenic or fluorescent probes, providing faster and more sensitive results than plate counting.[176] Changes in pH can be evidenced from bacterial growth using phenol red for instance and metabolically-active cells via resazurin.[123] They can be extrapolated to growth, division or antibiotic activity of/on bacterial cells.[176]

As ATP is the most common compound testifying of energy transfer in cell metabolism, it closely relates to cell count and could eventually prove a more quantitative approach than OD monitoring.[165] ATPase is first used to remove human ATP from clinical samples[165] and oxidation of luciferin to adenoxyluciferin with photon release can provide AST results in less than 4 hours.[165] Another bacterial-specific bioluminescence assay allows a bacterial count estimation within 2 hours at high sensitivity but still relies on bacterial growth.[165] While OD increases during bacterial growth but remains identical during lysis, ATP levels still reflect antibiotic efficacy once steady growth has been attained.[184] The qualitative output obtained discriminates between susceptible and resistant phenotypes rather than a quantitative MIC assessment.[165] A reported luciferase-based assay for bacterial viability has enabled a greater throughput for reduced time and costs.[38] Benefitting from a simple method and low-cost instruments, the ATP bioluminescence to assess antibiotic susceptibility

has the potential to be adapted in the clinic as running the assay does not require experienced staff, even if further validation is still needed.[165]

The growing use of nanomaterials has been mainly reported for sensitive diagnosis and has also applications for early stage detection and finer imaging or visualisation due to their sensitivity as well as more precise drug delivery without adverse reactions.[182] Optical methods benefit from mathematical modelling improvements, more miniaturisation and accuracy with a point-of-care format.[176] Progress from imaging methods will provide more information about individual cell processes.[176] Problems often encountered include non-transparent media, noise, interferences from cell debris, gas bubbles or micro-/nano- particles, time and cost efficacy, inhibition of fluorescent reagents.[176]

Costly fluorescent probing can be countered using microfluidics,[119] complementary with optical methods for sample processing or higher throughput.[176] Microarray systems provide a platform to screen samples at high throughput with fluorescence for instance.[119]

2.7.4 Mechanical and thermal detection

Droplet-based assays and piezoelectric sensors are also at the heart of multiple published platforms, call for little sample and provide a high sensitivity on antibiotic susceptibility testing.[119] By exerting a mechanical force on piezoelectric crystals, an electric signal is generated. The crystal is functionalised with a biorecognition element and the formation of a complex with its specific target induces a perturbation in the mass detected and therefore in the oscillation frequency detected as an electrical signal.[185] Quartz crystal microbalance (QCM) is a perfect illustration able to detect bacteria rapidly and in real-time.[121] More and more nanomechanical sensors are being developed.[119] Microcantilevers can also facilitate single cell analysis by the detection of cell mass and nanomechanical characteristics changes. Cantilevers allow the passage of microbes through small channels yielding a change in frequency through a weight variation.[176] Highly sensitive, fast, and easily miniaturisable, they need to operate in air, meaning testing in relevant matrices is

rarely reported.[186] Despite taking advantage of bacteria-surface interactions, nano-and micro-technologies struggle with precision, reproducibility and scalability.[119] Relying on enzyme activity, calorimetry senses heat produced or consumed during a reaction via a thermistor into an electrical output.[185] Microcalorimetry is based on heat generated by metabolic processes with reaction rates proportional to heat flow rates and the total heat production linked to the extent of the reaction, however non-specific.[176]

2.8 AST closer to the point of need

2.8.1 The case for rapid AST...

Diagnostic tests are an essential response strategy to antimicrobial resistance and rapid assays, critical to implement antimicrobial stewardship.[121] Rapid AST (rAST) would allow quicker prescription of appropriate antibiotics, the reduction of use of empiric broad spectrum drugs[165] and epidemiological surveillance.[158] Rapid AST can be defined as AST completed in an 8-hour workshift maximum - more realistic than in the ultrarapid method timeframe of 4 hours. rAST are either categorised as rapid single test or accelerated full AST. The former facilitates activity assessment of single antibiotics against defined microorganisms to discriminate susceptible from resistant phenotypes but still require full AST profiles as they are considered an add-on assay. The latter provides complete susceptibility profiles similarly to standard methods. In the case of MALDI-TOF MS, microbial identification has been accelerated and allows for infectious species to be known before phenotypic testing, which restricts the antibiotic panel to be screened. Even if MALDI-TOF MS has directly and positively impacted patient care, this workflow requires involved sample preparation.[123]

Only low-cost and user-friendly rAST has a chance to be widely adopted for routine diagnostics, more beneficial for patients and medical staff and financially attractive for the industry in terms of intellectual property. Feasibility of rAST is possible using inexpensive methods such as colorimetric tests. Metabolic-based AST has the potential to provide a shorter turnaround than culture-dependent methods, through the monitoring of ATP or macromolecule biosynthesis for instance.[165]

Additional features are multiplexed testing and the possibility of adding more samples to the queue while the assay runs.

Despite the universality of phenotypic rAST along with exact categorisation, results are still affected by inoculum effect, delayed resistance, lag phase and initial biomass increase from susceptible samples; however, the exact incidence is unknown.[123] More studies are needed to evaluate this risk and enable confidence in shorter time-to-result methods. Maintaining rAST assay conditions as close as possible to standardised methods is advised since incubation times are already a deviation, with a reference method as close and relatable as possible to the rAST being characterised.[123]

Innovative AST solutions are being proposed and can be implemented with currently existing platforms. A high degree of integration is needed for pretreatment steps and user-friendly interfacing but none is yet optimal.[121] Microfluidics, machine learning, and automation can all improve turnaround times, sample handling, required volume and throughput.[119] Microfluidics support point-of-care solutions, however their development into clinical solutions is slowed down by specific reagent costs.[119] The advantages behind microfluidics - minimal sample, reagents and power use, low cost, user-friendly handling, rapid turnaround time, integration (multimodal), automation, and portability[121] - are not fully exploited as the necessary preculture step yields sufficient material for analysis and automated AST solutions are available on the market. Machine learning is increasingly utilised to recognise antibiotic resistance from large datasets and contribute to a faster time-to-result. Limitations arise mainly from the programming knowledge of platform designers or insufficient sample set size.[119] Mobile phone readers have also made their way into AST from disc diffusion to plasmonic sensors.[117,119,187] Cost, ease of use, speed, accuracy, precision and ability to multiplex are all to be considered and balanced into new AST solutions. Most new platforms tick a majority of criteria but rare are those able to meet them all.[119]

Technological obstacles and organisational aspects are roadblocks as much as market competition.[123] The plethora of rAST published is not reflected in the clinic with no penetration in routine practices.[123] Despite new technologies being time-saving, conventional methods still prevail.[121] Manual AST products represented the largest share of the overall AST market in 2019. Disk diffusion held the biggest share for its low cost and the diversity of commercially available disks, with hospitals and diagnostic laboratories as main end users.[121]

2.8.2 ...at the point-of-care

As bodily fluids are almost exclusively handled by central laboratories, with blood being the gold standard sample matrix for biomarker and detection, bringing samples from patient to testing point contributes to delay results.[188] Cheaper, safer reagents and instrumentation are essential to bring testing out of the laboratory.[188] A point-of-care (PoC) assay is the best use of a rapid technique.[189] It limits sample transport, enables faster triage and medical decision-making, prevents broad-spectrum empiric prescribing and facilitates antibiotic treatment monitoring.[189] Nowadays, PoC applications can be envisioned in pharmacies, home-based care or telemedicine.[190] Telemedicine is a growing area that encounters a majority of infectious cases, especially as a result of the recent SARS-CoV-2 pandemic,[191] where PoC AST would support treatment decision-making by providing quick information to the medical professional. Since a teleconsultation interaction is short, no prior relationship exists between the patient and healthcare provider - not necessarily aware of local antibiograms -, preventing antibiotic misuse with maximal clinical outcomes is very challenging in this setting.[191] Point-of-care testing is crucial to restrict emergence and spread of antimicrobial resistance worldwide.[190]

Not only attractive costs will be decisive but also a better education of the general public concerning PoC tests and health benefits.[190] As national and international reimbursement schemes remain rare, patients without basic healthcare insurance might face the choice between paying for antibiotics or a PoC test.[190] First-line users are healthcare providers since directly dealing with patients and responsible to empirically decide on the use of a diagnostic test,[190] making it vital to

understand how the perception of clinicians impacts decision-making in an emergency situation and avoid inappropriate prescribing.[190]

While PoC tests compete on multiple fronts, they do not intend to fully supplant current diagnostic methods but allow an early screening to facilitate later analyses.[188] As antibiotic stewardship practices mainly target hospitals, primary care and long-term care settings,[191] adapted frameworks would be necessary for direct-to-consumer telemedicine to prevent rising antibiotic resistance in the community.[191] Since PoC tests could be used without medical/professional supervision, special assistance will have to be arranged via telephone or internet hotlines.[190] Innovators are therefore in charge of creating and maintaining efficient communication between interested parties to ensure PoC test adoption, appropriate use and improvement and make evidence-based medicine prevail over empirical practices.[190]

Hand *et al.* (2021) reported on the use of MicroGuide[TM], an application to support healthcare providers in their antibiotic prescription practices, help them follow guidelines and adhere to antimicrobial stewardship policies.[192] As the speciality of most doctors falls outside of microbiology and infectious diseases, infections are most often dealt with by non-specialists and the application provides convenient and timely access to key information for patient treatment, which participates in antibiotic stewardship.[192] The program is adaptable by each care facility for the most suited guidelines depending on epidemiology, clinical setting and location, and enhanced clinician user experience.[192] MicroGuide[TM] sorts decisive information and provides a fast access to antibiotic prescription data for a more prompt, supported and up-to-date clinical decision.[192] A regular update of antibiotic guidelines is highly important as well as monitoring on a more patient-centric level since appropriate antibiotics can vary on a case-by-case basis. A fear of medical de-skilling from using the application was raised, however the opposite was observed with improved knowledge of antimicrobials, even if empirical prescriptions remained.[192] Patterns of prescribing can also be informative to set and design meaningful antibiotic stewardship interventions[193] and an application is a familiar format that easily supports patients

and prescribers. Support is needed and welcome but changing everyone's behaviour is not easy.

Another consideration for PoC rAST is the decentralisation of data.[190] Collected results could be correlated with environmental, meteorological or entomological parameters, to predict the origin and spread of arising and current infectious diseases and release early warnings.[190] Furthermore, machine learning could feed decision support systems to improve healthcare outcomes by anticipating a physiological and more cost-effective response to treatment or drawing more personalised and regional antimicrobial resistance profiles.[190] All these could be implemented directly at the point of care using biosensors.

2.8.3 Biosensors

Biosensors are composed of a bioreceptor able to bind an analyte of interest, immobilised on a transducer to translate a binding event into a readable signal.[182] Selecting an appropriate biorecognition element, since each displays unique properties, is rooted in analyte and transducer features. Detailed below are the main strategies to bring selectivity and specificity to biosensors via enzymatic, affinity, and nanomaterial-based recognition (Figure 2.10).[182]
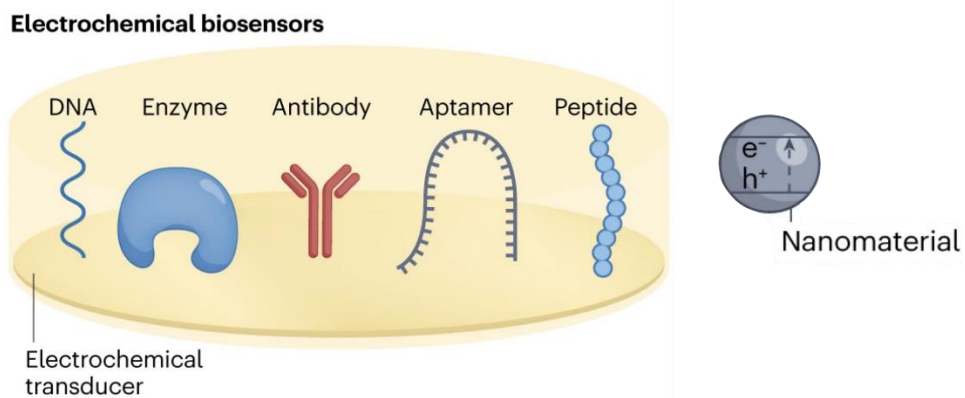
Figure 2.10 Electrode functionalisation possibilities for selective and specific recognition. Adapted from Wu, J., Liu, H., Chen, W. *et al.* Device integration of electrochemical biosensors. *Nat Rev Bioeng* **1**, 346–360 (2023).[194]

Enzymes were the first type of bioreceptor used in biosensing[195] and offer high binding affinity and specificity.[196] They catalyse a specific reaction, allowing measure

of either reactant or product[196] without alteration of the bioreceptor[195], and of the analytical signal obtained through monitoring the Faradaic current at constant potential.[195] Binding to the active site occurs through hydrogen, electrostatic or non-covalent interactions.[196] Enzyme immobilisation onto a highly conductive material provides stability, embedded in surface structures for short diffusion[196] and their nature implies reusability. Depth and density of surfaces need to be fine-tuned as deeper structures allow for denser packing but might result in less sensitivity with higher limits of detection and slower sensor responses.[196] Amperometric and potentiometric enzyme-based sensors are more often reported than impedimetric detection.[196] Oxidoreductases are of high interest as they catalyse reactions involving electron transfer. Oxidases are often employed for the detection of analytes such as glucose, ethanol or lactate.[195] The most successful example of enzymatic detection is the glucose sensor, first commercialised biosensor in 1975,[182] having evolved through four generations until now (Figure 2.11).[196]
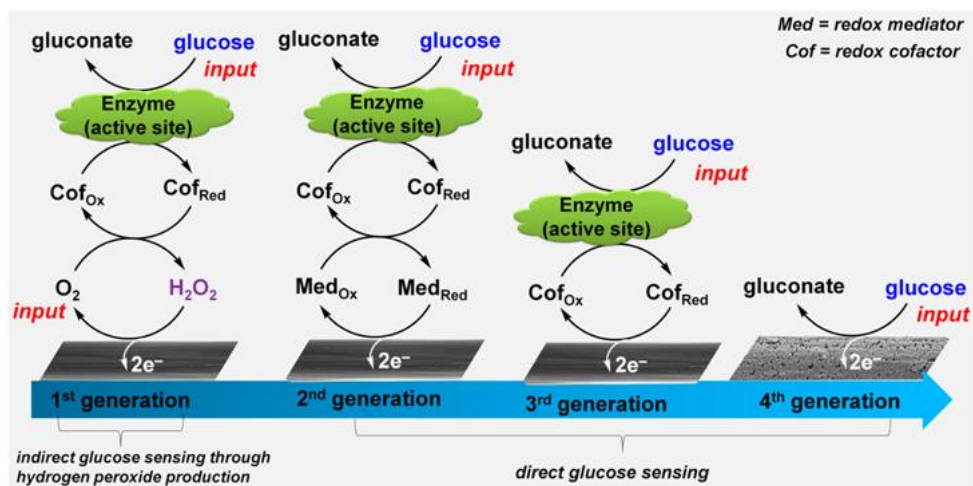
Figure 2.11. Four generations of glucose sensing strategies.[197] Reproduced under CC-BY 4.0 license from Kumar Das, S.; Nayak, K. K.; Krishnaswamy, P. R.; Kumar, V.; Bhat, N. Review—Electrochemistry and Other Emerging Technologies for Continuous Glucose Monitoring Devices. *ECS Sensors Plus* 2022, *1* (3), 031601.

The first generation used glucose oxidase, oxidising glucose into gluconolactone in aerobic conditions, yielding hydrogen peroxide and water, which then undergoes a second transformation into gluconic acid.[182] The presence of the FAD^+ cofactor is necessary for glucose oxidase activity, reduced to $FADH_2$. This demanded high operation potential and high selectivity and was limited by the

oxygen deficit, or its solubility in biological fluids.[182] To counter this, the second generation of glucose biosensor took advantage of non-physiological electron acceptors such as "ferrocene, ferricyanide, quinones, tetrathialfulvalene, tetracyanoquinodimethane, thionine, methylene blue, and methyl viologen".[182] The third generation of glucose sensing devices aimed to solve the mediator toxicity by detecting the direct electron exchange occurring between enzyme and electrode, providing great selectivity.[182] The fourth generation is sometimes qualified by nanotechnologies, sometimes by non-enzymatic glucose sensors.[182]

Enzymatic-based detection of antibiotics is reported but not necessarily with an AST focus.[198] Reports of their activity have been the focus of specific studies as well[199,200] but not as widely reported as affinity-based strategies.

Contrarily to catalytic-based recognition, affinity-based interactions rely mostly on thermodynamic forces such as enthalpy in the case of charge mediation or entropy when hydrophobicity is involved, highly influenced by solvents.[196] Bioreceptors employed for affinity binding encompass antibodies but also aptamers, MIPs, DNA, peptide nucleic acids (PNA)…

Antibodies remain a staple despite their "known and accepted limitations".[196] Antibodies are 3D Y-shaped natural proteins, which allow for highly specific recognition of an antigen, forming an immunocomplex upon binding.[196] Overall in the 150 kDa range,[196] they are constituted of two light and two heavy chains, with each light and heavy chain pair linked by a disulfide bond.[201] They can be monoclonal, specific for a single epitope or polyclonal, able to recognise multiple sites.[201] Passive adsorption of antibodies on electrode surfaces prevents any controlled orientation. This can be achieved by targeting sulfhydryl groups, covalently binding them to the electrode and forming a brush-like array,[196] or fragment receptor binding. Chemical modification of the antibody itself is also possible. Extensive reviews are available concerning electrochemical immunosensors targeting either antibiotics[202] or pathogens[203] more specifically. Identified from biochemical pathways, their isolation and purification comes at a non-negligible expense and so does their lengthy, *in vivo*

production.[196] Disadvantages of antibody-based biorecognition also includes limited stability and storage.[196] Demonstrated accuracy and reliability is not sufficient to move reported early-stage solutions closer to commercialisation.[204] Alternatives are being explored such as fragments or nanobodies, single chain antibodies discovered in the 1990s in camels.[196]

Synthetic molecules were designed to counter production drawbacks from natural molecules, mostly antibodies and enzymes, and offer flexibility of target analyte, stability and smaller size.[196] Artificial-binding proteins include affibodies, low molecular mass affinity proteins.[205] Their triple alpha helical structure enables specific and selective binding to a wide range of proteins.[196] Synthetic nucleic acids are complementary and unique strands of DNA, with a specific binding motif to the targeted bioanalyte.[196] After identification, they are artificially designed to be subsequently immobilised onto sensor surfaces.[196] Steric hindrances from nucleic acids limit sensitivity, which is why locked nucleic acids were developed,[196] with the 3' ribose locked for more rigidity and improved binding. Another alternative is PNA, oligonucleotides with repeating aminoethyl-glycine motifs linked by peptides that are neutrally charged for enhanced binding stability.[196] Better accessibility to binding domains enables a greater biosensing range and less sensor saturation.[196]

Aptamers are synthetic single-stranded oligonucleotides, developed for a wider range of analytes through the SELEX process. Their affinity challenges antibodies even for small molecules along with easy chemical modifications and selectivity.[196] The detection scheme is based on a conformational change upon target recognition, with possibilities of signal on or off assay development. Redox labelling is available but not imperative,[196] with methylene blue replacing ferrocyanide due to its hazardous nature and the labelling not being possible in buffer.[206] Available reviews covering aptamer-based sensors recognising antibiotics[207,208] or pathogens[209] are an easy find.

Molecularly-imprinted polymers (MIPs) are synthetic recognition elements with a templated polymer matrix, modulable depending on the combination of

monomer, cross-linker, solvent and target analyte. Similarly as enzymes, they can be embedded in surface structures on transducers. This enables low fabrication cost, ease of development and stability, however weighed down by low selectivity due to the nature of binding interactions, non-covalent, electrostatic or size inclusion or exclusion. Non-specific binding occurs more frequently with larger molecules, that increased cross-linking can partially solve since affecting binding and slowing down responses.[196] Published reviews using MIPs to detect antibiotics[210] and pathogens[211] account for their popularity.

Coating sensor surfaces with nanostructures heightens catalytic potential, upgrading sensitivity but driving specificity down. Cross-reactive sensors can benefit from a multiplicity of catalytic functionalisation, still compromising on a specific sensor response.[196] More specifically, gold nanoparticles covalently bond to thiol groups, hence their wide utilisation. Platinum and palladium in conjunction with carbon nanotubes are another popular option for better conductivity and electrocatalytic activity. Polymers, whether nanostructured or molecularly-imprinted are gaining more popularity. While nanostructured polymers are motifs at the microscale to facilitate surface immobilisation, MIPs are macrolevel synthetic structures able to bind specific targets. Despite MIPs numerous advantages such as low cost, ease of synthesis, stability in terms of chemistry, temperature and storage, and reusability, they lack electrocatalytic activity and conductivity. This has been improved by conjugation with carbon dots and carbon nanotubes for instance. Quantum dots are another alternative, semiconductor nanomaterials producing bright luminescence upon light or electrical excitation, directly correlated to their size with little toxicity. MXenes are a mix of transition metal and carbon or nitrogen layered in two nanodimensions, facilitating immobilisation. They allow improved electron transfer, catalytic activity and absorption and low resistance at the interface.[212]

Multimarker detection can be designed as various recognition elements immobilised onto one transducer, with distinctive detection windows or multiplexed

detection with a multiplicity of transducers, each associated to a single biorecognition molecule.

Molecular methods, amplifying genetic contents of lysed cells alongside microbiological culture methods are most common. Affinity-based biosensors prove to be an upcoming solution to provide ubiquitous testing. However, washing steps and tagging do not make them compatible for wearable options. Tedious and time-consuming sample preparation can be supplanted by microfluidic strategies, as hydrodynamic flow enhances mass transfer to the transducer, yielding better performance. Wireless connectivity represents the next step to manage data with Bluetooth, near-field communication (NFC) or internet of things (IoT) for instance. Equipment miniaturisation and sensor production should be picked up as follow-up studies to bring published solutions nearer commercialisation. Long term stability also needs better assessment and improvements. Precision and personalised medicine with point-of-care testing would allow patient data to be directly communicated from patient to clinician for real-time treatment monitoring and decision-making.[188]

Quantitative sensitivity and selectivity are most often the measures of success from early-stage sensors.[196] Sensitivity is the signal change measured as a function of analyte concentration and based on limits of detection.[196,182] Selectivity translates the ability of the sensor to only respond to the intended target. Poor selectivity results in high false positive rates, showing positive responses in negative samples. When selectivity is most important, antibodies and enzymes are the ideal recognition elements. Nucleic acids and aptamers suffer from non-specific electrostatic interactions due to their negative charge, countered by the neutrality of PNAs.[95] At an early development stage, biosensor features refined should be reproducibility and stability.[182] Fabrication of multiple identical sensors providing a consistent response shapes reproducibility. Factors impacting reproducibility include intrinsic variability from biorecognition elements, nature of surface attachment and inconsistencies in surface constructs. For instance, antibodies and enzymes can be easily degraded by pH or temperature changes, meaning transport and storage are key. Synthetic

bioreceptors such as MIPs or aptamers are not impacted by batch-to-batch variations compared to *in vivo*-produced antibodies. Sensor reusability is rarely reported, with the majority of sensors being developed for single use. Considering and testing regeneration through chemical, thermal or electrochemical strategies could be a future emphasis for PoC sensor development.[196] However, reproducibility and reusability are infrequently discussed, which could explain why sensor technology transfer from benchtop to benchside is stalling, along with selectivity in complex matrices not systematically reported. Out of the REASSURED criteria - Real-time connectivity/Ease of sample collection/Affordable/Sensitive/Specific/User-friendly/Rapid, robust/Equipment-free/Deliverable to end users - as well as the more focused requirements, meeting them all is challenging and trade-offs have to be made, knowing recognition elements limitations.[196] All criteria have their importance and setting standards appears to be a common suggestion to solve inconsistencies, assess reproducibility and reusability, to move sensor development to the next stage.[196]

Recent innovative techniques have fuelled the diagnostic clinical microbiology landscape. Sandwich immuno-assays have progressed into PoC tests, PCR scaled to high-throughput methods and automatization is adapted to more and more routine procedures. Point-of-care strategy aims to overcome the expensive, immovable, requirement for analytical equipment disadvantages for on-site, rapid and cost-efficient detection.[182] Focus on biomarkers - biological molecules found in blood, other bodily fluid or tissue indicative of normal or abnormal condition or diseases[182] - present at very low concentrations, do not solely serve the purpose of diagnosis and monitoring but also provide prognostics for treatment.[182] Electrochemical biosensors constitute cost-effective, miniaturisable and simple instrumentation subject to automation,[176] alternatives to the commonly used chromatographic, immunoassay and notably ELISA, one of the most important analytical detection method for analytes,[182] as well as microbiological culture methods, scoring high on cost reduction and/or time duration.[213]

The Global Use of Medicines report forecasts a growth up to USD 1.9 trillion by 2027, with cancer as the leading sales therapeutic area and diabetes ranking third.[214] Glucose sensing is the biggest market share for PoC solutions. In 2022, the global biosensor market value was estimated at over USD 27 billion, with a compound annual growth rate over 7% in the next 5 to 10 years.[215–217]

Unfortunately as a general trend, obesity is signalled as a forthcoming area for therapeutic sales, closely linked to diabetes,[214] setting a promising market opportunity not only in terms of sales but also innovation and investment. Taking advantage of innovations/equipment and available production facilities but also familiarity of the system and format both from patients and healthcare providers with electrochemical sensing would prove opportune to use electrochemical detection for AST. Components of an electrochemical system are detailed next.

2.9 Electrochemical detection principles

Electrochemistry allows for the analysis of interfacial properties through qualitative or quantitative detection of oxidation or reduction reactions involving ions, molecules of various nature and size such as drugs, hormones, nucleic acids, proteic biomarkers or even pathogens. Instead of using chromatography or spectroscopy, electrochemistry facilitates a cheaper, simpler, easier to miniaturise rapid and accurate detection.[218]

2.9.1 Electrochemical cell composition

2.9.1.1 Electrodes

Cell design and composition varies according to the studied sample and experiment conducted.[219] Electrochemical cells are commonly composed of three electrodes: the working electrode (WE) at which the reaction of interest takes place, the reference electrode (RE) with a constant composition giving a stable and reproducible potential via a bridge insulating from the sample and an auxiliary or counter electrode (CE) constituted of an inert conducting material.[219] The reference electrode is placed as close as possible to the working electrode.[219] Since no current

flows through the reference, the counter electrode allows to complete the current path (Figure 2.12).[219]
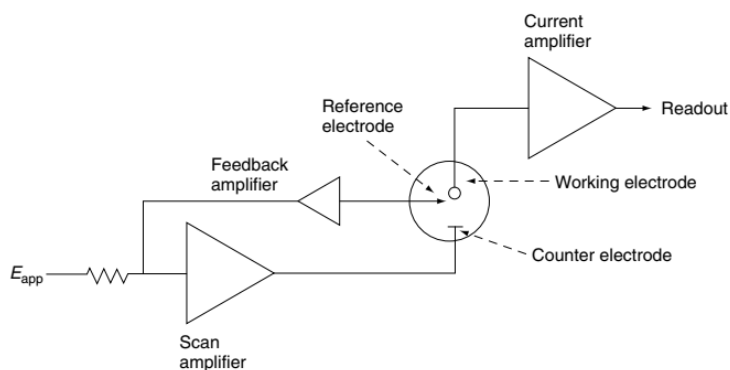
Figure 2.12. A three-electrode potentiostat.[219] Reproduced with permission from Wang, J. *Analytical Electrochemistry*; 2006.

The working electrode material is key for the performance of the measurement. This influences the signal-to-noise ratio as well as the reproducibility of the obtained response. The redox activity of the target analyte is primordial and so is the background current of the potential region but also the working potential window, electrical conductivity, surface reproducibility along with electrode mechanical properties, cost, availability or toxicity. The most popular electrode materials are mercury, carbon and noble metals such as gold and platinum. Due to toxicity and a limited anodic range, the use of mercury electrode has been abandoned. Silver, nickel and copper electrodes are reserved for more specific applications such as cyanide and sulfur-containing molecules for the former and amino acids or carbohydrates in basic environments for the latter materials.[219] Solid electrodes can be stationary or rotating and require pretreatment and polishing before use. Carbon electrodes allow measurements to be conducted in a broad potential window with low background current, a rich surface chemistry, chemical inertness at low cost with slower electron transfer than metal electrodes. The type of carbon, glassy carbon, carbon paste or carbon fibre for instance, and pretreatment greatly influence further analytical performance. Boron-doped diamond presents semi-conducting to semi-metallic properties with a wide potential window of nearly 3 V, low and stable background current, good electrochemical reactivity without pretreatment, low sensitivity to dissolved O_2 and extreme hardness. Metal electrodes

such as platinum and gold present very favourable electron transfer kinetics and large anodic ranges but more limited cathodic potential windows. High background currents however, can originate from the formation of surface oxide or adsorption of hydrogen layers. Gold is more inert than platinum, meaning less prone to oxide film formation or surface contamination. Copper, nickel and silver have been utilised for the detection of carbohydrates and amino acids. Bismuth film electrodes constitute an alternative to mercury electrodes, especially for stripping voltammetry of trace metals. Alloy electrodes are often employed to circumvent the adsorption or corrosion of one of their components.[219]

Along with material, electrode size plays a significant role in device performance. Using micro- over macro-electrodes provides a higher signal-to-noise ratio due to reduced electrode capacitance. The less linear and more radial diffusion leads to a higher current density, enhancing the mass transport rate.[220,221] As polarisation time is decreased, overall assay time is reduced which better supports *in vivo* monitoring.[220] However, micro-electrodes require additional cleaning and pretreatment, a sensitive current amplifier and their matrix is easily deactivated and reacts chemically with organic solvents.[220,222] Higher variability between devices also arises from reaching the performance limits of manufacturing processes.[220] Ultramicroelectrodes only provide a very small current using two electrodes which requires an efficient current measurement circuitry for good differentiation between Faradaic response and electronic noise with grounding and shielding of the instrument.[219]

The reference electrode is responsible to yield a stable and reproducible potential through a constant composition of both redox couple forms, regardless of sample composition.[219] The standard hydrogen electrode, even if being the primary standard due to the precision of their measurements, is not easy to handle. Mercury-based reference electrodes were reported but have been supplanted by Ag/AgCl for their simplicity and reproducibility. Silver/silver chloride references can also be used in microsystems.[223]

After deciding on the most appropriate composition for the electrochemical cell depending on the intended application, the electrochemical cell is placed in a solution to be analysed in the presence of electrolytes.

2.9.1.2 Electrolyte solution

The chosen medium, constituted of solvent and electrolyte is highly dependent on the analyte solubility and redox activity as well as conductivity, electrochemical activity and chemical reactivity of the solvent. Water is a commonly employed medium, triple distilled for trace or stripping analyses but double distilled otherwise, while non-aqueous solvents are also often reported. Electrolytes allow for a constant ionic strength, a lower solution resistance, prevent electromigration and are usually present at 0.1-1 M. They can be an inorganic salt, a mineral acid or buffer system such as acetate, phosphate or citrate when a stable pH is needed. In aqueous media, potassium chloride, nitrate, ammonium chloride, sodium hydroxide or hydrochloric acid are often reported as electrolytes while tetraalkylammonium salts are electrolytes for organic solvents.[219]

The electrochemical reduction of oxygen is a common interference to consider.[219] It consists of the formation of hydrogen peroxide and its reduction as described below:

$$O_2 + 2H^+ + 2e^- \rightarrow H_2O_2$$

$$H_2O_2 + 2H^+ + 2e^- \rightarrow 2H_2O$$
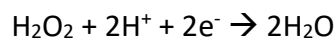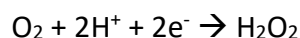
Purging the solution with an inert gas or the use of electrochemical or chemical zinc scrubbers, nitrogen activated nebulisers or chemical reduction using sodium sulphite or ascorbic acid can minimise this interference.[219]

2.9.1.3 Potentiostat

Electrodes are connected to a potentiostat to enable control and measure of the potential and current from the sample solution where electrodes are placed. Rapid advances in microelectronics have yielded major changes in electroanalytical instrumentation. Voltammetric analysers are composed of two circuits with a

polarising entity applying potential to the electrochemical cell and a measuring circuit to monitor the cell current.[219]

2.9.2 Measurements

An overview of the most common electrochemical measurements is provided in this section.
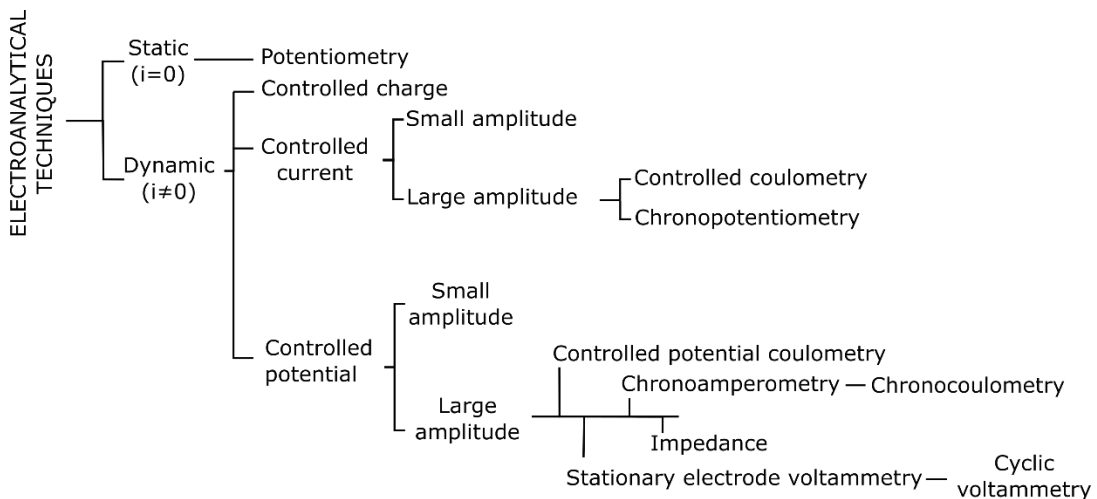
Figure 2.13. Possible categorisation of electroanalysis techniques.[224,225] Reproduced and adapted with permission from Scholz, F. Voltammetric Techniques of Analysis: The Essentials. *ChemTexts* 2015, *1* (4) and Kissinger, P. T.; Heineman, W. R. *Laboratory Techniques in Electroanalytical Chemistry, Revised and Expanded*; Informa, 1984.

2.9.2.1 Controlled current

Potentiometry entails the change in potential correlating to the target analyte when no current is generated (Figure 2.13) and obeys the Nernst equation: [218]

$$E = E^0 - \frac{RT}{nF} \, lnQ$$

where E represents the potential of the measured cell, E^0 the standard potential of the cell both in V, R the universal gas constant, T the temperature in K, n the number of electrons, F the Faraday constant and Q the reaction quotient corresponding to the instantaneous ratio of redox species concentration between anode and cathode.

Coulometry enables the performance of an exhaustive electrolysis of a target analyte thanks to the application of a constant potential to the working electrode (Figure 2.13) and prevents interferences by targeting a single reaction occurring at a specific potential.[218]

2.9.2.2 Controlled potential

Voltammetry focuses on the recording of the Faradaic current produced from a constant or varying potential.[218] The Faradaic current is defined by the electron transfer through electrode surfaces, enabling a quantitative analysis. It is divided into polarography, using mercury electrodes, and amperometry, measuring a redox reaction taking place at a constant potential.[218] Amperometry was the first electrochemical technique to be adapted to the microscale.[226] Voltammetry is much easier to implement now using devices enabled with more computing power to scan through potentials.[226]

2.9.2.2.1 Cyclic Voltammetry

Cyclic Voltammetry provides a linear scan of a working electrode potential by means of a triangular waveform (Figure 2.13). It allows a quick determination of electroactive redox potential and media effect.[219] Peaks in the cyclic voltammogram result from the diffusion layer formed close to the surface.[219] For a reversible reaction, the Randles–Ševčik equation defines the peak current at 25°C:[219]

$$i_p = (2.69 * 10^5) n^{1/2} A C D^{1/2} v^{1/2}$$

with n the number of electrons, A the electrode area in cm², C the concentration in mol/cm³, D the diffusion coefficient in cm²/s and v the scan rate in V/s.

Therefore, current has a linear relationship with concentration and increases with the square root of the scan rate, meaning the electrode reaction is governed by mass transport.[219] Peak position regarding the formal potential of the redox process studied can be expressed by:[219]

$$E^0 = \frac{E_{p,a} + E_{p,c}}{2}$$

The peak separation can be used to assess the number of electron transferred for a reversible couple:[219]

$$\Delta E_p = E_{p,a} - E_{p,c} = \frac{0.059}{n} V$$

For a fast process involving one electron, ΔE_p is equivalent to 59 mV.[219] It is worth noting that peak potentials are expressed independently of the scan rate.[219] For multiple electrons, there can be multiple peaks.[219] However, for a slow electron exchange or if associated to a chemical reaction, this can look different.[219] For irreversible processes, peak currents can appear lower with a wide separation. For a totally irreversible system, the peak potential is likely to shift depending on scan rate.[219]

$$i_p = (2.99 * 10^5)n(\alpha n_a)^{1/2}ACD^{1/2}v^{1/2}$$

where α represents the transfer coefficient and n_a the number of electrons taking part in the charge transfer.

In the eventuality of a quasi-reversible system, charge transfer and mass transport both control peak current.[219] The larger peak separation than for a reversible system mainly characterises cyclic voltammograms of quasi reversible systems.[219]

For an additional reaction before or after the electrochemical reaction, the exact value of the peak ratio can inform on the rate constant of this chemical reaction. The ratio of the rate constant to the scan rate directly impacts the peak ratio.[219]

Ultramicroelectrodes display a characteristic sigmoid voltammogram since mass transport is predominantly radial rather than linear and can reach much faster scan rates.[219]

Cyclic voltammetry also characterises the interfacial behaviour of redox-active compounds. Surface-confined, non-reacting species are defined by ΔE_p = 0 and 90.6/n mV for peak half-width. Surface coverage can be extrapolated from the area under the peak. A more negative or more positive pre-peak is observed if either the oxidised or reduced product is adsorbed. Adsorption can either be fast and controlled by mass transport or involving kinetics.[219]

Peak current measurements can also be utilised for quantitative measurements. Taking into account background reactions, the detection limit using cyclic voltammetry lies around tens of micromolar levels.[219]

2.9.2.2.2 Pulse voltammetry

Barker and Jenkin lowered the detection limits of voltammetric techniques through pulse voltammetry. Thanks to a bigger difference between Faradaic and non-Faradaic currents, quantification has been made possible down to tens of nanomolars.[219]

The sampled current-potential step, relating to chronoamperometric measurements, is turned into a sequence of steps for 50 ms. Following the potential step, charging current decays exponentially while Faradaic currents experience a slower decay. Sampling the current later in the pulse allows to accentuate the charging current.[219] Differences between pulse techniques lie in their excitation waveform and timing of current sampling.[219] Normal, differential pulse and square wave voltammetry are all pulsed techniques (Figure 2.14) but only the two most sensitive will be discussed here.

Differential pulse voltammetry (DPV) allows for a very effective background current correction, over an order of magnitude lower than normal pulse voltammetry.[219] While a sequence of pulses of increasing amplitude followed by successive drops at a preselected time near each drop end is characteristic of normal pulse voltammetry, the differential pulse method superimposes fixed magnitude pulses on a linear potential ramp right before the drop end.[219] The current is actually sampled twice, prior pulse application and when the charging current decays, resulting in a ΔI against potential plot where current peak height directly correlates to analyte concentration.[219] Tens of nanomolar or µg/L concentrations can be directly detected with an improved resolution between redox species with close redox potentials, which facilitates analyses of mixtures.[219] The half-peak width is given by:

$$W_{1/2} = \frac{3.52RT}{nF}$$

73

with R the universal gas constant, T the temperature in K, n the number of electrons and F the Faraday constant.

For a one electron reaction, the half-peak width is then equal to 30.1 mV.[219] Lower and broader peaks characterise irreversible systems.[219] When choosing pulse amplitude and potential scan rate of usually 25-50 ms and 5 mV/s, a trade-off occurs between sensitivity, resolution and speed.[219]

With peak currents respectively 4 and 3.3 times higher than DPV in reversible and irreversible cases, **square wave voltammetry** (SWV) is a large amplitude differential method allowing excellent sensitivity and discrimination against charging current. The waveform is a symmetric square wave superimposed on a base staircase potential. The current is also sampled twice, at the end of the forward and reverse pulse. The resulting peak shaped voltammogram presents symmetry at half wave potential and generates peak currents directly correlated to analyte concentration.[219] Speed is a major advantage of this technique, where the scan rate is equivalent to the square wave frequency times step height. This allows for an increased sample throughput that is also useful for kinetic studies.[219]
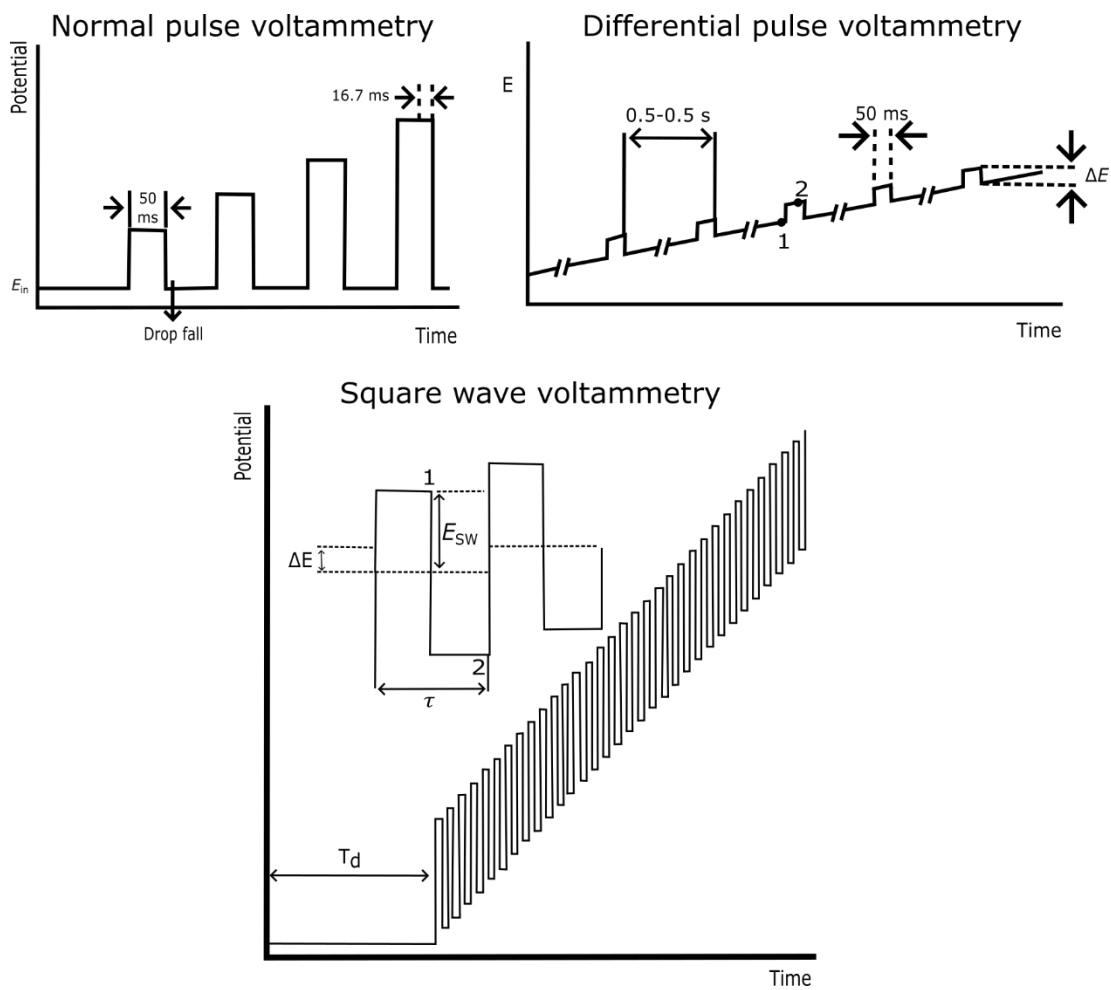
Figure 2.14. Differences in pulses from normal, differential and square wave voltammetry.[219] Reproduced with permission from Wang, J. *Analytical Electrochemistry*; 2006.

2.9.2.2.3 Electrochemical Impedance Spectroscopy

2.9.2.2.3.1 Characteristics and definition – AC vs DC

Electrochemical Impedance Spectroscopy (EIS) is considered one of the most sensitive analytical techniques, presenting low LODs with sensors able to reach atto- to femto-molar levels and a wide linear working range.[205] EIS constitutes the measure of the current resulting from an electrochemical cell interrogated via a sinusoidal voltage (Figure 2.15).[227] Firstly presented in the 1880s by Heaviside, impedance was then developed in terms of vector diagrams and complex description by Kennelly and Steinmetz less than fifteen years later and has evolved plenty since then.[61,228]

The exponential character of electrochemical cell responses is a consequence of the large range of voltages scanned using direct current governed by Ohm's

law,[218,227] while the small alternating current response from impedimetric measurements allows a possible linear approximation,[227] uncovering inductive and capacitive patterns. The small signal excitation required to measure impedance can also be expressed as a function of time:[218]

$$E_t = E_0 \sin(\omega t) \text{ where } \omega = 2\pi f$$

with E_t the potential at time t, E_0 the amplitude of the signal, ω the radial frequency and f the applied frequency.[218]

Frequencies scanned usually range between 0.1 and 10 000 Hz, with 20 to 50 frequencies logarithmically spaced. Working over many frequencies rather than a single one enhances accuracy and averages out noise.[61]

The phase shift acquired during the current response to a sinusoidal potential displays a sinusoidal behaviour at the applied frequency. Therefore, for a pseudo-linear system with a phase Φ:

$$I = I_0 \sin(\omega t + \Phi)$$

The impedance Z is then defined in terms of magnitude Z_0 and phase shift Φ by $Z = \frac{E}{I} = Z_0 \, e^{i\Phi} = Z_0 \, (\cos \Phi + i \sin \Phi)$; which can be simplified into real (Z') and imaginary components(Z''): $Z = Z' + iZ''$
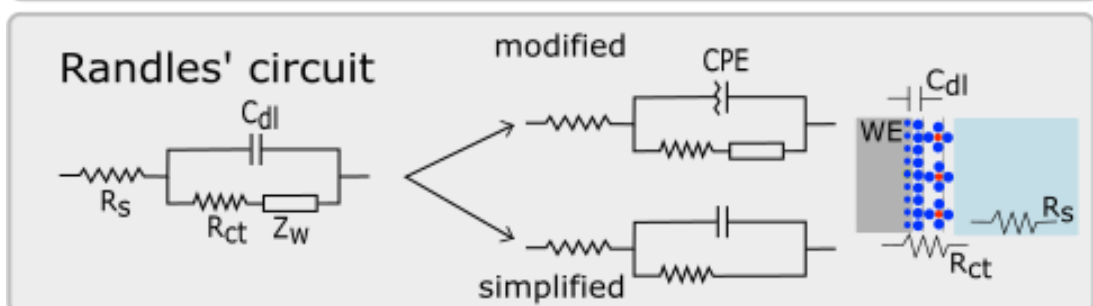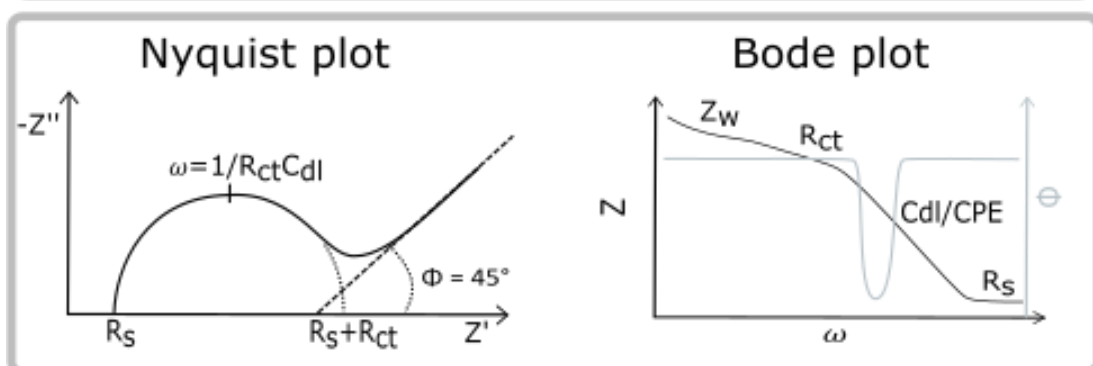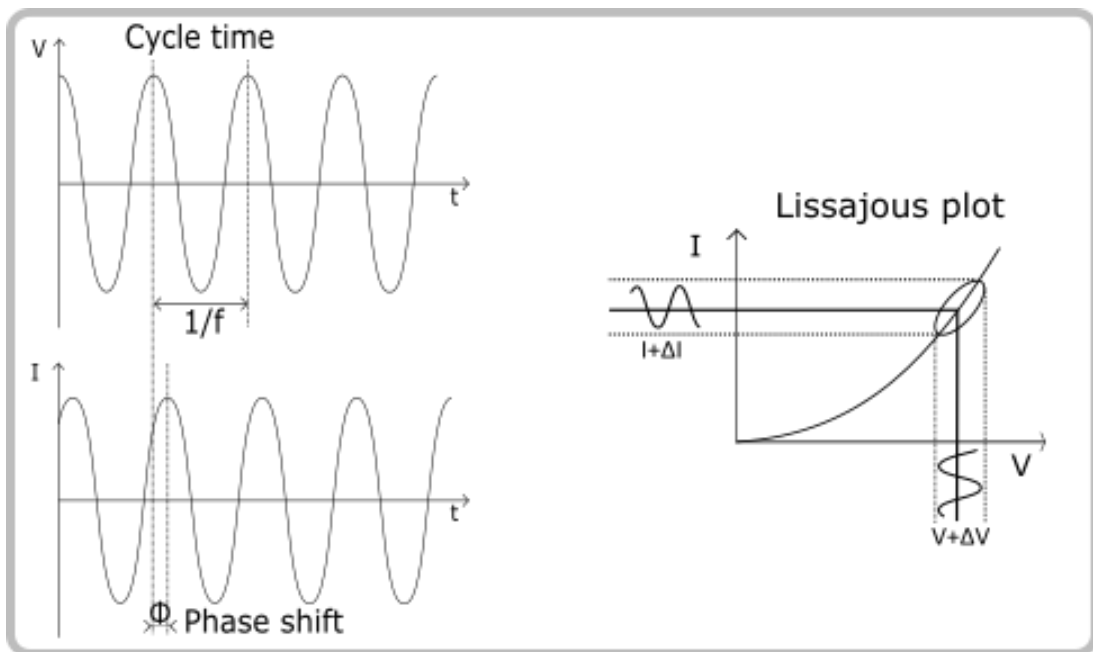
Figure 2.15. Graphical representations of EIS using the Lissajous plot,[61] Nyquist[226] and Bode plots and associated equivalent electrical circuits.[229] Reproduced with permission from Lvovich, V. F. Electrochemical Impedance Spectroscopy (EIS) Applications to Sensors and Diagnostics. *Encyclopedia of Applied Electrochemistry* 2014, 485–507, and under CC-BY license from Khan, N.I.; Song, E. *Micromachines* 2020, *11*, 220, and Magar HS, Hassan RYA, Mulchandani A. *Sensors*. 2021; 21(19):6578.

2.9.2.2.3.2 Electrical circuit

EIS allows the study of intrinsic material properties impacting conductance, resistance or capacitance, in a non-destructive fashion.[61,218] It demonstrates the ability of a circuit to resist the flow of current and at the same time, store electrical energy.[61] Impedance allows to explore mass transfer, charge transfer and diffusion[218] via fitting of the obtained response to an equivalent electrical circuit, building on the Randles' equivalent circuit model (Figure 2.15). Composed of the solution resistance, the double layer capacitance, the charge transfer resistance and the Warburg impedance,[227] the Randles' circuit is one of the most simple and common models, utilised for many aqueous, conductive and ionic solutions.[61] The solution resistance, R_s is placed in series since all current passes through the bulk solution.[226] The current chooses one or several "paths of least resistance" between electrodes under AC frequency, voltage amplitude, electrode geometry and configuration, sample composition and concentration of main conducting species, temperature, pressure, convection and external magnetic fields.[218] Two parallel paths are then possible at the electrode:electrolyte interface, either a Faradaic charge transfer or charge build-up from C_{DL}, often used as detection parameters.[226] At the working electrode, Faradaic processes take place according to Faraday's law through a redox mechanism, most often using either a redox-active probe or mediator contrarily to non-Faradaic processes which do not necessitate charge transfer.[230]

While C_{DL} models a perfect capacitor, C_{PE} replaces C_{DL} to represent a non-ideal capacitance, more realistic and reflective of surface roughness, heterogeneity and surface porosity.[218] The diffusion of analytes or redox species is modelled by an additional resistance in the Warburg element that is frequency dependent.[218] At high frequencies, the Warburg is low since reactants do not need to move far. However, at lower frequencies, its value is more consequent as molecules then possess the force to diffuse.[218] It is represented by a 45°-tilted line on a Nyquist plot and a 45° phase shift on the Bode plot called Warburg effect.[218] Building a good fitting model by component addition is feasible but not necessarily representative of the actual

studied electrochemical system and a minimal number of components is preferred based on theory.[61]

2.9.2.2.3.3 Graphical representations

The obtained bulk impedance, noted Z, can be divided into its real (Z') and imaginary (-Z'') components.[227] These are commonly displayed on a Nyquist plot where resistive phenomena appear on the real impedance axis while capacitive behaviours are displayed on the imaginary impedance axis (Figure 2.15).[227] The shape of the Nyquist varies depending on electrode composition and electrochemical response close to the working electrode surface or resulting from the bulk solution.[218] Nyquist plots are used for more resistive systems but do not contain any information on frequency,[61] while Bode plots depict capacitive systems with two distinct curves on a logarithmic scale, impedance magnitude and phase against frequencies (Figure 2.15).[218]

EIS measurements can be Faradaic or non-Faradaic, reflecting the presence of a redox mediator to sink electrons or its absence, with the potential for both to reach similar sensitivity.[227] Capacitive measurements, meaning without any redox mediator, rely on the ionic strength of the buffer and reach a maximal sensitivity using interdigitated electrodes.[227] When carrying non-Faradaic measurements, Cole-Cole complex capacitance plots are encountered, representing complex against real capacitance defined by: [205]

$$C^* = \ C' + jC'' = \frac{1}{j\omega Z} = \frac{-Z''}{j\omega|Z|^2}$$

The last 40 years have brought advances in electrochemistry equipment and computing technology for higher quality, better control and versatility.[61] Prior modern EIS instrumentation, namely lock-in amplifiers and frequency response analysers (FRA),[61] the Lissajous plot (Figure 2.15) constituted the single EIS representation via the sinusoidal current response against the applied sinusoidal voltage.[218] The resolution plot, depicting AC and DC potential against time allows to assess if sensitivity is sufficient and noise levels kept to their minimum.[205]

2.9.2.2.3.4 Applications and challenges

In terms of electrodes for EIS measurements, macro-, micro- and interdigitated electrodes are all frequently encountered with gold, platinum and carbon being the most frequently reported electrode materials and generally modified with conductive polymers, nanomaterials or antifouling layers. Nanomaterials enhance analytical features through an increase in surface area, sensitivity, selectivity, and rapidity of response.[218]

EIS reflects interfacial properties from selective biorecognition events through a phase and amplitude shift[205] based on: enzymatic activity, immunosensing, DNA hybridisation, and even whole cell detection.[218,227] Small molecule detection, including hormones, neurotransmitters or drugs using impedance is still challenging as their low molecular weight induces a minimal change, especially in complex samples where interferents of much larger sizes are present and responsible for non-specific signals. Aptamer-based impedimetric biosensors offer, for instance, a lower starting impedance compared to antibodies due to their smaller size and support higher sensitivity. A high probe density can also induce steric hindrance and not reflect specific binding.[205] Signal stability and drift either during operation or storage, the tendency of certain redox mediators to etch the electrode surface and inconsistencies in layer formation are common challenges faced when using EIS.[205,227] Issues with stability can originate from the reference electrode as it should remain non-polarisable.[205] Impedance high sensitivity can also lead to a high level of imprecision, doubly fed by difficulties in reproducibility. Mass production could improve reproducibility in terms of substrate and functionalisation.[205] Minimising non-specific binding for more robust performance in real samples is essential without increasing sample preparation or volume.[205] Despite its sensitivity, nanomaterials and analyte pre-separation can be necessary to operate in a label-free manner. The complexity of the technique added to the cruciality behind appropriate data interpretation and the difficulty of obtaining linearity, stability and causality in a home diagnostic solution are challenges faced on the development of a device and user interface level, operable by anyone.[205] Overcoming these limitations is crucial for

viable products relying on EIS to be commercialised. The future of impedance lies in its wide applicability[61] with an ideal analysis of several body fluids for one system.[205]

2.10 Electrochemical-based AST approaches

This section presents an overview of the current advances of the electrochemical detection of antibiotics and antibiotic susceptibility, via microbial growth or bacterial viability. Electrochemical sensors are widely reported to detect planktonic growth (Table 2.3) and biofilm growth (Table 2.4).[119] The impact of bacteria morphology on the current or the impact of current on bacterial behaviour is however, not well understood.[119] Changes taking place at the electrode surface or in the medium can be detected depending on inoculum size and conditions favourable for growth. Microbial growth enhances conductivity by the conversion of uncharged/weakly charged components of the medium to highly charged metabolic products such as amino acids, aldehydes or ketones.[176] Resistance will increase if microbes attach to the WE surface, hence why low conductivity medium support better evidence for microbial growth via EIS. Complex components of culture medium also influence electrochemical readouts, mainly in terms of accuracy and reproducibility and additional steps are necessary to get rid of the interference.[176] Voltammetric monitoring as well as conductivity in cell medium can be hindered by the synthesis of redox-active metabolic intermediates.[176]

Solutions for slow-growing pathogens, namely *Mycobacterium tuberculosis* aim to use a metabolic proxy to lower the time-to-result (Table 2.3). The pre-culture step is often necessary to ensure a high bacterial load and robust detection as low bacterial counts are more rarely reported since challenging with minimal sample preparation/culture/processing, reproducibility and tests in clinical samples, this can be an issue for infections needing urgent results such as sepsis.

A handful of redox mediators are commonly reported, potassium ferricyanide being the most popular and resazurin not far behind as an indicator of metabolic activity. A variety of materials are reported, and most mediator-free strategies use capacitance and interdigitated electrodes.

More and more studies test a wider array of antibiotics, screening different classes to find a working antibiotic since incidence of antibiotic resistance is increasing. Possibilities for faster, multiplexed results and decentralisation of tests come from equipment: mass production at minimal cost and disposability of electrodes, portability and user-friendliness.[188] Screen printing allowed to reduce

sample volumes from millilitres down to a few microliters, again being shrunk by expanding microfabrication techniques.[188] Screen-printed substrates for electrode fabrication have shown versatility, selectivity and sensitivity for antibiotic detection when modified with various recognition elements, nanomaterials, or even whole bacteria.[213] Bacterial identification is facilitated by affinity biorecognition elements, with antibodies still being the most popular options, with aptamers not far behind. The development of biorecognition elements uses dead or inactivated bacterial cells as targets, which might not suffice for AST as bacterial viability needs to be assessed to confirm antibiotic action and a culturing step is then highly recommended.[213] Alternatively, resazurin and other tetrazolium salts can fulfill this role (Table 2.3).

The contemporary focus is on setting higher sensitivity and selectivity, increasingly challenging while trying to maintain costs down. Integrating electrode modifications in manufacturing can help to keep sensor prices low since portable, on-field screening and detection of samples is on high demand.[213] Furthermore, few published sensor concepts allow live/dead differentiation, which has to be subsequently undertaken using classic culture methods.[213] *E. coli* and *S. aureus* are the main Gram-negative and Gram-positive bacteria tested in planktonic assessment and *P. aeruginosa* as a biofilm model (Table 2.3 and Table 2.4). Reports of mixed cultures and complex sample matrix testing, robustness and comparison with current methods for sensor validation are often overlooked.[213] Studying the system as a whole, whether for biofilms or metabolic assessment, could circumvent the time taken for a full culture step to be undertaken. Identification and emphasis on areas for improvements, when more systematically reported and tackled, are likely to bring developed sensors closer to marketable products.[213]

Table 2.3. Non-exhaustive comparison of electrochemical AST reported in the last 10 years based on planktonic phenotype of bacteria. TTR is for time-to-result (the presence of + indicates a pre-culture step), *E. c* and *S. a* are *Escherichia coli* and *Staphylococcus aureus*, modif. is short for surface modification, FFC means potassium ferri-/ferro-cyanide, bac. conc. and antibio. respectively refer to bacterial concentration and antibiotics.

TTR	Bacterial species			Electrode	Modif.	Technique	Mediator	Bac. conc./ density	Antibio.	
	E. c	*S. a*	Other							
30 min	√	√	*K. pneumoniae, A. baumannii*	Pt	-	Cytometry & Impedance	-	10^5 cells	5	[231]
30 min			*M. tuberculosis -* MPT64 protein	Au	Aptamers	Impedance	FFC	1 to 50 nM MPT64	∅	[232]
3-10 h	√			Contactless conductivity detector	-	Conductivity	-	10^3-10^9 CFU	3	[233]
4.5 h		√*		Au SPE	Antibody with alkaline phosphatase functionalised magnetic particles	DPV	p-amino-phenol	10^3-10^5 CFU/mL	1	[234]

TTR	Bacterial species			Electrode	Modif.	Technique	Mediator	Bac. conc./density	Antibio.	
	E. c	*S. a*	Other							
<300 min	√		*L. innocua*	SPCE	Carbon nanotube, Nafion and glutaraldehyde & HRP-tagged antibody	CV - Field effect enzymatic detection (FEED)	H_2O_2 via HRP	8-10 CFU/mL	2	[235]
12 h				Honeycomb net of silicon nanowires	-	Current	-	10^8 cells/mL*	3	[236]
-			*M. tuberculosis* - pyrazinoic acid (POA)	Au and Pt WE	-	Voltammetry	-	5-645 µM POA	1	[237]
5 min+	√	√	*A. baumannii, B. subtilis,*	Graphene-FET	Peptide probes	Resistance	-	10^4 cells/mL	1	[238]
15 min+	√		*B. subtilis*	ITO	L-lysine coated cerium oxide nanoparticle	CV	FFC	OD_{600} 0.1 and 0.3	3	[239]
30 min+	√	√	*P. aeruginosa*	GC	Wireless magnetic coupling	Permittivity	-	10^5 CFU/mL	5	[240]

TTR	Bacterial species			Electrode	Modif.	Technique	Mediator	Bac. conc./density	Antibio.	
	E. c	*S. a*	Other							
30 min+	√	√		Pt IDE	3-D copper-β-cyclodextrin-graphene oxide porous nanocomposite	CV & EIS	FFC	10 to 10^7 CFU/mL	1	[241]
20 & 60-80 min+	√	√	*K. pneumoniae*	Graphene-FET		Impedance	-	10^7 cells/mL	1	[242]
30-60 min+	√			Au microelectrodes	BSA	Impedance		10^4–10^8 CFU/mL	3	[243]
< 45 min+		√		Au SPE		EIS & DPV	FFC	50,000 CFUs	2	[244]
1 h+	√		*K. pneumoniae*	Pt		DPV	Resazurin	10^8 CFU/mL	3	[245]
1 h+	√			Graphite sheets & laser-induced graphene with Nafion		CV	Resazurin	OD_{600}=0.125±0.025	2	[246]
1 h+	√		*K. pneumoniae*	Au electrodes	-	DPV	Resazurin	100 CFU/µL	2	[247]

TTR	Bacterial species			Electrode	Modif.	Technique	Mediator	Bac. conc./ density	Antibio.	
	E. c	*S. a*	Other							
1 h+		√	*S. typhi, E. faecalis*	Pt-coated micro IDEs	-	DEP & Impedance	-	4250 cells/mm²	3	[248]
1 h+	√	√	*K. pneumoniae, A. baumannii, P. aeruginosa*	Pt IDE	-	Impedance	-	10^6 CFU/mL	6	[249]
1 h+	√			Au IDE	-	Impedance	-	$7*10^0$ to $7*10^8$ cells/mL	∅	[250]
< 90 min+	√	√		SPE Ag IDE	Antibody	Impedance	-	10^5 to 10^7 CFU/mL	6	[251]
90 min +	√			Carbon graphite SPE	-	DPV	Resazurin	10^8 CFU/mL	1	[252]
1.5 h	√		*P. aeruginosa*	3D printed graphite	LB agar	Impedance	Hexaammineruthenium	10^9 CFU/mL	4	[253]
90 or 150 min+	√	√	*A. baumannii, K. pneumoniae*	Glassy carbon with PMS		CV	Phenazine methosulfate	OD$_{600}$ 0.1	4	[254]
1-2 h+	√			TaSi$_2$	p(NIPMAM) microgels	Impedance	-	10^5-10^7 CFU/mL	1	[255]

TTR	Bacterial species			Electrode	Modif.	Technique	Mediator	Bac. conc./ density	Antibio.	
	E. c	*S. a*	Other							
2 h+	√			GC with Graphitized Mesoporous Carbon	-	LSV	-	OD = 0.1	2	[256]
2 h+		√		Au IDE	Antibodies	Impedance	-	10^9 CFU/mL	1	[257]
2 h+	√	√	*K. pneumoniae, S. saprophyticus*	Au	-	Electrical resistance	Resazurin	$5*10^5$ CFU/mL	2	[258]
2.5 h+	√			Au SPE		EIS	FFC	$1.75*10^7$ CFU	1	[259]
2.5 h+	√	√	*S. typhi, P. aeruginosa, S. epidermidis, B. subtilis*	Au	3-APBA	Capacitance	-	10^8 CFU/mL	5	[260]
2–3 h+	√		*K. pneumoniae, K. oxytoca, K. aerogenes, E. cloacae, C. freundii, S. marcescens*	Pt PCB		Oxidation Reduction potential	-	2–3 CFU/mL	7	[261]

TTR	E. c	S. a	Other	Electrode	Modif.	Technique	Mediator	Bac. conc./ density	Antibio.	
4 h+	√			Pt	-	Amperometry	FFC	10^6 CFU/mL	7	[262]
5 h+	√		16S rRNA for bacteria, Enterobacteriaceae, *P. mirabilis*, *P. aeruginosa*, *E. faecalis*	SPE	Oligonucleotides in hexanedithiol and 6-mercapto-1 hexanol monolayer	Amperometric	H_2O_2 via HRP	10^3 CFU/mL	1	[263]
6 h+	√			Gold	-	Impedance	-	Single cells	1	[264]
6 h+	√			Silicon nanowire FETs	-	Current	-	Single cells	3	[265]
6 h+			*A. baumannii, P. aeruginosa, K. pneumoniae, E. faecalis*	Au IDE	Aptamers	Capacitance	-	10^5 CFU/mL	7	[266]
+	√			Au	Aptamer	Capacitance	-	10-10^6	3	[267]
+			*P. aeruginosa*	SPCE	AuNPs/rGO	CV & DPV	Pyocyanin	1–100 µM		[268]

Table 2.4. Sample comparison of electrochemical AST reported in the last 10 years based on biofilm phenotype of bacteria. TTR is for time-to-result (the presence of + indicates a pre-culture step), bac. conc. and antibio. respectively refer to bacterial concentration and antibiotics.

TTR	Biofilm species	Mediator	Surface modification	Technique	Electrode	Bac. conc. /density	Antibio.	
2-4 h+	*P. aeruginosa*	Resazurin	-	SWV	Laser-induced graphene	OD_{600} 0.6–0.75	1	[269]
6 h+	*S. aureus, E. coli, P. aeruginosa*	rGO-AB	rGO-AB	OCP	Graphite	$10^4 - 10^5$ CFU/cm^3	$\emptyset$	[270]
24 h+	*S. aureus, S. epidermis*	-	-	Impedance	Au	$OD_{650} =$ 0·175	10	[271]
<2 days+	*P. aeruginosa*	-	-	Impedance	Au IDE	$OD_{600} = 0.1$	2	[272]

2.11 Scope of the thesis

Traditional antibiotic susceptibility tests are impacted by many drawbacks, however their applicability to a wide range of bacterial species and low running costs are some of the main arguments to improve these methods. Bringing AST from centralised laboratory facilities closer to the patient, with faster results to support clinical decisions and antibiotic stewardship practices is critical to tackle antibiotic resistance. As electrochemical biosensor advantages have been democratised with glucose monitoring devices, adapting the point-of-care, sensitivity and selectivity aspects to antibiotic detection and antibiotic susceptibility testing has become an attractive avenue to explore.

The overall aim of this thesis is to develop electrochemical detection assays based on a specific application using strategies to allow transferability for a wider range of uses and impact.

Electrochemically characterising actinorhodin, directly from bacterial culture, is the focus of Chapter 3. As *S. coelicolor*, which produces actinorhodin, is a widely utilised heterologous host for antibiotic production, its monitoring could be a proxy for specialised metabolite production optimisation. Screening various electrochemical measurements on gold, carbon and platinum and using two different electrolytes led to the necessity of scaling down complexity of this mixture, undertaken here via liquid-liquid extraction.

The recognition of moxifloxacin, a widely used antibiotic that is also a second-line treatment for resistant tuberculosis, via an aptasensor is the subject of Chapter 4. The sensing strategy was based on a hybridised complex formation, composed of an anchor sequence paired to an aptamer, the latter being displaced upon moxifloxacin binding. Since aptamers can be produced for any antibiotic, the concept could be applied in essence to any other sequence. Optimisation of the aptamer microenvironment and its impact on moxifloxacin recognition have been examined. Displacement of the aptamer sequence was verified by a redox label on the aptamer

sequence and stabilisation of its optimal binding conformation via its inclusion in a molecularly-imprinted matrix in Chapter 5.

Biofilm characterisation and antibiotic susceptibility are the focus of Chapter 6. Starting with the model biofilm producer*, P. aeruginosa*, and taking advantage of the production of pyocyanin, a pigmented redox-active unique biomarker, a dual system was developed using hyperspectral imaging and square wave voltammetry. Biofilm formation was assessed with electrochemical impedance spectroscopy. Transferring this system to biofilm-producing organisms, which do not produce redox active specific compounds, was undertaken using resazurin, testifying of active metabolism and therefore antibiotic susceptibility.

Chapter 3 Electrochemical characterisation of actinorhodin for an *in situ* antibiotic production monitoring

3.1 Introduction

3.1.1 Interest in Actinomycetes & *Streptomyces*

Of the >50 000 compounds known from microbes including 17 000 with antibiotic properties,[273–275] 61% of microorganism-derived, known natural substances come from actinomycetes, with a major contribution from the genus *Streptomyces*.[276] Actinomycetes were first considered an intermediate between bacteria and fungi until the 1950s[277,278] but are nevertheless Gram-positive bacteria comprised of more than 100 genera, of which *Streptomyces* is the largest with more than 1000 species.[279] Despite actinomycetes being known since the 19th century, interest in this order only grew considerably from 1943. This marked the isolation and identification of streptomycin as the first effective treatment against tuberculosis by Selman Waksman, earning him the Nobel prize in Physiology or Medicine almost ten years later and opening up the Golden Age of antibiotic discovery.[280] *Streptomyces* are nowadays responsible for the production of two-thirds[275,281,282] of commercialised antibiotics, including but not limited to terpenes, lactams, aminoglycosides, nonribosomal peptides and polyketides (Figure 3.1).[283]
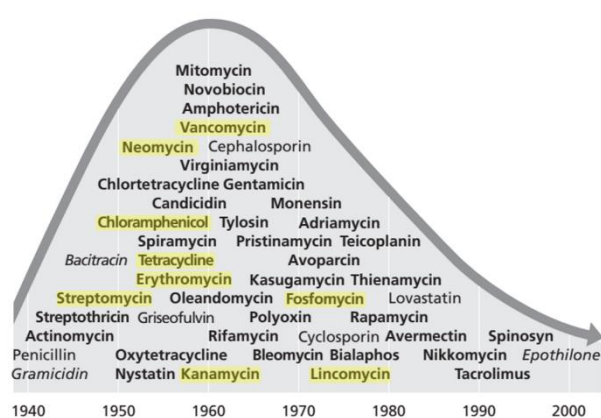
Figure 3.1. Discovery of antibiotics and other natural substances originating from actinomycetes and from *Streptomyces*, other bacterial phylum and fungi (respectively bold, bold highlighted, italics and normal font).[280] Adapted with permission from Hopwood, D. A. *Streptomyces in Nature and Medicine : The Antibiotic Makers*; Oxford University Press: New York, 2007.

3.1.2 Antibiotic discovery potential correlated with technological advances

To counter antibiotic resistance, finding new classes of antibiotics with different targets remains a pressing challenge.[284] With over 250 antibiotics in clinical use and produced commercially, the typical hit rate verges on 0.1%.[284] The more traditional top down strategy for secondary metabolite discovery has evolved towards a bottom-up approach relying on a variety of stresses to generate new compounds in their natural hosts (Figure 3.2).[281,285] Novel screening methods are a promising direction to discover new structures.[284] Genome mining emerged and exponentially evolved as an untapped source of novel antibiotics, especially attractive for unculturable microorganisms and silent gene clusters.[277,286] Genomic data accompanied by genetic modifications of producing organisms are now routinely conducted to screen hosts for novel secondary metabolite structures, possible new families and prospective antibiotics.[285]
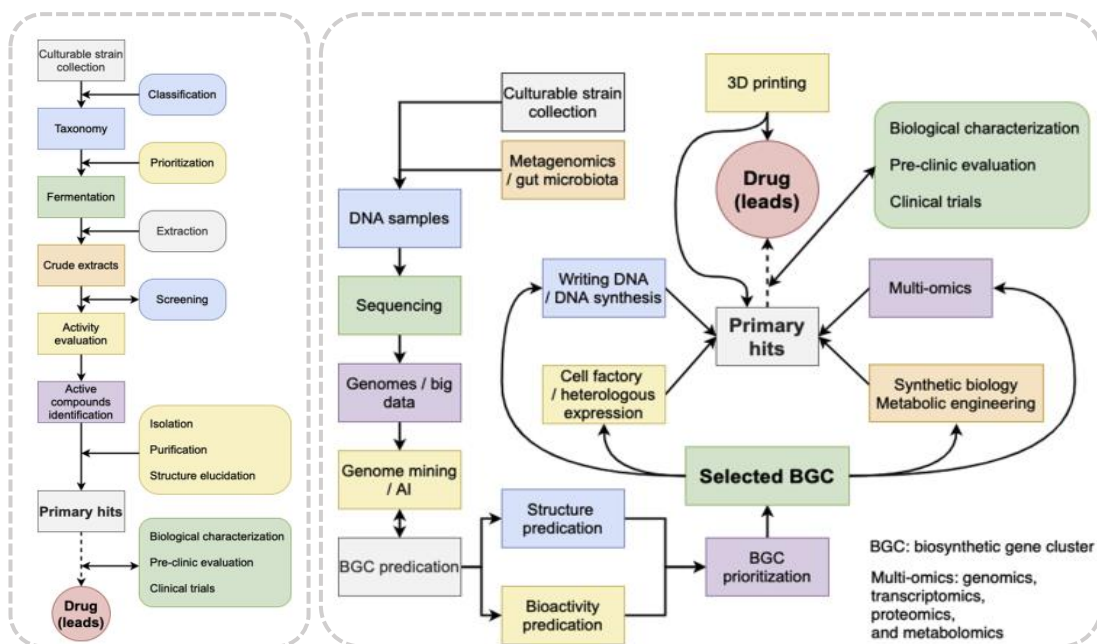
Figure 3.2. Natural product discovery : top-down and bottom-up approaches (respectively left and right when referring to drug leads).[277] Reproduced and adapted with permission from Tong, Y.; Deng, Z. An Aurora of Natural Products-Based Drug Discovery Is Coming. *Synthetic and Systems Biotechnology* 2020, *5* (2), 92–96.

To the best of knowledge, the *Streptomyces* genus alone is able to produce a better diversity of compounds than what has been chemically synthesised so far, on top of the selection through millions of years of evolution to specifically interact with biological targets.[287] Novel screening techniques have prompted multiple re-

evaluations of *Streptomyces* specialised metabolite repertoire. When the pre-genomics era assumed limited amounts of secondary metabolites per microbial species,[288] more recent estimates have attributed 30 secondary metabolites or more to each of the *Streptomyces* species. Considering the whole genus, *Streptomyces* potentially produce over 100 000 different antibiotics.[275] The decline in finding new antibiotics could therefore be attributed to waning effort and investment rather than the previously believed near completion of natural product knowledge,[280] or perhaps the necessity to search using novel strategies. In the past few years, artificial intelligence via deep learning algorithms has allowed more and more to explore at a faster and wider pace the chemical space. This has been beneficial for the discovery of abaucin, a narrow-spectrum antibiotic against *A. baumannii*,[289] halicin active against a range of pathogens including *M. tuberculosis* and carbapenem-resistant Enterobacteriaceae,[290] a compound active against methicillin-resistant *S. aureus* and vancomycin-resistant enterococci, [291] as well as six more compounds showing antibiotic activity against *A. baumannii* and several other pathogens[292].

3.1.3 *S. coelicolor* potential

Streptomyces coelicolor illustrates this progression quite well as a single species. Initially, it was attributed the production of five specialised metabolites: blue actinorhodins, red prodiginines, grey spore pigments, brown methylenomycin and calcium-dependent antibiotics. With the advent of genome mining, bioinformatic analyses revealed a possible additional 19 specialised compounds synthesised by this species. Further knowledge of its biosynthetic pathways has attributed *S. coelicolor* the ability to produce 32 original specialised metabolites. As secondary or specialised metabolites are a great source of antibiotics, a higher number of compounds means more potential antibiotics. *Streptomyces coelicolor* is a species of interest since being one of the earliest organism having its full genome mapped (Figure 3.3),[293] which has evolved into a thorough understanding of its secondary metabolic processes. Its single linear chromosome is divided in three main regions: a central core, representing half of the total size with genes responsible for growth and primary metabolism, the left and right arms, specific to each *Streptomyces* species and

responsible for proteins involved in secondary metabolism, terminated by terminal repeat sequences. With the *Streptomyces coelicolor* plasmid 1 (SCP1) mostly composed of specialised metabolite gene clusters, two-thirds of the total gene clusters of *S. coelicolor* are dedicated for specialised metabolism.[293]

3.1.4 *S. coelicolor*: a workhorse for antibiotic biosynthesis investigation and secondary metabolite discovery

Available background knowledge allowed *S. coelicolor* to be a model organism for bacterial differentiation and genome mining[294] but also the study of antibiotic synthesis and production.[295] The actinorhodin BGC contains the first mapped antibiotic gene[296] (Figure 3.3) and allowed the study of antibiotic production and regulation.[287] Most antibiotic gene clusters show an analogous organisation with gene(s) for self-resistance[296] and physical clustering of genes responsible for compound biosynthesis.[297] Additionally, possibly unidentified and cryptic natural products were unveiled, which prompted the expansion of sequencing efforts to more species along with the development of culture conditions for *in vitro* expression of these unexpressed regions.[287] BGC identification is now part of routine laboratory practices with available bioinformatic tools.[287]
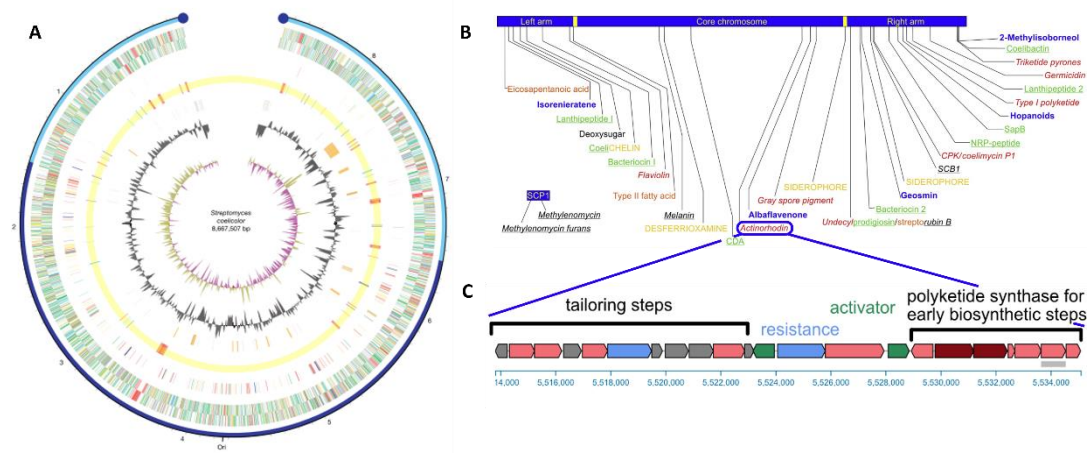
Figure 3.3. *Streptomyces coelicolor* genome with secondary metabolites gene clusters in red highlighted (A)[293], identified secondary metabolite gene coding regions (B)[298] and the actinorhodin biosynthetic gene cluster (C)[280]. Reproduced and adapted with permission from Bentley *et al.* Complete Genome Sequence of the Model Actinomycete *Streptomyces coelicolor A3(2). Nature* 2002, *417* (6885), 141–147; van Keulen, G.; Dyson, P. J. *Production of Specialized Metabolites by Streptomyces coelicolor A3(2).* ScienceDirect; and Hopwood, D. A. *Streptomyces in Nature and Medicine*; Oxford University Press, 2007.

3.1.5 Shifting *S. coelicolor* antibiotic production towards higher yields

Antibiotic production by *S. coelicolor* is typical of *Streptomyces* at large.

3.1.5.1 *Streptomyces* life cycle: favouring antibiotic production over sporulation

Streptomyces are ubiquitous, non-motile bacteria producing filamentous hyphae to reach for nutrients and producing aerial hyphae turning into spores to survive and thrive.[282,287] *Streptomyces* can be grown both in solid and liquid environments,[281] and behave differently in each (Figure 3.4). Their complex life cycle is closely embedded with secondary metabolite production.[281,287] The germination of unigenomic spore marks the start of the *Streptomyces* life cycle.[283] Apical growth then leads on to coverage by vegetative mycelia.[283] The formation of pellets and clumps in liquid cultures is widely accepted to correlate to secondary metabolite formation.[281] Activation of secondary metabolite production occurs upon the second multinucleated mycelium (MII) differentiation, triggered by Programmed Cell Death (PCD), with additional regulators called elicitors involved.[281] Enhancing PCD and MII differentiation, in the presence of elicitors, boosts secondary metabolite production. Environmental changes probe them to generate complex responses at the morphological and physiological levels for adaptation. In nutrient-limiting conditions, aerial hyphae are produced, forming septa and turning into mature spores.[283] Sporulation halts primary and secondary metabolism[281] and is tightly linked to antibiotic production (Figure 3.4).[298]
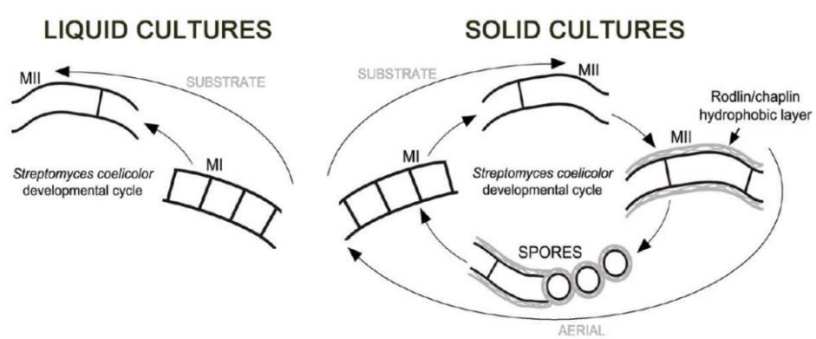
Figure 3.4. Liquid cultures prevent sporulation and secondary metabolism halting in *Streptomyces*.[299] Reproduced with permission from Manteca *et al*. Quantitative Proteome Analysis of *Streptomyces coelicolor* Nonsporulating Liquid Cultures Demonstrates a Complex Differentiation Process Comparable to That Occurring in Sporulating Solid Cultures. *Journal of Proteome Research* 2010, *9* (9), 4801–4811.

3.1.5.2 Influence of nutrients

In the natural environment, the function of antimicrobials is to limit competitors' growth, providing a selective advantage when nutrients become scarce and developmental growth is initiated in *Streptomyces.*[282] The production of bioactive compounds compensates for their non-motile characteristics and ensures sufficient nutrient supply during developmental growth.[287] Since *Streptomyces* are found in a wide range of environments, they have developed capacities to survive a diversity of nutrient supply and metabolise carbon, nitrogen and phosphate from a great range of sources.[287]

The yield of antibiotic production in their native hosts is often low since the evolutionary priority focuses on growth optimisation.[284] Secondary metabolism is more species-specific[283] and imposes constraints on primary reactions as there is a drain for one or a few precursors, disturbing the balance. The energetic cost of producing antibiotics for microorganisms explains why they are not naturally produced in high quantities. For a strain to be deemed good for large scale antibiotic production, cell mass needs to quickly reach a high biomass concentration. A successful example of yield increase is penicillin. Penicillin is commercialised as such and as a substrate to be chemically modified for the further production of ampicillin, amoxicillin and cephalexin.[284] Discovered in 1928, industrially produced from 1945, penicillin is nowadays produced at yields 100 000 times higher than upon discovery.[284]

A large number of antibiotics are produced by fermentation[284] and undertaken in industrial bioreactors, involving large flasks and bioreactors[299,280] since liquid cultures prevent sporulation in most *Streptomyces* species.[281] Consequent volumes are needed for wide spectrum antibiotics to match the worldwide demand for antibiotics.[284] Even for narrow spectrum compounds of which quantities needed might not be as consequent, cost-effective production calls for higher yields than what native hosts normally produce.

Changes in the external environment[300] constitute a leading cue to switch from primary to secondary metabolite production and antibiotic accumulation,

translated into a shift in transcriptional responses (Figure 3.5). Non-specific methods for yield improvement, mostly developed during the Golden Age of antibiotic discovery, include varying media composition (carbon, nitrogen sources, phosphate availability) and biophysical parameters such as pH, viscosity, oxygen availability and surface tension, metabolic engineering through increase of precursor availability, inducing stress responses[276] (heat and ethanol shocks) and selecting for overproducing strains through random mutagenesis (Figure 3.5).[281,301,302]
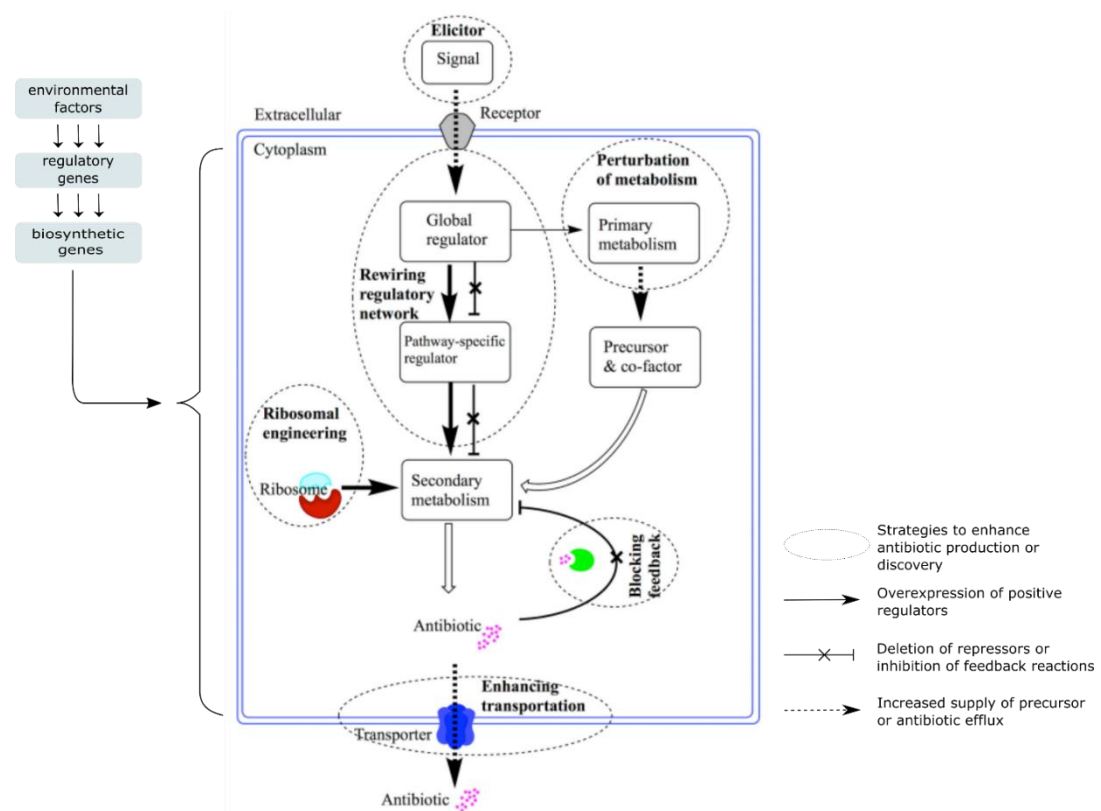
Figure 3.5. Improvements to antibiotic productivity via *Streptomyces* regulatory cascades.[276,280] Adapted from Hopwood, D. A. *Streptomyces in Nature and Medicine*; Oxford University Press, 2007. and Xia *et al*. The Application of Regulatory Cascades in *Streptomyces*: Yield Enhancement and Metabolite Mining. *Frontiers in Microbiology* 2020, *11.*

Improving classic strain yield is usually cost-effective and easily implementable, however non-specific in the nature of the approach.[281,284] Metabolic engineering stands as a more targeted solution, the hurdles being the requirement for extensive knowledge on the producer's physiology, biochemistry and genetics.[284]

3.1.5.3 Improving antibiotic production via metabolic engineering

Several metabolic engineering strategies have been used to improve antibiotic production from original hosts. Improving the flux biosynthetic pathway is one, through biosynthetic gene cluster multiplication, over-expression of positive pathway-specific regulators or on the contrary, disruption of their negative counterparts. Increasing precursor supply, coming from the central carbon metabolism, anabolic reactions or specifically synthesised is another approach along with the decrease of by-product formation to avoid wasting available carbon sources and lowering purification costs due to the formation of very similar and related compounds. The PEP-PYR-OAA node is a key metabolic engineering target, as it is a major junction between glycolysis, gluconeogenesis and the TCA cycle (Figure A.1).[283]

As the nature of original hosts, often slow growing actinomycete bacteria or filamentous fungi reaching limiting oxygen supply at higher cell densities in submerged cultures and not always easily handled efficiently through genetic engineering, these strategies are often undertaken in heterologous hosts. They can be superhosts, presenting a clean background (meaning no or little secondary metabolite production), with available precursors and efficient precursors and correct protein folding. *S. coelicolor* has been a long-used and reliable heterologous host for *Streptomyces* antibiotic production,[303] as is *E. coli,* both already optimised for high yields. Their rapid growth capabilities, well-known behaviour and ease of access to genetic tools justify their wide use challenged by differences in codon usage from GC-rich actinobacteria, where a consequent number of antibiotic come from. This is countered by either an optimisation of the gene sequence to reflect host patterns or an increase in the presence of rare transfer RNA pools. Increasing the production of microbodies from the host can also be beneficial for the release of the antibiotic of interest. Lastly, generating new products through the extension of product spectrum or combinatorial biosynthesis is an improvement strategy for antibiotic production. Cephalosporin is an example of chemical modification replaced by fermentation, proving to be a more cost-effective and greener production solution.

Combinatorial biosynthesis, using genome mining and synthetic biology to modify existing molecules embodies a more targeted approach.[281] It can take several forms, either relating to pathway engineering for one or multiple new products, or the combination of genes from various pathways yielding analogue libraries. For instance, a six module polyketide synthase (PKS) system is theoretically able to produce 100 000 unique structures. Implemented strategies include deleting, inserting or swapping modules or subunits, manipulating domains, varying glycosylation patterns. Daptomycin is one commercialised antibiotic resulting from true combinatorial synthesis. Isolation and characterisation of gene clusters have promised to bypass common issues with generated compounds such as lack of solubility, toxicity or side effects.[304] Increased understanding of secondary metabolism control has the potential to further unravel the 'silent majority' not expressed under classic laboratory conditions[281] and find appropriate conditions for unexpressed pathway activation,[287] uncovered by next-generation sequencing.[281] Among the wide variety of biosynthetic gene clusters in *Streptomyces*, many are defined as cryptic for encoding unknown or undetectable natural products, containing substantial novel antibiotic potential. Three approaches are used to attempt cryptic gene expression: through chemical elicitors, regulatory gene rewiring and ribosomal engineering. Elicitors are small molecules acting as diffusible signals to induce cryptic BGC and/or differentiation.[281] Co-cultures of microorganisms to mimic the natural environment is one strategy to serve this purpose[281] and have the potential to be conducted on a high throughput scale. Acting on the regulatory network can provide further understanding of the general complexity and help optimising antibiotic production as well as uncovering new structures.[276] Other strategies involve growing non-cultivated known bacteria and screening for new species from unexplored niches as well as researching primary metabolism and vegetative growth.[281]

3.1.6 Actinorhodin properties and mode of action

An important feature of *S. coelicolor* is the pigmentation of the originally known antibiotics,[274] that have served as "phenotypic biomarkers"[305] for a quick

visual and easily quantifiable cue, invalidating or confirming mutations and potential regulators altering secondary metabolite production.[274] Actinorhodin is one of them and has a litmus-like behaviour, displaying a blue colour above pH 7 with high solubility in polar solvents and a red pigmentation in more acidic conditions.[306] Actinorhodin is therefore an indicator in co-culture environment, used to mimic interaction and competition to favour new natural products production reflecting the non-producing organism defence mechanism if being degraded, monitor growth or secondary metabolism of its producing organism.[276,307] γ-actinorhodin production has been repressed when in presence of certain *Pseudomonas* species[308] whereas it can be stimulated if co-cultured with *Bacillus* spp.,[309,310] other actinomycetes,[311] *Myxococcus xanthus* and *Serrati*a spp..[310]

Actinorhodin has been isolated and known since 1947[312] but its full synthesis was only achieved in 2019.[313] This allows to purchase it as a standard from companies able to perform custom synthesis. Initial reports attributed actinorhodin antibacterial activity against *Staphylococcus aureus* present on the skin and in the human respiratory tract.[314] Exhibiting only a weak antibiotic activity has not generated much attention for actinorhodin to be brought down further the clinical trial or commercialisation route, with little information available and sparse research undertaken towards a deeper understanding of its biological activity.[298,305,315] More recent isolation of pure compounds has enhanced the reported antibacterial activity, whether in the case of Nass *et al.* (2017) with γ-actinorhodin[316] and Mak and Nodwell (2017)[315]. This means that actinorhodin is not produced at the same large scales as other commercialised antibiotics but could be in the future.

Actinorhodin is a naturally-occurring quinone, class of compounds that have previously shown bioreductive DNA-alkylating functions. *Staphylococcus aureus* exposed to actinorhodin has likely triggered three main stress cascades, oxidative, protein and specific DNA damages along with primary metabolism pathways. Extended screening against multiple bacterial and fungal strains revealed that actinorhodin's activity is specific to Gram-positive bacteria and bacteriostatic.[315] Actinorhodin could also be a catalyst for the production of toxic levels of hydrogen

peroxide.[305,317] Nishiyama *et al.* (2014) presented actinorhodin as an organocatalyst, a small molecule of non-metallic origin, with L-Ascorbic acid and L-Cysteine as substrates:[317]

$$\text{L-ASC} + O_2 \rightarrow \text{L-DHA} + H_2O_2$$

$$2\text{L-Cys} + O_2 \rightarrow \text{L-CSSC} + H_2O_2$$
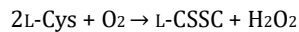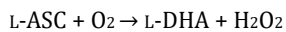
Accumulation of H_2O_2 was then proposed as the mechanism of action for actinorhodin's antibacterial activity, increasing linearly with temperature.[317] This was even proposed as a greener process in terms of chemistry to improve the H_2O_2 production process, removing the need for metal catalysts, high temperature and pressure.[317] Nass *et al.* (2017) findings later pointed to superoxide, rather than hydrogen peroxide, in the mediation of γ-actinorhodin antimicrobial activity. Electrons, generated from the quinone reduction, interact with molecular oxygen. $O_2^{\bullet-}$ is produced and further dismutated into reactive oxygen species such as H_2O_2 (Figure 3.6).[315] Oxidative damage caused by γ-actinorhodin to the electron transport chain was proposed as the mode of action, impacting the proton motive force of the bacteria and providing free electrons to generate superoxide.[305]
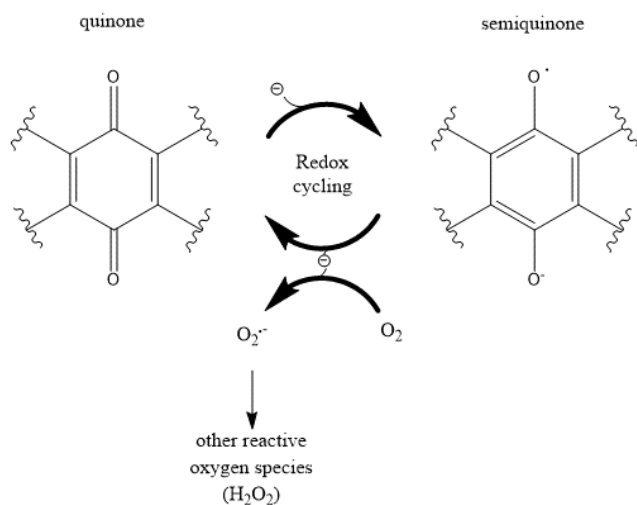
Figure 3.6. Actinorhodin proposed redox activity via radicals and reactive oxygen species from quinone moieties.[315] Adapted from Mak, S.; Nodwell, J. R. Actinorhodin Is a Redox-Active Antibiotic with a Complex Mode of Action against Gram-Positive Cells. *Molecular Microbiology* 2017, *106* (4), 597–613.

The reported organocatalyst properties of actinorhodin,[317] more potent in basic conditions, differ from Mak and Nodwell (2017), who demonstrated γ-

actinorhodin's optimal potency under acidic conditions and decreasing concomitantly as pH increases. They also refuted this first possibility due to the complexity of the observed response, suggesting that it would make it part of Pan Assay Interference Compounds (PAINS).[315] PAINS are compounds presenting high chemical reactivity but low specificity, not constituting suitable drug leads. Lastly, actinorhodin also shows redox-active properties (Figure 3.6).[315]

3.1.7 Specificities of actinorhodin production and export

The production of pigmented antibiotics, such as actinorhodin, by *S. coelicolor* acts as a proxy to evaluate growth and antibiotic production. Their relationship has been studied by multiple authors[318] including Elibol and Mavituna (1999)[319] (Figure 3.7).
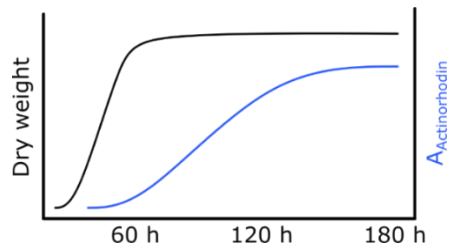
Figure 3.7. The production of actinorhodin is initiated at the later exponential phase and mostly occurs during the stationary phase of growth.[318] Adapted Abbas, A. S.; Edwards, C. Effects of Metals on *Streptomyces coelicolor* Growth and Actinorhodin Production. *Applied and Environmental Microbiology* 1990, *56* (3), 675–680.

S. coelicolor presents a particular pattern for antibiotic production. Instead of primary metabolism and growth occuring first followed by the takeover of secondary metabolism, antibiotic production starts at the end of the exponential growth phase and is maintained into the stationary phase, both processes occurring simultaneously.[319] This might be correlated to the activation of antibiotic production when an ample amount can be produced because of sufficient population numbers able to provide a significant competitive advantage.[286] Furthermore, sporulation in *S. coelicolor* does not occur in the typical large-scale antibiotic production settings of submerged aerated cultures.[281,298]

The export of actinorhodin and resistance in its producing organism has been inferred as a two-step process. Metabolic intermediates activate the expression of

export genes in order to prevent toxic accumulation in the cytoplasm and possibly speed the flux as a whole through the pathway. The presence of actinorhodin also feeds back to gene activation for higher expression and more sustained production while its removal could accelerate the whole metabolic pathway for production. The cognate export and resistance is supported by the three putative export pumps encoded in the same actinorhodin biosynthetic gene cluster.[320]

According to Byrstrykh *et al.* (1996), actinorhodin is produced and stored intracellularly for a pH of the growth medium around 5. When the growth medium pH nears 7, γ-actinorhodin is accumulated both intra- and extra-cellularly (Figure 3.8).
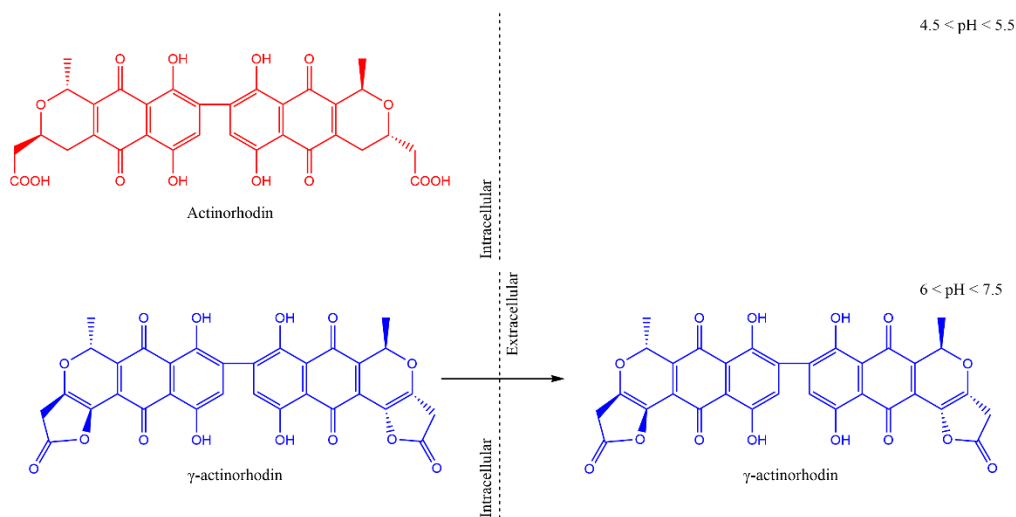
Figure 3.8. Red actinorhodin is accumulated intracellularly when the growth medium nears pH 5 while blue γ-actinorhodin is accumulated both intra- and extracellularly at a growth medium pH of 7.[321] Reproduced with permission from Bystrykh *et al.* Production of Actinorhodin-Related "Blue Pigments" by *Streptomyces coelicolor A3(2)*. *Journal of bacteriology* 1996, *178* (8), 2238–2244.

3.1.8 Actinorhodin detection

The production of actinorhodin is easily evidenced thanks to its pigmentation and mostly detected using spectrophotometry in the literature (Table 3.1), which involves a few manual sample processing steps before measurement.

Table 3.1. Reported characterisation methods for actinorhodin.

Characterisation	Ref.
Prism spectroscopy	322
Spectrophotometry	
UV	313,315,317,323,324
λ = 542 nm	321,325,326
λ = 588 nm	327 (λ-ACT)
λ = 602 nm	318
λ = 608 nm	300,328,329
λ = 633 nm	330–332
λ = 640 nm	302,333–343
λ = 644 nm	344
IR	305 (γ-Act.)
Fluorescence	307
Circular dichroism	345
NMR	305,322,324,345,346 (γ-Act.)
LC-MS or MS	305,315,317,323,347 (γ-Act.)

Despite the growing reported number of compounds constituting the actinorhodin family (Figure 3.9), the exact form detected is rarely specified (most likely γ-actinorhodin from the supernatant)[348] when spectrophotometry is the main detection method.
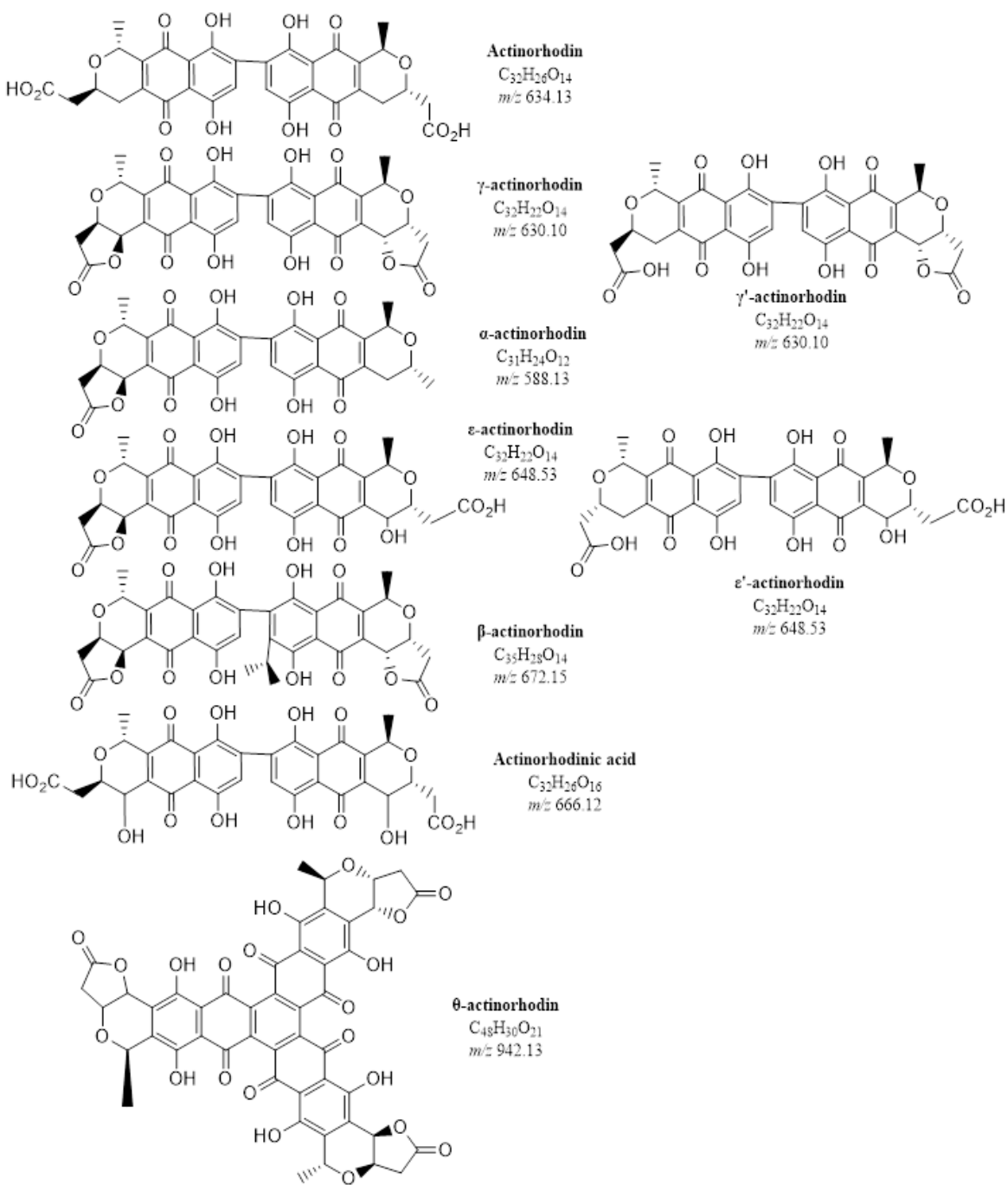
Figure 3.9. Compounds reported with the actinorhodin skeleton.[321,327] Reproduced with permission from Bystrykh *et al*. Production of Actinorhodin-Related "Blue Pigments" by *Streptomyces coelicolor A3(2)*. *Journal of bacteriology* 1996, *178* (8), 2238–2244 and Zhang, H.; Zhan, J.; Su, K.; Zhang, Y. A Kind of Potential Food Additive Produced by *Streptomyces coelicolor*: Characteristics of Blue Pigment and Identification of a Novel Compound, λ-Actinorhodin.

Echoing earlier difficulties, Nass *et al.* (2017) confirmed the challenge of separating actinorhodin forms with simple processes.[305] When not precisely stated, one or more specific forms of actinorhodin and even possible metabolic intermediates can be detected.[349] Polyketide lactones are not stable at very basic pH

and degrade to the actinorhodinic acid form.[321] Moreover, actinorhodin itself is insoluble in water or chloroform at neutral and acid pH while γ-actinorhodin is soluble in chloroform or methanol. Extracting and isolating γ-actinorhodin has shown fruitful in enhancing its reported bioactivity against *S. aureus*, which displays strong features of an antibacterial drug.[305]

Specific enzymes from the actinorhodin biosynthetic pathway (Figure A.1) would require lengthy production and purification procedures such as described in Kendrew *et al.* (1995) since none is produced at an industrial scale.[350] Strategies for electrochemical detection were therefore explored using actinorhodin reported redox activity (Figure 3.6) directly from the actinorhodin sample.

3.2 Rationale, aims and objectives

Despite a redox activity reported as possible antibiotic activity,[315,317] actinorhodin compounds have not been characterised electrochemically. They have the potential to be detected electrochemically based on the presence of quinone groups, the redox activity of quinones being central to respiration or anti-cancer drug mode of actions.[351] Moreover, commercial availability of actinorhodin is limited to companies able to perform custom synthesis, meaning that the production is not streamlined and continuous and comes at a high cost. Many obtain actinorhodin mostly from growing *S. coelicolor*.

Actinorhodin detection could serve as a proxy to optimise and monitor *S. coelicolor* secondary metabolism, as it is often used as a heterologous host for the production of many more antibiotics. Detecting and differentiating actinorhodin compounds would offer more information than a single wavelength spectrophotometer read of a group of analogues with the same test duration,[352] directly from the bacterial culture for a close to real-time feedback on antibiotic production as screen printed electrodes could be slotted in a Petri dish or in a liquid culture and prevent any disturbance from sampling, sample processing or having to undertake longer analytical characterisation. This chapter aimed at:

1) Electrochemically characterising actinorhodin compounds sampled from the culture medium on bare electrodes and,
2) Assessing if minimal sample preparation could be sufficient to clearly differentiate actinorhodin compounds electrochemically.

3.3 Material & Methods

3.3.1 *S. coelicolor* culture and actinorhodin harvest

To harvest secreted actinorhodin from *Streptomyces coelicolor* M145 (actinorhodin-producing as pictured in Figure 3.10) or M1152 (not producing actinorhodin), 10 Mannitol Soya Flour Agar plates[353] were inoculated with 1 x 10^6 spores of *S. coelicolor* and spread evenly across the surface. For the medium preparation, 20 g of mannitol were dissolved in a litre of water and 2 g of soya flour and 2 g of agar were added per flask (10 in total). 100 mL of mannitol solution were then dispensed in each flask then autoclaved.[353]

Plates were grown at 30° C for 7 days. The agar and bacterial growth were then removed from all plates and resuspended in an equal volume of sterile distilled water (~ 250 mL). The agar and water mixture was agitated at room temperature for 2 h, before the liquid was decanted. Actinorhodin solution was subsequently filtered with 0.2 µm syringe filters to yield the final actinorhodin solution. Samples were handed over at this point from P A. Hoskisson (SIPBS). Following this, they were then either stored at 4°C, -20°C or -80°C for longer term storage. Further dilutions tested were carried from the stock solution in 0.1 M KCl or 10 mM PBS, either at pH 2, 7 or 11. Due to the difficulty in purchasing actinorhodin, a control with standard concentrations was not available. The control used in place was the non-producing actinorhodin species *Streptomyces coelicolor* M1152.
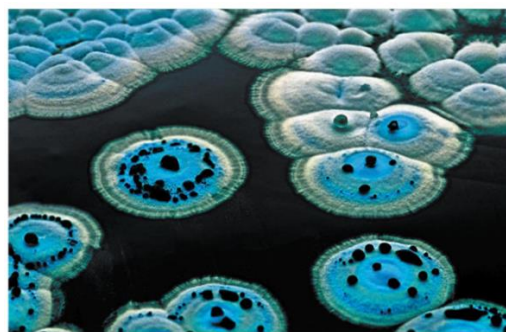
Figure 3.10. Actinorhodin-containing exudates from *S. coelicolor*. Reproduced with permission from Thompson, C.J., Fink, D. & Nguyen, L.D. Principles of microbial alchemy: insights from the *Streptomyces coelicolor* genome sequence. *Genome Biol* **3**, reviews1020.1 (2002).

3.3.2 Mass spectrometry (MS)

Actinorhodin samples were filtered with PES (5190-5098 Crawford Scientific) or PTFE membranes (5190-5086 Crawford Scientific) and transferred in amber vials to avoid photodegradation, and only in one instance purposefully in clear vials.

The Agilent Technologies 1200 Series HPLC coupled to an Agilent Technologies 6130 Quadrupole was used to acquire MS data with a single wavelength UV detector and an electrospray ionisation (ESI) source. The wavelength was set at 254 nm to target benzene rings unless stated differently. A standard screening method was used where 10 µL of sample were injected per run and eluted at 1 mL/min through an Agilent Infinity Lab Poroshell 120 C_{18} reverse phase column, 4.6x100 mm, 2.7 µm with a column temperature of 40°C with water and acetonitrile, supplemented with 0.1% formic acid or 5 mM ammonium acetate (Figure 3.11).
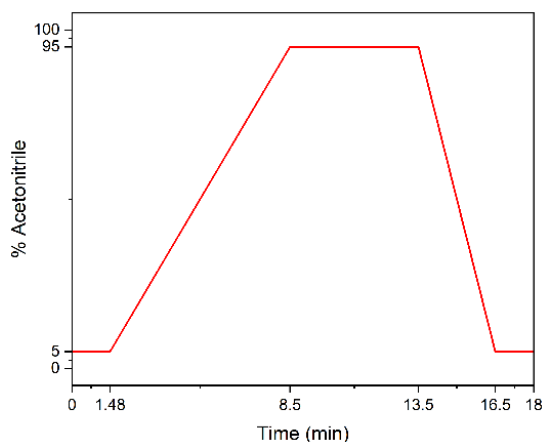
Figure 3.11. Standard solvent gradient for the HPLC-MS data acquisition.

Concerning mass spectrometer parameters, the mass range was set to 100-1000 Da with positive and negative MS spectrum acquired in one HPLC run, fragmentor 70, gain EMV 1.0 and threshold 150.

3.3.3 Electrochemical activation and electrode characterisation
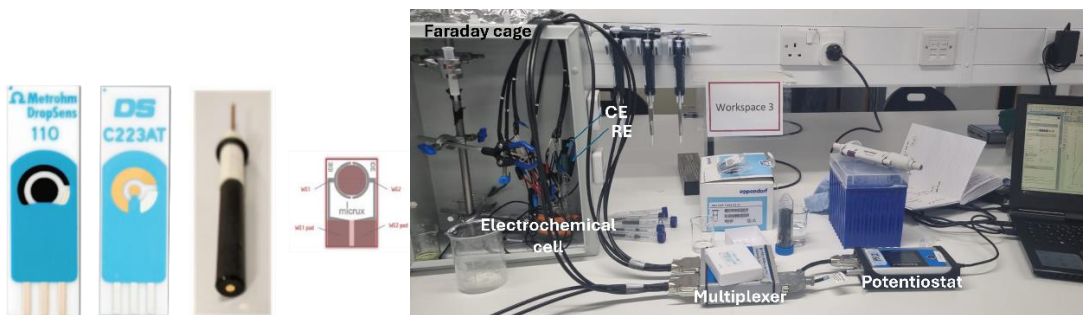
Figure 3.12. Sample of electrode formats screened for actinorhodin characterisation and electrochemical setup on the right. From left to right: carbon (WE ⌀ 0.4 cm) and gold (WE ⌀ 0.16 cm) screen-printed electrodes (3.38 cm long, 1.02 cm wide and 0.05 cm thick, polycrystalline gold electrode (⌀ 0.2 cm) and interdigitated gold microelectrode. Electrochemical set-up composed of macroelectrodes, Pt counter (CE) and Ag/AgCl reference (RE) electrodes located in a Faraday cage and connected to a multiplexer linked to a potentiostat.

Macro-electrodes, namely glassy carbon, polycrystalline gold (Figure 3.12) and platinum, were polished for two minutes using 0.03 µm alumina powder and rinsed with deionised water. Except for glassy carbon (a few seconds only), electrodes were then sonicated for 2 minutes in water for the remaining slurry to come off. All electrodes were dried with an inert gas. A platinum counter and Ag/AgCl reference electrodes constituted the electrochemical cell (Figure 3.12). The potentiostat used was a PalmSens 4 (Alvatek) with a multiplexer (MUX8-R2, Alvatek). Polycrystalline gold and platinum electrodes were immersed for 15 minutes in a piranha solution, composed of 3 parts H_2SO_4 and 1 part H_2O_2 (v/v), rinsed then dried. Gold and platinum electrodes as well as gold screen-printed electrodes were activated by potential cycling from [-0.3 ;1.5] V in 0.1 M H_2SO_4 for 20 and 10 scans, respectively. Glassy carbon and carbon screen-printed electrodes were activated in 10 mM PBS with potential cycling between [0;1.2] V for 10 scans. Electrodes were then rinsed with deionised water and dried before characterisation in either 0.1 M KCl or 10 mM PBS and 1 or 5 mM $[Fe(CN)_6]^{3-/4-}$.

Actinorhodin samples were diluted in either 0.1 M KCl or 10 mM PBS at pH 2 (acidic), 7 (neutral) or 11 (basic) when specified.

Potential windows for voltammetric measurements can be found for each specific experiment in the figure captions. Cyclic voltammetry interrogation were performed for 3 scans at 0.1 V/s and a step of 0.01 V. At an identical step and scan rate, additional parameters for DPV were 0.025 V and 0.05 s pulses. Concerning SWV, an 0.01 V step with 0.1 V amplitude and a 10 Hz frequency were set by default. Any change is mentioned for the specific section.

One LSV was performed on a clean electrode in actinorhodin or actinorhodin-free samples followed by five SWV. LSV and SWV parameters are listed in Table 3.2 for the voluntary polymerisation studies.

Table 3.2. Polymerisation study - parameters for LSV and SWV techniques.

	LSV		SWV
Equilibration time (s)	1.0 V for 120 s		
Potential window (V)	[-1 ;1]	Potential window (V)	[-1 ;1]
Step (V)	0.001	Step (V)	0.01
Scan rate (V/s)	0.05		
		Amplitude (V)	0.1
		Frequency (Hz)	1

For EIS measurement, E_{dc} and E_{ac} were respectively set at 0 and 0.01 V, scanning through 40 frequencies between [0.1 :100000] Hz.

3.3.4 Liquid-liquid extraction of actinorhodin sample

The extraction procedure followed van Dissel and van Wezel (2018)[354] protocol using chloroform or ethyl acetate to replace chloroform[355]. Succinctly, the pH of actinorhodin extracts was adjusted to 2-3 using 5 M HCl. A 1:1 CH_3OH: $CHCl_3$ was added at half the extract volume, further centrifuged for 10 minutes at 5000 rpm. The organic phase was dried and resuspended for analysis.

3.4 Results & Discussion

3.4.1 Analysis of the actinorhodin sample sampled from solid cultures

Streptomyces coelicolor A3(2) was grown on mannitol soya flour agar at 30°C for 7 days. The bacterial growth and agar were removed and resuspended in 250 mL of sterile distilled water, agitated at room temperature for 2 h, before the liquid was decanted. The actinorhodin solution was filtered and ready to use.

3.4.1.1 Determination of the stock extract concentration

The concentration of the actinorhodin stock was determined by an absorbance read at 633 nm using a Biochrom WPA S1200+ Visible Spectrophotometer and the following extinction coefficient ε = 15135 $M^{-1}.cm^{-1}$ against a water blank.[356] An average of 3 measurements of the stock solution gave A_{633} = 2.446 and A_{633} = 0.496 when diluted 10 times. Using the Beer Lambert equation with a path length of l = 1 cm:

$$A = \varepsilon * l * C \Leftrightarrow C = \frac{A}{\varepsilon * l} = \frac{0.496}{15135*1} = 3.28*10^{-5} \text{ M for the 0.1 stock solution.}$$

The concentration of the stock solution was therefore 0.328 mM, equivalent to $3.28*10^{-4}$ * 634.5 = 0.208 g/L. These estimations are correct for an environment where only actinorhodin absorbs at this wavelength, which can be considered as an order of magnitude rather than an exact value here. The concentration obtained was between the reported 1.3 mg/L for another *S. coelicolor* J802 in Hobbs *et al.* (1984)[353] up to 3 g/L for *S. coelicolor* 100 in similar sporulation culture conditions.[357]

3.4.1.2 Mass Spectrometry analysis of actinorhodin samples

The actinorhodin obtained sample was also analysed using mass spectrometry. Two volatile salts were tested, ammonium acetate and formic acid, the former more adequate for physiological conditions and the latter acidifying the mobile phase more preventing the formation of negative ions.

Compounds eluted before the gradient were not retained in the column. Separation is efficient for the C_{18} for the duration of the solvent gradient. Anything eluted at the final solvent change was retained by column.

By the multiplicity of peaks observed on the UV trace and in the total ion chromatograms, Figure 3.13 highlighted the non-purity of the sample. Figure 3.13 and Figure A.2 in Chapter 3 Appendices allowed the comparison between two different filter composition, respectively polyethersulfone (PES) and polytetrafluoroethylene (PTFE). The main difference observed lied in the major peak at 9.3 min (Figure A.3 in Chapter 3 Appendices), present but not as intense when the sample was filtered with PES as a membrane (Figure 3.13). Other notable divergences were the UV peaks at 6 min, of same intensities using PTFE (Figure A.3 in Chapter 3 Appendices) compared to the difference using PES (Figure 3.13) and the peak after 8 min with a PES filter not evidenced when using the hydrophobic PTFE.
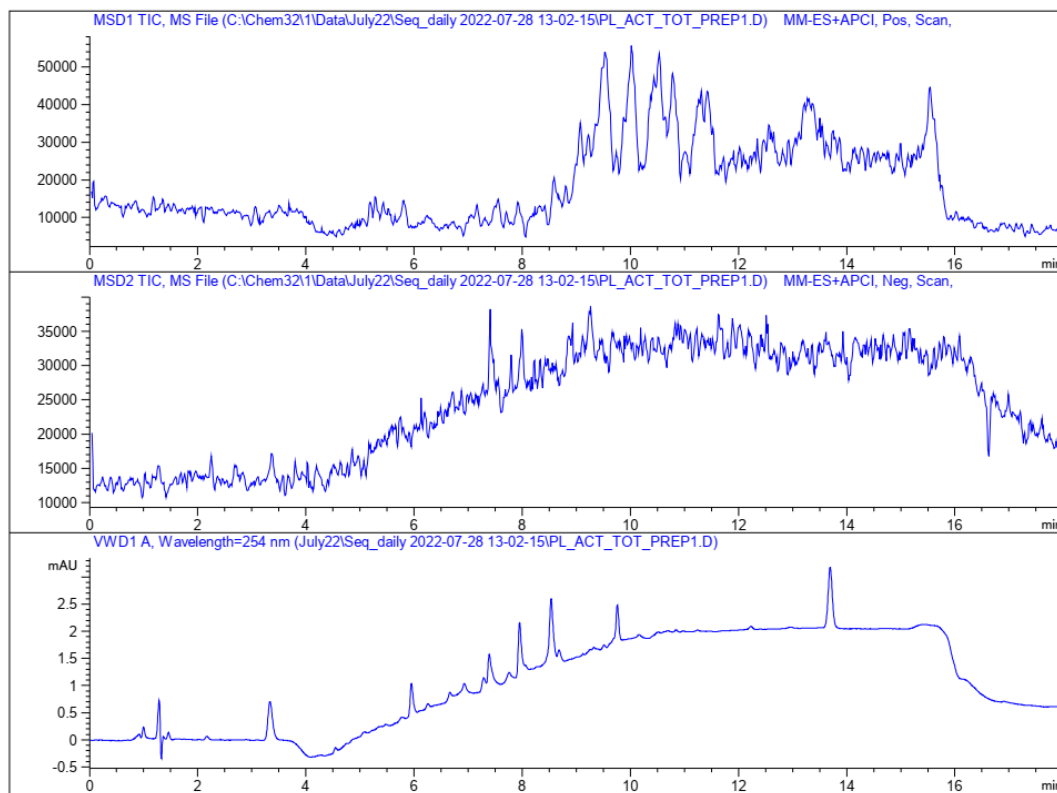
Figure 3.13. Total ion count (TIC) chromatogram in positive (top) and negative ionisation modes (middle) of the total actinorhodin sample at 16.4 µM using PES filter and UV chromatogram at 254 nm (bottom) and ammonium acetate as a solvent additive.

Figure 3.13 and Figure A.2 in Chapter 3 Appendices differ in the solvent additive, ammonium acetate for the former and formic acid for the latter. Formic acid provides a more acidic pH of the mobile phase and prevents the formation of ions in negative mode for weak acids. Ammonium acetate provides an environment closer

to a neutral pH.[358] This was reflected in the UV profiles, with an absence of the 3 min peak in , a more abundant variety of compounds between 4 and 5.5 min and less peak separation but higher signals between 6 and 7 min for the formic acid samples (Figure A.3). Major compounds are still evidenced at 7.7, 8.5 and 9.7 min in both cases, with a much smaller peak at 13.8 min compared to the rest of the signals in the formic acid conditions.

Drawing from Byrstrykh *et al.* (1996), actinorhodin itself would not be soluble in water at neutral and acidic pHs, which was the environment set by the solvent additives. This standard method was not the most optimal to evidence the presence of actinorhodin and a combination of both solvent additives with a more optimised solvent gradient was reported by Marshall and Carlson (2023).[352] Moreover, γ-actinorhodin tends to degrade into actinorhodinic acid at high pH values, originating from the unstability of the polyketide lactone groups. This compound, however, is soluble in chloroform or methanol.[321]

Photosensitivity was also compared using Figure 3.13 and Figure A.4 in Chapter 3 Appendices. The most affected compounds were behind the peak at 6 min, lower after light exposure as well as those after 8 min and close to 10 min. More compounds before 6 min appeared post light exposure, possibly due to degraded by-products (Figure A.4).

PES filtration was preferred to avoid sample contamination as PTFE is a common contaminant. The low intensities recorded for the total samples could come from a low solubility of actinorhodin compounds in organic solvents. Equivalent samples tested electrochemically did not undergo the filtration step, which have possibly affected background signals recorded on electrodes. Amber vials were used when analysing samples with MS and electrochemical interrogation was conducted in a Faraday cage to avoid sample degradation/modification from light exposure. More extensive method development to favour more stable conditions for actinorhodin or γ-actinorhodin or solvent additives supporting negative ion formation could benefit compound identification and quantification[352].

Coming from a bacterial culture and a species able to produce an array of secondary metabolites (Figure 3.3), samples were analysed in the mass spectrometer to assess if a major compound was evidenced and identifiable, which was not the case using this standard gradient and wavelength. The mixed nature was confirmed with multiple peaks, whose identity was inferred but not confirmed as requiring purification for clearer mass spectra (Chapter 3 Appendices (A. I)).

A control condition is to be ran next in MS and spectrophotometrically with an extract coming from a bacterial mutant culture, whose actinorhodin gene cluster has been knocked out. This would provide a landscape of possible interfering compounds and validate recorded signals as emanating from actinorhodin compounds. Electrochemical assessment of the actinorhodin sample has been undertaken next.

3.4.1.3 Electrochemical characterisation

Since direct detection of actinorhodin has not been previously reported in the biosensing literature, different electrode materials in various formats were assessed, namely polycrystalline gold, glassy carbon and platinum electrodes with an external Pt counter and an Ag/AgCl reference as well as gold and carbon screen-printed electrodes. Additionally, electrochemical measurements were also carried out on gold microelectrodes (Figure 3.12).

The results are presented from least to most catalytically active materials - first carbon, then gold and finally platinum - using phosphate and potassium chloride electrolyte solutions.

3.4.1.3.1 Carbon

3.4.1.3.1.1 Glassy Carbon Electrodes

Glassy carbon electrodes were characterised in Figure A.5 in Chapter 3 Appendices. A voltammetric approach has been first tested with actinorhodin samples. Cyclic voltammetry was the reference method, followed by differential pulse voltammetry and conducted first on concentrated dilutions to evidence an obvious signal from the main compounds.

Using PBS as a background electrolyte, the various potential windows scanned on GCE did not display any potential redox activity that could be attributed to actinorhodin by being present in actinorhodin- but absent from actinorhodin-free samples (Figure 3.14).
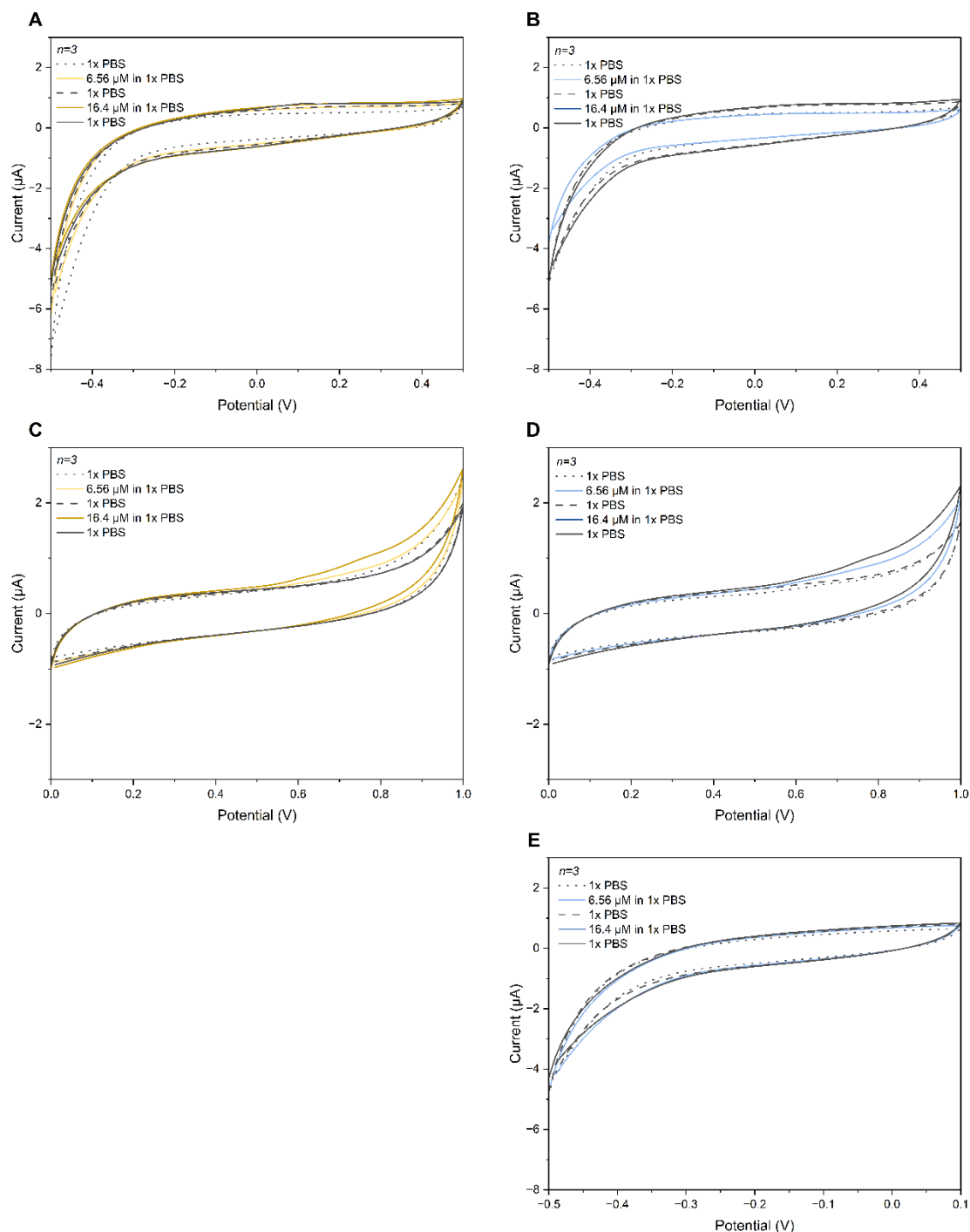
Figure 3.14. CV on GCE of actinorhodin-free and actinorhodin samples in 10 mM PBS respectively with [-0.5;0.5] V (A&B), exclusively positive (C&D) and negative (E) potential windows.

Higher signals were recorded from some actinorhodin-free samples compared to samples were actinorhodin was present with DPV (Figure 3.15A-B). Minor peaks at - 0.4 and 0.4 V were uncovered next, absent from actinorhodin-free samples and possibly proportional to sample concentration (Figure 3.15B and E). The presence of compounds at 0.6 and 0.7 V overlapping with components of the culture medium could also be likely (Figure 3.15C-D and Figure 3.14C-D).
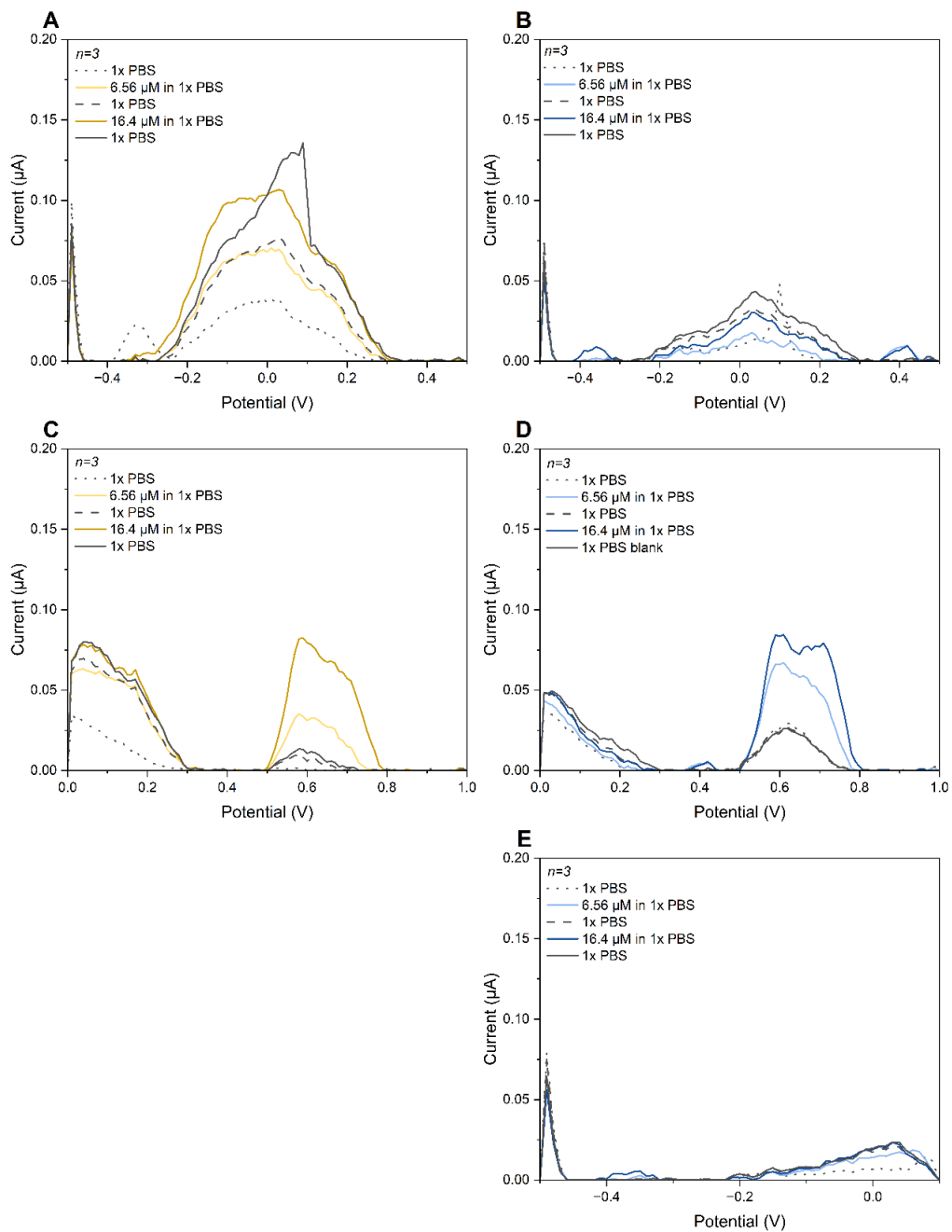
Figure 3.15. DPV on GCE of actinorhodin-free and actinorhodin samples in 10 mM PBS respectively with [-0.5;0.5] V (A&B), exclusively positive (C&D) and negative (E) potential windows.

The chosen potential windows at 0.1 V/s were not suitable to specifically attribute any electrochemical activity to actinorhodin using CV in a potassium chloride background as no characteristic peak varying from actinorhodin-free samples was detected in actinorhodin extracts (Figure 3.16). Concerning DPV, peaks recorded around 0.1 V, 0.25 and 0.5 V at the lower actinorhodin sample concentration seemed to differ from the actinorhodin-free samples in the positive only potential window (Figure 3.17C&D). High DPV blank signals appeared more consequent from the negative potential regions up until 0.2 V (Figure 3.17B-C-D).
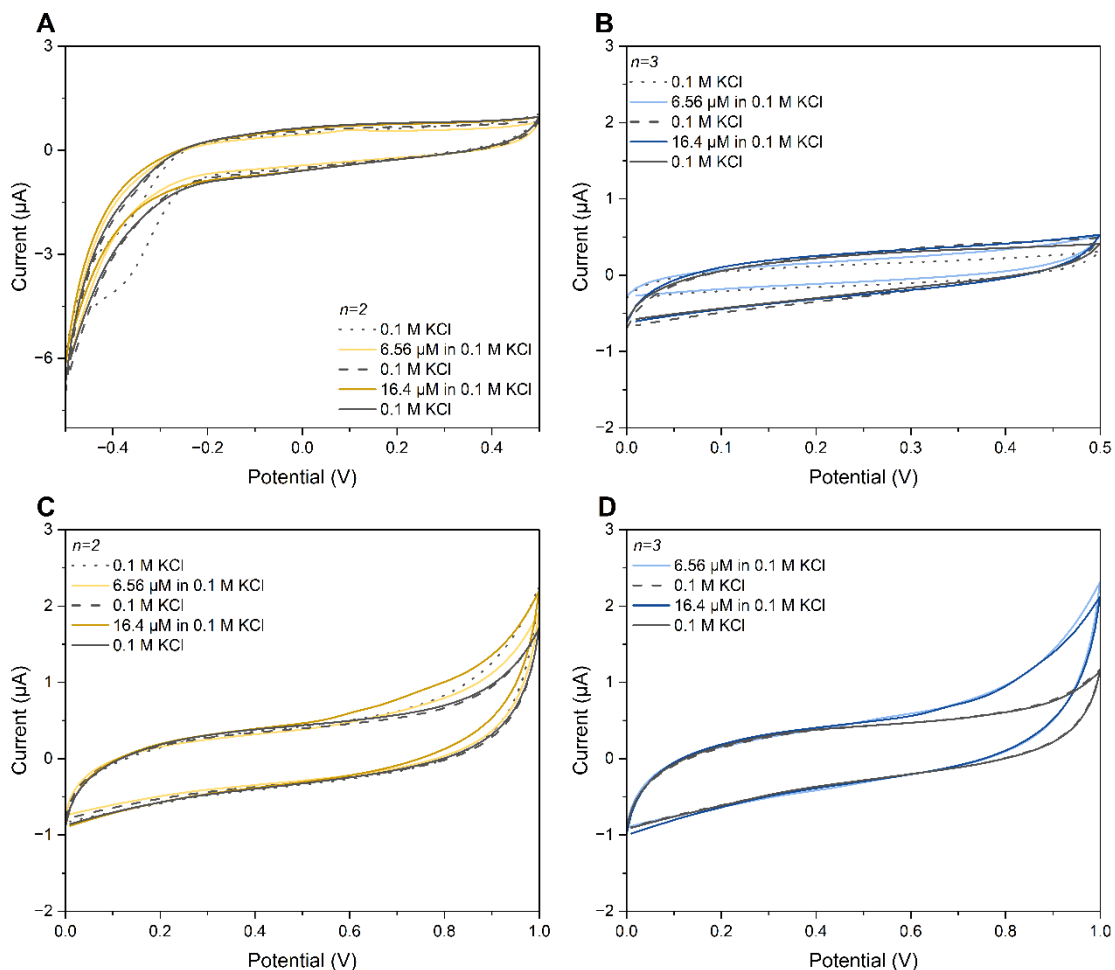
Figure 3.16. CV on GCE of actinorhodin-free (left) and actinorhodin samples (right) in 0.1 M KCl respectively with [-0.5;0.5] V (A&B) and exclusively positive (C&D) potential windows. Each trace is the average of 2 electrodes for actinorhodin-free samples and 3 electrodes for actinorhodin samples.
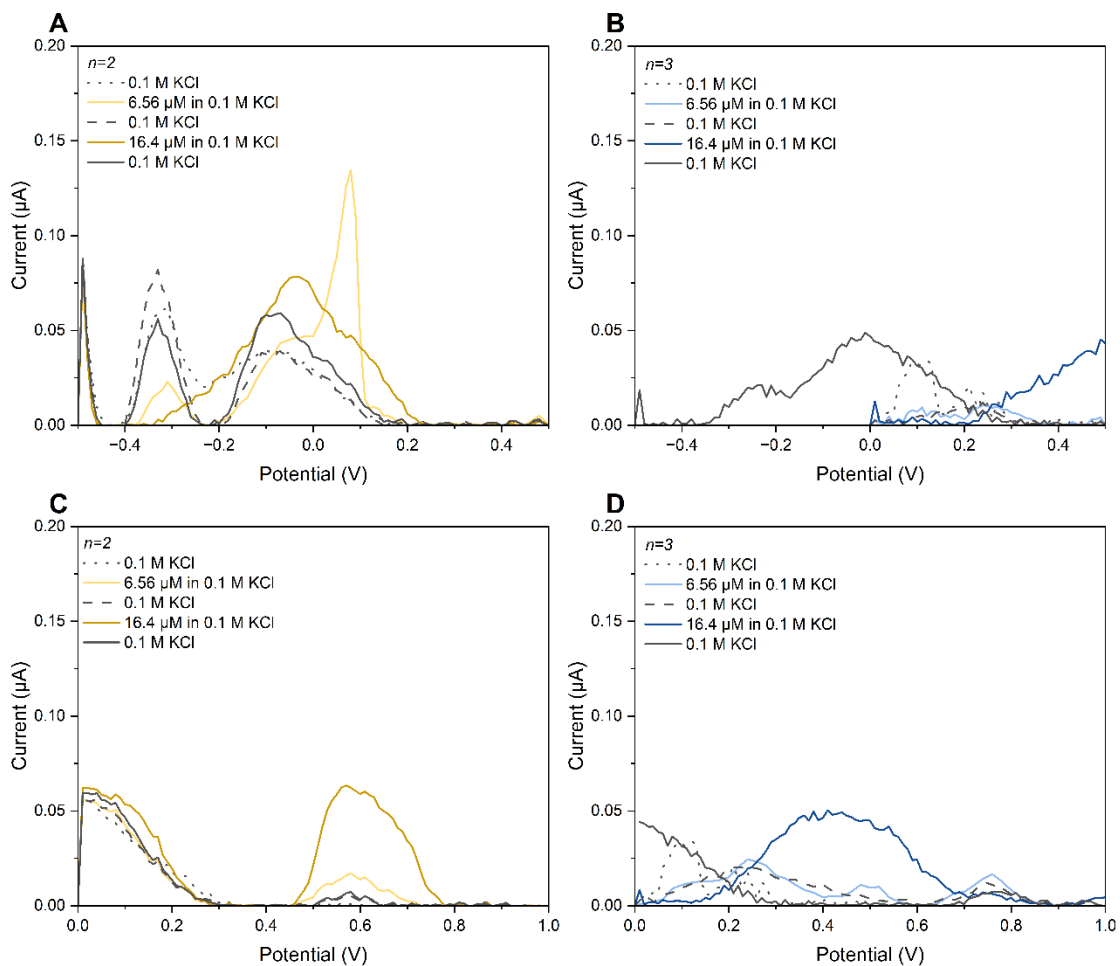
Figure 3.17. DPV on GCE of actinorhodin-free (left) and actinorhodin samples (right) in 0.1 M KCl respectively with [-0.5;0.5] V (A&B) and exclusively positive (C&D) potential windows.

3.4.1.3.1.2 Screen-Printed Electrodes

Using a carbon SPE electrode format, actinorhodin samples were also interrogated in a background of PBS (Figure 3.18) or KCl (Figure 3.19). Characterisation of the activated electrodes was presented in Figure A.6 in Chapter 3 Appendices.
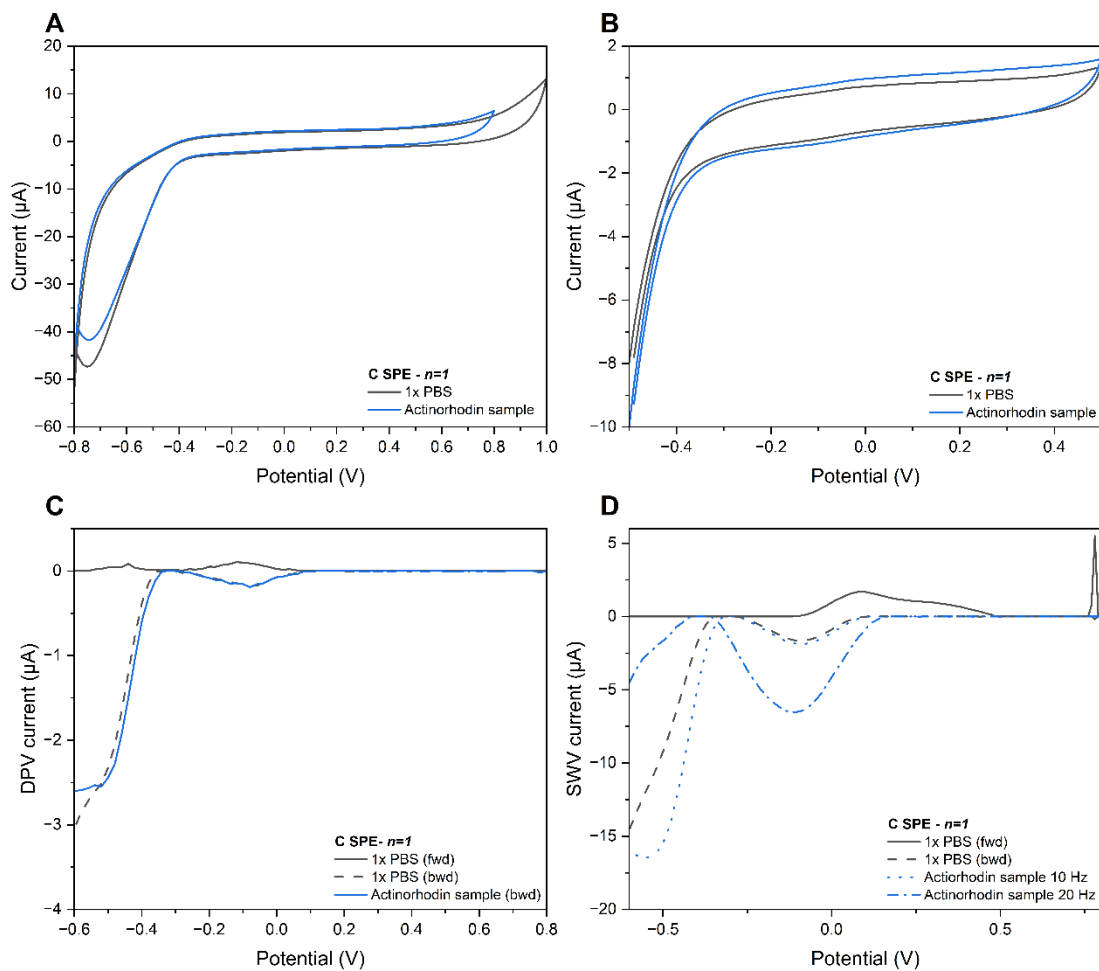
Figure 3.18. Analysis of the actinorhodin sample on carbon SPE in 10 mM PBS with CV (A&B), DPV (C) and SWV (D).

Cyclic voltammograms did not show distinctive redox peaks in any of the electrolyte solutions tested (Figure 3.18A-B and Figure 3.19A).

Peaks recorded in PBS corresponded to sample peaks when electrodes were interrogated with DPV (Figure 3.18C). Prompted with different SWV frequencies, the reducing peak amplitude at - 0.1 V increased (Figure 3.18D). A defined peak appeared with PBS samples around - 0.1 V (Figure 3.18C-D), confirmed in KCl solutions via SWV (Figure 3.19C). Small peaks were also recorded in KCl between [0.4;0.6] V. with pulsed voltammetry (Figure 3.19B-C). Published by Bellin *et al.* (2014) on pyocyanin, where compound differentiation and peak resolution depending on the direction of the potential window screened informed the initiative to obtain signals for Figure 3.18C-D.[359]
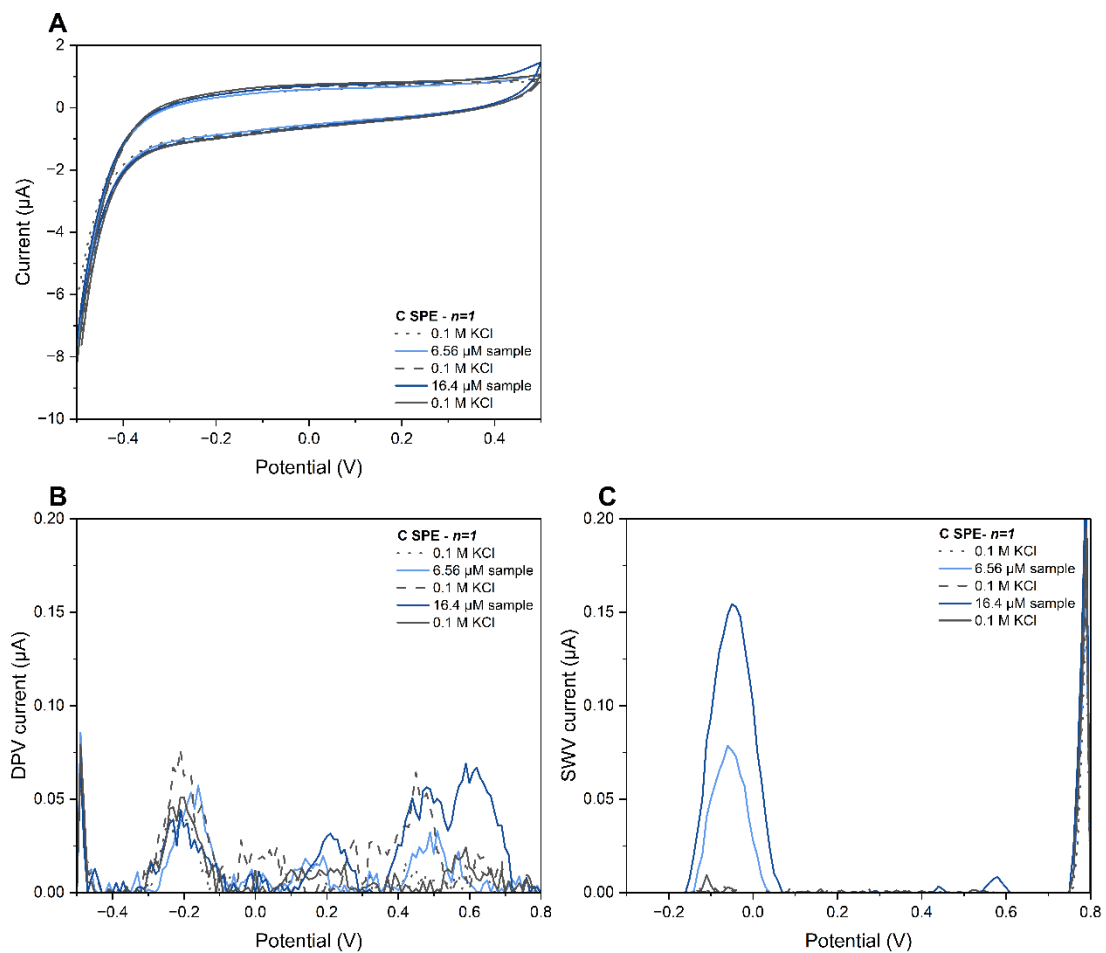
Figure 3.19. Analysis of the actinorhodin sample on carbon SPE in 0.1 M KCl with CV (A&B), DPV (C) and SWV (D).

Across the two different concentrations of actinorhodin extract tested, no characteristic peak was detected using CV on a carbon SPE, that also displayed a higher peak amplitude than the blank electrolyte solution (Figure 3.20A&C). DPV peaks in the potential window tested were better differentiated using the less concentrated solution (Figure 3.20B). Two major peaks at -0.7 and -0.2 V were evidenced in the first run, with a growing peak at -0.4 V upon the second measurement (Figure 3.20B). At least two peaks could be identified when scanning the potential from positive to negative, with a decrease in current amplitude of the more negative peak (Figure 3.20B). The three maximum peak amplitudes could be found in from the more concentrated solution in both oxidative and reductive potential screening windows (Figure 3.20D). All DPV peak amplitudes recorded were above electrolyte only solutions (Figure 3.20B&D), which had a similar profile as samples suggesting an electrode adsorption of major peaks.
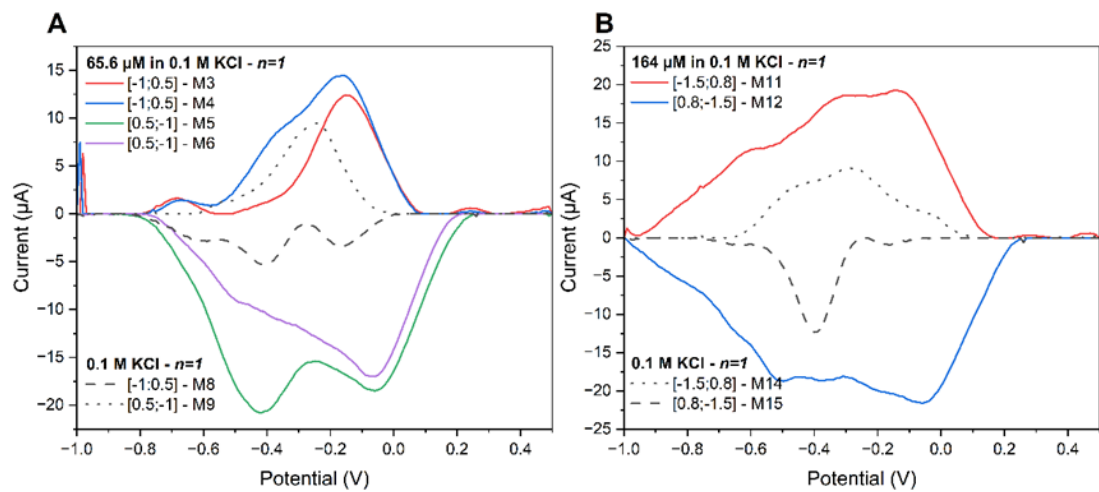
Figure 3.20. DPV characterisation on carbon SPE of an actinorhodin solution in 0.1 M KCl at 65.6 µM (A) and 164 µM (B).

Table 3.3. Summary of peaks detected on carbon electrodes. Peaks included have a different potential than actinorhodin-free samples and their amplitude reaches higher currents than at least the first electrolyte blank solution tested.

Potential region (V)	Electrode format		Electrolyte		Measurement			Fig.
	GCE	SPE	KCl	PBS	CV	DPV	SWV	
-0.65		√	√			√		Figure 3.20
-0.4	√			√		√		Figure 3.15
		√	√			√		Figure 3.20
-0.2		√	√			√		Figure 3.20
-0.1		√		√			√	Figure 3.19
			√			√	√	
0.25	√		√			√		Figure 3.18
0.4		√	√			√	√	Figure 3.19
	√			√		√		Figure 3.15
0.5	√		√			√		Figure 3.17
0.55-0.6		√	√			√	√	Figure 3.19
0.6	√			√		√		Figure 3.15
0.7-0.75	√			√	√	√		Figure 3.15

3.4.1.3.2 Gold

Actinorhodin and actinorhodin-free samples were next tested on a less inert electrode surface than carbon, namely gold electrodes.

3.4.1.3.2.1 Polycrystalline Gold Electrodes

PGE were cleaned and activated and their characterisation displayed in Figure A.7 in Chapter 3 Appendices.

The cyclic voltammograms presented in Figure 3.21 showed a reduction peak around -0.3 V for actinorhodin-free and -0.2 V for actinorhodin samples. Other peaks detected might come from the medium as they were found in both actinorhodin and actinorhodin-free samples.
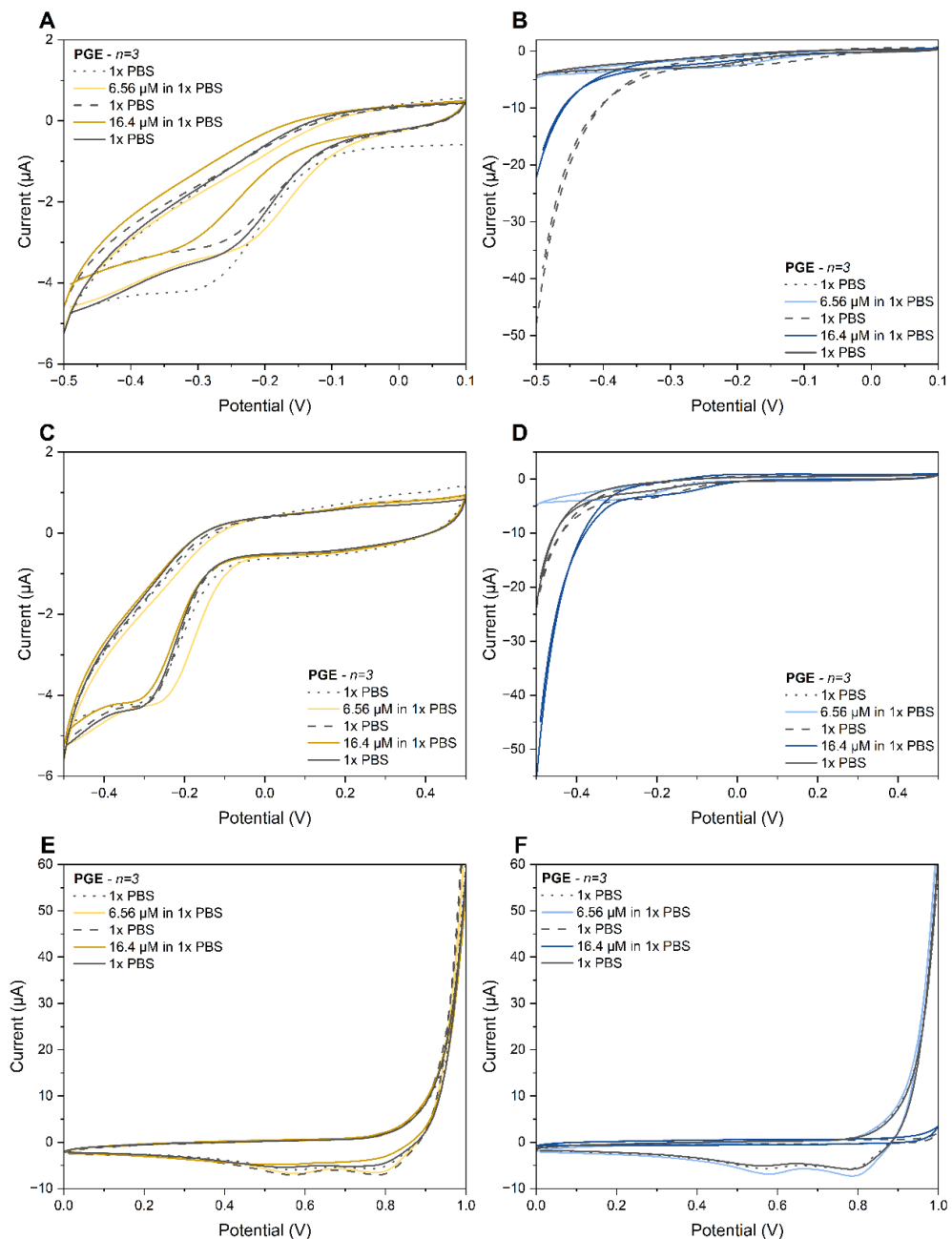
Figure 3.21. CV on PGE of actinorhodin-free and actinorhodin samples in 10 mM PBS respectively mostly negative (A&B), [-0.5;0.5] V (C&D) and exclusively positive (E&F) potential windows.

Differential pulse voltammetry measurements have also been attempted with the aim of achieving higher sensitivity. Three peaks were recorded around -0.25, 0.25 and 0.5 V that both showed up in actinorhodin and actinorhodin-free samples (Figure 3.22). Peak amplitudes decreased with increasing sample concentrations and showed compound accumulation at the electrode surface, impacting sensitivity upon repeated measurements and electrode uses (Figure 3.21 and Figure 3.22). Blanks

were required in between each measurement to assess compound adsorption on the electrodes, observed from the little difference between peak amplitudes (cite) of the 6.56 µM and 16.4 µM concentrations. Scan rate studies might have enabled an assessment of the reversibility of redox processes occurring.[219]
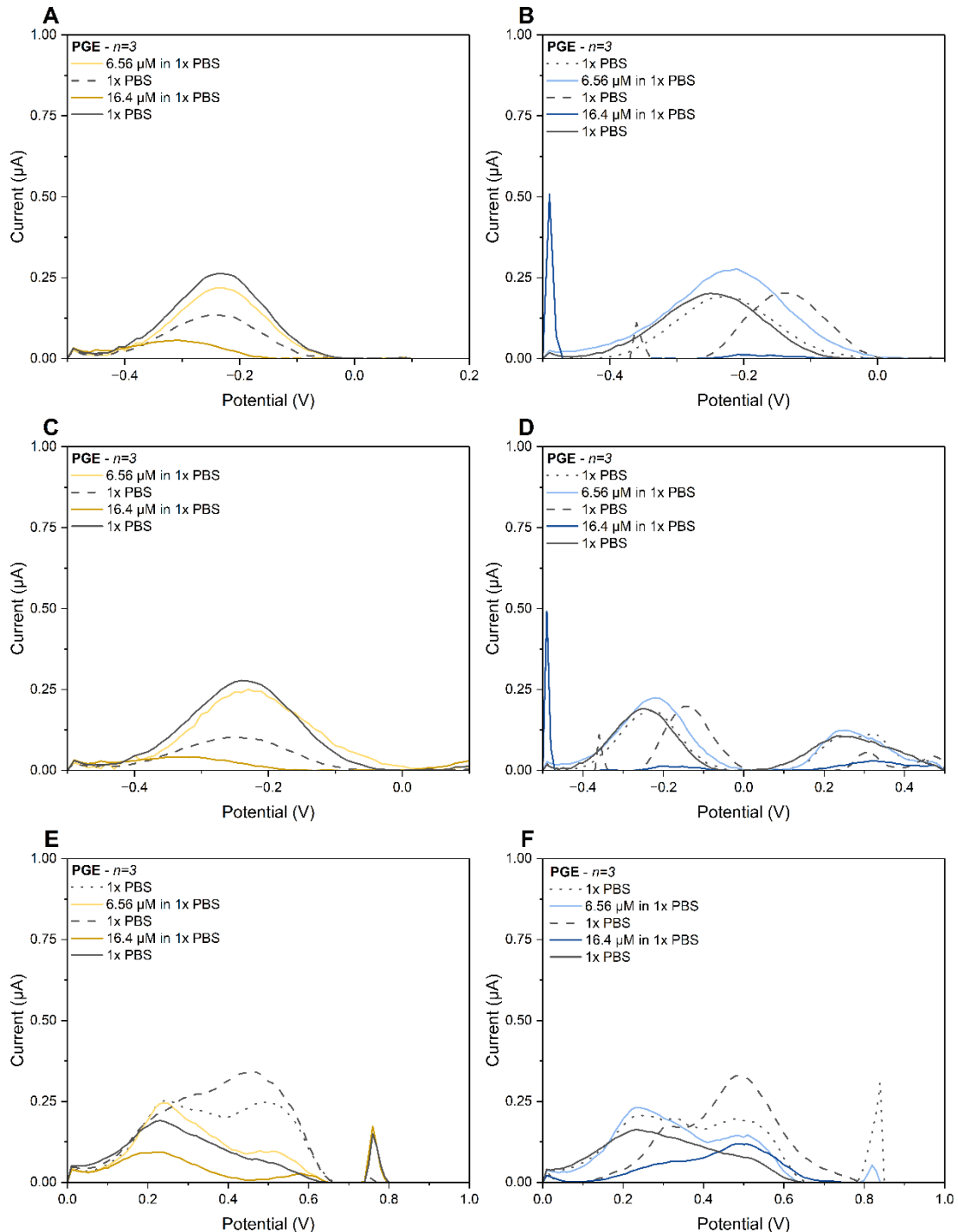
Figure 3.22. DPV on PGE of actinorhodin-free and actinorhodin samples in 10 mM PBS respectively mostly negative (A&B), [-0.5;0.5] V (C&D) and exclusively positive (E&F) potential windows.

Actinorhodin dilutions were tested next in KCl (Figure 3.23). Small peaks at -0.1 and 0.1 V were noticed with the potential window scanning negative and positive potentials (Figure 3.23D). A shift in potential was observed in actinorhodin samples (0.5 V) compared to actinorhodin-free solutions (0.6 V) (Figure 3.23).
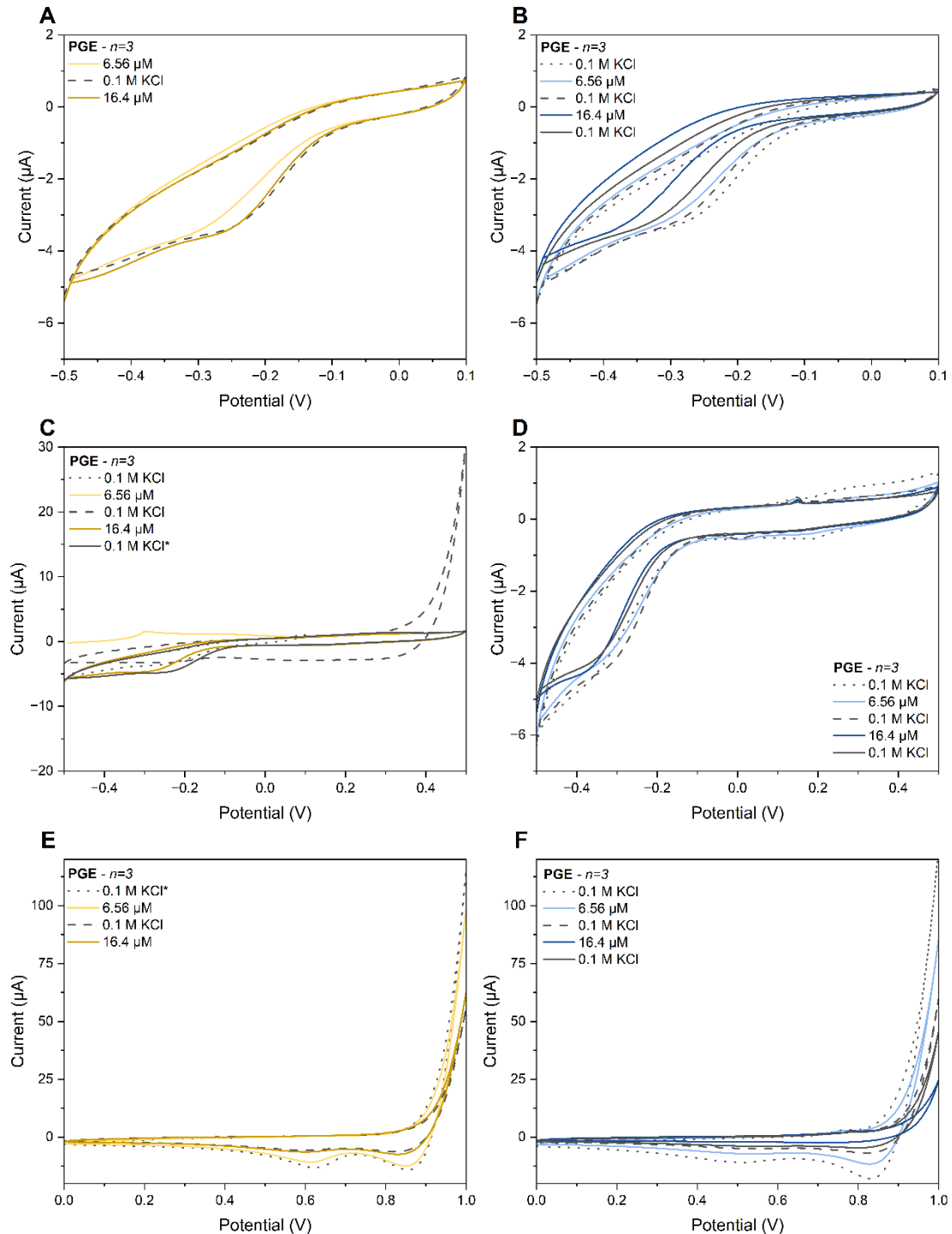
Figure 3.23. CV on PGE of actinorhodin-free and actinorhodin samples in 0.1 M KCl respectively mostly negative (A&B), [-0.5;0.5] V (C&D) and exclusively positive (E&F) potential windows. * indicates *n=2*.

Concerning DPV on PGE in 0.1 M KCl, no peak recorded appeared to be differing in actinorhodin compared to actinorhodin-free samples and above blank samples (Figure 3.24). Reiterating observations from PBS samples on the same electrode material and format, lower peak amplitudes were recorded for increasing concentration of actinorhodin samples (Figure 3.24B-D-F), which was not as consequent in actinorhodin-free solutions (Figure 3.24A-C-E). This highlights compound accumulation at the electrode surface driven by actinorhodin-like compounds over other components (Figure 3.25).
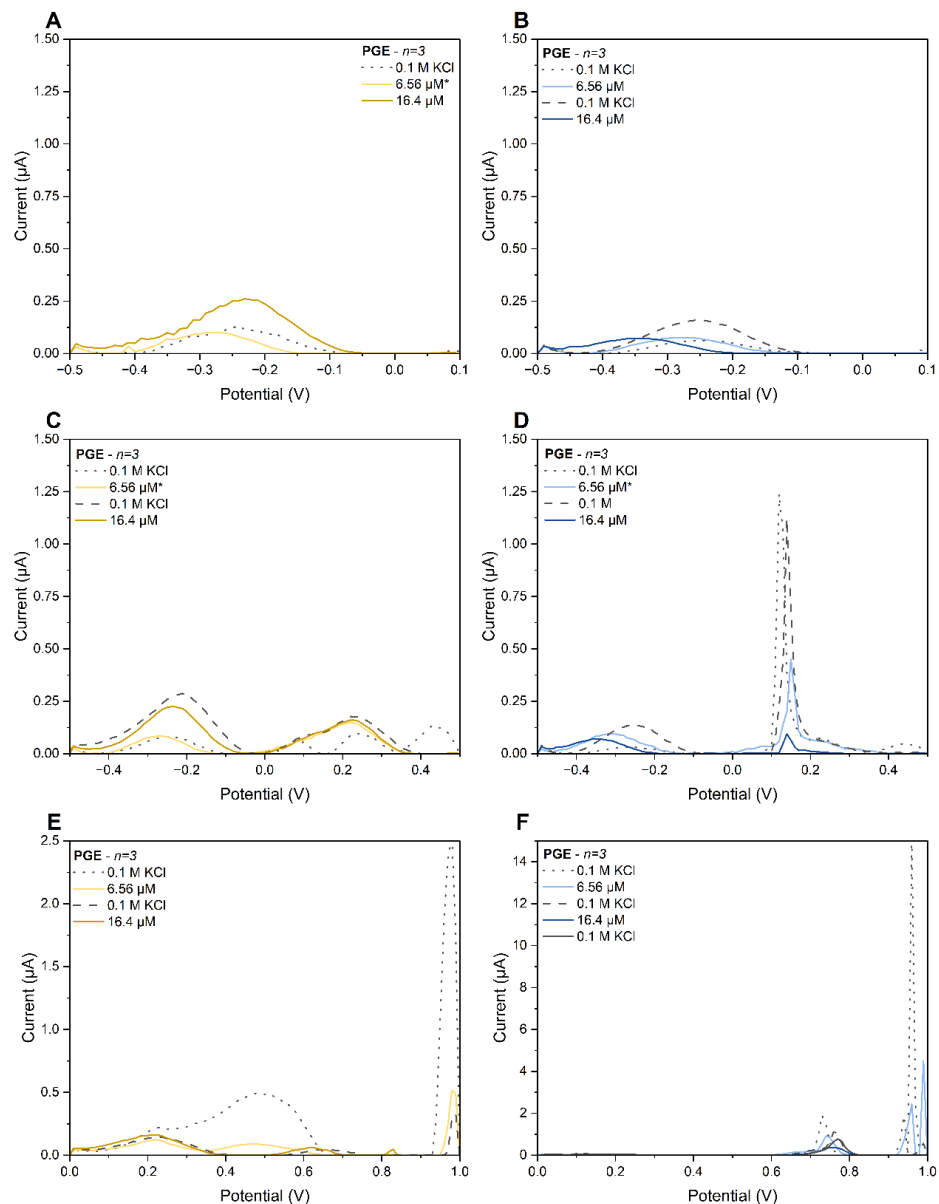
Figure 3.24. DPV on PGE of actinorhodin-free and actinorhodin samples in 0.1 M KCl respectively mostly negative (A&B), [-0.5;0.5] V (C&D) and exclusively positive (E&F) potential windows. * indicates *n=2*.

Figure 3.25. Evidenced actinorhodin non-systematic adsorption on gold PGEs following electrochemical measurements.

After analysing actinorhodin solutions on PGE, the next electrode format to be screened was a screen-printed gold format with on-chip gold counter and Ag/AgCl reference electrodes.

3.4.1.3.2.2 Screen-Printed Electrodes

Clean and activated screen-printed electrodes were characterised in Figure A.8 in Chapter 3 Appendices. On gold SPE and in a PBS background, a shifted reduction peak compared to blank samples was recorded in the − 0.2/- 0.3 V region (Figure 3.26A-B). Several DPV peaks differentiating from the PBS blank in potential and amplitude were present in the forward scan, with peaks at − 0.65, - 0.4 and 0.1 shifted to 0.2 V, the latter in the backward scan (Figure 3.26C-D-E).
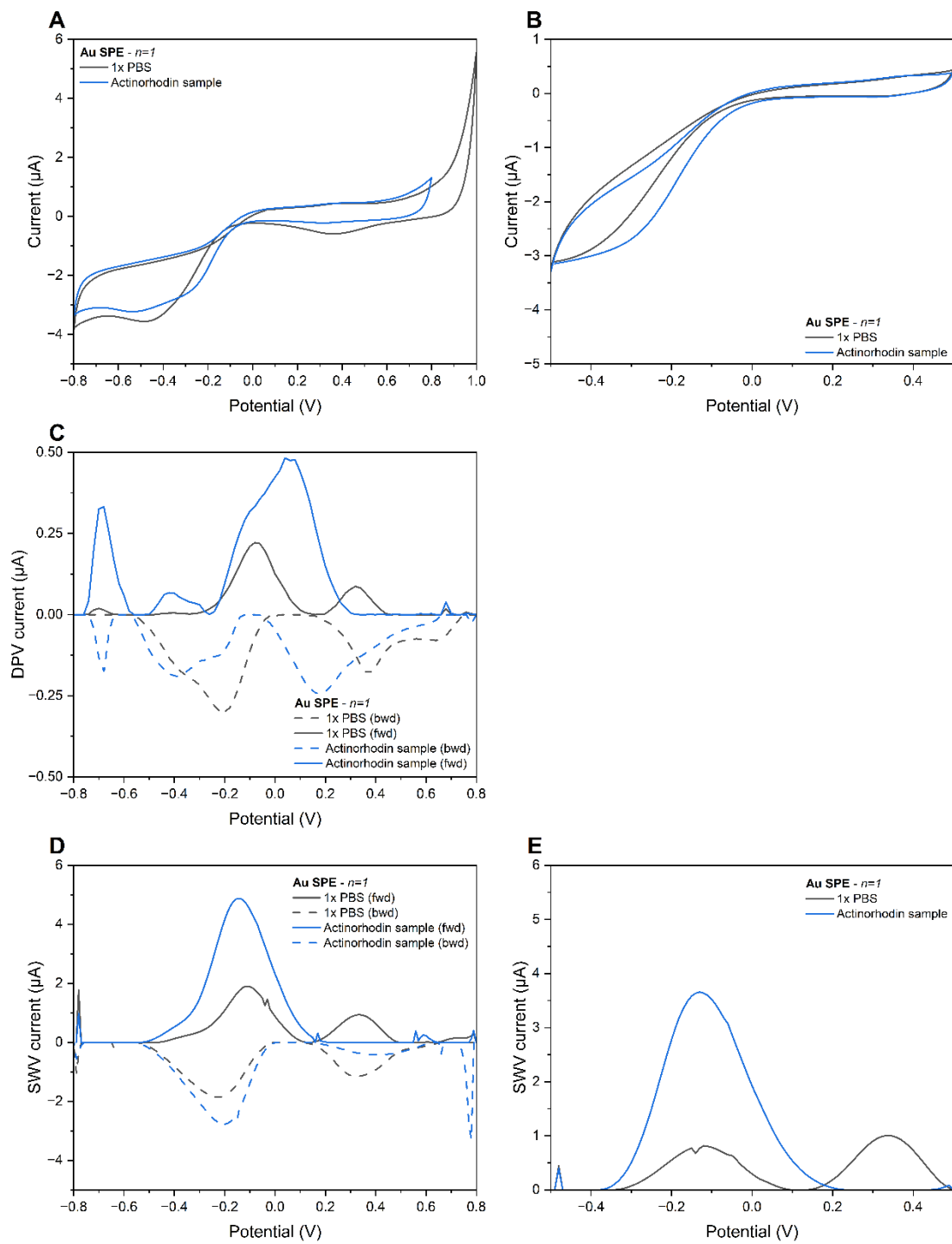
Figure 3.26. Analysis of the actinorhodin sample on gold SPE in 10 mM PBS with CV (A&B), DPV (C) and SWV (D&E) with *n=1* for each trace.

Concerning the KCl dilutions, oxidation and reduction peaks were recorded at 0.1 and − 0.1 V in the cyclic voltammogram (Figure 3.27A), confirmed with DPV and SWV (Figure 3.27C-D). An additional peak, proportional to sample concentration was recorded in SWV close to 0.35 V (Figure 3.27D).
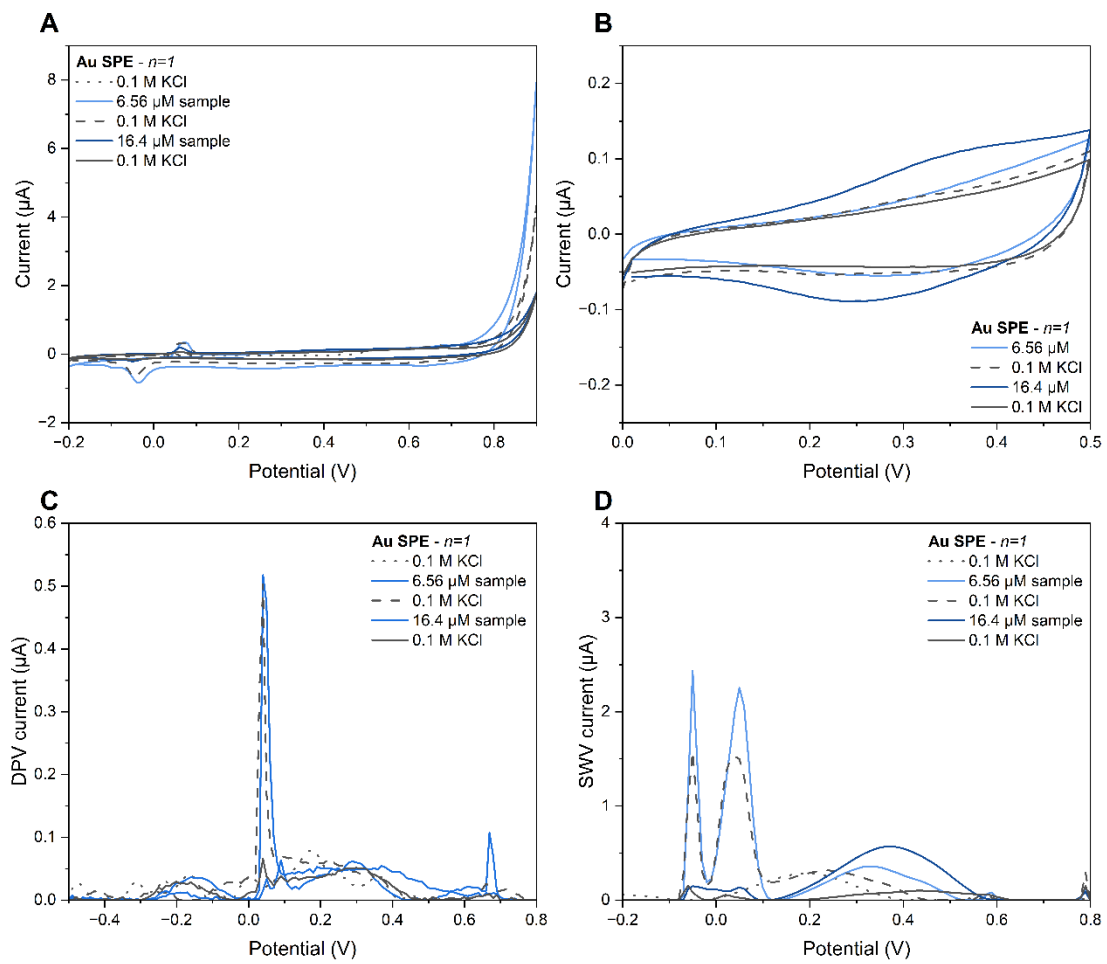
Figure 3.27. Analysis of the actinorhodin sample on gold SPE in 0.1 M KCl with CV (A&B), DPV (C) and SWV (D) with *n=1* for each trace.

Assessing if electrolytes present in the medium would be sufficient, a concentrated actinorhodin solution was interrogated on gold SPE (Figure 3.28). Upon the first CV, an oxidation and a reduction peak were recorded respectively around 0.2 and -0.15 V (Figure 3.28A). A few major compounds were evidenced next via DPV and SWV and upon reinterrogation via CV using the same electrode, no oxidation or reduction peak appeared anymore (Figure 3.28).
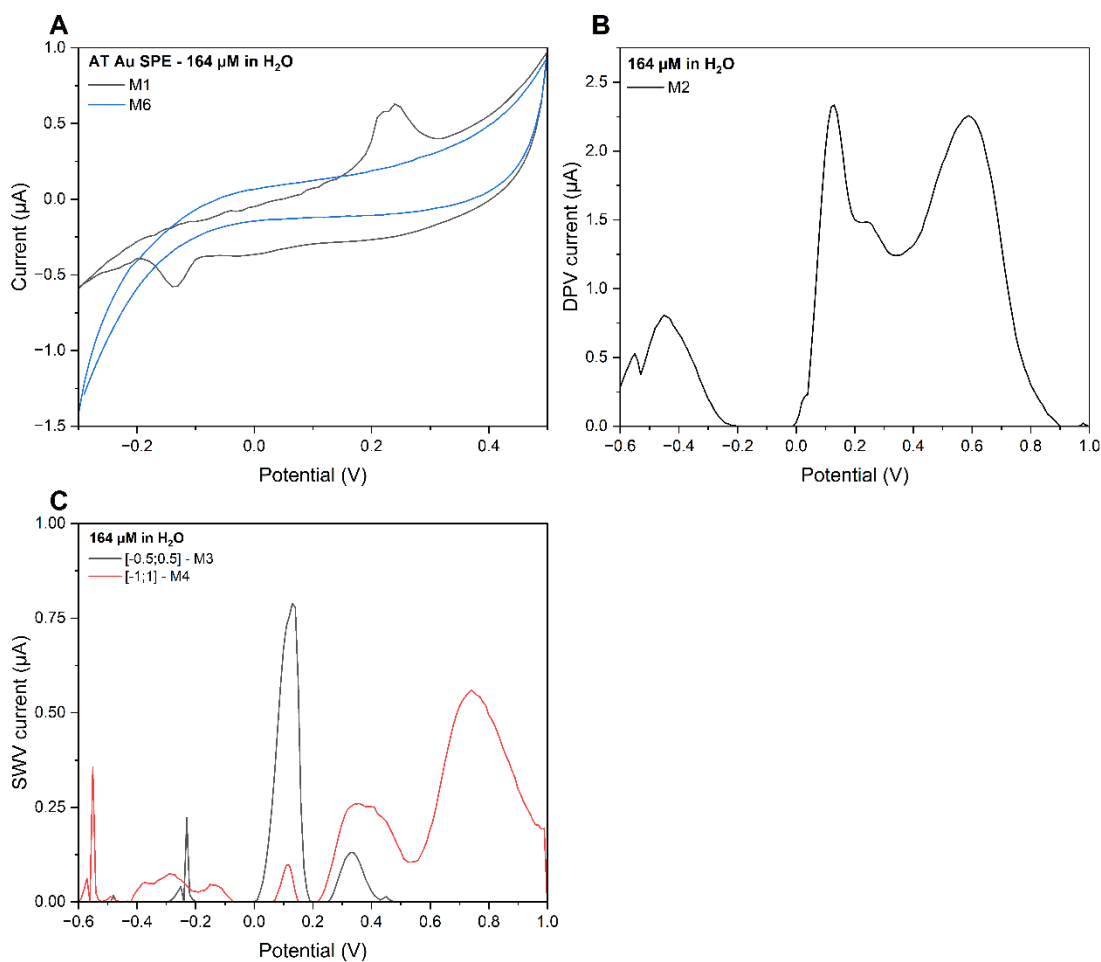
Figure 3.28. CV (A), DPV (B) and SWV (C) characterisation of a 164 µM actinorhodin solution in water. The number after M in the legend corresponds to the order in which measurements were carried out.

A lower electrolyte concentration has been tested for both PBS and KCl and a 1 mM KCl background has confirmed the observed phenomena from Figure 3.28.

One oxidation and two reduction peaks at least were evidenced with the first CV cycle used to characterise the 164 µM actinorhodin solution in a 1 mM KCl background. Subsequently widening the potential window led to lower peak amplitudes. Peaks appeared in the blank measurement, suggesting once more a possible adherence on the electrode surface (Figure 3.29 and Figure 3.30).
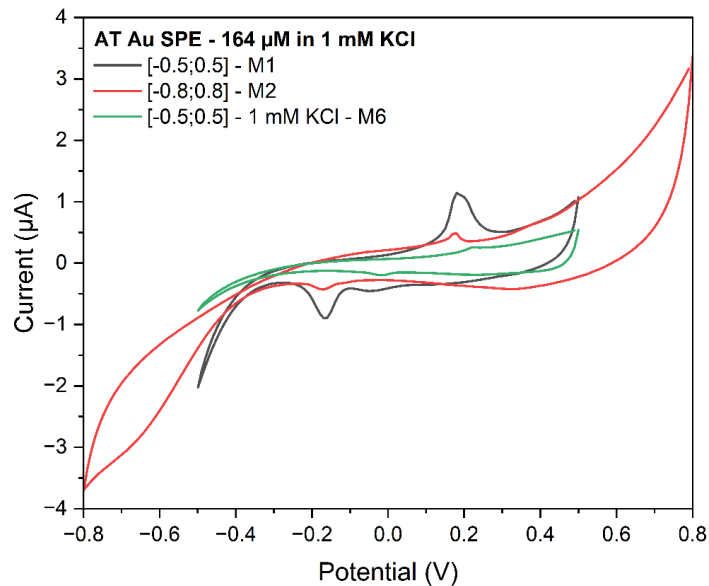
Figure 3.29. Characterisation of a 164 µM actinorhodin solution in 1 mM KCl on Au SPE (*n=1*). CV (A&B), DPV (C) and SWV (D). The number after M in the legend corresponds to the order in which measurements were carried out.

Figure 3.30. Evidenced actinorhodin adsorption on gold SPEs following measurements.

Finally, interdigitated gold microelectrodes were evaluated to assess if a clear and repetitive detection could be obtained.

3.4.1.3.2.3 Interdigitated Electrodes

Three different gold thin-film interdigitated microelectrode models were tested, namely IDE1, IDE2 and IDE3 (Micrux). Electrodes were cleaned using a plasma asher for 1 min at 50% and 0.3 mbar for 3 cycles and their characterisation in $[Fe(CN)_6]^{3-/4-}$.reported respectively in Chapter 3 Appendices in Figure A.9, Figure A.10 and Figure A.11.

A 10 µL deposit of 65.6 µM of actinorhodin solution was assessed with cyclic voltammetry first, then differential pulse voltammetry. A [-0.5 ;0.5] V potential

window was not sufficient to evidence actinorhodin oxidation or reduction (Figure 3.31A and B). Extending the potential window to [-1.0 ; 1.0] V allowed to record an oxidation peak at 0.1 V and a reduction peak at -0.1 V using a scan rate of 0.5 V/s at three occurrences using the same electrode (Figure 3.31C). The higher scan rate appears to be crucial, as evidenced with subsequent measurements of the stock solution (Figure 3.31E). Concerning DPV, the more positive peak amplitude increased overall (Figure 3.31D). Differentiation between the more cathodic peak and the more anodic peak was only evidenced upon the first measurement, at 65.6 and 328 µM. Moreover, the lower DPV current amplitude from the more concentrated solutions indicated a possible fouling of the electrode (Figure 3.31D and F).
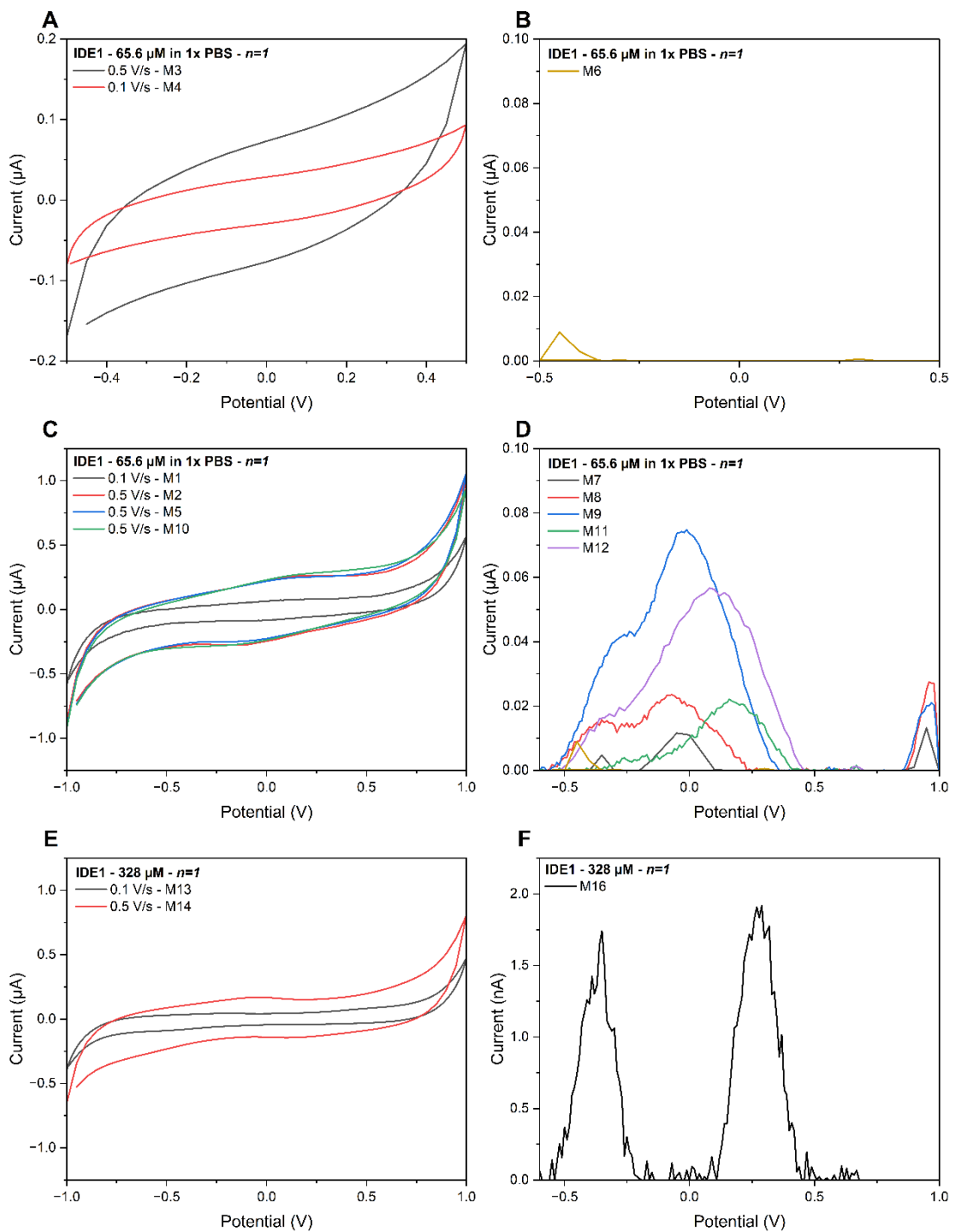
Figure 3.31. Characterisation using IDE1 of a 65.6 µM actinorhodin solution respectively for [-0.5 ;0.5] V and [-1.0 ;1.0] potential windows using CV (A&C) and DPV (B&D) and 328 µM actinorhodin extract at the largest potential window with CV (E) and DPV (F). The number after M indicates the order in which the measurements were conducted.

Repeating the same tests using KCl might have been beneficial for comparison along with additional repeats for each condition. With IDE2, neither oxidation nor reduction events were captured by cyclic voltammetry at various scan rates using PBS

as a background electrolyte (Figure 3.33A). On differential pulse voltammograms, some activity is recorded between [-0.25 ;0.25] (Figure 3.32C). With KCl as an electrolyte and a wider potential window, at least one reduction peak at -0.52 V and one oxidation at 0.5 V are evidenced (Figure 3.32B). Similar peaks are recorded in the first DPV in 0.1 M KCl, merged into one for the next two measurements (Figure 3.32D). Using a wider potential window with DPV, both peaks are recorded in the two electrolytes tested and better resolved in KCl than PBS (Figure 3.32E and F). To confirm the existence and location of these peaks, a more concentrated stock solution was tested next, with KCl as a background electrolyte only (Figure 3.33). Recorded at similar potentials (-0.53 and 0.53 V), a lower amplitude (0.8 and 0.7 µA in Figure 3.33A compared to 1.4 and 1.3 µA in Figure 3.32B) indicated a possible adhesion onto the electrode.
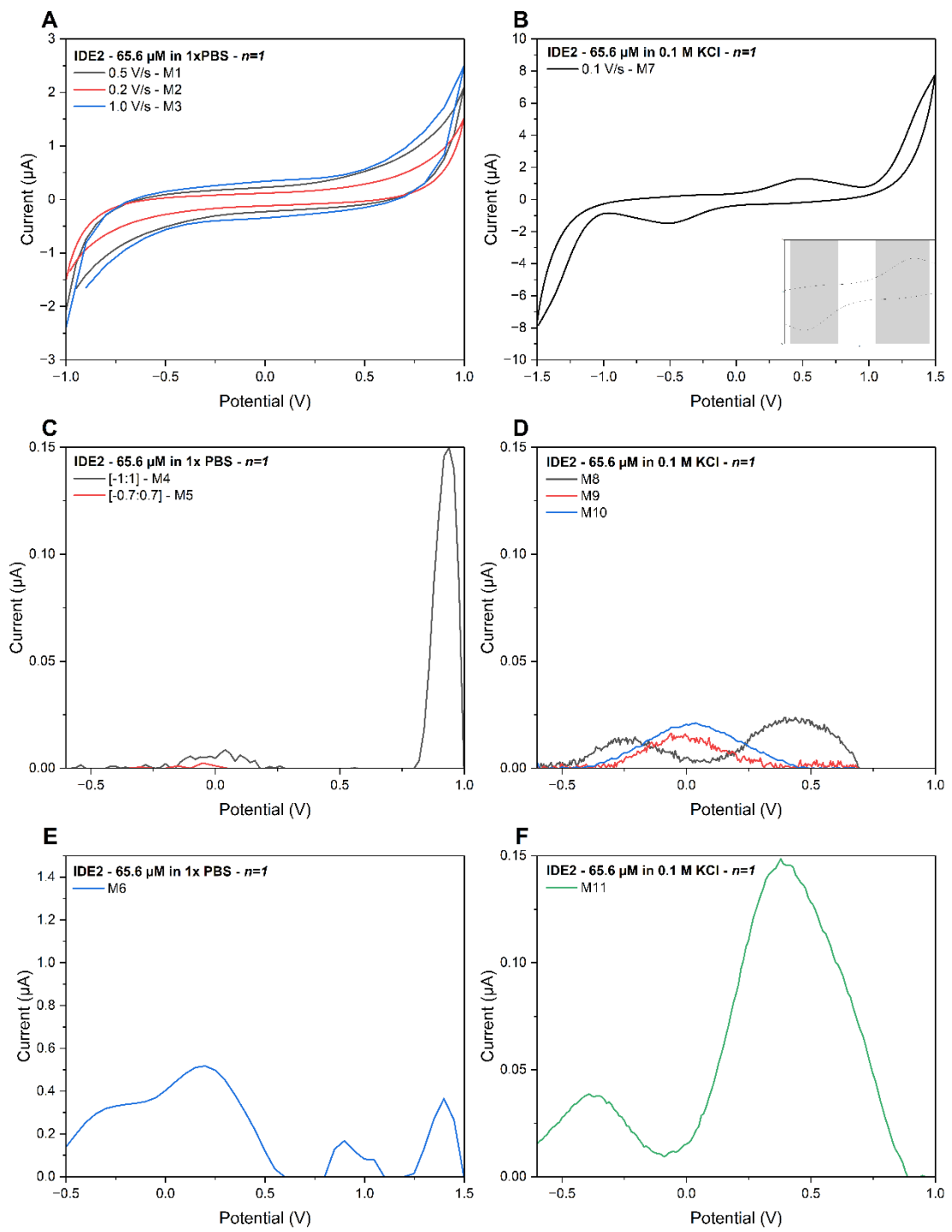
Figure 3.32. Characterisation using IDE2 of a 65.6 µM actinorhodin extract in 10 mM PBS using CV (A) and 0.1 M KCl (B) and DPV using [-1.0 ;1.0] (C&D) and wider potential windows (E&F) using respectively PBS or KCl as background electrolytes. The number after M in the legends indicates the order in which the measurements were conducted.

137
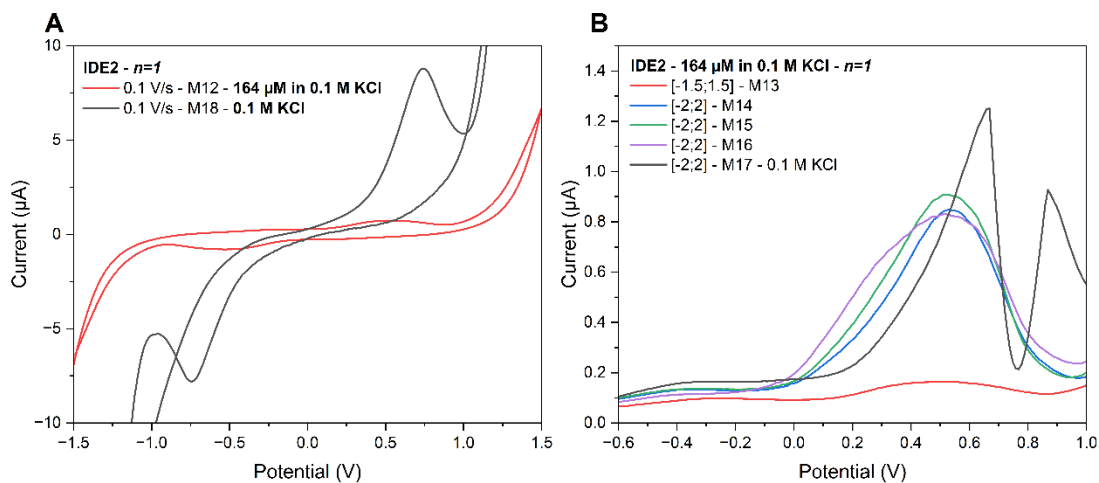
Figure 3.33. Characterisation using IDE2 of a 164 µM actinorhodin extract in 0.1 M KCl using CV (A) and DPV (B). The number after M in the legends indicates the order in which the measurements were conducted.

Cyclic voltammograms of actinorhodin samples using IDE3 were inconclusive on detecting electrochemical activity in actinorhodin samples. DPV of 65.6 µM solutions in a PBS background repeatedly showed at least one peak at a slightly negative potential. The potential window was narrowed from [-1 ;1] to [-0.7 ;0.7] V in an attempt to preserve electrode integrity and conserved for the next measurements (Figure 3.34). To be noted as well is the difference in order of magnitude in peak amplitude between Figure 3.34A and Figure 3.34B, 100 times lower for the first measurement. Peak amplitudes recorded in a 164 µM actinorhodin solution with 0.1 M KCl as a background electrolyte displayed initially a peak current in the 10 µA range, which grew up to over 60 µA for the same solution by repeating measurements (Figure 3.34C). A decrease in peak amplitude was recorded upon interrogation of the same electrode with a 65.6 µM actinorhodin solution in 0.1 M KCl (Figure 3.34D). Blank electrolyte solutions were tested after sample testing to attempt identifying the recorded peak. The same signal was evidenced despite the absence of actinorhodin in the solutions tested (Figure 3.34E). The potential windows scanned might have been damaging for the electrode as well, however earlier results prevented recording of peaks from a narrower potential window (Figure 3.32A&B). The DPV was only ran once, so the peak might have decreased upon repeated measurements. Moreover, these were the results of a single repeat, which might have benefitted from more replicates. Adsorption of actinorhodin onto electrodes, decreasing the sensitivity of

the electrode is another possibility as reported by Mazur and Haroon with Frenolicin B[360] and evidenced by the electrode aspect after testing (Figure 3.35). In addition, sample concentrations were high, which could have favoured adsorption as well.
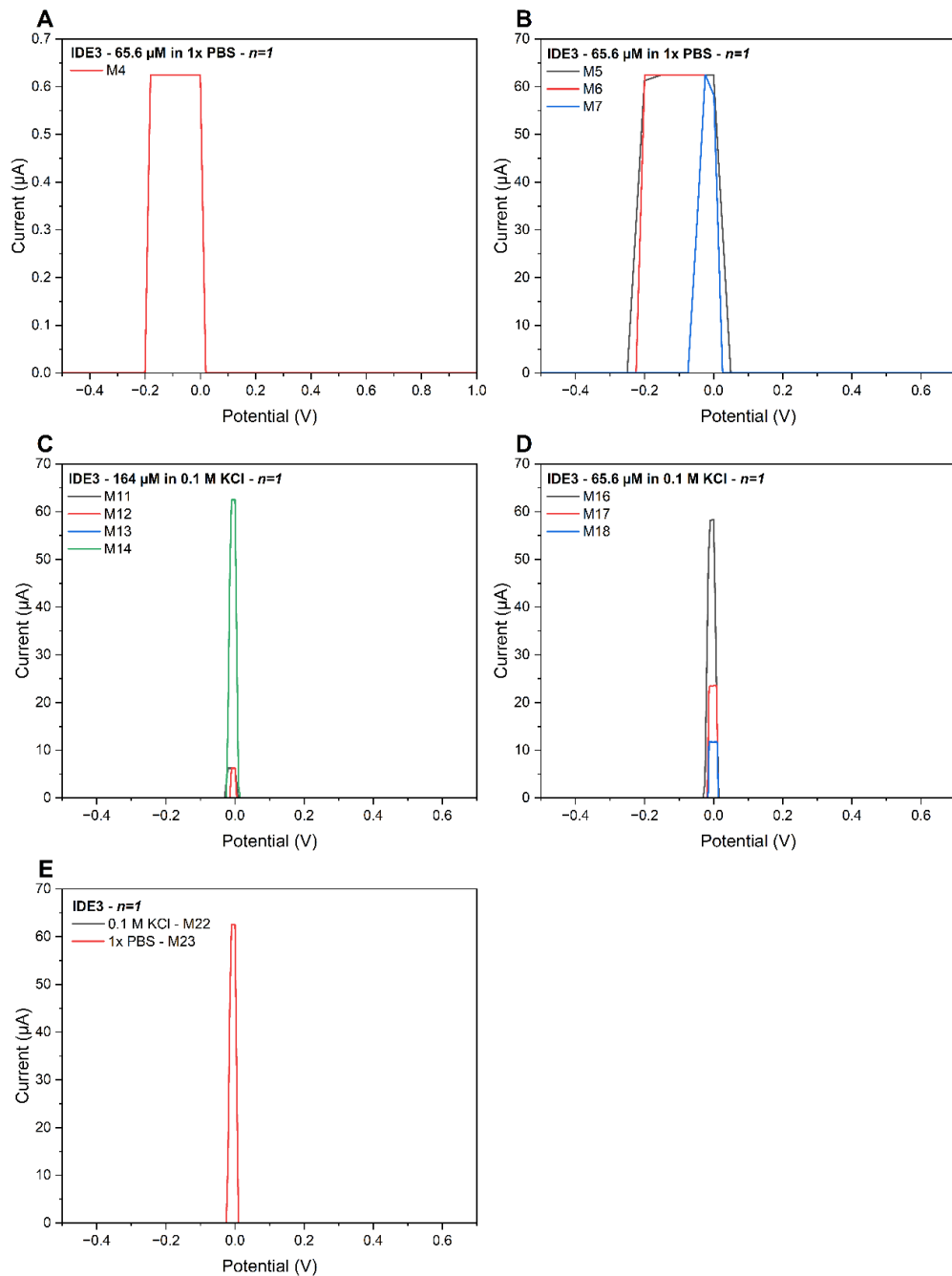
Figure 3.34. DPV characterisation using IDE3 of a 65.6 µM actinorhodin sample in 10 mM PBS for a wider (A) and more narrow potential window (B). DPV of 164 µM (C) and 65.6 µM samples in 0.1 M KCl (D) with final electrolyte-only measurements (E). The number after M in the legend corresponds to the order in which measurements were carried out.

The electrochemical signal seemed to decrease between increasing concentrations. Most often, the recorded blank signal appeared higher than any other signal. Electrodes were coated after first voltammetric measurement, which is why the signal was decreasing rather than being proportional to concentration. The high signal too from blanks led to inferring that either the background medium components or actinorhodin precursors played a role on the polymerisation. Polymerisation did not always occur similarly, considering location on the electrode or spread of the film (Figure 3.35, Figure 3.30 and Figure 3.25).

Figure 3.35. IDE1, IDE2 and IDE3 after measurements of actinorhodin samples (respectively left, middle and right). A blue hue is noticeable on IDE1, much lighter on IDE3 and dark and advanced on IDE2.

A summary of peaks detected via electrochemical methods on gold electrodes is reported in Table 3.4.

Table 3.4. Peak detection for actinorhodin samples on gold electrodes. Peaks included have a different potential than actinorhodin-free samples and their amplitude reaches higher currents than at least the first electrolyte blank solution tested.

Potential region (V)	Electrode			Electrolyte		Measurement			Fig.
	PGE	SPE	IDE	KCl	PBS	CV	DPV	SWV	
-0.55			√	√		√			Figure 3.33
-0.4		√					√	√	Figure 3.25
			√	√	√	√	√		
-0.25/-0.3				√	√		√		Figure 3.26
			√						Figure 3.32
		√				√		√	Figure 3.33
-0.15				√		√			Figure 3.28
			√						
		√			√			√	

Potential region (V)	Electrode			Electrolyte		Measurement			Fig.
	PGE	SPE	IDE	KCl	PBS	CV	DPV	SWV	
-0.2	√				√	√			Figure 3.21
		√			√	√		√	Figure 3.26
		√				√			
-0.1	√				√	√			Figure 3.21
	√			√		√			Figure 3.23
		√		√	√	√	√	√	
			√	√	√		√		
		√				√			
0.1	√			√		√			Figure 3.23
	√			√		√	√		Figure 3.24
		√			√		√		Figure 3.26
		√		(√)		√	√	√	
			√		√	√			
0.25		√		(√)		√	√		Figure 3.28
0.35/0.4		√						√	
			√	√		√		√	Figure 3.27
0.5	√			√		√			Figure 3.23
			√	√		√	√		
0.6		√					√		Figure 3.28
0.7	√			√			√		Figure 3.24

3.4.1.3.3 Platinum

Platinum macroelectrodes were characterised after cleaning and activation in Figure A.12 in Chapter 3 Appendices. From the CV in PBS on platinum electrodes, no oxidation or reduction peaks were attributable specifically to actinorhodin-like compounds (Figure 3.36). The reduction peak around -0.1 V on CV in KCl experienced a slight potential shift in actinorhodin samples compared to actinorhodin-free solutions and were proportional to concentration (Figure 3.37).
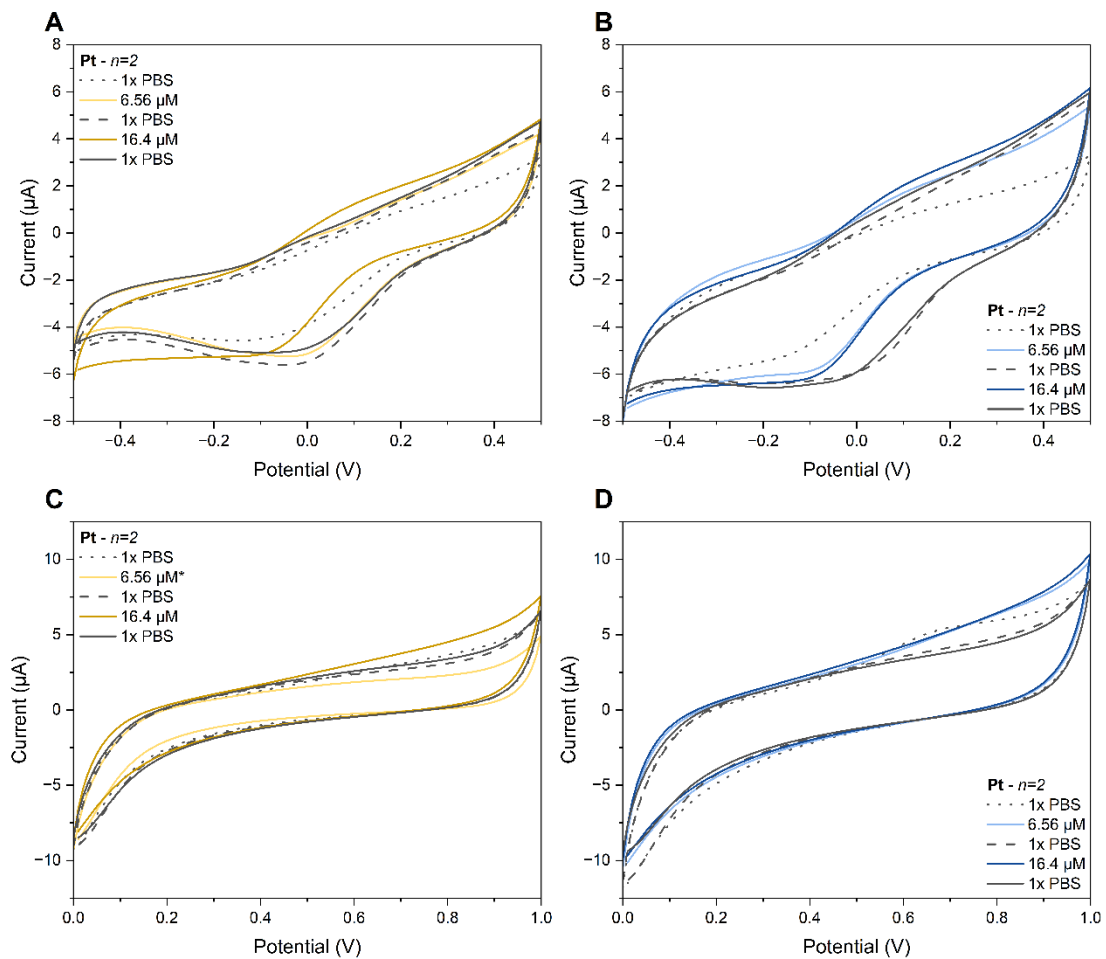
Figure 3.36. CV on Pt electrodes of actinorhodin-free and actinorhodin samples in 10 mM PBS respectively [-0.5;0.5] V (A&B) and exclusively positive (C&D) potential windows. * indicates *n=1*.
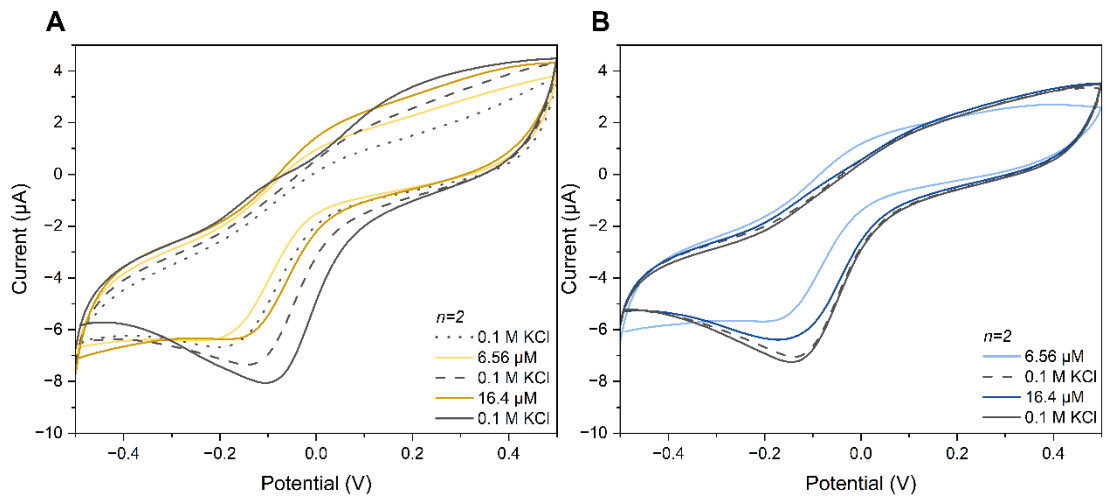
Figure 3.37. CV on Pt electrodes of actinorhodin-free (A) and actinorhodin samples (B) in 0.1 M KCl between [-0.5;0.5] V.

142
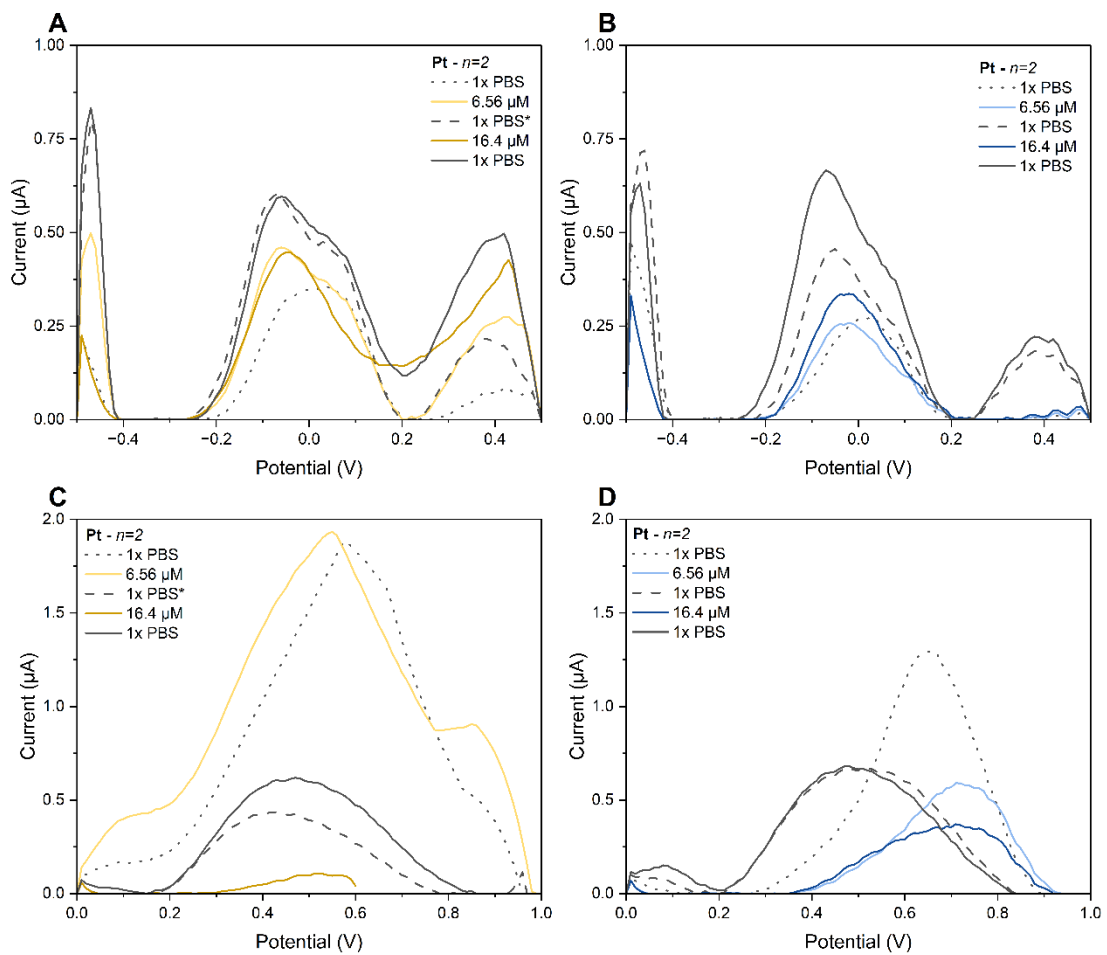
Figure 3.38. DPV on Pt electrodes of actinorhodin-free and actinorhodin samples in 10 mM PBS respectively [0.5;0.5] V (A&B) and exclusively positive (C&D) potential windows. * indicates *n=1*.

On the DPV in PBS, modest sample signals were recorded above electrolyte blanks (Figure 3.38 and Table 3.5). None of the DPV signals in KCl from actinorhodin and actinorhodin-free samples were recorded above electrolyte blanks (Figure 3.39 and Table 3.5).
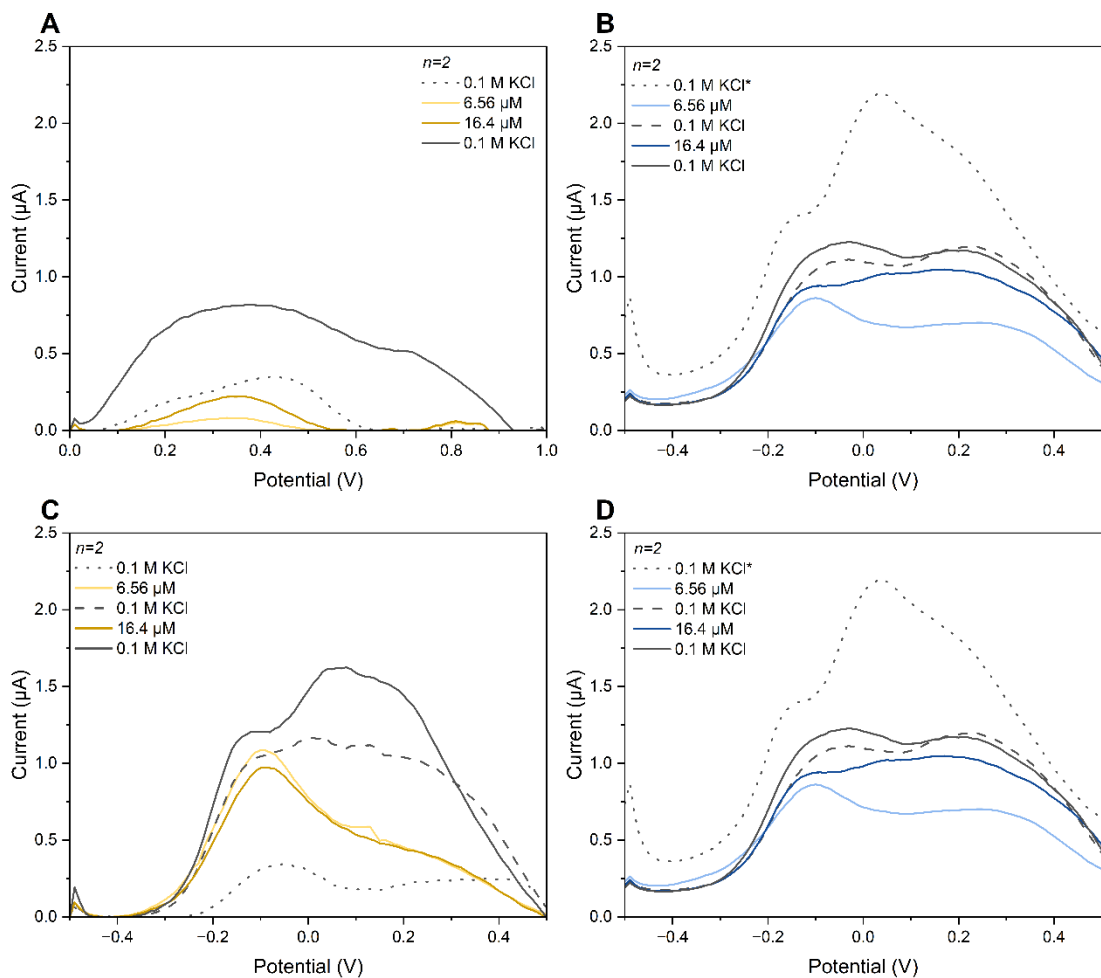
Figure 3.39. DPV on Pt electrodes of actinorhodin-free and actinorhodin samples in 0.1 M KCl respectively [0.5;0.5] V (A&B) and exclusively positive (C&D) potential windows. * indicates *n=1*.

Table 3.5. Peak detection for actinorhodin samples on platinum electrodes. Peaks included have a different potential than actinorhodin-free samples and their amplitude reaches higher currents than at least the first electrolyte blank solution tested.

Potential region (V)	Electrode	Electrolyte		Measurement			Fig.
		KCl	PBS	CV	DPV	SWV	
-0.1	Pt	√		√			Figure 3.36

Different electrodes were used for each electrolyte dilution but only regenerated before the first electrolyte blank. Cyclic voltammetry was performed prior DPV. As platinum is more catalytically active than gold, electrodes might have readily been coated by either actinorhodin-like or other components of the samples upon potential cycling and prevented an accurate DPV and further CV depiction of

144

sample contents. Degassing solutions might have enhanced signal recording as well for this electrode material.[219]

A few recurring patterns were noticed across all electrode materials (Table 3.3, Table 3.4 and Table 3.5). As the electrode material had decreasingly inert properties, currents recorded for blank thresholds became higher than currents recorded for actinorhodin and actinorhodin-free samples and were not dependent on sample concentration. Running experiments in a degassed environment could offer more stability for actinorhodin compounds.

Noticed visually on the electrodes (Figure 3.25, Figure 3.30, Figure 3.35) as well as on the voltammograms, components of the mixture adsorbed on the electrode area after the first few scans, impairing the electron exchange as well as signal acquisition. The high chemical reactivity of actinorhodin compounds has been previously reported,[315] as well as a similar phenomenon with the close metabolite Frenolicin B.[360] The newly characterised theta-actinorhodin has been reported as unstable and isolated as a film, which could be responsible for the inconsistent polymerisation behaviour.[352]

Further trials, with lower concentrations have explored the resemblance with dopamine polymerisation. An explanation for the mechanism of polydopamine formation has been provided by Dreyer *et al.* (2012) (Figure 3.40) with a 1:1 benzoquinone and diol complex formation followed by π-stacking of quinhydrones yielding multidimensional polymeric materials.[361]
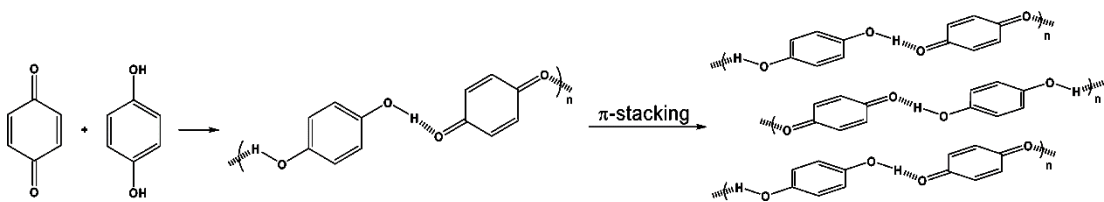
Figure 3.40. Dopamine polymerisation mechanism.[361] Reproduced with permission from Dreyer *et al*. Elucidating the Structure of Poly(Dopamine). Langmuir 2012, 28 (15), 6428–6435.

Redox active centres of actinorhodin are constituted of the same motifs that could possibly interact to form a similar structure and form more easily at the electrode surface due to the flow of electrons enhancing chemical reactivity. Occurring solely at negative potential, around -540 mV, exclusively positive potential windows have also been tested for actinorhodin samples. The presence of oxygen in solution is another trigger for dopamine to polymerise and could be one for actinorhodin too.

As actinorhodin compounds possess quinone moieties, whose electrochemical activity is highly dependent on pH, this could explain the differences observed between samples of different pH. The use of aprotic solvents might have limited proton availability as quinones in aqueous media behave in a complex manner[362], involving 9 possible species and increasing the complexity of phenomena observed.[351] The slow electron transfer kinetics of quinones could have been improved by an anodic pretreatment.[362] Additionally, some quinones show little stability overlong term storage,[363] also mentioned for theta-actinorhodin.[352] This could constitute partly why electrochemical signal observed were not consistent.

The biological activity of quinone-based compounds relies on the stability of its intermediate form, semiquinone, which is possible to study using electrochemistry.[364] Quinones are not defined as aromatic and only become so after a minimum one electron reduction. Aromaticity is dependent on multiple parameters relating to electronic, steric, hydrophobic, hydrophilic, and hydrogen-bonding properties.[351] With quinones of similar radii, different substitutes have been shown to impact stability and structure of intermediates.[364] Quinone species with a hydrophobic tail more substantial in size compared to the quinone ring(s) do not tend to impact electron exchanges. Aqueous systems tend to present more complexity since protons are involved and equilibrium could be reached closer to neutral pH values.[365] In this study, authors examined several quinone substitutions in a dry aprotic solvent environment, restricting the number of intermediate species encountered. A greater number of aromatic rings present in quinone compounds increase the difficulty to reduce the quinone to its semiquinone intermediate. In the

case of paraquinones, reduction becomes more difficult with aromatic rings on both sides of the quinone. Moreover, differentiation between different reduced and oxidised intermediate states is more challenging with a greater number of rings, unless a sulfur atom is present. Substituent location is crucial as ortho-quinone reduction has been found easier than para-quinones. In the case of benzoquinones, since any substituent is in ortho position, the oxygen electron-withdrawing effect occurs in most cases. When in presence of naphthoquinones, they tend to inhibit electron transfer to other quinones and do not accept electrons.[365] This could explain the difficulty in recording and assigning electrochemical signature to actinorhodin compounds and mean that assessing electrochemical activity of actinorhodin compounds using another redox mediator would be more appropriate using a non-quinone species. When distance between electron donor and acceptor grows because of steric hindrance, the electron transfer is affected since donor and acceptor orbitals cannot overlap anymore. This shifts to outer-sphere transfer phenomena, less affected by steric hindrance with weaker complexation between electron donor and acceptor. Unhindered donors can undertake electron transfer via charge-transfer bonds and can be described as inner sphere. Steric encumbrance is therefore a key parameter in electron exchange processes for quinone compounds alongside solvent, temperature and salt, all influencing intermediates and compounds formed.[366] Steric hindrance from actinorhodin compounds' structure might prevent the recording of electrochemical activity directly by affecting their catalytic activity[367] and further strategies using more well-known and characterised mediators might be suitable to indirectly characterise their behaviours.[368]

Attempted next was to induce the polymerisation of actinorhodin-like compounds in a reproducible and consistent manner. Taking into account scan rate observations and potential window specificities, linear scan voltammetry (LSV) has been explored along with SWV for similarities with voltammograms obtained previously.

3.4.1.3.4 Voluntary polymerisation with LSV & SWV

3.4.1.3.4.1 Preliminary trials

Both positive and negative controls were diluted at the same factor, 1 in 50. This is equivalent to 4 mg/mL for the actinorhodin containing sample, based on the spectrophotometric reading.

From linear stripping voltammograms, a peak at 0.13 V on both gold and platinum electrodes was observed in the actinorhodin samples and absent from the actinorhodin-free samples (Figure 3.41).

For gold, the peak observed in the LSV is also present on square wave voltammograms (Figure 3.42). Since each condition only corresponded to one electrode, this prompted further concentration tests for reproducibility and quantitative assessment.
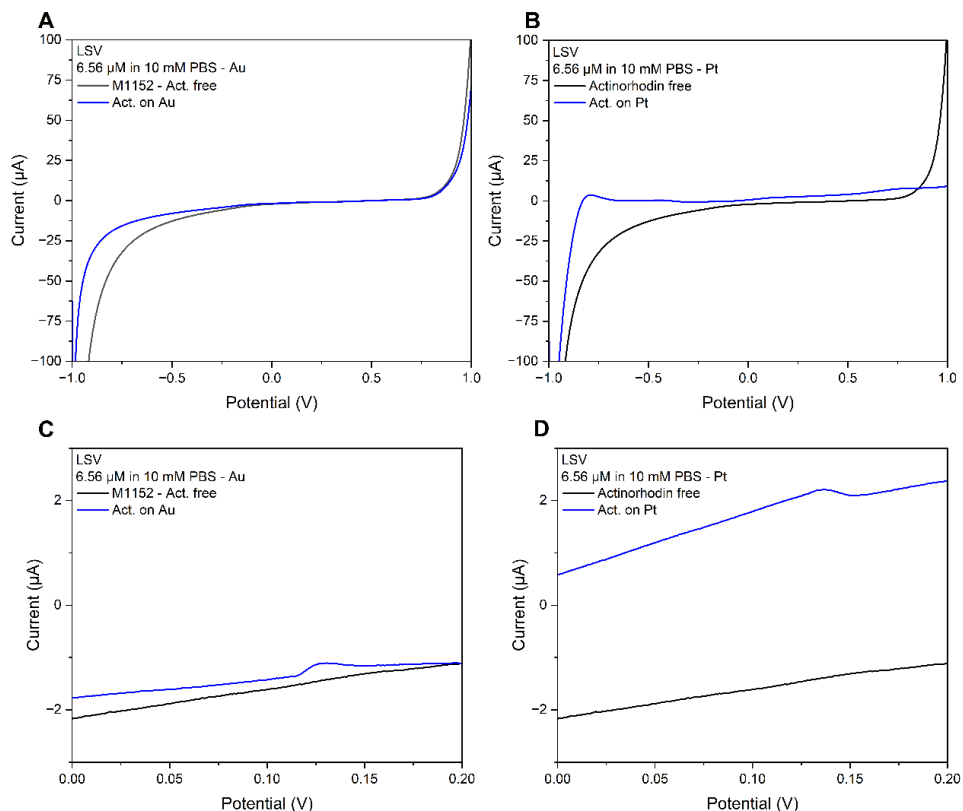
Figure 3.41. LSV on Au and Pt electrodes of actinorhodin and actinorhodin-free samples (respectively A and B) with corresponding close-ups for Au (C) and Pt (D) of the 0 to 0.2 V region to evidence the presence of peak in actinorhodin samples, absent from actinorhodin-free samples.
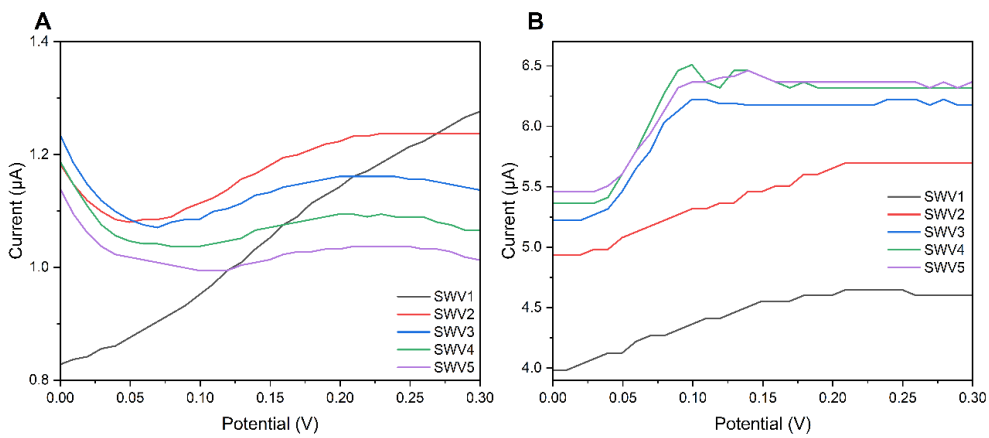
Figure 3.42. SWV iterations of the actinorhodin-free sample and actinorhodin sample on gold (respectively A and B). *n=1* for each trace.

3.4.1.3.4.2 Dose-dependent and repeatable polymerisation

The LSV and SWV measurement suites were performed on clean electrodes four to five times. Since samples were available in limited quantities, replicates were assessed from the same solution. A single electrode was dedicated for each concentration and cleaned in between each replicate to reduce variability.

The previously observed peak at - 0.1 V was observed only in the lowest solution concentration with and without blank subtraction but not systematically for every replicate (Figure 3.43B). This was at a much lower than the 6.56 µM on first exploratory work (Figure 3.41). The blank was diluted at the highest concentration, which might have hindered peak detection when subtracted. However, since the lowest concentration only showed a peak in the region of interest, the impact of blank subtraction might be different than expected. Visually, on the electrodes, a film formed but not consistently. When a peak around 0.1-0.2 V is present, the film formed appeared much darker (Figure 3.25).

Repeating the several dilutions tested in a different electrolyte, for instance KCl, might uncover different behaviour from actinorhodin-like compounds. Testing isolated compounds from the mixture could help to understand which compound(s) is/are responsible for the polymerisation as well and which conditions favour or prevent it.

149
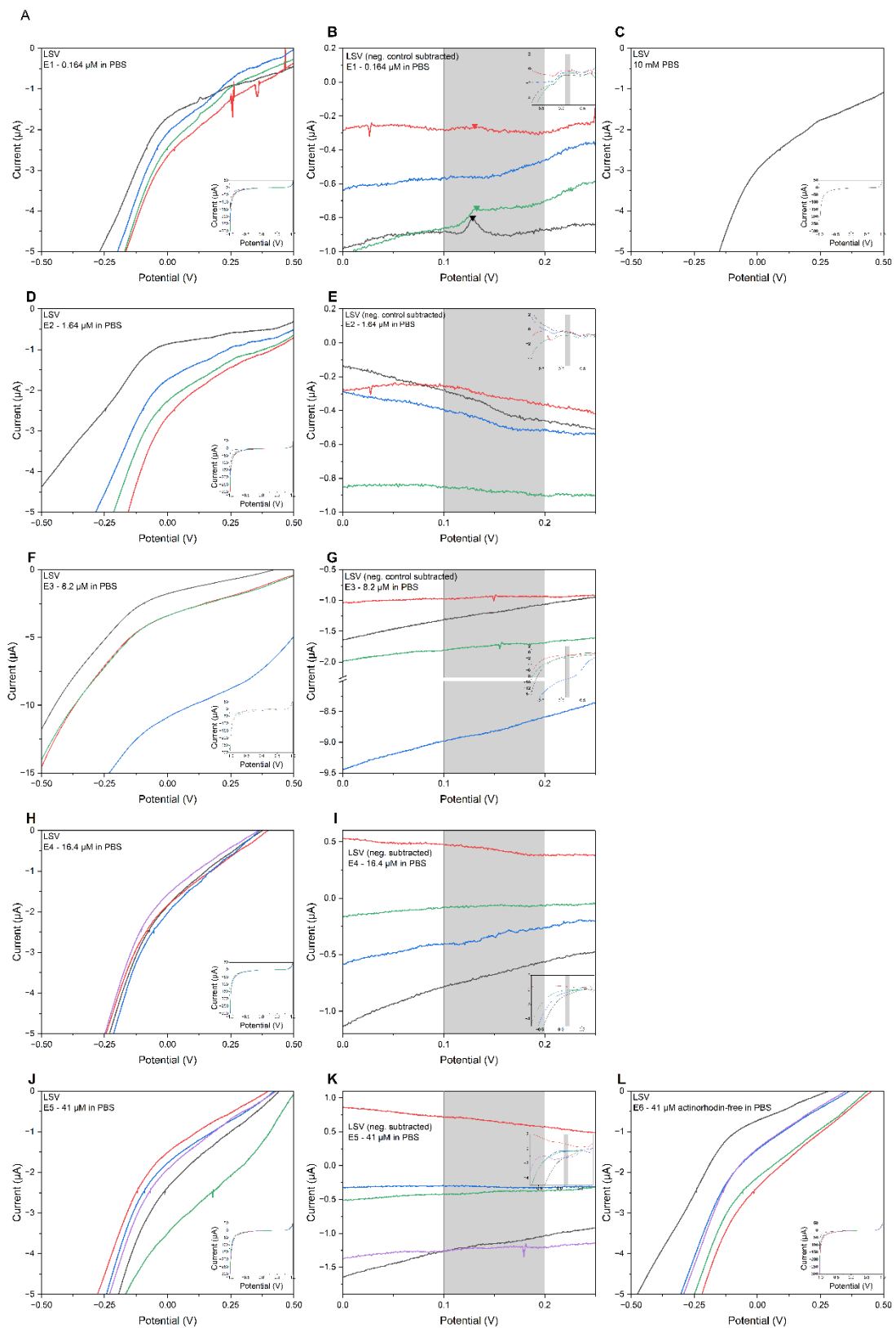
Figure 3.43. LSV on PGE of actinorhodin samples (left), with actinorhodin-free sample subtracted (middle) with increasing concentrations: 0.164 µM (A-B), 1.64 µM (D-E), 6.2 µM (F-G), 16.4 µM (H-I) and 41 µM (J-K). LSV of corresponding negative controls, namely electrolyte blank (C) and actinorhodin free sample at 41 µM (L). Traces represented per plot indicate the number of replicates per concentration tested.

The series of 5 SWV to assess PGEs after polymerisation did not provide a clear identification of changes between actinorhodin and actinorhodin-free samples. The four compounds detected below 0 V were also present in the actinorhodin-free sample. The second most cathodic peak could be an actinorhodin-related peak as its amplitude in the blank was lower than in actinorhodin samples. Moreover, these two cathodic peaks were more resolved in the actinorhodin-free compared to the actinorhodin samples, possibly hindering at least another peak/compound. The two peaks around 0.25 and 0.5 V were evidenced at the lowest two actinorhodin concentrations (Figure 3.44A-B), 16.4 μM (Figure 3.44D) and 41 μM (Figure 3.44E) but not differentiated at 8.2 μM (Figure 3.44C). Nevertheless, they were detected in the blank sample as well, even if at lower current amplitude (Figure 3.44F). The most anodic peak appeared in most samples and at a very close potential in the blank. However, peak amplitude did not seem to correlate directly with concentration (Figure 3.44). Attempting this measurement series on carbon and platinum, as well as with different electrolytes could help to identify responsible compound(s) for polymerisation. Isolation of compounds from the mixture and test them separately would be highly beneficial for peak assignment and understanding phenomena behind surface fouling.

The same series of polymerisation experiment were conducted in an acidic electrolyte background. The two major peaks in the negative potential region also appeared in the PBS blank. However, peak amplitude was lower with a higher sample concentration, possibly meaning that the electrodes were coated with compounds showing in this potential region. More electrochemical activity was recorded in the positive region and seemed related to sample concentration (Figure 3.45). Comparing to the neutral electrolyte solution, similarities occurred in the positive region and the most anodic peak was evidenced at a slightly more positive potential. Less peak separation was observed in the negative potential region with a shift in amplitude ratio between the major peaks recorded (Figure 3.44 and Figure 3.45).

Evidence of polymerisation has arisen visually (Figure 3.25, Figure 3.30, Figure 3.35) and with signal intensities decreasing inversely to sample concentration.

Samples appeared to behave similarly after the series of LSV and SWV, with the intermittent presence of a detectable compound (Figure 3.43). This could be the results of the instable theta-actinorhodin, degrading quickly and isolated as a thin film.[352]
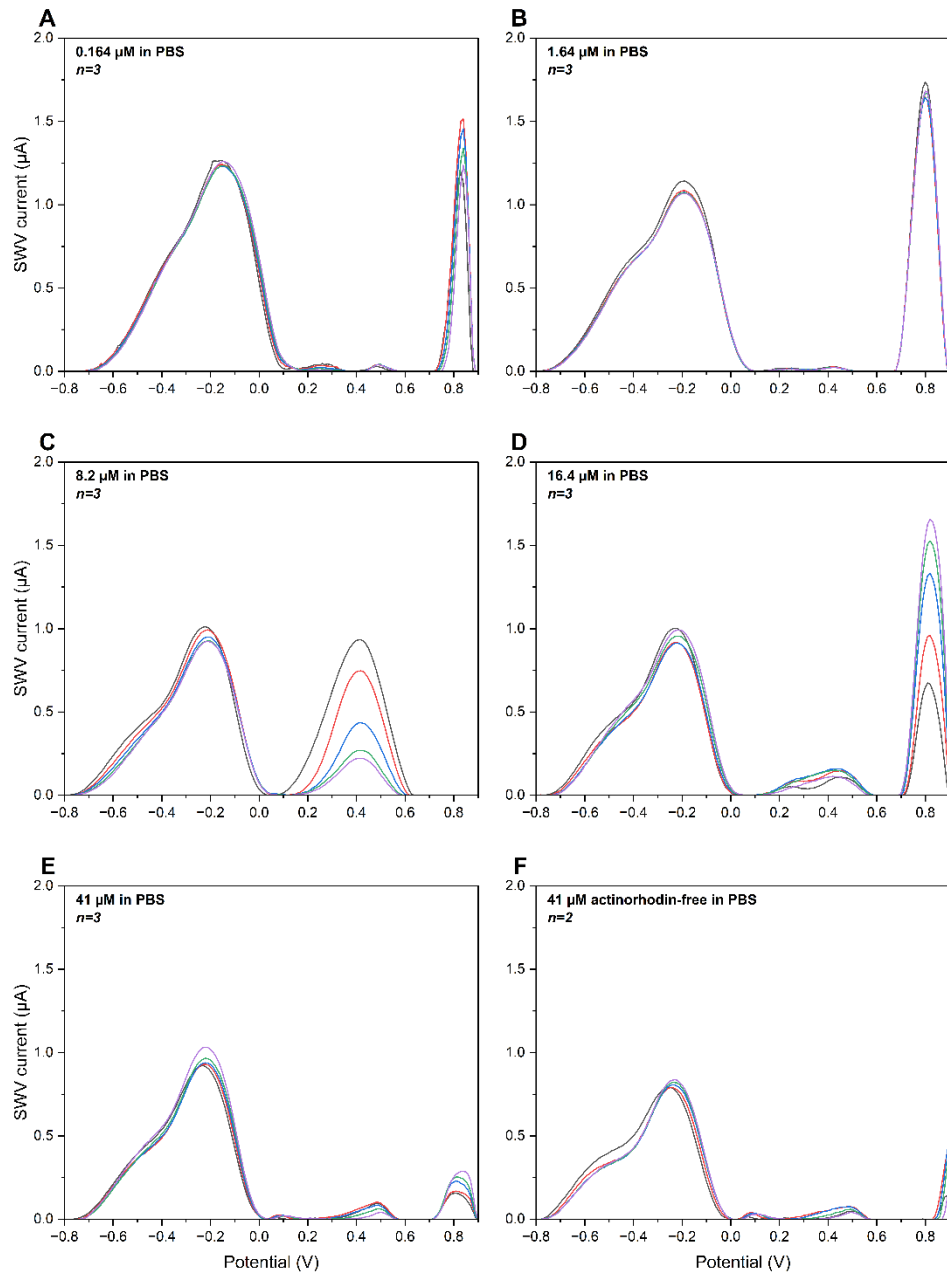
Figure 3.44. SWV performed after LSV treatment on PGE for increasing concentration of actinorhodin samples, 0.164 µM (A), 1.64 µM (B), 6.2 µM (C), 16.4 µM (D), 41 µM (E) and 41 µM (F) of actinorhodin-free sample.
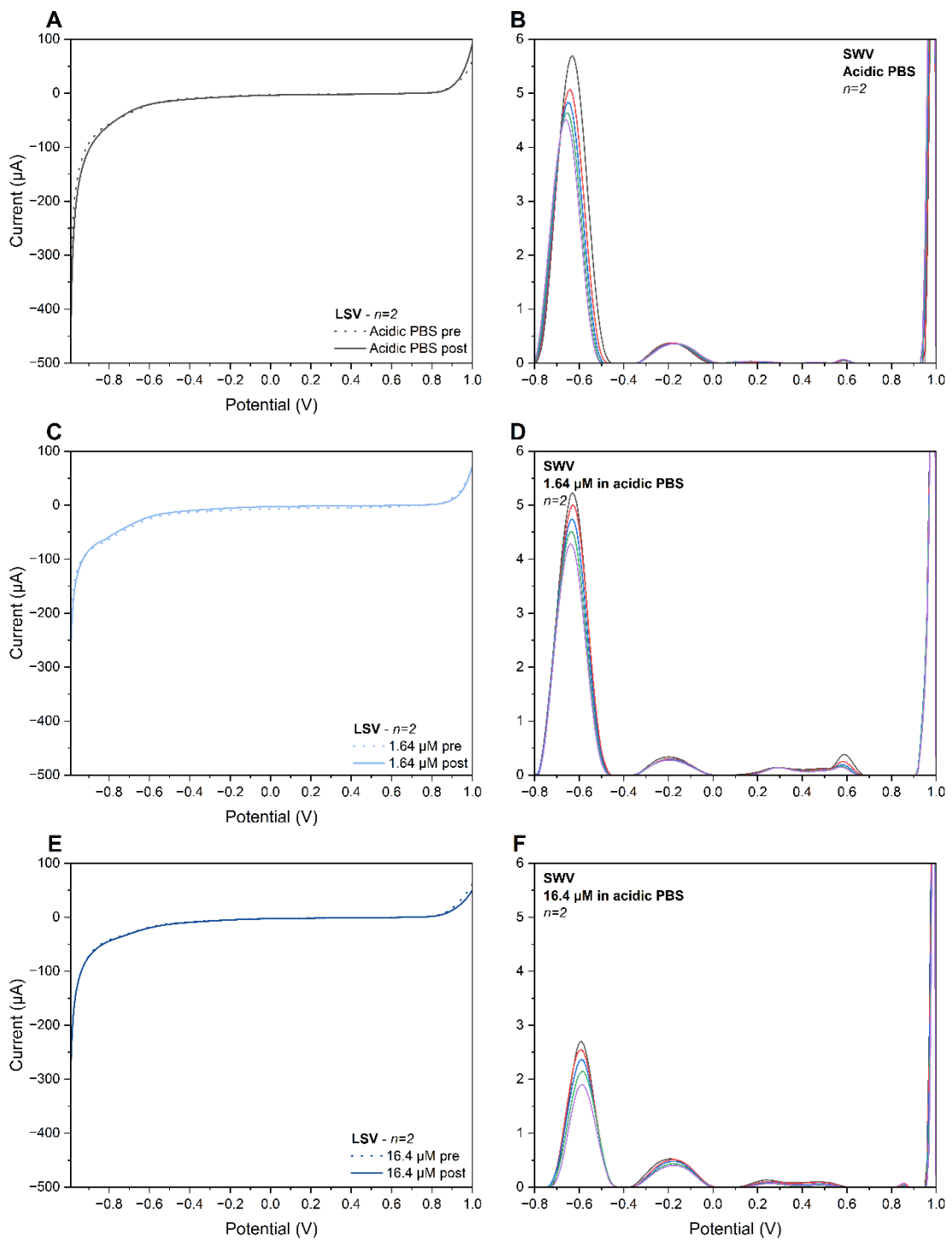
Figure 3.45. LSV performed with acidic PBS and subsequent SWV on PGE for actinorhodin samples at 0 μM (A-B), 1.64 μM (C-D) and 16.4 μM (E-F).

3.4.1.3.4.3 EIS

PGE were polished, sonicated then dried with argon. Immersion in a piranha bath for 15 minutes followed. Gold surfaces were then activated in 0.1 M H_2SO_4 and characterisation of clean electrodes was performed in 5 mM $[Fe(CN)_6]^{3-/4-}$ in 10 mM PBS. EIS was then measured before LSV. 3 SWV were ran for one series of replicates. Another EIS assessment with identical parameters was undertaken last to assess the impact of polymerisation of actinorhodin and actinorhodin-free samples (Figure 3.48).

From the OCP difference after LSV and SWV, it could be inferred that the polymerised film is electroactive, especially at higher actinorhodin concentrations (Figure 3.46). The blank, meaning the actinorhodin-free solution, was equivalent to the highest actinorhodin sample dilution. Providing a blank equivalent corresponding to each sample dilution could be more accurate in providing a detection threshold. Running SWV measurements in series following the LSV therefore amplified OCP differences and probably impacted the nature of the compounds aggregated close to the electrode surface.
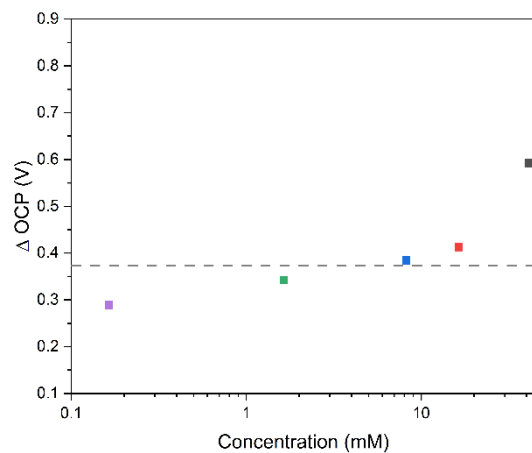
Figure 3.46. OCP difference measured post LSV in relation to actinorhodin concentration. The blank sample is represented by the dashed line and each data point is the average of 3 replicates.

Across concentrations, the general trend observed for impedance was a decrease following LSV and SWV. R_{ct} variability resulting from bare electrodes decreased after the voltammetric treatment. Sensible circuit fitting from Nyquist plots negatively impacted the accuracy of the fit for the constant phase element. The

decline in both R_{ct} and Q built on to the possibility of an electroactive rather than fully insulating film formed at the electrode surface (Figure 3.48). Electrochemical activity observed in the SWV from Figure 3.44 did not allow to specifically assign the compound adsorption to a specific compound or group of compounds as most peaks recorded in actinorhodin samples were present in the actinorhodin-free samples, even if at lower amplitudes. The peak at 0.8 V was solely evidenced in the first SWV when present, testifying of the changing nature of the obtained samples ().
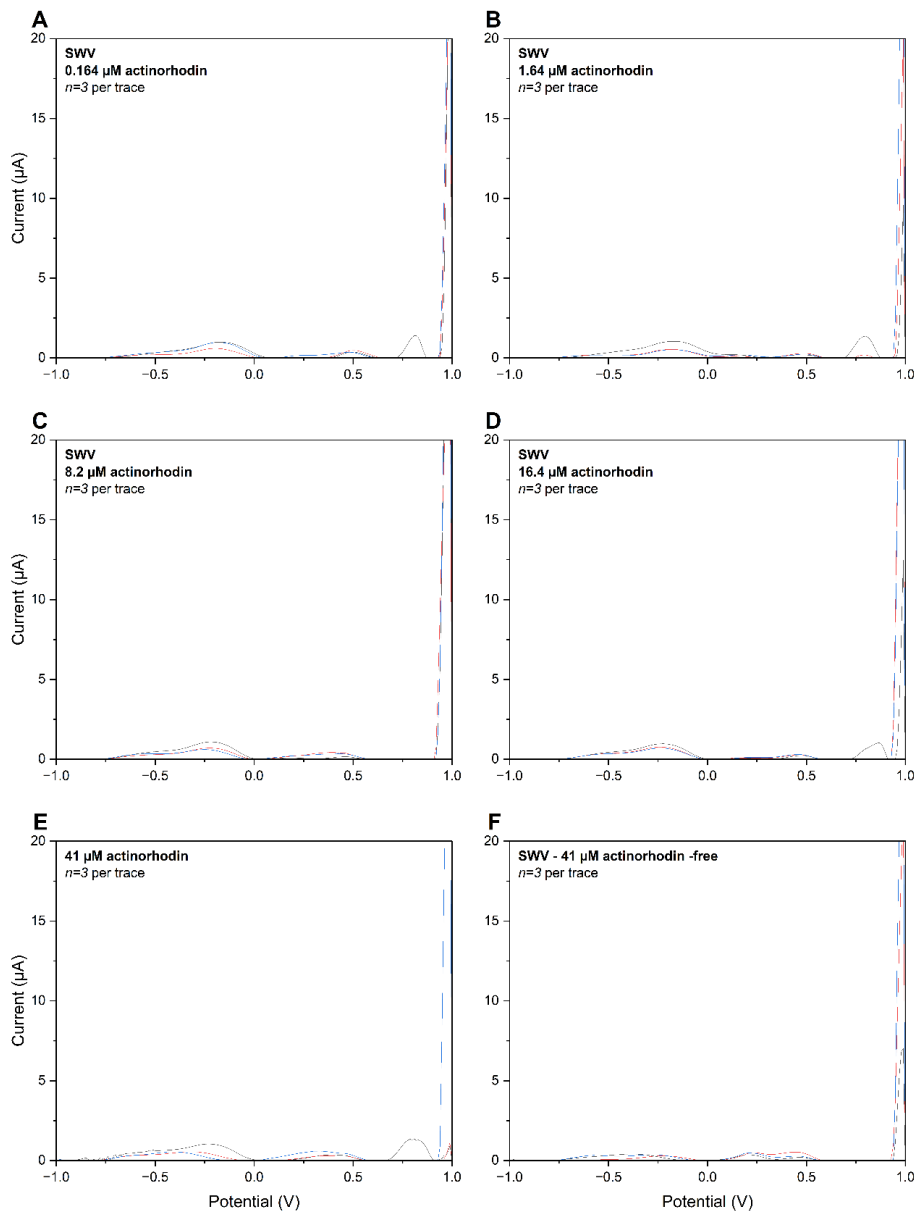
Figure 3.47. Sequential SWV measurements after LSV in increasingly concentrated actinorhodin and actinorhodin-free samples: 0.164 (A), 1.64 (B), 8.2 (C), 16.4 (D), 41 µM (E) actinorhodin samples and 41 µM actinorhodin-free sample.
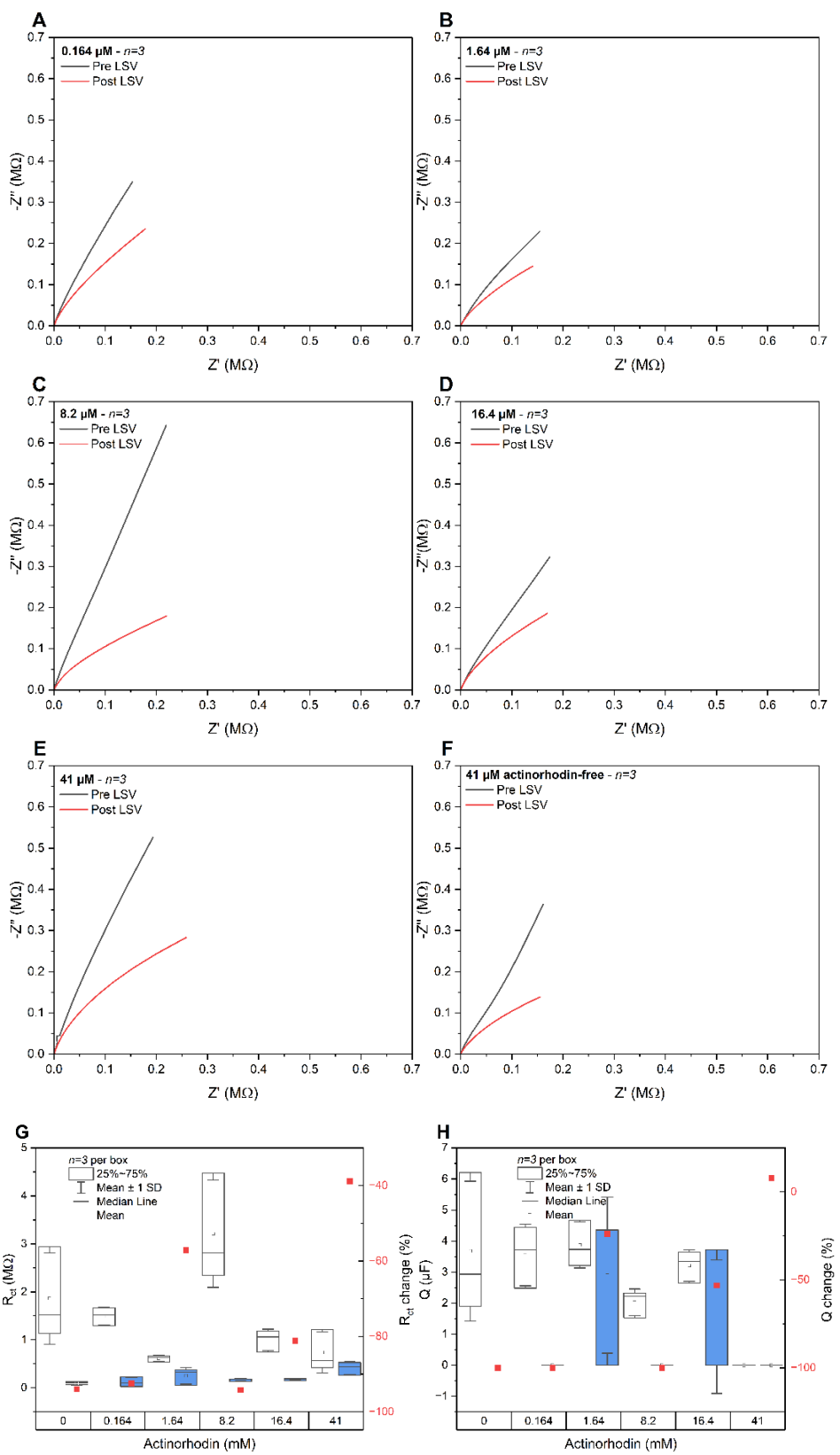
Figure 3.48. Nyquist plots of PGE before and after running LSV and SWV measurements in 0.164 (A), 1.64 (B), 8.2 (C), 16.4 (D), 41 μM (E) actinorhodin samples and 41 μM actinorhodin-free sample. R_{ct} values and corresponding changes (G) and Q values and associated changes (H) for a simplified (before) and modified (after LSV) Randles' circuit fit.

EIS was also used to assess the impact of hyperspectral imaging (HSI) measurements detailed in Chapter 3 Appendices (A. IV). HSI was used more extensively as part of Chapter 6 and scoping experiments were undertaken here applied to actinorhodin compounds. As the OCP difference observed was not null, this showed that the actinorhodin sample was not stable during the HIS measurement. This could result from the HSI setup but also from the sample instability as well.

To the best of our knowledge, electrochemical characterisation of actinorhodin has not been reported previously. Redox behaviour along with liquid chromatography of a close compound, Frenolicin B, has been reported by Mazur and Harron (1995). Contrarily to the sample used here, they extracted the compound to obtain a standard, dissolved in a medium polarity anhydrous solvent. Moreover, electrode modification using zinc chloride was needed due to loss of sensitivity. The preparation of the zinc chloride electrodes required to apply a -1.0 V potential for up to 8 hours to enable Frenolicin B reduction at lower potentials. This could irreversibly damage gold and carbon electrodes. Moreover, these electrodes required the removal of oxygen.[360] As sample preparation for biosensing purposes is ideally absent or minimised, review of the literature for existing methods has been conducted next with reassessment of extracts electrochemically as well as with mass spectrometry.

3.4.2 Analysis of extracted samples

3.4.2.1 Choice of extraction method

Liquid-liquid extraction was conducted as a desalting method prior analysis of extracts with mass spectrometry since non-volatile salts can damage the equipment and hinder signals[369]. Desalting based on filtration was not conducted as molecular weight cut-offs commercially available were not low enough to separate salts and compounds below 1 kDa.

From the various actinorhodin extraction methods reported (Table 3.6), the use of organic solvents was favoured along with minimal sample processing.

Table 3.6. Non-exhaustive reports of actinorhodin extraction from bacterial culture.

Solvent	Steps	Ref.
H₂O with NaOH	–	300,318,319,328,329,331,333,334,341,356
H₂O with NaOH & HCl	-	327,345
H₂O with KOH	-	335,336,339,343,347,370,371
H₂O with HCl & CH₃OH/CHCl₃	7	372
	3	354
Miscellaneous	>10	334,342,373
	5 (most efficient extraction)	355

The chosen procedure followed van Dissel and van Wezel (2018)[354] method using chloroform, also used elsewhere or ethyl acetate in acidic or neutral conditions, taking advantage of the pH-responsiveness feature of actinorhodin (Figure 3.49).[294,325,353] Based on immiscibility of two solvents, salts soluble in the aqueous phase would be separated from specialised metabolites in the organic phase. Reported solvent polarity being 10.2 for water, 4.4 for ethyl acetate and 4.1 for chloroform, layer differentiation as well as compound extraction was more efficient with chloroform than ethyl acetate.[374]
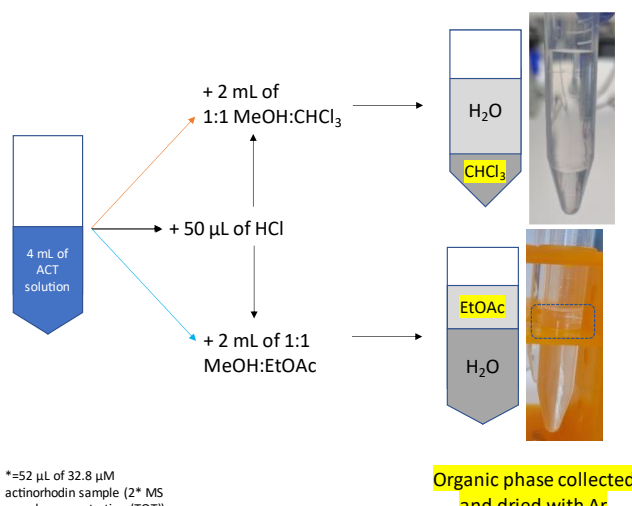
Figure 3.49. Liquid-liquid extraction conditions and obtained samples.

3.4.2.2 Mass Spectrometry analysis of extracted actinorhodin samples

Extracts obtained via the protocol presented in Figure 3.49 were also analysed with mass spectrometry. Results for the more basic samples extracted in chloroform were presented in this section. Results for the chloroform extracts in acidic conditions and ethyl acetate extracts are gathered in Chapter 3 Appendices (A. VI).

The chloroform extract in more basic conditions depicted in Figure 3.50, displayed little compounds in terms of either ion count or UV signal before 5 min and after 8.5 min. Peaks between 5 and 6 min were not as intense as in the acidic conditions but a major compound at 6.1 min ionised in the negative mode and other main ions at 11.8 min in the positive mode. The chloroform extract in acidic conditions presented in Figure A.18 in Chapter 3 Appendices, showed a compound absorbing at 254 nm at 4.5 min not evidenced before as well as an interesting region between 5 and 6 min, strongly ionising in the positive mode. When a few compounds might be detected at 4 min with the ammonium acetate method, the formic acid protocol enabled higher intensity of more than two (Figure A.19 in Chapter 3 Appendices). The intensity of the peaks eluting in the gradient was not as pronounced for the more basic compared to acidic conditions based on signal order of magnitude. Testing solvent additives enabling ionisation mainly in the negative mode could improve detection and identification of compounds not detected in the positive mode. Compounds inferred from this extract were gathered in Table 3.7 and corresponding mass spectra reported in Figure 3.51 and Figure 3.52.
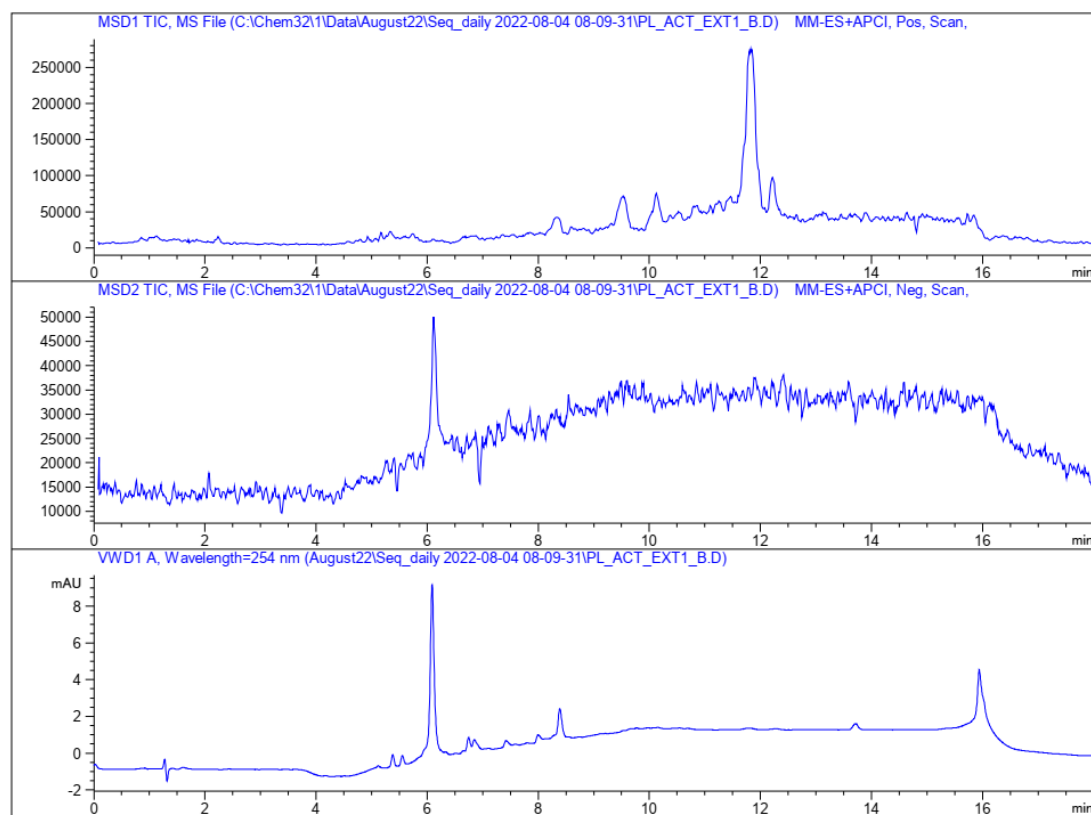
Figure 3.50. Total ion count (TIC) chromatogram in positive and negative ionisation modes of the chloroform extract of the total actinorhodin sample (respectively top and middle) and UV chromatogram at 254 nm (bottom) with ammonium acetate as a solvent additive.

Table 3.7. Possible compound identification from the chloroform extract of the total actinorhodin sample with ammonium acetate (AA) as a solvent additive.

Rt (min)	Sample	Method	Ion	Compound
6.1	EXT1_B	AA	$[M+ACN+Na]^-$	Actinorhodinic acid
8.3	EXT1_B	AA	$[M+NH_4]^+$ $[M+ACN+Na]^+$	Actinorhodin
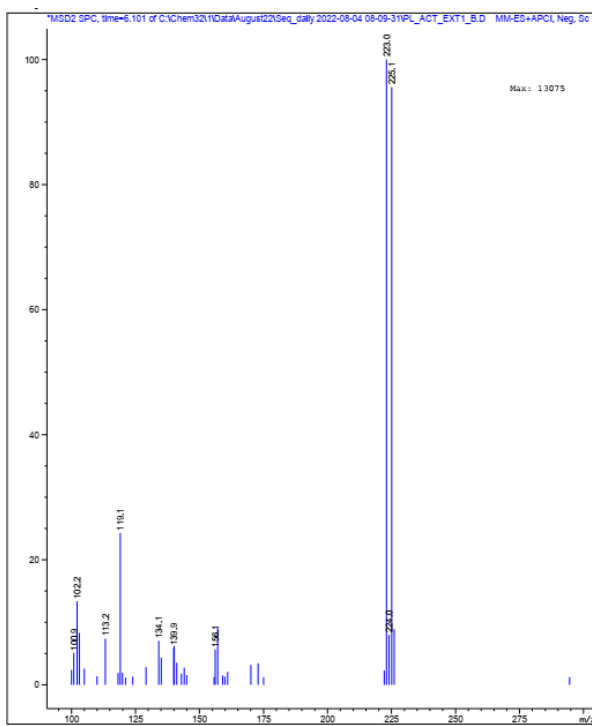
Figure 3.51. Mass spectrum of actinorhodinic acid at 6.1 min in the total actinorhodin sample using ammonium acetate as a solvent additive.
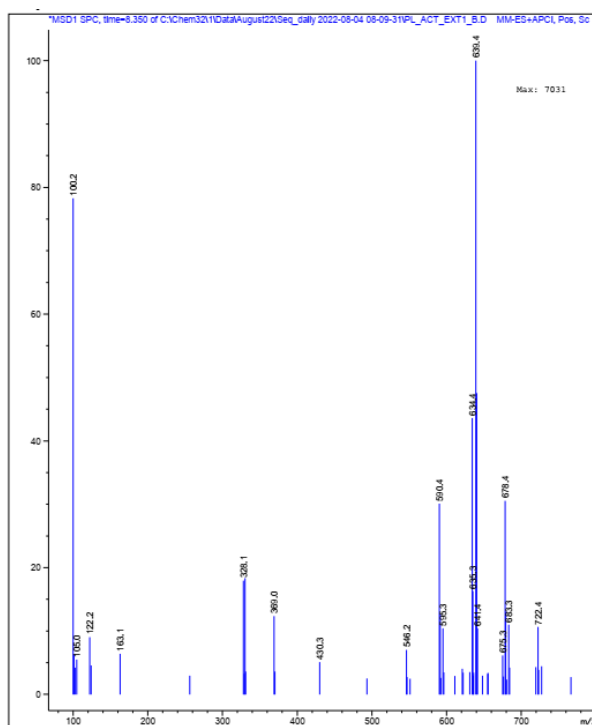
Figure 3.52. Mass spectrum of actinorhodin at 8.3 min in the total actinorhodin sample using ammonium acetate as a solvent additive.

The ethyl acetate extracts in acidic and basic conditions respectively presented in Figure A.20 and Figure A.21 both in Chapter 3 Appendices, showed a similar profile

in the solvent gradient region. None of the major compounds observed in the chloroform extract in more basic conditions (Figure A.19) with higher intensity were clearly evidenced in the corresponding ethyl acetate extract (Figure A.21). Using ethyl acetate compared to chloroform yielded more ionisation in the non-polar step of the method (Figure 3.50 and Figure A.20) whereas the more polar compounds eluted between 4 and 6.5 min were more efficiently extracted with chloroform (Figure A.18, Figure A.19 in Chapter 3 Appendices and Figure 3.50).

Possibly, the actinorhodin-compounds could have interacted with the mobile phase or volatile salts for instance and underwent modifications before reaching the MS detector. Compounds evaluated in the MS and electrochemically might differ.

Extracts from the solvent partitioning process were subjected to a standard MS method that could have been further refined. Optimised compound separation and purification using HPLC along with further analysis via NMR, MS and IR of pure isolated compounds and comparison with actinorhodin-free samples are the logical next steps to enable compound identification, characterisation and electrochemical peak attribution from pure solutions. Next, assessing the behaviour of pure and mixed solutions could provide an understanding of the polymerisation process observed upon electrochemical interrogation.

3.4.2.3 Electrochemical characterisation of chloroform extracts

The four extracts, obtained in chloroform and ethyl acetate in acidic and neutral/basic conditions, were then diluted with either PBS or KCl as electrolytes and tested on gold and carbon SPEs. Chloroform was the reported solvent for the reported actinorhodin extraction method followed[354] and allowed for a better phase differentiation compared to ethyl acetate. Results for ethyl acetate extracts analysed in PBS are presented in Chapter 3 Appendices (A. VI).

3.4.2.4 PBS as a background electrolyte

After chloroform evaporation, extracts diluted with PBS were analysed electrochemically with CV, DPV and SWV.

Low redox activity was detected in the acidic extract on gold around 0.4 V (Figure 3.53A). Widening the potential window to [-0.8 ;0.8] V allowed to record peaks at slightly shifted potential from the electrolyte blank on gold, at -0.7, -0.5 and 0.5 V (Figure 3.53C). An oxidation peak at 0.6 V (Figure 3.53B) and a reduction peak in the -0.6 V region were recorded with the wider potential window on carbon SPEs and absent from the blank sample (Figure 3.53D).
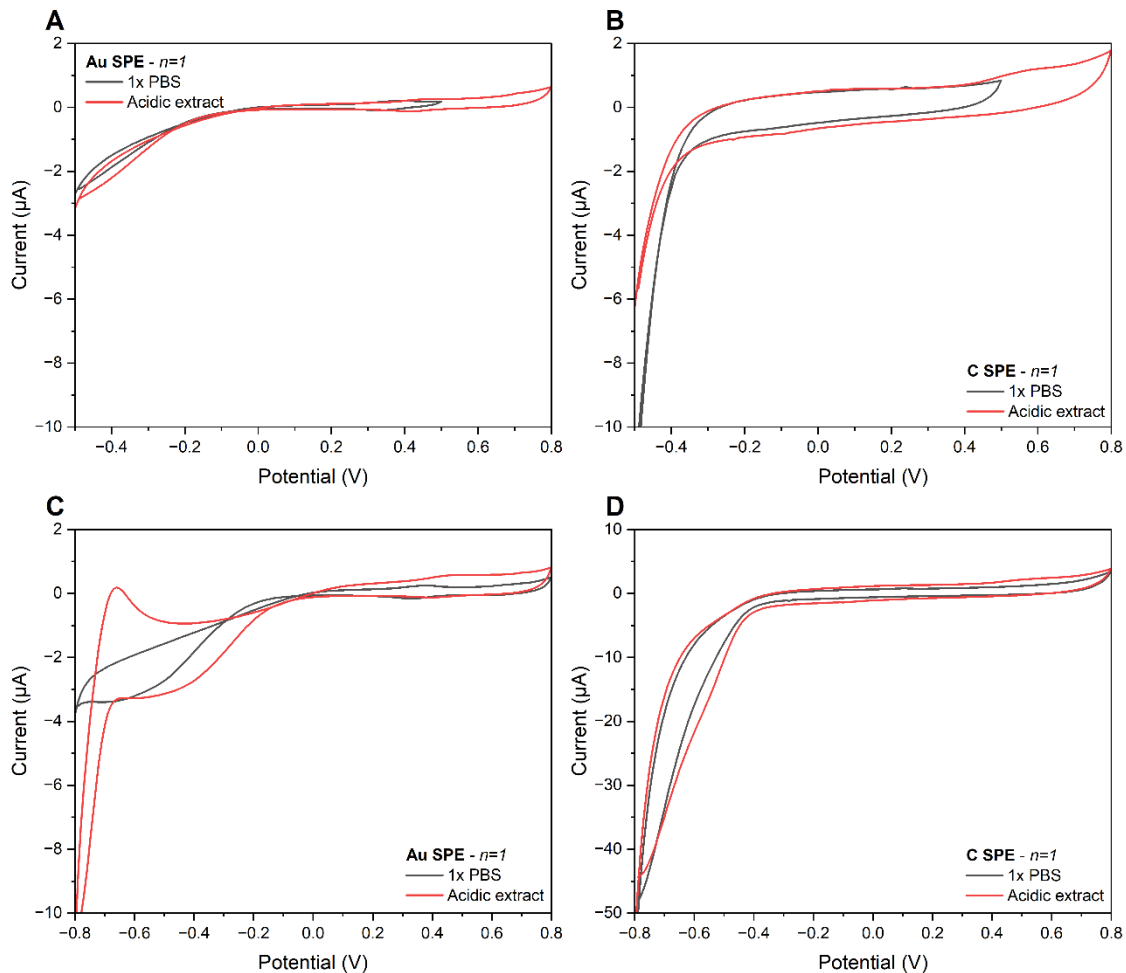
Figure 3.53. CV analysis of the acidic actinorhodin extract in 10 mM PBS on gold (A&C) and carbon (B&D) SPE respectively with [-0.5;0.8] and [-0.8;0.8] voltage windows.

Concerning DPV on gold, a slightly shifted peak compared to the blank was present at 0.4 V in both forward and backward scans (Figure 3.54A), matching up with similar events recorded with CV (Figure 3.53). On carbon, three main regions, could be defined, especially on the forward scan at around -0.4, between -0.2 and 0.2 and

close to 0.5 V (Figure 3.54B). For SWV on gold, most peak heights were recorded below PBS, maybe due to absorption of compounds on electrodes, except for the most cathodic wide peaks at - 0.7 V in the forward and backward scans. Electroactive regions were observed around -0.3 and 0.35/0.4 V in the backward scan, -0.1 broad and 0.45 V in the forward scan (Figure 3.54). SWV on carbon allowed a clearer differentiation between blank electrolyte and samples. Two main electroactive regions were noticed at - 0.45 and -0.05. A peak at 0.4 V was recorded in the more narrow potential window only on the forward scan and another peak in the - 0.7 V region on the backward scan and a wider potential window (Figure 3.54D-E).
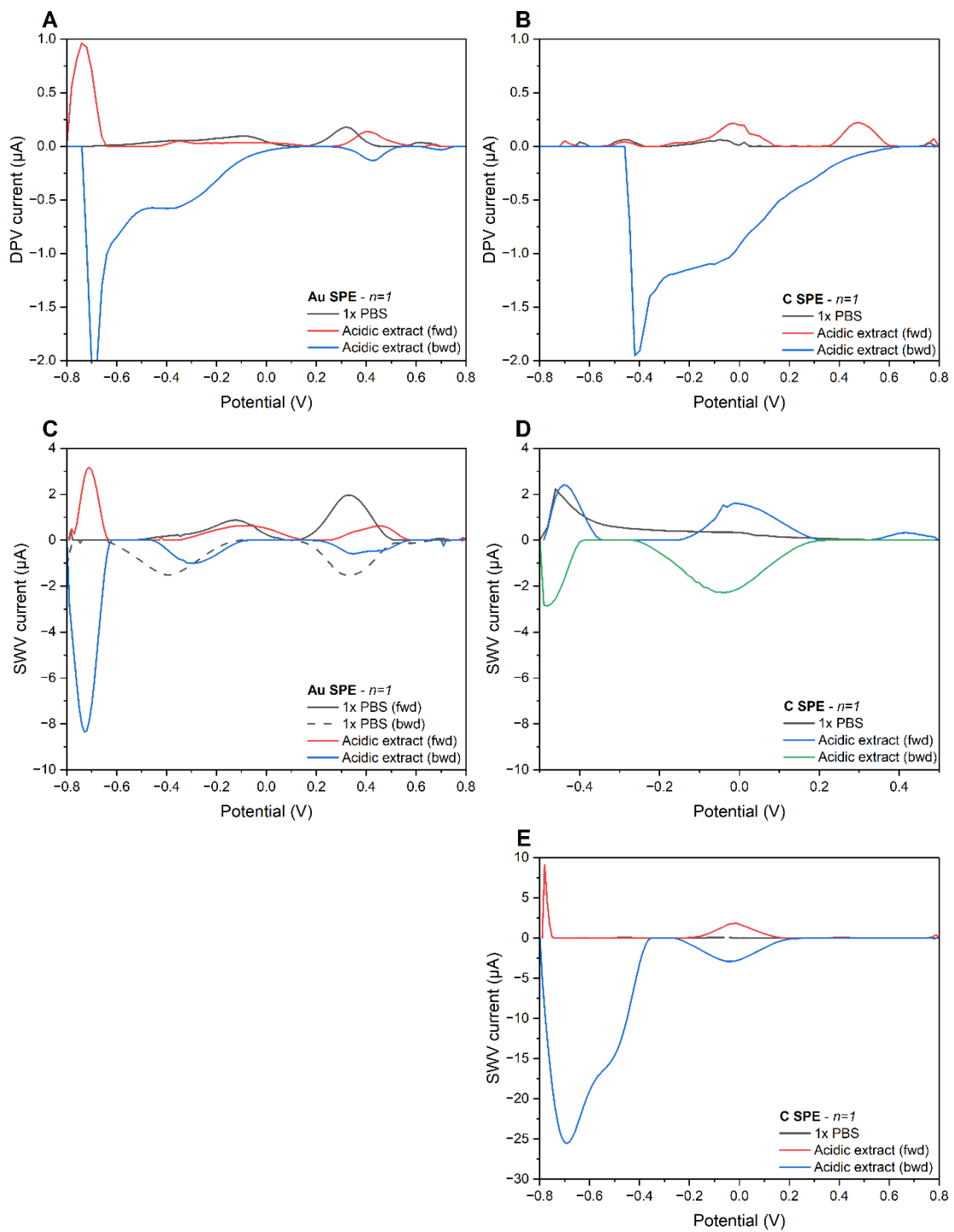
Figure 3.54. Pulse voltammetry of an acidic extract in 10 mM PBS. DPV on gold (A) and carbon (B) SPEs. SWV within [-0.5;0.5] V on carbon (D) and a wider potential window for the gold (C) and carbon SPE (E).

Moving to more basic chloroform extracts, the small oxidation peak at 0.5 V on carbon corroborated with the redox reaction observed on gold in the same region (Figure 3.55A&C). A slight shift of the oxygen reduction peak on gold in the - 0.6 V region with the same redox peaks observed in the sample and blank solutions were

detected (Figure 3.55B). These resembled the more acidic extract profiles obtained in the same solvent and electrolyte (Figure 3.53).
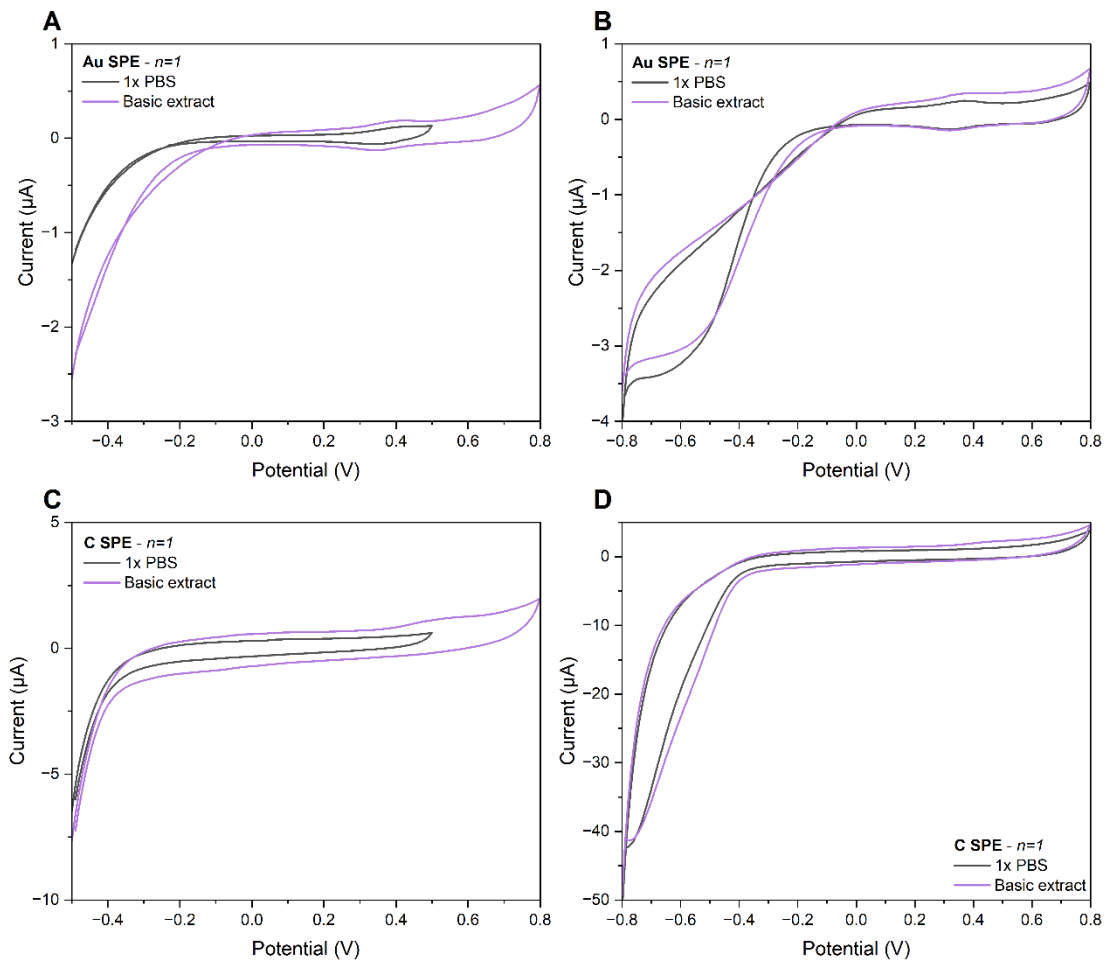
Figure 3.55. CV analysis of the basic actinorhodin extract in 10 mM PBS on gold (A&B) and carbon (C&D) SPE respectively with [-0.5;0.5] and [-0.8;0.8] voltage windows.

DPV of these chloroform more basic extracts uncovered the same redox active regions on gold and carbon SPEs. The backward scan on gold showed a corresponding reduction peak to 3 out of four oxidation peaks observed (Figure 3.56A). This was true for analysis on carbon electrodes except for the most anodic peak at 0.4 V (Figure 3.56B). Similar profiles were recorded on gold for the SWV regardless of the potential window (Figure 3.56C-E), with lower compound differentiation compared to the DPV which could be the result of the order in which measurements were taken either altering compounds close to the electrode surface, favouring adsorption or requiring more optimisation of the SWV parameters. Regarding SWV on carbon SPEs, three main compounds were identified at first, matching DPV observations (Figure 3.56B-

D), the more anodic peak absent from the wider potential window SWV (Figure 3.56F) and the backward scan of the more narrow potential window (Figure 3.56D), which correlated to observations made for the more acidic extract in Figure 3.54.
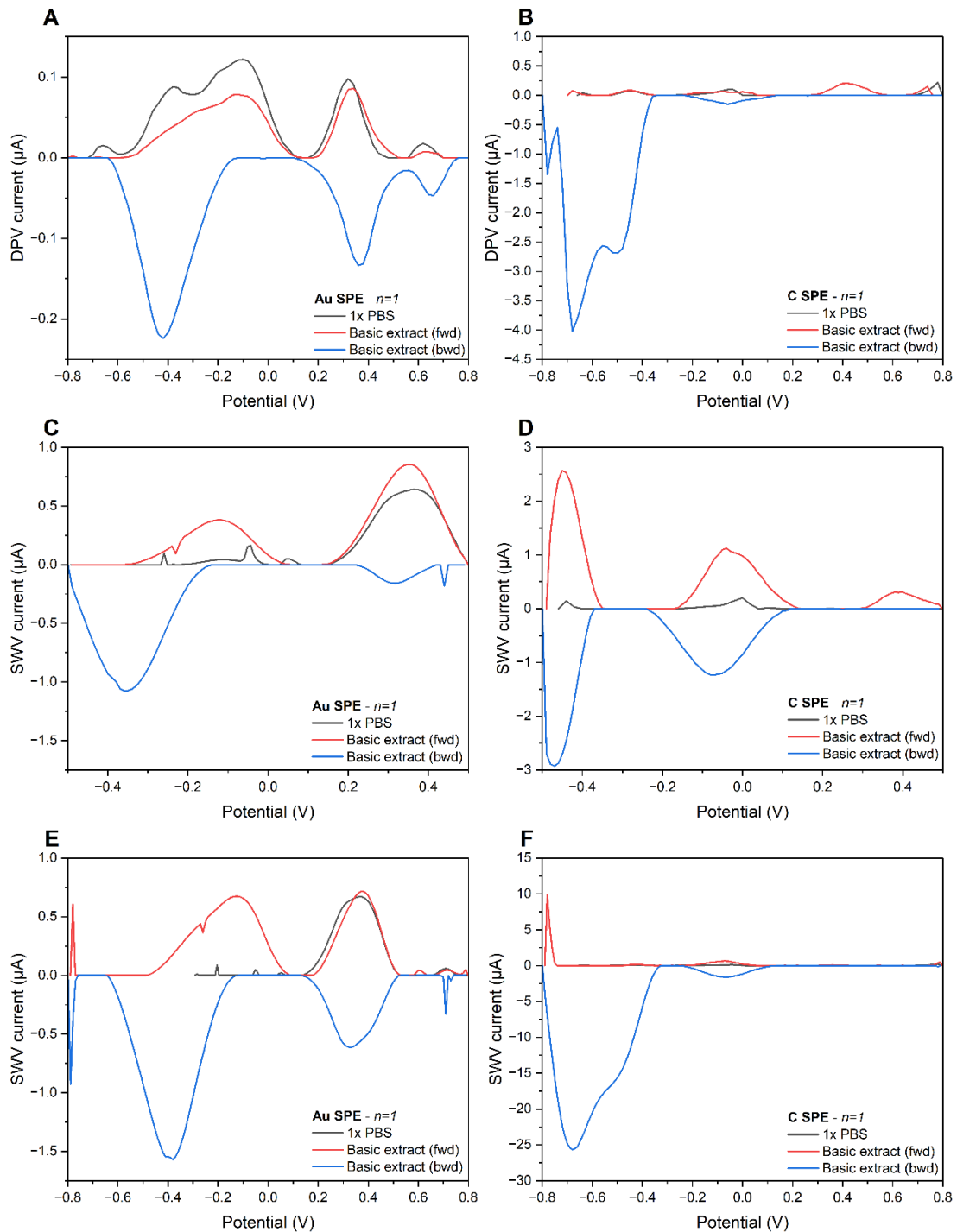
Figure 3.56. Pulse voltammetry of a basic extract in 10 mM PBS. DPV on gold (A) and carbon (B) SPEs. SWV within [-0.5;0.5] V on gold and carbon SPEs (C&D) and a wider potential window for each electrode material respectively (E&F).

The peak detection summary presented in Table 3.8 highlights the complexity of the mixture analysed in this section, given the diversity of peaks detected from extracts compared to the whole sample (Table 3.3, Table 3.4 and Table 3.5). They could be related to single unique compounds or multiple oxidised and reduced forms of a more limited amount of molecules.

Table 3.8. Actinorhodin extracted samples on gold and carbon SPE in PBS. Peak potentials included show higher amplitude currents than at least the first electrolyte blank solution tested. Highlights indicate peaks detected on the same electrode material with the same electrolyte in the whole sample. Fwd = forward scan from negative to positive potentials and bwd = backward scan from positive to negative potentials.

Potential region (V)	pH		Electrode material		Measurement			Fig.
	<7	>7	Au	C	CV	DPV	SWV	
-0.6	√		√		√			Figure 3.53
-0.5	√			√			√ (bwd)	Figure 3.54
		√		√		√ (bwd)		Figure 3.56
-0.45	√			√		√ (fwd)	√ (fwd)	Figure 3.54
		√		√		√(fwd)	√ (fwd&bwd)	Figure 3.56
-0.4	√		√			√ (bwd)	√ (fwd)	Figure 3.54
				√		√ (bwd)	√ (bwd)	Figure 3.54
		√	√	√		√ (bwd)		Figure 3.56
-0.35		√	√				√ (bwd)	Figure 3.56
-0.3			√				√(bwd)	Figure 3.54
	√			√		√ (fwd)		
-0.1	√		√				√	Figure 3.54
	√			√		√ (bwd)		Figure 3.56
		√	√	√		√ (fwd	√(fwd)	
-0.05	√			√		√ (fwd)	√ (fwd&bwd)	Figure 3.54
		√		√			√ (fwd&bwd)	Figure 3.56
0.3		√	√		√	√ (fwd)	√ (bwd)	Figure 3.55& Figure 3.56
0.35	√		√				√ (bwd)	Figure 3.54

		√	√		√	√ (bwd)	√ (fwd)	Figure 3.55 & Figure 3.56

0.4	√					√ (fwd&bwd)	√ (fwd) √ (fwd) √ (fwd)	Figure 3.54 Figure 3.55 Figure 3.56
			√	√				
		√	√	√	√	√(fwd)		
0.5	√			√		√ (fwd)		Figure 3.54
0.6		√	√			√ (bwd)	√ (fwd)	Figure 3.56

3.4.2.5 KCl as a background electrolyte

Using KCl as a background electrolyte, a reduction peak at -0.2 V was observed on gold using a mostly negative potential window (Figure 3.57) with cyclic voltammetry of acidic extracts. For more basic extracts, redox events at 0.6 and 0.7 V on gold electrodes are the most notable characteristic signals detected (Figure 3.58).
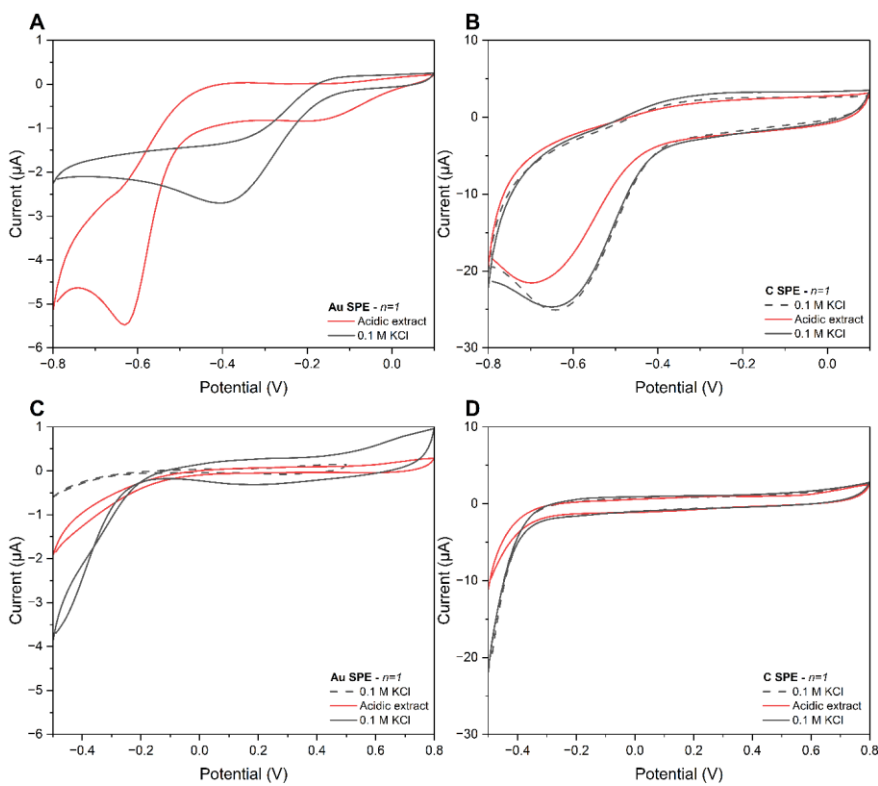
Figure 3.57. CV analysis of the chloroform acidic actinorhodin extract in 0.1 M KCl on gold (A&C) and carbon (B&D) SPE respectively with [-0.8;0.1] and [-0.5;0.8] voltage windows.
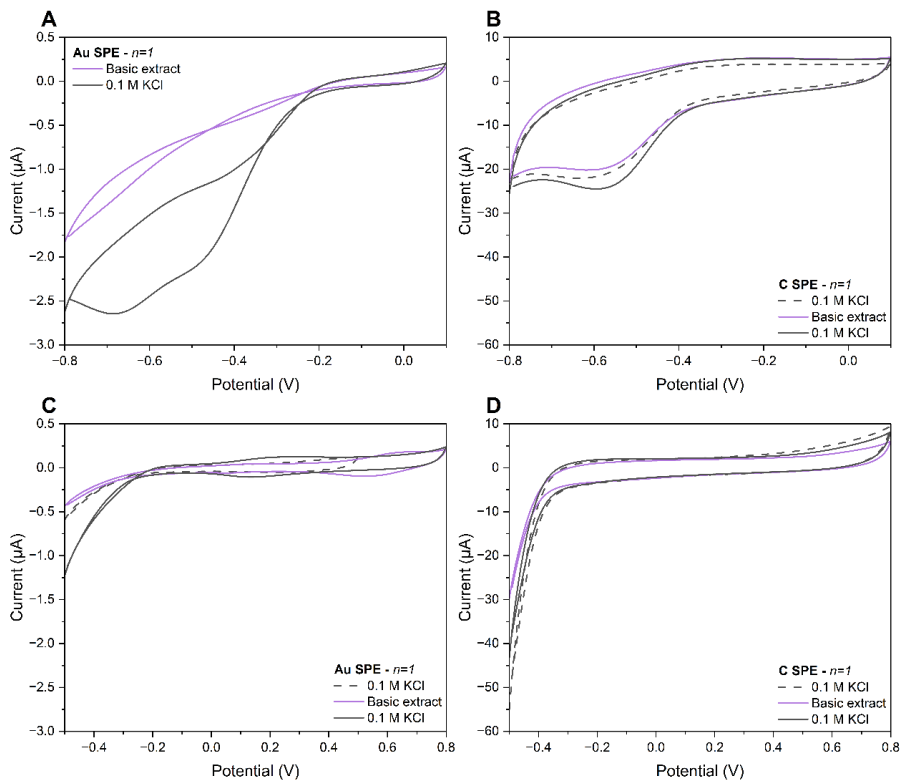
Figure 3.58. CV analysis of the chloroform basic actinorhodin extract in 0.1 M KCl on gold (A&C) and carbon (B&D) SPE respectively with [-0.8;0.1] and [-0.5;0.5] voltage windows.

A major asymmetric peak between -0.3/-0.2 and 0.4 V was displayed on the acidic extract DPV and SWV profiles on carbon SPE, unlikely to be the result of only a single compound (Figure 3.59). The basic extract on the same electrodes showed initially two peaks in the negative potential region, with only the least anodic one remaining when scanning more positive potentials (Figure 3.60B-D). DPV of acidic extracts on gold SPEs uncovered at least 6 peaks, of which SWV displayed three (Figure 3.60A-C). DPV of more basic extracts on gold was characterised by two major peaks and a minor one, also found in the SWV profile from negative to positive potentials. Moreover, the peak at 0.15 V seemed to reversibly oxidise and reduce (Figure 3.60A-C).
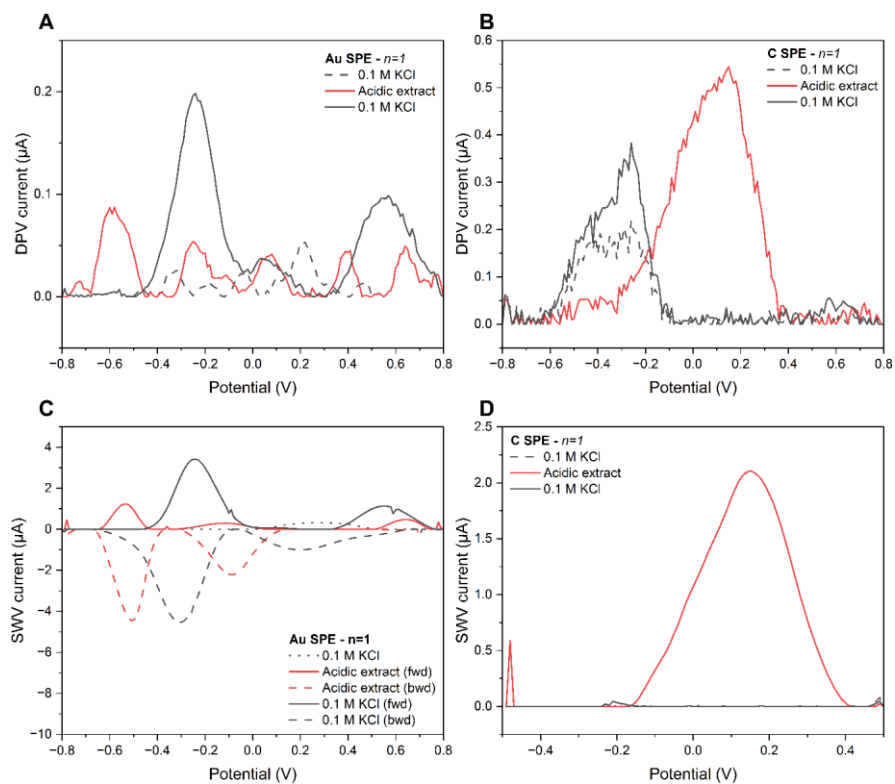
Figure 3.59. Pulse voltammetry of a chloroform acidic extract in 0.1 M KCl. DPV on gold (A) and carbon (B) SPEs. SWV on gold and carbon SPEs (C&D).
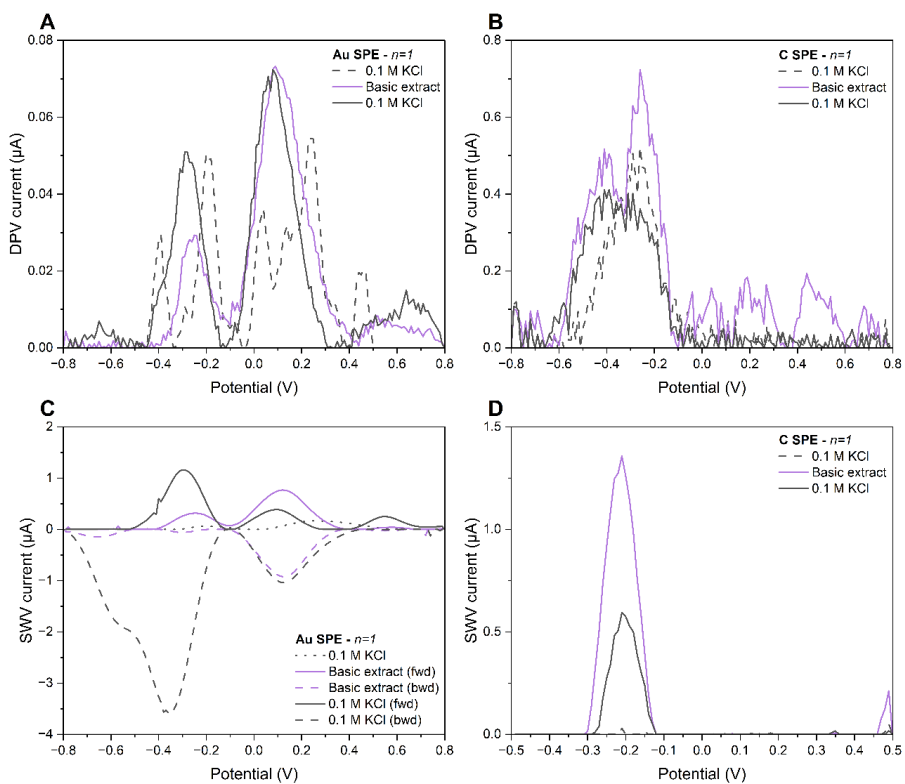
Figure 3.60. Pulse voltammetry of a chloroform basic extract in 0.1 M KCl. DPV on gold (A) and carbon (B) SPEs. SWV on gold and carbon SPEs (C&D).

A summary of peaks recorded electrochemically with signal above blanks on screen printed electrodes is presented in Table 3.9.

Table 3.9. Actinorhodin extracted samples on gold and carbon SPE in KCl. Peak potentials with higher amplitude currents than at least the first electrolyte blank solution tested. Fwd = forward scan from negative to positive potentials and bwd = backward scan from positive to negative potentials.

Potential region (V)	pH		Electrode		Measurement			Fig.
	<7	>7	Au	C	CV	DPV	SWV	
-0.5	√		√				√ (fwd&bwd)	Figure 3.59
-0.4	√		√		√			Figure 3.57
		√		√		√		Figure 3.60
-0.25	√		√			√		Figure 3.59
		√	√			√	√ (fwd)	Figure 3.60
		√		√		√		Figure 3.60
-0.2	√		√		√			Figure 3.57
		√		√	√		√	Figure 3.60
-0.1	√		√			√	√ (fwd&bwd)	Figure 3.59
-0.05		√		√		√		Figure 3.60
0.05		√	√		√			Figure 3.58
		√		√		√		Figure 3.60
0.1	√		√			√		Figure 3.59
		√	√			√	√ (fwd&bwd)	Figure 3.60
0.15		√	√		√			Figure 3.58
	√			√		√	√	Figure 3.59
0.2		√		√		√		Figure 3.60
0.25		√		√		√		Figure 3.60
0.3	√			√	√			Figure 3.57
0.45		√		√			√	Figure 3.60
0.5		√	√		√			Figure 3.58
0.6	√		√			√	√ (fwd)	Figure 3.59
0.7		√	√		√			Figure 3.58
	√		√				√ (bwd)	Figure 3.59

Using KCl as a background electrolyte also confirmed the prevalence of DPV and SWV sensitivity over CV to detect and differentiate redox-active processes from this complex mixture. Overlapping compounds with total actinorhodin samples are located between -0.4 and 0.45 V, which reflected overall sample composition more accurately than using PBS as a background electrolyte. Increasing the replicate count to verify the reproducibility of the obtained results is also crucial.

The extracts electrochemically analysed on gold and carbon SPEs were 10 times more concentrated than the samples analysed by MS. It would have maybe been more accurate to directly test the extracts in the solvents they were obtained and adjust the required electrolyte. Indeed, similarities observed between acidic and more basic extracts could stem from the electrolyte and solvent they were tested in rather than the method the compounds were extracted with. Certain compounds preferring an organic solvent might not be as soluble in an aqueous phase.

Extracting the actinorhodin-free samples with the same procedures could also have enabled peak assignment to actinorhodin-like compounds electrochemically and would be next to conduct.

3.4.2.6 Suggestions for electrochemical peak assignment

Gathering electrochemical data and mass spectrometry data, inferences could be made for the possible nature of recorded peaks. First, the nature of compounds found in MS was summarised (Table 3.10).

Table 3.10. Summary of possible compound identification from mass spectrometry data obtained for actinorhodin samples and chloroform and ethyl acetate extracts of the actinorhodin samples using acidic and more basic environments.

Rt (min)	Sample			Solvent additive		Possible compound			
	TOT	CHL	EtOAc	AA	FA	Act.	α-act.	β-act.	Act. acid
4.1/10.6	√				√				√
4.4	√				√			√	
6.1		√		√					√
8.3		√		√		√			
5.5		√ (acidic)		√			√		
5.6		√ (acidic)		√		√			
7.0		√ (acidic)		√				√	
9.5		√ (acidic)		√					√
4.2		√			√			√	
4.655		√			√		√		
9.4		√			√				√
5.5			√ (acidic)	√					√
6.9			√ (acidic)	√				√	
8.3			√ (acidic)	√		√			
5.5/8.3			√		√	√			
6.9			√		√			√	
9.5			√		√				√

Peak potential regions common to total and extracted samples recorded on SPEs were then gathered in Table 3.11 and could potentially be attributed to actinorhodinic acid and/or β-actinorhodin since those two compounds are found in acidic and more basic extracts both in chloroform and ethyl acetate (Table 3.10). However, these would need confirmation of their absence in an actinorhodin-free sample using MS. Moreover, α-actinorhodin was not found in the total sample using

formic acid as the solvent additive but in all extracted conditions. Based on the MS analysis, actinorhodin was found in both chloroform extracts but not when using ethyl acetate. The number of peaks detected in chloroform but not in ethyl acetate extracts is very limited and considering the approximation from samples being a mixture rather than pure solutions, no definite inference can be made as to which potential region actinorhodin could be detected at for this specific electrode format using these parameters for electrochemical measurements performed. A more exhaustive dataset could have enabled a more certain peak assignment. Nevertheless, sample purification, compound isolation and characterisation still remain the only absolute certainty to attribute specific peaks to compounds.

Table 3.11. Summary of peaks detected electrochemically common to actinorhodin samples and actinorhodin extracted fractions tested on gold and carbon SPEs.

Potential region (V)	Sample		pH		Electrolyte		Electrode	
	CHL	EtOAc	<7	>7	KCl	PBS	Au	C
-0.4			√			√	√	
	√			√	√			
	√							√
		√	√			√		√
		√		√		√	√	
-0.2	√		√		√		√	
-0.1	√			√		√	√	
	√		√		√		√	√
		√		√		√	√	
0.1	√		√		√		√	
	√			√	√		√	
0.3				√	√		√	
	√	√	√			√	√	
		√		√		√	√	
0.45	√			√	√			√

Findings from this chapter are summarised in Figure 3.61.

Actinorhodin sample

- Concentration of actinorhodins determined using A_{633}
- Using MS, evidence of a complex mixture resulting from the bacterial culture
- Electrochemical screening of the actinorhodin sample:

 -Inconsistency in the peaks detected on a single electrode format/material and across the range tested

 -Adsorption/polymerisation observed on gold mostly

Actinorhodin extract obtained with chloroform or ethyl acetate

- Detection of actinorhodinic acid and actinorhodin compounds with one lactone group, possibly deriving from the degradation of lactone-possessing actinorhodins

- Purity and consistency not sufficient to assign electrochemical peaks

Purification and isolation of compounds from the bacterial sample necessary to enable MS characterisation and identification as well as electrochemical characterisation

- MS method to be optimised taking account of pH conditions for more suitable ionisation and better separation
- Electrochemical scan rate study to determine if the detection is adsorption controlled and using organic solvents
- Degradation/stability assessment of actinorhodins for appropriate storage/assessment

Figure 3.61. Chapter 3 findings with next steps in the dashed box.

3.5 Discussion

The motivation behind attempting to electrochemically characterise actinorhodin stemmed from its possible mechanism of action based on redox activity, the presence of quinone moieties, well-studied electrochemically and responsible for the activity of several commercialised drugs and the monitoring of secondary metabolite production for a heterologous antibiotic production host.

Electrochemical techniques tested here used standard voltammetric parameters to analyse actinorhodin samples. Compound detection might have benefitted from a more specific fine-tuning and carrying on further experiments using optimised values, taking the example of scan rate in cyclic voltammetry (Figure 3.31) to identify the presence of an adsorption- or diffusion-controlled electron exchange or square wave voltammetry frequencies (Figure 3.18). Further data processing with peak deconvolution using SWV could also help to distinguish signals obtained from different compounds overlapping.[375]

A key component of the electrochemical cell is the electrolyte. pH control with more adequate buffers might have provided more reproducible results (Figure 3.29 and Figure 3.32). For instance, hydrochloric acid for acidic conditions, sodium acetate for more neutral pH values and sodium hydroxide[219] in a basic environment as actinorhodin is reported as a pH-responsive compound[306] and electrochemistry of quinones is highly dependent on pH conditions. Another difficulty lied in the low number of repeats for extracted samples and reproducibility lacking between repeats even when averaged (section on Voluntary polymerisation with LSV & SWV). This was in part due to compound accumulation in the vicinity of the electrode surface and visibly coating it (Figure 3.25 and Figure 3.30). However, the scarce understanding of conditions favouring or preventing polymerisation initiation limited the number of electrode uses since evidenced current amplitude was not proportional to sample concentration anymore (Figure 3.22) and the nature of peaks recorded might have resulted from the modification of compounds accumulated at the electrode surface rather than components in solution (Figure 3.31 and Figure 3.32). The use of aprotic solvents might have been beneficial to limit proton availability as quinones in aqueous

media behave in a complex manner,[362] involving 9 possible species.[351] The slow electron transfer kinetics of quinones could have benefitted from an anodic pretreatment as well.[362] Repeats for an identical sample concentration using a given electrolyte were often analysed in the same bulk solution, considering a limiting quantity of material to be tested. These would have ideally been separate preparations or at lower concentrations. That was why SPEs were chosen to analyse extracted samples, as a small sample drop of less than 100 μL is needed for analysis compared to the several mL for the macroelectrode system. Degassing solutions to avoid sample overlaps with oxygen reactive regions on the various electrode materials could be informative to perform next. Concerning electrode use and cleaning, one macroelectrode was dedicated to the same sample set, either actinorhodin or actinorhodin-free sample and tested with increasing concentrations using voltammetry, then polished and activated again before repeating the procedure again. One SPE was dedicated to each different extract in a specific electrolyte to minimise interferences due to compound aggregation/polymerisation at the electrode surface. Additionally, some quinones show little stability overlong term storage,[363] also mentioned for theta-actinorhodin.[352] This could constitute partly why electrochemical signal observed were not consistent as storage and degradation has not been carefully studied and might have been inappropriate in this study.

Challenges have also arisen when using mass spectrometry. Potentially, the compounds from both actinorhodin total and extracted samples could have interacted with the mobile phase, the volatile salts[369] or between each other, knowing the mixture to be reported as containing possibly 10 compounds,[357] and underwent modifications, as being reported as a PAINS compound.[315] Compounds detected in MS might not have been an exhaustive and accurate depiction of sample composition examined in electrochemical profiles. An optimisation of the separation method concerning gradient as well as wavelength detection could provide better peak resolution and identification. Purification and isolation of individual compounds is still necessary for accurate identification and electrochemical behaviour assessment.

Screening the literature for close compounds characterised electrochemically has returned scarce results since a spectrophotometric assessment is short, convenient and widely used (Table 3.1). As part of the actinorhodin metabolic pathway and similar to one of the actinorhodin moieties, Frenolicin B characterisation has proved challenging to by Mazur and Haroon (1995) and required zinc electrodes with modifications.[360] As dihydrokalafungin is the half moiety and is more widely available as a commercial standard, this compound might constitute a pure intermediate for electrochemical assessment.

Taking advantage of more reported bacterial mutants[353] with specific genes knocked out is another possibility for peak identification and assignment. Another possibility could be to grow intended bacterial strains directly above electrodes[376,377] and monitor electrochemical activity at key time points of actinorhodin production to avoid fouling and prevent accurate measurement from continuous electrochemical interrogation. To complement reported spectrophotometric detection (Table 3.1) and attempts at oxidation and reduction of the actinorhodin samples (Chapter 3 Appendices (A. V)), spectroelectrochemistry could also provide a direct combination of both methods to interpret observed changes.[375] For a more specific and indirect detection, actinorhodin bioorganocatalyst function[317] could be used and coupled to a horseradish peroxidase tag that would use the hydrogen peroxide generated. However, complex sample composition with direct culture measurements might require testing of individual compounds. Using its catalytic properties could be supported by the use of nanoparticles combined to a specific detection scheme as Raykova *et al.* (2023).[378] Taking advantage of actinorhodin pH-responsiveness could also bring more light into observed changes. Ionic liquids for their high stability and high conductance as well as wide potential windows would be another avenue to explore for actinorhodin and actinorhodin-like detection.[379] Spontaneous reaction of quinones with glutathione lead to an irreversible excretion from cells,[363] which could differentiate actinorhodin and γ-actinorhodin in a solution.

Developing a biosensor for a specific target is generally undertaken by increasing the sample complexity: first characterising the specific signal obtained by

one or more set-ups for the chosen target regardless of the size from standards, either commercially available or through verified/reported methods and then rising the number of interferents/components to confirm that a specific signal (and ideally quantitative) is maintained to reflect real sample composition. From a bacterial medium perspective, the works of Oziat *et al.* using the well-characterised *P. aeruginosa* illustrates this point well.[380–382] Considering possible small molecule mixtures and differentiating close compounds, sensors in the forensic field detecting illicit substances also follow a similar scheme for increasing complexity.[383] Affinity and enzymatic bioreceptors immobilised on electrodes offer a specific detection in a complex mixture from a complex mixture with possibilities for multiple measurements in blood for glucose[384] or nasopharyngeal fluids for SARS-CoV-2[385] deployed at wider scales.

As actinorhodin's reported bioactivity did not yield any more interest in pursuing further mode of action studies or was screened at a wider scale, efforts to either synthesise it or develop a wider commercial scale production have not emerged as a priority. Since pure actinorhodin or actinorhodin-like compounds cannot be purchased, investing in the development of specific bioreceptors for any actinorhodin or actinorhodin-related molecule has not been feasible. The absence of commercially available standard, enzyme from actinorhodin's biosynthetic pathway or antibody prevented the possibility of electrode functionalisation, which would have possibly prevented biofouling and enabled a direct detection from the actinorhodin sample.

The classic pathway to purify a mixture and isolate its components using analytical chemistry involves different extraction and partitioning steps as well as further separation often using HPLC. As optimisation can be required, this process might be time-consuming depending on the nature of the molecules and their ability to be separated. Characterisation using MS and NMR adds to the skilled expertise needed. Nevertheless, obtaining pure compounds allows for wider bioactivity screening and understanding of the mode of action. depending on domains of expertise, synthesising the molecule of interest when available in the literature can

be another route. These may as well uncover new compounds with different biological activity that could be of interest for the general antibiotic discovery sphere.[386] Moreover, the impact of advances in one field of research benefit many more such as how genetics informed and allowed the modulation of antibiotic production.[387]

Consequent efforts and investments, mostly in terms of industrial and public strategies, fundings and time, are necessary. High risk and little return on investment due to low hit rates are critical reasons why industries have turned away from antibiotic discovery. Known compounds with little reported bioactivity have not been pursued further down the commercialisation route in the past lack key data, namely full chemical synthesis, a thorough understanding of the biological targets and mode of action, pharmacokinetics and pharmacodynamics to cite a few. There are available and possible prospects but they require tremendous pushes for action to only generate a few potential solutions. Actinorhodin compounds, produced by *Streptomyces coelicolor*, are a great example showing how an initially reported weak antibacterial activity slowed down research efforts towards investigating it as drug-like compounds but taking advantage of its pigmentation depending on pH-responsiveness and early knowledge and mapping of its biosynthetic gene cluster and production drove a growing understanding of antibiotic production across the bacterial kingdom but still lagging considering the actual compound themselves.

3.6 Conclusion

The chapter findings are summarised in Figure 3.61. As the electrochemical characterisation of actinorhodin and actinorhodin-like compounds had not been reported, actinorhodin and actinorhodin-free samples from bacterial culture were tested in aqueous solutions on unmodified common electrode materials (carbon, platinum and carbon) using different formats and electrolytes, namely phosphate-buffered saline and potassium chloride. Cyclic and pulsed voltammetric analyses were undertaken, with standard parameters. **The reactivity of actinorhodin and compounds alike were evidenced from assessing different scan rates and also visible polymerisation occurring at the electrode surface upon interrogation.** An attempt at understanding this dopamine-like polymerisation was conducted, assuming a specific compound might have been responsible for it. However, using linear stripping voltammetry and repeated square wave voltammetry did not result in a consistent observation of the phenomenon and neither the ability to define a threshold separating its occurrence from its absence. To benefit the parallel mass spectrometry analysis of sample and support compound identification, a simple liquid-liquid extraction procedure on actinorhodin samples was performed. **Extracted samples were then analysed electrochemically on gold and carbon screen-printed electrode formats. Based on single replicates and the available set of conditions tested, definitive electrochemical peak assignment was not possible. Nevertheless, assumptions could be made as to the potential compounds responsible for the recorded redox activity.**

Without pure compound standards and selective bioreceptors, purification of actinorhodin samples and at least main – if not all – compound isolation is necessary for further chemical and electrochemical characterisation. Sensing directly from the bacterial culture to monitor and optimise antibiotic production might be achievable without electrode modification, providing a better understanding of compound aggregation and polymerisation at the electrode surface but most likely using specific recognition of compounds of interest.

Chapter 4 Systematic development of an aptasensor to detect moxifloxacin using differential pulse voltammetry and electrochemical impedance spectroscopy

4.1 Introduction

4.1.1. Point-of-need monitoring of one of the most prescribed antibiotics: a case for the development of an electrochemical aptasensor for moxifloxacin detection

4.1.1.1. Presence of moxifloxacin residues in different sample matrices

Active pharmaceutical ingredients are emitted into the natural environment during their manufacture, use and disposal.[388] Antibiotic residues can still exert activity on surrounding microorganisms, select for and make the environment, a reservoir for antibiotic resistant bacteria.[389] Limiting antibiotic use and release is critical to decrease the risk for human exposure to AMR[389] and prevent antibiotic resistance arising faster.[390]

Fluoroquinolones are widely prescribed antibiotics due to their spectrum of activity, good tolerance and pharmacokinetic profile in humans[391] but also as infection prevention added to livestock feed.[392] Since they are not fully metabolised by either human or animal bodies, fluoroquinolones are excreted into the environment. They are poorly biodegradable and can transfer from soil to plants where they are stored. Consumed in food, they present toxic side effects[393] such as bacterial infections and gastrointestinal inflammation.[394]

Moxifloxacin is a fourth generation fluoroquinolone and one of the most prescribed antibiotics globally.[391] Moxifloxacin is used to treat sinus and lung infections caused by Gram-positive and Gram-negative bacteria and cases of bacterial conjunctivitis.[395] Moxifloxacin is also used as a second-line treatment for resistant tuberculosis (TB)[396] and listed on the World Health Organisation (WHO) Essential Medicines List 2023 for this specific use. As part of the Watch category, moxifloxacin presents higher potential for resistance, and should be a key targets of stewardship

and monitoring initiatives.[397] In 2019 alone, 10 million people were newly diagnosed with TB, of which 330 000 were resistant to first-line antibiotics.[396] Additionally, over 17% of existing cases in 2019 developed resistance,[396] relying on limited treatment options such as moxifloxacin. When taken orally or intravenously, almost half of the moxifloxacin dose is excreted unchanged,[395] given that antibiotic regimens to treat tuberculosis can last from 6 to 18 months and strict adherence is essential.[398] There is a need to measure moxifloxacin blood levels to monitor response to therapy in TB patients.

Involuntary exposure to undetected moxifloxacin likely fuels resistance to a much-needed treatment. In addition, China and India report the highest global incidence of resistant tuberculosis.[397] These regions of the world concentrate a major part of the world's active pharmaceutical ingredient production[399,400] where little regulation is in place for pharmaceutical industry waste disposal with a lack of wastewater treatment facilities. Wilkinson *et al.* (2022) reported a correlation between the most contaminated sites in terms of antibiotic levels with areas with poor wastewater and waste management infrastructure, and pharmaceutical manufacturing.[388] This emphasises the need to monitor antibiotic residues in complex samples to mitigate exposure, antibiotic resistance emergence and increase. Additionally, there is no standardised experimental approach in place to determine selective concentrations of antimicrobials and dose response correlations linking exposure to antibiotic resistant bacteria with negative health consequences.[401] More reports in that sense would support decision-making in regulation and antibiotic resistance mitigation measures.[389]

4.1.1.2. Answering detection challenges with electrochemical biosensors for on-site monitoring

Nowadays, routine detection methods for antibiotic presence are comprised of microbiological methods, such as the disk diffusion, colorimetric method and analytical techniques. Sterility requirements as well as specialised facilities are drawbacks of microbiological methods despite low costs and colorimetric assays taking only a few hours.[402] Current analytical techniques for antibiotic detection

include capillary electrophoresis, spectroscopic, spectrometric and chromatographic methods, which require sample preparation, are costly, time-consuming and require specialist expertise for equipment operation.[392,393,403–405] Moreover, high-pressure liquid chromatography (HPLC) operation uses organic solvents, gas chromatography (GC) the ability of compounds to transform into a gaseous phase and mass spectrometry (MS), possible ionisation of studied molecules. High specificity and a time to result under an hour is counterbalanced by high costs. Hyphenated techniques combine advantages and disadvantages of individual methods. Enzyme-linked immunosorbent assay (ELISA) tests possess the high specificity of antibodies as an advantage but also have high costs and other drawbacks.[406] A variety of alternatives, including microfluidics and paper-based assays have been proposed for antibiotic detection, but none has been deployed on a wider scale. Simultaneous detection of a range of analytes is desired but commonly involves additional sample preparation, increasing analysis time and cost as well as the risk to introduce contamination or alter analyte concentration, translating into more potential diagnostic errors.[402]

Electrochemical biosensors offer a potential route towards faster on-site analysis owing to advantages such as low amount of analyte and little pre-treatment, with the ability for high sensitivity and specificity for accurate analysis.[403] Biosensors provide a low-cost platform amenable to miniaturisation and mass production. Electrochemical biosensors offer the possibility for detection even in non-transparent samples that are more challenging for optical techniques.[406,407] They can be designed for minimal impact by pH or temperature.[405] EIS is particularly suited to enable low mass molecule,[408] such as antibiotics, or ion detection[402] with minimal sample amounts, reflect changes in self-assembled monolayers[390,409] with high sensitivity and offers the possibility of label-free recognition[410].

The variety in chemical structures of antibiotics, considering size or functional groups for instance, is a hurdle to develop simple and universal spectroscopic or electrochemical detection methods.[390] Moreover, environmental samples pose challenges in terms of the diversity of sample matrices, variations coming from

sampling locations and the presence of metabolised compounds along the original parent molecule.[411] Fluoroquinolones have only been focused on in the last decade for electrochemical detection (Table 4.1).

Unmodified electrodes can detect fluoroquinolones. However, complex samples analysed at the point of need require higher selectivity, rendered possible and consistent by catalytic or affinity bioreceptors.[392] The widespread use of antibodies has not resulted in a wide deployment of more point-of-care platforms due to their shortcomings.[412] Thanks to the variety in functionalisation strategies and the intrinsic advantages from electrochemical sensors, aptasensors offer adequate features to adapt to antibiotic variety and combine high specificity with low costs, detection under an hour and the use of antifouling strategies to minimise interferences.[406]

Table 4.1. Electrochemical detection strategies reported for fluoroquinolones.[392]

Method	LoD	Detection range	Advantages	Disadvantages
Direct detection at Hg electrodes	pM /nM	pM-μM	High sensitivity, low limits of detection when used in a stripping mode, renewable surface, resistance to fouling.	Toxicity of the transducing element (Hg), limited portability of the sensing infrastructure.
Direct detection at carbon-based electrodes	nM /μM	nM-μM	Simple and redox based read-out, no modification, low-cost sensing solutions (screen printing).	Limited selectivity, susceptible to fouling.

Method	LoD	Detection range	Advantages	Disadvantages
Electrodes modified with nano-, carbon-based and polymeric materials	pM	pM-μM	Improved sensitivity compared to non-modified electrodes, higher selectivity, variety in developed working solutions.	Frequently subjected to overcomplicated surface engineering, elevated fabrication costs.
Electro-chemical aptasensors	pM/ nM	pM-μM	High selectivity or even specificity, simple surface decoration protocols.	Bioelements susceptible to lose function in complex environments, elevated fabrication costs.
Molecularly-imprinted polymers	fM/ pM	pM-μM	Very high selectivity or even specificity, low limits of detection	Synthetic effort, elevated fabrication costs from electrode surface modification.
Enzymatic sensing	pM/ nM	pM-μM	Very high sensitivity and selectivity, existence of signal amplification strategies.	Possible loss of function in complex environments, frequently subjected to complex decoration, elevated fabrication costs.
Ion selective electrodes	μM	μM-mM	Simple signal processing, high selectivity, detection over few orders of magnitude.	Limited number of ionophores dedicated to fluoroquinolone detection.

Method	LoD	Detection range	Advantages	Disadvantages
Electrified liquid – liquid interface	nM/μM	μM	Signal based on the simple ion transfer reaction, selectivity governed by molecular partitioning, direct insights into molecular partitioning coefficients.	Toxicity of the organic phase, limited stability of the liquid-liquid interface, requires specific instrumentation.
Complexation-based solutions	nM	nM-μM	Simple electroanalytical studies providing physicochemical insights into drug-metal ions; drug-drug and drug-DNA interactions.	Low selectivity, limited practical applicability.

4.1.2. Potential advantages associated with aptamers

4.1.2.1. Characteristics

Aptamers were first reported in the 1990s, with RNA aptamers discovered two years before DNA aptamers.[413,414] RNA sequences are mostly preferred for their ability to be expressed intracellularly while DNA aptamers are less prone to degradation.[402]

Aptamers are single strand oligonucleotides, usually 20 to 80 nucleotides long,[415] selected to bind a wide range of targets with high affinity and selectivity.[416]

Target recognition occurs through a conformational change, with a complex stability and interaction surface comparable to antibodies (≈2600 Å).[415] Depending on the recognition strategy, aptamers can permanently[402] fit or reversibly bind a given biomolecule.[412,417] Secondary structures can be predicted from aptamer sequences and determine target binding locations.[418] Geometrical complementarity allows for strong target binding and recognition usually mediated by polar, hydrogen bonding[418] or van der Waals forces[409,419]. Aptamers are designed to adopt more complex 2D and 3D structures than DNA probes, such as loops, hairpins, pseudoknots, bulges and G-quadruplexes,[402,418–420] directly translating the presence and/or quantity of an analyte.[417]

Aptamers are now utilised in a diversity of fields such as drug delivery, as a replacement for antibodies in assays,[402] separation science or a complement to antibodies, the most popular biorecognition element,[421] thanks to their small size and lower cost production, allowing for chemical modification and multi-labelling.[402,405,416,422–424] Antibodies have generated only a handful of accomplished technologies[423] due to their drawbacks (Table 4.2), which explains the ever-lasting research for adequate replacement.[424] Aptamers also play an important role in point-of-care tests as recognition elements in lateral flow assays. As artificial ligands, aptamers enable a wider range of smaller targets than their antibody counterparts such as small molecules and ions.[422] Even if the recorded affinity of aptamers developed for smaller molecules is lower than for larger proteins, this could also be due to the sensitivity of the technique used to determine the K_D and could benefit for more sensitive strategies. Their potential for simultaneous target recognition is equally appealing for complex sample analysis.[412]

Aptamers are versatile biorecognition elements for biosensor functionalisation.[416,423,424] The 5' end is often modified with a chemical group allowing immobilisation and orientation of the sequence onto the transducer while the 3' end is usually dedicated to fluorescent tags[402] or redox labelling[417]. Among many other advantages, aptamers can refold after denaturation[412,418] and offer chemical, thermal and conformational stability.[405,406,424] Where antibodies fail to maintain activity outside

of physiological environments, aptamers are not limited by these constraints[423,424] since their kinetic parameters are strictly selected to bind specifically the target of choice.[424]

Table 4.2. Comparison between aptamers and antibodies characteristics.[425] Reproduced and adapted under CC BY license with permission from Odeh, F. *et al.* Aptamers Chemistry: Chemical Modifications and Conjugation Strategies. *Molecules* 2019, *25* (1), 3.

	Aptamers	Antibodies
Synthesis	Chemically synthesised and easy to produce	High cost and complexity of production[412]
Size	Small compared to antibodies	Large
Stability	Prone to nuclease degradation	Short biological half-life
Targets	Wide range of targets, starting from ions to whole living cells	Produced only against immunogenic molecules, which limits the range of targets
Toxicity and immunogenicity	Low toxicity and non-immunogenic	Immunogenic
Binding specificity	Comparable	Comparable
Binding affinity	pM/nM	pM/nM[426]
Clearance rate	Rapid circulation clearance	Low clearance rate
Chemical conjugation	Easy to conjugate to nanoparticles and drugs	More difficult to conjugate[422]
Chemical modification	Tolerant to chemical modifications to enhance structural and functional properties	Modifications often lead to reduced activity[422]

4.1.2.2.   A synthetic production process shaping aptamer adaptability

Aptamer selection has been qualified as the "Darwinian evolution at the molecular level"[424]. Aptamer sequences with the best affinity to a chosen target are selected through SELEX, the Systematic Evolution of Ligands by Exponential enrichment. A starting pool of 10^{14} to 10^{16} of DNA or RNA oligonucleotides is placed in contact with the chosen target immobilised onto a solid matrix.[424] Separation of free oligonucleotides is undertaken by size exclusion filtration, affinity or capillary chromatography, flow cytometry or using magnetic beads. Target-sequence complexes are then dissociated and variations in ionic strength, temperature or chaotropic agents elute the aptamers.[415] Complexed oligonucleotides undergo PCR amplification.[424] The resulting multiplied double strand nucleotides are further separated into single strand ones or used as templates to be transcribed *in vitro*.[424] This enriched pool goes into the next selection cycle that operates similarly.[424] with gradual increased pressure, shorter incubation periods and more stringent conditions.[402,424] In total, 8 to 15 cycles are usually performed with the best candidates each sequenced.[424]

SELEX is a lengthy process which does not always yield successful outcomes. Shortening the process duration and increasing affinity are continuously investigated since it is considered slow, strongly biased and can be automated only to a small extent.[402] A multitude of variations of SELEX have been developed for more specific applications.[402,418,424]

Several key issues have been raised such as bias in the starting pool or structural instability resulting in conformation shift and loss of binding affinity. Higher affinity aptamers can be obtained through SELEX parameters fine-tuning. The optimisation of primary sequences and stabilisation of aptamer conformations are the main approaches to aptamer sensitivity and selectivity. Improving aptamer affinity include the optimisation of various conditions such as ionic strength and composition, pH, temperature and lifting limitation of molecular diversity in the initial library. Sequence optimisation involves determination of binding sites based on secondary structure predictions and sequence truncation.[418] Modified nucleotides to

provide hydrophobic properties or amino-acid mimicking functional groups and prevent exonuclease activity are also part of primary sequence optimisation.[418] Dimerisation of sequences has been shown to improve affinity and increase complex stability as well as the number of possible binding sites,[402,418] with multivalent interactions producing higher binding affinities than their corresponding monovalent interactions.[418]

At later clinical stages, aptamer stability is threatened by nuclease degradation especially in serum and renal filtration with an *in vivo* half-life of tens of minutes compared to several days for antibodies.[427] Overall, industrial efforts seem minimal compared to academic reports, where antibodies benefit from consequent funding.[427]

Optimised aptamers make ideal candidates for small molecule recognition,[415] due to their relatively lower size in comparison to other biorecognition elements such as antibodies or enzymes and can be the basis for a variety of strategies for sensor functionalisation.

4.2 Rationale, aims and objectives

As one of the most used antibiotics, including for the treatment of resistant tuberculosis, monitoring moxifloxacin residues from surrounding environmental samples could inform on possible involuntary exposure and increased risk to develop resistance. This could steer antibiotic treatment choices within communities to maximise chances for treatment success. Moreover, this could inform preventative measures to implement if antibiotic residue levels need to be lowered.

This study demonstrates the development and optimisation of a voltammetric and impedance-based aptasensor for moxifloxacin, functionalised with a DNA aptamer selective for this antibiotic, presenting a K_D of 325 nM.[428] The aptasensor entails a commercially protected sequence from Aptamer group, whose sequence composition, 2D or 3D structure and therefore interaction with the target has not been shared by the company. EIS was chosen for its sensitivity as it has been reported that aptamers binding small molecules were more challenging than when the specific target was a bigger molecule and DPV as a sensitive voltammetric technique to cross-check recorded EIS trends as non-specific events can overtake recorded events.

The versatility of the aptamer system would have the potential to be adapted with aptamers raised for different antibiotics, making rapid, low-cost, and convenient monitoring practices possible to avoid unnecessary exposure, inform local healthcare practices and eventually mitigate existing and emerging antibiotic resistance.

The following objectives were set:

1) Screen and select a functionalisation method, electrode format and electrochemical measurement for the optimisation of moxifloxacin recognition,
2) Fine-tune parameters involved in self-assembled monolayer (SAM) formation for an optimal moxifloxacin detection,

Obtain a quantitative estimation of moxifloxacin in a buffer and more complex environment using the optimised aptasensor.

4.3 Material & Methods

4.3.1 Electrode cleaning and characterisation

Three types of gold electrodes were employed in this chapter (Figure 4.1).
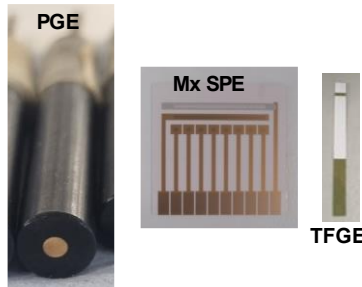
Figure 4.1 Electrode formats used in this chapter: polycrystalline gold electrodes (PGE), multiplexed gold screen-printed electrodes (Mx SPE) and thin-film gold electrodes (TFGE) from left to right.

Polycrystalline gold electrodes (PGE) with a 2 mm diameter (IJ Cambria, Llanelli, UK), were mechanically polished for two minutes with 1 µm diamond powder, sonicated for two more in deionised water then taken through a polish and sonication cycle with 0.05 µm alumina slurry. PGE were subsequently left in piranha solution (1:3 H_2O_2:H_2SO_4) for 15 minutes. After a deionised water rinse and argon dry, they were electrochemically cleaned in 0.1 M H_2SO_4 by scanning the potential between − 0.05 and 1.1 V vs. Ag/AgCl for 25 cycles. A thorough rinse with deionised water and argon drying followed. Surface cleanliness was assessed by a characterisation with EIS and DPV in 1 mM $[Fe(CN)_6]^{3-/4-}$ (10556412 and 10216460 Fisher scientific**).**

Thin Film Gold Electrodes (TFGE) (FlexMedical Solutions, Livingston, UK) performed best without any mechanical, chemical or electrochemical treatment.[429]

For both PGE and TGFE, an external Pt counter (PT.SHEET Metrohm) and Ag/AgCl reference electrodes (012167 IJ Cambria) constituted the electrochemical cell.

Multiplexed gold screen-printed electrodes (Mx SPE) were rinsed with deionised water and argon dried. Three methods were selected and compared[430] : deposition of ethanol for 30 minutes, overnight incubation in 0.1 M H_2SO_4 and potential cycling using CV in 0.1 M H_2SO_4 (400 µL to cover the electrodes in this case)

for 10 scans at 0.1 V/s. After a water rinse and argon drying, they were characterised with CV, SWV, EIS and DPV in 5 mM $[Fe(CN)_6]^{3-/4-}$, then rinsed and dried.

4.3.2 Aptamer specifications & buffer composition

Aptamer sequences were provided by Aptamer Group with specifications listed in Table 4.3.

Table 4.3. Oligonucleotide specifications.

	Support (Supp.)	Aptamer (Apt.)	Thiolated aptamer (SH-Apt.)
Modification	5'-thiol	-	5'-thiol
Length	12 bp	42 bp	42 bp
Molecular weight (g/mol)	5,432	12,904.4	13,230.8

A 5x aptamer buffer stock was prepared, further diluted with water of molecular biology grade (10505854 Fisher scientific). This buffer results from the selection process of the aptamer for moxifloxacin during SELEX but does not contain any aptamer in this case. The exact composition for a 1x preparation contains 20 mM Tris (T1503 Sigma Aldrich) pH 7.4, 100 mM NaCl (S9888 Sigma Aldrich), 5 mM KCl (A11662.0B Fisher), 2 mM $MgCl_2$ (M8266 Sigma Aldrich) and 1 mM $CaCl_2$ (442909 Sigma Aldrich). The aptamer buffer was used as a background electrolyte for oligonucleotide immobilisation and rinses following these steps. 10 mM PBS (P4417 Sigma Aldrich) was used otherwise.

4.3.3 Aptasensor functionalisation

Prior immobilisation, aptamer sequences or 1:1 aptamers to oligonucleotide supports in aptamer buffer were heated to 95°C for 5 minutes and immediately cooled to 4°C. Thiolated sequences were reduced with 1 or 5 mM Tris (2-carboxyethyl) phosphine (TCEP) (C4706 Sigma Aldrich) for 45 minutes and TCEP filtered out using NAP-10 (17085402 Cytiva) columns or NAP-25 (17085201 Cytiva) following supplier recommendations and eluting with aptamer buffer when specified. An overnight or

hour co-immobilisation on clean sensor surfaces of reduced sequences (0.228 μM oligonucleotide support or aptamer) with 6-Mercapto-1-hexanol (MCH) (451058 Sigma Aldrich), 0.1% BSA (A9418 Sigma Aldrich) or other specified SAM-forming molecules [2-mercaptoethane-1-sulfonic acid (J63989.09 Thermofisher Scientific), 3-mercapto-1-propanol (405736 Sigma Aldrich), 1-undecanethiol (510467 Sigma Aldrich) or 1H,1H,2H,2H-Perfluorodecanethiol (660493 Sigma Aldrich)] at a 1:100 ratio if unspecified.

A one-hour blocking step with 1 mM MCH or the corresponding SAM component allowed to obtain fully functionalised electrode surfaces either prior or following aptamer hybridisation at 2.28 nM or 0.228 μM from 4.4.2. Functionalised sensors were then exposed to concentrations of moxifloxacin for 30 minutes, rinsed with 10 mM PBS then interrogated.

Where temperature was not specified, incubations were carried out at room temperature. . Electrochemical interrogation occurred after each modification (unless otherwise stated) using EIS and DPV in 1 or 5 mM $[Fe(CN)_6]^{3-/4-}$ in PBS for PGE and TFGE and aptamer buffer after 10 minutes of stabilisation for Mx SPE. A thorough rinse of each sensor prior and following each set of measurement was carried out with the specified electrolyte.

4.3.4 Experimental specifics per electrode format

Concerning Mx SPE particularities included each tested condition dedicated to a single chip, or half a chip, with *n=4* per condition, when accounting for chip variability. 2 μL were deposited on each working electrode at each step, compared to the 50 μL on PGEs and 15 μL on TFGE

Functionalised sensors were exposed to concentrations of oxacillin, as a negative control of close molecular weight, and/or moxifloxacin for 30 minutes, both in a background of aptamer buffer, then rinsed and electrochemically tested.

4.3.5 Electrochemical measurements parameters

DPV was acquired between - 0.4 and 0.6 V at 0.1 V/s with 0.01 V step and a pulse of 0.025 V every 0.05 s. EIS was recorded against Open Circuit Potential (OCP)

with E_{ac} = 0.01 V in a 1 to 100 kHz frequency range at 9.8 frequencies per decade. R_{ct} values were obtained from fitting Nyquist plots to a modified Randles' circuit (Figure 4.2), replacing the conventional double layer capacitance by a constant phase element (CPE) to represent surface unevenness and a more realistic heterogeneous SAM. Diffusion processes of $[Fe(CN)_6]^{3-/4-}$ were modelled by the presence of a Warburg element.[420]
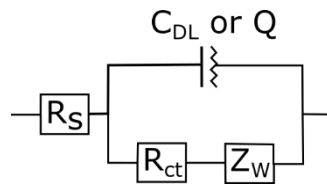
Figure 4.2. Modified Randles circuit to fit EIS responses.

Percentage changes were calculated according to the following formula where $X_{[conc.]}$ is the DPV peak current or R_{ct} obtained after exposure of the sensor to a specified concentration and X_{SAM} the DPV peak current or R_{ct} obtained after SAM formation:

$$\% \text{ change vs SAM} = 100 * \frac{X_{[conc.]} - X_{SAM}}{X_{SAM}}$$

Statistically significant differences were obtained by performing paired sample t-tests using Origin.

4.4 Results & Discussion

This study presents the development and optimisation of a voltammetric and impedance-based aptasensor for moxifloxacin, functionalised with a DNA aptamer selective for this antibiotic, presenting a K_D of 325 nM.[428] Binding of moxifloxacin to the aptasensor relies on EIS for its sensitivity regarding events occurring at the electrode interface and DPV as a sensitive voltammetric technique to cross-check recorded EIS trends as non-specific events can overtake signal changes.

4.4.1 Comparison of immobilisation strategies & gold substrates

4.4.1.1 Polycrystalline gold electrode functionalisation

Three immobilisation strategies were tested on PGE using the **thiolated aptamer sequence**, a **pre-hybridised complex** composed of a 5'-thiol-modified short

oligonucleotide paired with the aptamer strand and a **sequential assembly of the complex** with thiol-modified support immobilisation followed by aptamer hybridisation (Figure 4.3). Displacement of the aptamer strand from its oligonucleotide support was verified by Maugi *et al.* (2021).[431] The duplex oligonucleotide functionalisation scheme was previously reported as a successful detection and signal enhancement strategy[432] for small molecules such as glucose,[433] dopamine,[433,434] cortisol,[435] steroids[436] and tetracycline[437]. Self-assembled monolayer formation was adapted from Sypabekova *et al.* (2019).[232]
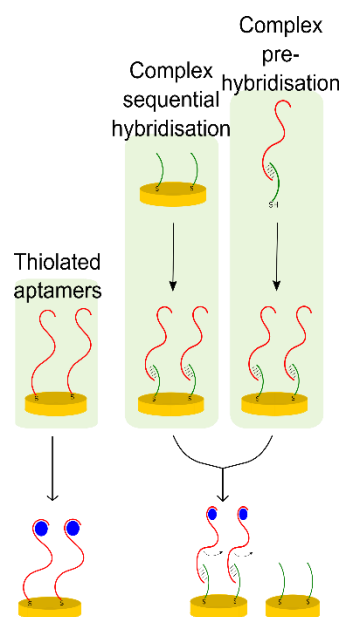
Figure 4.3. Aptamer immobilisation strategies with the direct immobilisation of the thiolated aptamer sequence, the complex sequential hybridisation method which consists in immobilising a support oligonucleotide (green) prior hybridisation to the aptamer sequence (red) or pre-hybridisation of the same complex before its immobilisation on gold. Both support:aptamer complex methods undergo a complex sequential hybridisation of the aptamer sequence upon moxifloxacin recognition and enhance electron transfer whereas the direct sequence immobilisation should remain attached to the gold and moxifloxacin binding decreases electron transfer efficiency.

Layer formation and negative controls differed for the three tested strategies. Only the support sequence without the paired aptamer served as a negative control for complex sequential hybridisation and pre-hybridisation strategies. Concerning the direct immobilisation, only the background solution deprived of moxifloxacin gave a negative control response at this stage since a scrambled sequence was only provided

later on (Chapter 5). Steps were designed to avoid any non-specific interaction when heating the aptamer sequence, hence the differences in order for the three strategies. Concentrations of moxifloxacin tested were in the detection range of reported levels in wastewater samples.[438,439]

DPV peak amplitude changes showed an overall decrease for the three methods compared to their respective negative controls (Figure 4.4C&F&I). Complex sequential hybridisation and pre-hybridisation methods showed opposite trends between positive and negative target exposures (Figure 4.4C&F). Only the complex sequential hybridisation method resulted in a signal change proportional to moxifloxacin concentration (Figure 4.4B) correlating with the direction of the trend observed when directly immobilising thiolated aptamers on the gold (Figure 4.4F). An opposite signal change upon target exposure for the complex sequential hybridisation method was noticed compared to the pre-hybridised complex method (Figure 4.4I). The 15-minute stabilisation time seemed to enable a better differentiation between absence and presence of target and/or probe (Figure 4.4C-F-I).
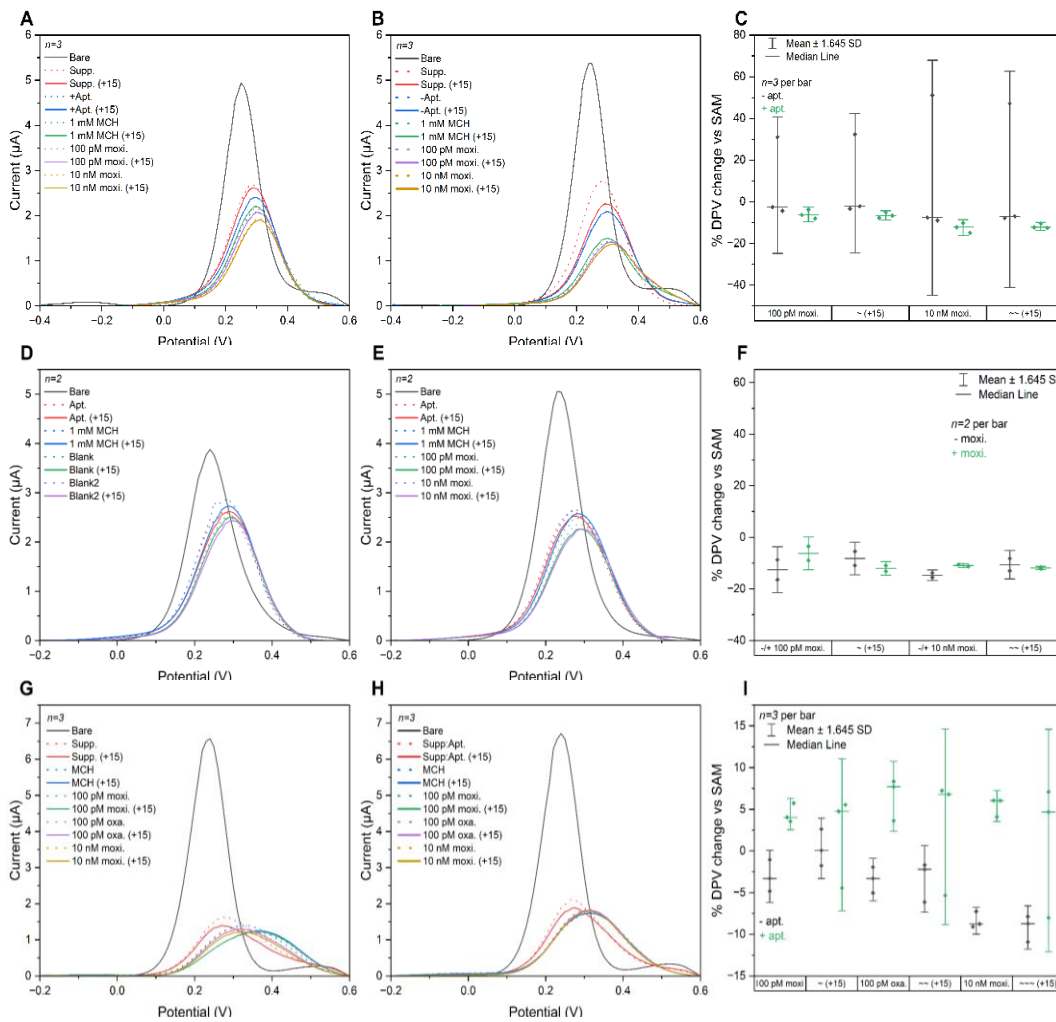
Figure 4.4. Average DPV peak amplitude of 5 mM [Fe(CN)$_6$]$^{3-/4-}$ in 10 mM PBS on PGE after each surface modification and fifteen minutes of stabilisation and associated percentage change after moxifloxacin exposure against functionalised sensors blocked with MCH for the complex sequential hybridisation (A-C), thiolated aptamer sequences (D-F) and prehybridised complex (G-I) methods.

R$_{ct}$ values were obtained from fitting Nyquist plots to a modified Randles' circuit (Figure 4.2). Overall, an increase in R$_{ct}$ was observed upon surface functionalisation for all methods (Figure 4.5). The R$_{ct}$ trends were in agreement with the DPV trends for all methods as well (Figure 4.4). Negative control conditions generated higher signal changes than positive conditions (Figure 4.5C&F&I). Higher R$_{ct}$ changes were recorded for the thiolated aptamer sequences (Figure 4.5) and almost none for the pre-hybridisation complex formation. High recorded variability motivated the use of the aptamer buffer throughout most experimental steps to provide the best functional environment for target recognition in the next trials. The

complex sequential hybridisation method yielded higher R_{ct} values upon increasing concentration of target compared to the more stable blank solutions (Figure 4.5).
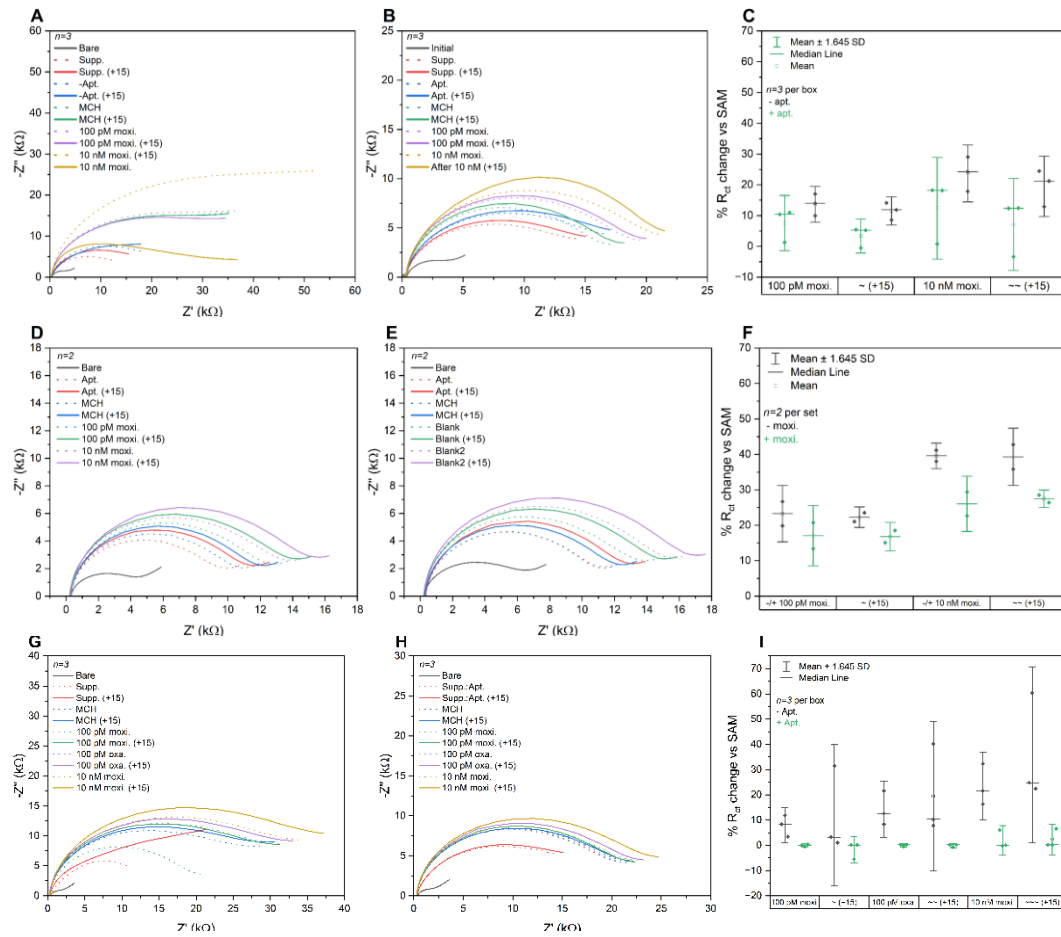
Figure 4.5. Nyquist plots obtained in 5 mM $[Fe(CN)_6]^{3-/4-}$ in 10 mM PBS after each surface modification and fifteen minute stabilisation and percentage R_{ct} change after moxifloxacin exposure against functionalised sensors with MCH block for the complex sequential hybridisation method (A-C), thiolated aptamer sequences (D-F) and pre-hybridised complex (G-I) on PGE.

The opposite trends between presence and absence of aptamer using DPV as well as the increasing R_{ct} changes proportional to moxifloxacin concentrations led to the selection of the sequential hybridisation as the better scheme for moxifloxacin detection and further optimisation on PGE.

According to supplier information, folded aptamer sequences only retain their functional shape for a limited time. The direct immobilisation of thiolated aptamer sequences as well as the prehybridised complex (Figure 4.5) with an overnight electrode functionalisation might have reached this limit and this could have affected target recognition performance. Using high temperature buffer has been reported

detrimental to signal acquisition using EIS,[432] which is partly why heat treatment followed by cooling was performed prior aptamer immobilisation. Considering SAM formation, the sequential assembly of the complex allowed for an extra hour of layer stabilisation with aptamer hybridisation, impacting the lower signals recorded for the negative control conditions. Indeed, MCH SAM reorganisation occurred for over 12 hours recorded as an EIS drift, impacting the magnitude of the signal change recorded,[432] supporting the initial overnight immobilisation. Stabilisation in the measurement buffer was also advised,[432] hence the repeated measurements after 15 minutes. These showed a better differentiation between presence and absence of aptamer, however not showing any statistically significant difference, notably for the complex sequential hybridisation method (Figure 4.5).

4.4.1.2 TFGE functionalisation

These experiments tested if a developed assay[429] using aptamers from Aptamer group selectively binding SARS-CoV-2 S1 could be transferred to these sequences aimed at smaller molecule recognition on the TFGE format. Briefly, reduced oligonucleotides were co-immobilised on TFGE with BSA, and further blocked with BSA (after aptamer hybridisation depending on the functionalisation method). Functionalised sensors were then exposed to two increasing concentrations of moxifloxacin. The TFGE format employed here possesses several advantages, being mass produced for little cost, enabling a lower reagent volume and being readily usable in comparison with polycrystalline gold electrodes.[429]

Out of the three immobilisation strategies, the most consequent DPV change after probe immobilisation was observed for the complex sequential hybridisation method given the decrease tin DPV current amplitude in presence of aptamer compared to a blank solution(Figure 4.6A). DPV changes showed an increasing behaviour after moxifloxacin exposure in the case of thiolated aptamer sequences (Figure 4.6). This could be because moxifloxacin bound to the full aptamer sequence enhances electron transfer due to the redox activity of fluoroquinolones,[392] showing selectivity towards this class of antibiotics compared to oxacillin for instance.
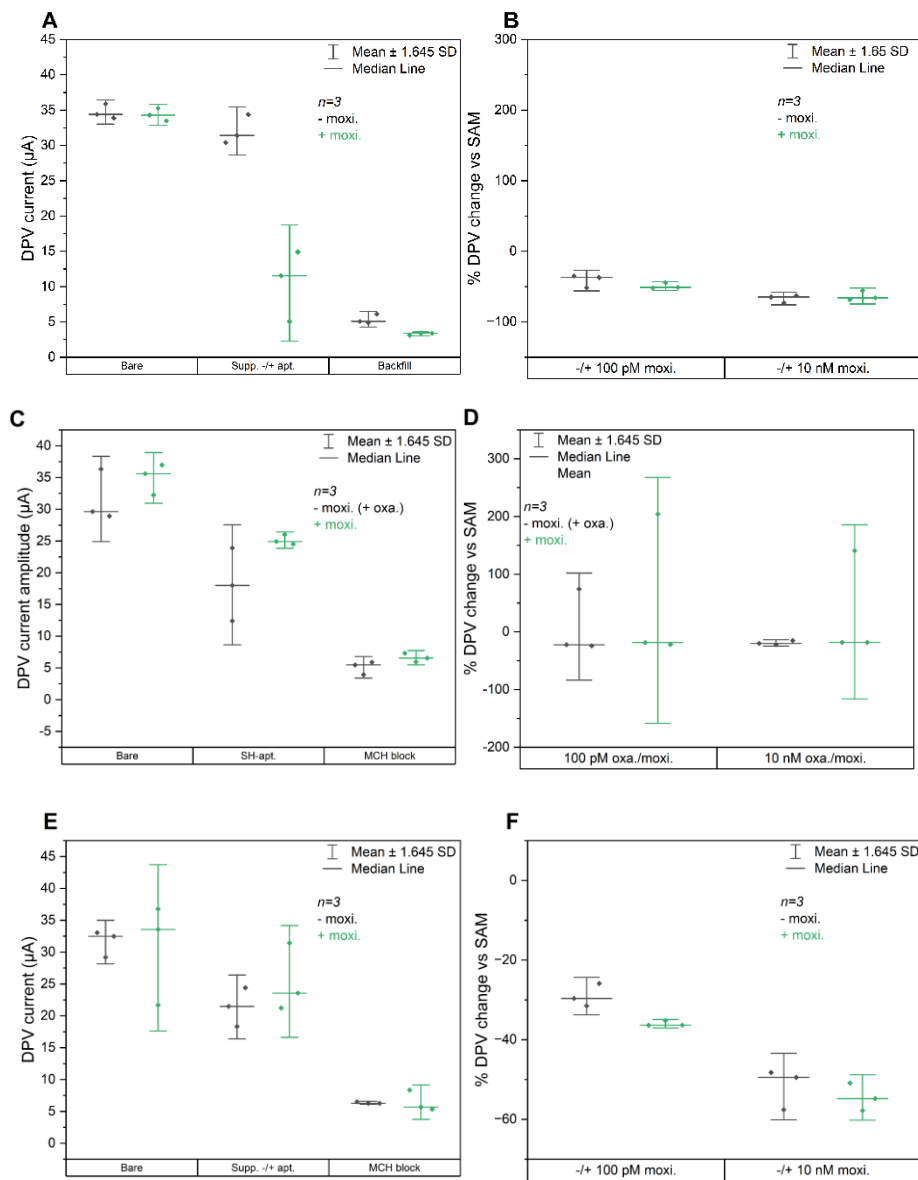
Figure 4.6. DPV peak amplitude of 5 mM $[Fe(CN)_6]^{3-/4-}$ in 10 mM PBS reflective of SAM formation with a BSA block and sensor performance with moxifloxacin through calculated percentage change using the complex sequential hybridisation (A&B), thiolated aptamer sequences (C&D) and pre-hybridisation (E&F) functionalisation methods on TFGE.

A decreasing trend for functionalisation involving a duplex formation (Figure 4.6B-F) was observed, both proportional to moxifloxacin concentration. The complex sequential hybridisation of the aptamer sequence from its support upon target recognition would supposedly enable an easier electron exchange close to the electrode and an increase in DPV current amplitude, when a decrease is instead observed (Figure 4.4B-F). If the aptamer sequence did not detach from its

oligonucleotide support, the complex as a whole might be blocking current even more when bound to moxifloxacin and explain the decrease recorded for the complex sequential hybridisation and pre-hybridisation methods (Figure 4.4B&F). With a DNA probe charged negatively, charge can increase or decrease depending on the charge of the target.[420] Change in conformation from the bound complex between probe and target may either block electron transfer close to the electrode or allow a better ion permeability.[420] No statistically significant difference between positive (moxifloxacin) and negative (absence of aptamer for the complex or oxacillin) was observed using DPV (Figure 4.6). Moreover, variability obtained with the thiolated aptamer sequences prevents differentiation between positive and negative controls (Figure 4.6B).

R_{ct} changes all increased over time regardless of the functionalisation method (Figure 4.7), which correlated with the increasing DPV trends between duplex formation and thiolated aptamer sequences (Figure 4.6). Immobilisation of aptamers can show an overall increase in impedance upon target binding to the aptamer sequence,[390] especially for the sequential complex formation in line with previous observations. Despite a higher R_{ct} increase with aptamer sequences present, a higher signal change was recorded without aptamer for the complex sequential hybridisation method (Figure 4.7A).

Miodek *et al.* (2015) observed different R_{ct} trends depending on the target concentration: increase in R_{ct} at low concentration and a decrease when higher concentrations are tested.[420] Concerning the thiolated aptamer sequences, moxifloxacin exposure yielded an almost null percentage change with high standard deviation in presence of aptamer and an average higher signal change in absence of specific target (Figure 4.7D). This might come from the little difference between bare and functionalised surfaces (Figure 4.7C). Using the pre-hybridisation functionalisation, the lower concentration of moxifloxacin yielded a higher signal change in presence than absence of aptamer, which was not repeated with the subsequent concentration (Figure 4.7F). This could result from inefficient washes to disrupt the specific binding of moxifloxacin to the aptamer strand.
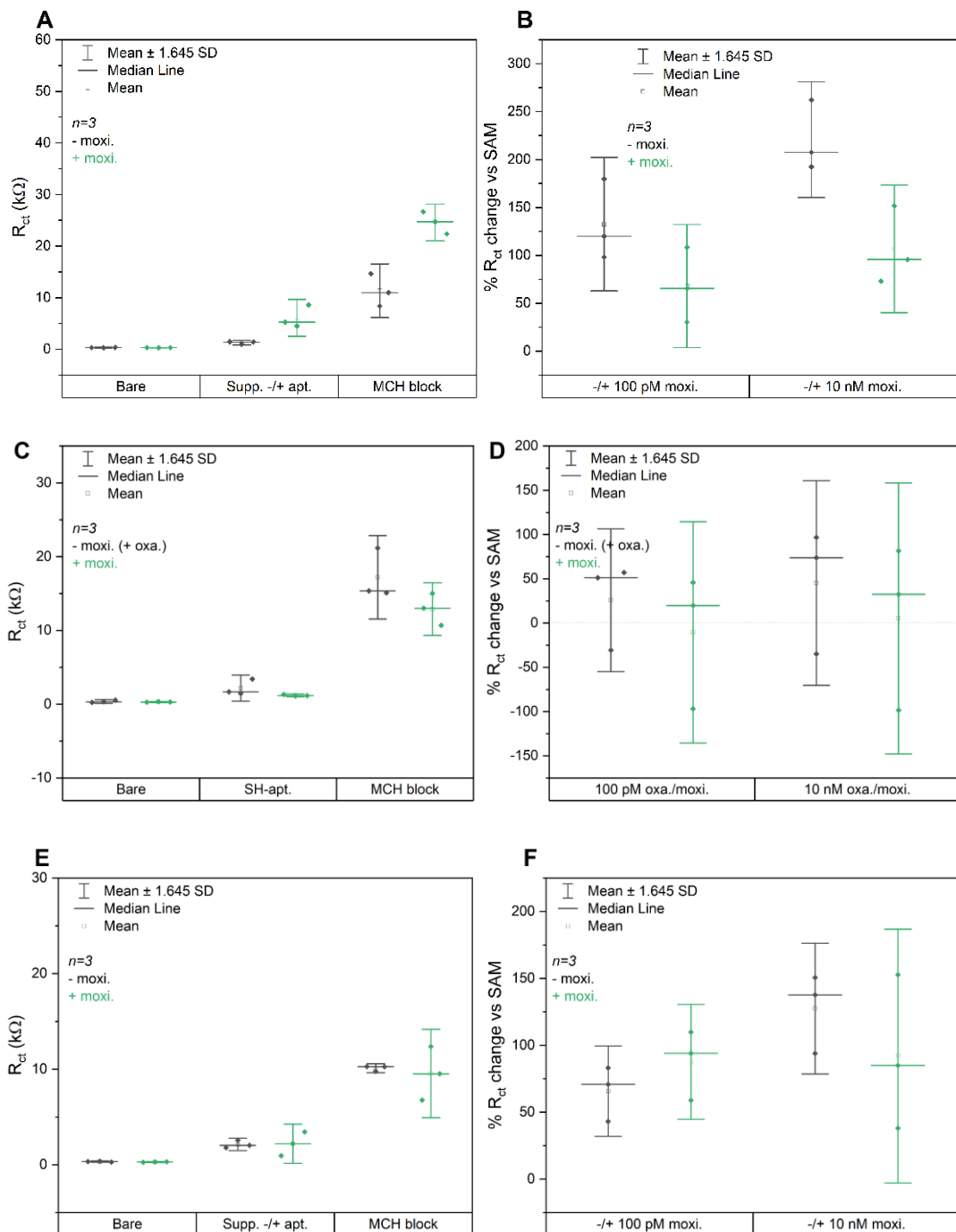
Figure 4.7. R_{ct} values and calculated percentage change against functionalised sensors after increasing concentrations of moxifloxacin on TFGE with BSA as the blocking agent in 5 mM $[Fe(CN)_6]^{3-/4-}$ in 10 mM PBS. Modified Randles' circuit fitting of Nyquist plots for the complex sequential hybridisation (A&B), thiolated aptamer sequences (C&D) and prehybridised complex assembly (E&F).

Considering the complex sequential hybridisation and pre-hybridisation methods, a decrease in R_{ct} was expected as the aptamer sequence recognising moxifloxacin would be displaced from its support. Reusing sensors would mean rehybridisation of aptamers to their support to provide a quantitative response in samples of unknown moxifloxacin concentration, which could partly explain the observed lower percentage change after the second concentration of moxifloxacin for the prehybridised method (Figure 4.7F). In addition, the TFGE sensors used here were initially designed for single use glucose determination. Repeated measurements favoured contact pads wear-out, impacting the timing and quality of later recorded signals.[440]

Hybridisation of the aptamer for the complex sequential hybridisation method might have been hindered by the size of BSA as a block agent compared to the smaller common alkanethiols used to block gold surfaces. Moreover, high hybridisation yields have been reported for low DNA surface coverage as a consequent negative charge density from DNA close to the electrode, forming an electrostatic barrier impeding duplex formation.[441]

Developing aptasensors targeting small molecules is challenging compare to larger proteic targets, with lower reported affinities.[415] Comparing the target-to-aptamer size ratio between our previously reported work[429] with the 140 kDa SARS-CoV-2 S1 domain against its 10,747.2 Da optimised aptamer sequence (13.03) versus this study using the 401.431 g/mol moxifloxacin and either the 13,230.8 Da thiol-modified aptamer (0.03) or 18,876.4 Da (0.02) support-aptamer complex respectively yield a 430 to 650 times difference, providing a possible reasoning behind the difference in magnitude of observed signal changes.

Probe packing density impacts sensitivity with possible steric hindrance depending on target size, minimised with small molecules such as antibiotics.[390,406,442] TCEP filtration resulted in the dilution of aptamers;[443] using higher starting concentrations would raise the cost per experiment/test and limit optimisation possibilities.

MCH improves probe orientation and layer packing as it displaces non-specifically adsorbed aptamer regions and orient them upright, through repulsion between negatively charged DNA and the net negative dipole of the MCH alcohol end group. This leads to optimal aptamer density, reproducibility and improved access to binding sites.[409]

Our published functionalisation scheme for SARS-CoV-2 S1 using TFGE did not yield successful DPV and EIS monitoring of moxifloxacin recognition using this specific aptamer sequence. As target and block agent sizes differed, the following optimisation for moxifloxacin detection was conducted with MCH as a SAM component.

4.4.1.3 Optimisation of conditions for aptamer functionality on TFGE

All three aptamer immobilisation strategies were performed on TFGE; the main variables studied being using aptamer buffer instead of PBS for rinsing and MCH instead of BSA as a block agent. TCEP filtration was undertaken with a NAP-25 column instead, yielding a final volume of 2.5 from 1.475 mL.

Overall smaller magnitude of changes for all methods were recorded (Figure 4.8) compared to the previous functionalisation using BSA (Figure 4.7 and Figure 4.6). Little differences between absence and presence of aptamers for the duplex methods (Figure 4.8A&E) might explain why both DPV current and R_{ct} increased after moxifloxacin exposure. Thiolated aptamer sequences showed an increase in DPV current and decrease in R_{ct} with moxifloxacin exposure (Figure 4.8E and G). Layers formed seem quite stable after both target concentrations in absence of aptamer for DPV and EIS (Figure 4.8B and F). Pre-hybridisation of the complex gives lower DPV and R_{ct} change in presence rather than in absence of aptamer. Despite no statistically significant changes, the complex sequential hybridisation method shows opposite trends for moxifloxacin recognition between presence and absence of aptamer, with proportional signal change increase to target concentration for DPV and EIS (Figure 4.8).
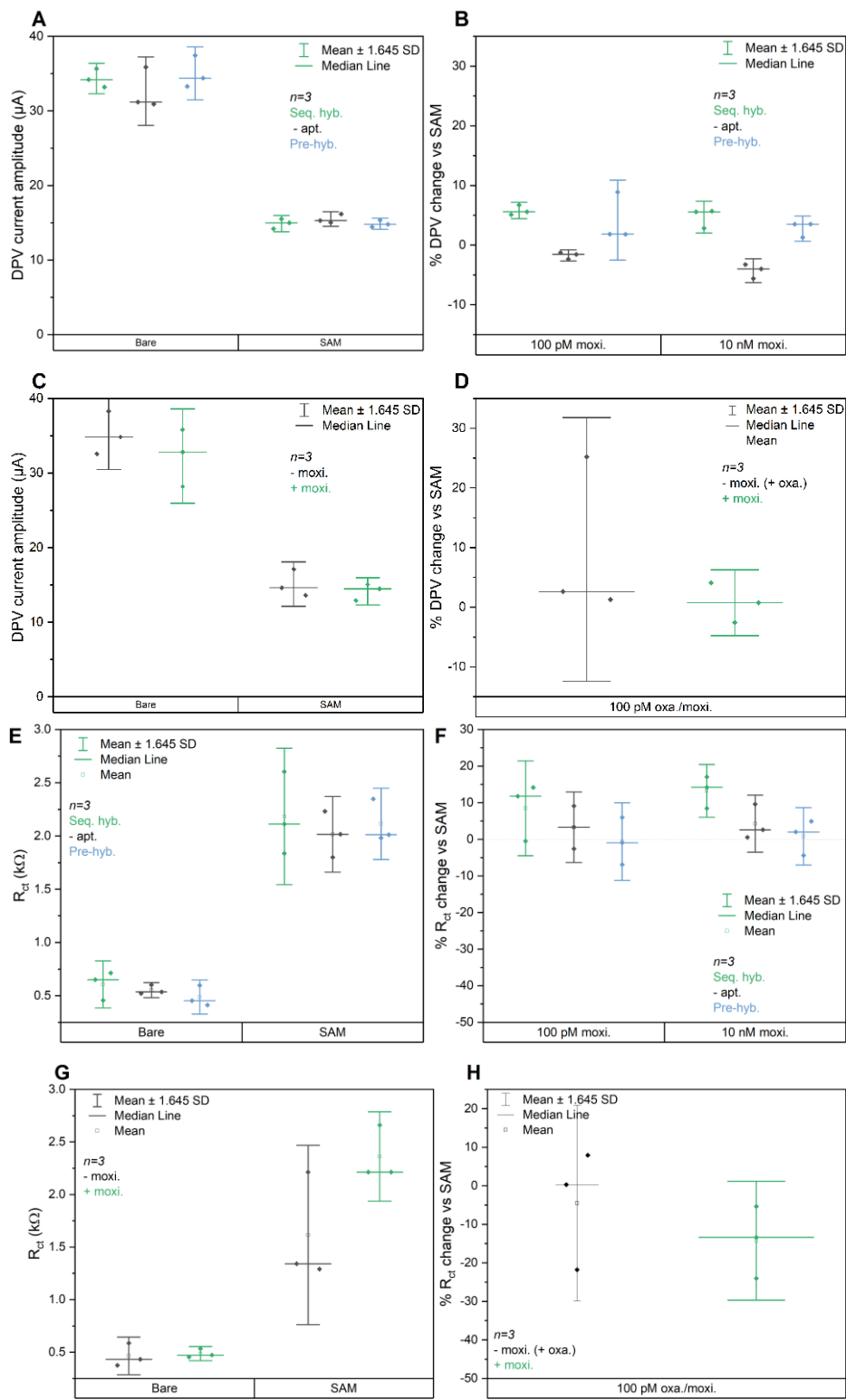
Figure 4.8. DPV and R_{ct} responses in 5 mM $[Fe(CN)_6]^{3-/4-}$ in 10 mM PBS on TFGE blocked with MCH. Current amplitude (A&B) and associated percentage changes (C&D) against fully functionalised layers for the complex sequential hybridisation (se. hyb.), prehybridised complex (pre-hyb.) and thiolated aptamer sequences. R_{ct} values and percentage changes respectively for the complex sequential hybridisation and pre-hybridised complex (E&F) and thiolated aptamer sequences (G&H) in the same conditions.

Observed sensor behaviour for the thiolated aptamer sequences produced opposite trends, namely a decreasing DPV current amplitude and an increasing R_{ct} with target concentration for thiolated aptamer sequences. However, the increasing DPV for the duplex formation methods was not matched by a decreasing R_{ct}. As the aptamer sequence displaces from the support when binding moxifloxacin, electron flow would supposedly be improved with a less crowded layer closer to the electrode surface, which was seen by the increasing DPV with moxifloxacin binding (Figure 4.8). This might result from electrochemical activity of moxifloxacin, possibly penetrating the layer and interacting non-specifically with the SAM. This has been studied through target immobilisation in the layer by Liu *et al.* (2021).[444] R_{ct} increases have also been reported systematically after voltammetric interrogation[432], which could be the case here. A long conditioning of the electrode in the measurement solution, over 12 hours, to counter the short term R_{ct} increase and reflect the longer term decrease can also reflect more accurately recorded signal changes.[432] Aptamer complex sequential hybridisation upon moxifloxacin exposure might have induced SAM reorganisation as well.[409,432]

Magnitude of signal changes for this functionalisation scheme was also lower than when using PGE (Figure 4.4 and Figure 4.5), which is possibly due to probe amount immobilised (), since the filtration step inevitably led to oligonucleotide dilution, however potentially beneficial for enhanced duplex formation,[441] but not confirmed by the data obtained in Figure 4.8.

Based on the results from the two different electrode formats, the complex sequential hybridisation method showed more consistent signal changes upon moxifloxacin exposure, compared to the other two detection strategies and these changes were more often proportional to target concentration (Figure 4.3B, Figure 4.4B, Figure 4.5B and). The complex sequential hybridisation functionalisation and detection scheme was therefore retained for optimisation of moxifloxacin recognition.

Table 4.4. Summary DPV and R_{ct} responses on PGE and TFGE obtained for three support:aptamer complex formations: complex sequential hybridisation (S+A), thiolated aptamer sequences (A) and pre-hybridisation of the aptamer:support complex (SA). |-A|<|+A| translates to a greater signal change (absolute value) observed in presence than absence of aptamer or moxifloxacin when the A is replaced by moxi. % change || [moxi.] refers to a greater percentage change upon subsequent exposure to increasing moxifloxacin concentration.

Format	Complex assembly	Block	Average DPV change		Average R_{ct} change	
			|-A| <|+A|	Change || [moxi.]	|-A| <|+A|	Change || [moxi.]
PGE	S+A	MCH				Yes
PGE	SA	MCH				
TFGE	S+A	BSA	Yes			
TFGE	SA		Yes	Yes	Yes	
TFGE	S+A	MCH			Yes	
TFGE	SA	MCH				
			|-moxi.| <|+moxi.|	Change || [moxi.]	|-moxi.| <|+moxi.|	% change || [moxi.]
PGE	A	MCH		Yes	Yes	Yes
TFGE	A	BSA	Yes	Yes		Yes
TFGE	A	MCH	Yes		Yes	Yes

4.4.1.4 Mx SPE cleaning and characterisation

After the polycrystalline gold electrodes (PGE) and thin film gold electrode (TFGE) formats, multiplexed screen-printed gold electrodes (Mx SPE) were assessed (Figure 4.9). PGE characterisation has been previously reported,[445,446] and so has TFGE.[429] As the Mx SPE were newly designed and locally produced, their cleaning and characterisation have been undertaken here.
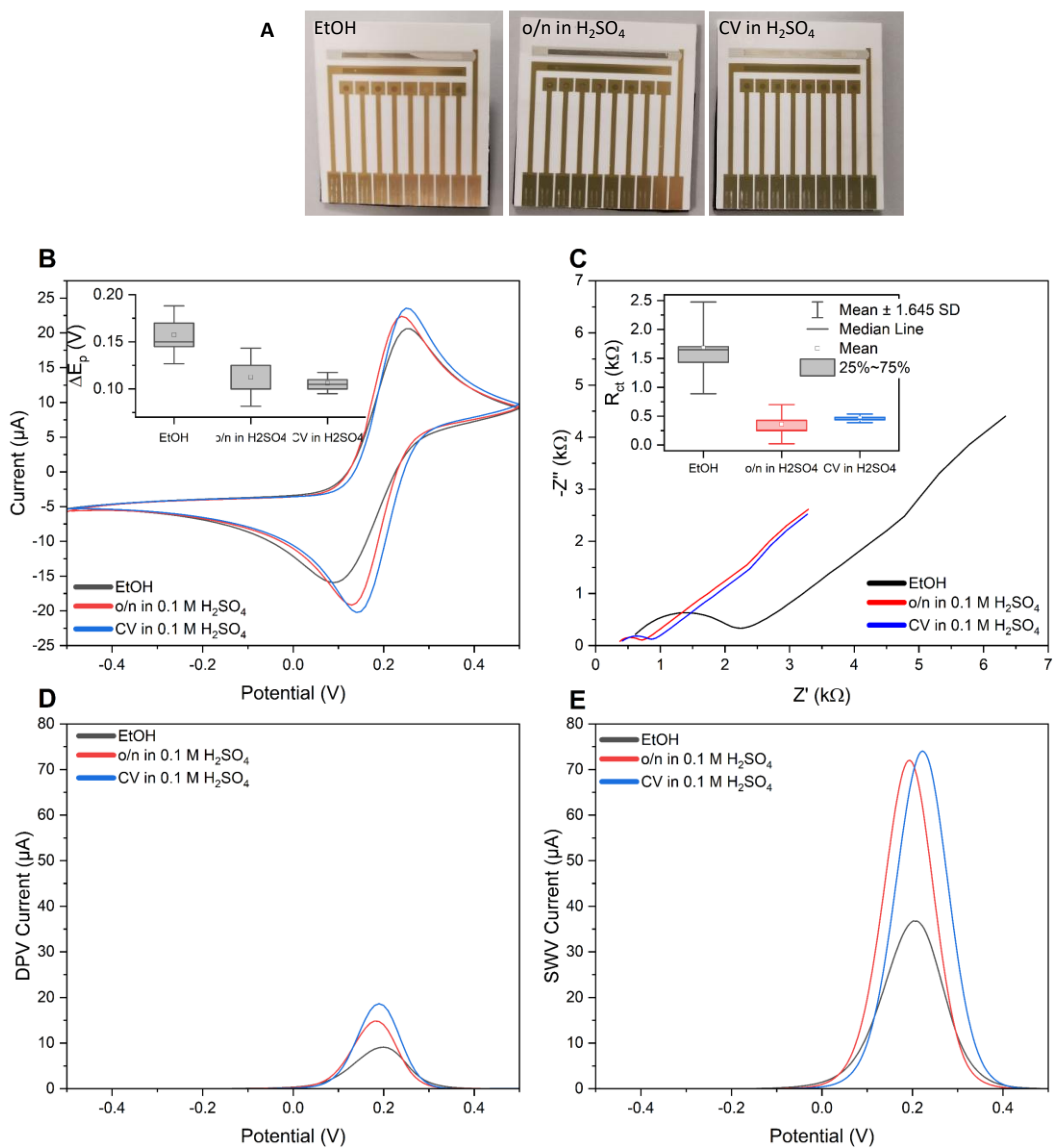
Figure 4.9. Comparison of cleaning methods for Mx SPE in 5 mM [Fe(CN)$_6$]$^{3-/4-}$ in 10 mM PBS (A) through chip integrity post cleaning and CV (B) with ΔE_p in inset, EIS (C) and inset average R$_{ct}$ values, DPV (D) and SWV (E) with *n=8* for each trace/box.

Among Fischer *et al.* (2009) cited methods,[430] three cleaning techniques were selected for their ease of execution and lesser damage to surface integrity: deposition of ethanol for 30 minutes, overnight incubation in 0.1 M H_2SO_4 and potential cycling in 0.1 M H_2SO_4. Considering the obtained voltammetric and impedimetric measurements $[Fe(CN)_6]^{3-/4-}$ (Figure 4.9), the chip cleaned with ethanol performed the least well after cleaning. Both sulfuric acid cleaning methods yielded similar results. CV cycling allowed for slightly higher peaks looking at both pulse voltammetry results (Figure 4.9D-E) along with less variability in the potential difference between oxidation and reduction peaks (Figure 4.9B inset) and R_{ct} values (Figure 4.9C inset). Finally, looking at the integrity of the electrodes, CV cycling allowed for less disintegration of the Ag/AgCl reference electrode coating compared to the overnight incubation. These electrodes were connected to the PalmSens 4 potentiostat using the external 8 WE DropSens connector with an edge connector. As the electrodes were much thinner than the proprietary electrodes it was designed for, layers of tape were added to ensure adequate contact. Wearing of the contact pad deposits occurred readily after a few measurements (Figure 4.9A), which is why the number of measurements were minimised to ensure accurate signal acquisition. Based on the closest ΔE_p to 59 mV and lowest standard deviation, higher peak amplitude from pulsed voltammetry and the least variability in R_{ct} as well as reproducibility between chips (Figure 4.10), the cyclic voltammetry scan iteration in 0.1 M H_2SO_4 was the best performing method to clean the gold chips and retained for next experiments. Having arrived at an acceptable cleaning technique it was next necessary to test electrodes' ability to support surface bio-functionalisation.
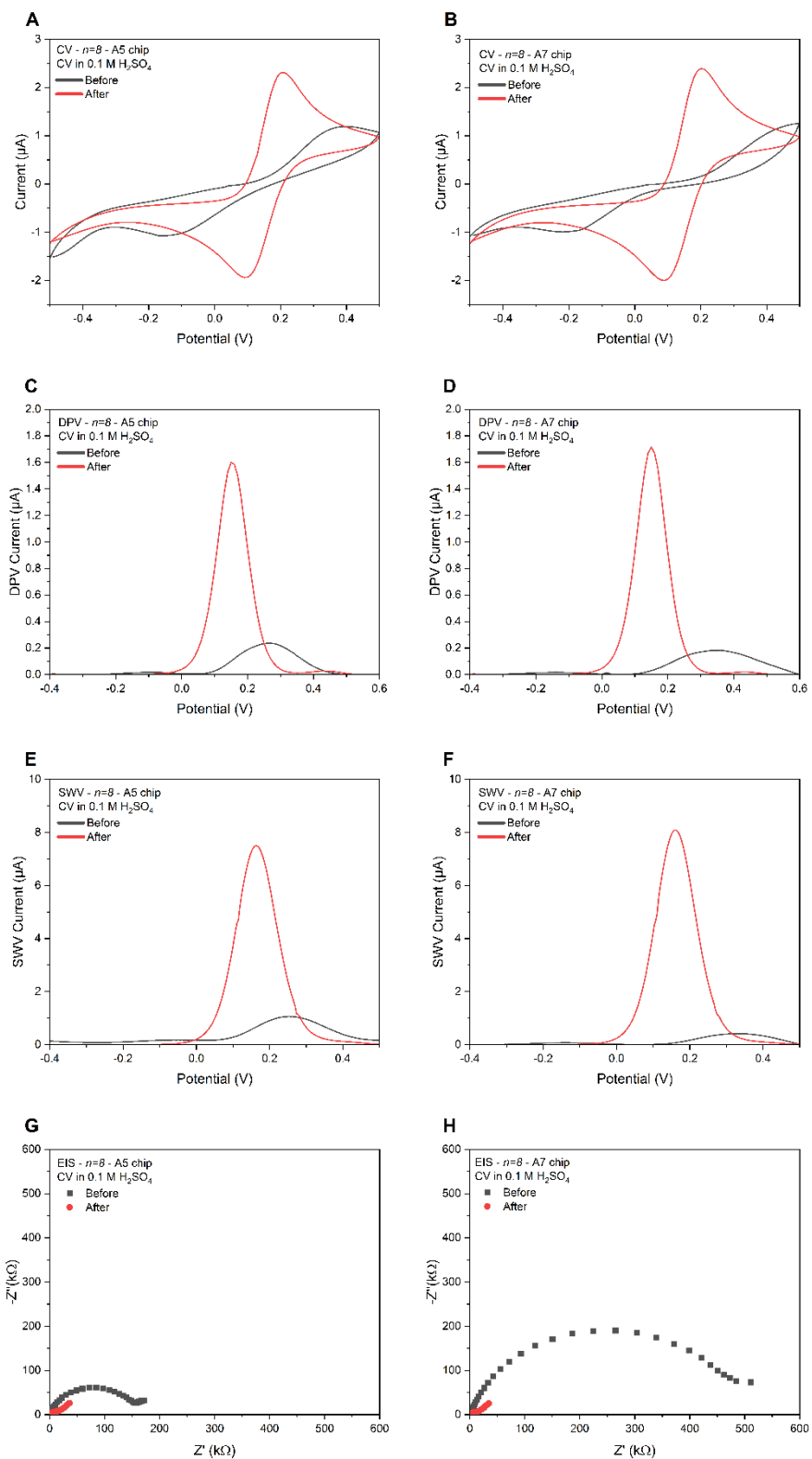
Figure 4.10. Characterisation of Mx SPE with 5 mM $[Fe(CN)_6]^{3-/4-}$ in 10 mM PBS. Two independent chips from the same production batch before (black) and after (red) CV cycling in 0.1 M H_2SO_4 with CV (A&B), DPV (C&D) and SWV (E&F) and Nyquist plots (G&H).

4.4.1.5 Mx SPE functionalisation

Once the Mx SPE cleaning procedure optimised, working electrodes were functionalised, 230 nM of reduced oligonucleotide supports were co-immobilised with MCH at a 1:100 ratio. Aptamers at a 1:1 ratio to their supports were subsequently hybridised, and a blank solution of aptamer buffer only in the negative control case. The remaining free gold surfaces were blocked with 1 mM of MCH. Sensors functionalised with the complex sequential hybridisation method were then exposed to 1 µM of a non-specific target, oxacillin, prior to 1 µM of moxifloxacin. A higher concentration of moxifloxacin was tested compared to previous trials, to ensure detection of the moxifloxacin binding events in relation to the aptamer's K_D.

An equivalent DPV response was observed after oxacillin exposure in presence and absence of aptamer (Figure 4.11B). Upon moxifloxacin incubation, a DPV current decrease was observed, slightly more consequent in the presence of aptamer and opposite to the increase upon oxacillin exposure.

Concerning R_{ct}, a small response was noticed when exposed to oxacillin but less consequent than the increase in R_{ct} after moxifloxacin incubation, slightly more significant in presence of aptamer (Figure 4.11D).

Loose moxifloxacin molecules possibly penetrate and disturb the monolayer, which can be counteracted, when the detection scheme allows, by including it in the monolayer.[444] Both loose antibiotics interact differently with the layer as observed by the differences in trends recorded (Figure 4.11B and D). Differences in layers formed for the full and incomplete SAM were not recorded by DPV (Figure 4.11A), however the difference between aptamer absence and presence upon moxifloxacin recognition was picked up by DPV (Figure 4.11B). DPV decreases were matched with R_{ct} increases, indicating that moxifloxacin recognition was reflected by signal changes rather than differences in layers formed. However, variability was too consequent to enable a statistically significant difference.

Additionally, the percentage change magnitude was lower than when exposing TFGE sensors to 10 nM and 10 pM of moxifloxacin (Figure 4.7B and F),

possibly from the higher R_{ct} values of the SAM formed on Mx SPE (Figure 4.11C) compared to the ones formed on TFGE (Figure 4.7A and E). As the moxifloxacin concentration tested was high, optimisations were further studied to enable increases in signal changes and lower detection of antibiotics.
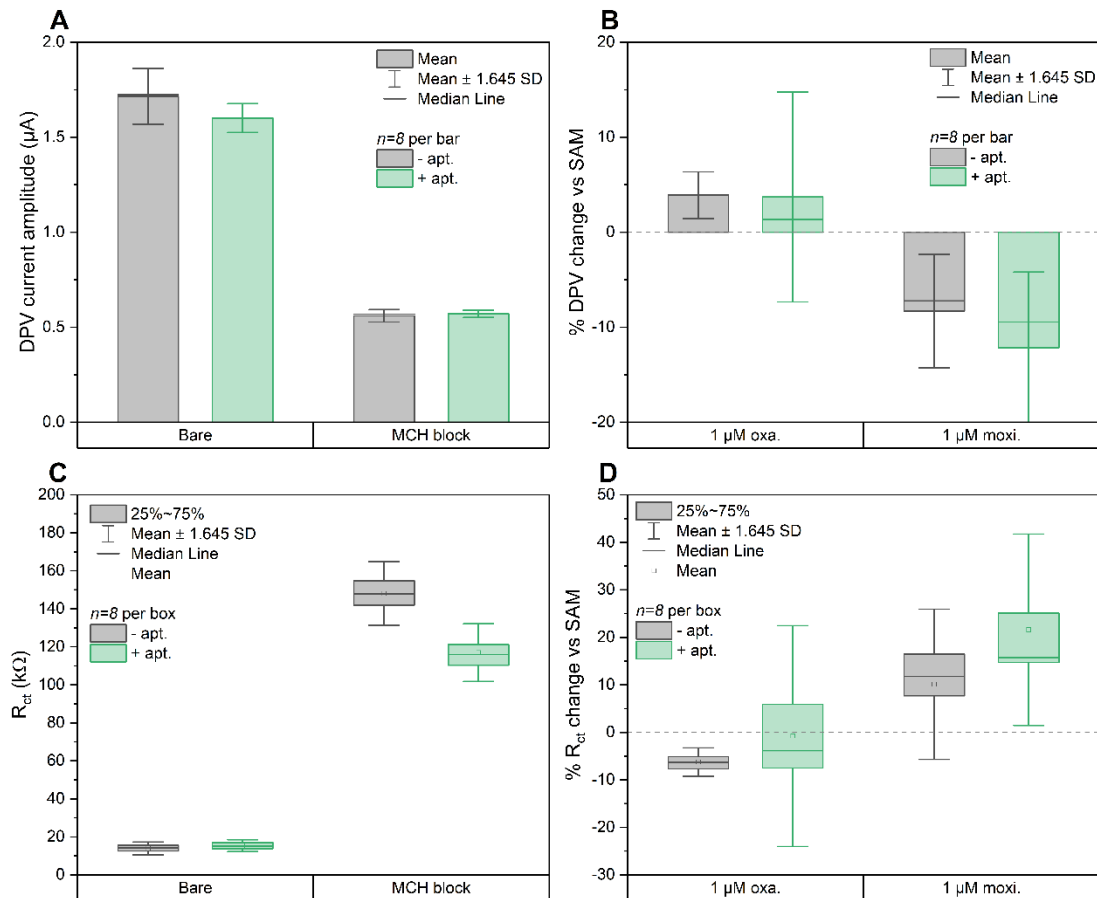
Figure 4.11. DPV and R_{ct} responses using the complex sequential hybridisation functionalisation on Mx SPE in 5 mM $[Fe(CN)_6]^{3-/4-}$ in 10 mM PBS. Peak current (A) and R_{ct} values (C) and associated percentage changes (B&D) after target exposure.

4.4.1.6 Increasing probe concentration for enhanced Mx SPE performance

In the attempt of increasing signal change, the functionalisation strategy employed on Mx SPE was repeated with a hundredfold more duplexes, at 219.85 µM support co-immobilised with MCH and 3.26 µM aptamer. A block step with 1 mM MCH ensured all remaining free sites were blocked to minimise non-specific interactions. Sensors were then exposed to 1 nM of oxacillin, an equivalent concentration of moxifloxacin and 1 µM of moxifloxacin to enable a comparison with the previous attempt.

Oxacillin gave almost no DPV response without aptamer but a decrease with aptamer (Figure 4.12B). This can be due to non-specific interactions with the aptamer sequence. DPV peaks decreased with moxifloxacin concentrations in presence of aptamers more than without aptamer sequence (Figure 4.12B) reflecting the slight difference in layer recorded in Figure 4.11A. Corresponding increasing R_{ct} trends confirmed moxifloxacin detection (Figure 4.12D). Moxifloxacin seemed to interact non-specifically with the support as higher concentration of moxifloxacin yielded a R_{ct} increase in absence of aptamers as well. The overall magnitude of signal changes observed, 83.6% vs 21.6% previously for R_{ct} changes after 1 µM of moxifloxacin in presence of aptamers and -38.6% vs -12.2% for DPV in the same respective order, compared to the previous experiment was 4 times higher for the 1 µM target exposure (Figure 4.11), even if it was the first moxifloxacin concentration tested in the previous trial and the second concentration tested here.
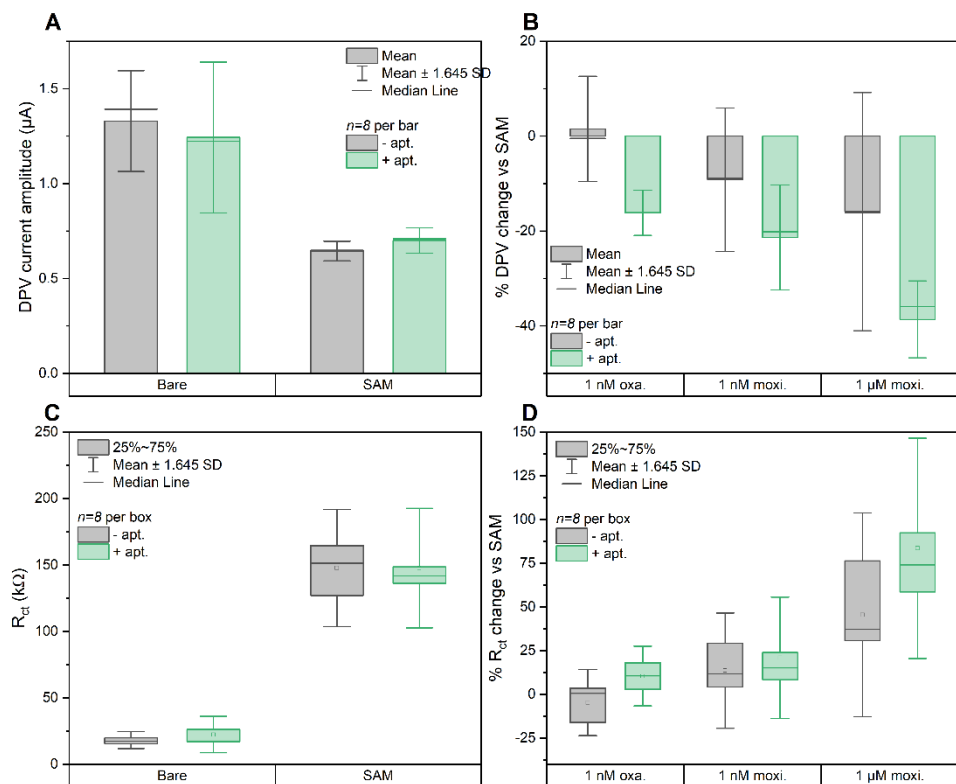
Figure 4.12. Repeatability of the complex sequential hybridisation approach on Mx SPE through DPV (A) and R_{ct} (C) values and associated percentage changes (B&D) against functionalised sensors after target exposure in 5 mM $[Fe(CN)_6]^{3-/4-}$ in 10 mM PBS.

Since the functionalisation scheme on Mx SPE proved successful for average moxifloxacin recognition (Table 4.5), systematic optimisation of the SAM was undertaken next. The focus electrochemical method was put on EIS for its sensitivity as well as its minimal layer disturbance. The complex sequential hybridisation method was preferred for its possible transferability to other aptamers and signal enhancement potential.[437]

Table 4.5. DPV and R_{ct} trend summary based on complex packing density. |-A|<|+A| translates to a greater signal change (absolute value) observed in presence than absence of aptamer or moxifloxacin. % change ‖ [moxi.] refers to a greater percentage change upon subsequent exposure to increasing moxifloxacin concentration.

Electrode format	Support : aptamer	Average DPV change		Average R_{ct} change	
		|-A| <|+A|	% change ‖ [moxi.]	|-A| <|+A|	% change ‖ [moxi.]
Mx SPE	0.23 μM : 0.23 μM	Yes	Yes	Yes	Yes
Mx SPE	219.85 μM : 3.26 μM	Yes	Yes	Yes	Yes

4.4.2 Optimisation of layer formation

4.4.2.1 Effect of complex density and aptamer concentration on moxifloxacin recognition

Mx SPE were functionalised using the complex sequential hybridisation method by co-immobilising 100:1 MCH:reduced support oligonucleotide strands at 3 different concentrations, namely 228, 22.8 and 2.28 μM overnight. Corresponding 1:100 aptamer:support concentrations were hybridised for an hour, respectively 3.26, 0.326 and 0.0326 μM and 1 mM MCH blocked for another hour. Functionalised sensors were finally exposed to 1 nM moxifloxacin, then 10 nM oxacillin and 1 μM of moxifloxacin, each for 30 minutes and all in a background of aptamer buffer.

Oligonucleotide support and MCH co-immobilisation have homogenised the disparities recorded from bare surfaces with DPV responses (Figure 4.13A). The difference between support only and full duplexes were maintained after block for the lower and higher probe concentrations when referring to DPV signals and

resulting to higher peak current and lower R_{ct} values (Figure 4.13A-C). Hybridisation has been reported as an increase or decrease in R_{ct}[447] and has been seen as mostly a R_{ct} increase (Figure 4.5, Figure 4.7, Figure 4.13) and DPV decrease (Figure 4.4, Figure 4.6, Figure 4.8) across electrode formats so far.
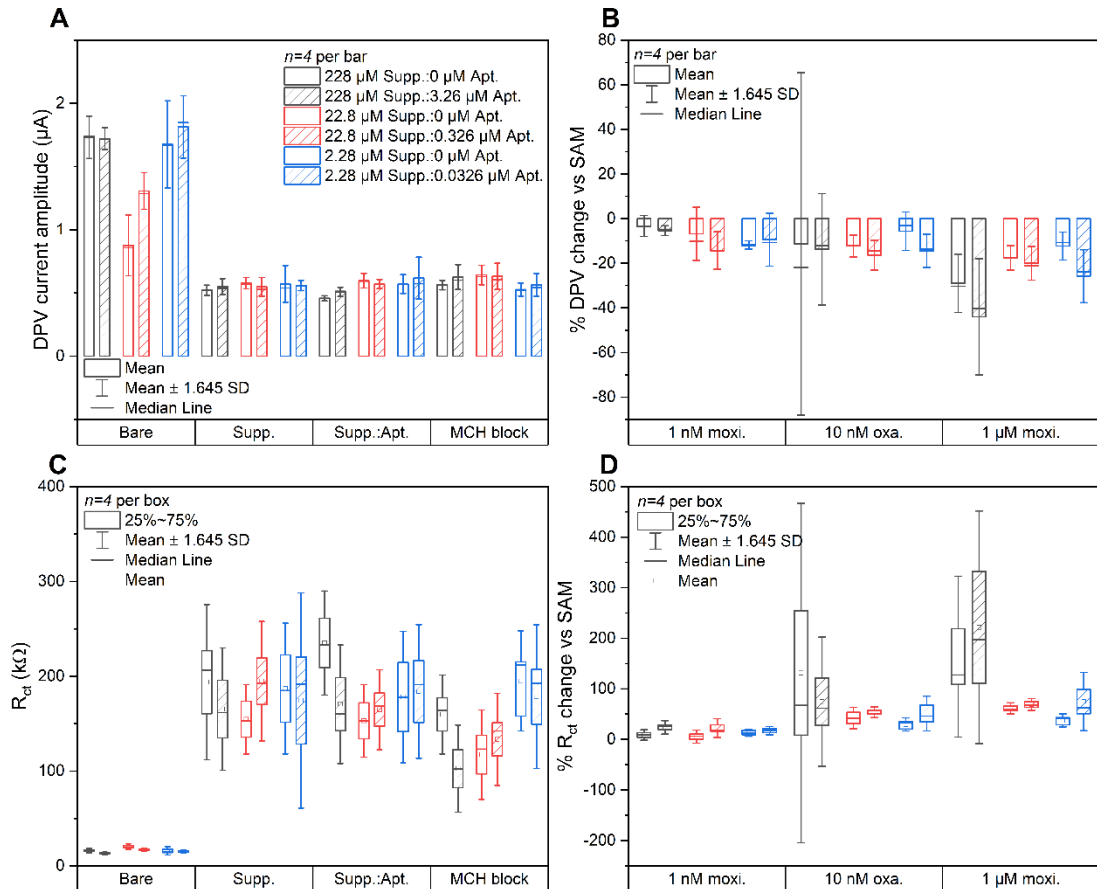
Figure 4.13. Monolayer density comparison using DPV (A) and R_{ct} (C) values and respective changes against functionalised sensors after moxifloxacin (moxi.) or oxacillin (oxa.) exposure (B&D) with the complex sequential hybridisation approach on Mx SPE in 5 mM $[Fe(CN)_6]^{3-/4-}$ in 10 mM PBS.

Concerning sensor performance (Figure 4.13B-D), the lower concentration of duplex recorded the higher DPV peak current and R_{ct} signal changes, nevertheless accompanied with the highest variability. The lower duplex concentration performed similarly with lower values whereas the middle duplex concentration showed little change over moxifloxacin and oxacillin concentrations tested. Keighley *et al.* (2008) reported lower hybridisation efficiency with higher DNA probe concentrations,[447] which can explain the lower moxifloxacin recognition performance of the middle complex dilution compared to the lowest dilution in Figure 4.13B&D (Table 4.6).

Testing against oxacillin generally raised R_{ct} values, independently of ratio concentration (Figure 4.13D), with possible non-specific interactions disturbing the layer. DPV decreasing trends were matched with R_{ct} increases, with signal changes positively correlated with higher moxifloxacin content.

Comparing average DPV changes obtained here (Figure 4.13B) after 1 nM and 1 µM of moxifloxacin with previously obtained results (Figure 4.12B) shows a degree of repeatability between DPV decreases and their magnitude (Table 4.6). The better differentiation between averages in absence and presence of aptamer of the previous attempt can be attributed to the order in which oxacillin and moxifloxacin were tested and the minimal interrogations conducted throughout layer formation, enabling minimal system perturbations. DPV and R_{ct} percentage changes after 1 nM of moxifloxacin for the middle complex dilution (Figure 4.13B), were equivalent to the previous functionalisation trial (Figure 4.12B and Figure 4.11B). For Figure 4.11B and the middle complex dilution in Figure 4.13B, the aptamer concentration was within the same order of magnitude and tenfold higher for Figure 4.12B. This might mean that the signal change is maximal for this specific aptamer and 1 µM of moxifloxacin. Indeed, more aptamer in Figure 4.12 and Figure 4.13 yielded a more consequent signal change for these moxifloxacin concentrations and the lower complex dilution with the smallest aptamer concentration tested in Figure 4.13 resulted in less consequent DPV and R_{ct} signal changes (Table 4.6).

Table 4.6. Comparison of complex concentration on specific recognition of moxifloxacin (Antibiotic +) and non-specific oxacillin response. |-A|<|+A| translates to a greater signal change (absolute value) observed in presence than absence of aptamer.

Fig.	Support : aptamer	Antibiotic	Average % DPV change	Average % R_{ct} change
			|-A.|<|+A.|	|-A.|<|+A.|
Figure 4.11	0.23 μM : 0.23 μM	1 μM oxa.		
		1 μM moxi.	Yes	Yes
Figure 4.12	219.9 μM : 3.3 μM	1 nM oxa.		
		1 nM moxi.		
		1 μM moxi.	Yes	Yes
Figure 4.13	219.9 μM : 3.3 μM	1 nM moxi.		
		10 nM oxa.		
		1 μM moxi.	Yes	Yes
Figure 4.13	22.0 μM :0.33 μM	1 nM moxi.		
		10 nM oxa.		
		1 μM moxi.	Yes	Yes
Figure 4.13	2.2 μM : 0.033 μM	1 nM moxi.		
		10 nM oxa.		
		1 μM moxi.		Yes

Signal changes recorded in absence of aptamer or for oxacillin were higher than expected. In some cases, namely for Figure 4.11 and Figure 4.13 higher and lower complex dilutions, the presence of aptamer seemed to "shield" the SAM by providing a lower R_{ct} signal change than in absence of aptamer, which was only reflected in the DPV changes for Figure 4.11. Intending to consider chip variability, layers formed with and without aptamer sequence hybridised were localised on the same chip for each complex ratio, which could have induced some cross-reactivity and decreased the replicate number from 8 to 4. Since working electrodes are close to each other, initial 2 μL deposits possibly merge and do not provide expected differentiation between layers formed. This could also be the case at the moxifloxacin

stage, where the aptamer strand is being displaced from its anchor and interact specifically or non-specifically with other possible free sites. The variability, depicted by standard deviation, in sensor responses prevented statistically significant differentiation from both positive and negative control conditions tested, namely moxifloxacin in presence and absence of recognition element and with a non-specific target of similar size.

As the equipment used acquired measurements in a sequential rather than simultaneous manner, the delay between the first and last working electrode measured ranged between 10 and 15 minutes for EIS especially. This meant that SAMs on the last electrode measured had more time to stabilise from the physical disturbance of washes and solution changes compared to the first ones. This was countered by the stabilisation time in redox buffer to introduce a degree of repeatability between experiments.

The DPV potential window was chosen to avoid thiol reductive, below - 0.5 V, and oxidative desorption above 1 V.[448] Minimising voltage-induced desorption can be countered by a restrictive potential window between - 0.2 and 0.2 V, which is not always possible depending on peak location from the electrochemically-active marker.[449] Moreover, oxygen reduction on gold yields hydrogen peroxide, potentially damaging immobilised aptamers, occurring over 0.3 V when chloride ions are in the solution.[432,450]

Longer-chain alkanethiols for SAM formation slows down thiol desorption since they are more electrochemically stable but form thicker and more insulating layers.[409,448] Enzymatic degradation of the DNA is another reason for irreversible signal loss,[448] tampered by the use of nuclease-free water to make the aptamer buffer and dilute most solutions, which prevents damage at this stage of the sensor development.

As R_{ct} proved more sensitive to layer formation and binding events through magnitude of signal changes compared to DPV, it has been chosen, along with the

highest oligonucleotide complex concentration, as the main focus for subsequent optimisation to reflect moxifloxacin binding with minimal perturbation.

4.4.2.2 Taking advantage of spontaneity of the thiol adsorption on gold for shorter functionalisation

As thiol desorption might have impacted previous results (Figure 4.13) through continuous voltammetric interrogation along with SAM reorganisation, a one-hour SAM immobilisation was compared to the longer overnight step through EIS monitoring only. As Aptamer group stated a limited duration for aptamer shape retention following heat-treatment, the one-hour hybridisation remained unchanged. Clean Mx SPE were functionalised with the support oligonucleotide at 228 nM and 1:100 MCH either for an hour or overnight. 2.28 nM of aptamers were then hybridised and remaining free surfaces blocked for an hour with 1 mM MCH block. Sensors were then all tested with 100 µM moxifloxacin spiked directly in the redox mediator solution and left for 10 minutes before measurement.

Aptamer hybridisation was clearly observed for the hour SAM (Figure 4.14A). R_{ct} values yielded a statistically significant difference between absence and presence of aptamer after 100 µM moxifloxacin exposure when aptamers were hybridised for an hour (Figure 4.14A), contrasting with previous attempts without any statistically significant difference. However, the R_{ct} change from the overnight immobilisation led to a slightly more consequent decrease in presence than absence of aptamer. R_{ct} values provided a more statistically significant difference than calculated R_{ct} change (Figure 4.14). Furthermore, an overall decrease is observed here in comparison with the previous increases (Table 4.6). As aptamer sequences specifically bind moxifloxacin, they should displace from support strands, reflecting an easier electron exchange close to the electrode surface, hence justifying a decrease in R_{ct}. However, the decrease is more consequent in absence than presence of aptamer, the denser layer probably shielding the gold from etching by CN⁻ anions from the redox mediator (Figure 4.14).[409,451]
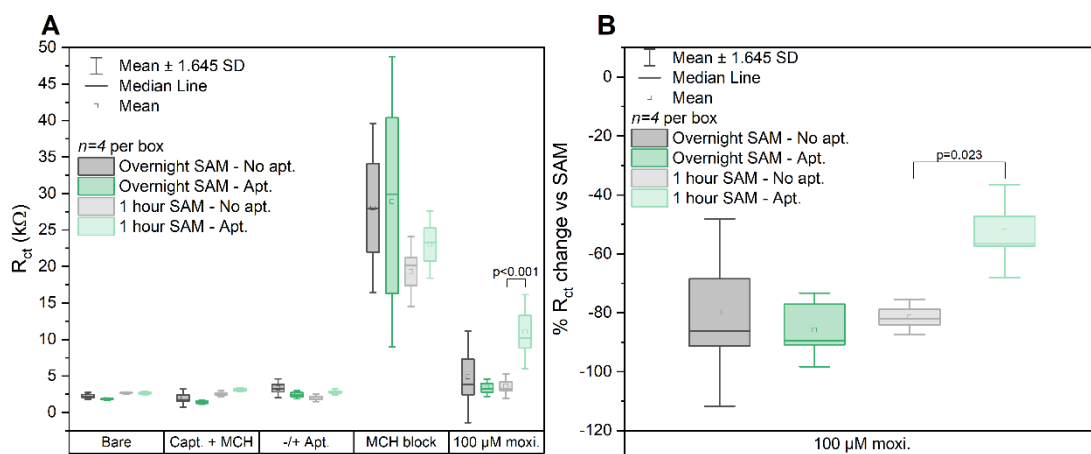
Figure 4.14. Comparison of sensor performance after overnight and one-hour SAM immobilisation on Mx SPE in 5 mM $[Fe(CN)_6]^{3-/4-}$ in 10 mM PBS via R_{ct} values (A) and calculated percentage changes (B).

SAM formation over the course of an hour has led here to a more successful aptamer hybridisation, compared to an overnight functionalisation. Sensor performance for 100 µM moxifloxacin showed statistically significant differences of $p < 0.001$ between presence and absence of oligonucleotide recognition elements at a lower duplex concentration on the electrode surface (Figure 4.14) and aptamer-free and -full duplexes located on the same chip.

4.4.2.3 SAM composition and assembly

To evaluate the effects of the alkanethiol components on signal acquisition and change, different SAM components with varied alkane chain length but also diverse end groups were compared (Figure 4.15).
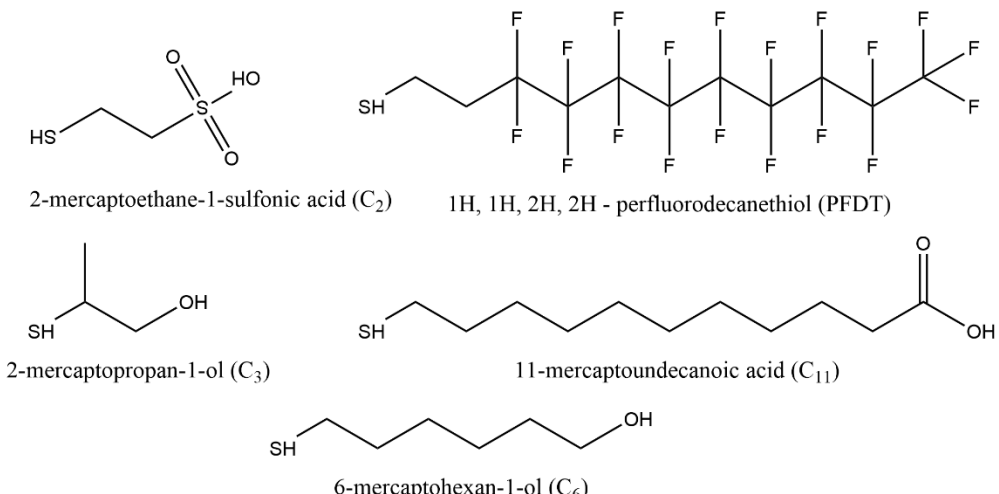
Figure 4.15. Chemical structure of SAM components tested.

Co-immobilisation of the support strand at 0.228 µM with a SAM component occurred over the course of an hour on clean Mx SPE. The widely used 6-mercaptohexan-1-ol (C_6)[450] was replaced by 2-mercaptoethane-1-sulfonic acid (C_2), 3-mercapto-1-propanol (C_3), 1-mercaptoundecanethiol (C_{11}) or 1H,1H,2H,2H-Perfluorodecanethiol (PFDT) (Figure 4.15). Complex assembly was also evaluated with hybridisation of 2.28 nM aptamers occurring either before or after blocking the remaining exposed electrode areas, since this complex concentration enabled recording of statistically significant R_{ct} signal change when challenged with 100 µM moxifloxacin (Figure 4.14). Three consecutive concentrations of moxifloxacin were incubated each for 15 minutes: 10, 50 and 100 µM for most configurations with probe attachment negative and positive conditions located on the same chip.

The C_2 and C_3 conditions, respectively with the blocking step last and first, displayed the lowest starting R_{ct} for each set. This would set up for better performance, as the electrode can detect increases in R_{ct} easily as well as decreases from low concentrations as no upper threshold was yet reached. When co-immobilising support and SAM component, an overall R_{ct} increase was observed for carbon chains above 6 and a decrease for carbon chains below 6 (Figure 4.16A&B). Even if longer chain thiols yielded the most consequent percentage change upon co-immobilisation and blocking step, smaller resistance changes would be more difficult to capture, either resulting from aptamer hybridisation or even target recognition, considering antibiotics relatively smaller size compared to the alkanethiol.

Concerning aptamer hybridisation, a more consequent change in presence rather than absence of aptamer supposedly reflected a more successful hybridisation. This was observed for C2 where aptamers were hybridised before block (Figure 4.16A), C6 and PFDT in the case of aptamer hybridisation as the last SAM formation step (Figure 4.16B) and 11-mercaptoundecanoic acid (Figure 4.16A&B) in both SAM assemblies. Aptamer hybridisation was assumed successful to a degree when the average R_{ct} was absolutely superior to the identical condition without aptamer or having an opposite trend (bold values in the hybridisation section of Table 4.7), the most successful being C_{11} where aptamer pairing occurred after block. A consistent

R_{ct} increase across several moxifloxacin concentrations tested, differentiated from the conditions without aptamers (Figure 4.16D&F and bold values in the moxifloxacin section of Table 4.7) was evidenced by C_{11} and C_3, both where aptamer pairing occurred after block. Most other SAM composition and assemblies either only performed on the first concentration since all probes might have been displaced from the micromolar range of moxifloxacin, or not at all (Figure 4.16D&F and Table 4.7).
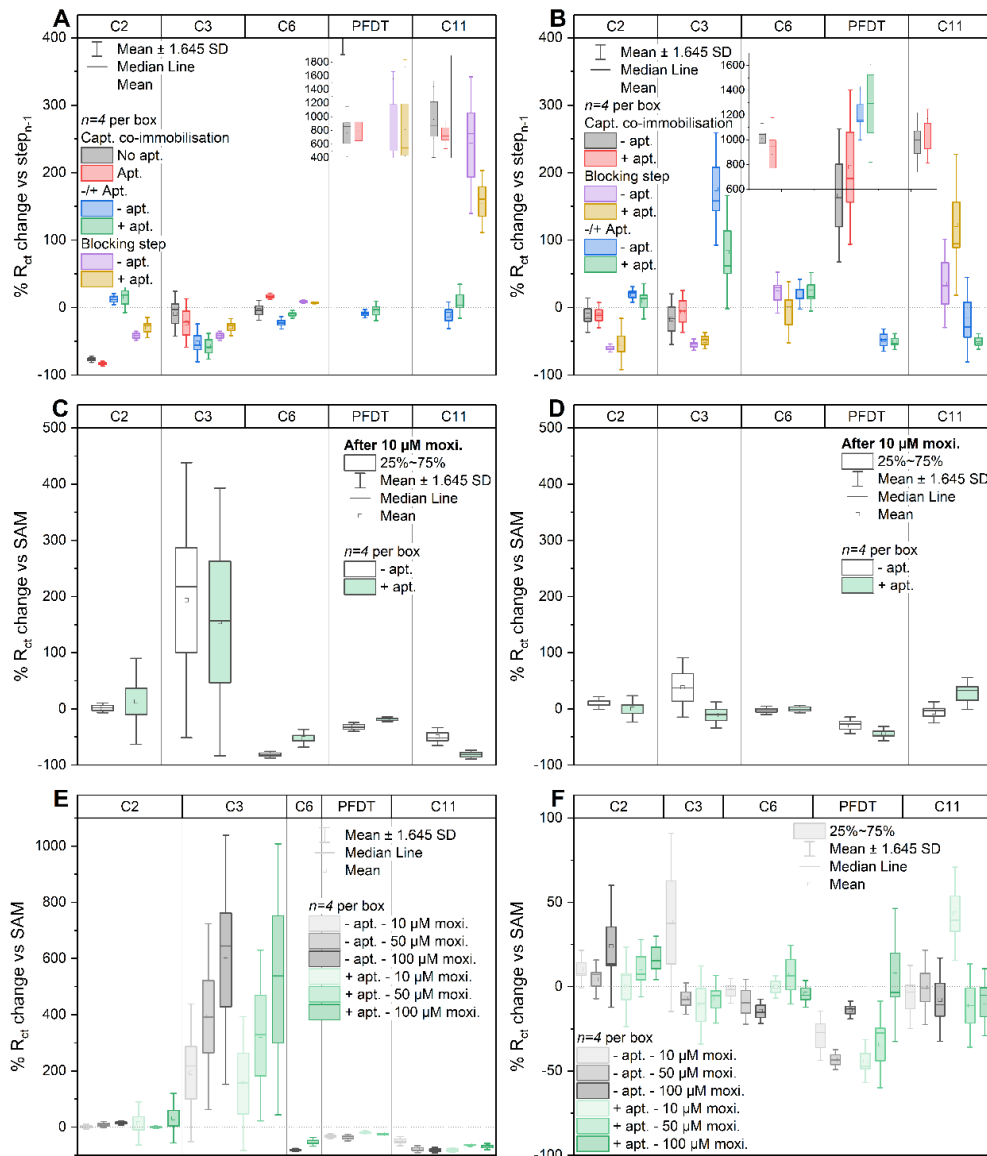
Figure 4.16. Optimisation of SAM composition and formation on Mx SPE in 5 mM of $[Fe(CN)_6]^{3-/4-}$ in aptamer buffer - Evolution of R_{ct} changes for SAM formation with aptamer hybridisation before (A) and after block (B); sensor performance after the first concentration of moxifloxacin with aptamer hybridisation before (C) and after block (D); sensor performance after a series of increasing concentrations with aptamer hybridisation before (E) and after block (F).

Table 4.7. R_{ct} change summary for SAM composition and formation. |-A|<|+A| translates to a greater signal change (absolute value) observed in presence than absence of aptamer or moxifloxacin. Trend across concentrations translates into a sustained increase or decrease for the concentrations tested and opposite trends refers to either a negative percentage for -A. and a positive change for +A. or vice versa.

Alkane-thiol	Hybridisation	Moxifloxacin			Trend across concentrations	Opposite trends for -A. and +A.
		10 µM	50 µM	100 µM		
C$_2$	Yes	Yes		Yes		
C$_2$			Yes		Yes	
C$_3$	Yes					
C$_3$			Yes		Yes	Yes |-A.|>0 & |+A.|<0
C$_6$						
C$_6$	Yes					
C$_6$	Yes					
PFDT					Yes	
PFDT	Yes	Yes			Yes	
C$_{11}$	Yes	Yes				
C$_{11}$	Yes	Yes	Yes	Yes	Yes	Yes |-A.|<0 & |+A.|>0

SAM formation in aqueous rather than ethanolic solutions results in more densely packed monolayers.[450] Shorter and longer alkanethiol choice compared to 6-mercaptohexan-1-ol were based on literature reports for 2-mercaptopropan-1-ol,[445,446] 6-mercaptohexan-1-ol,[445,452] PFDT[453] and 11-mercaptoundecanoic acid[454]. Monolayer end groups impact electrochemical signals and other possibilities could have been carboxyl-, sulfonate-, or amine as well as methyl-terminated alkanethiols, the latter enabling tightly packed SAMs with little defects.[450] Hexanethiol, the methyl-terminated version of 6-mercaptohexan-1-ol, has also shown increased stability when continuously interrogated, however more prone to fouling in biological fluids, and necessitating a mixed monolayer.[450]

To our knowledge and understanding of this system so far, aptamer sequences displacing from their support upon target recognition was best captured by decreasing R_{ct} trends (Table 4.7), which is why the 2-mercaptopropan-1-ol SAM, with aptamer hybridisation occurring last was the optimisation that was retained moving onwards. Moreover, three carbon monolayer yielded a maximal signal gain for Dauphin-Ducharme and Plaxco (2016) using aptamers binding aminoglycoside antibiotics.[455]

4.4.2.4 Striking the right balance between maximal probe packing and steric hindrance via optimisation of the probe:alkanethiol co-immobilisation ratio

Since 2-mercaptopropan-1-ol (MCP) is approximately half the size of the previously used MCH, 228 nM of the reduced support:alkanethiol ratio was reassessed. Lower ratios, namely 1:10, 1:25, 1:50[456] were compared against the 1:100 previously reported[232,456,457] and tested, immobilised on clean Mx SPE for an hour, to ensure the least steric hindrance and facilitate conformation change recording upon target recognition. The SAM was complete after aptamer hybridisation, hybridised to a 1:1 ratio regarding oligonucleotide support concentrations. Sensors were exposed to 10 μM moxifloxacin for 15 minutes.

Both duplex conditions, aptamer-free and hybridised, were located on the same chip with four replicates per condition. Before aptamer hybridisation (red, blue

and yellow boxes on Figure 4.17A), little difference between positive and negative conditions should be occurring. Maximal difference was therefore expected upon aptamer pairing to its support compared to a blank solution, which was the case for the 1:25 and 1:100 ratios. Among these two conditions, the average R_{ct} increase after aptamer hybridisation was respectively of 24.5% and 82.2 % for the 1:25 and 1:100 support:MCP ratio respectively and of -36.6 and +175.8% after blank at the corresponding step.
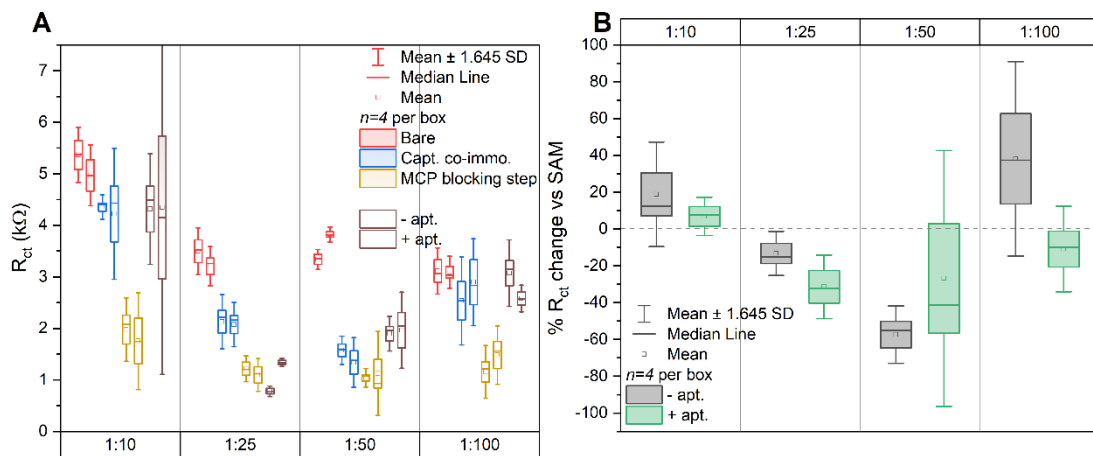
Figure 4.17. Comparison of R_{ct} values for various initial ratios of immobilised support strand to MCP and sensor performance after 10 μM moxifloxacin exposure (respectively A and B) on Mx SPE in 5 mM of $[Fe(CN)_6]^{3-/4-}$ in aptamer buffer.

When examining sensor performance, 1:10 and 1:50 ratios exhibited a lower performance after moxifloxacin exposure in presence compared to absence of aptamer (Figure 4.17B). For the 1:100 ratio, the decrease after target testing in presence (-10.9%) and increase in absence (+38.1%) of aptamer nevertheless displayed a less consequent change in presence of recognition probe compared to the 1:25 ratio (-31.4% against -13.3%).

Since the 1:25 condition testified through R_{ct} changes of successful aptamer hybridisation and target recognition, this was further used for sensor functionalisation. Ratios for co-immobilisation strategies of DNA sequences to alkanethiols vary,[420,447,458] and Keighley *et al.* (2008) reported the most optimal hybridisation for a 1:5 ratio,[447] close to the tested range for this section.

4.4.2.5 Assessing the effects of deposit evaporation and alkanethiol reduction prior block on aptamer hybridisation and sensor performance

Reproducibility of the 1:25 support:MCP results was assessed next along with the effect of TCEP reducing the alkanethiol prior surface blocking, ensuring immobilisation of single molecules onto gold and best SAM packing. Sensors were functionalised by oligonucleotide support and MCP co-immobilisation at a 1:25 ratio, followed by MCP block then aptamer hybridisation before being tested with moxifloxacin. Co-immobilised MCP was not reduced as its molecular weight is too close to TCEP and would have been filtered out. Furthermore, deposit volume was also compared for each condition between 2 µL, equivalent to a droplet per working electrode and 400 µL, providing an ample coverage of 8 working electrodes and minimising evaporation. Reduced and non-reduced SAM-forming alkanethiol conditions were run on different chips.

Bare R_{ct} values were all comprised between 2 and 5 kΩ, showing homogeneity in the cleaning method (Figure 4.18A). 400 µL deposits yielded a higher R_{ct} increase after aptamer hybridisation in presence of TCEP, possibly due to minimised evaporation and overall, more available molecules to bind the gold. The variability of responses between electrodes in terms of aptamer hybridisation was also more consequent, the least variability obtained by 2 µL deposits with SAMs containing reduced alkanethiols (Figure 4.18A). Upon moxifloxacin exposure, sensors all showed an increase in R_{ct} as seen in Table 4.6, respectively 32.6 and 57.3% for non-reduced and reduced MCP SAMs using 2 µL deposits and 87.5 and 76.6% using 400 µL deposits contrasting with the previously obtained decrease (Figure 4.16 and Figure 4.17). Regardless of R_{ct} trends upon aptamer hybridisation, moxifloxacin exposure yielded an increase in R_{ct} (Figure 4.18B). It is worth adding that due to the initial small change upon aptamer hybridisation for most of the chips of this figure only, an extra half hour incubation with a tenfold concentrated aptamer solution has been performed, against which percentage changes have been calculated.
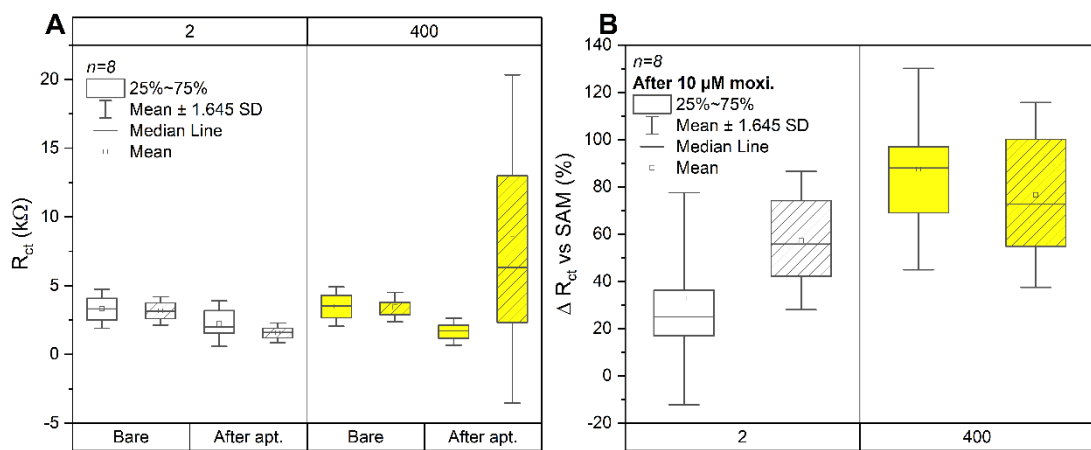
Figure 4.18. Effect of deposit volume and alkanethiol reduction (hashed) before block on aptamer hybridisation through R_{ct} values (A) and percentage changes after moxifloxacin exposure (B) on Mx SPE in 5 mM of $[Fe(CN)_6]^{3-/4-}$ in aptamer buffer.

TCEP and DTT reduce disulfide bonds between thiolated DNA, the sulfur group having a tendency to oxidise and dimerise in solution containing oxygen.[459] This allows control over orientation of oligonucleotides to be immobilised on gold surfaces.[459] As DTT contains a thiol group, it competes with reduced oligonucleotides for gold immobilisation and needs to be removed.[443] On the contrary, TCEP is devoid of sulfur groups and does not necessitate the additional separation step, hence its better suitability for gold biosensor applications.[443] The oxidation of TCEP occurs in a single step and irreversibly,[443] meaning there is an accumulation of the product that could interact non-specifically.

Using the 2 versus 400 μL deposits containing TCEP also contributed to prevent deterioration of the pseudo-reference electrode. Overall, the reduction of alkanethiol for SAM formation induced a more consequent signal change after moxifloxacin exposure (Figure 4.18B). Negative controls, either non-functional aptamer or monolayers without aptamer hybridised, to assess the specificity in moxifloxacin recognition were missing here, meaning conclusions are to be considered carefully.

4.4.2.6 Optimisation of the ionic strength conditions

Improving aptamer binding affinity in a biosensor format can take many forms including buffer, pH or temperature optimisation.[418] Different ionic buffer strengths were tested here to optimise aptamer hybridisation, functionality, stability and sensor

performance through target recognition. Concentrations of aptamer buffers tested ranged from five- and ten-fold more concentrated and diluted as well as 10 mM PBS diluted in molecular biology water. These were substituted in washes, solution dilutions as well as in the redox mediator background. Clean sensors were functionalised first with 228 nM support and MCP at a 1:25 ratio, further blocked with 1 mM of reduced MCP and 1:1 support:aptamer hybridised thereafter. Sensors were then exposed to 10 µM of moxifloxacin to assess performance. Positive and negative controls were ran on the same day on dedicated multiplexed screen-printed electrodes and different buffer dilutions on separate days.

Sensor performance neared 0% for the PBS and 5x aptamer buffer conditions, which was confirmed by little difference at the aptamer hybridisation step between aptamer and blank solution for these two conditions (Figure 4.19A). Despite an apparent difference at the probe hybridisation step for the twofold-diluted aptamer buffer condition, the previous step also showed a consequent differentiation when layers were at an identical stage. Bare R_{ct} values average at approximately 6,300 Ω and 10,560 Ω for the twentyfold buffer dilution chips to be respectively tested without and with aptamer. When normalised against R_{ct} of formed SAMs, sensors tested with the twofold aptamer buffer dilution do not provide a specific response to moxifloxacin (Figure 4.19B). Aptasensors functionalised with a background of 10x aptamer buffer performed better on aptamer hybridisation (253.5% vs 44.4% change in presence and absence of aptamer) compared to the tenfold dilution (141.4% and 52.6% change with and without aptamer hybridised) and moxifloxacin recognition with a p<0.001 versus p=0.043 between R_{ct} of the full and partial complex. Moreover, the magnitude of change resulting from the tenfold-diluted aptamer buffer provided more range for quantitative assessment of moxifloxacin than the tenfold buffer concentration for a consequent moxifloxacin level. As PBS yielded the smallest percentage change (8%) for the negative condition, it is then used forward as a background solution for moxifloxacin.
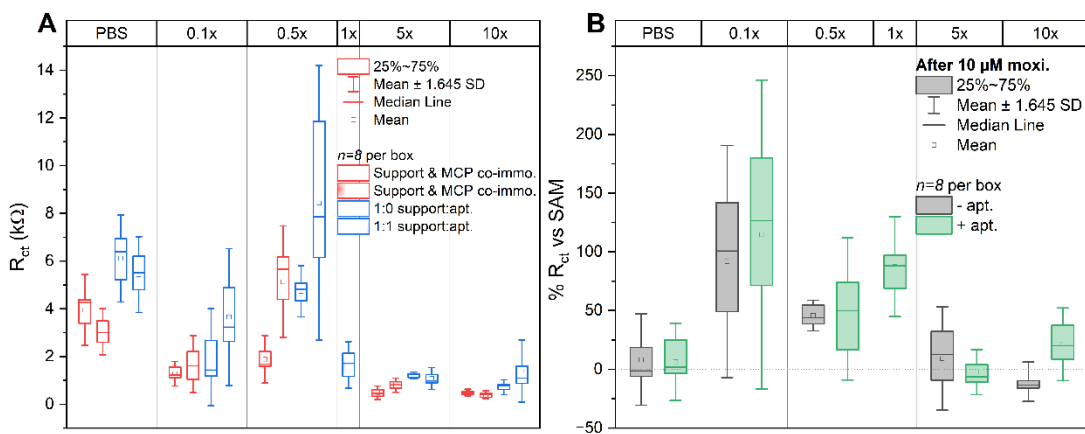
Figure 4.19. Comparison between buffer environments for aptamer hybridisation and moxifloxacin recognition through R_{ct} values (A) and changes (B) on Mx SPE in 5 mM of $[Fe(CN)_6]^{3-/4-}$.

Ionic strength influences redox mediator electrostatic interaction with the aptamer sequence.[409] Moreover, affinity for the target is driven by ionic strength as well as ions present in the sample.[460] For instance, concentrations of KH_2PO_4 above 0.4 M allow a reduction in electrostatic repulsion between DNA sequences.[461] The SELEX buffer was found optimal for measurements by other studies[232]. Divalent cations such as Mg^{2+} seem to be essential for aptamer functionality[420] according to Miodek *et al.* (2015) and can impact aptamer conformation, and consequently target interaction.[417,442] However, the signal-to-noise ratio was found to be the most significant with buffers where divalent cations were absent, such as $MgCl_2$ for Amor-Gutiérrez *et al.* (2020).[417] Moxifloxacin was diluted in a background of PBS as the aptamer buffer contained $MgCl_2$. This balanced out with destabilising the aptamer structure, shown to be intensified with divalent cations present in the buffer.[420]

4.4.2.7 Reviewing gold surface integrity

Before assessing the quantitative potential of the optimised layer, electrode cleaning was reassessed to guarantee a more precise recording of moxifloxacin recognition in presence of aptamer due to the possible access to a plasma asher. Moreover, the changes in R_{ct} trend for aptamer hybridisation and moxifloxacin recognition did not provide confidence in a robust recording of antibiotic binding by immobilised aptamers. Oxygen plasma cleaning for 62 s at 50% power[462] was therefore compared to 0.5 and 0.1 M H_2SO_4 CV cleaning for 20 scans.

Sensors were then functionalised identically as the procedure from the previous section. Due to supply availability, NAP-25 columns were replaced by NAP-5, allowing for overall lower reagent use. An attempt to enhance differentiation between presence and absence of aptamer was also tested by first exposing sensors to 10 mM PBS for 15 minutes followed by 10 µM of moxifloxacin in PBS for 15 minutes.

Prior aptamer hybridisation, SAM formation was similar across both sets of electrodes. Rct values post SAM formation averaged around 1000 Ω for the chip cleaned using the plasma asher whereas the one cleaned with sulfuric acid showed differences between the two groups of electrodes (Figure 4.20A). The O2 plasma treatment affected the hydrophobic coating present on screen-printed electrodes and made the 2 µL deposits merge and spread on the chip. Reference electrode coatings were also affected, and changes noticed visually throughout the duration of experiments. Aptamers have hybridised to their support more successfully on the plasma-treated chip (160.4% vs 2.3% change in presence and absence of aptamer respectively) compared to the sulfuric acid cleaned chip (40.2% vs 64.7% change in presence and absence of aptamer respectively) (Figure 4.20A). Between the absence and presence of aptamers when exposed to PBS, electrode responses were below 100% change for all conditions (Figure 4.20B). Variability in the system without aptamer after moxifloxacin exposure was lower for the oxygen plasma treated electrodes, and the opposite was true for the fully hybridised complex (Figure 4.20B).
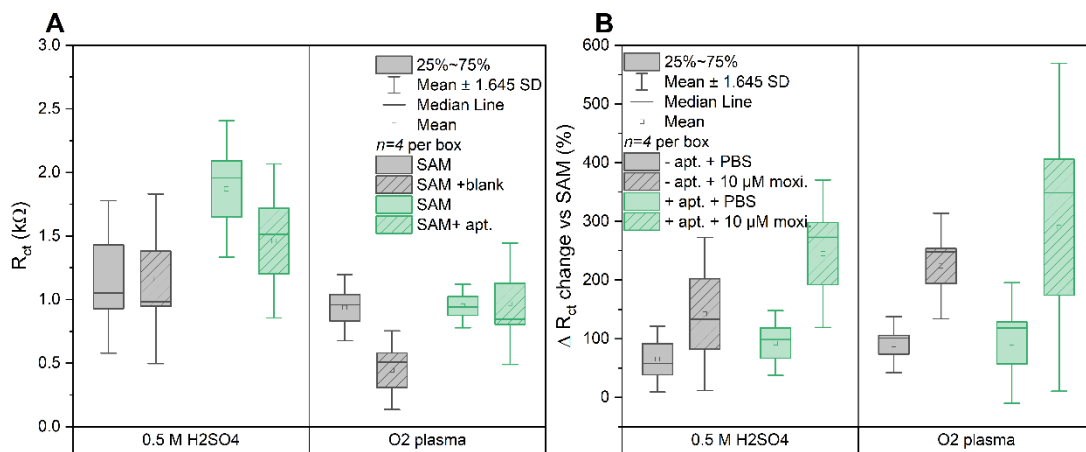
Figure 4.20. Comparison of 0.5 M H_2SO_4 and O_2 plasma cleaning through sensor functionalisation and performance using R_{ct} values (A) and percentage changes (B).

Overall, slightly higher percentage responses were recorded compared to the sulfuric acid cleaned chip for target recognition. Statistically significant differences were present between R_{ct} values mostly below $p<0.01$ and $p<0.001$ between conditions, however not discriminative enough between conditions for meaningful conclusions. The oxygen plasma method has been retained for its ease of use and speed, reverting to 400 µL deposits (Figure 4.18B) and one condition per chip to provide better differentiation between conditions. Overall R_{ct} increases dominated target recognition, even in absence of aptamer. Non-specific interactions and SAM reorganisation possibly dominated the signal change recorded rather than specific moxifloxacin binding. Longer stabilisation times might be required,[432] or a non-matching aptamer sequence hybridised to free support sites.[463] Another parameter that could impact the stability of the 2D and 3D aptamer structures is the heat treatment. Heat-treated aptamers were taken to room temperature for half an hour before hybridisation by Savory *et al.* (2010)[464] and Jolly *et al.* (2016)[465] for more stable aptamer structure instead of a cold shock, as per supplier recommendation here.

Table 4.8 summarises the conditions tested for layer optimisation and the R_{ct} magnitude of changes obtained, both for the positive and negative conditions, i.e. in presence and absence of aptamer. A R_{ct} decrease after target recognition was observed until the aptamer buffer dilution was chosen as the best ionic strength environment (Table 4.8).

Table 4.8. R_{ct} changes summary across layer optimisation parameters. |-A|<|+A| translates to a greater signal change (absolute value) observed in presence than absence of aptamer or moxifloxacin.

	µM of moxi.	|-A.|<|+A.|	Parameter
Figure 4.14B	100 µM moxi.		Overnight
Figure 4.14B	100 µM moxi.	**Yes**	1 h
Figure 4.17B	10 µM moxi.		1:10 support:MCP
Figure 4.17B	10 µM moxi.	**Yes**	1:25 support:MCP
	µM of moxi.	**|-A.|<|+A.|**	**Parameter**

Figure 4.17B	10 µM moxi.		1:50 support:MCP
Figure 4.17B	10 µM moxi.		1:100 support:MCP
Figure 4.20	10 µM moxi.		PBS
Figure 4.20	10 µM moxi.	**Yes**	Aptamer buffer 0.1x
Figure 4.20	10 µM moxi.		Aptamer buffer 0.5x
Figure 4.20	10 µM moxi.		Aptamer buffer 1x
Figure 4.20	10 µM moxi.		Aptamer buffer 5x
Figure 4.20	10 µM moxi.		Aptamer buffer 10x
Figure 4.21	10 µM moxi.		0.5 M H_2SO_4
Figure 4.21	10 µM moxi.	**Yes**	O_2 plasma

4.4.3 Assessing the quantitative response of the developed aptasensor

4.4.3.1 Concentration range from pM to M

Oxygen plasma treated Mx SPE were submitted to one cycle of 62 s at 50% power. Sensor functionalisation followed the previously described protocol of reducing the support with 10 mM TCEP for an hour, NAP-5 filtration, 1:25 MCP addition and co-immobilisation on electrodes for an hour. Surfaces were blocked for a subsequent hour with 1 mM MCP, previously reduced with 5 mM TCEP for 60 minutes. Heat-treated and cold-shocked aptamers were then hybridised to support oligonucleotides for an hour. With the full SAM, sensors were exposed to one moxifloxacin concentration diluted in PBS for 30 minutes. After each step, sensors were rinsed with tenfold-diluted aptamer buffer (3*500 µL) and electrochemically interrogated in 5 mM $[Fe(CN)_6]^{3-/4-}$ in a tenfold aptamer buffer dilution after a ten-minute stabilisation.

The first set of concentrations (dark squares - Figure 4.21) from 1 pM to 1 mM did not yield any clear-cutting quantitative trend. The best fit obtained, with a reduced X^2 of 0 and adjusted R^2 of 1 is pictured in Figure 4.20A and is represented by the equation below:

$$y = 40.91118 + \frac{(134.60138 - 40.91118)}{1 + (\frac{0.00374}{x})^{-0.59446}}$$
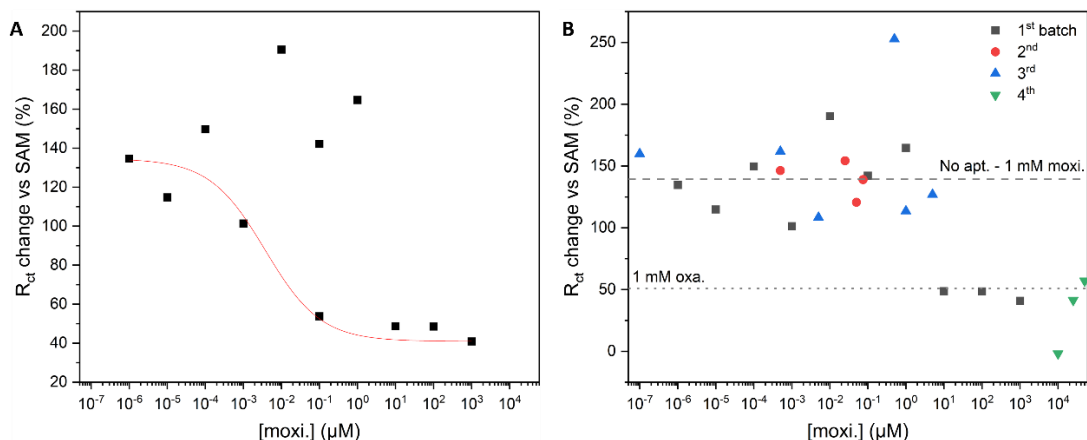
Figure 4.21. Evaluating the quantitative and reproducible sensor response. R_{ct} change against functionalised sensors after the first series of moxifloxacin concentrations (A) and after three more series for repeatability and range extension (B) including oxacillin control (dotted line) and 1 mM of moxifloxacin in absence of aptamer (dashed line). Each data point is the average of 8 replicates.

Most data points in the 0.1 nM to 0.1 µM range were not included in the fit, despite being located in the linear working range. Therefore, additional concentrations were tested (Figure 4.20B). The second set (red circles) attempted to refine the concentration interval where datapoints were located outside the fit. Since the yielded responses did not converge towards the initial fit, the further two attempts (blue and green triangles) widened the tested range, repeating certain concentrations for reproducibility across various chips but did not decipher for a clear quantitative trend. Consequently, recorded signal changes did not reflect specific and quantitative moxifloxacin recognition. A background of aptamer buffer rather than PBS might have been a former condition to go back to or a SAM component with a longer chain such as 1-undecanethiol (Figure 4.16) proving more stable but requiring longer experimental immobilisation/stabilisation, direct measurements in the sample solution (Figure 4.14). Observed changes might however have been the result of buffer variations, overpowering the sensitive EIS recording over the more subtle changes yielded by small molecule recognition. The size ratio between probe & target

for signal change might explain the difference between signal changes observed here and the spike aptamer for similar immobilised probe concentrations.[415,429,463]

4.4.3.2 Ensuring maximum oligonucleotide support site occupation by aptamer sequences

Since disparities between datasets have been observed (Figure 4.21), optimal complex formation was ensured by incubating 10, 25 and 50 times more aptamers. Reproducibility of the two higher concentrations was assessed once more on Mx SPE and PGE, where the most promising condition in presence of aptamer was compared to its homologue without aptamer. Sensors were functionalised with a 1:25 support:MCP ratio at 228 nM, blocked with 1 mM of reduced MCP and heat-treated aptamers hybridised at three concentrations, all for an hour. Aptasensor performance was then tested following a 30-minute incubation in 10 μM moxifloxacin in a background of PBS.

Instead of a 1:1 support:aptamer ratio (Figure 4.11, Figure 4.17) or 1:100 (Figure 4.15) at the hybridisation step, excess aptamer ratios were tested to ensure maximal signal change for the tested support concentration immobilised. Higher starting R_{ct} values for the second and third repeats compared with the first revealed chip variability (Figure 4.22), providing that even PGE reached a lower R_{ct} for repeat three (Figure 4.9A). The SAM layer homogenised surfaces after functionalisation (Figure 4.22B). Aptamer hybridisation from R_{ct} change was most successful for the 1:25 ratio of the second repeat with $p<0.001$ relative to the associated negative control without aptamer. However, this was not confirmed with target recognition, yielding a statistically significant difference for this condition only for the first repeat. Moxifloxacin recognition by the 1:50 support:aptamer ratio also produced a statistically significant difference respective to their corresponding negative control of $p<0.01$ (Figure 4.22C). These results highlighted the sensitivity of the system to chip and buffer variability, making it difficult to reproduce obtained trends and results but also the importance of running negative control conditions.
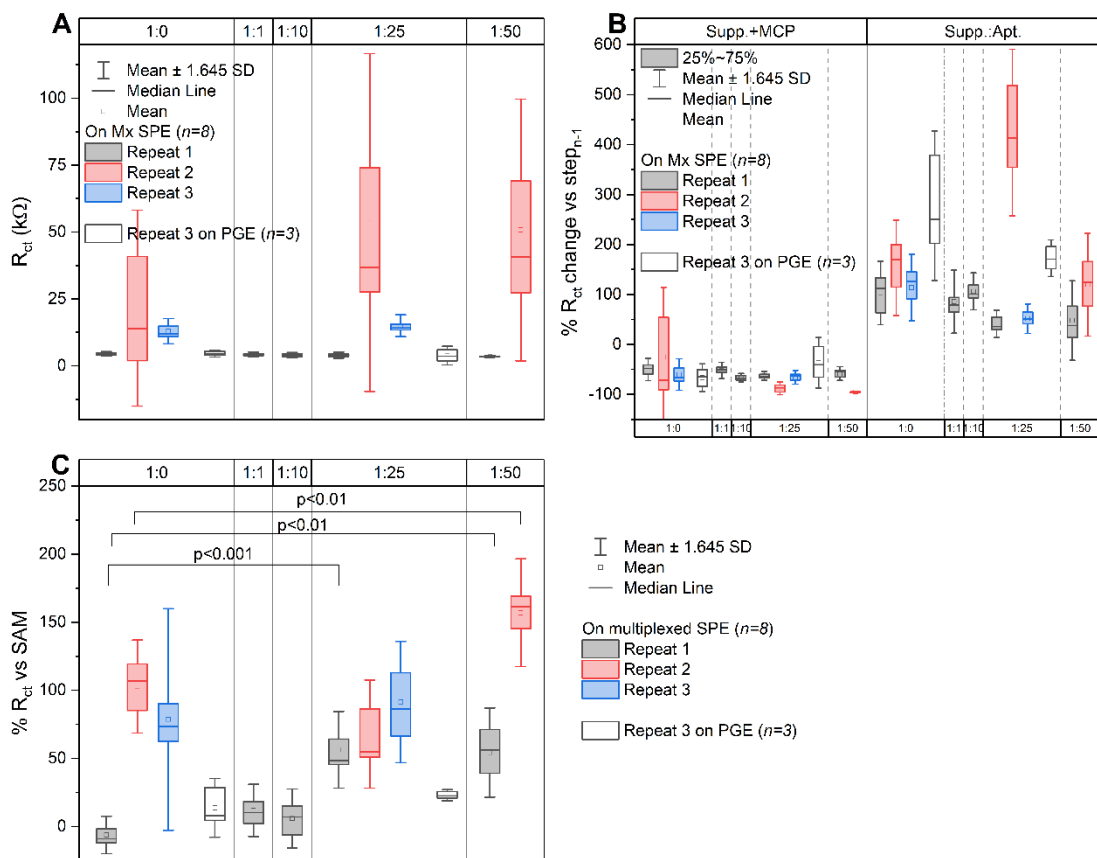
Figure 4.22. Ensuring maximal aptamer hybridisation for immobilised support. R_{ct} values of bare clean electrodes (A) and R_{ct} signal changes through signal changes against previous step for homogeneous layer formation and aptamer hybridisation (B) and after 10 µM moxifloxacin testing (C).

A better control for the non-recognising sequence would be a scrambled aptamer sequence hybridised to the support. However, since not in possession of the sequence, this was only supplied at the next batch received (Chapter 5). Since the support is much shorter than aptamers, SAM without aptamers are more sensitive to buffer changes as well as cyanide etching from the redox mediator.[432,463] Indeed, SAM defects are likely to create easier access to the gold surface for $[Fe(CN)_6]^{3-/4-}$.[451] Non-specific electrostatic interaction close to the electrode seemed to have dominated signal change and could explain the higher signal change for the control without aptamer (Figure 4.22C) rather than hybridised duplexes due to the presence of unreacted sites as Garrote *et al.* (2019) have highlighted.[463] Moreover, the system might have had needed much more stabilisation time in between rinses and buffer changes to get over SAM reorganisation phenomena.[432] Longer stabilisation times also mean that aptamer functional shape retention could have been compromised.

On a final note, aptamer buffer was made using Tris-Base. Even if the pH was adjusted, it might have tended to more basic condition and altered target recognition signal changes compared to Tris-HCl. Accurate and repeatable probe concentration on gold surfaces with efficient hybridisation was not reached and sensor performance could not be assessed quantitatively.

4.4.3.3 Ensuring optimal complex assembly

Since the response recorded between 0.1 pM and 50 mM did not yield a clear trend to allow for quantitative recognition of moxifloxacin (Figure 4.21), complex formation was verified using complex pre-assembly before immobilisation, and saturation of support available binding sites with the optimal 1:25 ratio of support:aptamer (Figure 4.22).

Pre-forming the support:aptamer complex prior co-immobilisation with mercaptopropanol did not generate the highest R_{ct}, as was expected,[451] when comparing functionalised electrodes after SAM formation (Figure 4.23A), most likely due to the observed effect of MCP consistently yielding a decrease in R_{ct}.(Figure 4.16A&B and Figure 4.17A). Moxifloxacin recognition, for a concentration located in the linear range of the fit (Figure 4.21A), showed a more consequent but more spread increase from the preformed complex. However, regardless of SAM assembly, R_{ct} percentage changes were slightly above but not significantly different from the condition without aptamer (119.1 % after moxifloxacin exposure without aptamer vs 378.5%, 182.2% and 190.5% respectively in the same order as Figure 4.23B). These findings confirmed that aptamer hybridisation for this support concentration occurred to its optimal level and yielded a consistent response after moxifloxacin exposure of the system in PBS.
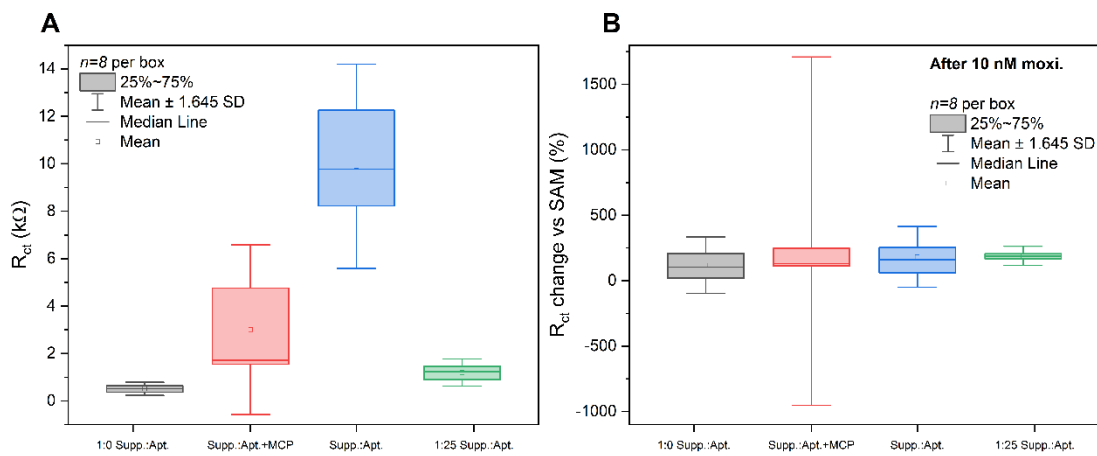
Figure 4.23. R_{ct} value comparison after SAM formation (A) and corresponding sensor performance of various layers composition and SAM assembly (B) after 10 nM of moxifloxacin with *n=8* per box.

4.4.3.4 Chip variability and ionic strength

Since inter-chip variability was observed in the previous section (Figure 4.22), gold surfaces functionalised with and without aptamers were tested on the same 8 working electrode chip once more. This enabled testing of the two most successful ionic strength conditions (Figure 4.19), a tenfold concentration and tenfold dilution of aptamer buffer with maximum hybridisation of support with aptamers at 25 times the support concentration (Figure 4.19).

If considering R_{ct} increasing as a reflection of aptamer hybridisation, it was slightly better in a tenfold-diluted (74.1%) rather than a tenfold-concentrated aptamer buffer environment (43.7%) when also considering a lower signal change in absence of aptamer (Figure 4.24B&D). Presence and absence of aptamer on the same chip (Figure 4.24B&D) did not allow for better differentiation at the target recognition stage between positive and negative conditions compared to dedicating one chip per tested condition (Figure 4.24C). Gold functionalisation enabled surface homogenisation at the SAM formation stage (Figure 4.24B&D), allowing a minimal impact of chip intervariability on signal change recording, but not enough to be conclusive on a differentiation between absence and presence of aptamer.
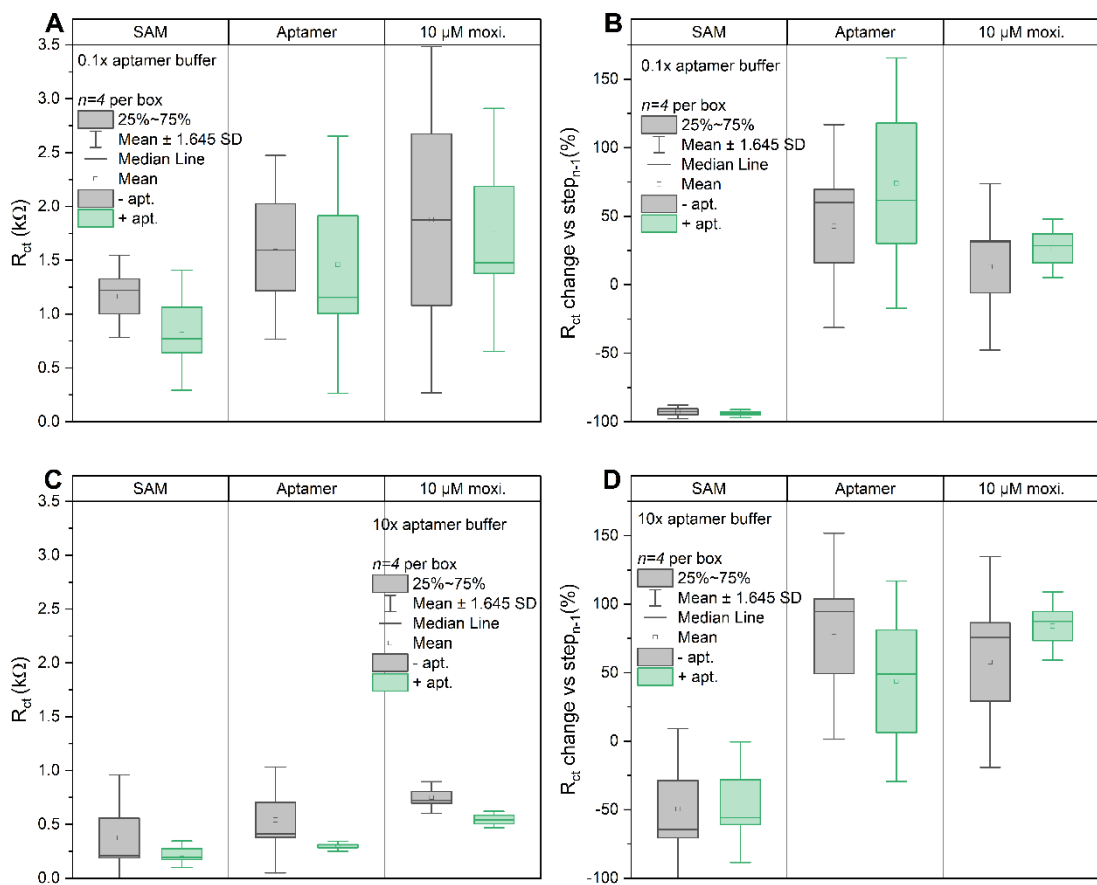
Figure 4.24. Aptamer buffer environment comparison and minimisation of chip intervariability through R_{ct} values (A&C) and corresponding percentage changes (B&D) using the 1:25 support:aptamer ratio for 0.1x (A&B) and 10x aptamer buffer (C&D).

4.4.3.5 Verification of probe packing and steric effects on target recognition

Since aptamer hybridisation occurred consistently and to its most optimal rate, complex concentration was studied to understand if aptamer support concentration and consequently aptamer concentration, were responsible for the absence of consistent quantitative recognition of moxifloxacin (Figure 4.21). Sensors were functionalised as in the above section, only with a tenfold-diluted support and aptamer complex.

Figure 4.25 allowed to compare sensors being functionalised with the 30 nM concentration of support and aptamer with sparser layers functionalised with 10 times less complexes. The signal change was 2.5 times lower with a denser layer, correlating most complex concentrations at a 1:100 aptamer:support ratio tested previously (Table 4.6), and the overall response from 8 working electrodes seemed

242

more consistent with smaller error bars than the lower complex concentration (Figure 4.25). Furthermore, sensor responses across those three concentrations appeared to follow a similar trend and increasing, which could mean non-specific interactions dominated the signal change observed, a lower moxifloxacin range was needed or the complex sequential hybridisation phenomenon did not yield the expected response.
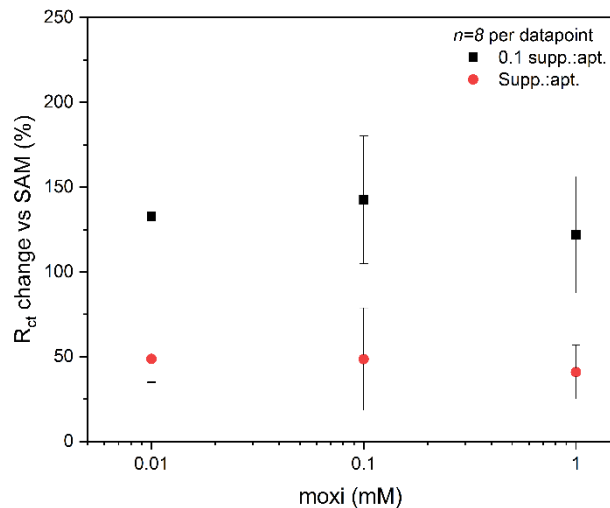
Figure 4.25. Sensor performance before and after moxifloxacin exposure for sparser and denser SAMs (respectively dark squares and red circles) through R_{ct} change with *n=8* behind each mean and error bars representing one standard deviation.

Miodek *et al.* (2015) mention the importance of aptamer concentration immobilised on the surface, higher values likely to cause steric hindrance resulting in R_{ct} change not directly proportional to target quantity.[420] Daprà *et al.* (2013) add that steric hindrance from the small sized antibiotics would not affect device sensitivity due to surface coverage and conformation change.[390]

The density of aptamers on the surface has been shown to affect signal gain as well as equilibration time. For an aptamer recognising a small molecule, White *et al.* (2008) reach a maximal density for 0.3 µM of aptamer, steric and negative charge repulsion likely responsible for this saturation phenomenon. [466] They showed that signal gain was maximal and equilibration time minimal (~10 minutes) for a lower probe density, correlating with earlier findings (Figure 4.13). Shorter equilibration times for lower packing aptamer densities were confirmed by Ricci *et al.* (2007).[467] They investigated more conductive SAMs as a better support for lower probe density

on the electrode surface by increasing the signalling current. However, signal gain with a C_3 compared to C_6 SAM is 20% lower.

Finally, using an Invitrogen Qubit 4 fluorometer, the concentration of reduced and filtered support oligonucleotide was checked for available datasets (Figure 4.26). This revealed that variability in observed signal changes also came from variability in immobilised support concentrations, due to the filtration process, and possible degradation from exonucleases.
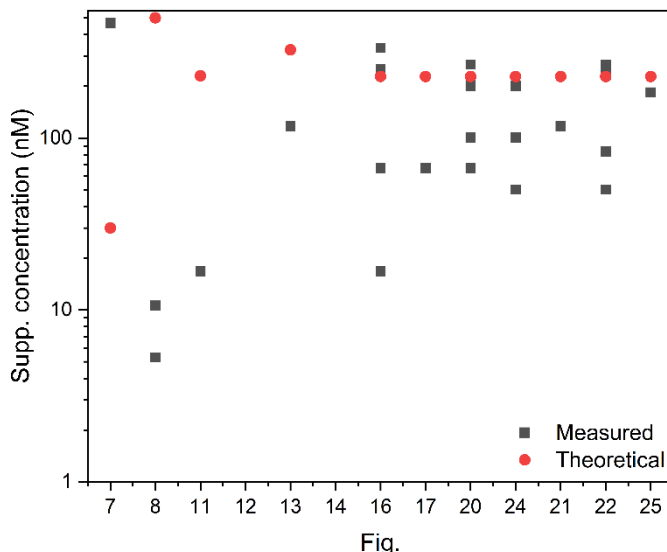
Figure 4.26. Calculated support concentration (red dots) vs measured concentrations (black squares) from Qubit reads of reduced and filtered oligonucleotide supports.

4.4.3.6 Gold surface cleanliness

In a non-cleanroom environment, gold surfaces are sensitive to surrounding contaminants, later impacting thiol binding.[430] Moreover, variability coming from the electrode production process also needs to be taken into account.[468] Therefore, available R_{ct} values obtained after gold surface cleaning, whether cycled in H_2SO_4 or O_2 plasma treated were compared across datasets from this chapter (Figure 4.27).
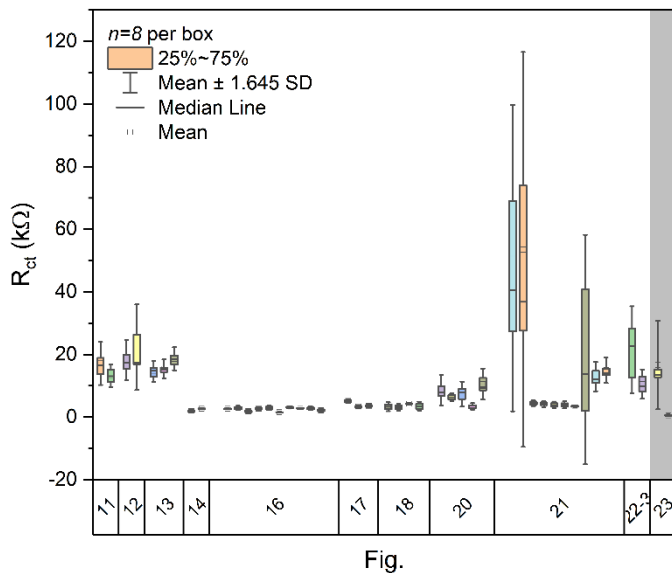
Figure 4.27. R_{ct} values of Mx SPE in 5 mM $[(FeCN)_6]^{3-/4-}$ after H_2SO_4 cleaning and plasma asher cleaning (grey band).

From repeat 2 of Figure 4.19, starting R_{ct} values average around 15 kΩ or above mostly (Figure 4.20A). The plasma asher treated electrode presented a starting R_{ct} on average close to 10 kΩ (Figure 4.20B), lower than the later sulfuric acid cleaned electrodes but not as low as obtained previously, on average below 5 kΩ. The manufacturing process might have had an influence on the starting R_{ct} as this matches the start of a newly ordered batch. Additionally, the O_2 plasma treatment affected the hydrophobicity of the surface and pipetting precisely 2 μL deposits onto each working electrodes without merging became very challenging.

4.5 Discussion

Aptamers selected for smaller molecules often have lower reported affinities than when specifically recognising molecules of bigger size.[415] This results in a smaller body of literature in the sensing sphere compared to aptasensors for the recognition of proteins. With the first reported electrochemical aptasensor dating back from 2004[469] and EIS use in a biosensing design following shortly after,[470] both labelled and label-free detection strategies are being employed. The redox properties of guanine are sometimes being taken advantage of to remove the need for sequence modification, which limit these sensors to single use and often give a weak signal. Therefore, labelling the aptamer sequence or using a soluble redox mediator, in our case $[Fe(CN)_6]^{3-/4-}$, is more often adopted for higher sensitivity of target recognition events, either based on hybridisation or change in conformation.

Immobilisation of the biorecognition element on or close to the electrode is also key to preserve its biological activity.[471] Among the most common immobilisation strategies for aptamers are physical adsorption by electrostatic interaction, covalent attachment by carbodiimide conjugation, affinity interaction using streptavidin and biotin[415] and chemisorption through thiol groups, the latter being a popular choice.[461,472] The aptamer is either directly modified with a thiol group and the remaining free gold surfaces blocked or attached to low-molecular weight linkers, such as cysteamine, 3-mercaptopropionic acid, Lomant's Reagent, or aromatic thiols for instance.[415]

TCEP and DTT are used to reduce disulfide bonds between thiolated DNA strands, the sulfur group having a tendency to oxidise and dimerise in oxygenated solutions.[459] This allows control over orientation of oligonucleotides to be immobilised on gold surfaces.[459] As DTT possesses a thiol group, it competes with reduced oligonucleotides for gold immobilisation and needs removal.[443] On the contrary, TCEP is devoid of sulfur groups, without the additional separation step required, hence its better suitability for gold biosensor applications.[443] The oxidation of TCEP occurs in a single step and irreversibly,[443] the product then accumulates and could interact non-specifically. The filtration step was maintained throughout the

trials to avoid any potential signal interference (Figure 4.26). In terms of costs and sensor preparation along with improving layer reproducibility, removing the filtration step is strongly considered.

Immobilisation on gold electrodes, following reduction of the oligonucleotide sequence, occurred in a self-assembled monolayer (SAM). SAMs on gold are reported easy to form and control, stable and reproducible[451] and allow to mimic the microenvironment of biological membranes.[473] They prevent non-specific adsorption from proteins on electrodes when testing complex samples[474] or introducing them *in vivo*[475]. Physisorption on gold resembles a disorganised ensemble with van der Waals interactions mostly dominating while chemisorption of the sulfur atom involves loss of hydrogen and binding to three gold atoms. The tilt of the bound chain by 20-40° is compensated by the alignment of molecules on the electrode via van der Waals, repellent, steric and electrostatic tail-tail interactions for ordered and orientated SAMs.[409] Contrarily to most reports, Inkpen *et al.* (2019) have demonstrated that chemisorbed thiols were not prevalent upon solution deposition on gold and physisorption prevailed,[476] which could explain the instability of monolayers formed throughout this study.

SAMs are most often composed of organosulfur compounds (alkanethiols) in pure or mixed layers.[472] Stable alkanethiol SAMs are tied to the cleanliness of the gold, which has proved inconsistent throughout this work (Figure 4.27). Mercaptohexanol (MCH) is commonly employed to space probes and passivate non-sensing regions while retaining permeability to electrons.[417,474,477,478] It also ensures upright orientation of aptamers through the complex sequential hybridisation of non-specifically adsorbed regions via multiple nitrogen atoms, for higher density and accessibility of the target to the binding region and better reproducibility of functionalised sensors. When simultaneously immobilised, aptamer and alkanethiol should reach an optimal density that is maximal in terms of sensitive detection but also allowing adequate folding of the oligonucleotide.[415] With an unknown sequence and 2D structure, determining optimal packing density and interpreting results becomes much more challenging,[479] which could be evidenced here.

MCH is also known to induce the formation of DNA islands.[409] Bigger alkanethiol end groups such as carboxylic acid or ferrocene reduce packing and order on the electrode surface.[409] A certain degree of disorder and missing molecules create heterogeneity and defects in SAMs as pinholes.[409] They can result from thiol desorption, often observed as the result of repeated electrochemical interrogation,[480] which is partly why solely impedance was used for SAM optimisation. Reorganisation within MCH-based SAM also influences recorded Nyquist plots and fitted R_{ct} values.[409] The hydrophilic character of MCH layers elevates their rate of desorption in aqueous media compared to hydrophobic 1-hexanethiol monolayers for instance, and accelerating signal loss.[449] All these have likely impacted recorded signals and calculated changes presented throughout this chapter.

Signal drift is another common challenge for electrochemical aptamer-based sensors.[443] This can be the result of biofouling or desorption of the SAM due to repetitive electrochemical interrogation as well as irreversible redox reaction of the reporter or DNA being degraded. In the work of Leung *et al.* (2021), the drift observed in the exponential phase results from the complex sample matrix and desorption of monolayer driving the complex sequential hybridisation of the redox-tagged DNA probe.[448] Normalisation of the electrochemical signal enables to correct for the observed drift. Moreover, the applied potential window can also affect the stability of the gold-thiol bond. Potentials below - 0.5 V induce reductive desorption while oxidative desorption takes place above 1 V, so narrowing the scanned potential window can therefore slow down desorption. Square wave frequency optimisation can also prevent signal loss. If the drift observed is induced by fouling, this can also be reverted in part with detergents and denaturants.

Monolayers composed of longer-chained molecules have shown to be more stable with a slower electron transfer. The opposite trend with shorter chains is equally true.[448] The choice of 3-mercapto-1-propanol over longer chain alkanethiols intended a recording of the antibiotic binding event from a size perspective with a less insulating layer.[481] In this case, a longer stabilisation time might have been favourable to the stability of the monolayer as over 24 h are recommended for shorter

alkanethiol chains.[409] This has been hinted in Figure 4.14 where ours, despite a statistically significant difference for moxifloxacin recognition after the hour stabilised SAM, the more significant signal in presence than absence of aptamer was obtained for the overnight SAM. Enhancing SAM stability has also been proposed through multi-dentate anchoring, cross-linking and hydrophobic thiols.[480] Inversion of signalling behaviour between MCH and hexanethiol monolayers during calibration[480] could explain the R_{ct} increase seen using a 1-undecanethiol, the longer chain being more hydrophobic, and advocate for this molecule as a more optimal SAM component for moxifloxacin recognition using this aptamer system.[450]

Appropriate characterisation of aptamer binding and carefully selected controls are essential to ensure observed binding is specific, which has been shown problematic in a variety of aptamer sequences reported.[481,482] Here, the signal changes recorded for non-specific target or in absence of recognition element were often more consequent in specific conditions. This could be due in part to the low concentrations of moxifloxacin tested, in regard to the aptamer K_D of 325 nM.[428] Instability from the support strand being loose and unstable compared to the anchor-aptamer complex could be another possibility, along with fluoroquinolones electrochemical activity[392] and non-specific interactions with either the support strand or SAM-forming molecules. Another possibility is oxacillin having a similar behaviour as unbound moxifloxacin, disturbing the SAM and playing a role in electron exchange. The full thiolated aptamer sequence, with the binding site theoretically closer to the electrode, might have provided better signal changes than the support and aptamer complex. Again, signal amplification through this method might be more successful for bigger size targets. The unknown sequence composition created a delay in obtaining a scrambled sequence from the supplier. Moreover, uncovering more binding site and interaction information could have been helpful to guide the SAM optimisation. A non-folded aptamer to block the free support sites was not a possibility since, it might not have bound the oligonucleotide support and the signal changes obtained were not clear enough to differentiate specific from non-specific target binding.

On deciphering which trend to expect from target recognition, Miodek *et al.* (2015) observed different R_{ct} trends depending on target concentration: increase in R_{ct} at low concentration and a decrease when higher concentrations are tested.[420] DNA probes are charged negatively. Depending on the charge of the target, the charge increases or decreases knowing that for proteins, it is case-dependent. Change in conformation from the bound complex between probe and target allowing a better ion permeability can also lead to lower R_{ct}. Both were observed through the course of optimisations in this study, with R_{ct} increases predominating later on.

Another important parameter for further testing is physiological temperatures for SAM formation and target exposure.[420] Temperature of the buffer might have had an impact when preparing solutions or used for rinses, as it was stored at 4°C and might not have been brought back to room temperature completely. Moreover, room temperature varies throughout the year. In addition, a more thorough examination of moxifloxacin incubation time might have maximised the signal-to-noise ratio, as longer durations were found optimal in other reports.[417,442]

The impact of using $[Fe(CN)_6]^{3-/4-}$ on gold as the redox mediator has also impacted signal recording. It can interact with aptamers via electrostatic interactions, bind in the grooves or intercalate.[409,483] Partial degradation of $[Fe(CN)_6]^{3-/4-}$ leads to CN^- anions, etching the gold electrode surface.[451] Increasing concentrations of $[Fe(CN)_6]^{3-/4-}$ seem to take over other reactions and increase layer packing.[451]

To ensure further and wider point-of-need applications, high signal-to-noise ratio and reproducibility have been prioritised for method optimisation along with statistically significant difference between positive and negative conditions where present.[407] As this was not observed consistently throughout the study quantitatively in a buffer environment, more complex and real samples have not been tested.

Reports of gold functionalisation strategies with aptasensors devoid of signal enhancement are rare for comparable size targets. An aptasensor using a complementary strand and exonuclease strategy to detect streptomycin has been reported with LoD values in the nanomolar region in complex samples thanks to cyclic

voltammetry monitoring.[484] Targeting kanamycin and using EIS, Zhou *et al.* reached nanomolar to millimolar working range in milk.[485] Obtaining a sub-nanomolar sensitivity to detect ciprofloxacin with EIS was possible using nanoparticles and carbon nanotubes, as reported by Hu *et al.* (2018).[486] Nevertheless, signal enhancement with micro or nanoelectrodes requires better signal sources as well as deoxygenated buffers.[461] Relying solely on aptamers as the detection probe can lead to high LoD and low selectivity. Combined approaches, using antibodies for instance, accompanied by a secondary reporter are being increasingly considered. Nanomaterials and nanoparticles with their large surface area, strong plasmon, and SAM convenient functionalisation provide a better signal-to-noise ratio with lower LoD and better selectivity.[415]

Aptamer selection is conducted by life scientists while aptamer-based assays are being developed by analytical scientists with a reduced number of aptamer sequences.[424] Szeitner *et al.* (2014) advised along with Zhu *et al.* (2023) that a selection process of the aptamers involving real samples to be targeted could fine-tune the sensitivity and affinity of final synthesised oligonucleotides.[424,487] Moreover, the detection of a specific unique target has not proven sufficient, and the benefit of multiplexed detection in a single run could benefit food analysis, disease diagnosis and environmental monitoring.[417] Assay integration with microfluidic and microelectronics enabling solutions at the point-of-care are the way forward for testing outside central laboratories.[415] Gaps between research at the academic level and commercial availability of these solutions remain omnipresent.[405] Therefore, collaboration at an earlier stage between aptamer producers and aptamer users could highly benefit the development of robust and sensitive commercial aptasensors for point-of-need use.[424]

4.6 Conclusion

Three functionalisation strategies for aptamers binding moxifloxacin were tested on polycrystalline gold electrodes, thin film gold electrodes and in-house designed 8 working electrode gold SPEs, locally produced. The latter format initiated promising recognition of the target antibiotic in aptamer buffer, allowing for greater number of replicates to be tested at once. The sequential hybridisation method, where the aptamer sequence was bound to an oligonucleotide support, immobilised onto the gold surface through a thiol group, showed the most encouraging response early on with potential for quantitative assessment of moxifloxacin compared to the thiolated aptamer alone or prehybridisation of the complex prior immobilisation on electrodes. DPV and EIS monitoring of SAM formation and sensor were undertaken, the impedimetric strategy performance being retained for further optimisation due to its sensitivity to surface processes. **The complex sequential hybridisation method on multiplexed gold SPEs allowed to test for reproducibility of functionalisation and moxifloxacin recognition using DPV and EIS.**

Complex density of 22.0 µM support:0.33 µM aptamer provided the best moxifloxacin recognition with a 1:100 aptamer:support ratio with DPV and R_{ct} trends matching and more consequent signal change upon moxifloxacin recognition by the matching aptamer. **An hour co-immobilisation of the support and alkanethiol** yielded **a more statistically significant response to micromolar levels of moxifloxacin** compared to an overnight stabilisation. Four **other SAM components** of various chain lengths and function instead of the typical six-carbon MCH were tested along with the prime aptamer hybridisation time, namely before or after surface blocking. **The most promising results based on generated signal change post antibiotic exposure were obtained with mercaptopropanol and 11-mercaptoundecanethiol**. Differentiation between absence and presence of aptamer binding sequence after the first moxifloxacin concentration seemed more promising at the time, with an increase in R_{ct} upon hybridisation and recorded decrease when sensors were interrogated with moxifloxacin. The initial 1:100 co-immobilisation ratio of support:MCP was reassessed due to the difference in chain length compared to MCH with lower amounts allowing

for more probe spacing. The **1:25 co-immobilisation ratio** enabled to maintain the R_{ct} decrease upon moxifloxacin recognition and a minimal response without aptamer. To ensure the best surface packing, **additional reduction of the SAM components was introduced prior surface blocking** and deposition volume optimised accordingly in further steps when necessary. Ionic strength of the background buffer for rinses, incubations and measurement solutions was tested with the l**owest ionic strength yielding the most consequent moxifloxacin response.** This was verified later on again and the lower ionic buffer strength provided a more beneficial aptamer hybridisation.

Quantitative assessment of the aptasensor response upon moxifloxacin recognition was tested and highlighted a non-specific response of the optimised system. This resulted from blanks and negative conditions displaying more consequent signal changes than positive conditions, without any statistically significant difference as well as high variability in recorded signal changes even within conditions in an experiment or between studies. **Inconsistency and difficulty to obtain reproducible trends have prevented the quantitative detection of moxifloxacin using chosen parameters.** Aptamer hybridisation was tested as only R_{ct} increases upon moxifloxacin exposure were observed. Functionalisation with a longer chain alkanethiol might have homogenised surfaces. Differences between calculated oligonucleotide concentrations and obtained readings have affected reproducibility of probe concentrations, possibly due to the filtration process or exonuclease degradation before immobilisation or hybridisation. Higher saturating concentrations proved more efficient and statistically different; however, reproducibility issues were made apparent. Integrity of the bare gold surfaces was also investigated and variability between production batches were uncovered.

Overall, R_{ct} changes from small molecule binding aptamers seemed to have been overtaken by non-specific interactions. Strategies to enable the behaviour of the aptamer sequence upon moxifloxacin binding would help to refine the most optimal environment for quantitative moxifloxacin detection, for instance through redox labelling of the aptamer sequence. Stabilisation of the aptamer conformation could also provide more reproducibility in the observed signal changes.

Chapter 5 Tracking a moxifloxacin aptamer behaviour through use of a redox-active tag and conformation stabilisation through a molecularly-imprinted matrix

5.1 Introduction

5.1.1. Improving electrochemical signal from electrode size and surface modification angles

Obtained signals in biosensors are proportional to probe loading. In the previous chapter, signal changes upon hybridisation did not provide clear differentiation between absence and presence of probe to inform on later sensor performance. As a result, many amplification strategies aim to increase the specific electrode area.[488] Enzyme-like nanomaterials are a popular strategy and satisfy the need of electrochemical biosensors for fast electron transfer between working electrode and biorecognition element.[489]

Carbon-based nanomaterials present good conductivity and the ability to complex with electron donor groups through charge transfer.[230] Carbon nanotubes (CNT) are rolled-up graphene sheets, with modifiable single or multiple walls, used to improve surface area and show good biocompatibility along with high mechanical strength and good chemical stability.[230,490] Zhou *et al.* (2012) have successfully detected tetracycline using multi-walled CNT (MWCNT) and aptamers on glassy carbon electrodes (GCE) in a linear range between 10 nM and 50 µM with a LoD of 5 nM.[491] With a larger surface area than single-walled CNT, graphene is composed of sp^2 hybridised carbon at an atom thickness.[230] Its properties include elasticity, high mechanical strength, thermal conductivity and little dispersion in aqueous environments.[230] Graphene possesses the ability to absorb unfolded aptamers via π-π stacking[230] and is a popular modification for aptasensors gathered in review publications.[492,493] Graphene oxide catalytic activity has even been reported as higher than the native horseradish peroxidase as well as more cost effective. Peroxidase-like activity also characterises single walled carbon nanotubes.[494] Among the five types of

nanoparticles (magnetic, metal, semiconductor, polymeric and hybrid), the metal and hybrid types are the most commonly utilised for electrochemical biosensing. The popularity of gold nanoparticles comes from the ability to covalently bond thiols while the use of platinum and palladium in conjunction with CNT improves electrocatalytic activity and conductivity.[230] Prussian blue nanoparticles possess the ability to scavenge oxygen reactive species towards peroxidase, catalase and superoxide dismutase activities while being biocompatible, biodegradable low-cost with control over shape and present good electrochemical activity.[494] Quantum dots (QD) are manufactured semiconductor nanomaterials generating bright colours upon light or electrical excitation.[230] Energy absorption or emission is dependent on their size.[230] They present low toxicity, high luminescence and narrow emission.[230] They can be used as a graphene sheet modification for instance.[230] MXenes have shown better performance in electron transfer, catalytic activity and absorption with lower interfacial resistance compared to graphene.[230] These 2D layered nanomaterials are composed of a transition metal and carbon or nitrogen and provide an efficient immobilisation medium.

Nano and micro-electrodes are another way to enhance signal-to-noise ratio as well as lowering required sample volume, the double layer capacitance and effects from the ohmic drop. Buffer deoxygenation is important to ensure the real amplitude of the observed phenomenon. Signal enhancement can also take the form of novel redox molecules or improving measurement procedures.[495]

5.1.2. Enhancing signal change via modification of the recognition probe

5.1.2.1. Redox labelling

Since aptamers are not intrinsically redox-active, redox activity can either come from an external mediator or a label. Labelled sensing approaches require additional preparation steps, translating into longer procedures with higher costs[496] and less scalability[494]. However, heightened sensitivity,[496] minimal cross-reactivity and interferences counterbalance these drawbacks, explaining why probe labelling is often used in electrochemical biosensors.[494] Lack of scalability and reproducibility,

however, slow down possible perspectives of commercialisation,[494] that have nevertheless been translated to *in vivo* preclinical studies.[497]

Attachment of the redox reporter to the aptamer sequence is of covalent nature and target recognition induces conformational changes affecting the spatial positioning of the tag towards the electrode.[497] When tagged with a redox label, the conformational change from the aptamer enables the redox tag to be brought closer or further from the electrode surface, magnifying the signal change (Figure 5.1).[230]
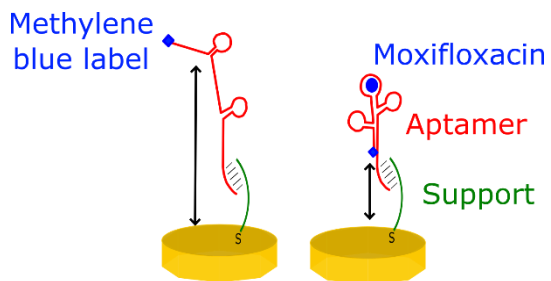
Figure 5.1. Impact of conformation change on electron transfer of redox-tagged aptamers immobilised on sensor surfaces upon moxifloxacin recognition.

Redox reporters are chosen based on their possible attachment to the aptamer sequence and electron transfer kinetics, usually between 1-1000 s^{-1}.[497]. Moreover, absence of reaction to oxygen and no dependency to pH are essential features.[498] Ferrocene and its derivates, ferrocyanide, methylene blue, benzoquinone and N-methyl phenazine are among the most reported labels.[498] Methylene blue and anthraquinone experience a reversible two-electron, one proton reaction respectively at - 0.26 and - 0.44 V against an Ag/AgCl reference. Ferrocene undergoes a one-electron exchange at 0.22 V vs Ag/AgCl and its oxidised state, ferrocenium easily reacts with chlorides found in the environment.[497] While potentials used for the detection of ferrocene are prone to damaging the electrodes, anthraquinone potential is found in a similar potential region as oxygen reduction on gold.[497] The stability of methylene blue electron transfer and its ideal reduction potential away from possible backgrounds reactions is the most employed tag, even though it is pH-sensitive.[497]

Sensor lifetime is tightly linked to the chemical stability of reporters either upon continuous interrogation but also in relevant complex matrices.[497] As most

reports focus on the methylene blue tag, this generates a bottleneck to translate into multiplexed detection.[497] An advantage of electrochemical aptamer-based (E-AB) sensors is the fast time-to-results that possibly enable real-time monitoring of target concentrations *in vivo.*[497] Enabling monitoring of drug and metabolite concentration simultaneously through decentralised diagnostics and multiplexed detection using redox-tagged aptamers could offer tailored drug dosing for instance while monitoring patients' response.

5.1.2.2. Increasing specificity to target through molecular imprinting

Improving sensitivity (true positives)[499] and selectivity (recognition of several analytes compared to specificity recognising only one analyte[500]) is central to the current challenges of PoC sensing, most importantly while keeping the solution design simple and at minimal costs.[498] Enzyme-like nanomaterials offer more stability than natural enzyme but do not compete yet for selectivity.[494] Artificial biorecognition elements support an extension of the overall possible detection portfolio with low costs and fast time-to-results.[230] Molecularly-imprinted Polymers (MIPs) are artificial bioreceptors with improved selectivity and specificity(true negatives),[494,499] making use of shape, size and functionality for target recognition.[501] They can be generally synthesised with monomers introduced to the template with crosslinking agents and form a complex once the polymerisation started around the imprint of a chosen target showing specific recognition.[494] MIPs can be obtained from potentially any template[494] and both interact via covalent or non-covalent bonds, such as hydrogen, ionic, hydrophobic or van der Waals interactions.[494] Pulse voltammetric methods (DPV, SWV) and EIS are commonly reported in MIPs biosensing.[501] Thermal, chemical, long-term stability and reusability are part of their advantages. Despite their attractive flexibility in terms of targets, MIPs have not yet delivered in the commercialised biosensing field.[494] Their low conductivity and electrochemical activity encouraged combinations with other materials such as CNT, carbon dots or graphene oxides for better stability and sensitivity.[494] To improve sensitivity, aptamer sequences can be included in the polymers for the detection of various size molecules as shown Figure 5.6.

Table 5.1. Electrochemical sensors using Apta-MIPs as biorecognition elements. Thiol modification at the 5' end of the aptamer sequence are indicated by SH-Apt. whereas a modification at the 3' end is written Apt.-SH. Abbreviations for electrode modifications comprise Glassy Carbon Electrodes (GCE), Graphene Oxide (GO), fullerene (C_{60}), Multi-Walled (MW) Carbon Nanotubes (CNT) and Nanoparticles (NP). Reproduced with permission and adapted from Ali, G. K.; Omer, K. M. Molecular Imprinted Polymer Combined with Aptamer (MIP-Aptamer) as a Hybrid Dual Recognition Element for Bio(Chemical) Sensing Applications. Review. *Talanta* 2022, *236*, 122878.[502]

Monomers for MIP	Aptamer (Apt.) nature	Electrode material/ modification	Measurement	Substrate	Linear range LoD	Ref.
Dopamine	SH-Apt.	Au	EIS	PSA	100 pg/mL-100 ng/mL 1 pg/mL	503
Dopamine	SH-Apt.	Au	FET	PSA	0.1 pg/mL-1 ng/mL 0.1 pg/mL	504
O-aminophenol	Carbon dot-tagged Apt.	GCE GO-AuNP	ECL	Lincomycin	5.0 pM-1.0 nM 0.16 pM	505
Dopamine	NH_2-Apt.	GCE AuNP@C_{60}	EIS	2,4,6-trinitrotoluene (TNT)	0.01 fM-1.5 μM 3.5 aM	506
N,N'-methylene diacrylamide + methacrylic acid	Apt.-SH	GO-AuNP on Au	DPV	Carbofuran	0.2–50 nM 67 pM	507
Dopamine	SH-Apt.	GCE AuNP	EIS	Tetracycline	0.5–100 pM and 1–1000 nM 144 fM	508

Monomers	Aptamer	Electrode material/modification	Measurement	Substrate	Linear Range LoD	Ref.
Dopamine	Apt.	MWCNT-Chitosan modified GCE	DPV	Hepatitis C virus core antigen	5.0 fg/mL-1.0 pg/mL 1.67 fg/mL	[509]
Resorcinol	NH$_2$-Apt.	3-ampy-GO on GCE AgNP	EIS	Chloramphenicol	1.0 pM-1.0 nM 0.3 pM	[510]
O-phenylenediamine	SH-Apt.	GCE GO-AuNP	DPV	Thrombin	2.5 pg/mL-1.3 ng/mL 0.16 pg/mL	[511]
Dopamine	SH-Apt.	AuNP/CNT/GCE	EIS	Urea	500 nM 900 fM	[512]
Pyrrole & TCEP	SH-Apt.	GCE GO-AuNP	DPV	Dopamine	50 nM– 10 µM 47 nM	[513]
O-phenylenediamine	SH-Apt.	AuNP/CO$_2$H-CNT/GCE	DPV&EIS	Histamine	0.46–35 nM and 0.35–35 nM 0.15 nM and 0.11 nM	[514]
N,N'-methylenebis acrylamide, methacrylic acid, methacrylamide	SH-Apt.	GCE GO-AuNP	DPV	Amyloid-β oligomers	5 pg mL– 1-10 ng/mL 1.22 pg/mL	[515]

5.2 Rationale, aims and objectives

The previous chapter on moxifloxacin detection using the complex sequential hybridisation of an aptamer sequence from its oligonucleotide support, mainly through the monitoring of R_{ct} with $[Fe(CN)_6]^{3-/4-}$ as a redox mediator has not proven successful in the quantitative detection of the fourth-generation fluoroquinolone. As the chosen signal amplification strategy explored in the chosen microenvironment, namely complex sequential hybridisation of the aptamer sequence upon moxifloxacin binding, has not led to conclusive results (Chapter 4), two other alternatives have been explored: labelling the moxifloxacin aptamer sequence with a redox-active group and stabilising the aptamer in its optimal binding conformation in a molecularly imprinted matrix for improved affinity.

1) Understand the behaviour of the moxifloxacin aptamer upon moxifloxacin binding via the presence of a methylene blue label on the 5'-end of the aptamer and,

2) Using AptaMIPs and NanoMIPs containing the moxifloxacin aptamer with a higher affinity than the aptamer sequence alone to detect moxifloxacin binding in buffer and bacterial culture.[428]

5.3 Moxifloxacin recognition with a methylene blue-labelled aptamer sequence

5.3.1 Material & Methods

Modified aptamer sequences specifications are presented in Table 5.2.

Table 5.2. Methylene blue-modified oligonucleotide specifications.

	Support (Supp.)	Aptamer (Apt.)	Scrambled Aptamer (Scr-Apt.)
Modification		5'-MB	5'-MB
Molecular weight (g/mol)	5432	20649.6	20649.6
Length	12	66	66

Methylene blue was incorporated as a phosphoramidite (Glen Research, 10-5961-02). The dye is not stable to conditions used in standard oligonucleotide

deprotection protocols, so ultramild conditions were used during the synthesis - i.e. ultramild amidites for A, G, and C nucleotides, phenoxyacetic anhydride for Cap A, and deprotection using 0.05 M potassium carbonate in methanol for 4 hours at room temperature.

Polycrystalline gold electrodes were polished in a 0.03 µM alumina slurry for 2 minutes, sonicated in water then rinsed and dried with argon. They were then immersed in a piranha bath (1:3 H_2O_2:H_2SO_4) for 15 minutes before being rinsed and dried once again with argon. Finally, electrodes were scanned from - 0.2 to 1.3 V with cyclic voltammetry in 0.1 M H_2SO_4 before a final rinse in H_2O and dried with argon.

Thiolated oligonucleotide supports were reduced in 1 mM TCEP, filtered through a NAP-5 column (17085301 Cytiva) and electrodes functionalised overnight with 15 nM or 1 µM of reduced supports at a 1:25 ratio with 2-mercaptopropan-1-ol (MCP). The following day, remaining surfaces were blocked with 1 mM MCP and methylene blue-tagged sequences hybridised to the oligonucleotide supports for an hour. Two types of sequences were tested: one binding moxifloxacin and a scrambled sequence, not binding specifically moxifloxacin. Functionalised sensors were incubated in PBS for 30 minutes and subsequently with 10 µM of moxifloxacin or oxacillin in PBS.

All steps were performed at room temperature. 50 µL of solution were incubated per working electrode, in a ventilated environment for steps involving thiolated molecules and in the dark because of the methylene blue tag light sensitivity.

Rinses after each incubation consisted of 3*500 µL of aptamer buffer (Chapter 4). All measurements were acquired in 10 mL of aptamer buffer against Pt counter and Ag/AgCl reference electrodes in a Faraday cage.

DPV parameters employed were the following: - 0.8 to 0.2 V at 0.1 V/s with a step of 0.01 V, a pulse of 0.025 V every 0.05 s. Concerning EIS, a frequency range of 0.1 Hz to 10 kHz was screened at 3.8 per decade with E_{ac} = 0.01 V, measured against OCP for 10 s.

Percentage changes were calculated according to the following formula where $X_{[conc.]}$ is the R_{ct} obtained after exposure of the sensor to a specified concentration and X_{SAM} the R_{ct} obtained after SAM formation: % R_{ct} change vs SAM $= 100 *$

$$\frac{X_{[conc.]} - X_{SAM}}{X_{SAM}}$$

Statistically significant differences were obtained by performing paired sample t-tests using Origin.

5.3.2 Results & Discussion

5.3.2.1 Overnight immobilisation of aptamers at high and low concentration for response characterisation

Figure 5.2 reports on the monitoring of DPV and R_{ct} using polycrystalline gold electrodes functionalised with the complex sequential hybridisation method (Figure 4.3) with 15 nM of thiolated oligonucleotide support and by extension, aptamers. Two types of sequences with a methylene blue tag located at the 5' end were hybridised for an hour to the support strand and MCP layer stabilised overnight: one denominated aptamer, selected for its ability to selectively bind moxifloxacin and one designated as scrambled, corresponding to the moxifloxacin-binding strand with the same nucleotides in a different order. The negative control condition was therefore improved, enabling a closer SAM to the selective aptamer compared to the oligonucleotide support alone used in the previous chapter.

The potential region for the methylene blue peak is commonly found around - 0.25 V using a similar electrochemical set-up.[498] The possible peak attributed to methylene blue here was found at - 0.4 V (Figure 5.2A and B). This would have to be confirmed by assessing methylene blue solutions with this specific electrochemical set-up. The presence of the peak after moxifloxacin exposure indicated the presence of the tagged sequence, meaning the complex sequential hybridisation has taken place but not been displaced. Moreover, the peak amplitude observed for the sequence binding moxifloxacin (Figure 5.2B) compared to the scrambled strand (Figure 5.2A) was more consequent, indicating a degree of specificity in moxifloxacin binding but also of non-specific interactions through a recorded methylene blue

current for the scrambled sequence (Figure 5.2A and B). A higher variability in R_{ct} signal change was recorded for the scrambled aptamer sequence compared to the moxifloxacin-binding layer, respectively 3,015% after PBS and 176% after moxifloxacin for the non-complementary strand and -13.8% after PBS and 52% after moxifloxacin for the complementary sequence (Figure 5.2), suggesting that non-specific interactions overtook the recorded signal.
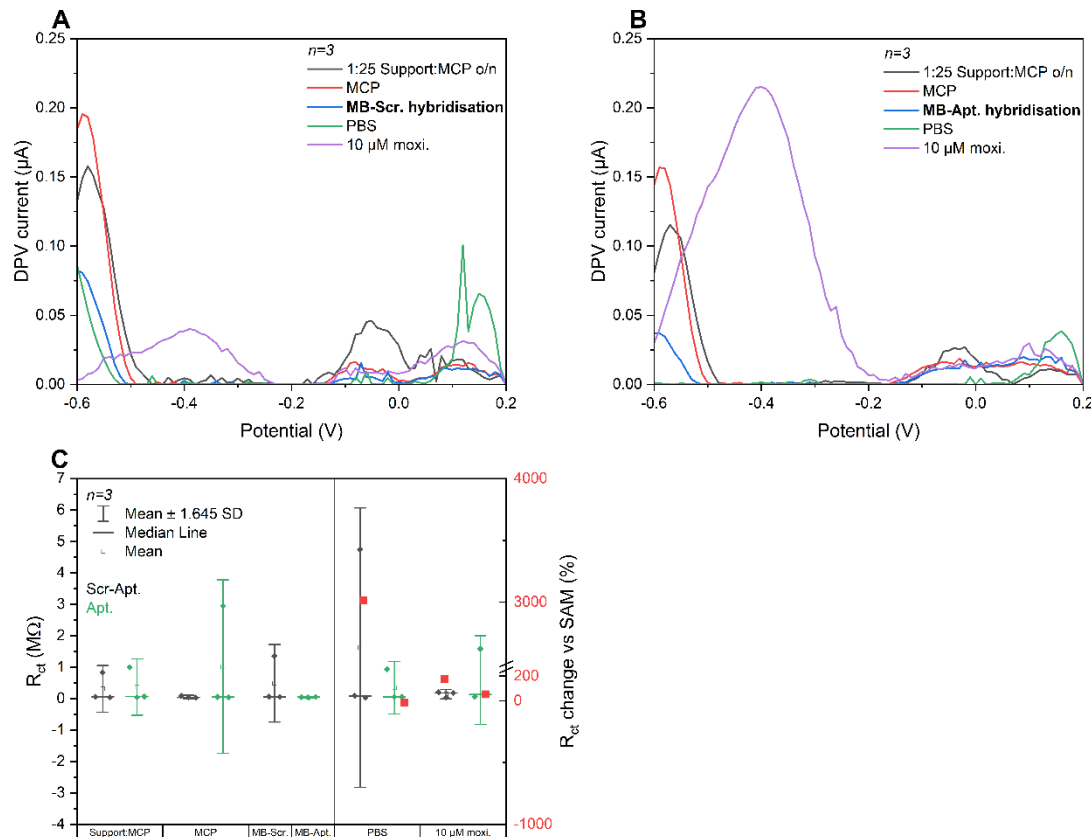
Figure 5.2. Responses of PGE functionalised with an overnight SAM and 15 nM of aptamer sequences in aptamer buffer. DPV of methylene-blue tagged scrambled (A) or moxifloxacin-binding (B) sequences along with R_{ct} values and changes (C) acquired against Pt counter and Ag/AgCl reference.

In order to ensure the recording of moxifloxacin binding events, a higher aptamer concentration was tested next at 1 µM and responses shown in Figure 5.3.
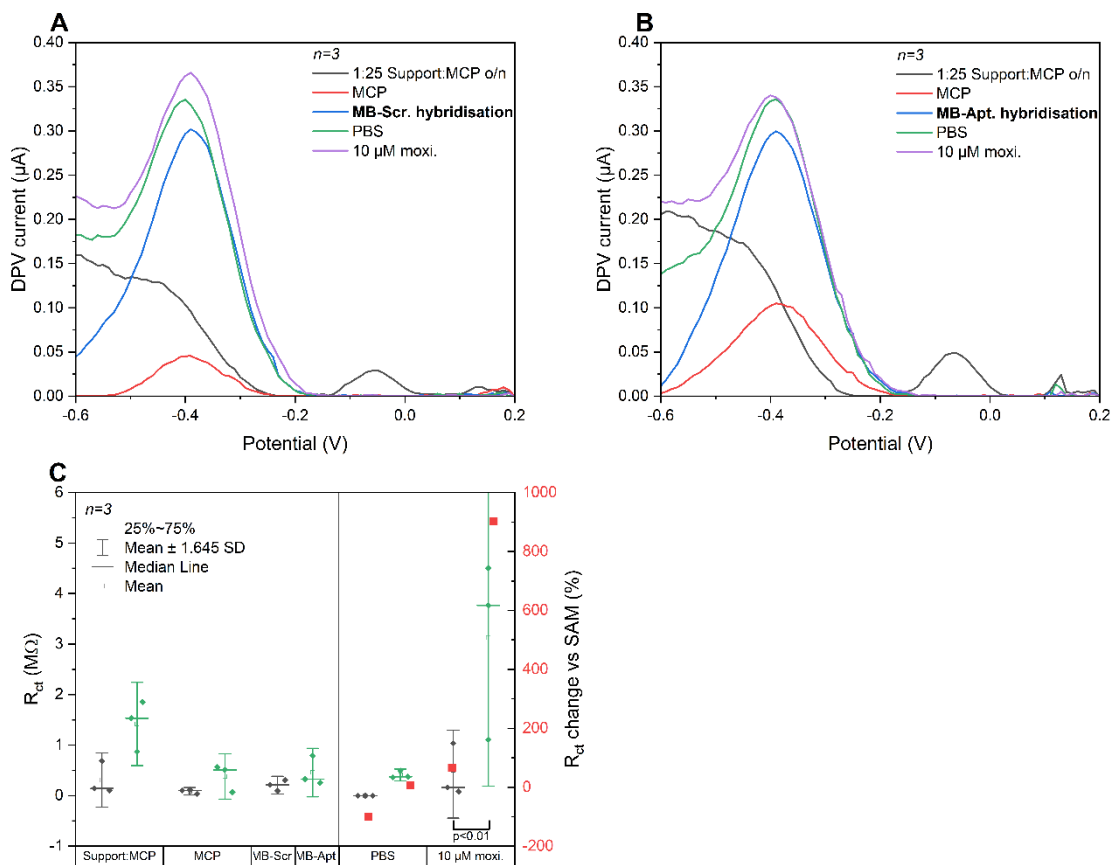
Figure 5.3. PGE functionalised with an overnight SAM and 1 µM of methylene-blue tagged scrambled or moxifloxacin-binding sequences. DPV traces (respectively A and B) along with R_{ct} values and changes (C) acquired for the moxifloxacin aptamer in green and scrambled sequence in black in aptamer buffer against Pt counter and Ag/AgCl reference.

Figure 5.3 reports on the monitoring of DPV and R_{ct} using polycrystalline gold electrodes functionalised with the complex sequential hybridisation method (Figure 4.3) with 1 µM of thiolated oligonucleotide support and by extension, aptamers. The MCP and oligonucleotide support layer was stabilised overnight and aptamers were subsequently hybridised for an hour to the support strand.

Peaks attributed to methylene blue were apparent at a consequent amplitude from the aptamer hybridisation step (Figure 5.3A and B) compared to the 15 nM aptamer functionalisation tested previously (Figure 5.2). The peak amplitude increase was higher from the PBS alone for both systems than after moxifloxacin exposure (Figure 5.3A and B). Stabilisation of the system in the different electrolyte composition and using PBS to rinse might have benefitted the recording of a more accurate baseline and signal change. Considering R_{ct} responses, moxifloxacin

exposure to the binding aptamer sequence yielded a statistically significant difference from the scrambled sequence, with low variability when testing a blank solution beforehand (Figure 5.3C). Optimisations for the aptamer microenvironment from the previous chapter with an overnight SAM stabilisation were able to provide an adequate recognition environment for moxifloxacin using R_{ct} but not DPV, at a higher immobilised aptamer concentration.[497] Both aptamer concentrations, 15 nM and 1 µM, were then immobilised only for an hour and DPV and R_{ct} responses assessed and compared.

5.3.2.2 Comparison with a low aptamer concentration immobilised over an hour

The DPV response from the one-hour SAM containing 15 nM methylene blue-tagged sequences showed little behaviour difference between moxifloxacin-binding and non-binding layers (Figure 5.4A and B). The non-specific signal change obtained from the scrambled strands after moxifloxacin were more consequent than for the binding sequences, with values closer to accumulated change from non-specific interactions resulting from PBS (Table 5.3). These trends were partly reflected in the R_{ct} behaviour with more consequent differences for the moxifloxacin-binding sequences upon PBS than moxifloxacin exposure (Figure 5.4C). However, scrambled sequences yielded R_{ct} changes closer to 0, correlating with expectations from a negative control. From these observations, 15 nM of aptamer sequences for an-hour long SAM immobilisation were not sufficient in yielding a specific moxifloxacin recognition response using DPV or EIS.

Testing a higher concentration of methylene-blue tagged aptamers with an hour SAM would have confirmed if a higher concentration of aptamers was required. High non-specific signal changes generated upon PBS exposure indicated that the aptamer buffer might have been a better background for moxifloxacin or rinses including a surfactant might have eliminated non-specific binding (Table 5.3).
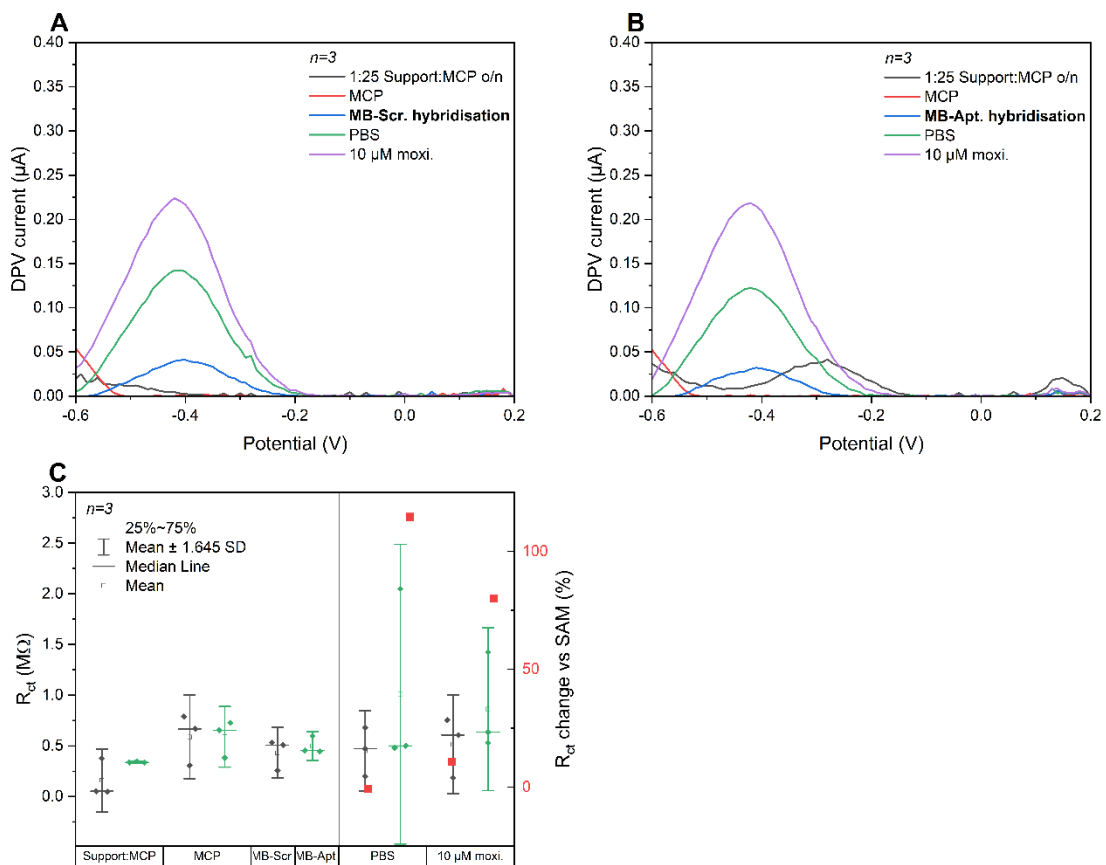
Figure 5.4. PGE functionalised with a 1-hour SAM and 15 nM of methylene-blue tagged scrambled or moxifloxacin-binding sequences. DPV traces (respectively A and B) along with R_{ct} values and changes (C) acquired in aptamer buffer against Pt counter and Ag/AgCl reference.

Table 5.3. DPV signal changes for overnight and one hour-long functionalisation of PGE with methylene blue-tagged, moxifloxacin-binding (Apt.) and non-binding (Scr.) sequences. Systems challenged with PBS blank solutions (-) and 10 μM moxifloxacin in a PBS background.

	Overnight				1 hour	
	15 nM		1 μM		15 nM	
	-	+	-	+	-	+
MB-Scr.	-	3,908.7	11.1	21.3	276.5	580.4
MB-Apt.	-	15,021.3	12.1	13.5	247.8	446.5

5.3.2.3 Repeatability of the layer showing the most significant moxifloxacin recognition

Finally, since the overnight 1 μM aptamer immobilisation yielded the best moxifloxacin recognition, the repeatability of these conditions was tested and reported in Figure 5.5. Recorded DPV peak amplitudes did not reach the same peak

heights as in Figure 5.3. PBS seemed to introduce more signal change than moxifloxacin, with -22.4% and 43.4% changes respectively for conditions corresponding to Figure 5.3A and Figure 5.3B, when at this stage, difference between layers had not been introduced. These changes were also more consequent than the previous attempt reported in Table 5.3. Upon oxacillin and moxifloxacin exposure, DPV changes were respectively of 8% and 24%, again higher than the previously recorded changes.

Considering R_{ct}, both layers formed showed a difference that was carried along most steps (Figure 5.5C). As R_{ct} changes obtained including all replicates did not reflect the overall observed trends from R_{ct} values, the main outlier for the sensors to be exposed to oxacillin was removed (dark squares in Figure 5.5D) to reveal an equivalent R_{ct} change for both layers after exposure to a blank PBS solution, of 35 and 30% for the oxacillin and moxifloxacin sensors. Exposure to moxifloxacin yielded a 14% change while the same amount of oxacillin resulted in a -0.6% R_{ct} change (Figure 5.5D), much lower than the statistically significant difference of 7% post PBS and 902% post 10 μM moxifloxacin obtained in Figure 5.3.
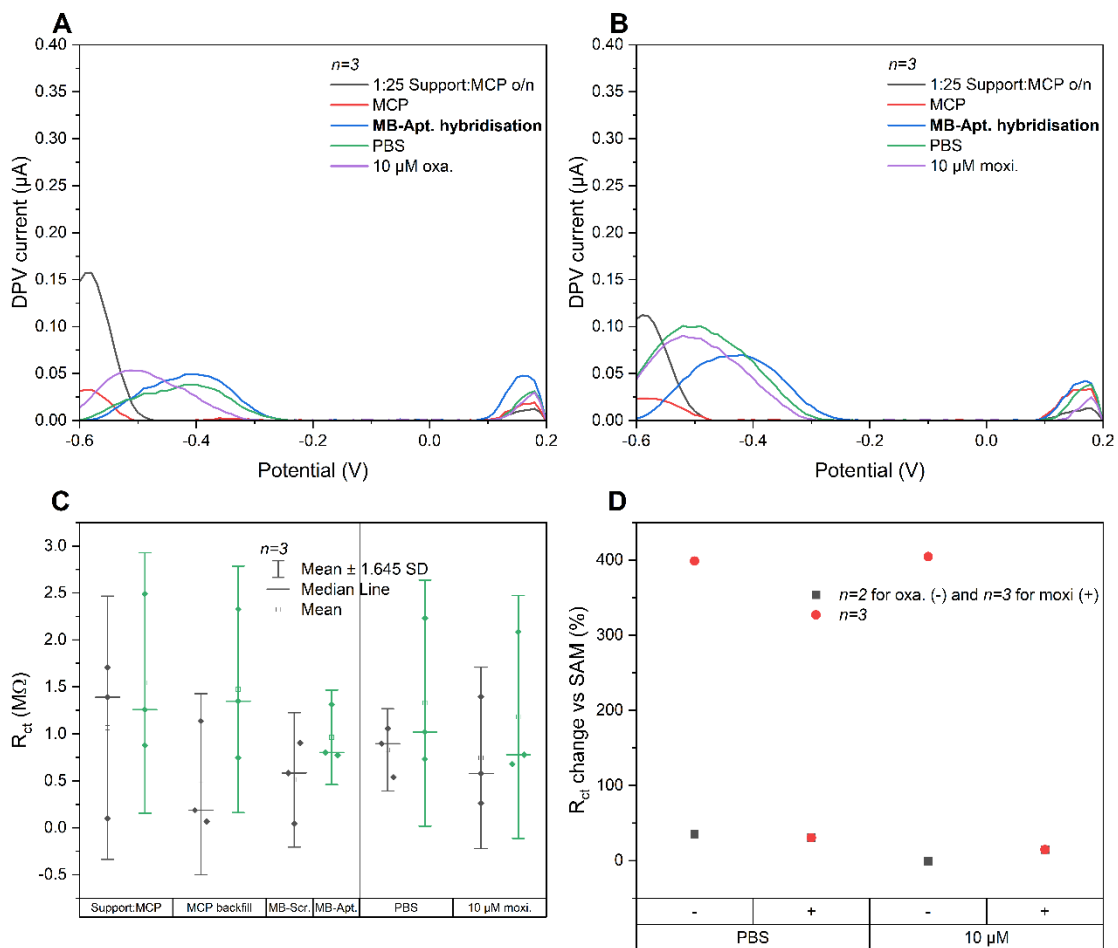
Figure 5.5. PGE functionalised with an overnight SAM and 1 μM of methylene-blue tagged moxifloxacin-binding sequences exposed to oxacillin or moxifloxacin. DPV traces (respectively A and B) along with R_{ct} values (C) and associated changes (D) acquired in aptamer buffer against Pt counter and Ag/AgCl reference.

5.3.3 Discussion & Conclusion

Compared to publications from the works of Plaxco,[497] 1 μM was above the more common 500 nM aptamer concentration immobilised on electrodes, while 15 nM below previous reports[516–518]. Differences in aptamer sequences, with spacers, a methylene blue tag at the 3' end instead of 5' end in our case and HPLC purified sequences[516–520] as well as an hour equilibration of prepared sensor to buffer prior use[517] are differences that contributed to their functionalisation and detection scheme working more consistently and sensitively. Their gold roughening protocol in decreasing concentrations of H_2SO_4, brought further with surface wrinkling, also maximised surface area and efficient probe packing.[520]

Voltammograms obtained in Figure 5.2-Figure 5.5 showed a peak at - 0.4 V instead of the reported - 0.25 V, located in the oxygen reduction region[521] which can result from exposed gold as a consequence of thiol desorption. In addition, the presence of the methylene blue at the 5' end of the aptamer sequence might affect the binding to the oligonucleotide support, with an average base number close to other reported aptamer lengths. Since the methylene blue-tagged sequences were over 40 base pair long, the conformation change occurred at a distance from the electrode where it was immobilised and might have impaired signal recording upon target recognition, taking into account the small size of the antibiotic target and the sensitivity of EIS to non-specific binding.[522]

Redox-tagged aptamer sensors, thanks to their consistent and characteristic signal, tend to be less affected by non-specific binding and repeated electrochemical interrogation, even in complex body fluids. A number of voltammetric methods can be employed, to report on target-binding events from the induced aptamer conformation change such as CV or SWV for instance, the latter even enabling the possibility of either signal-on or signal-off responses, depending on the frequency.[516,519] Faster measurements, reaching sub-second signal acquisition, are obtained using chronoamperometry[519] or intermittent pulse amperometry[517]. Thanks to the combination of an affinity recognition element with a redox reporter, reagent addition is not necessary and washing steps can be removed.[516]

The recorded methylene blue peak post moxifloxacin exposure indicated the non-displacement of the aptamer sequence upon target recognition. The methylene-blue tag on the aptamer sequence did not provide a consistent and reliable signal amplification solution to record repeatably moxifloxacin binding events using DPV and EIS in the chosen micro-environment. Further possible optimisations could come from the sequence purification, including a spacer, changing the position of the label or increase buffer equilibration time prior measurement.

5.4 Using a molecularly-imprinted polymer containing the moxifloxacin aptamer sequence to detect *A. baumannii* susceptibility to this antibiotic

An efficient strategy to improve aptamer stability, in terms of protection against nuclease degradation or thermal sensitivity is its inclusion in a molecularly-imprinted polymer matrix. By substituting a thymine with an equivalent nucleotide bearing a polymerisable group such as vinyl or acrylamide groups, the aptamer sequence is anchored into its most adequate structure to specifically bind its target.[428,523] Sullivan *et al.* (2021) kindly supplied their synthesised Apta- MIPs for moxifloxacin, that showed a 100-fold increase in affinity towards moxifloxacin compared to the aptamer alone, namely 3.65 against 325 nM, and the NanoMIPs without aptamers.[428]

The assay developed in this section targeted *Acinetobacter baumannii* antibiotic susceptibility. *Acinetobacter* species,[524] and more specifically *A. baumannii,*[525,526] have been reported for the past 20 years as a leading source of hospital-acquired infections such as meningitis, endocarditis, pneumonia, respiratory and urinary tract infections.[526,527] *A. baumannii* also appears on the WHO priority list of multidrug-resistant organisms[526] and on the Centre for Disease Control (CDC) urgent threat to public health[525]. The main practice for treatment relies on antibiotics, including fluoroquinolones,[524,526,527] to which *A. baumannii* is becoming increasingly resistant. Several resistance mechanisms have been reported, overexpression of efflux pumps being one.[526,528] If moxifloxacin penetrates *A. baumannii*'s membrane and does not get effluxed, there is less moxifloxacin available to bind for the Apta-MIPs added later on (Figure 5.6). If *A. baumannii* pumps out the antibiotic, then detection of Apta-MIPs binding moxifloxacin can be detected. If Apta-MIPs are present in the bacterial culture with moxifloxacin, growth of *A. baumannii* should be minimally impaired as moxifloxacin would bind to Apta-MIPs and would not be available to act on *A. baumannii*.
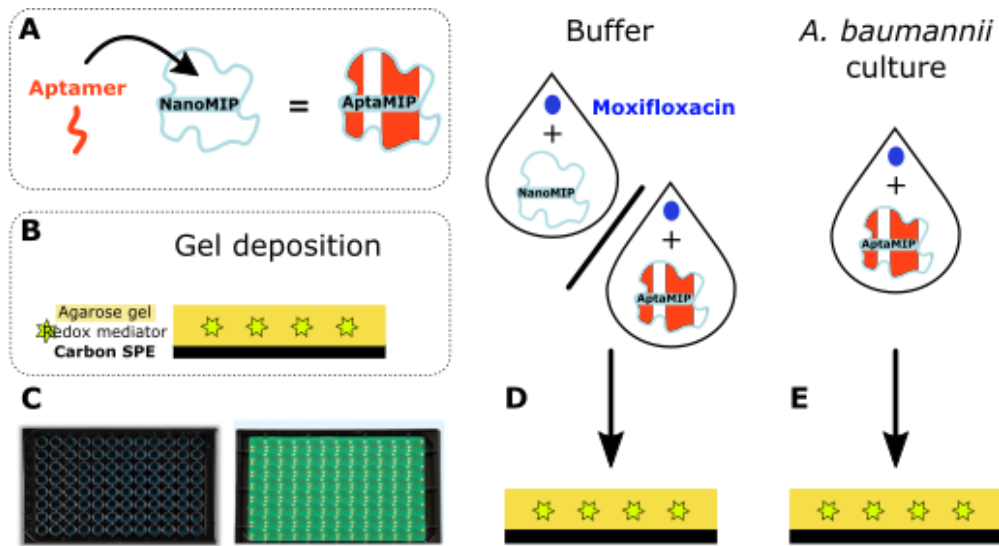
Figure 5.6. Summary of AptaMIP testing specific for moxifloxacin recognition. (A) Integration of the moxifloxacin aptamer sequence in the NanoMIP molecularly imprinted polymer matrix to obtain the AptaMIP. (B) Deposition of agarose gels on carbon screen-printed electrodes in a 96-well microtiter plate format (C - top and bottom view). Detection of moxifloxacin binding NanoMIPs or AptaMIPs in buffer (D) and *A. baumannii* inoculum (E).

5.4.1 Material & Methods

96-well plates with screen-printed carbon working and counter electrodes and Ag/AgCl reference electrodes (96X110 Metrohm) at the bottom were used with their dedicated connector (CONNECTOR96X Metrohm) through a multiplexer (MUX8-R2 Alvatek) to a PalmSens 4 (Alvatek) (Figure 5.7). Each well was cleaned with 10 to 20 scans of 20 mM NaCl using cyclic voltammetry at 0.5 V/s. Wells were then rinsed with deionised water and dried with argon or nitrogen. Electrodes were characterised with either 1 mM of $[Fe(CN)_6]^{3-/4-}$ or 1 mM of $[Ru(NH_3)_6]^{3+/2+}$ (262005 Sigma Aldrich) in 0.1 M KCl (A11662.0B Fisher), rinsed with deionised water and dried again with argon or nitrogen.
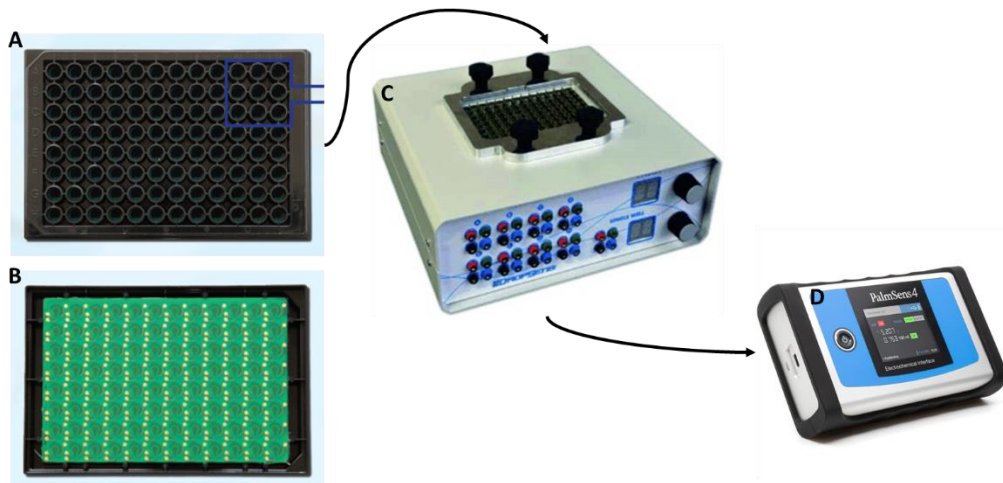
Figure 5.7 Experimental set-up using 96-well screen-printed carbon electrodes (A front and B back) linked to a box connector (C) leading to the potentiostat (D).

Gels were composed of 1% w/v agarose (A6877 Sigma Aldrich), KCl and 2.5 % w/v LB (L3522 Sigma Aldrich) in a water background, autoclaved with either 1 mM of $[Fe(CN)_6]^{3-/4-}$ ((10556412 and 10216460 Fisher scientific) or 1 mM of $[Ru(NH_3)_6]^{3+/2+}$ added and mixed right before deposition. 70 µL of gels were pipetted onto electrodes while still hot and liquid and left to solidify for a couple of minutes. Background DPV and EIS characterisations were undertaken to assess the quality of the deposits.

MIPs were solubilised in deionised water at 0.015 µg/mL and the moxifloxacin stock solution prepared in an aptamer buffer background and 0.22 µm filter-sterilised. Next, 70 µL of MIPs and moxifloxacin were deposited in each well to be tested and wells sealed.

For bacterial samples, *A. baumannii* was grown overnight in LB at 37°C under agitation. *A. baumannii* was tested at a final OD_{600} = 0.1, supplemented with moxifloxacin and/or Apta-MIPs diluted in LB. Wells were then sealed and placed at 37°C.

Additional gels deposited as backups had excess LB pipetted on to avoid drying (since located in the same plate and sealed).

DPV measurements were acquired in a suitable potential window for each redox mediator, namely [- 0.1; 0.7] V for $[Fe(CN)_6]^{3-/4-}$ and [- 0.5; 0.2]V for $[Ru(NH_3)_6]^{3+/2+}$; both at 0.1 V/s with a 10 mV step, 25 mV and 0.05 s pulse. For EIS, E_{ac}

272

was set at 0.01 V, and 20 frequencies between 0.1 and 10,000 Hz scanned against OCP. Statistically significant differences and percentage changes were obtained following 5.3.1 . in the previous section.

After bacterial samples and gels were discarded, the plate was rinsed with 70% ethanol, dried and placed under UV for 15 minutes to be sterilised and reused.

5.4.2 Results & Discussion

5.4.2.1 AptaMIPs and NanoMIPs binding of moxifloxacin recording on $[Fe(CN)_6]^{3-/4-}$ gel-modified carbon SPEs

Building on work published by Hannah *et al.* (2019, 2020)[244,259] and Domingo-Roca *et al.* (2022)[529], a 96-well plate format with carbon screen-printed carbon electrodes at the bottom was used. Gels containing bacterial culture medium and redox mediator were dropcasted on the bottom of the well and once solid, the binding of either NanoMIPs or Apta-MIPs to moxifloxacin was monitored in aptamer buffer and then in bacterial culture (Figure 5.6).

The first trials were undertaken at room temperature and intended to assess the possibility of a quantitative electrochemical signal reflective of MIPs binding moxifloxacin. From Sullivan *et al.* (2021), AptaMIPs presented a higher binding affinity than NanoMIPs to moxifloxacin, due to the integration of the aptamer sequence providing a supplementary affinity dimension to the molecularly-imprinted polymer. Dissolution of the dry AptaMIPs and NanoMIPs occurred in aptamer buffer under prolonged sonication and they were both used at a concentration of 0.015 µg/mL, which was the dilution at which the solution was clear and MIPs appeared in solution. MIPs and moxifloxacin solutions were mixed right before deposition on gel-modified electrodes and interactions monitored every 15 minutes, as this was close to the duration of performing a DPV and EIS measurement for 8 wells from a single column. Figure 5.8 shows DPV responses and Figure 5.9, R_{ct} values from fitting circuits to EIS responses thanks to a modified Randles' circuit. All values presented are normalised against the initial value obtained right after gel deposition and solidification, as these showed variability resulting from manual pipetting.

DPV peak current mainly decreased over the 45-minute monitoring, regardless of conditions. Apta-MIPs exposed to 5 nM of moxifloxacin facilitated electron exchange compared to the bare gel as evidenced by the only DPV increase whereas most other concentrations with Apta-MIPs or NanoMIPs led to lowering peak intensities. After 45 minutes, a plateau was discernible for all moxifloxacin concentrations with Apta-MIPs thanks to their second order fits (Table B. 7.9).

Apta-MIPs with 5 nM of moxifloxacin showed more positive DPV changes than each component alone (Figure 5.8A). The change was less consequent than 50 nM of moxifloxacin alone but more than Apta-MIPs on their own for Apta-MIPs with 50 nM of moxifloxacin (Figure 5.8C) and more consequent in the negative range with 500 nM of moxifloxacin (Figure 5.8E). These trends were similar using NanoMIPs, however at a smaller order of magnitude (Figure 5.8B, D, F). These observations converged as a confirmation of the higher affinity of Apta-MIPs to moxifloxacin compared to NanoMIPs.
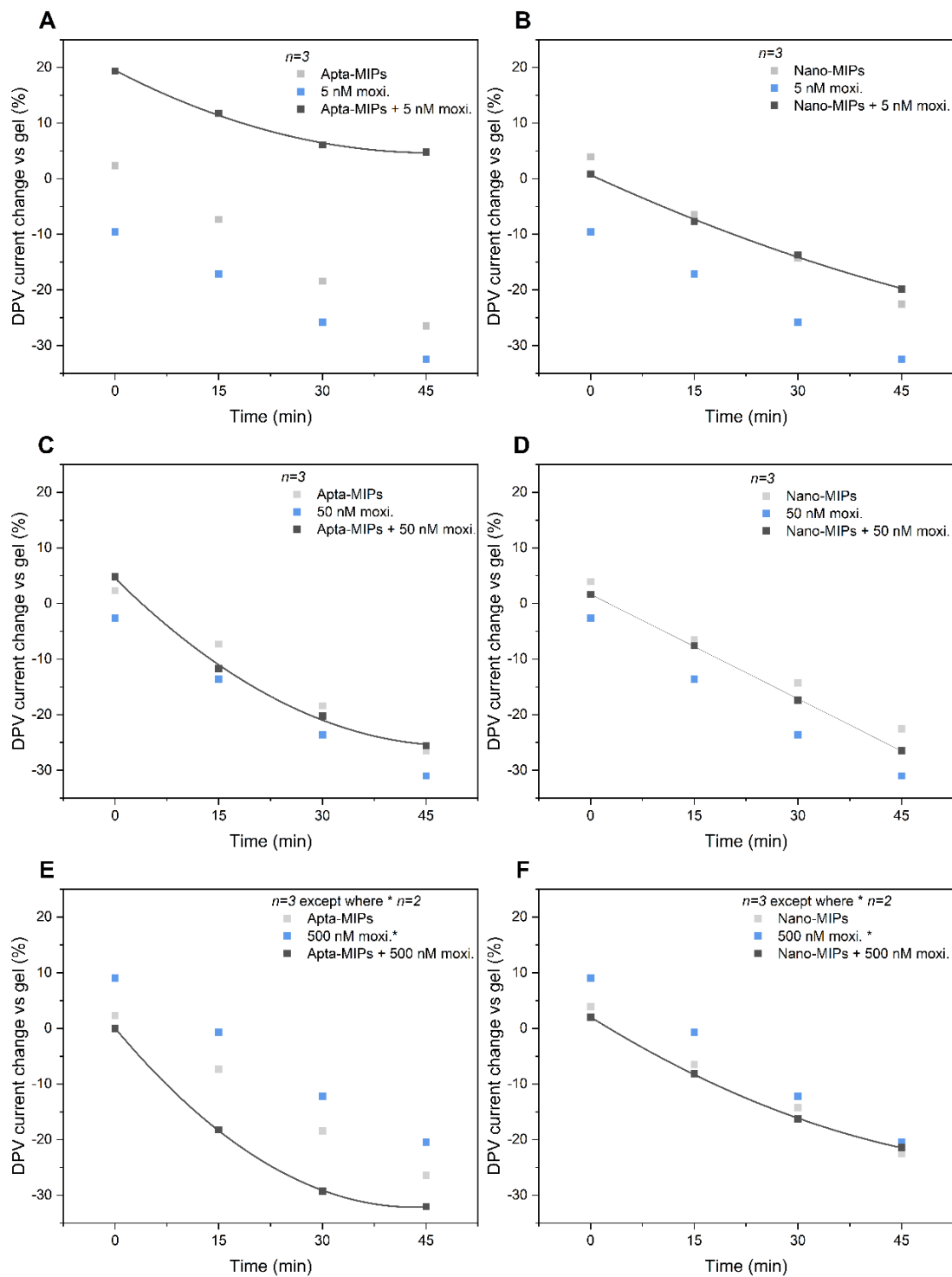
Figure 5.8. DPV monitoring on 1 mM [Fe(CN)$_6$]$^{3-/4-}$ gel-modified carbon SPEs of 0.015 µg/mL Apta-MIPs or NanoMIPs binding 5, 50 and 500 nM of moxifloxacin (A, C, E and B, D, F).

Concerning R$_{ct}$ monitoring, an overall increasing trend over the monitored duration was recorded for AptaMIPs and moxifloxacin (Figure 5.9A-C-E). Apta-MIPs with moxifloxacin displayed a more positive change than their separate conditions,

with a range of recorded percentage changes decreasing with increasing moxifloxacin concentrations. NanoMIPs did not display notable differences between moxifloxacin concentrations with close to constant trends, however always more consequent than their individual controls (Figure 5.9B-D-F). Additionally, datapoints seemed to gather around a fit more closely in the case of Apta-MIPs at higher moxifloxacin concentrations (Figure 5.9A-C-E and Table B. 7.9, Table B. 7.10 and Table B. 7.11).
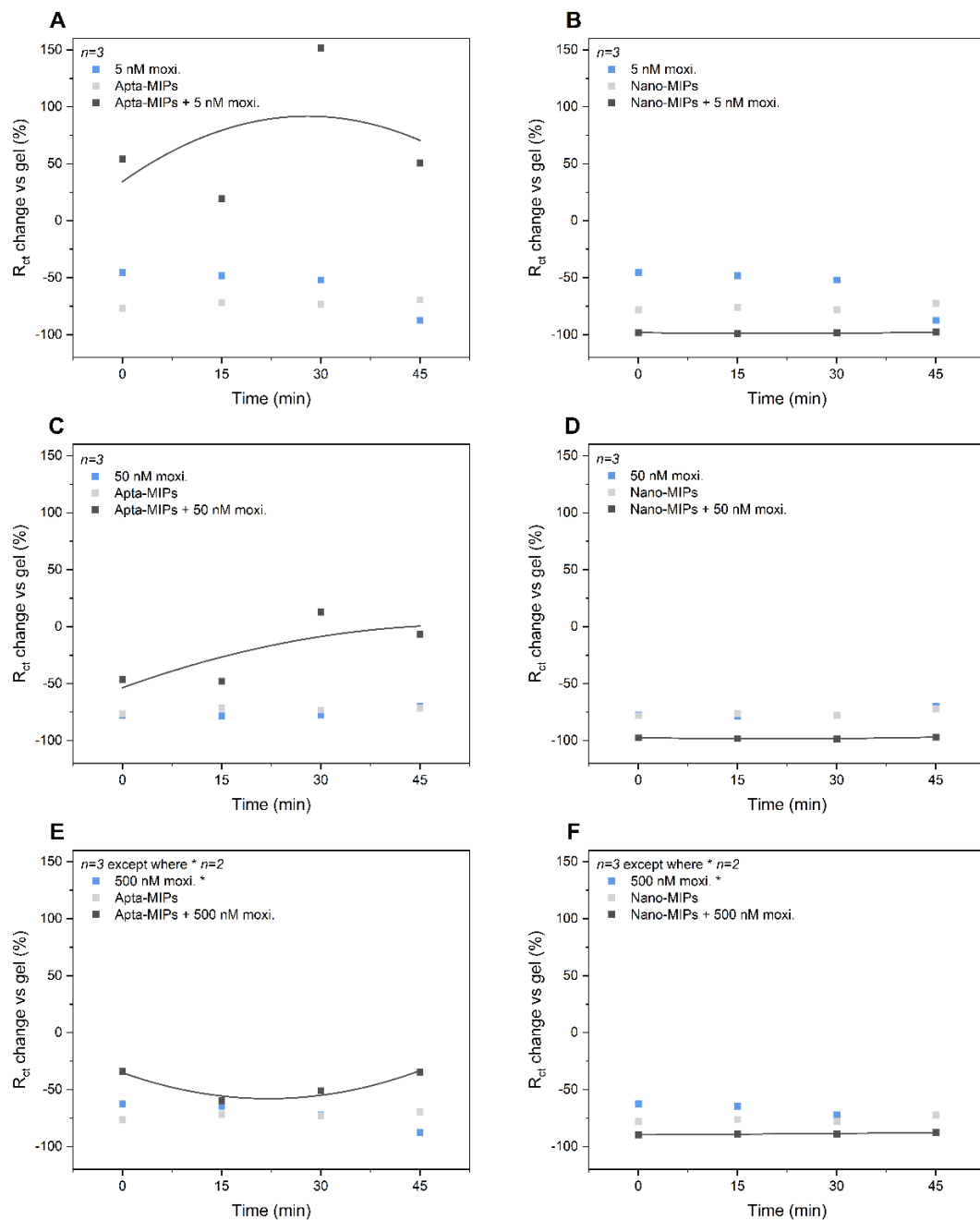
Figure 5.9. R_{ct} monitoring on 1 mM $[Fe(CN)_6]^{3-/4-}$ gel-modified carbon SPEs of 0.015 µg/mL Apta-MIPs or NanoMIPs binding 5, 50 and 500 nM of moxifloxacin (A, C, E and B, D, F).

The higher affinity of AptaMIPs for moxifloxacin was confirmed through R_{ct} monitoring as well as DPV with better differentiations between moxifloxacin concentrations compared to NanoMIP performance. Additionally, it is possible that unbound moxifloxacin impacted the recorded electron exchanges by penetrating gels. Calibration of the system for both polymers over a wider range of antibiotic concentrations would be beneficial for later susceptibility assessment, along with carrying it in LB rather than aptamer buffer and at bacterial growth temperature for more accurate comparison. Longer monitoring times could enable the confirmation of the existing plateau and equilibrium being reached between MIPs and moxifloxacin (Figure 5.9). This time interval aimed at being close to *A. baumannii* doubling time, the chosen microorganism to be tested based on conclusions obtained from results shown in Chapter 5 Appendices (B.II).

5.4.2.2 Evidencing bacterial growth differentiation on [Fe(CN)6]3-/4- gel-modified electrodes

A. baumannii cultures were tested at a final concentration of OD_{600} = 0.1 to match the MIC assessment (Chapter 5 Appendices (B.II)). The chosen moxifloxacin concentration was set at 0.1 µM (0.04 µg/mL) to match the order of magnitude of available data from earlier calibration, despite it being undertaken at room temperature instead of 37°C at the time. 70 µL of *A. baumannii* with or without moxifloxacin were deposited on gel-modified electrodes, either containing 1 mM of $[Fe(CN)_6]^{3-/4-}$ or $[Ru(NH_3)_6]^{3+/2+}$.

Figure 5.10B confirmed the ability to detect a difference in *A. baumannii* growth, impacted by the presence of 0.1 µM moxifloxacin, using R_{ct} on $[Fe(CN)_6]^{3-/4-}$ gels over the course of multiple doubling times, ranging from 20 to 40 minutes for one replication.[530] Longer monitoring times might be required to record a more notable difference using the DPV peak current, as the last datapoints at 120 minutes started to dissociate (Figure 5.12A).
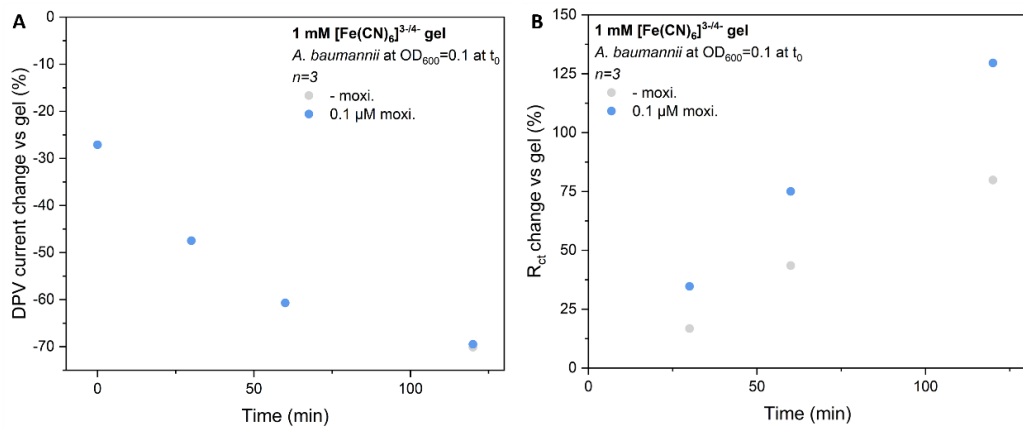
Figure 5.10. *A. baumannii* growth monitoring via DPV (A) and R_{ct} (B) on 1 mM $[Fe(CN)_6]^{3-/4-}$ -gel modified carbon SPEs.

5.4.2.3 Impact of repeated interrogation in relation to deposit volume and redox mediator choice

As longer monitoring times were to be further implemented, stability of the redox mediator signal in relation to the electrode material and previous reports[529] were conducted. 1 mM of $[Fe(CN)_6]^{3-/4-}$ or $[Ru(NH_3)_6]^{3+/2+}$ were compared.

$[Ru(NH_3)_6]^{3+/2+}$-loaded gels exhibited more stability than $[Fe(CN)_6]^{3-/4-}$ deposits (Figure 5.11). Testing more concentrations of redox mediators, mainly higher ones could also help in stabilising the $[Fe(CN)_6]^{3-/4-}$ signal across time using an excess but risking hindering small signal changes. The importance of freshly made gels and avoiding reheating that could deteriorate redox mediators is to keep in mind. It is of interest to note that voltammetric interrogation was undertaken prior impedance measurements, which might have affected the stability of obtained R_{ct} values. Recorded R_{ct} values might have been more stable if EIS measurements would have been run before DPV. The little number of replicates is also to be underlined, which originates from using a 96-well plate with few available wells despite intensive chemical and electrochemical electrode regeneration.[531] Bacterial trials were run with a fresh 96-well plate. Repeated electrochemical interrogation has accelerated $[Fe(CN)_6]^{3-/4-}$ signal degradation and highlighted the need for minimal measurements. The total number of measurements undertaken here was exceeding the quantity performed over the course of later tests with *A. baumannii*.
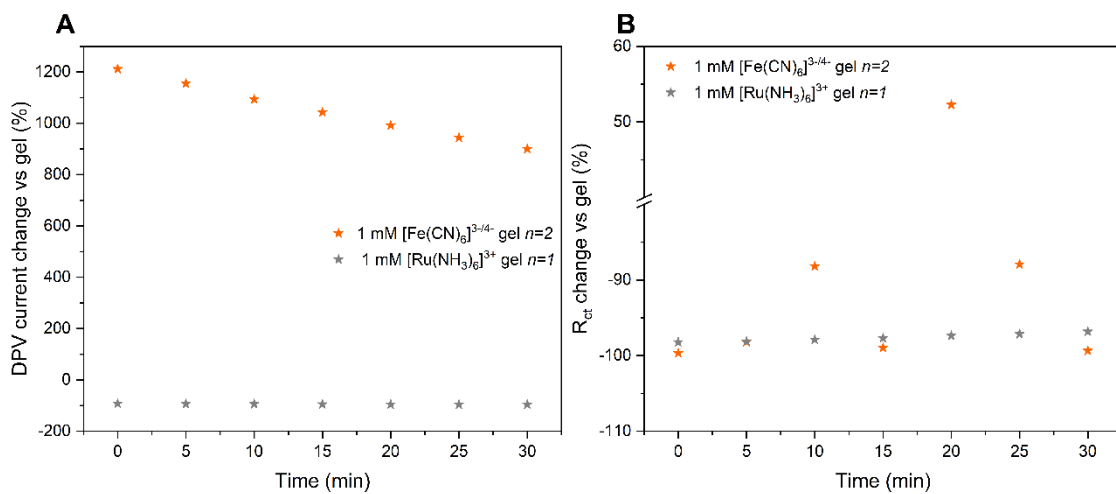
Figure 5.11. Repeated electrochemical interrogation on the stability of 1 mM $[Fe(CN)_6]^{3-/4-}$ or $[Ru(NH_3)_6]^{3+/2+}$ gel-functionalised electrodes with DPV (A) and R_{ct} (B).

Both redox-mediator loaded gel compositions were further tested, as calibration was performed using $[Fe(CN)_6]^{3-/4-}$ and $[Ru(NH_3)_6]^{3+/2+}$ gels offered more stability and less disturbance from repeated interrogations.

5.4.2.4 Comparison of redox mediators at recording variability in *A. baumannii* growth profiles impacted by moxifloxacin in presence of Apta-MIPs

Since $[Ru(NH_3)_6]^{3+/2+}$ showcased in Figure 5.11 better stability when repeatedly interrogated compared to $[Fe(CN)_6]^{3-/4-}$, both gel compositions have been tested in their suitability to record *A. baumannii* growth patterns in presence of moxifloxacin, either bound or unbound to Apta-MIPs. The presence of redox mediator in the agarose gel has not significantly altered bacterial growth as shown by Hannah *et al.* (2019, 2020)[244,259] and Domingo-Roca *et al.* (2022)[529].

The decrease in DPV was more consequent for $[Fe(CN)_6]^{3-/4-}$ gels in comparison with $[Ru(NH_3)_6]^{3+/2+}$ deposits accounting for the presence or absence of Apta-MIPs in *A. baumannii* samples with 0.1 µM moxifloxacin (Figure 5.12A and C). This might have been impacted by the frequency of measurements but not only, as the most consequent difference was recorded in the first hour. Moreover, both conditions converged to reach a plateau over the second hour on $[Ru(NH_3)_6]^{3+/2+}$ gels whereas the difference was maintained on $[Fe(CN)_6]^{3-/4-}$ gels.
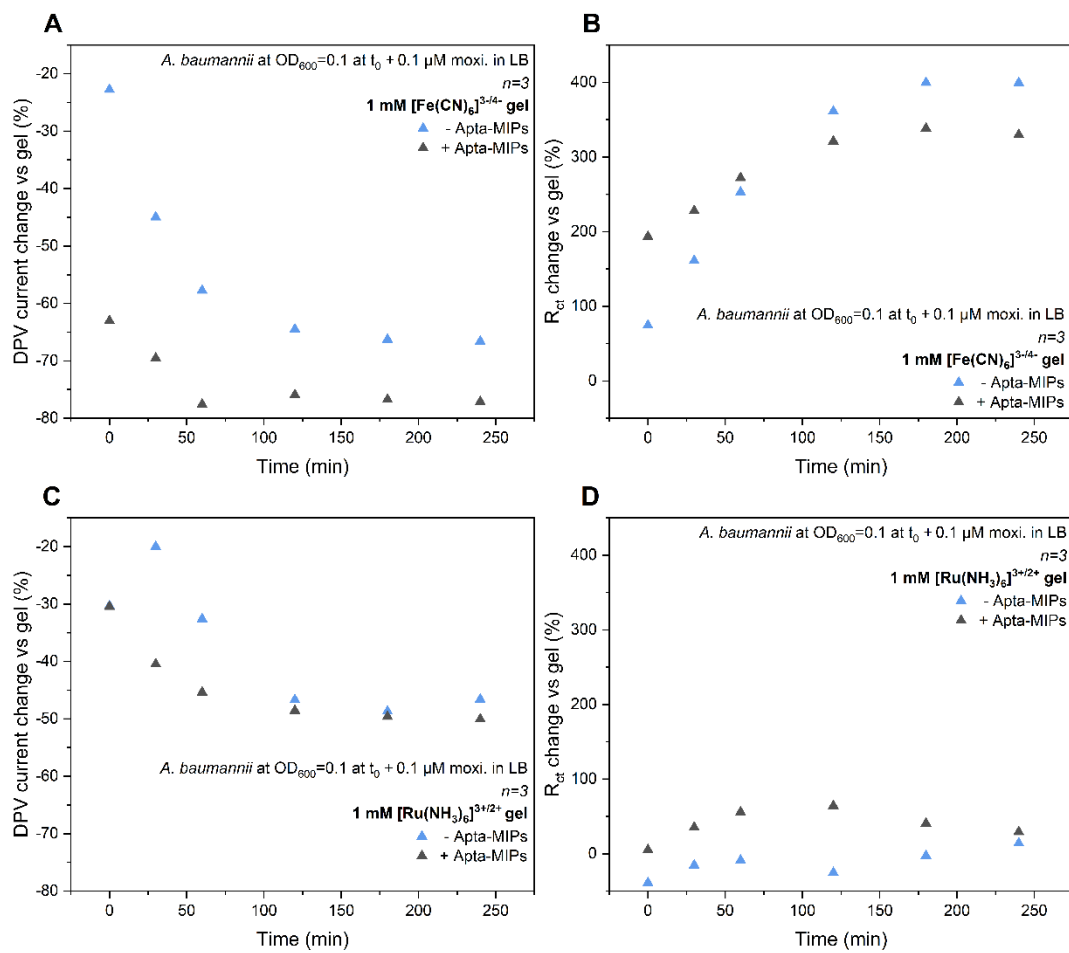
Figure 5.12. Influence of the presence of Apta-MIPs on *A. baumannii* growth under moxifloxacin on 1 mM [Fe(CN)$_6$]$^{3-/4-}$ and [Ru(NH$_3$)$_6$]$^{3+/2+}$ gels via DPV (A,C) and R$_{ct}$ (B, D) monitoring. Concerning R$_{ct}$ trends, overall increases were observed regardless of gel compositions or Apta-MIP presence, correlating with Figure 5.11B with bacteria in samples and diverging from Figure 5.9 decreases without bacteria. Both Apta-MIP conditions on [Ru(NH$_3$)$_6$]$^{3+/2+}$ gels showed a similar trend, namely negative changes without AptaMIP and positive changes with Apta-MIPs binding moxifloxacin, and converging after 4 hours (Figure 5.12D). R$_{ct}$ of [Fe(CN)$_6$]$^{3-/4}$ gels experienced a shift, from a higher change before the first doubling time for the presence of Apta-MIPs to a lower rate than in their absence over the next 3 hours (Figure 5.12B). This could indicate an action of unbound moxifloxacin on bacteria compared to moxifloxacin bound to Apta-MIPs and would make [Fe(CN)$_6$]$^{3-/4}$ gels more suitable for this assay. Corresponding fits were summarised in Table B. 7.12. Controls ran with *A. baumannii* and MIPs without antibiotics are needed to confirm that the presence of Apta-MIP in the bacterial

medium did not impact microorganism growth. Often reported are either MIPs detecting antibiotic residues[505,508,510] in complex matrices or MIPs binding whole bacteria,[532] which challenges any confirmation from the literature on the impact of the presence of MIPs on bacterial growth. However, this emphasises the novelty of the assay strategy to detect antibiotic susceptibility directly from bacterial cultures.

Testing of the NanoMIPs in bacterial culture, to provide a comparison of their performance against AptaMIPs are to be conducted next. Additionally, as bacterial growth in the 96-well plate is undertaken statically, it might be beneficial to check, using for instance crystal violet staining, if *A. baumannii* remained in a planktonic phenotype or has formed a biofilm. Trials assessing different concentrations of antibiotics to enable a MIC determination could be an interesting next step. Instead of MIPs being present from the beginning of the monitoring, they would need to be added after a defined time.

5.4.3 Conclusion

Carbon screen-printed electrodes in a 96-well microtiter plate format were coated with gels containing a redox mediator, either 1 mM of $[Fe(CN)_6]^{3-/4-}$ or $[Ru(NH_3)_6]^{3+/2+}$. Apta-MIPs and NanoMIPs binding to moxifloxacin in solution, deposited on the gels, were monitored using DPV and R_{ct}. **AptaMIP superior binding affinity compared to NanoMIPs was evidenced on $[Fe(CN)_6]^{3-/4}$ gels and in *A. baumannii* culture medium.** The stability of $[Ru(NH_3)_6]^{3+/2+}$ over $[Fe(CN)_6]^{3-/4}$ gels concerning repeated measurements (Figure 5.11) was reflected in the magnitude of changes observed in complex media. Despite increasing monitoring durations and additional control conditions needed, $[Fe(CN)_6]^{3-/4-}$ gels supported Apta-MIP binding moxifloxacin recording in buffer and bacterial culture. This highlighted the **possibility of early differentiation in bacterial growth patterns under antibiotic treatment using Apta-MIPs.** Adding the polymer at a later time could also inform on the antibiotic uptake or efflux, and by extension susceptibility or resistance of *A. baumannii* to moxifloxacin. The presence of MIP, and more specifically Apta-MIPs, enabled the detection of a small molecule and yielded a more consequent change thanks to its nanometre size.

Chapter 6 Electrochemical assessment of monospecies biofilms aided by hyperspectral imaging

6.1 Introduction

6.1.1 Biofilm-related infections and current treatment strategies

6.1.1.1. Estimated incidence, variety of infections and symptoms

Despite using vaccines and antibiotics to control the acute diseases they cause, bacteria take increasing advantage of biofilm formation to maintain their ubiquitous presence and infection potential.[23,533] The burden of biofilm disease as a health issue is deemed important[533] yet cannot be accurately estimated since neither properly diagnosed, detected, nor reported or treated. A current estimate from the National Biofilms Innovation Centre evaluates the worldwide annual cost of biofilms to human health at US$387 billion, representing five percent of global health expenditure[534] with 65[535] to 80%[536] of all infections being attributed to biofilms.

Biofilms stimulate the immune response mostly through antibody production. Recruited antibodies cannot penetrate the biofilm matrix but aggregate at the surface, likely causing more damage to the colonised tissue.[23] Infection can lead to biofilm development which, once established, can give rise to periods of acute infection where antibiotics may have some efficacy but in the longer term, recurrent infections are possible. This directly translates into bacterial biofilms being the most difficult to eradicate with natural surfactants, phagocytosis or antimicrobial agents. Estimates range from 500 times as the earliest report[533] to at least 1000 times[21] more antibiotic resistant character than free-floating species.

Biofilm disease can be subdivided into device-related, non-device related chronic infection or biofilms provoking device malfunction. Clinicians are aware of biofilms as a common cause for medical device infections.[22] Biofilm sampling from the device or surrounding fluids and tissues is challenging.[23] The singularity or multiplicity of bacterial species in an infection-related biofilm varies according to different factors such as anatomic location, nature of the device and duration of use.

Staphylococci are one of the most commonly isolated species from biofilm-infected samples, correlating with their major prevalence as nosocomial pathogens. *Candida albicans, Pseudomonas aeruginosa, Klebsiella pneumoniae* and *Enterococcus faecalis* are also frequently identified as causative agents of biofilm diseases[23,537] with *P. aeruginosa* being a model organism for biofilm formation and studies.[538] Among other ESKAPE pathogens, *Acinetobacter baumannii* is able to form highly infectious biofilms, responsible for extensive antibiotic resistance and high mortality rates.[539]

Considering an increasing number of implantable medical devices, indispensable to patients, bacterial attachment and colonisation readily occurring within 2 to 24 hours of implantation[537] and rising antibiotic resistance, effective treatment and prevention strategies, become pressingly and critically needed as the risk for biofilm infections is heightened.[23]

6.1.1.2. Existing control strategies and treatments

Preventing biofilm formation and development is the most effective approach to control biofilm formation.[23] Currently employed strategies to lower infection rates, morbidity and mortality encompass sterile and aseptic precautions during interventions, prevention of early colonisation by diffusion-controlled release of antimicrobials from the implanted device or innovative biomaterials, and antimicrobial infusion to dislodge an established biofilm.[23]

When access to the infection site is possible and of relative discomfort to the patient, in the case of anti-biofilm surgical acts and non-healing wounds for instance, existing and accepted practices for biofilm elimination include desloughing and debridement.[22,23] Ultimately, removal and replacement of infected devices, when possible, are the most effective last resort treatment, not devoid of physical or physiological consequences on the patient.[22]

Nevertheless, infectious biofilms cannot always be physically removed. Antibiotics currently used to treat biofilm infections were developed, tested and dose-tailored for free-floating microorganisms and would require reassessment of their potency against biofilm phenotypes of the same species.[23,21,22] Therefore,

prescribed antimicrobial treatment temporally allows for infection symptom relief by killing mostly planktonic bacteria shedding from the biofilm rather than embedded cells. The biofilm matrix physically shields constituting bacterial cells, for instance by hindering penetration for aminoglycosides from charge interaction with exopolysaccharides. Antibiotic resistance can also occur by single-point mutation for rifampin or insufficient activity against non-dividing *P. aeruginosa* from colistin,[23] a last resort antibiotic for extensively drug-resistant (XDR) Gram-negative infections with delicate dosing and detrimental side effects.[540] When a biofilm is not completely eradicated after an antibiotic treatment, chances for the biofilm to form again and resistance to arise are much higher, resulting in prolonged antibiotic courses at high concentrations possible adverse side effects as well as incurred costs.[22,23,535]

6.1.2 Fundamental differences between motile and sessile bacteria and the challenges of drugging biofilms

The fundamental differences between planktonic and biofilm phenotypes from their composition, formation and evolution and plasticity all contribute to resist antibiotic action.

6.1.2.1 Biofilm constitution is unfavourable to antibiotic action

Biofilms enable a "confined mode of survival"[541] in optimal hydrated conditions as they provide a physical and chemical retention barrier[23,533] against host defences such as antibodies, phagocytes or surfactants as well as biocides, ultraviolet radiation and antibiotics.[542] From a composition standpoint, less than 10% of the biofilm is constituted by microorganisms with the exopolysaccharide (EPS) matrix equivalent to 90% of the biofilm biomass.[537,543,544] The EPS is mainly constituted of polysaccharides, proteins , extracellular DNA and insoluble constituents.[544,545] The exact composition is variable with a mixture of charged and neutral constituents, with charge heterogeneity reflected spatially in biofilms.[533,542] Thus the EPS holds a key role in extracellular electron transfer[544,546] through outer membrane vesicles, physical interaction between cells and quorum sensing.[547] As sub-MIC levels of the most common antibiotics (such as aminoglycosides, β-lactams, fluoroquinolones, glycopeptides, rifamycins and tetracyclines) trigger the formation of biofilms by a

range of bacteria *in vitro,* inadequate treatment, in terms of antibiotic or dose, is likely to cause more harm than good.

6.1.2.2 Formation and evolution of optimal communities to shelter and host bacteria

Biofilms can form as microaggregates, on biotic or abiotic substrates and at solid, liquid and air interfaces.[542] Bacterial adhesion is favoured on surface with charge, chemistry, topography or mechanic heterogeneities when encountering nutrient abundance.[548] Adhesion leads to modifications in expressed phenotypes and development of the biofilm architecture, supported by exopolysaccharide (EPS) and extracellular DNA production.[545] A micro-environment is shaped for each bacterium and biofilm microorganisms find themselves in single- or mixed-species microcolonies, defined as the basic biofilm unit,[533] with variable growth rates. Cooperation between biofilm microorganisms benefit maturation and lead to coordinated microbial communities.

Biofilms are mature and stable when cell division is halted by quorum sensing mechanisms once an optimal thickness is reached. Shedding of planktonic cells then occurs at a steady frequency,[533] which can be potentially targeted by antibiotics. However, they have been reported to cause higher cytotoxicity and mortality than "purely" planktonic specimens;[23,549,550] possibly due to horizontal gene transfer and intrinsic mutagenesis.[23]

6.1.2.3 Biofilms do not remain in a comfort zone, adaptability is enabled through architecture, accepting and hosting diversity and metabolic changes

Biofilms offer bacteria the optimal species- and substrate-specific architecture to efficiently support complex communities, enabling adaptation to external stresses.[533] Enhanced homeostasis compared to a planktonic state, physiological cooperation and coordinated metabolism provide an optimal microenvironment for the most favourable prokaryotic genome expression.[533] Other factors at play include biofilm substrate, taking advantage of localised heterogeneities, biofilm maturity and composition[23] as well as the ability to respond to stress.

The impact of selective pressures is not only localised but distributed among biofilm organisms.[551] The EPS matrix is mostly responsible for the regulation of metabolism, nutrient exchange and communication. Within a single biofilm, several chemical microenvironments coexist, multiplying possible reactions to changes.[533] Peripheral biofilm constituents might be more affected by external variations than those located at the core but have in contrast, a closer access to nutrients and oxygen.[551] If nutrients become scarce, biofilms persist using their trapped energy sources, with new peripheral cells shed.[533] Balancing a high oxygen concentration at the interface with the external environment, oxygen availability tends to equate to none in the deeper trenches of the biofilm,[548] where fastidious anaerobes can be encountered. Stress response can also lead to spatial reorganisation within the biofilm, with altered production of metabolites and signalling molecules.[551] Cooperative or competitive quorum sensing[23] between bacteria takes place through the production of small molecule intermediates.[547] Hence, possible universal models to test novel compounds and standardise treatments targeting biofilms or the EPS are challenging to develop due to variability in composition, metabolic processes and location[542]. Investigations are necessary both at genotypic but also at phenotypic levels.[533]

Biofilms favour the emergence of heterogeneous structures and phenotypes.[548] Dormant cells in a biofilm could either be preexisting or generated in response to environmental stimuli.[23] Either in a slow growth or no-growth mode, they are able to survive in the eventuality of nutrient or oxygen shortage.[23] Antibiotics are able to bind to dormant cells but not exert their action since they target biomolecule synthesis occurring in an active metabolism.[23] For instance, penicillin, ampicillin and later generation classes such as β-lactams, aminoglycosides or fluoroquinolones have a reduced activity against them.[22] This unique and protected phenotypic expression can therefore tolerate high bactericidal antibiotic levels,[23] the energetic toll for tolerance being non-proliferation.[23] Excluding the EPS matrix and any presence of resistance gene, antibiotics theoretically kill all biofilm cells except dormant ones. Once the treatment stops, dormant cells also called persisters are able to switch back

to their growing active phenotype to reconstitute the biofilm and enable a return of the infection.[23]

6.1.2.4 Shaping future treatment strategies

The microenvironment of the biofilm, including nutrient and oxygen availability, metabolic state of bacteria, bacterial species as well as the impact of the external environment on the biofilm and its constituents contribute individually and as a whole to antibiotic resistance.[23] Consequently, new strategies and treatments are needed to provide a sustainable and efficient solution to treat biofilms since current ones are not appropriate. Future treatments might be combinatorial instead of based on a single compound.[23] Combination of agents to target both active (ciprofloxacin, tobramycin or β-lactams) and slower metabolism (colistin) is a promising way to explore.[23] Biofilms are seen as an added barrier for drugs to pass in order to reach their target.[23] Increasing biofilm penetration is another considered direction. Topical application in avascular areas could avoid negative side effects from high dosages, provide local concentrations with minimal loss compared to parenteral administration and minimise the risk of antibiotic tolerance, illustrated by the antibiotic lock technique.[23] For disruption or complete eradication, treatments aim at the exopolysaccharide matrix, in order to weaken the structure as a whole.[537] In terms of preventative options, inhibition or disruption, when a biofilm has already settled, target quorum sensing (QS) mechanisms, to intercept communication between biofilm specimens and inhibit further biofilm development. Nevertheless, little of these alternatives have been implemented at the clinical stage.[552,553]

Effective biofilm treatment is crucially important, developing strategies for this would improve antibiotic efficacy. On a broader scale, not all biofilms are infectious or troublesome. Because of their ubiquity and the breadth of their impact upon various fields, their control is highly sought after. *In vitro* MIC testing and resulting PK/PD parameters, the current accepted methods, are not relevant to decide on biofilm infection treatment. Plus, there is no standardised method to test if a potential drug lead could inhibit biofilm formation or eradicate established ones.[23]

6.1.3 Successful treatments also rely on robust diagnosis: the lack of support from available detection methods, standards and regulatory framework

6.1.3.1 A plethora of detection possibilities without possible comparison and comprehensiveness

Confocal laser scanning microscopy (CLSM) is often cited as the best confirmation for biofilm presence, despite its time-consuming aspect and specialised skill requirements.[22,548] The use of fluorescent stains provides additional information on examined samples, such as viability compared to crystal violet or biofilm thickness for example.[24] Little consensus exist on image acquisition and result analysis, which cannot be subjected to validation, nor reproduced[24] with method comparison seldom undertaken.[24] High equipment costs and sample destruction are disadvantages also shared by other microscopy techniques such as scanning electron microscopy (SEM), transmission electron microscopy (TEM), atomic force microscopy (AFM) and scanning transmission X-ray microscopy (STXM).[554]

Culture-dependent methods are routinely performed to analyse biofilms such as colony forming unit (CFU) counts after serial dilution.[24] Multiple steps are involved in biofilm formation followed by compound testing, results taking several days to be obtained.[21] Traditional culture methods for biofilm organism assessment do not provide an accurate depiction of biofilms as the relationship between aggregates and colony forming units is not proportional, certain species' nonculturable character *in vitro* along with dormant or anaerobic bacteria.[23,533] Despite the awareness of methods not being suitable for biofilm infection assessment, they are still routinely used and most likely feed resistance on a frequent basis.[23] Microfluidic and higher throughput systems based on culture methods are available such as the Antibiofilmogram[555,556] or the BioFilm Ring Test requiring expensive and/or specialised equipment,[21] and the less high throughput Calgary Biofilm Device, using a large amount of laboratory consumables.[557]

Chemical evidence of biofilms include staining biofilm components. Colorimetric assays allow the conversion of a substrate into a pigmented compound, quantified by spectrophotometric readouts. Crystal violet staining is a widespread

method taking advantage of culture methods.[24] Crystal violet, from the Gram staining protocol, enables coloration of the bacterial membrane, is low cost and convenient to use.[21] However, crystal violet does not enable a distinction between live and dead cells as it stains all biological material containing DNA and proteins including the EPS,[21] needing additional procedures to assess antibiotic susceptibility.[21] This approach is laborious, leads to subjective results and inconsistencies and does not account for biofilm structure as such, since the detection is focused on single microorganisms.[24] Colorimetric assays also include tetrazolium salts or resazurin, enabling an assessment of the metabolic activity of bacteria through respiration. Tetrazolium salts, 3-(4,5-dimethyl-2-thiazolyl)-2,5-diphenyl-2H-tetrazolium bromide (MTT) and 5-cyano-2,3-di-(ptolyl)-tetrazolium chloride (CTC) being the most common ones respectively for eukaryotic and prokaryotic viability tests, are converted from colourless to coloured and lipophilic formazan products[558] whereas blue resazurin is converted to the pink resorufin. The latter, also known under the Alamar blue denomination, has shown increased sensitivity, quick result turnaround, lower cytotoxicity and cost than the tetrazolium salts. The limit of quantification remains low nevertheless and EPS components are not accounted for. Phospholipid-based biomass analysis can complement biofilm assessment to colorimetric methods as well as light microscopy, however lack of reproducibility and sensitivity are often reported.

Combinatorial methods using anti-EPS antibodies or EPS extraction also rely on further microscopy, therefore depending on equipment and reagent costs. Similarly, the continuous monitoring capacity of Fourier-Transform Infrared (FTIR) is also outbalanced by tedious sample preparation.[554]

Omics methods are an emerging avenue for biofilm understanding rather than routine detection. Transcriptomics focuses on the transcriptome, providing an overview of gene regulation under studied specific conditions[542] relying on quantitative PCR (qPCR), or higher throughput techniques such as micro-array and RNA-sequencing.[542] Further molecular studies or complementary proteomics or metabolomics are required as mRNA is only a first stage account in gene expression[542] and translation into proteins as well as post-translational modifications include

variations in phenotypic expression.[542] Proteomics analyse proteins expressed by an organism at a set time in specific defined conditions.[542] Gel-based approaches used earlier on are being replaced by gel-free proteomics based on MS.[542] Drug resistant and persister phenotypes have been assessed using proteomics to bring more understanding on biofilm resistance.[542] There is no broad consensus from a proteomic point-of-view on the importance of the EPS and polysaccharide content.[542] This can be explained by extracellular matrix proteins being difficult to recover and polysaccharides being a better fit to metabolomics studies.[542] Metabolomics is defined as the end-point, more exhaustive report of the metabolome.[542] It enables detection, identification and quantification of primary and secondary metabolites with a direct link to phenotypes, contrarily to genes and proteins.[542] The variety of organisms, EPS composition, metabolic states and external conditions involved in biofilm occurrences highlights the difficulty to draw global metabolite blueprints and the requirement for case by case analysis.[542] Compound extraction methods are limited by compound solubility, and call for a variety of approaches for comprehensiveness.[542] The use of MALDI-TOF MS circumvents those limitations by enabling whole bacterial cell studies immobilised on matrices.[542] Integrating data from different omics approaches is the next step in deepening biofilm understanding.[542] Nevertheless, large omics datasets still require standard deposition in global shared platforms.[542] Hurdles for implementation come from the intensity of the computational process and differences in data types requiring normalisation.[542] Unsupervised or supervised data integration can be performed and the latest artificial intelligence improvements hold the promise for predictions of specific phenotypes through metabolic pathways and markers.[542]

Among physical methods, ultrasonic time-domain reflectometry and dry mass weighing are limited by their sensitivity. Nuclear Magnetic Resonance Imaging requires time-consuming sample preparation and consequent equipment costs. Electrochemical methods and visible and near infrared (VNIR) on the contrary, call for little sample preparation and possibilities to bring low cost sensitive solutions closer to the point of care.[554]

Electrochemical approaches have been reported for characterisation of biofilms and their composition at least since biofilms were defined by Costerton *et al.*[533] Given the complexity of natural multi-species formations, single-species biofilms have been the focus of most studies.[533] Electrochemical methods are convenient in terms of cost, rapidity of measurement and procedure, compared to chromatography and spectrophotometry, to detect QS processes linked to early biofilm establishment. Biofilm accepted complexity leads to the conclusion that a single method would not be sufficient to characterise biofilm formation and evolution.[21] Optical visualisation of metabolites and signalling molecules are informative to understand spatial organisation and progression, especially upon stress exposure without being invasive. Hyperspectral imaging enables recording of a spectrum for each pixel of an image, enabling a 3D measurement that is also non-destructive compared to metabolite mapping with mass spectrometry.[548]

6.1.3.2 The absence of standards, models and regulations discourages new system development and leaves little solutions for doctors facing biofilm-based infections

Coming to a consensus and more widely applicable method would provide a lever to assess effectiveness, compare and support anti-biofilm strategies, test more clinical samples and ultimately provide better guidance to clinicians and treatment solutions for patients.[22,23]

Despite the breadth of methods reported, there is no unified procedure to characterise biofilms[23,559,537] (except for *P. aeruginosa* biofilms *American Society for Testing and Materials (ASTM)* Methods[22]) or assess anti-biofilm activity, which hinders diagnosis, infection treatment, anti-biofilm drug discovery and development.[22] Indeed, part of the clinical guidelines to diagnose biofilm infections are infection persistence and inefficacy of antibiotic courses.[560] Commonly, laboratories use microtiter plates and staining methods or CLSM to estimate biofilm biomass.[22] Once the time and financial investments are undertaken, reassessment of testing procedures and equipment are generally unlikely.[22]

Additionally, no standard is available to check anti-biofilm efficacy against, meaning the widely accepted practice is complete biofilm eradication.[22] Based on standards set for planktonic antimicrobial activity, a reduction over $3 \log_{10}$ in reference to the reproducibility standard deviation is accepted as bactericidal.[561] Effectiveness for an anti-biofilm drug would also need to link biofilm reduction with decreased symptoms and better patient outcomes.[22] However, the term biofilm is rarely mentioned as part of new drug/device documentation, more often restricted to curing or preventing infections, when regulatory bodies do require clinical data to decrease infection rates.[22] Replicating results within and between laboratories, since standards cannot be referred to, is almost impossible.[22]

The currently available biofilm models are tested *in vitro* but not validated *in vivo.*[22] As biofilm samples are in the micro- to milli-metre range at most, they are difficult and fiddly to sample[560] resulting in gaps[562] between research being undertaken *in vitro* and lack of *in vivo* applications.[22] *In vitro* data is furthermore for a pharmaceutical regulatory body to approve and make a drug available.[22] Potential assay development able to accurately reproduce *in vivo* conditions of biofilm evolution are challenged by the diversity of biofilms.[22] Biofilm resistance to antibiotics is associated to a range of factors or biomarkers, making it difficult to target universal assay or treatment options.[22] This translates into the absence of a single assay or biomarker to attribute a biofilm as the cause of infection.[22]

The lack of anti-biofilm (universal) drugs/treatment combinations[21] feeds the absence of existing regulatory framework for drug assessment and approval.[22] Little standards and absence of regulation to lean on do not form an appealing environment for the pharmaceutical industry to invest more in anti-biofilm research and compounds.[22] Hence, this disinterest hinders financial support for the development of standard methods.[22] Doctors and clinicians are left, when faced with a biofilm infection if detected, without anti-biofilm drugs and laboratory guidance to rely on.[22]

Case-by-case assessment and solutions, or at least more personalised, with multi-faceted, systems-level approaches[542] arise as more pertinent.[22] By taking

divergence into account, efforts to develop a universal strategy to tackle biofilm characterisation and treatment could be directed towards « standardised adaptations (calibrated) » assays to improve clinical outcomes.[22] Complexity and variability of biofilms should be reflected within the solution with a degree of repeatability between laboratories.[22] Ideally, solutions with reproducible, rugged, responsive and quantitative[22] features alongside being as close to *in vivo* biofilms as possible are the ultimate aim.[22]

6.2 Rationale, aims and objectives

As was described, biofilms represent a serious threat to patients and are already a significant challenge to healthcare providers since they complicate the implantation of many medical devices and are responsible for the majority of failed procedures. The nature of the problem and the need to improve success rates for procedures means it is crucial to develop new technologies which enable both the study of biofilm formation, their behaviour and drugability, and the assessment of real infections with the aim of achieving optimal treatments.

As no standard method is widely adopted to characterise biofilms, this chapter aimed to provide a dual and close to real-time monitoring of biofilm formation and evolution as well as capturing their antibiotic susceptibility. The final application would be to enable antibiotic susceptibility of infectious patient samples relying on experimental rather than empirical decisions.

P. aeruginosa was tested with the dual system because of its well-known ability to form biofilms and its production of pigmented redox active secondary metabolites (pyocyanin, pyoverdine etc.) which could facilitate direct electrochemical and hyperspectral detection.

Once the system was established, its transferability to 'electrochemically inert' pathogens was evaluated, i.e. one that is incapable of producing redox active metabolites for direct detection, using resazurin. As resazurin conversion to resorufin is directly linked to active metabolism, this also reflected metabolically active bacteria, more likely to be targeted by antibiotics (Figure 6.1).

The objectives of this chapter were:

1) Design a combined hyperspectral and electrochemical detection platform to evidence biofilm formation,

2) Establish proof of detection from both hyperspectral imaging and electrochemistry with standard pyocyanin,

3) Perform detection experiments with *P. aeruginosa* isolates and establish performance level of the platform,

4) Adapt the detection strategy for other ESKAPE pathogens which **do not** produce redox active secondary metabolites using resazurin.

As part of a collaborative funding, work related to objectives 1 to 3 has been published in Sensors & Diagnostics with a joint first co-authorship between R. D. Dunphy and P. Lasserre. Experimental work pertaining to hyperspectral camera set-up and use, hyperspectral imaging data acquisition and processing and data interpretation was contributed to by the author. Data acquired for Figure 6.6 was performed by L. Riordan.
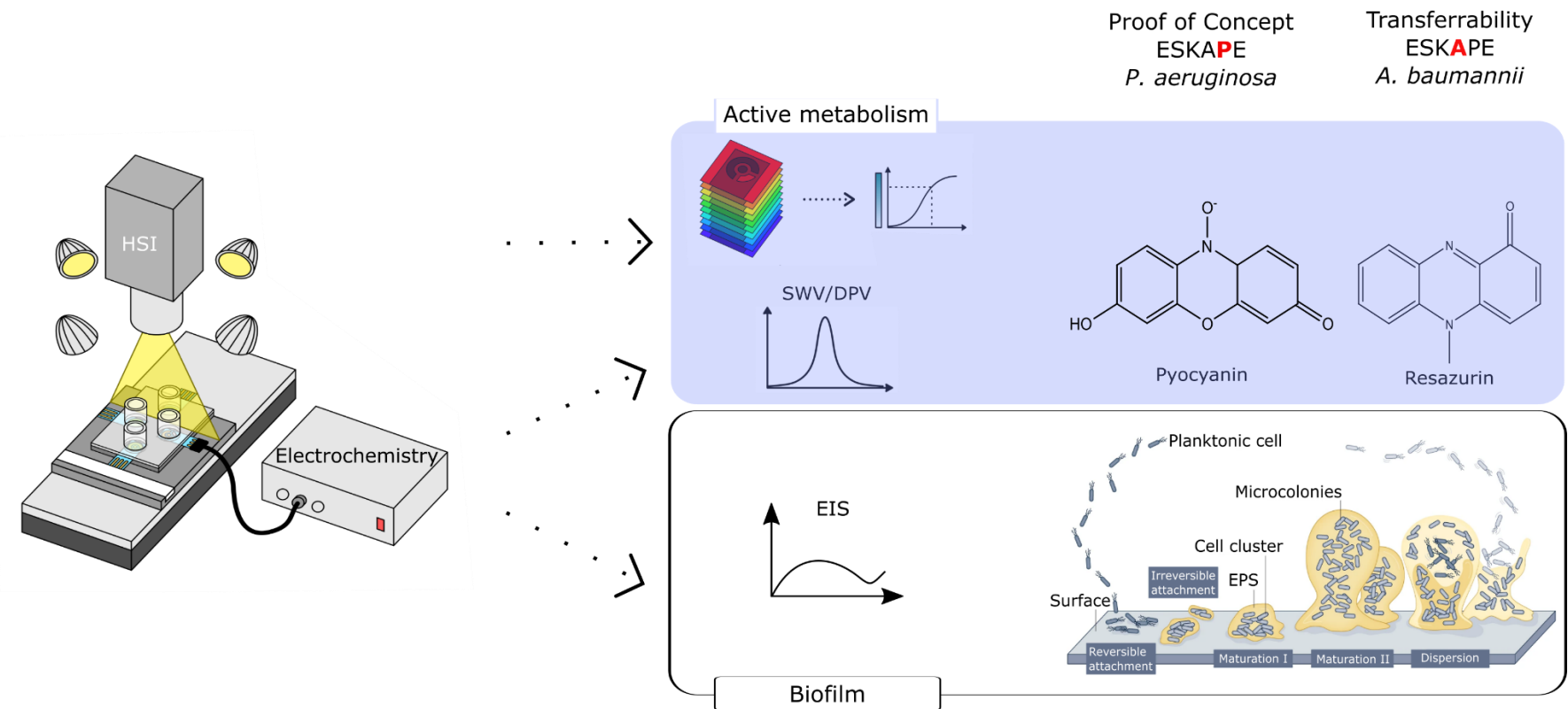
Figure 6.1. Biofilm monitoring assay design using HSI and DPV and SWV for antibiotic susceptibility and EIS for biofilm formation and evolution assessment with *P. aeruginosa* and *A. baumannii* [563] Reproduced and adapted with permission from Sauer, K.; Stoodley, P.; Goeres, D. M.; Hall-Stoodley, L.; Burmølle, M.; Stewart, P. S.; Bjarnsholt, T. The Biofilm Life Cycle: Expanding the Conceptual Model of Biofilm Formation. *Nature Reviews Microbiology* 2022, *20* (10), 608–620.

6.3 Combining hyperspectral imaging and electrochemical sensing for the detection of *Pseudomonas aeruginosa* through pyocyanin production

Pseudomonas aeruginosa is a World Health Organization priority (WHO) pathogen,[564] and one of the most commonly associated pathogens in hospital-acquired infections (HAI).[565–568] It is responsible for acute infections in healthy subjects and its pathogenicity in immuno-compromised patients often results in chronic infections because of its resistance to antibiotics and to the host immune response.[566] Pyocyanin is ubiquitously produced by *P. aeruginosa* and one of its main virulence factors, characteristically produced by this bacterial species in a biofilm phenotype, its most efficient survival strategy.[565,569–571] As a well-characterised compound across the electrochemical literature, pyocyanin has led to a wide range of sensing strategies through amperometric, voltammetric, or impedance-based detection.[569,571–573]

Hyperspectral imaging (HSI) is a photographic imaging technique that captures detailed spectral information for each pixel of an image. The resulting hyperspectral datacube can be thought of as a collection of greyscale images corresponding to narrow bands of the electromagnetic spectrum. This effectively allows a complete reflectance spectrum to be constructed for each pixel of an image, enabling computer-assisted analysis of processes that are detectable in the visible or infrared spectrum. HSI enables the detection of specific substances by matching absorption bands to known spectral signatures. HSI has the advantage over UV spectroscopy and other analytical techniques that it allows identified compounds to be localised over the area of an affected sample. Hyperspectral techniques applied to biofilms include hyperspectral fluorescence imaging, which has been used to assess *E. coli* and *Salmonella* spp. biofilms on stainless steel.[574] Due to their non-destructive nature, hyperspectral methods are particularly well suited for time series studies, and have been used to monitor the effect of antibiotics on biofilm growth.[575]

In this study, we propose a robust and multifaceted combined HSI and electrochemical sensing approach to the detection of the *P. aeruginosa* virulence factor pyocyanin.

6.3.1 Materials & Methods

6.3.1.1 Custom-built test cell design

A 3D-printed custom-built test cell was designed and manufactured in-house to facilitate the image capture and electrochemical monitoring of *P. aeruginosa* pyocyanin production and biofilm formation. The design allows for samples to be grown, imaged from above before electrochemical measurements are taken using the potentiostat without disruption. The plate consists of a base plate with four slots to position screen-printed electrodes, which is bolted to a clear acrylic enclosure with wells around the electrode measuring area. Acrylic cylinders were inserted into the enclosure wells and sealed with O-rings to reproduce the shape of a 96-well microtiter plate, as this is the most common format for biofilm measurements.[576] The base plate and the enclosure are bolted together after sliding electrodes into the designated slots. The custom-built test cell was cleaned with 70% ethanol in distilled water (v/v). Figure 6.2 shows close-ups of a well of the custom-built test cell containing Lysogeny Broth (LB) medium (Figure 6.2B) and *P. aeruginosa* biofilm (Figure 6.2C).
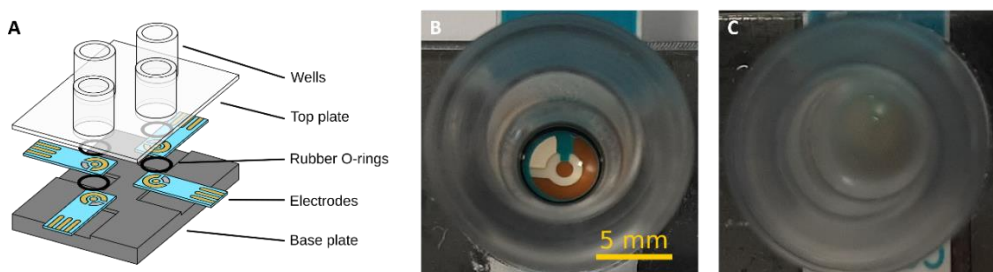
Figure 6.2. Biofilm formation in the custom-built test cell. (A) Exploded view of the test cell, (B) *P. aeruginosa* in LB medium at 0 h and (C) after 6 h of incubation. Reproduced with permission from Dunphy, R. D. *et al.* Combining Hyperspectral Imaging and Electrochemical Sensing for Detection of *Pseudomonas aeruginosa* through Pyocyanin Production. Sensors & Diagnostics 2022, *1* (4), 841–850.

6.3.1.2 Pyocyanin calibration

Pyocyanin standard (P0046) and LB medium (L3522) were purchased from Sigma. Pyocyanin was dissolved in 100% ethanol at a concentration of 10 mg/mL.

Further dilutions were prepared in triplicates, in LB medium at the following concentrations: 10, 5, 2.5, 1, 0.50, 0.25, 0.10, 0.05, 0.025 and 0.01 mM.

Screen-printed gold electrodes (C223-BT DropSens, Oviedo, Spain) with a 1.6 mm diameter working electrode were used to conduct experiments. 50 µL of overnight *P. aeruginosa* culture (LB, 250 rpm, 37°C) or media blank were deposited onto electrodes. The custom-built test cell was placed on a lateral translation stage located under the VNIR hyperspectral camera and illuminated by four 60 W halogen lamps. The plate was positioned to align each well with the lens of the camera as it was being imaged, minimising differences in illumination that might otherwise have been caused by the relative position of the well, camera and lamps. To avoid inconsistent illumination resulting from the edges of the plate, the outermost wells were not used. For each sample, an image was first captured, and electrochemical measurements followed directly after.

Hyperspectral images were captured using a Hamamatsu CCD/Specim C8484-05G VNIR pushbroom hyperspectral camera system, with 2x2 pixel binning used to compensate for sensor noise and an exposure time of 0.04 s. 512 wavelength bands in the range 386-1006 nm were measured, of which 440 bands in the range 379.6-909.9 nm were retained for analysis as bands outside of this range are negatively impacted by sensor noise. The spectral reflectance was obtained from the raw hyperspectral data using one-point calibration for each image, according to the formula:

$$R = \frac{S-D}{W-D} \ (1)$$

where S is the sample data, D is a dark reference point obtained by capturing an image with the lens covered, and W is a white reference point, obtained from a Spectralon calibration tile imaged alongside the sample.[577]

Mean reflectance spectra were calculated from a region of each hyperspectral image corresponding to the location of the reference electrode, which had the most Lambertian spectrum of any portion of the samples. The spectra were normalised to

a mean of μ = 0 as in (2). The mean reflectance for the corresponding area of a control sample containing only LB was used as the baseline reflectance spectrum and subtracted from each of the sample spectra.

Square wave voltammograms were acquired following settings previously described, with a 5 A current, a 3 mV step potential, and a 15 Hz frequency.[578] The potential ranged from -0.7 V to 0.0 V vs. Ag/AgCl. For EIS data generation, frequencies were scanned between 0.1 Hz and 100 kHz at a 0.01 V AC potential with 11 frequencies per decade at 67 frequencies. EIS spectra were measured against open circuit potential (OCP). EIS and SWV data were acquired with a PalmSens potentiostat and analysed with Origin.

6.3.1.3 *P. aeruginosa* monitoring in a 96-well plate format

Wells were inoculated with an OD_{600} value of 0.5 or 1 (Eppendorf Biophotometer 6131) adjusted with from an overnight *P. aeruginosa* culture (LB, 250 rpm, 37°C) of either PA14 or LESB58 respectively (obtained from K. R. Duncan). Distilled water was added to any empty well, ensuring sufficient ambient water availability to avoid sample concentration. Images of the plate were taken first, and sampling of each well occurred in sterile conditions where well contents were transferred to 0.5 mL sterile microcentrifuge tubes and stored on ice until SWV and EIS acquisition. 50 μL were pipetted onto the electrode area of gold screen-printed electrodes and tested with SWV with a wider potential window from -0.7 to 1.0 V and EIS. Hyperspectral images were normalised using the standard normal variate (SNV) approach, and adjusted relative to the LB baseline, with the formula:

$$X = \frac{R - \mu R}{\sigma R} - XLB \ (2)$$

where R is the calibrated image, μR is the mean of all data points in R, σR is the standard deviation of R, and XBL is the SNV of the baseline spectrum. Finally, a feature map F was defined by scaling the resulting scores between the normalised spectra for the pyocyanin solutions and LB:

$$F = \frac{X - XLB}{XPYO - XLB} \ (3)$$

where XLB is the normalised score for the LB sample, and $XPYO$ is the normalised score for the 1.0 mM pyocyanin positive control sample. OD_{600} measurements were taken every 15 minutes over 24 hours as a growth check by a plate reader.

6.3.1.4 *P. aeruginosa* biofilm monitoring in the custom-built test cell.

The custom-built test cell was assembled with the electrodes in the slots. An overnight *P. aeruginosa* (PA14 and LESB58) culture was inoculated in 200 µL of LB medium in each well of the 96-well plate, at an initial OD_{600} value of 0.5 or 1, placed at 37°C. When antibiotic susceptibility was assessed, gentamicin was added after 24 hours and a blank solution to mimic the disturbance instead for the negative controls.

6.3.2 Results

Since the aim of the study was to develop a combined HSI and electrochemical system for measurement of biofilm formation it was first necessary to establish the system through calibration exercises, correlation or electrochemical and HSI result with standardised solutions of pyocyanin. The next sections present this work before moving on to more advanced tests involving detection of live bacteria and real time biofilm formation.

6.3.2.1 SWV and HSI standard pyocyanin calibration

A pyocyanin standard calibration curve was first established with SWV and HSI with 50 µL deposits on screen-printed electrodes contained in the custom-built test cell. Images of increasing pyocyanin concentrations were captured and immediately followed with the acquisition of a square wave voltammogram.[579] As different oxidised and reduced forms of pyocyanin itself have different pigmentations (Figure 6.3),[580] HSI was always performed prior SWV to capture images before any sample modification could occur at that specific time point. Since SWV took place at each time point as well, pyocyanin produced could have undergone oxidation or reduction. In that case, HSI was able to measure newly formed pyocyanin more accurately whereas SWV assesses the overall production diffused in the culture medium.
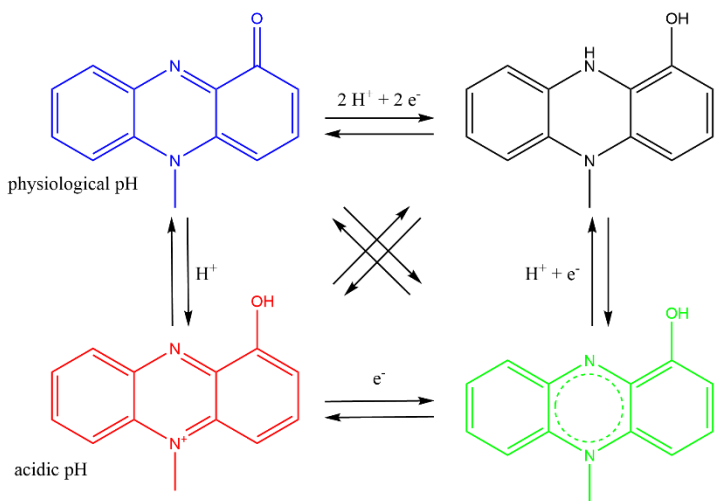
Figure 6.3. Pyocyanin oxidised and reduced states and their corresponding colours with the black molecule representing a transparent state. Adapted with permission from Glasser, N. R.; Saunders, S. H.; Newman, D. K. The Colorful World of Extracellular Electron Shuttles. Annual Review of Microbiology 2017, *71* (1), 731–751. [580]

As extensive work has been conducted on pyocyanin electrochemical detection, its purpose here serves as a basis for interpretation of hyperspectral observations. Additionally, its peak potential is distinct from possible common confounding compounds,[535,581,582] and is also distinguishably detected in polymicrobial environments.[583] The average SWV current responses obtained for one order of magnitude are depicted in Figure 6.4A for trend visualisation and readability. SWV responses for each concentration tested were extrapolated into a dose response curve. An approximately linear relationship was observed between pyocyanin concentration and SWV peak current (Figure 6.4B). One trend noticed with calibration is the shift in potential at which the pyocyanin peak occurs. This can be attributed to pH dependent changes as demonstrated previously[579] or use of a quasi Ag/AgCl reference electrode rather than a fritted system.[584,585]
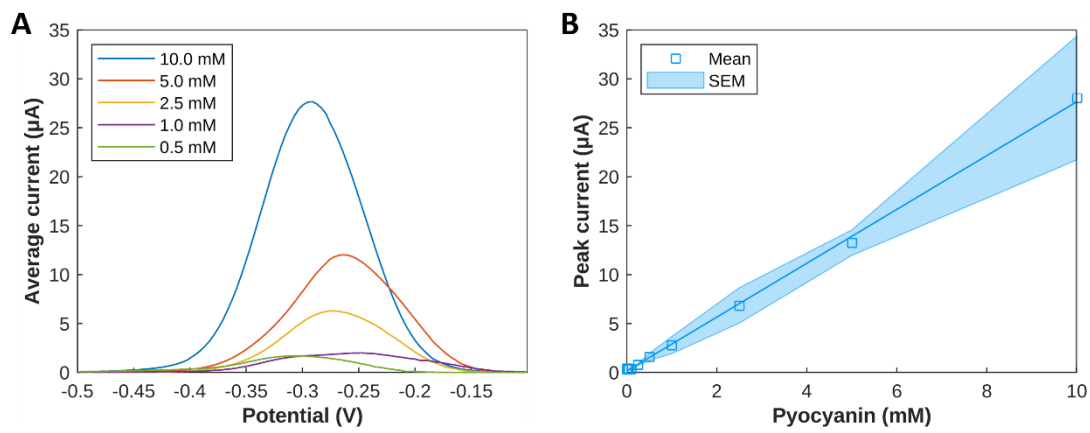
Figure 6.4. SWV characterisation of pyocyanin. (A) Average current amplitude for pyocyanin solutions from 0.5 mM to 10 mM (*n=3*) (B) Peak amplitude response to increasing pyocyanin concentrations between [- 0.35: - 0.15] V. Reproduced with permission from Dunphy, R. D. *et al.* Combining Hyperspectral Imaging and Electrochemical Sensing for Detection of *Pseudomonas aeruginosa* through Pyocyanin Production. Sensors & Diagnostics 2022, *1* (4), 841–850.

The calibration curve obtained for the HSI data, shown in Figure 6.5, reveals local maxima in the difference between the responses at the highest and lowest concentration at the wavelengths 395 nm, 638 nm, 703 nm, and 872 nm, with the 638 nm band corresponding to the centre of the main red absorption band. These curves are derived from the mean reflectance of known pyocyanin concentrations imaged in a 96-well plate placed on top of a Spectralon tile. Figure 6.5B shows the SNV with the mean LB reflectance subtracted. On this plot, an ideal LB sample should be represented by a line with a constant adjusted reflectance of 0. Deviations from this at the edges of the spectrum are caused by sensor noise and variation in the samples. Figure 6.5C shows the response at 638 nm as a function of concentration. An exponential decay curve of the form $y = ae^{-bx+c} + d$ was fitted to this data. The exponential curve was chosen to account for the diminishing change in the spectrum as the solution approaches the saturation point, in line with the Beer–Lambert law, which states that the transmittance of a sample at a given wavelength is a function of the exponential of its concentration.[586] The constant term d accounts for the reflectance. This curve fits the data with R² value of 0.98 (Figure 6.5C and Figure C. 1). The trend obtained for the SWV response is in line with HSI results for each sample.

6.3.2.2 SWV and HSI pyocyanin detection from *P. aeruginosa* inoculum in a 96-well plate format
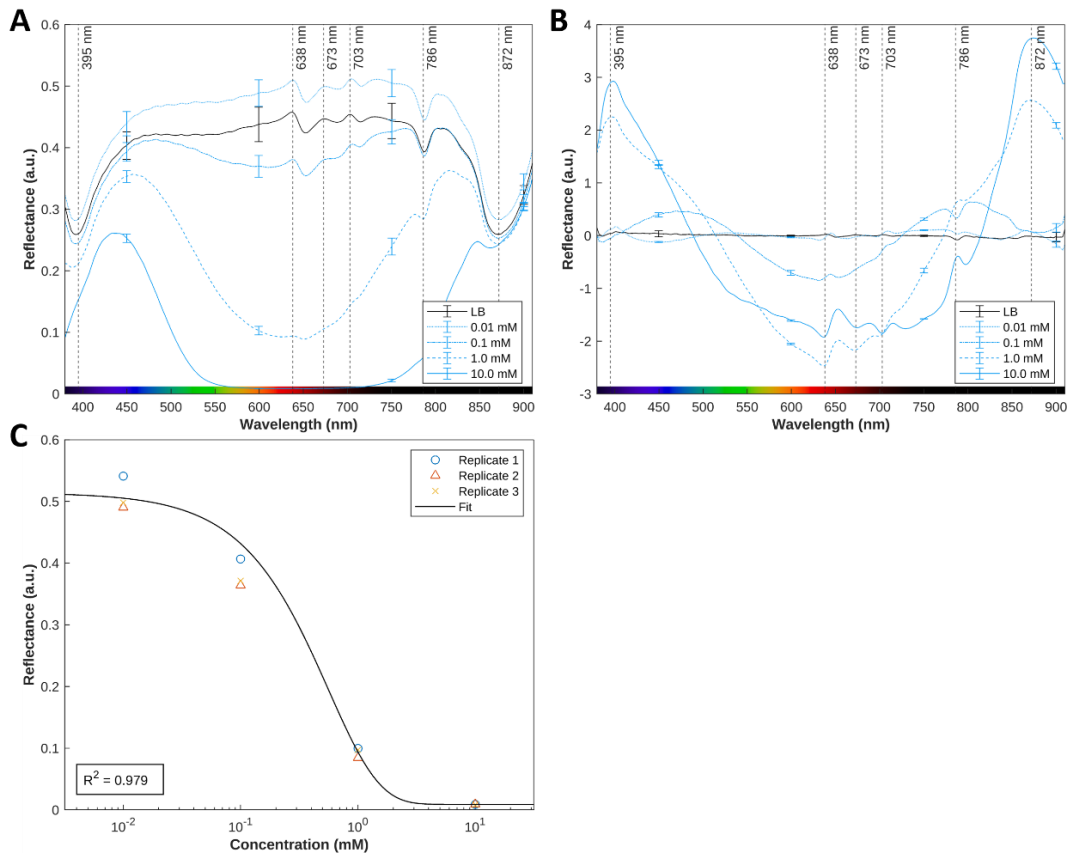
Figure 6.5. HSI response of pyocyanin samples(A) Mean reflectance spectra of pyocyanin in LB at four concentrations. Error bars representing the standard deviation have been included at 150 nm intervals, and a plot of the individual replicates can be found in Figure C. 3. (B) The same spectra normalised using SNV and baseline subtraction. (C) Exponential curve fit to calibration data for 638 nm. Reproduced with permission from Dunphy, R. D. *et al.* Combining Hyperspectral Imaging and Electrochemical Sensing for Detection of *Pseudomonas aeruginosa* through Pyocyanin Production. Sensors & Diagnostics 2022, 1 (4), 841–850.
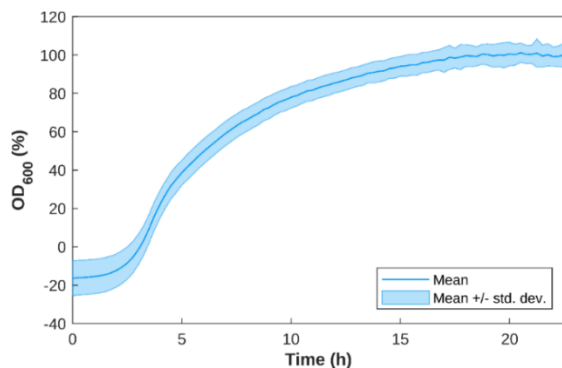
Figure 6.6. Growth curve of *P. aeruginosa* over 24 hours. Y axis shows optical density measured at 600 nm, normalised against the negative control (LB only). Note that growth reaches a stationary phase at ~15 hours. Reproduced with permission Dunphy, R. D. *et al.* Combining Hyperspectral Imaging and Electrochemical Sensing for Detection of *Pseudomonas aeruginosa* through Pyocyanin Production. Sensors & Diagnostics 2022, *1* (4), 841–850.

Figure 6.6 showed the growth curve of *P. aeruginosa* samples over a 24-hour period. The operation was repeated in triplicate following the same image capture and SWV and EIS settings established in the above section at 0, 24 hours and 48 hours.

After defining pyocyanin detection profiles with SWV and HSI, the growth of two strains of *P. aeruginosa*, PA14 and LESB58, was monitored with both approaches to detect and assess pyocyanin production. A transparent 96-well plate format was used to optimise bacterial culture and sample repeatability while allowing for higher throughput placed at 37°C and left static. Hyperspectral images were captured from the 96-well plate and wells were then sampled in sterile conditions for transfer onto gold screen-printed electrodes for SWV. Time points were chosen to ensure sufficient time for bacterial growth, pyocyanin production and biofilm formation.[587–590] LESB58, known to be the more virulent strain of the two tested,[591] produced on average more pyocyanin than PA14,[592] when assessed at two initial seeding concentrations.

Pyocyanin standards and *Pseudomonas* spp. cultures were in a background of LB medium. As reported,[579] LB is a complex culture medium which shows an intense oxidation peak at 0.85 V. This peak is not reproducible across samples and time, meaning the potential window of detection considered will be between -0.7 V and 0.6 V since pyocyanin and other signature metabolites are detected below 0.6 V.

For LESB58 samples (Figure 6.7A), two overlapping peaks (peak 2) are initially present at -0.25 V, which do not exactly overlap the pyocyanin standard (peak 1). Their amplitude is proportional to the initial bacterial inoculation concentration, the less concentrated samples at the level of the control and the more concentrated at double the amount of the control. After 24 hours, both LESB58 culture concentrations have produced a culture medium containing > 2 mM pyocyanin as evidenced by the two peaks at - 0.25 V overlapping the pyocyanin standard curve. After 48 hours, pyocyanin quantities have slightly decreased for the initially less concentrated LESB58 samples and dropped at the higher concentrations (Table C. 1).

Concerning PA14 samples (Figure 6.7B), the less concentrated PA14 samples show the presence of pyocyanin at the same potential whereas PA14 samples at a

higher concentration exhibit a slightly shifted peak (numbered 2) in the same potential region. After 24 hours, all PA14 samples contain approximately 0.5 mM pyocyanin (peak 1). The less concentrated samples have produced pyocyanin while the more concentrated one has converted the most likely precursor (phenazine-1-carboxylic acid) into pyocyanin. Pyocyanin levels decreased after 24 hours, possibly because of culture conditions[593] or irreversible oxidation[594].
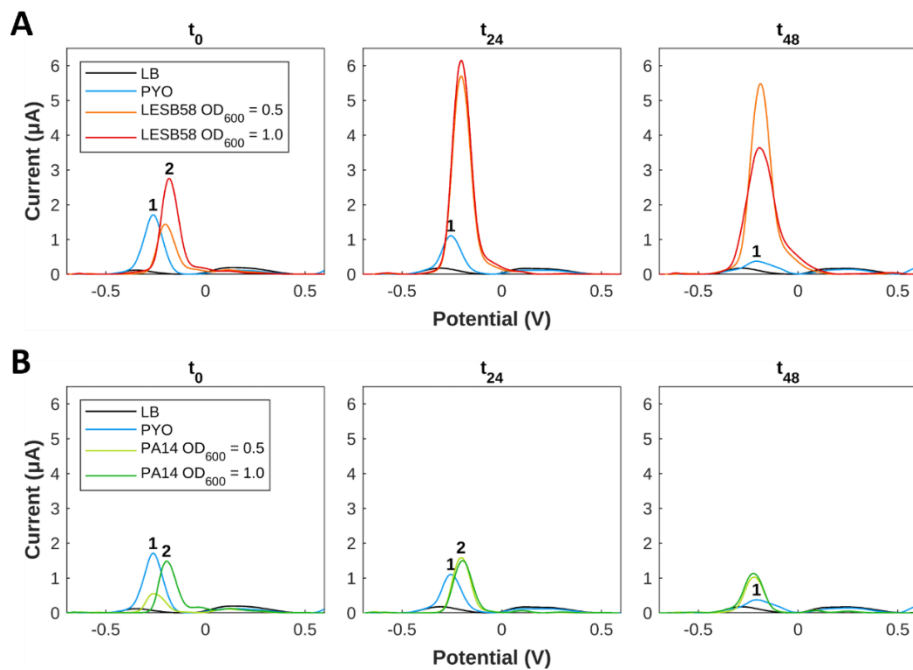
Figure 6.7. SWV evolution of two species of *P. aeruginosa* grown in a 96-well plate. (A) LESB58 samples at two initial seeding concentrations after 0 h, 24 h and 48 h. (B) PA14 samples at two initial seeding concentrations after 0 h, 24 h and 48 h. Peaks numbered 1 are associated to pyocyanin and 2 to pyocyanin precursors. Reproduced with permission from Dunphy, R. D. *et al.* Combining Hyperspectral Imaging and Electrochemical Sensing for Detection of *Pseudomonas aeruginosa* through Pyocyanin Production. Sensors & Diagnostics 2022, 1 (4), 841–850.

Other possible peaks present (Figure 6.7) can be attributed to 5-methylphenazine-1-carboxylic acid (5-MCA) around - 0.1 V, a direct precursor of pyocyanin within the *Pseudomonas* Quorum Sensing pathway: its presence testifies of bacterial growth and communication between bacteria.[359,595] For PA14 samples, the *Pseudomonas* Quinolone Signal (PQS) is detected around + 0.2 V (Figure 6.7).[359,579,595]

From SWV monitoring extrapolated into pyocyanin estimations, PA14 and LESB58 show different behaviours in terms of pyocyanin production: LESB58 samples

showing more pyocyanin production than PA14 (Table C. 1), confirming earlier reports.[592] Furthermore, pyocyanin production by both strains reflects previous reports of higher production within the first hours of growth, followed by either a plateau or decrease in pyocyanin production.[579] This has been linked to *P. aeruginosa* exoproduct synthesis being heightened to establish infection during acute phases,[570] further evolving towards a decrease at chronic stages.[596] Overall, pyocyanin production trends were in agreement with previous reports.[585,590,597]

The presence of pyocyanin detected by SWV correlates with pigmentation observed in the HSI data, as shown in Figure 6.8. The pyocyanin absorption band centred around 638 nm can be clearly seen in the mean spectra for the positive control samples, which is increasingly approached by the spectra of the LESB58 samples over time. Two smaller absorption bands at 395 nm and 872 nm that are present in all samples are produced by LB. The 395 nm band overlaps with an absorbance band in the UV range that increased over time in the bacterial samples and may be indicative of biofilm growth. This could be associated to the Soret band, related to heme proteins[598] which can correlate to biofilm growth.[599,600] Further work is required to confirm the source of this feature. Table 6.1 shows an estimation of the quantity of pyocyanin in representative samples based on the fit found for 638 nm of $y = 0.49\ e^{-1.78x+0.39} + 0.0089$ to the 96-well plate calibration data, as shown in Figure 6.5. Estimated values for PA14 before 48 h were lower than the error margin of the method. Negative values were adjusted to 0.
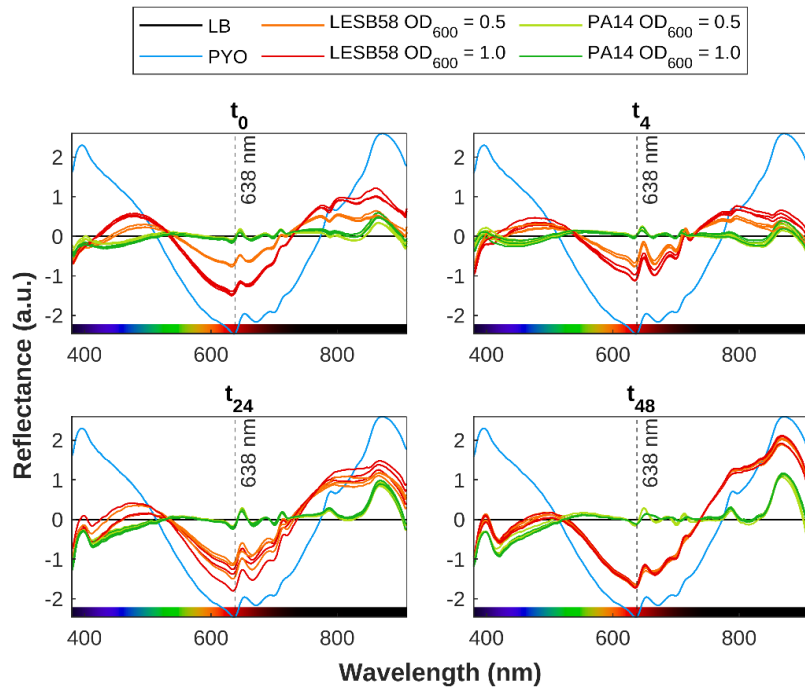
Figure 6.8. Time series of reflectance spectra for samples, compared with the positive control (PYO) and negative control (LB), normalised using SNV, with mean LB spectrum subtracted. There is clear indication of pyocyanin production in LESB58 samples, with a lower initial concentration in the OD$_{600}$ 0.5 samples. from Dunphy, R. D. *et al.* Combining Hyperspectral Imaging and Electrochemical Sensing for Detection of *Pseudomonas aeruginosa* through Pyocyanin Production. Sensors & Diagnostics 2022, 1 (4), 841–850.

Table 6.1. Estimated pyocyanin quantity (µM) using mean HSI calibration curve at 638 nm. Mean of three replicates per value.

	T = 0 h	T = 4 h	T = 24 h	T = 48 h
LESB58 OD$_{600}$ 0.5	60.6	80.0	225.3	524.5
LESB58 OD$_{600}$ 1.0	160.8	153.6	283.5	544.2
PA14 OD$_{600}$ 0.5	0	0	16.7	45.9
PA14 OD$_{600}$ 1.0	0	0	28.3	48.3

Figure 6.9 shows a heat map of the differential feature map F for the 638 nm absorption band as calculated by (3), showing an increase in the amount of pyocyanin over time for the LESB58 samples, with initially greater production in the centre of the well. Pyocyanin production in the PA14 samples was below the detection limit of this method. Four small artefacts are visible around the centre of each well, which are caused by specular reflection from the surface of the liquid. These areas were omitted from the analysis.
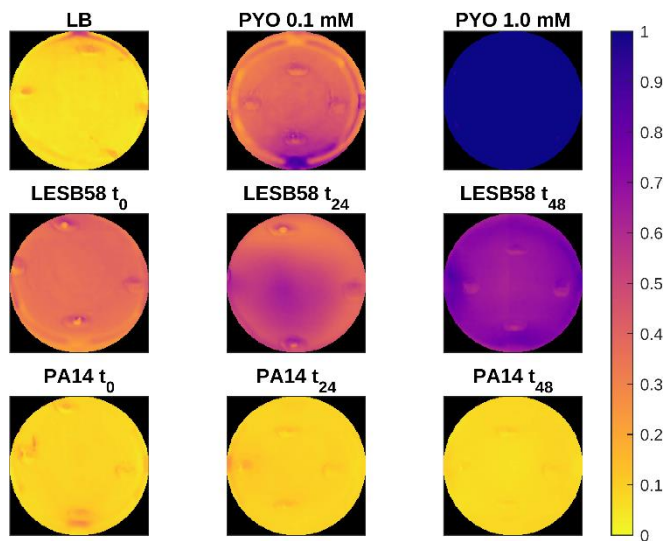
Figure 6.9. Spatial distribution of relative similarity to positive and negative controls for samples of the LESB58 and PA14 strains at OD_{600} = 0.5 at the start and after 24 and 48 h. Higher values indicate higher relative spectral similarity to the positive control (pyocyanin in LB). Reproduced with permission from Dunphy, R. D. *et al.* Combining Hyperspectral Imaging and Electrochemical Sensing for Detection of *Pseudomonas aeruginosa* through Pyocyanin Production. Sensors & Diagnostics 2022, 1 (4), 841–850.

The combined detection of pyocyanin through electrochemical methods along with HSI has enabled the reliable detection of *P. aeruginosa* presence through its electroactive and pigmented biomarker. Furthermore, pyocyanin quantities were detected within the clinically relevant range.[570] However, differences in trends and estimations were observed between both approaches, which could result from the data acquisition angle and nature of tested sample. It has been reported that biofilms form layers and gradients.[601] Imaging occurred from the top of the plate, where the biofilm forms and the most oxygenated form of pyocyanin, in its blue form, is the most concentrated.[602] Contrastingly, SWV measurements were taken after pipetting samples on screen-printed sensors, deposits being a mix of biofilm and diffused pyocyanin in the medium, in its transparent form as the growing biofilm gradually shields the liquid medium from optimal oxygenation, which might explain the diverging trends.

The detection of pyocyanin relies only on the relative absorption of light over a small number of representative wavelengths, opening up the possibility of developing a low-cost sensor that leverages the transmittance at those specific wavelengths. Such a sensor would be limited to settings where the presence of

confounding pigments can be ruled out, whereas HSI has the ability to distinguish between spectrally distinct pigments.

6.3.2.3 Integrated *P. aeruginosa* biofilm detection in a custom-built test cell

After calibrating with pyocyanin standards and confirming detection in bacterial inoculum, EIS was used to demonstrate the presence of biofilm formation when bacterial samples were grown in the custom-built test cell (37°C, LB, static) (Figure 6.2A). Being able to grow biofilms directly above the sensor and simultaneously imaging the interface maintained the coherence of the bacterial structure as much as possible for detection. Limiting the number of samples per support minimised movement and temperature disturbances.

EIS measurements were analysed but not presented at the previous stage since biofilm integrity was disrupted by sample pipetting from wells onto screen-printed electrodes.[601] SWV results shown in the supplementary materials (Figure C. 2) showed more variability between replicates and the likely presence of other metabolic products than pyocyanin alone, with higher peak amplitudes, suggesting that other metabolic pathways were favoured over pyocyanin production. Pyocyanin metabolic precursors are characterised by diverse and distinct pigmentation profiles.[603] This could lead to an overall alteration of sample spectra, however a response from the chosen detection wavelengths from pyocyanin confirmed with electrochemical detection is a confident validation. As the hyperspectral data focused on pyocyanin and almost none was detected in the custom-built test cell (Figure C. 2), the focus here was to detect biofilm formation with EIS, as the direct correlation between these two virulence factors still remains to be demonstrated.[604]

Nyquist plots (Figure C. 4) were fitted to a modified Randles equivalent circuit.[605] The evolution of LB across time was very distinct from pyocyanin and *P. aeruginosa* samples (Figure 6.10), which might result from a slow evaporation process occurring over time. Indeed, the LB condition with added gentamicin after 24 hours shows a more steady trend. The pyocyanin standard exhibits a decrease in charge transfer resistance (R_{ct}) over the first 24 hours followed by an increase over the next

24 hours, closer to the behaviour of LB alone. Both bacterial strains display identical R_{ct} trends: a steep decrease within the first 24 hours maintained at a slower rate over the next 24 hours (Figure 6.10). It appears that the initial R_{ct} value and its change over the first time period could be specific to the *P. aeruginosa* strain, reflecting the synthesis of electroactive secondary metabolites, attributable to phenazine compounds or PQS. A decrease in R_{ct} over time has previously proven to be indicative of biofilm extent.[601] The biofilm was formed at the air liquid interface[606] - visually confirmed and absent at t=0 as coming from an overnight culture under agitation - more distant from the electrode measuring area in this experiment than in previous demonstrations, which likely explains the fewer observed changes. Using the custom-built test cell to grow and characterise *P. aeruginosa* biofilm, it was possible to monitor biofilm formation in both strains using impedance measurements. Biofilm formation occurred within the timeframe of previously published work.[587] Antibiotic additions after the 24-hour measurement of 100 μg/mL, provoked a slight R_{ct} increase for PA14, possibly testifying of bacterial death and/or biofilm reduction. In this case, PA14 appears mildly susceptible to the gentamicin dose, even in a biofilm phenotype. LESB58 gentamicin treated condition behaviour differs from PA14. Its initial slow growth does not reflect its non-treated counterpart. However, the addition of gentamicin triggers a decrease in R_{ct} after 48 hours, inferring a possible resistance from LESB58 to gentamicin and favouring biofilm formation. At 48 h, statistically significant difference of $p < 0.034$ and $p < 0.033$ is recorded between no growth conditions of LB supplemented with gentamicin and biofilm growth respectively for LESB58 (Figure 6.10C) and PA14 (Figure 6.10D). Further work is required to establish whether a hyperspectral approach can be used to differentiate between *P. aeruginosa* in biofilm and in planktonic form.
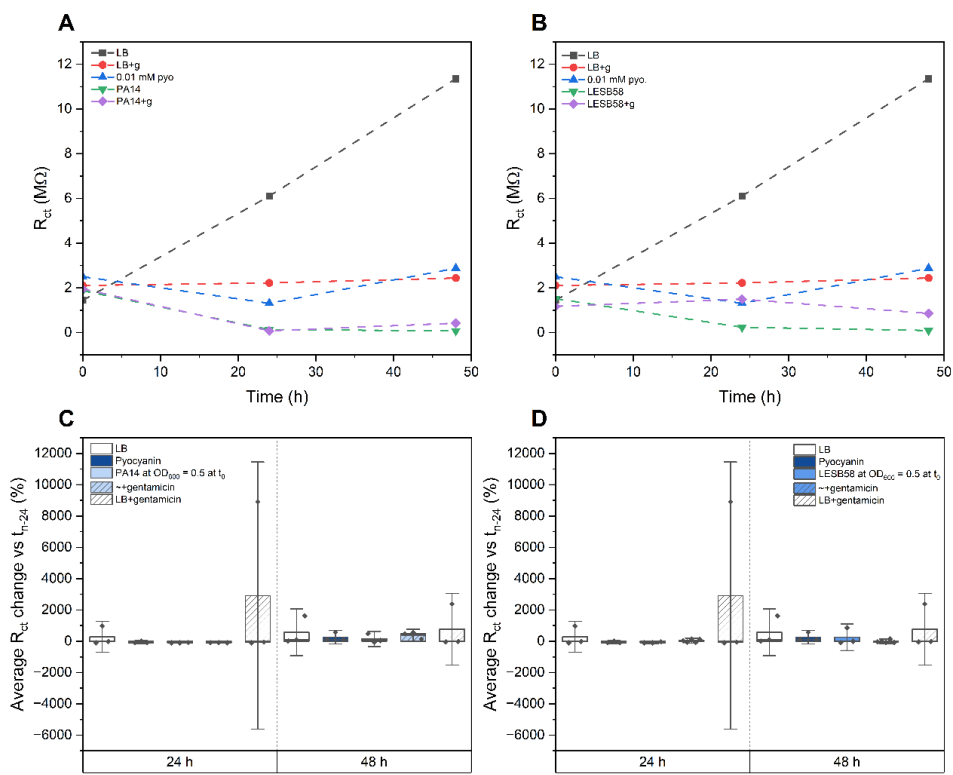
Figure 6.10. Electrochemical monitoring at 0, 24 and 48 h in the designed custom-built test cell of biofilm growth of R_{ct} of PA14 and LESB58 (respectively A and B) at initial OD_{600} = 0.5 and corresponding percentage changes between two subsequent time point reported in (C) for PA14 and (D) for LESB58. Adapted with permission from Dunphy, R. D. *et al.* Combining Hyperspectral Imaging and Electrochemical Sensing for Detection of *Pseudomonas aeruginosa* through Pyocyanin Production. Sensors & Diagnostics 2022, 1 (4), 841–850.

6.3.3 Discussion

EIS was chosen to enable surface assessment of the electrode, useful for further transfer of the method to bacterial biofilms where no redox mediators are produced, having only tested our system with one ESKAPE pathogen; *P. aeruginosa*, which is an outlier in this respect because of its production of redox active secondary metabolites. Further research is required to establish whether the presented method will work with multi-species biofilms, which are more reflective of clinical or even environmental cases,[533] for testing in later clinical samples. Relating measured bacterial density to colony counts should be performed as well as controlling the purity of the cultured bacteria. More extensive tests are required to confirm the absence of contamination between experiments and update the decontamination procedure.

In contrast to other spectroscopic methods that do not have a spatial component, such as UV spectroscopy, HSI can be used to gain an understanding of

the spatial distribution of metabolites produced by pathogens. Due to diffusion through the liquid culture in relatively small wells, the differences seen in Figure 6.9 are not pronounced, but more distinctive distribution patterns may be found in other settings. While of limited use in a clinical setting, this approach may allow for further research to increase understanding of how bacterial pathogens interact with their environments and disperse over time, which may be of interest for biofilm characterisation.

While HSI relies on large and expensive equipment, identifying wavelengths that correspond to diagnostic spectral features can allow the development of cheaper filter-based multispectral imaging (MSI) sensors that only capture the relevant wavelengths. These sensors could be simplified and miniaturised as electrochemical equipment is also prone to integration and miniaturisation, outlining the perspectives of detection and identification of specific microorganisms that are frequent causes of infection and implementation at the point of care.[607] Additionally, the strategy presented could be easily translated into low-cost mass-manufacturable screen-printed electrodes, with small reagent and sample volumes.

Proposing an engineering scenario to serve clinical purposes,[556] our combined biosensing approach aligns with future biofilm detection strategies highlighted by leaders of the biofilm field.[608] Despite an initial culture step, the application envisaged could directly assess the patient/clinical sample.

Detecting biofilm growth directly from the sputum of cystic fibrotic patients could be another possibility to identify chronic infections caused by *P. aeruginosa,*[608] enabling additional surgery procedures to be supplied where necessary.[595] With the combination of the three techniques, biofilm profiles could be added to a library to quickly identify the most common pathogens and assess treatment options. Having an "electrochemical fingerprint"[609] of various strains with a hyperspectral profile would allow for quick identification and guidance for more time-consuming and accurate sequencing downstream methods.[595,609,610]

Adapting sample volume could help bring biofilms closer to the electrode and reduce differences in compound quantifications. Earlier and later time points, as well as more frequent monitoring would also bring a heightened understanding of biofilm dynamics and formation by providing a full understanding of sample behaviour. The combined detection by hyperspectral and electrochemical methods provides more reliability and confidence in the final result, saving time by avoiding the need to perform an array of methods.

Finally, the combination of EIS with HSI and SWV allows a full range of measurements capable of metabolite detection and differentiation, identification and biofilm growth assessment. While HSI characterises pigmented secondary metabolites, SWV detects redox active secondary metabolites. Having both sensing modalities along with EIS to monitor biofilms provides a greater range of sensing opportunities.

6.3.4 Conclusion

This study demonstrates that **VNIR-HSI can be used in conjunction with electrochemical methods to detect pyocyanin within the clinically significant range for *P. aeruginosa*,** and furthermore that regression of key spectral bands may aid in the detection and characterisation of *Pseudomonas* spp. presence and growth through pyocyanin production. The wavelengths at which the greatest differentiation of pyocyanin is detected are outlined, suggesting **the possibility of developing a low-cost narrowband sensor for detecting *P. aeruginosa*. SWV in conjunction with EIS confirmed pyocyanin presence and quantity, as well as biofilm formation over gold screen-printed electrodes in an integrated custom-built test cell.** Designing and validating a method for combined use of these techniques with reference to *P. aeruginosa*'s well-documented tendency to produce pigmented redox active compounds has the potential to translate to a wider range of biofilm-forming infectious pathogens in future. Finally, the nature of the two technologies employed (HSI and electrochemical sensing) means that the system can be deployed in a range of formats, including a platform to better study biofilm development and for detection purposes at the point of care.

6.4 Adapting the developed electrochemical biofilm sensing strategy for the detection of redox-inactive bacteria using resazurin

As *P. aeruginosa* is a unique case in its production of distinctive electrochemically active biomarker, the assay developed in the previous part would not enable detection of bacterial growth or metabolite synthesis related to biofilm formation by most other bacterial species. Commonly used to assess metabolic activity in bacteria, resazurin was introduced as an electrochemically active substitute for bacteria without distinctive redox-active biomarkers. Resazurin is fast, inexpensive and can be scaled up for high-throughput screening, compared to the direct estimation from time-consuming and labour-intensive plating methods.[611] Its reduction from the blue resazurin to the pink resorufin (Figure 6.11) is proportional to the amount of metabolically active cells in a sample.[611] This provides antibiotic susceptibility information as metabolic activity shifts could be due to either biofilm formation and cells entering dormancy or metabolically active cells to be targeted by antibiotics even if in a biofilm phenotype. Its blue or pink coloration also enables later HSI characterisation.

Figure 6.11. Irreversible reduction of blue resazurin to pink resorufin and reversible redox reaction with transparent dihydroresorufin. [612]Reproduced with permission from Fan, Y.; Hao, R.; Han, C.; Zhang, B. Counting Single Redox Molecules in a Nanoscale Electrochemical Cell. *Analytical Chemistry* 2018, *90* (23), 13837–13841.

The developed electrochemical detection strategy was optimised in this section with resazurin for bacterial growth and biofilm formation with *Klebsiella pneumoniae* and *Acinetobacter baumannii*, as ESKAPE opportunistic pathogens and non-redox metabolite producers. *Acinetobacter baumannii* is on the WHO priority pathogen list for its incidence and resistance to even last-resort carbapenems.[564] Infections often cause high morbidity and mortality, up to 60%.[613] *A. baumannii* is often isolated from polymicrobial infections with *Klebsiella pneumoniae* , another opportunistic pathogen and they are both notorious biofilm producers.[614]

6.4.1 Material & Methods

6.4.1.1 Characterisation of the electrochemical response of resazurin on gold SPEs

Four concentrations of resazurin (199303 Sigma-Aldrich) in LB (Tryptone T7293 Sigma-Aldrich, Yeast extract Y1625 Sigma-Aldrich, NaCl 10316943 Fisher) were set up : 0.02%, 0.01%, 0.002%, and 0% based on literature reports[615]. Four *B. subtilis* concentrations (as an available non-pathogenic bacterial species) were tested as bacterial samples: OD_{600} 0.0625, 0.125, 0.25 and 0.375 with added resazurin to 0.002% (1:1 bacteria:resazurin+LB in 200 µL). A positive control consisted of *B. subtilis* at OD_{600} 0.375 without resazurin. Each condition was prepared in hexaplicate, one series dedicated to hyperspectral imaging and one series to sample for electrochemistry testing. Hyperspectral imaging was performed prior electrochemical interrogation of samples to remain consistent with the previously published assay[377]. The plate was then placed at 37°C for 24 hours and tested again.

6.4.1.2 Antibiotic susceptibility of biofilms formed by *A. baumannii* and *K. pneumoniae* with broth microdilution

Acinetobacter baumannii and *Klebsiella pneumoniae* were grown overnight in LB at 37°C, 250 rpm. A two-fold bacterial dilution series was tested from OD_{600} = 0.5 to 0.001 with both species and only two specific optical density values at 600 nm were tested for the last trial with *A. baumannii*: 0.25 and 0.05, the latter matching the earlier MIC testing and the former enabling a comparison with published data[377]. All conditions were tested in triplicates. Samples were assessed at different time points from static growth at 37°C in a 96-well plate: at 0, 4, 24 and 48 hours in the case of antibiotic treatment. Each replicate was exclusively sampled at the intended time point, meaning biofilm formation and maturation would not be disturbed until assessed.

6.4.1.3 Antibiotic treatment

After 24 hours, allowing for biofilm formation, set conditions were treated with gentamicin (G1264-50MG) at 128 µg/mL, representative of twice the MIC concentration of 64 µg/mL, to ensure *A. baumannii* in its planktonic state gets killed.

Antibiotic-free controls were treated with LB instead, to allow an assessment of sample disturbance independent of antibiotic action.

6.4.1.4 Resazurin addition and electrochemical parameter settings

For every time point, 50 µL were taken out of each well to be electrochemically interrogated. Series of wells to be imaged were not sampled. Resazurin was then added to a final concentration of 0.02% to sampled wells and completed with LB for the remaining volume. Following an additional 30 minutes at 37°C, 50 µL were sampled once more for further electrochemical assessment.

Potential windows for voltammetric measurements were based on Mishra *et al.* (2019)[616] narrowed interval from - 0.6 to - 0.1 V for characterisation and extended to - 0.9 to - 0.1 V for subsequent trials. Three scans were ran at 0.1 V/s with a 0.01 V step. DPV pulse parameters were set at 0.025 V and 0.05 s. SWV was run at a 0.005 V step, 0.05 V amplitude and 20 Hz frequency. EIS was acquired against OCP for 10 s with E_{ac} = 0.01 V and scanned 40 frequencies from 0.1 Hz to 10 kHz. Hyperspectral imaging capture was run alongside electrochemical measurements.

Nyquist plots were fitted to one of two circuits (Figure 6.12).
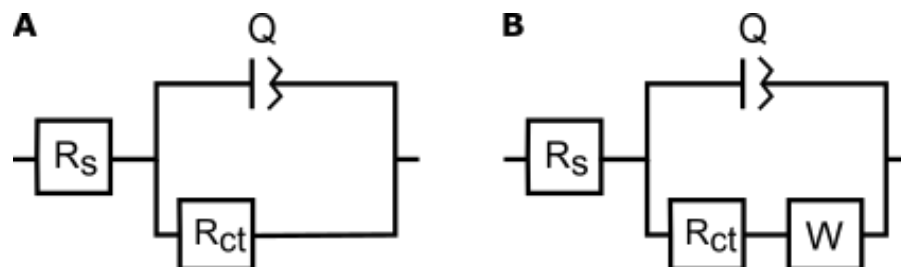
Figure 6.12. Electrical circuits modelling studied systems above electrodes. (A) Randles' circuit and (B) a modified version[590] where R_s designates the solution resistance, Q the constant phase element, R_{ct} the charge transfer resistance and W the Warburg element.

6.4.1.5 Bacterial growth and biofilm formation controls

Two control methods were ran alongside the second and third trial: using a specific 96-well plate to grow *A. baumannii* and *K. pneumoniae* biofilms for the same time duration as the electrochemical samples and taking OD_{600} reads at each sampled time point as well as a crystal violet assessment at all time points except 0 as it is

assumed that the biofilm could not have formed from inoculum grown under constant agitation.

For crystal violet staining, wells dedicated for imaging were used. Each condition was assessed in triplicate. Wells were emptied, washed once with distilled water and air-dried empty for 15 minutes. A matching sample volume of 0.1% crystal violet (C5168 Sigma Aldrich) was added to each well and incubated for 15 minutes. Wells were subsequently washed twice with PBS and air-dried empty for another 15 minutes. A matching sample volume of 95% ethanol was pipetted into each well to solubilise trapped crystal violet and the absorbance read at 570 nm following agitation by the plate reader for homogenisation.[21]

6.4.1.6 MIC assessment

A. baumannii was grown in LB overnight, at 37°C under agitation. Amikacin (A1774-250MG) and gentamicin dilutions in LB were performed in a 96-well plate followed by the addition of bacterial inocula to a final OD_{600} of 0.005 in each well. No antibiotic was added to the positive (bacteria in LB) and negative controls (LB blank). Each condition was prepared in triplicate. The absorbance was measured at 600 nm after 24 hours at 37°C.

6.4.2 Results

6.4.2.1 Electrochemical characterisation of resazurin behaviour

Firstly, the electrochemical characterisation of resazurin was conducted on the Dropsens gold screen-printed electrodes using voltammetry and EIS in bacteria-free dilutions (Figure 6.13). Two characteristic peaks occurred in resazurin samples, a smaller one around - 0.45 V and a higher one around - 0.25 V with DPV and at higher amplitude and similar potential in SWV (Figure 6.13C and D). The first cathodic peak results from the irreversible conversion of blue resazurin to pink resorufin and the more anodic peak reflects the reversible conversion of resorufin to the transparent dihydroresorufin (Figure 6.13).[617]

Peak amplitude increased linearly with resazurin concentration, confirming the possibility of a quantitative bacterial active metabolism assessment (Figure 6.13C

and D). At the lowest concentration of resazurin tested, the amplitude of the more negative peak cannot be clearly differentiated from the baseline (Figure 6.13C and D). Besant, Sargent and Kelley (2015) have emphasised the importance of evidencing an increasing or decreasing trend in peak detection rather than peak differentiation,[618] and so have Crane *et al.* (2021).[619] The Nyquist plot with R_{ct} values obtained from modified Randles circuit fitting shows the least change over 24 hours for the lowest concentration of resazurin tested (Figure 6.13B). Monteiro *et al.* (2012) conclude on 0.002% for their assays[615] and kept it below 0.01% moving forward,[620] this resazurin concentration was also chosen for the subsequent bacterial assessment based on R_{ct} values for 0.002% resazurin being close to LB and likely less toxicity to cells. This allowed for better differentiation for hyperspectral imaging at low bacterial concentration since aiming for early bacterial settlement detection.
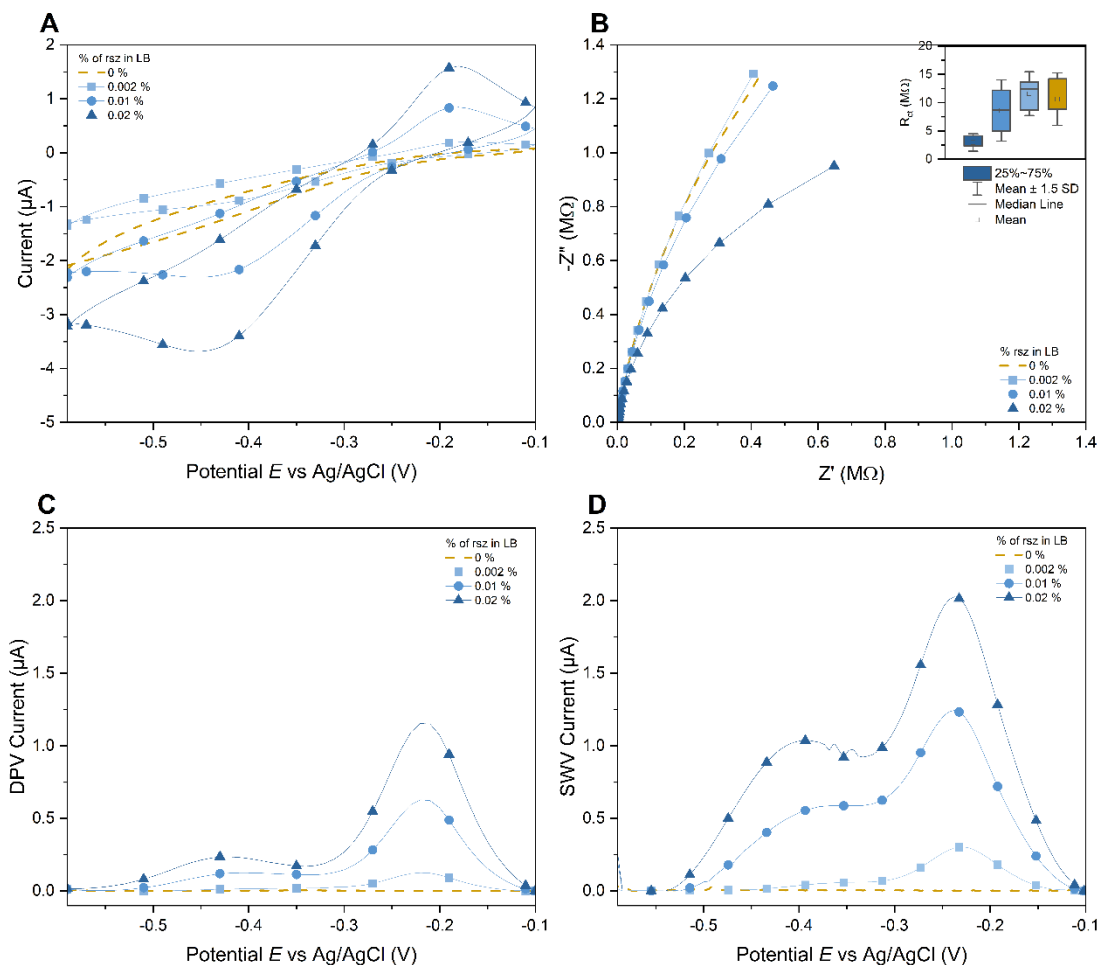
Figure 6.13. Characterisation of resazurin electrochemical behaviour on gold SPE. (A) CV, (B) EIS with fitting to a Randles' circuit (inset), (C) DPV and (D) SWV. Each trace is an average of three different electrode responses.

The data represented in Figure 6.13 comes from measurements after 24 hours as the ones taken right after resazurin addition showed higher noise and decreased peak resolution. Data presented in the following figures after result from the half hour resazurin addition, not directly after resazurin equivalent to the more noisy time after assessment. In subsequent trials, samples awaiting measurement were placed at 4°C and would not be processed immediately due to equipment capacity and experimenter handling limitations, being closer to the later resazurin measurements presented in Figure 6.13. Moving forward, resazurin was only added to the samples post bacterial/biofilm growth and incubated for 30 minutes at 37°C before measurement. Additional plates were prepared for biofilm assessment with crystal violet and OD_{600} for bacterial growth as a confirmation of observed electrochemical and hyperspectral trends. Here, samples to be interrogated electrochemically were pipetted out of the 96-well plate before hyperspectral imaging.

6.4.2.2 Assay optimisation on electrochemical parameter screening

6.4.2.2.1 Resazurin is an endpoint assessment of metabolic activity

After the electrochemical characterisation of resazurin in LB, biofilms were grown over 24 hours in 96-well microtiter plates. Metabolic activity was assessed at 4 and 24 hours by adding resazurin. The colour shift in bacterial samples occurred within the first few minutes of adding resazurin. Samples to be tested electrochemically at time 0 were kept at 4°C, slowing down bacterial growth while imaging was undertaken. Resazurin conversion was visually different for similar bacterial concentrations measured with the two different techniques (Figure 6.14). Conversely, the hyperspectral camera was set up in a housing and lit up by halogen lamps, raising the temperature surrounding the plate above 37°C in a few minutes upon adjusting parameters, speeding up active metabolism and resazurin colour change. After 24 hours, upon transferring samples for electrochemical testing, only the positive control, without resazurin, formed a biofilm. The colour of the wells did not visually change from the previous day. Images obtained and analyses related to the bacterial data set were therefore used as indication and for optimisation purposes rather than drawing conclusions.
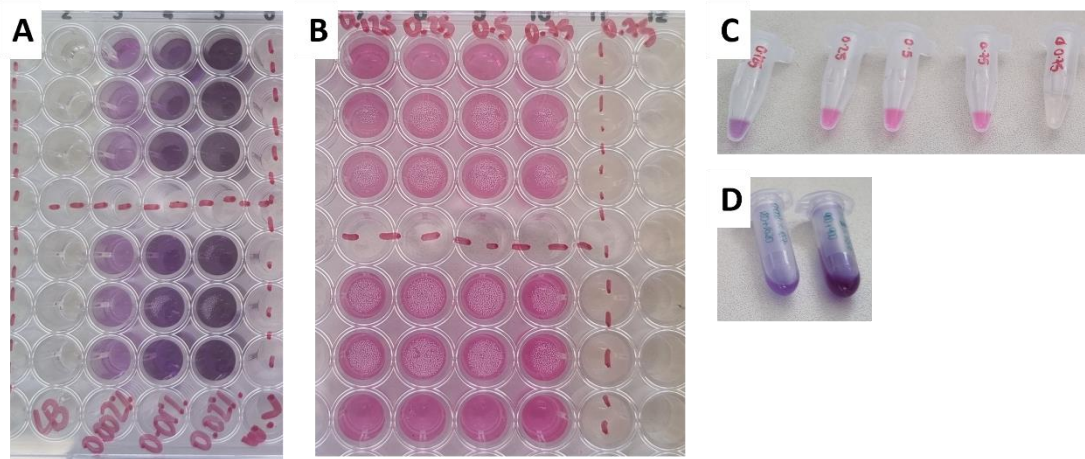
Figure 6.14. Resazurin visual colour changes in presence of bacteria. (A) Resazurin dilutions in LB (0.002, 0.01 and 0.02%) and (B) colour changes upon increasing bacterial concentrations (OD_{600} 0.125; 0.25; 0.5; 0.75) for HSI analysis. in comparison to no addition of resazurin at the highest bacterial concentration. Corresponding bacterial samples (C) and resazurin dilutions (D) stored at 4°C prior electrochemical interrogation.

Resazurin is irreversibly reduced upon metabolic activity to resorufin[621] (Figure 6.11), which explains why adding resazurin at time 0 would only reflect the bacterial population at this specific time point. A much higher concentration of resazurin would be required to enable monitoring over long time periods, which would more likely be toxic. Resorufin can be reversibly reduced to the colourless dihydroresorufin (Figure 6.11), which is also highly toxic.[621] Dihydroresorufin can be oxidised to resorufin with a lower reaction rate.[621] The potential presence of dihydroresorufin might have prevented bacterial growth and even survival. A more detailed explanation of reduction mechanisms of resazurin and resorufin can be found in previous work from Cakir and Arslan (2010)[617].

6.4.2.2.2 Bacterial and biofilm growth controls within assay conditions

Two ESKAPE pathogens other than *P. aeruginosa,* namely *K. pneumoniae* and *A. baumannii*, were selected for their infectious biofilm prevalence and critically reported antibiotic resistance.[564] They were grown at 37°C for 24 hours at various starting concentrations and sampled at 4 and 24 hours to a new plate for crystal violet staining. Biofilm samples for crystal violet assessment were grown and tested in the same 96-well plates, assessed only with hyperspectral imaging and not electrochemically.

An increasing trend correlated to increasing starting OD_{600} for biofilm formation is observed after 4 hours for both bacterial species, with higher absorbance values for *A. baumannii* (Figure 6.15A). After 24 hours, differentiation between starting bacterial concentration for both species does not seem possible anymore in terms of biofilm formation (Figure 6.15B). *A. baumannii* appears to be a better early biofilm producer than *K. pneumoniae*, given the higher absorbance values after 4 hours (Figure 6.15).
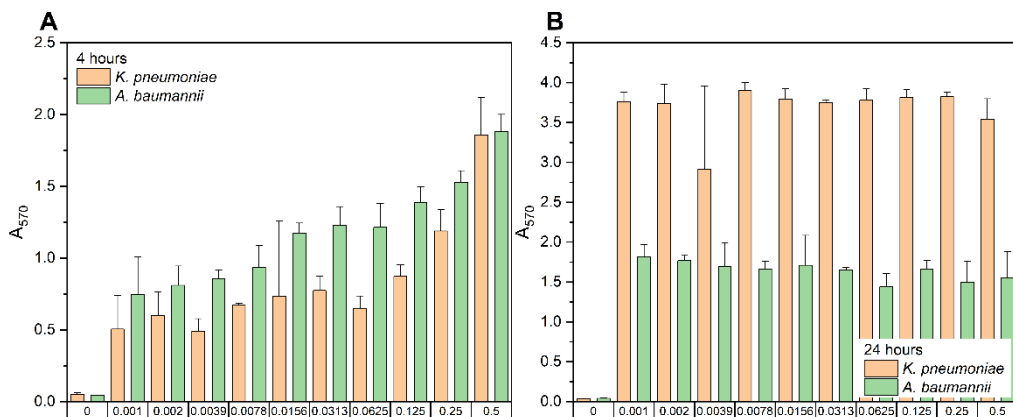
Figure 6.15. Absorbance at 570 nm following crystal violet assay for biofilm assessment of *A. baumannii* and *K. pneumoniae* at increasing OD_{600} values after (A) 4 and (B) 24 hours (B). 0 represents a blank withou bacteria (here 0.002% resazurin in LB). Each bar is the average of three samples.

K. pneumoniae showed lower values at the cellular level than *A. baumannii* in terms of absorbance values (Figure 6.16), maybe due to their difference in individual size (1–3 × 0.5–1 µm for the former and 1.0–1.5x1.5–2.5 µm for the latter).[622,623] Differentiation between initial seeding concentrations is possible within a wider concentration range after 24 hours for *A. baumannii* than *K. pneumoniae* (Figure 6.16A-D). Variation arising from sampling and measuring conditions did not seem to occur as both A and B series overlap for most time points for *A. baumannii* and *K. pneumoniae* (Figure 6.16E&F). The higher OD_{600} values at 4 hours versus 24 hours for higher bacterial concentrations might result from the stage of biofilm formation. Colony counting on agar plates could provide a standard verification for those differences.
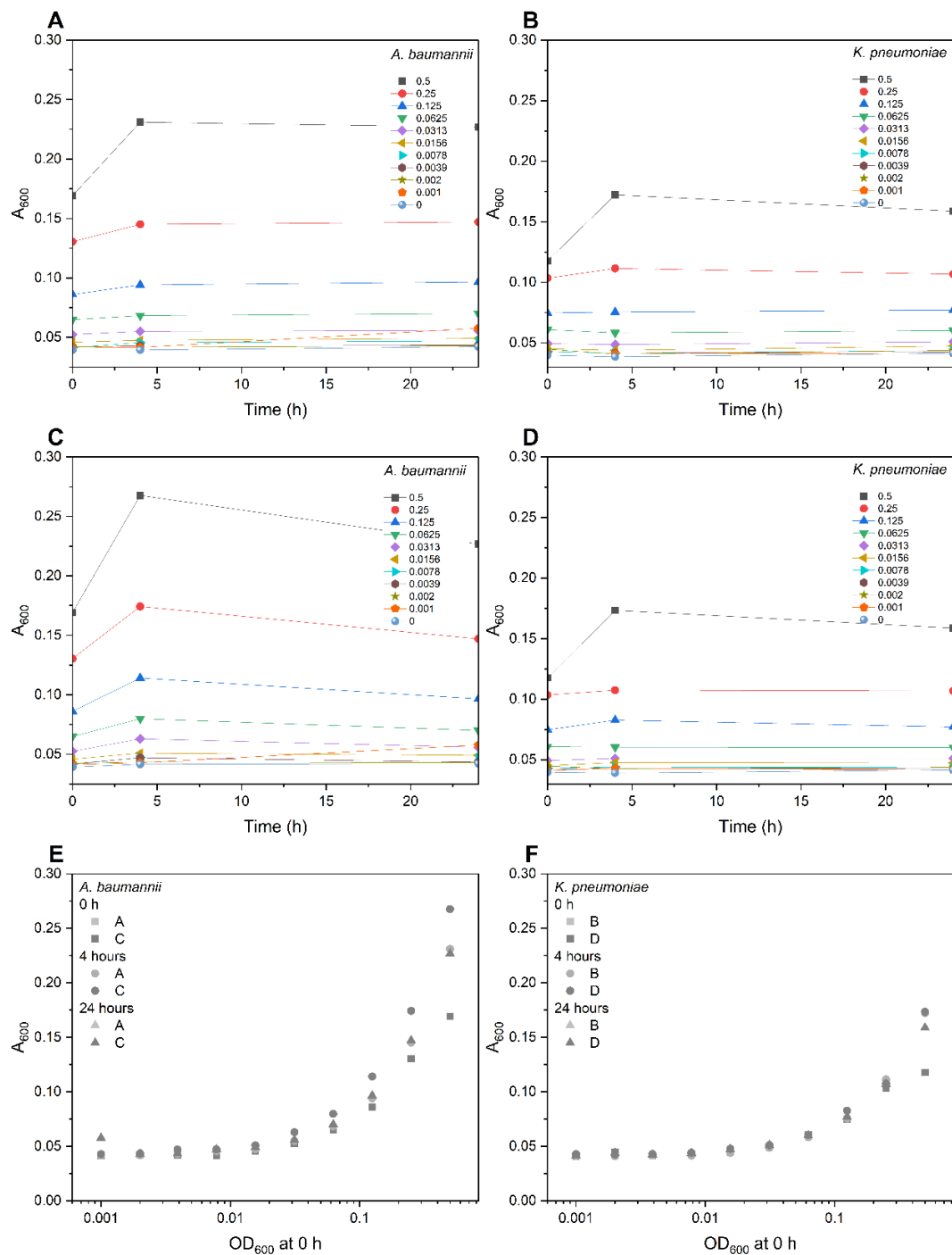
Figure 6.16. Impact of experimental perturbations on bacterial growth. Growth curves of the plates dedicated to HSI and crystal violet for *A. baumannii* (A) and *K. pneumoniae* (B) and plates dedicated to electrochemical, HSI and resazurin testing for the same pathogens (respectively C and D). Assessment of growth perturbation depending on experimental purpose for *A. baumannii* (E) and *K. pneumoniae* (F). Each data point is an average of three replicates.

Electrochemical assessment prior resazurin addition confirmed the absence of electrochemically-active compound(s) being produced in the resazurin region of interest from either *K. pneumoniae* or *A. baumannii* (Figure 6.17.).
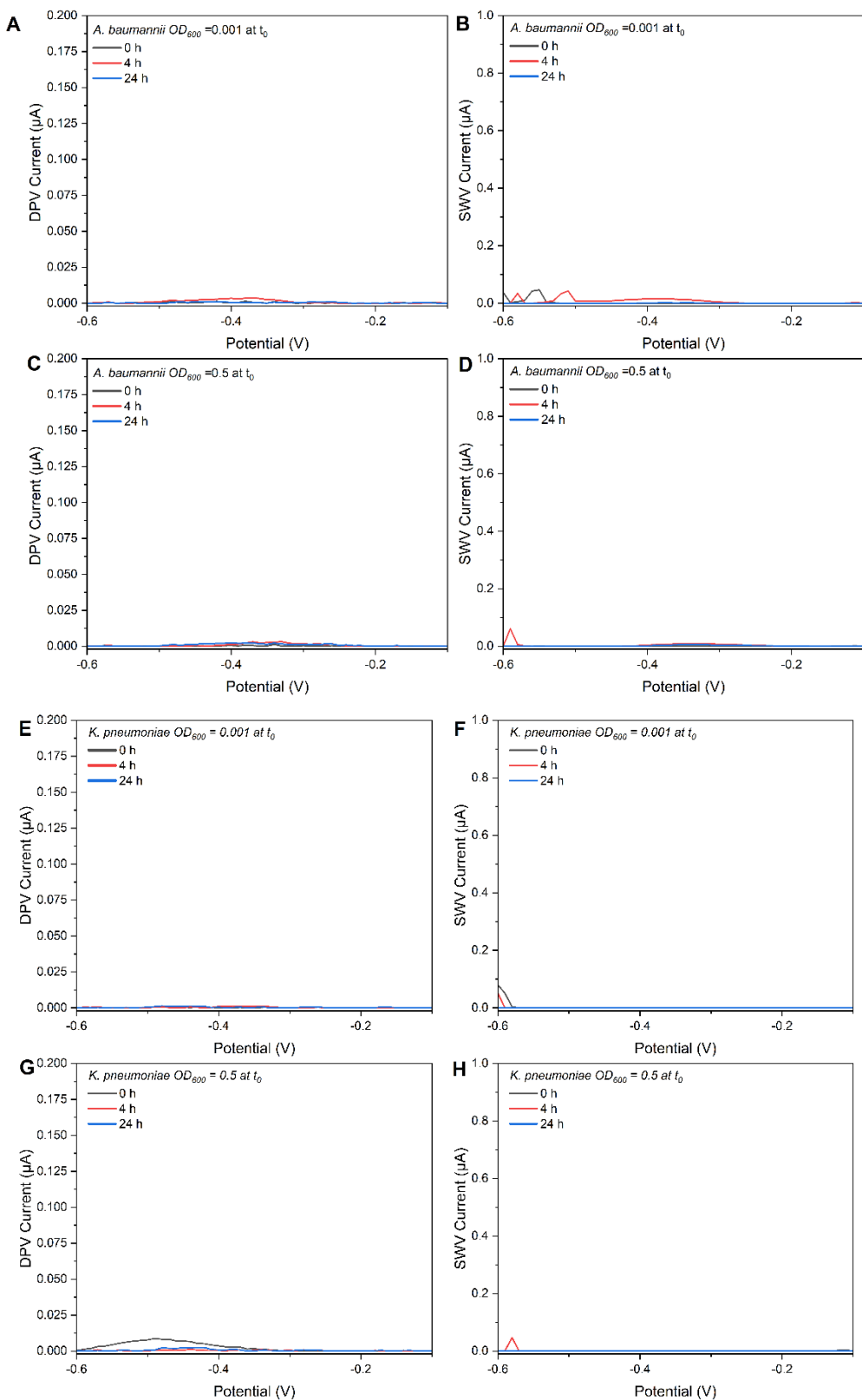
Figure 6.17. Absence of electrochemical activity using DPV (left) and SWV (right) in the studied potential window for *A. baumannii* (A-D) and *K. pneumoniae* (E-H) at the lowest (OD$_{600}$ = 0.001) and highest (OD$_{600}$=0.5) inoculated concentrations without resazurin. Each trace is an average of 3 samples.

6.4.2.2.3 Electrochemical monitoring of *Acinetobacter baumannii* biofilm and metabolic assessment via resazurin

Samples to be tested with resazurin were split between electrochemical testing and image capture before and after resazurin addition. The voltammetric response after biofilm formation and resazurin addition for *A. baumannii* at each sampled time point is depicted in Figure 6.18. The more cathodic peak in the LB control shows a higher amplitude than in the bacterial samples at most time points, whereas the more anodic peak displays lower amplitudes than for the bacterial samples. This confirms the conversion of resazurin (most cathodic peak) into resorufin (most anodic peak) (Figure 6.18) through active metabolism. The SWV parameters require more optimisation as detection of the more negative peak is more distinct with DPV than SWV, which is not in accordance with the sensitivity of each method. Peak amplitude for both pulsed techniques is higher after 24 hours compared to the previous time points (Figure 6.18A-D). However, reported peak current does not show a clear correlation to initial concentration for these trials (Figure 6.18E-F). This might be due to the amount of samples to be processed, delaying sample collection to electrochemical assessment during which the reaction might have continued and reached a maximum.

Considering the EIS response, two circuits (Figure 6.12) were fitted to the Nyquist plots and the R_{ct} values monitored (Figure 6.19). Both circuits seem to yield similar trends over time for the *A. baumannii* concentrations tested (Figure 6.19A&C vs. B&D). The presence of the Warburg element impacts on the range of R_{ct} values at 4 and 24 hours (Figure 6.19A&C). Consequently, calculated R_{ct} changes are slightly higher for the circuit including a Warburg element at 4 but not 24 hours. The decrease after 24 hours seems stable and concentration independent (Figure 6.19B&D). This implies that there is a high potential for early detection at 4 hours with possible EPS formation, and biofilm integrity is then essential since more fragile. However, it was compromised here as assessment were not yet conducted in the integrated system but manually pipetted to different wells and on the electrodes but taken into consideration for further optimisation.
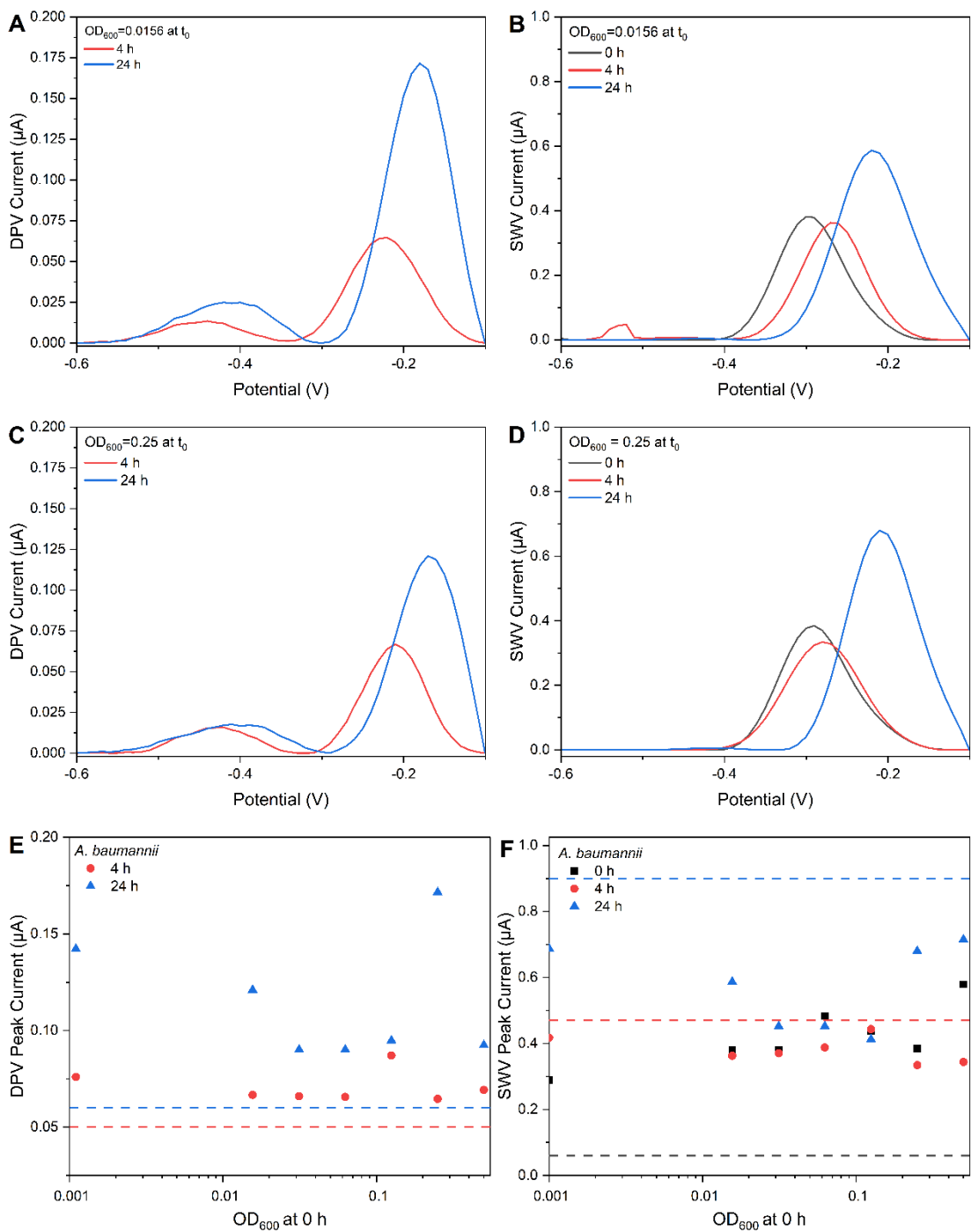
Figure 6.18. DPV (left) and SWV (right) responses of *Acinetobacter baumannii* at 0, 4 and 24 hours for lower (A&B) and higher (C&D) bacterial concentrations with correlation between peak amplitude against bacterial concentration for DPV (E) and SWV (F). Each datapoint is the average of 3 individual samples. Blank samples, only constituted of the growth medium, are represented with dashed lines with the colour corresponding to the appropriate time point.
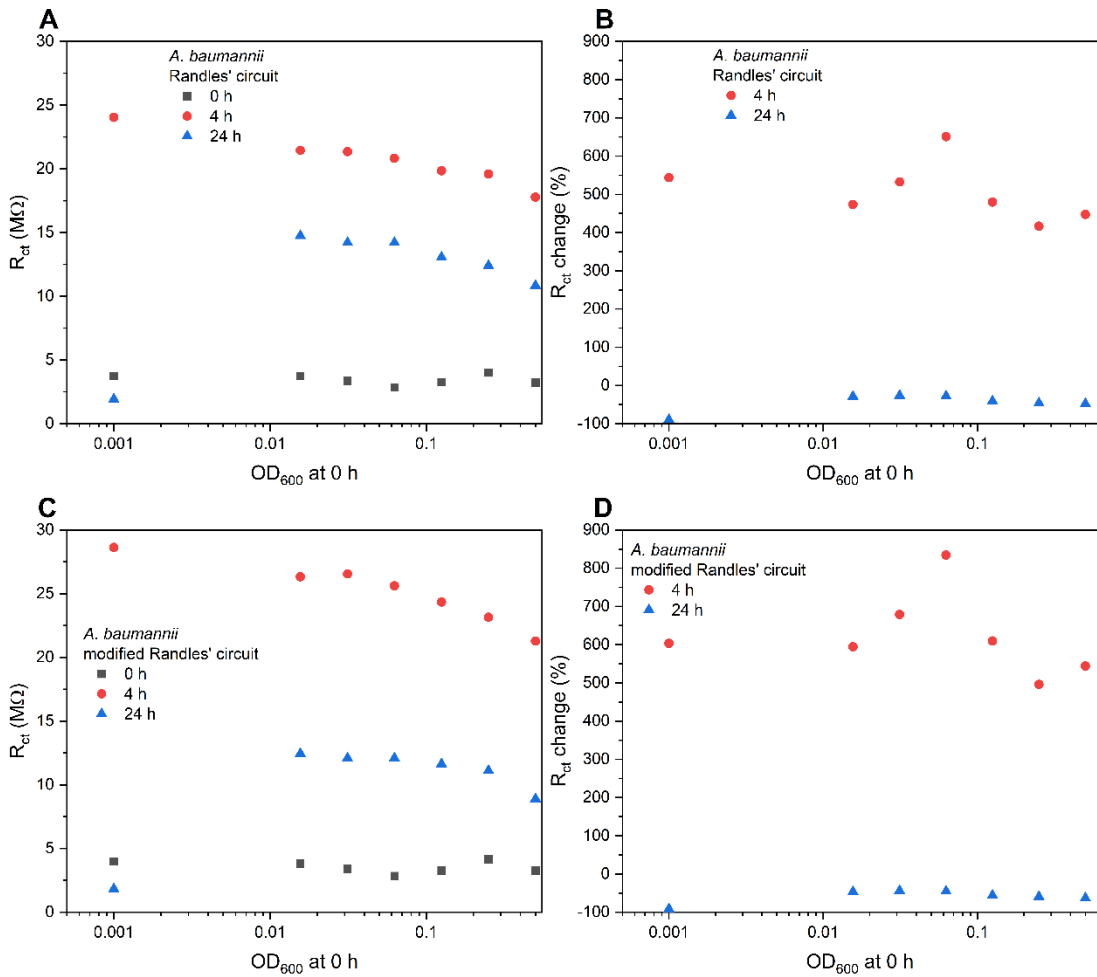
Figure 6.19. R_{ct} values of *A. baumannii* samples for circuit without (A) and with Warburg element (C) and percentage change against previous time point for respective circuits (B&D). Each data point represents the average of three samples.

6.4.2.2.4 Electrochemical monitoring of *K. pneumoniae* biofilm and metabolic assessment via resazurin

K. pneumoniae samples were treated similarly as *A. baumannii*. Samples were split between electrochemical testing and further image capture before and after resazurin addition.

The higher peak amplitude of the more anodic peak at 24 hours is also observed for *K. pneumoniae* (Figure 6.20A-D). DPV peak trends between time points do not display a consistent correlation to bacterial concentration (Figure 6.20E). The dashed lines represent LB medium without bacteria, which seemed contaminated for

SWV at 24 hours due to its higher peak current and could be due to insufficient rinsing of electrodes between sample interrogation or sample handling operations. The lowest concentration might be too low for accurate detection with these methods as recorded signals are equivalent to the next concentrations, more than an order of magnitude above (Figure 6.20E-F). Moreover, samples were all assessed in triplicates at OD_{600} values at 0 h twice diluted between of 0.5 and 0.001 and absence of datapoint at some of these values result from no positive peak being detected in the [- 0.3; - 0.1] V window.
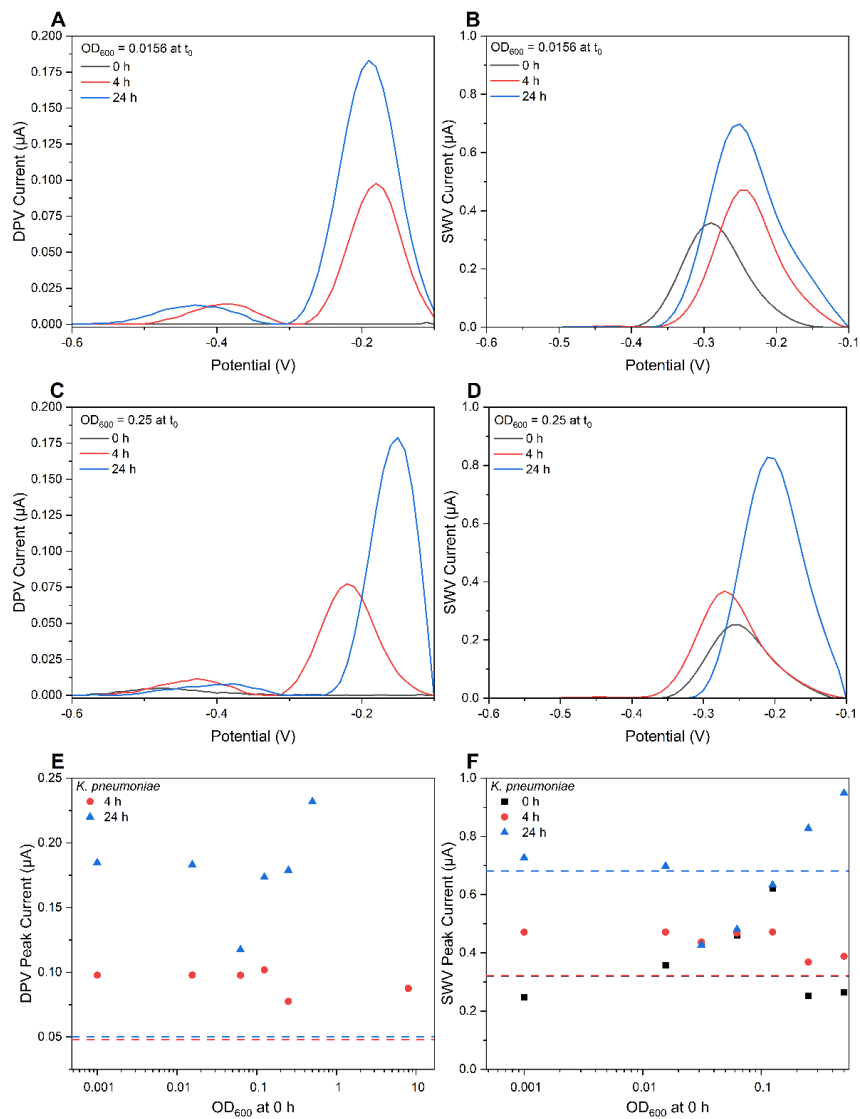
Figure 6.20. DPV (left) and SWV (right) responses of *Klebsiella pneumoniae* at 0, 4 and 24 hours for lower (A&B) and higher (C&D) bacterial concentrations with correlation between peak amplitude against bacterial concentration for DPV (E) and SWV (F). Each data point or trace represents the average of three samples. Blank samples, only constituted of the growth medium, are represented with dashed lines with the colour corresponding to the appropriate time point.

Concerning R_{ct}, highest values recorded at 4 hours for all concentrations of *K. pneumoniae* (Figure 6.21A&C) confirmed a similar behaviour for both bacterial species tested (Figure 6.19A&C). The higher magnitude of changes observed at 4 hours for the modified Randles' circuit (Figure 6.21B&D) correlated with *A. baumannii* observed pattern (Figure 6.19B&D) and the general decrease after 24 hours. Overall R_{ct} values for *K. pneumoniae* show more variability between time points (Figure 6.21A&C), especially after 4 hours compared to *A. baumannii* (Figure 6.19A&C), which could result from the difference in biofilm composition.
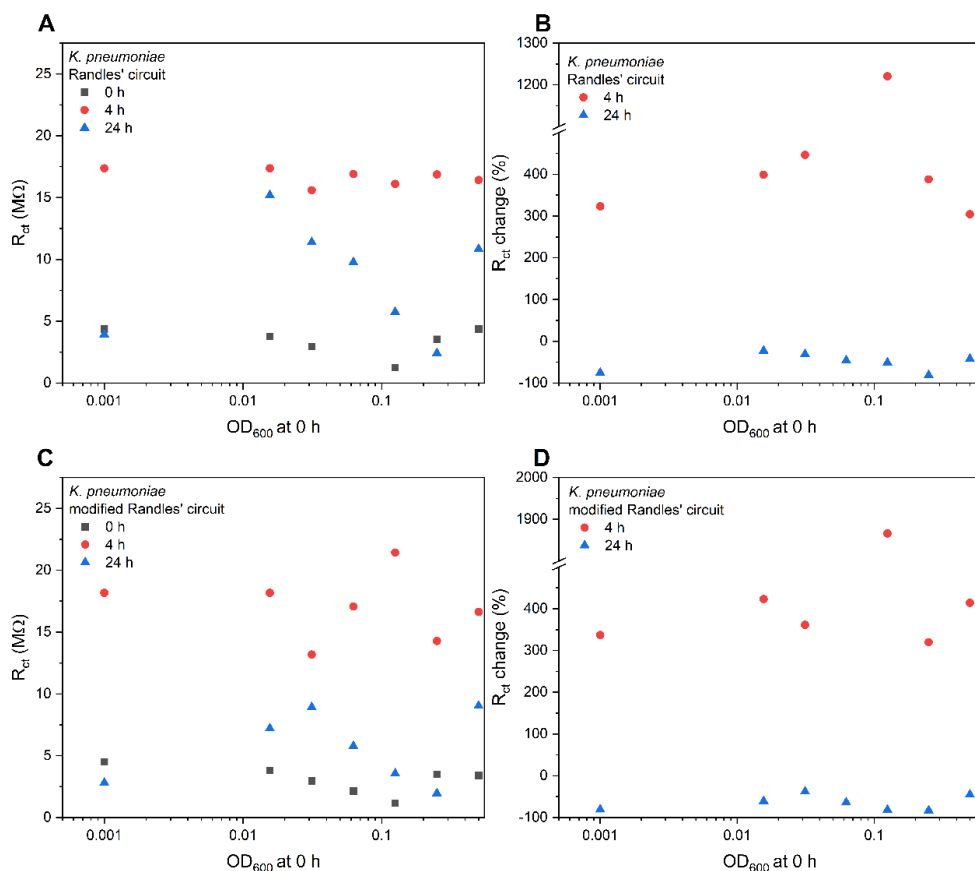
Figure 6.21. R_{ct} values of *K. pneumoniae* samples (left) for circuit without (A) and with Warburg element (C) and respective percentage change against previous time point (B&D). Each data point represents the average of three samples.

The ability to differentiate between biofilm formation early at 4 hours from higher absorbance values with crystal violet assessment (Figure 6.15), the differentiation between time points in R_{ct} values trends (Figure 6.19 compared to Figure 6.21) and the better consistency and correlation between initial bacterial

concentration and R$_{ct}$ made *A. baumannii* the candidate retained for following experiments; including HSI data (Figure C. 6 and Table C. 1).

6.4.2.3 Sample handling for a more accurate electrochemical monitoring

As mentioned earlier, resazurin is irreversibly converted into its pink resorufin form, reflective of active metabolism in live cells.[611] Despite multiple reports of its lesser toxicity compared to other metabolic indicators,[611] resazurin still hinders normal microorganism growth and is used for end-point estimation rather than continuous monitoring.[624] Furthermore, due to manual sample handling and output limitations, sampled wells could not be all measured at the exact time point and were placed at 4°C until tested. More distinct colour changes led to the assumption that resazurin conversion carried on at a slower rate, even though stored at a lower temperature. Measurements were relative to one another over time rather than strictly quantitative. Moreover, the hyperspectral imaging set-up included an enclosure with 2 halogen lamps directed at the plate, raising the surrounding temperature and enabling the reaction to continue if several images were taken. This means that samples analysed with the two methods were more and more divergent.

Hence the need arised for a supplementary sample processing step to stop the reaction. Taking into account the existing sample complexity, maintaining bacterial cell integrity and minimal interference to the microenvironment, metabolite or antibiotic by an added compound were crucial. Several options were considered such as stopping the reaction by adding an inhibitor at an excess amount or removing one of the reactant, a temperature shock, separation by centrifugation, or a reduction in sample number to enable a nearer real-time assessment. The former was not pursued as it raised the cost of the assay and added an extra variable that might have changed the electrochemical profile. Access to a - 80°C freezer or liquid nitrogen was not readily available in the same laboratory, which would have increased contamination and safety risks from transportation.

Therefore, attempts for mechanical sample separation were conducted by plate centrifugation. Bacteria would be pelleted with minimal damage while secreted

and excreted metabolites would remain in the culture medium, without the necessity to add any more reagent. A microtiter plate material that would stay intact throughout and after the centrifugation was also needed.

A. baumannii inocula at OD_{600} of 1, 0.5, 0.1 and 0.01 from an overnight culture were pipetted in triplicates in a 96-well plate. One was centrifuged at 3000 g for 10 minutes, another at 4000 g for the same duration. Supernatants were transferred to the empty wells below and absorbance values measured at 630 nm. Resazurin was then added to the wells to a final concentration of 0.002% for visual differentiation and kept at 37°C overnight.

Centrifugation speeds tested originated from published reports.[625] The reason for testing 3000 g resulted from 96 well plate sides breaking after 10 min at 4000 g, meaning plates could not be held properly in the plate reader tray anymore, and did not provide reliable results. Polypropylene 96-well plates (3355 Corning) were used instead of the standard polystyrene (10748692 Fisher Scientific).[626] However, their bottom was opaque, only allowing an absorbance read from the top. A different spectrophotometer had to be used, which only allowed fixed wavelengths and 630 nm was the closest one available to 600 nm.

The absorbance of the pellet increases in correlation with bacterial concentration after both centrifugations (Figure 6.22). The maximal absorbance was higher for the slower centrifugation speed at the highest bacterial concentration tested. This is potentially explained by supernatants being pipetted out with a single channel pipette, the multichannel instrument having shown less control, introducing more variability due to the viscosity of biofilms. All other bacterial concentrations are equivalent in absorbance values, whether considering the supernatant or pellet. No discrimination between the negative control and the two lowest bacterial concentrations is observed (Figure 6.22). After 24 h, all wells, including controls, were equally pink, meaning that the resazurin reaction carried on.
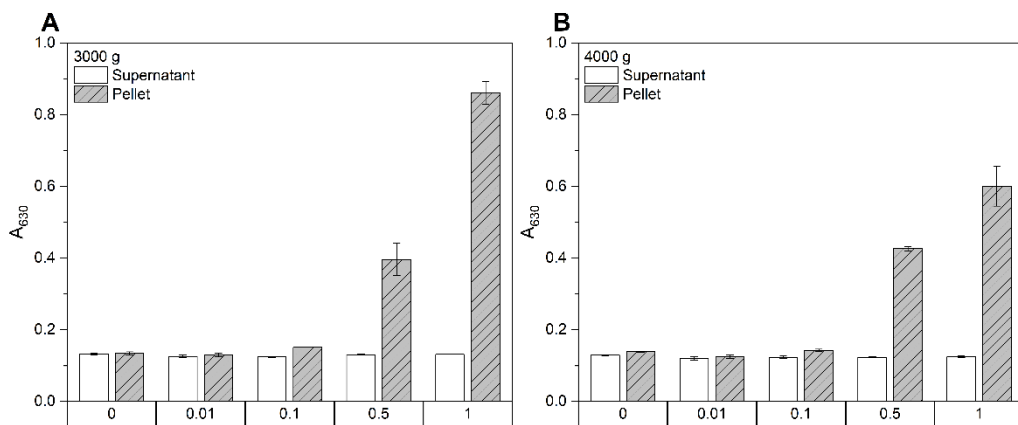
Figure 6.22. Absorbance at 630 nm of *A. baumannii* dilutions after centrifugation at 3000 g or 4000 g (respectively A and B), with pellet and supernatant separated and left overnight at 37°C. Bars represent the average of 3 samples with error bars indicating one standard deviation.

Centrifugation of samples, with subsequent manual separation of supernatant and pellet did not provide the sufficient possibility to slow down resazurin conversion and generated additional sources of contamination and more manual handling. As a result, the number of samples was consequently reduced to enable electrochemical measurement at the specified time points.

6.4.2.4 Antibiotic susceptibility assessment of *A. baumannii* biofilms through voltammetric and EIS monitoring using resazurin

Final adjustments with a lower sample output mostly constituted the final trial in the microtiter plate, for equivalent conditions to be tested after in the integrated test support. *A. baumannii* was inoculated at two starting OD_{600} values: 0.05 and 0.25. Electrochemical interrogation occurred at 4, 24 and 48 hours after resazurin addition and a 30-minute incubation. Gentamicin was added after the 24-hour measurement and its action assessed 24 hours later. Its concentration was based on a broth dilution-based MIC assessment and further data interpretation correlated with crystal violet assay and bacterial growth through absorbance at 600 nm.

6.4.2.4.1 *A. baumannii* MIC assessment for bactericidal antibiotic selection and dosage

MIC assessment for *A. baumannii* aimed at selecting an active antibiotic and its concentration for further electrochemical susceptibility testing on biofilms with SWV and EIS.

MIC determination was undertaken for *A. baumannii* using two antibiotics, gentamicin and amikacin. Activity of these aminoglycoside antibiotics was monitored and reported by EUCAST. A bactericidal activity was preferred to enable maximal trend differentiation (Table 6.2).

Table 6.2. Reported EUCAST breakpoints for MIC interpretation of *A. baumannii.* Inoculated at $5*10^5$ CFU in Mueller-Hinton broth.[627]

Antibiotic	Bactericidal?	Susceptible	Resistant
Amikacin	√	≤8 mg/L	>8 mg/L
Gentamicin	√	≤4 mg/L	≥4 mg/L

The recommended 18-hour incubation[627] was extended to 24 to match our assay conditions. Amikacin showed no antibiotic activity against *A. baumannii* whereas the observed MIC for gentamicin is 64 µg/mL (Figure 6.23). Therefore, gentamicin was selected for the following experiment, above the MIC at 100 µg/mL.
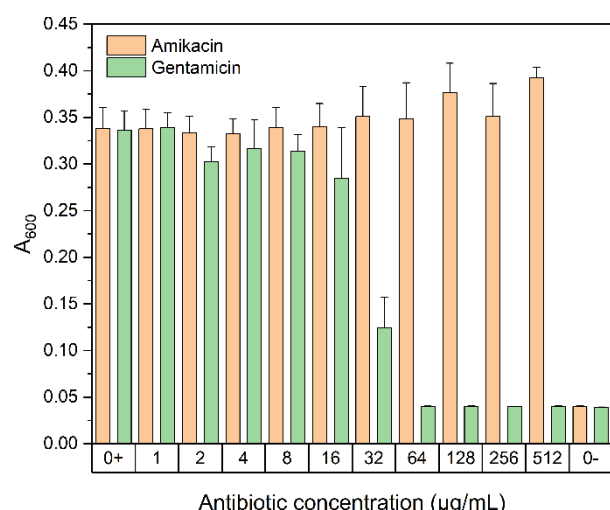
Figure 6.23. Absorbance at 600 nm after 24 hours for MIC determination of amikacin and gentamicin against *A. baumannii* with each bar representing an average of 3 samples and the error bar indicating one standard deviation.

6.4.2.4.2 Biofilm and bacterial growth controls

Crystal violet testing was undertaken is separate 96-well plates, one dedicated for each time point as this is an end-point assessment. Based on crystal violet controls, *A. baumannii* biofilms have grown proportionally to starting bacterial concentration over the first 4 hours and increasingly over the first 24 hours (Figure

6.24A 24h columns). A decrease in absorbance was observed after 48 hours (Figure 6.24A 48h columns) partially due to the addition of LB creating a physical disturbance. This decrease was intensified by the antibiotic treatment (respectively for 0.05 and 0.25, - 30% and - 45% without gentamicin and - 55% and - 58% with treatment). Concerning the increase after the 24-hour LB addition measured at 48 hours, this could be the result of variations between plates, well staining or a contamination as the OD_{600} values also increased after 48 h (Figure 6.24 and Figure 6.25). The possibility of wells being stained seemed more unlikely with the statistically significant difference recorded. Biofilm formation was evidenced from the crystal violet assay (Figure 6.24) and bacterial density increased proportionally to initial seeding density after 4 hours, without possible differentiation anymore after 24 hours (Figure 6.25). Antibiotic activity was detected with a decrease for both bacterial densities using absorbance measurements (Figure 6.25) and a lower statistically significant difference between antibiotic-treated and blank samples at 48 h compared to antibiotic-free bacterial samples with crystal violet (Figure 6.24).
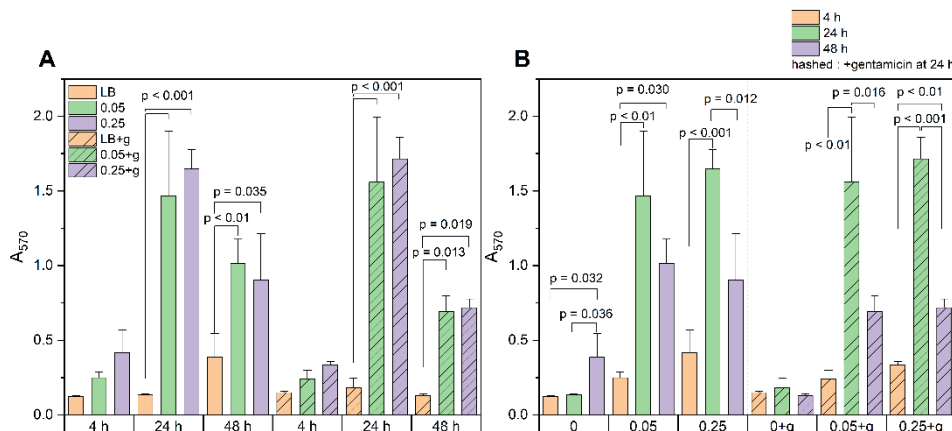
Figure 6.24. Absorbance at 570 nm after crystal violet assessment of *A. baumannii* biofilms for two starting bacterial densities at 4, 24 and 48 hours untreated and treated with gentamicin after 24 hours (hashed). Representations per bacterial densities (A) and time point (B) show the different statistically significant differences. Each bar represents the average of three independent replicates and the error bars indicate one standard deviation.
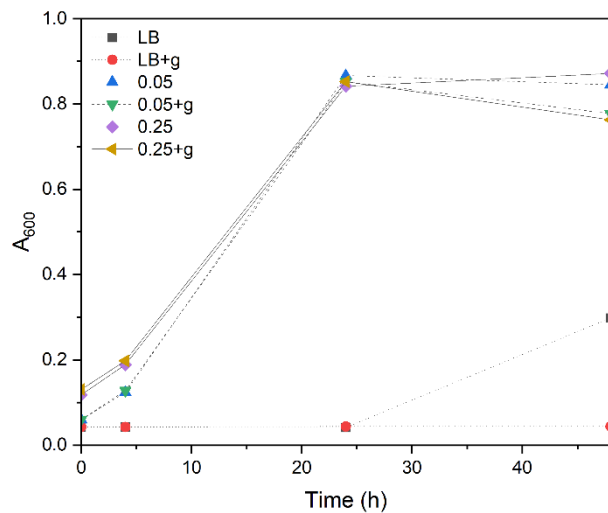
Figure 6.25. Absorbance at 600 nm of *A. baumannii* at 0, 4, 24 and 48 hours untreated and treated with gentamicin (g). Each datapoint represents the average of three replicates.

6.4.2.5 Antibiotic susceptibility of *A. baumannii* biofilms

Firstly, DPV responses of *A. baumannii* biofilms were analysed. LB contamination was noticed in the controls after 48 hours (Figure 6.24 and Figure 6.25). A difference in peak intensity was consistently noticed between 0 and 4 hours for the higher bacterial concentration (Figure 6.26E&F). At 24 hours, the difference in peak amplitude between the more cathodic and more anodic peaks was more consequent than for the blank samples and despite the same treatment for all samples, samples to be treated with antibiotics adopted a slower bacterial growth or less metabolically active biofilms compared to untreated ones (Figure 6.26). After 48 hours, a decrease in peak ratio was evidenced with LB treated samples (Figure 6.26A&C&E), translating into less overall metabolic activity whereas the antibiotic treated group underwent an increase in peak amplitude difference proportional to initial seeding concentration (Figure 6.26B&D&F), correlating to more active metabolism and susceptibility to the antibiotic treatment (Figure 6.24 and Figure 6.25).
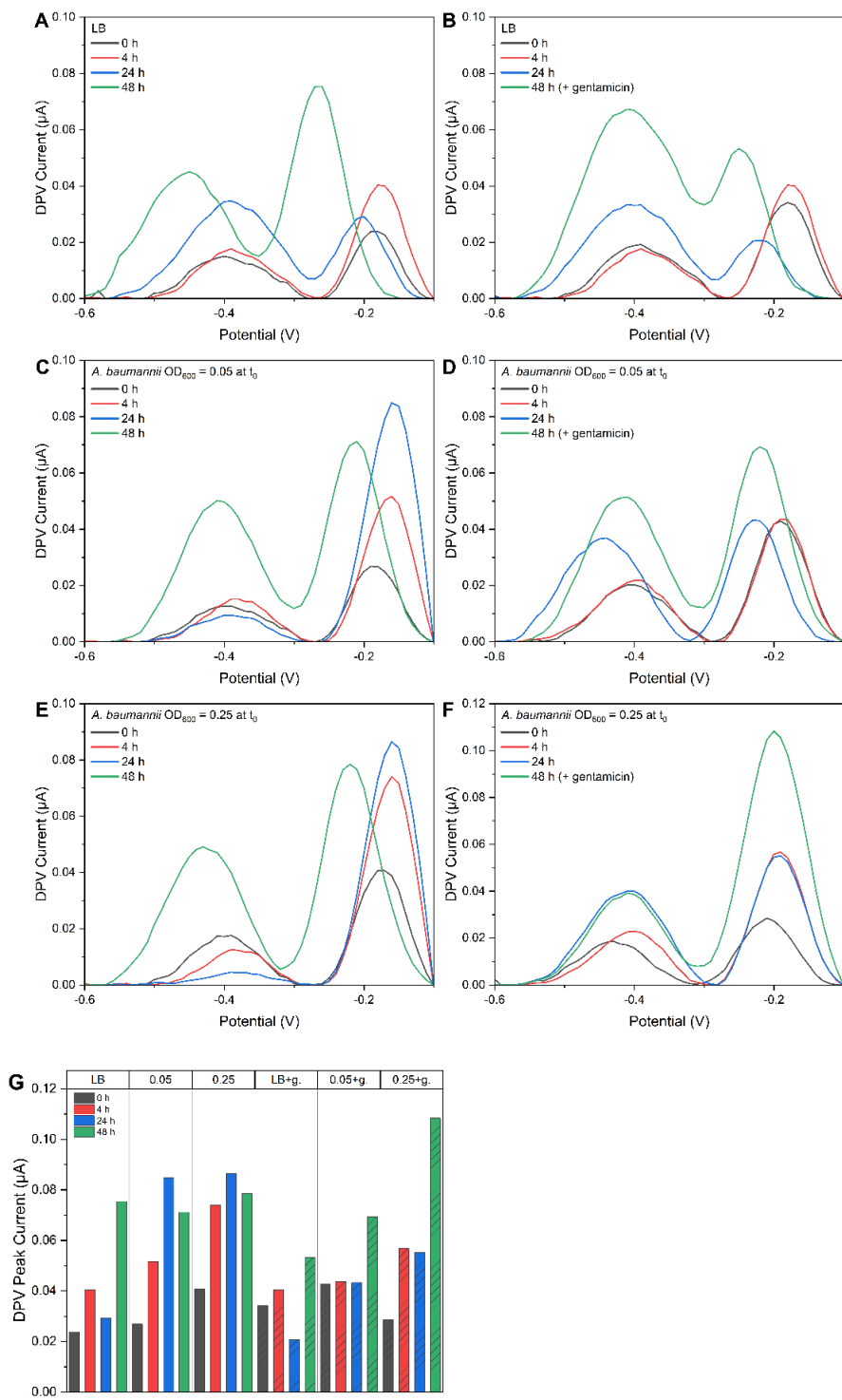
Figure 6.26. DPV traces of *A. baumannii* at 0, 4, 24 and 48 hours respectively without (left) and with (right) antibiotic treatment for a blank solution (A&B), initial OD_{600} of 0.05 (C&D) and 0.25 (E&F) with the peak current summary of the most positive peak (G). Each trace or bar represents an average of three samples.

An increase in peak amplitude difference over 24 hours and a decrease after 48 hours could indicate bacterial/biofilm growth over the first 24 hours through

bacterial growth and maturation of the biofilm over the next day with reduced metabolic activity (Figure 6.26).

Since control methods were conducted on different wells than the ones electrochemically measured, and wells assessed were different for each time point, bacterial variability impacted observed results. Running the resazurin-treated samples directly through the plate reader might have been best to correlate a control method with electrochemically interrogated samples. Real-time monitoring without affecting bacterial and biofilm growth with resazurin is not possible as it is an end-point assay. Even further use of the test support, bacterial variability between tested wells will have to be accounted.

Secondly, SWV peak current from control samples reached similar amplitudes than bacterial samples. Peak differentiation was not as resolved as with differential pulse voltammograms. Current changes did not reflect trends in the controls as well as DPV did, requiring more parameter fine tuning (Figure 6.27).

Despite Besant, Sargent and Kelley (2015)[618] along with Crane *et al.* (2021)[619] emphasising on increasing or decreasing trend in peak detection rather than peak differentiation which is valid for the SWV results, the DPV peak current here provides information not only on bacterial/biofilm growth but also metabolic activity and antibiotic response behaviour, which fulfil our aims.
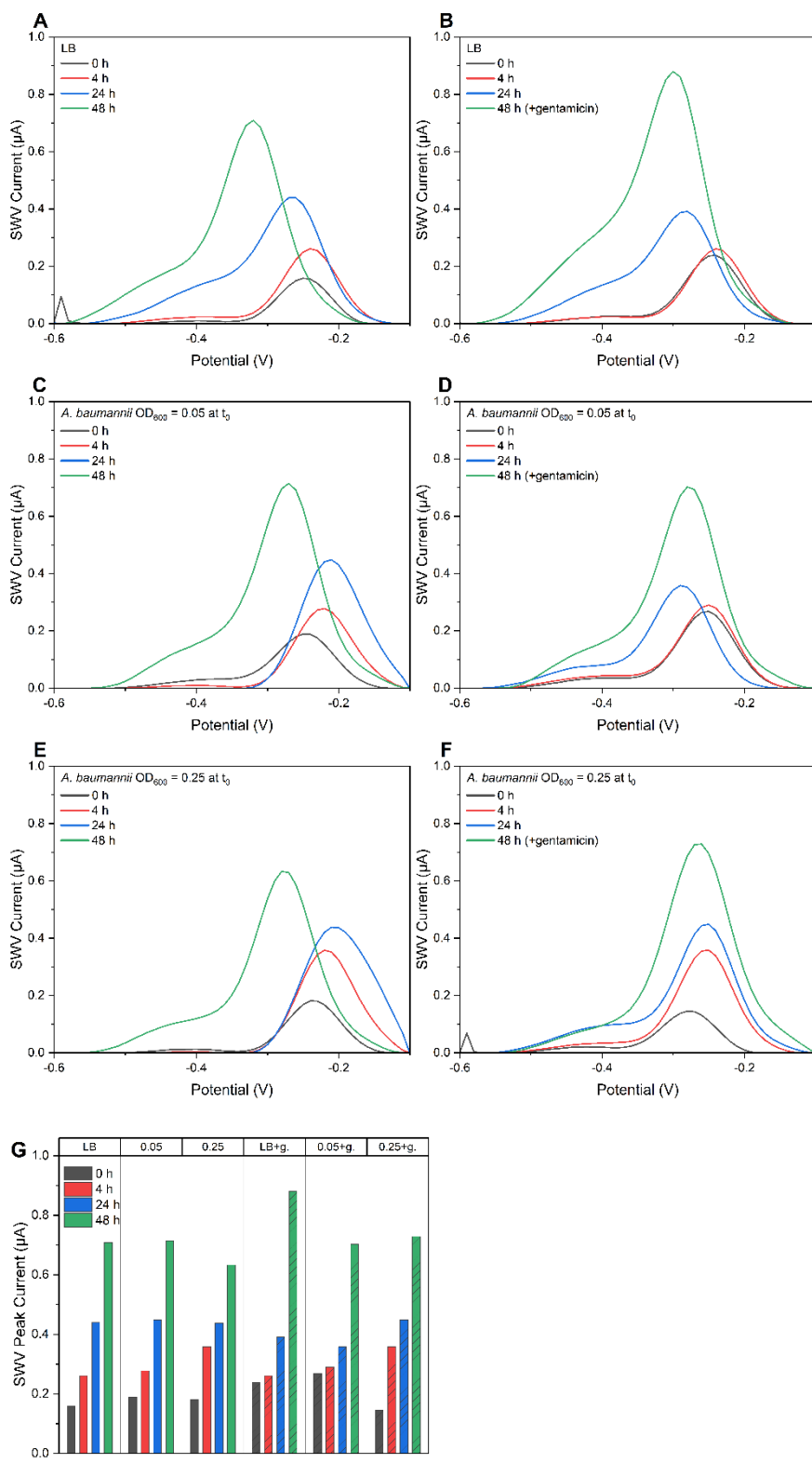
Figure 6.27. SWV traces of *A. baumannii* respectively without (left) and with (right) antibiotic treatment for a blank solution (A&B), initial OD_{600} of 0.05 (C&D) and 0.25 (E&F) with the peak current of the most anodic peak (G). Each trace or bar represents an average of three samples.

Thirdly, Figure 6.28 presents R_{ct} monitoring of *A. baumannii* biofilms treated either with LB or gentamicin after 24 hours, using resazurin. The R_{ct} decrease from both 0.05 and 0.25 (Figure 6.28) correlated with observed patterns in *P. aeruginosa* (Figure 6.10), possibly reflecting quorum sensing for biofilm establishment as secondary metabolites such as pyocyanin facilitate electron exchange but could also be due to the multiplication of planktonic bacteria as bacteria carry a net negative charge. Samples to be treated with antibiotics seemed to have a different biofilm formation pattern, with a R_{ct} increase for the least concentrated samples and similar behaviour as LB for the more concentrated ones and a slight decrease after antibiotic treatment. At 48 h, untreated samples showed an R_{ct} increase proportional to the initial seeding concentration and possibly biofilm growth, however not as consequent as for the 24-hour samples. Antibiotic-treated LB underwent a minor increase and antibiotic-treated bacterial samples showed a decrease. The antibiotic exerted its activity as the biofilm might not have progressed as much but did not fully stop bacteria to divide and expand (Figure 6.28).
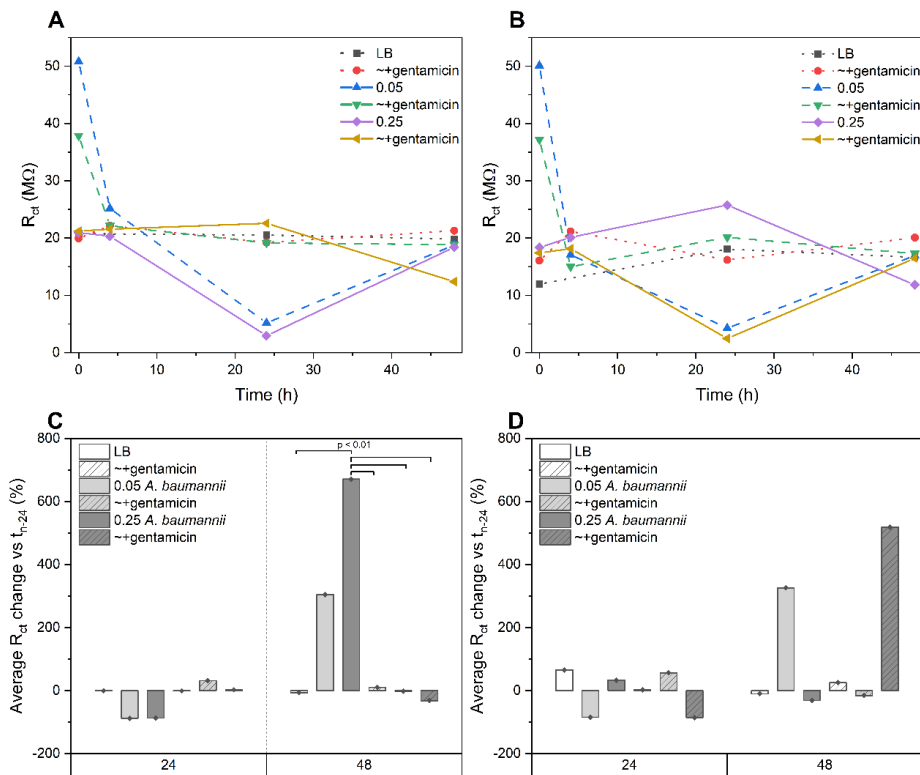
Figure 6.28. R_{ct} values and corresponding percentage change against previous time point of *A. baumannii* samples for Randles and modified Randles circuit fittings (respectively A&C and B&D). Each data point is the average of three replicates and each bar represent the percentage change between the R_{ct} average of three replicates.

Circuit fitting without the Warburg element provided more statistically significant difference between growth and no growth results for this data set (Figure 6.28C-D). Using resazurin as the redox mediator to monitor biofilm growth and their antibiotic susceptibility has therefore proved promising for *A. baumannii* biofilms treated with gentamicin in a 96-well microtiter plate. However, running the assay in a 96-well microtiter plate constituted the intermediate step, the final step consisting in the integrated test support use; yet to be conducted. A modified Randles' circuit might then be a more suitable fit given that the biofilm would be grown directly above the electrode, taking into account diffusion, and without physical or mechanical disturbance, in line with the previous publication.[377]

6.4.3 Discussion

Presented here is an integrated assay, first on the model organism *P. aeruginosa* due to its specific pyocyanin production, that is both electrochemically active and detectable using hyperspectral imaging thanks to its blue pigmentation. The possible influence of passing an electrical current and favouring biofilm development[533][545] has been countered by minimising the number of measurements recorded. The assay provides information on *P. aeruginosa* biofilm development in near real time and has clear potential for translation into clinical use.

To ensure low component costs and take advantage of mass production potential, we aimed for direct detection of biofilm without electrode functionalisation with screen-printed electrodes. Carbon is a widely reported electrode material for *P. aeruginosa* biofilms such as Ward *et al.* (2014), using carbon SPE for the monitoring of *P. aeruginosa* biofilms.[590] Gold was preferred here over carbon, considering that some bacterial species show low electroactivity and carbon's inertia could hinder their detection. Despite microelectrodes and interdigitated arrays enabling a better surface area and higher signal-to-noise ratio, this would have generated a consequent increase in cost. Biofilm immobilisation on gold electrodes has been reported and monitored via cyclic voltammetry on a gold working electrode against a platinum counter and Ag/AgCl reference electrodes.[628,629] Multispecies biofilms were detected using a similar electrochemical set-up in terms of electrode materials in conjunction

with EIS.[629,630] Concerning impedimetric detection of biofilms on unmodified gold, more studies have been published.[629,631]

If the biofilm does not cover the entire electrode measuring area, this could impact the conclusions drawn from acquired data.[541] This also relies on the rate at which the biofilm to be detected grows. The overarching strategy of combining the hyperspectral imaging method with electrochemistry was to provide a visual/optical characterisation of biofilms, countering this issue, which has not been achieved within the timeframe of this project. However, further experiments are considered in this direction since it has successfully been reported[632]. Designing the support with biofilm grown over the electrode and able to be monitored easily as well as imaged as a whole could integrate within an established laboratory screening for antibiofilm compounds or antibiotic susceptibility of infectious biofilms without much change to existing procedures and consequent financial investment on the electrochemical side. The hyperspectral camera can be simplified for a decrease in cost. Moreover, testing the patient sample as a whole would also account for diversity in terms of biofilm composition, infections and patients to facilitate more personalised, targeted and efficient antibiotic treatment.

Many studies using *P. aeruginosa* never go beyond, which is not reflective of the diversity of biofilm infections, with a multiplicity of constituting microorganisms. Monospecies biofilms are the main focus of research for antibiotic activity assessment, which does not reflect reality in the clinic,[23,633] where most infections result from polymicrobial biofilms. *In vivo* phenomena with wild-type pathogens might differ from *in vitro* studies.[23] Biofilm sampling would still be necessary unless electrodes would be implemented in the implanted device and localised where the biofilm settles. Our overarching aim is to obtain a fingerprint of commonly reported infectious biofilm producers to enable faster identification within complex samples. Studies of dynamics within polymicrobial studies would precede and therefore enable improved patient outcomes.[633]

To assess antibiotic susceptibility, resazurin was chosen for its colour change in presence of metabolically active cells, required for antibiotics to be effective as well as its pigmentation in both forms for hyperspectral imaging. Van den Driessche *et al.* (2014) demonstrated that the optimisation of a microtiter plate-based assay using resazurin to quantify metabolically active cells in established biofilms would enable a lower limit of detection from 10^6-10^8 down to 10^3-10^8.[611] This was achieved by dissociating biofilm cells from the structure rather than staining the biofilm directly in the wells they were formed.[611] Ren *et al.* (2020) have also successfully used resazurin for antibiotic susceptibility testing of *Salmonella gallinarum* on screen-printed carbon electrodes modified with multiwalled carbon nanotubes and gold nanoparticles.[634] Achieving a lower limit of detection allows antibiofilm treatments to be assessed more accurately.[611] Resazurin reflects the number of metabolically active bacterial cells present in the sample, not the total cell number. Because samples are being grown without shaking to form biofilms, it is possible that some cells enter a dormant state and would not be accounted for in these measurements aligned with the target of this assay being to detect and assess the presence of bacterial cells susceptible to antibiotics. A limitation of resazurin is non-fermenting Gram-negative bacillus unable to metabolise it, where tetrazolium salts could be a suitable alternative.[607]

Using *in vitro* bacterial growth still bears the same drawbacks as routine microbiological culture methods of viable but non culturable (VBNC)[635] or anaerobic bacteria or long time-to-result, which is why the measurement after 4 hours could provide early insights and help decision making. Anaerobic organisms are rarely reported, since culturing them *in vitro* remains currently challenging. However, they are abundant in the oral cavity, gastrointestinal and human genitourinary tracts, which could lead to misdiagnosing biofilm causative agents and targeting treatments at the wrong microorganism, further fuelling the persistence of infectious biofilms and fuelling possible antibiotic resistance.[23]

For biofilms grown in the 96-well plate, samples are each only tested once, at their dedicated endpoint, which might introduce variability between wells. It does not

attest of biofilm structure at its best and is only an intermediate step. Testing more ESKAPE pathogens with the test support using resazurin as well HSI correlation would constitute near future tests, since only preliminary testing was run (Figure C. 5 and Figure C. 6). An increase in replicate numbers and running the assay with a standard fluorescence detection in parallel are to be considered next. Moreover, additional control methods to testify of biofilm formation could provide confirmation of biofilm formation and obtained electrochemical results.

Results from all ESKAPE pathogens biofilm growth are alarming when considering clinical conditions. *P. aeruginosa*, *A. baumannii and K. pneumoniae* were all able to form detectable biofilms within 4 hours. Once settled, *K. pneumoniae* is able to form biofilms after 24 hours considering the data obtained, regardless of the initial population. The lower *A. baumannii* initial concentration is, the more biofilm it is able to produce (Figure 6.15, Figure 6.24 and Figure C. 7). Addition of antibiotics at an earlier time point or at various concentrations before biofilm establishment could harness the benefits of early detection over biofilm control. Assessing multispecies biofilms for a better reflection of clinical cases as well as patient sample testing would help moving this test closer to the clinic, which is a commonly reported flaw of many published AST strategies.

Costerton's words in 1996 to officially describe and define biofilms and the possibilities to characterise them has not evolved much since then. It does prove the quality of his work with conclusions still valid today. Almost 30 years later, with the technological advances in terms of equipment as well as availability and access of information, the methods have not changed showing the complexity and variability of biofilms still to be elucidated. The gaps in knowledge concerning biofilms, infectious potential and antibiotic resistance add to the biofilm detection and characterisation challenges. This assay has been designed for phenotypic testing, and maybe future species profiling and identification.

Trends observed such as the influence of the environment still require more investigation to be understood and explained fully. Moving towards appropriate

antibiotic treatment of biofilms requires lifting unknowns on the correlation between genotypic and phenotypic resistance in biofilms with a more comprehensive approach of environmental factors at play.[23]

Further research to understand the causes and effects of mechanisms leading to antibiotic tolerance of biofilms will support better solutions. *In vivo* sampling, sequencing and omics methods are expected to shine a light on unknowns.[23]

Antibiofilm agents are a pressing need as current available antibiotics have been developed for their activity against planktonic bacteria, which do not show as efficient at eradicating biofilms, leading to persistent infections.[636] To enable their successful development, robust biofilm characterisation methods need to support antibiofilm activity assessment.[611]

Since current options for biofilm disease treatment are unsuccessful, tomorrow's assay and treatment development need to proficiently reach and act on resident bacteria.[23] Personalised solutions for the patient and implant could be a possibility. However, biofilm vaccines, tailored to the patient seem a long way off and to be quite costly, unless improvements of vaccine manufacturing process in small batch becomes affordable and fast.[23] The balance to reach between standard methods and reproducibility versus case-by-case diagnosis and treatment is a fine but necessary point to reach. Research methods allow flexibility to advance new therapeutic strategies toward biofilm-associated infections but cannot be advanced without a degree of standardisation. The lack of standard methods due to variability from infections and patients has provided a roadblock comparing the medical field with the biocide/industrial field regarding biocide claims.[22,23] Local and systemic consequences of complete biofilm eradication have different levels of acceptance.

6.4.4 Conclusion

An integrated assay was developed using a custom-made test support to enable the detection and characterisation of standard pyocyanin and pyocyanin produced by *P. aeruginosa* with hyperspectral imaging and electrochemistry in the previous section. This platform also enabled the detection of biofilm formation using EIS. **Application of the assay to bacterial species unable to produce electroactive biomarkers was successful with electrochemical methods on *A. baumannii* biofilms and resazurin.** Its conversion to resorufin in the presence of metabolically active cells enabled antibiotic susceptibility assessment and showed promise with additional ESKAPE pathogens such as *K. pneumoniae*. This assay would allow sample testing directly from patient samples and could offer a screening of potential treatments by accounting for biofilm variability and personalised solutions for patients.

Chapter 7 Discussion & Conclusion

7.1 Discussion

The discussion is structured with a focus on each experimental chapter followed by a more general account of how AST biosensing might evolve and the main stakeholders at play.

7.1.1 On actinorhodin direct detection

Since no commercially available bioreceptor could be obtained for specific actinorhodin detection, the direct detection of actinorhodin, the blue pigmented antibiotic produced by *S. coelicolor*, without electrode functionalisation was explored for minimal sample processing. Despite using various voltammetric and impedimetric measurements, different electrolyte solutions and electrode materials, no clearly repeatable profile was obtained. Minimal sample preparation, using liquid-liquid extraction was undertaken, informed by additional analytical chemistry reference methods, but not sufficient to clearly confirm actinorhodin electrochemical behaviour with available data.

The colour change from antibiotic production is so striking with the naked eye and extensively through spectrophotometric assessment (Table 3.1). However, precisions on which compound each wavelength refers to are rarely mentioned, given the multiplicity of compounds existing from the same family (Figure 3.9) and the lack of exact chemical characterisation from the literature.[372]

Repeatability between replicates or experiments proved challenging, especially observed with polymerisation trials (3.4.1.3.4). Promising quantitative results were observed using OCP after polymerisation (Figure 3.46), even if process repeatability was not apparent. Attempts to avoid or induce polymerisation consistently were set back by unknowns around a possible polymerisation mechanism or even exact sample composition. Well-characterised and widely used electrode materials were selected with different catalytic properties but again, no clear electrochemical actinorhodin profile could be identified.

Missing conditions such as analysis of liquid-liquid extraction on the actinorhodin-free samples could have been beneficial for peak comparison and was constrained by time. More appropriate buffers/electrolyte supporting solutions such as H_2SO_4 or NaOH for higher and lower pH could have provided a more stable equilibrium for some actinorhodin-like compounds.

Overall, Chapter 3 provided insights into difficulties encountered when revisiting known but non-commercialised compounds. Depending on the use that has been made over time, characterisation data and synthesis are not always available, obtaining the compound of interest can be complicated and its purity might vary, which can appear dauting when being outside of researchers' field of expertise or necessitating access to different equipment. Testing for known compounds and screening for a different (biological) activity is not a straightforward process (2.4.2.1).[637] Informed rather than random screening, either from promising new evidence or knowledge built in a specific area, is more likely to be fruitful.[638] Multiple avenues could be explored to isolate actinorhodin-like compounds and characterise them electrochemically, but standard reference data is necessary as little electrochemical literature background is reported, even for close compounds (3 citations for Mazur and Haroon (1995)[360]).

7.1.2 On developing an impedimetric aptasensor for moxifloxacin

Obtaining a specific, repeatable, reproducible and quantitative recognition of moxifloxacin by the developed aptasensor was a major issue. No LoD calculations or testing in complex samples have been undertaken since the detection scheme did not provide a reliable output. The multiplicity of unstable parameters, from the electrode surface (Figure 4.27) to the probe immobilised (Figure 4.26) and SAM formation, along with the efficiency of complex hybridisation were piled on to the reported problematic sensitivity of EIS.[639] Variability of the electrodes might have been accentuated by the use of potassium ferri-/ferro-cyanide as a redox mediator as cyanide ions have been previously reported as etching the gold.[432] Understanding of the system based on supplier information did not consistently match observed trends. Elucidation of certain unknowns such as how the sequence folds or how long it retains

its shape for could inform better probe spacing[640] required between recognition probes or sensor functionality duration.[479]

Even if this signal amplification technique was reported,[641–643] it is not the most widely adopted. Many others have preferred a methylene blue label at the 3' end and voltammetric measurements. Methylene blue was placed at the 5' end here and influence on binding to either the anchor probe or moxifloxacin and pairing schemes were unknown and electrochemical detection in the tested environments did not provide consistent responses. Reducing the uncertainty brought by a high number of variables might have benefitted the optimisation scheme. This elegant system might need sequence optimisation with a shorter probe or a different microenvironment to improve its stability. A sensitive and specific detection of small molecules via aptasensors is a known challenge compared to bigger macromolecules.[644] Moreover, the reproducibility of published sequences is problematic and starts to be increasingly highlighted.[645,646] The aptaMIP format, which removed the complex and provided an increased affinity yielded more promising results.

7.1.3 On biofilm electrochemical characterisation

A dedicated detection platform was designed and used to characterise *P. aeruginosa* biofilms electrochemically and using HSI. The system was then adapted with other ESKAPE pathogens which do not produce redox active secondary metabolites, *A. baumannii* mainly here, using resazurin. The absence of electrode functionalisation is an advantage of the developed biofilm detection method and has been also reported in other studies (Table 2.4). The use of resazurin to monitor viability is increasing (Table 2.3) for planktonic bacteria. The novelty lies in the use of resazurin to assess antibiotic susceptibility of biofilms.

Only pure cultures have been tested at this stage and a limited amount of time points to avoid disturbing biofilm formation. The possibility of early detection of biofilms has been reported in the literature.[647] A higher throughput with enhanced platform design could support more antibiotic concentrations, antibiotic-bacteria

combinations and allow for the determination of limits of detection. Ultimately, testing directly from patient samples would be ideal to avoiding any pre-culture and maximise early detection and treatment for higher chances of biofilm eradication.

Confirming biofilm formation with HSI as well would provide more confidence in the end result, which has not been achieved during this study but is possible since reported by Wang *et al.* (2020), Lee *et al.* (2021) and Le *et al.* (2014).[648–650]

Bacteria have been isolated and grown in more and more standardised conditions, to measure, categorise and compare between laboratories or countries. However, bacteria do not only exist as planktonic specimen but establish biofilm communities to thrive and survive more efficiently external stressors. As this form of life is predominant, involves communication between bacteria and is responsible for a major amount of infections,[88] these constitute an area of interest to uncover key intermediates to stop proliferation or avoid virulent factors to be produced for instance. Since early detection supports more efficient biofilm eradication or prevent systemic infections, increased monitoring could be a promising strategy to prevent biofilm-related infections and expand antimicrobial coatings span of efficiency. Putting more time into co-culture or studying samples from microbes lining different parts of the human body through metabolomics against pure cultures could generate more insights into behaviour of individual bacteria/species within various communities or environments.

7.1.4 Improved understanding of bacterial behaviour towards AST relevance

With current AST, bacteria have been isolated from their overall environments and some of their traits were extrapolated as generalities. Nevertheless, their community behaviour and interactions/phenotypes are greatly variable. It might not be possible to take it all into account as the complexity would be enormous but starting to include more variables to translate native conditions better as automated equipment alleviate labour-intensive and time-consuming routine protocols and artificial intelligence helps us process more data, faster to uncover hidden patterns and generate predictions. This could allow for instance to adapt standards for culture

media or counts depending on the identified site of infection or nature of the clinical sample obtained.

Antibiotics are in essence a death message from one microorganism to a bacterium. However, they are not constantly produced and only target other specific species. Which conditions have selected for this additional effort to be conserved by a certain strain? What prevented it before, and can we target that trigger or use it with different species/extracellular conditions? Maybe attempting to understand how they switch from a non- virulent to a pathogenic behaviour and target those cues could be another approach to antibiotics. The vocabulary used in AMR literature relates to war and a fight against bacteria, which are trying to survive - just like us. We only send signals to bacteria using very narrow terms (= antibiotics) and expanding this communication to avoid settlement plus prevent infectious phenotypes, to reach their targets could be more thorough.

7.1.5 Translation of AST systems

Novel AST platforms are increasingly taking into account the necessity to screen more antibiotics already at the proof-of-concept (Table 2.3 and Table 2.4). Many early solutions using *E. coli* and *S. aureus* as planktonic models and *P. aeruginosa* for biofilm models, are not pursued with more following-up pathogens. The emergence of biorecognition elements for wider identification in multiplexed platforms shows again the integration of stated current needs from encountered hurdles in the patient sample workflow. More and more solutions allow for a reduced turnaround but the necessity of the pre-culture step largely remains (Table 2.3). This leads to the divergences between stated turnaround times, only considering part of the sample pathway in most cases, which impacts comparisons between solutions or possible impact in the microbiology sample processing pathway and on patient care.[651] More clarity around the use of specific terms could therefore be beneficial for the development and positioning of novel solutions but also comparisons of existing ones since improving this metric is key for antibiotic susceptibility tests.[651] Obtaining results directly from patient samples in a more adequate time will require more time and investments, consequently new solutions might not be available promptly. The

timid use of ML and AI is likely to pick up and uncover earlier patterns for detection, facilitate result generation and analysis. As these PoC solutions are not an entire substitute for extensive screening, patient sample transport from remote places to central facilities might need to be improved, for instance with the use of drones.

The point-of-care growth has so far been more lateral than progressive, with many publications and patents but little commercial viability.[652] Despite numerous reports, only a handful of studies are tested with patient samples or report enhanced patient outcomes.[25] This highlights the major challenge of moving early stage solutions towards commercialised products.

Setting aside the scientific and technological challenge, industrial and institutional problematics are also prominent.

Desensitising bacteria to antibiotics like humans do with addictive substances such as drugs, coffee or sugar is not possible. Several vital steps to mitigate and control the emergence of resistance have been laid out: a more restricted use in farming practices and lowered levels in wastewaters, tackling the inappropriate consumption contrasted with access issues to antibiotics in countries with poor access to healthcare, better antimicrobial stewardship, infection prevention and control by healthcare facilities, managing patient expectation and the need for support from new technologies.[653] Vaccines, whether existing or new, may help but the clinical antibacterial pipeline is not sufficient in any way because of high development costs, cheap alternatives available in the form of generics, the small market for new drugs and the low economic incentives.[653] CARB-X, the Repair Impact Fund or GARDP were set to boost the antibiotic pipeline outside of the solely industrial financing schemes but might not be sufficient as isolated enterprises to generate the push needed to keep up with emerging resistance. Without a clear path to secure consequent returns on investment, new technologies, even if promising, will not make it to the market. The example of Achaogen is striking, with the commercialisation of their new antibiotic, plazomicin, to treat multidrug resistant infections in 2018 followed by their bankruptcy in April 2019.

PoC solutions are not only left to the patient, needing medical advice and guidance. They could provide support to the healthcare professional for the patient to believe and trust the treatment decision and maybe stricter treatment adherence.

The use of health technology assessment can help to estimate cost-effectiveness of new medical technology as well as if the product can be reimbursed. It can also be used to assess the price to be paid, called value-based pricing. Getting HTA right is all the more important as smaller countries follow larger ones in terms of access, pricing and reimbursement. Moreover, an inappropriate assessment is likely to impact manufacturers return on investment.

Most therapeutic medical technologies only benefit individual patients however, antimicrobial agents along with diagnostics and vaccines indirectly benefit the wider society. Moreover, the low price of antibiotics diminishes the value people associate to them, leading to more misuse. If the antimicrobial manufacturer is paid by dose, the return on investment generated is lower than when considering the additional societal value in the assessment. Reimbursement schemes need to value the current availability of antibiotic to control outbreaks of resistant pathogens in the future. The negative externality when increasing the consumption goes hand in hand with a higher selection pressure for resistance.

7.1.6 Institutional obstacles

The default framework for disease detection in health technology assessment is non-communicable diseases. HTA applies the same criteria to all health technologies. As these rules fit primarily non-communicable diseases, they are not suitable to fight infectious diseases. Moreover, the timeframe of modelling is the lifetime of the patient receiving treatment or even shorter which does not match infectious diseases' ones that can be longer than patient's lives. In the UK, a new format of antibiotic subscription purchasing model has been set up on two newly marketed products where an annual lump payment rewards companies based on the full range of benefits provided by the available drug. In Norway, the societal value of AMR is now part of health technology assessments.

The current processes for Health Technology Assessment (HTA) present three main deficiencies: a methods-centric rather than a problem-focused approach, a lack of tools adapted to changing patterns of infections and an absence of methods to tackle epidemiological risks. To address, these, a wider epidemiological toolkit is necessary, a better design and communication of analyses to broader users and implementation of long-term policy goals.

A reminiscent theme in health economics is the difficulty of assessing medical care. Characterising the uncertainty in evidence base and keep generating data while putting technologies in the hands of patients is at the heart of the problem. Epidemiological risks include the understanding and modelling the spread of resistance. Most infectious disease models are considered at the population level which differs from non-communicable disease models. Indeed, they include contact, transmission and disease progression as factors, prove more difficult to validate and follow non-linear dynamics with the fitness cost of resistance as a critical determinant. Moreover, the expertise to interpret models might lie outside of HTA agencies.

7.1.7 Drivers of change

The ability to destroy markets and create new ones comes through overcoming restriction using high technological capabilities.[654] Being mindful of how a shift in AST technology is going to impact users and countries is important and it should be acknowledged that not all changes will be equal which could impact negatively on quality of health and worsen the problem. That is why transferrable and adaptable systems were intended in this thesis, point-of-care solutions to minimise the need for specialised laboratory equipment and centralised facilities and bring the diagnostic closer to the patient. More education would be required from healthcare providers to patients which could be beneficial in the global understanding of the AMR issue.

Vaccines as a solution for AMR show most beneficial long-term effects but might be outpaced by bacteria evolving different resistance mechanisms. However,

taking the example of Covid-19 and the roll out of boosters, it was able to adapt fast and benefit the whole world with accelerated approval. However, it required efforts from the whole world, governments and companies, all funds possible to develop and roll out one. The parallel can be made with antibiotics developed and approved at industrial scale production as the result of a world war economic and social landscape while VITEK-2 was the result of space exploration. These unusual times provided pushes for more disruptive innovation. Since then, it seems that innovation around AST has been a lot more incremental.

With the SARS-CoV-2 pandemic, the accelerated approval of PoC tests and vaccines and major efforts, all contributing to the same common challenge proved that it was possible to develop solutions in record time and bend approval pathways. This has in some ways familiarised the general population more with hygiene practices, self-testing and more drastic infection prevention measures.

This could provide a basis for AMR costs, development timeframes or translating regulatory frameworks. One of the major differences, however, is the absence of cure or vaccine available for SARS-CoV-2 when there are (still) some antibiotic options for resistant pathogens. Once the time and financial investments are undertaken, reassessment of testing methods is rarely undertaken and this also applies to AST. Getting people moving and acting is as difficult compared to the high and worldwide impact of the SARS- CoV-2 pandemic. Illustrating this are the previous SARS and MERS epidemics, that did not affect the West. Preparedness and contingency plans could have been put in place as well as efforts earlier on to look harder for treatments as people affected by SARS and MERS previous epidemics reside in some of the most densely populated areas in the world, which should have been of major concern already. Financial, governmental and regulatory means were fully mobilised to search for solutions only when the major stakeholders were completely stuck despite their major involvement in international organisations such as WHO, the World Bank or the United Nations.

The slow and gradual impact of AMR can also be treated as a parallel with climate change (with less campaigns). A change in the way of life only occurs when pro-environmental choices are enabled by government policies.[654] Changes in individual behaviour can need upfront investments from individuals for long-term benefits with government subsidies and loans needed.[654] Public action is required because trusting individuals to make the right decision is not effective.[654] Changes in perspective and practices have to be socially adapted through changes guided by institutions.[654]

7.2 Next steps & Limitations

Future steps following on from three different strategies developed during this thesis are described in this section.

Despite visually evident presence of actinorhodin-like compounds in collected samples from *S. coelicolor* cultures, the definite electrochemical characterisation of actinorhodin and close compounds was not successful without extensive sample pre-treatment as unsupported by neither existing literature, commercial standards or available affinity or catalytic bioreceptors.

To build a solid background on actinorhodin production, isolation and characterisation of compounds forming the mixture is crucial. It can be time-consuming and might need reassessment for each modified strain as the excreted metabolome is a complex mixture added to components of the growth medium. This can be coupled with analysis of samples from various *S. coelicolor* strains where specific genes responsible for antibiotic production have been inactivated. Once pure compounds are obtained, electrochemical characterisation can take place with pure samples to be able to identify obtained peaks on different electrode materials. Interactions between compounds can also be studied to understand polymerisation patterns. Degradation studies need to be considered and samples assessed as soon as possible after production. Electrochemical interrogation can also be assessed in organic solvents with appropriate electrolytes and at a range of scan rates, preferably

on carbon electrodes. Possible comparison with dihydrokalafungin, as more widely available as a close standard could help understanding electrochemical behaviours.

The signal enhancement strategy based on the complex sequential hybridisation of the aptamer sequence from its support upon target recognition, namely moxifloxacin, did not lead to a consistent, reproducible and quantitative recognition using EIS. Studies on the stability of the complex between aptamer and support strands as well as of the aptamer conformation would be informative. Tagging the support probe could serve as evidence for surface immobilisation, spacing and confirm hybridisation with the aptamer sequence. A different electrochemical technique could be used to detect moxifloxacin binding and as a reference to optimise EIS detection and optimise for a lower limit of detection. Sequence optimisation, for enhanced binding and bringing the system closer to the electrode might be of interest, along with making use of the full aptamer sequence only. Specific recognition, as well as assessment in complex matrices is required next. Once the most sensitive and robust strategy is secured, translation to other sequences recognising different antibiotics can be undertaken.

Concerning the aptaMIP strategy, all calibration steps occurring at 37°C and on a longer timescale are needed, along with additional controls assessing impact of aptaMIP presence on bacterial growth. Improving reproducibility and optimising measurements to increase the multiplexing capability of the assay are the next focus point.

For the biofilm characterisation approach, final assessment in the test support is the ultimate step to conclude the possible monitoring of *A. baumannii* biofilms using resazurin. The production of a test support solution allowing for more samples to be analysed simultaneously is the nearest priority. Additional time points, ideally early to reduce the assay duration are to be examined, along with more bacterial starting concentrations or antibiotic concentrations. This could therefore support a direct MIC or MBEC assessment, directly from patient samples ideally as the pre-culture step delays results. Implementing a bacterial identification component or at

least a differentiation between Gram-positive and Gram-negative specimens could narrow the antibiotics to assess.

Overarching limitations include sample heterogeneity, reproducibility in terms of sensors, functionalisation microenvironments and non-specific interactions and biofouling. Additional colony counting, sample/culture purity check are necessary to confirm observed results and conclusions but lacking throughout the work. This would enable an accurate comparison of the developed methods with gold standard techniques.

The possible non-homogeneity of actinorhodin solutions due to dilutions or the compounds that had adsorbed on the electrodes differently might be responsible for differences observed and using sample preconcentration for instance could help to gather elements to be detected close to the electrode. Bacterial variability, in terms of environmental conditions due to nutrients available, other microorganism present and response to stressors might impact observed responses. Moreover, metabolised antibiotics could also be present depending on surrounding medium composition and could impact their biorecognition. Interferents, arising from real sample matrices, whether bodily fluids or water samples for instance, could hinder the specific response either from non-specific interactions or biofouling, and are necessary to be assessed before moving to more advanced stages.

Reproducibility is another challenge, arising from batch-to-batch variations impacting the quality of the sensing surface but also functionalisation schemes. Taking the example of self-assembled layers, their homogeneity is impacted greatly by pinholes but also their rearrangement upon solution changes can overtake specific signals. Their hydrophobic or hydrophilic properties, depending on end groups of main molecules also impacts the possible interaction with complex matrices components.

The sensitivity of EIS allows for analyte detection at very low levels but suffers from background noise and can prevent recording of the targeted binding event. Despite signal enhancement strategies tested, scarce information about the

356

biorecognition system and target-to-receptor size ratio prevented recording of moxifloxacin recognition. Additional recognition sites and a bigger receptor in the form of aptaMIP provided a more reliable and specific recognition of the antibiotic, which is to be pursued.

Electrochemical point-of-care devices are not intended to fully replace either microbiological culture methods or analytical techniques but rather provide a quick estimation of antibiotic quantity, or faster triage or screening of patient samples to get a more appropriate treatment and support the clinical decision making. However, the benefits to users, whether considering patients or healthcare practitioners needs to be consequent to drive behaviour changes. Most often driven either by cost or by legal requirement, rethinking workflows, trainings to use novel devices and adoption take time and effort. Raised awareness and extensive communication, as well as the impacts of a worldwide pandemic have not drastically led to full behaviour changes. When considering the climate change problematic, with much more communication and public sensibilisation, the current witnessing of effects and how difficult it is for people, industries and governments to change, it is therefore possible that moving away from empiric prescribing and fully relying on traditional culture-based AST to reap the benefits from point-of-care tests could only be seen on a longer timescale unless very disruptive events or methods surface.

7.3 Conclusion

This thesis has explored three different approaches to detect antibiotics and antibiotic susceptibility using electrochemical sensing strategies.

The electrochemical detection of actinorhodin, not reported in the literature previously, was attempted here without electrode functionalisation and from direct sampling of *S. coelicolor* cultures. Conclusive results have not been obtained using either carbon, gold or platinum in biological electrolyte environments (KCl and PBS). Sample preparation via liquid-liquid extraction of the obtained samples was not sufficient to clearly attribute recorded electrochemical activity to specific signals. More in-depth analytical characterisation is required to pursue any identification and enable a clear attribution of electrochemical activity and polymerisation behaviour.

Using the hybridised aptamer to a support oligonucleotide and impedimetric detection did not provide quantitative and reproducible detection of moxifloxacin. Validation of the system's behaviour is needed for a better understanding of its behaviour and observed signal changes. More promising results were acquired when the aptamer was immobilised in a molecularly-imprinted matrix.

Biofilm evolution was undertaken in an integrated platform including electrochemical monitoring. This was conducted for *P. aeruginosa* and its electroactive virulence factor pyocyanin as well as for *A. baumannii* as an electrochemically inactive pathogen and a redox mediator reflective of active metabolism, resazurin.

Throughout this work, non-electrochemical techniques have been used to inform on events and phenomena occurring at the electrodes to enable more convenient and accessible detection of antibiotics and antibiotic susceptibility.

This work has contributed to inform future studies aiming to develop antibiotic and antibiotic susceptibility sensing using electrochemical detection and helped to advance knowledge on elaborating transferrable assays to support antibiotic stewardship initiatives.

A. Chapter 3 Appendices

I. Actinorhodin biosynthetic pathway

.
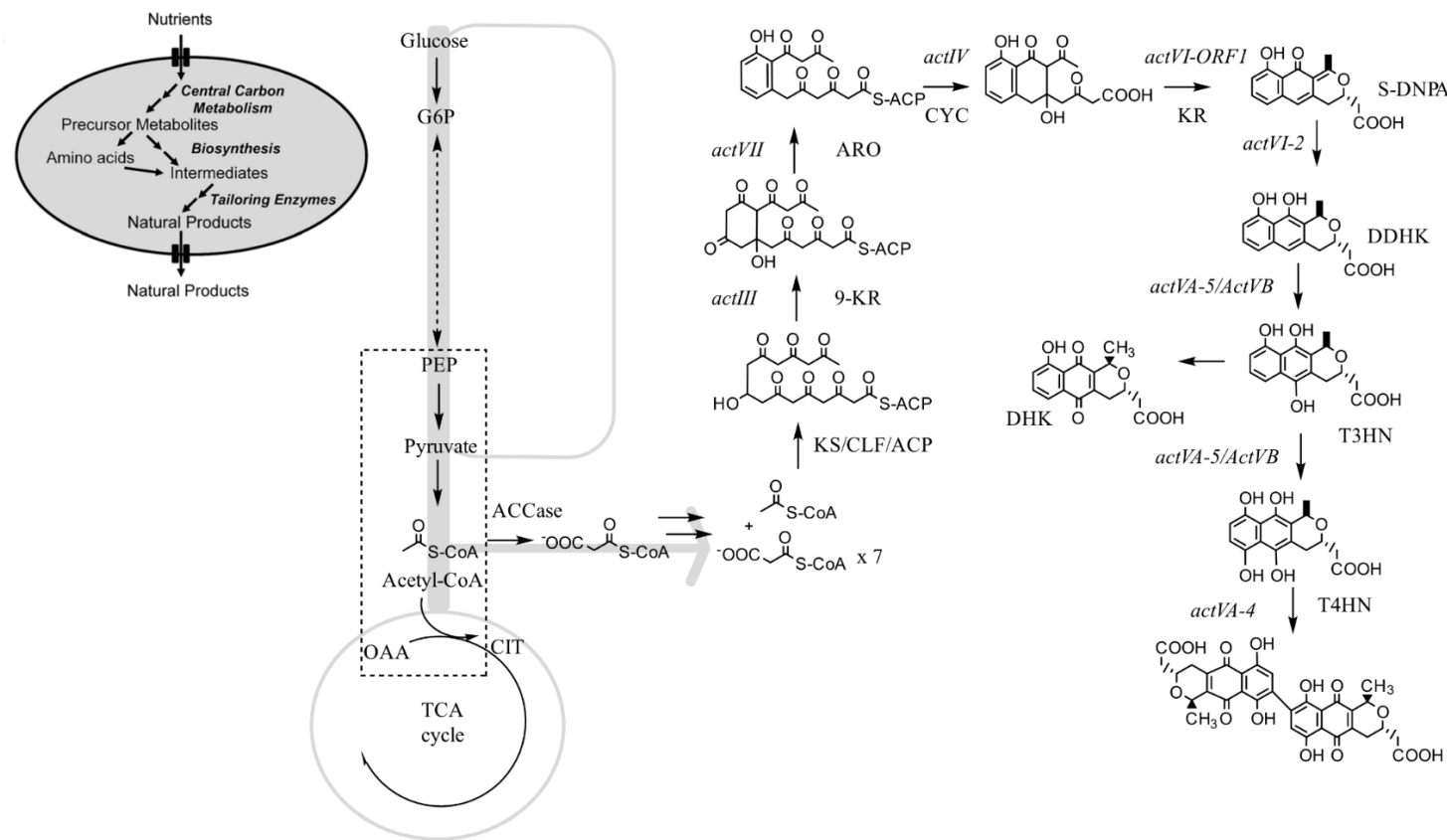
Figure A.1. Pathway to actinorhodin with an overview of the general steps[655] (top left) and the flux shift from primary to specialised metabolism[284] at the PEP PYR OAA key metabolic junction[283] (centre) and the specific reactions from acetyl-CoA to actinorhodin with genes involved in italics and their corresponding enzymes in capital letters (right).[656–658] Reproduced and adapted with permission from Nielsen, J. Cell Factory Engineering for Improved Production of Natural Products. Natural Product Reports 2019, 36 (9), 1233–1236; Rokem, J. S.; Lantz, A. E.; Nielsen, J. Systems Biology of Antibiotic Production by Microorganisms. Natural Product Reports 2007, 24 (6), 1262; Hiltner, J. K.; Hunter, I. S.; Hoskisson, P. A. Tailoring Specialized Metabolite Production in *Streptomyces*. ScienceDirect; Rohr, J.; Hertweck, C. 1.07 - Type II PKS. ScienceDirect; Das, A.; Khosla, C. Biosynthesis of Aromatic Polyketides in Bacteria. Accounts of Chemical Research 2009, 42 (5), 631–639; and Korman, T. P.; Ames, B.; Sheryl) Tsai, S.-C. 1.08 - Structural Enzymology of Polyketide Synthase: The Structure–Sequence–Function Correlation. ScienceDirect

II. Mass spectrometry analysis of actinorhodin sample

Figure A.2 showed a main peak at 9.4 min forming a positive ion, not detected at 254 nm. No compound was inferred from extracted peaks in the chromatograms. , using formic acid instead of ammonium acetate as a solvent additive, displayed a different profile with possible compounds listed in Table A.7.1.
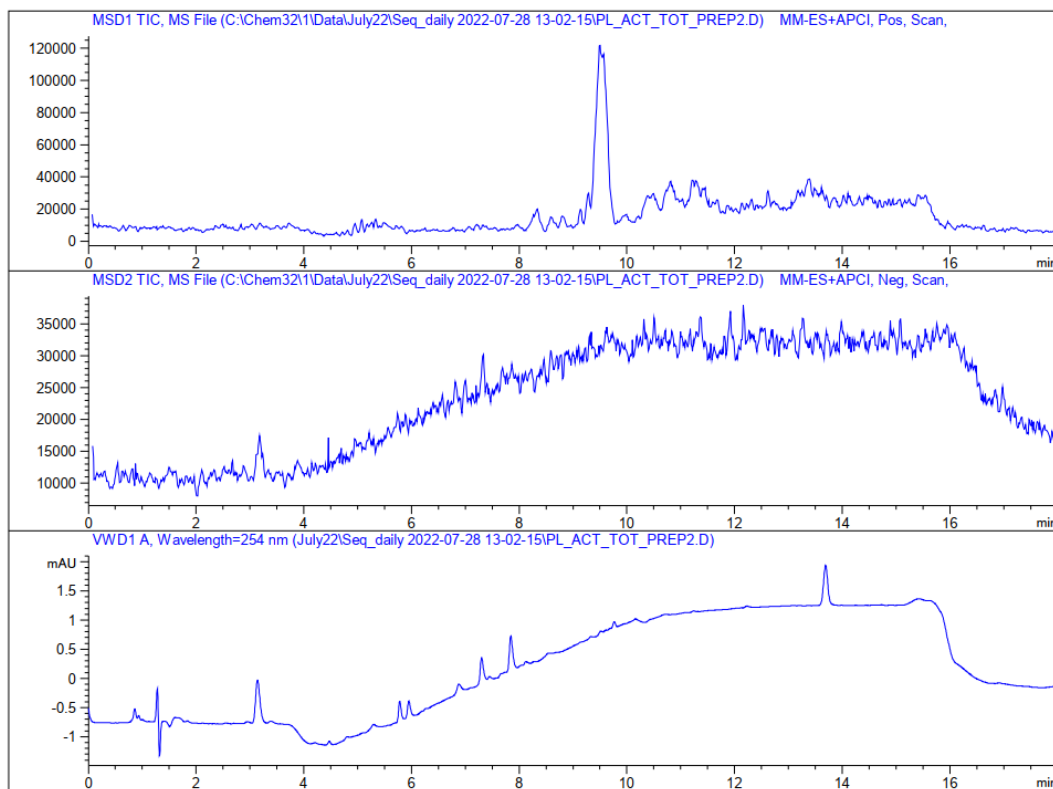
Figure A.2. Total ion count (TIC) chromatogram in positive (top) and negative ionisation modes (middle) of the total actinorhodin sample at 16.4 µM using PTFE filter (respectively top and middle) and UV chromatogram at 254 nm (bottom) and ammonium acetate as a solvent additive.
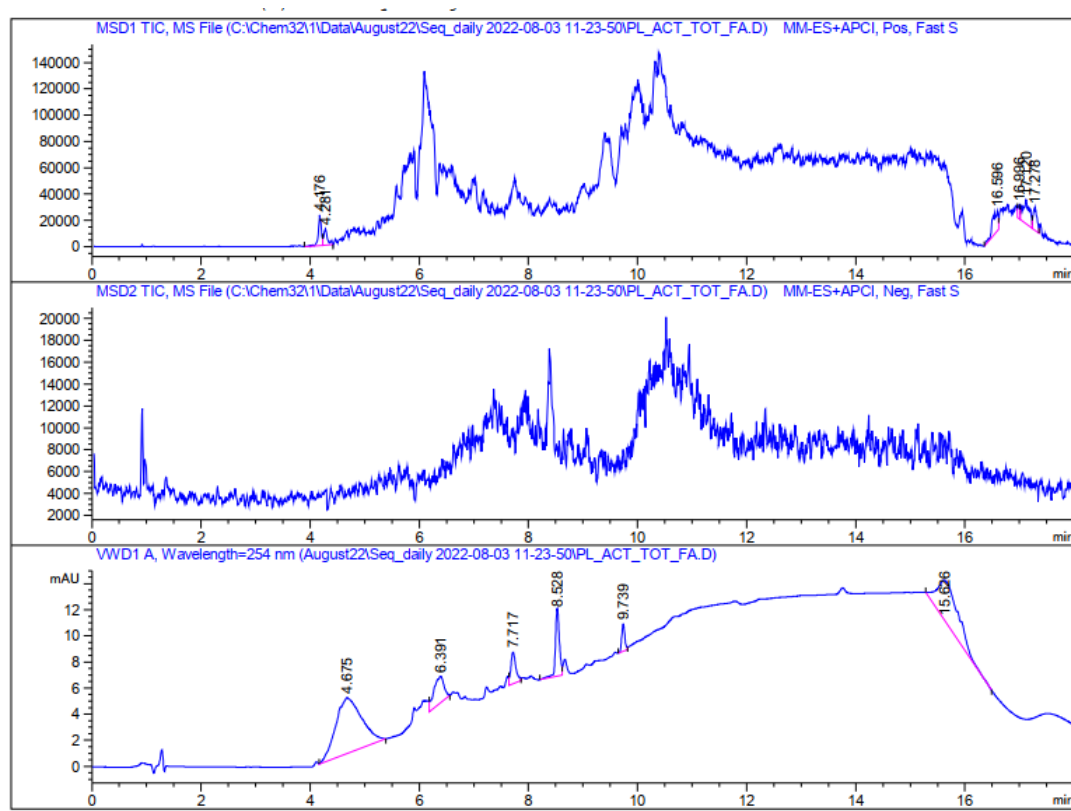
Figure A.3. Total ion count (TIC) chromatogram in positive and negative ionisation modes of the total actinorhodin sample at 16.4 μM using PES filter (respectively top and middle) and UV chromatogram at 254 nm (bottom) formic acid as a solvent additive.

Table A.7.1. Possible compound identification from the total actinorhodin sample with formic acid (FA) as a solvent additive.

Rt (min)	Sample	Method	Compound
4.1 (+) & 10.6 (+)	Total actinorhodin sample	FA	Actinorhodinic acid
4.4 (+)	Total actinorhodin sample	FA	β-actinorhodin
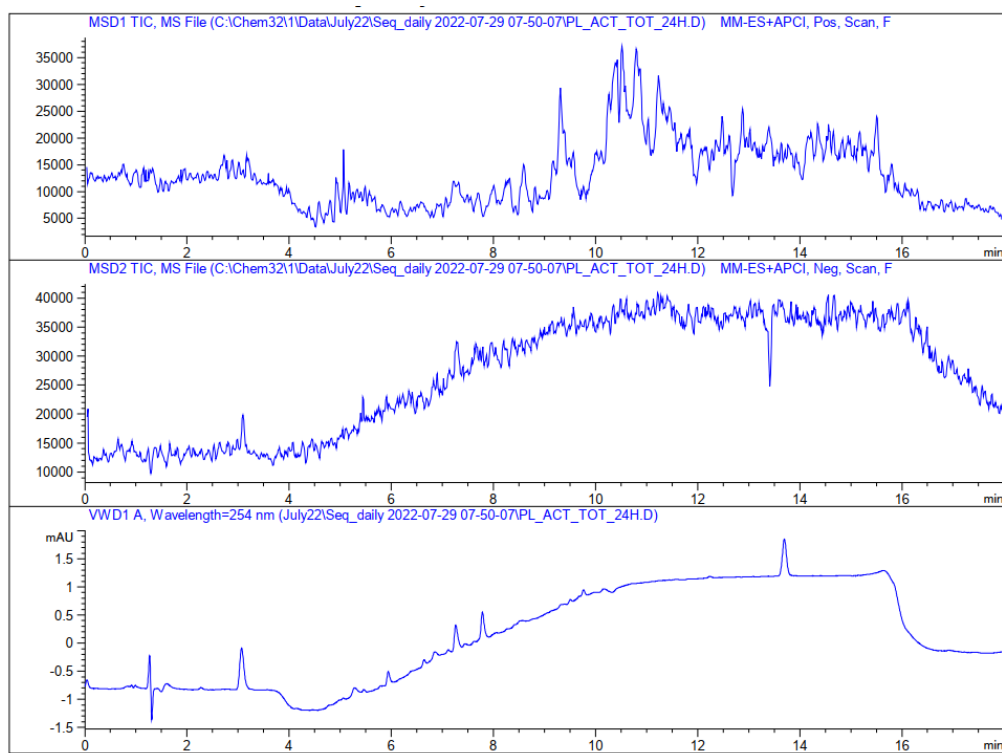
Figure A.4. Total ion count (TIC) chromatogram in positive and negative ionisation modes of the total actinorhodin sample at 16.4 μM left for 24 h in daylight (respectively top and middle) and UV chromatogram at 254 nm (bottom) using ammonium acetate as a solvent additive.

Comparing Figure A.4 left in the daylight over 24h compared to a freshly prepared solution analysed in , the main difference lies in the absence of the main peak at 9.4 min In the positive ionisation mode, suggesting that this main compound is photosensitive.

III. Electrode characterisations

i. Glassy carbon electrodes
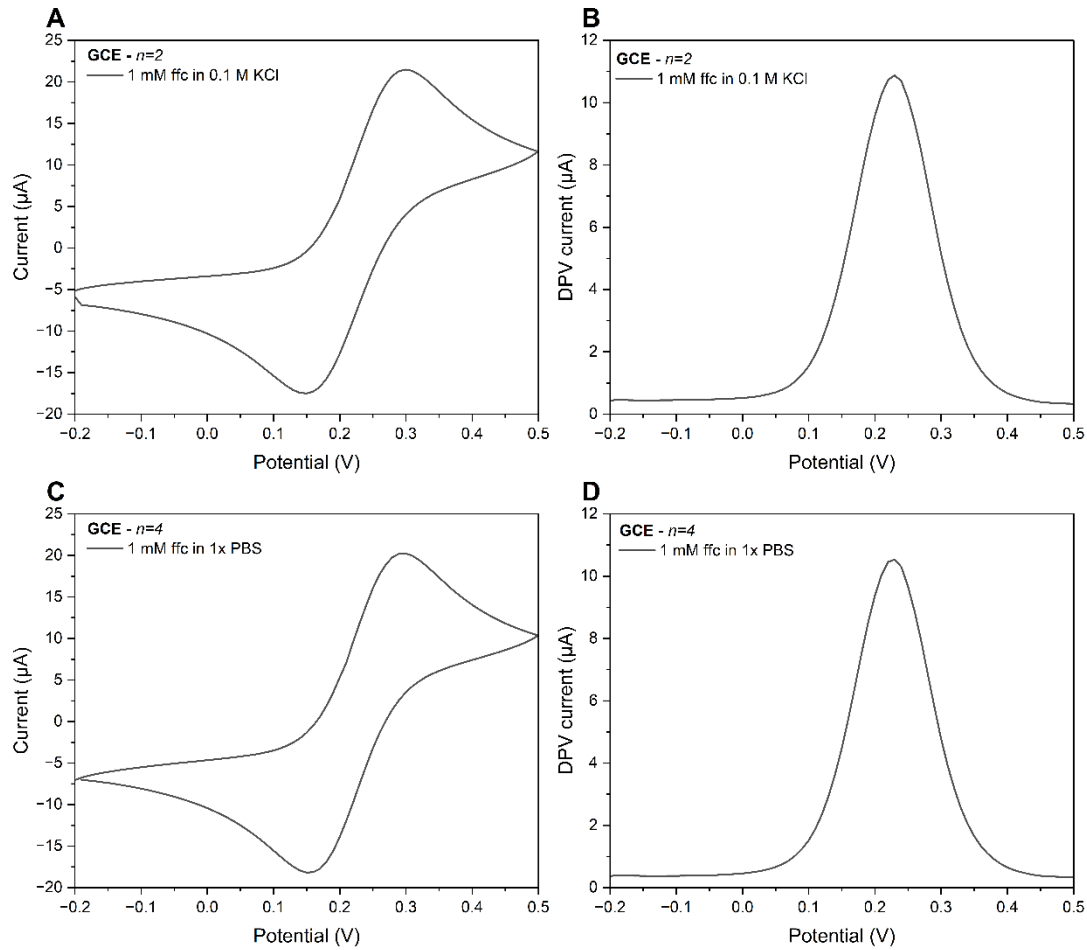
Figure A.5. Glassy Carbon Electrodes (GCE) characterisation with 1 mM $[Fe(CN)_6]^{3-/4-}$ through CV (A) and DPV (B) in KCl and PBS (respectively C&D) electrolyte backgrounds.

ii. Screen-printed carbon electrodes

Carbon SPEs were activated in 20 mM NaCl for 10 CV at 0.1 V/s between [0 :1.4] V following Hannah *et al.* (2020)[659] and characterised using 5 mM $[Fe(CN)_6]^{3-/4-}$ in 0.1 M KCl in Figure A.6.
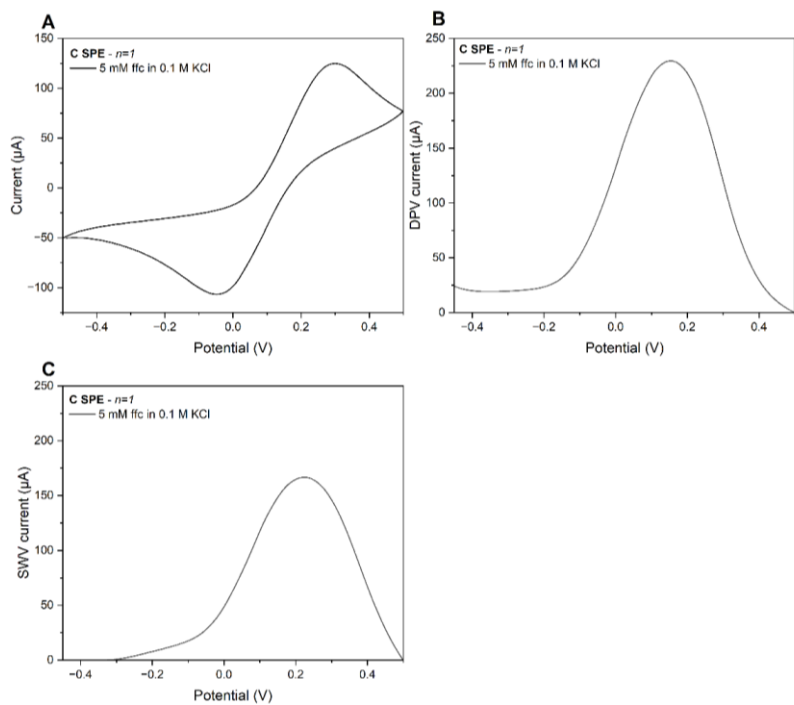
Figure A.6. Carbon SPE characterisation in 5 mM $[Fe(CN)_6]^{3-/4-}$ in 0.1 M KCl. CV (A), DPV (B) and SWV (C) after NaCl activation.

iii. Polycrystalline gold electrodes
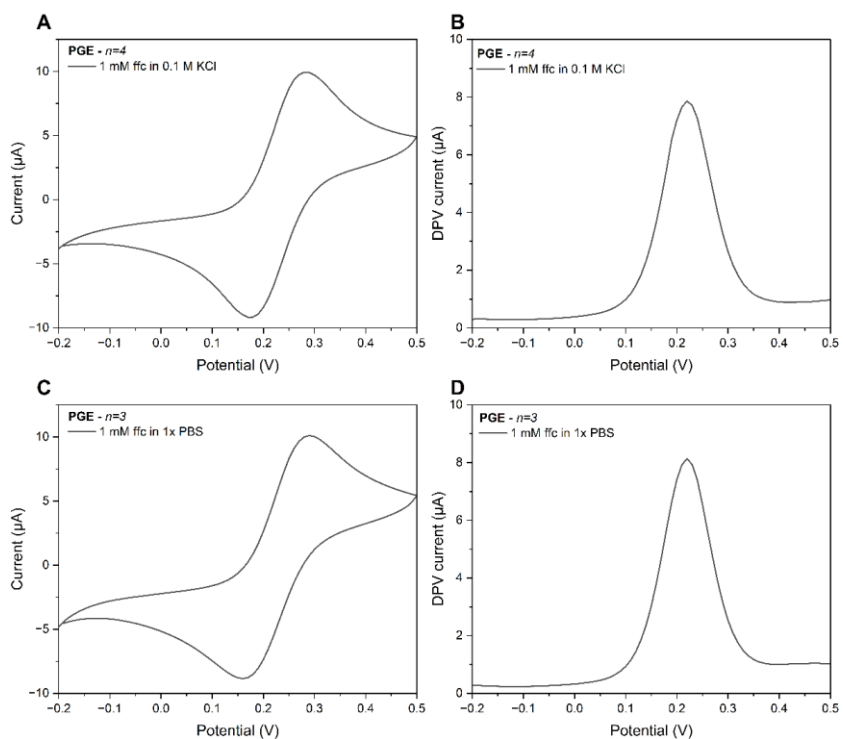
Figure A.7. Polycrystalline Gold Electrode (PGE) characterisation with 1 mM $[Fe(CN)_6]^{3-/4-}$ through CV (A) and DPV (B) in KCl and 0.01 M PBS (respectively C&D) electrolyte backgrounds.

iv. Screen printed gold (AT) electrodes
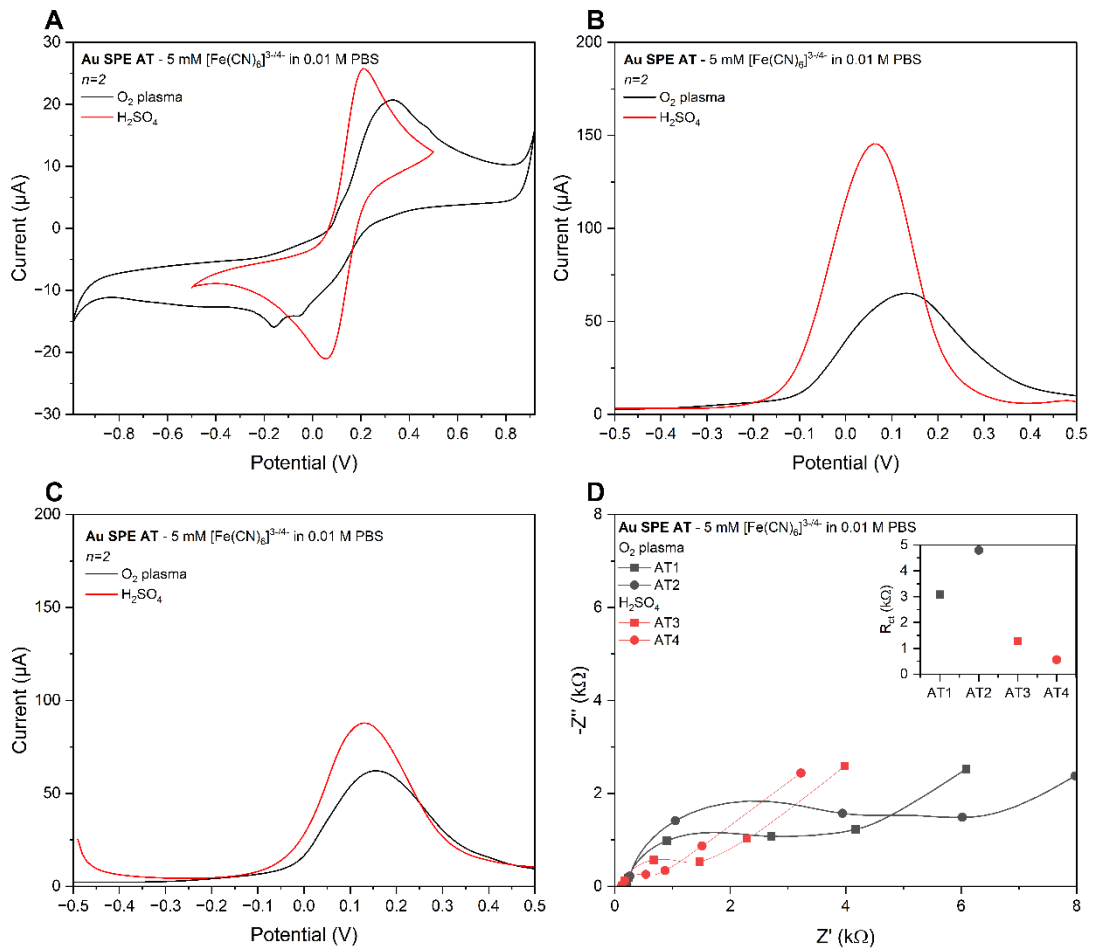
Figure A.8. Characterisation of commercial Au screen-printed electrodes (AT) in 5 mM $[Fe(CN)_6]^{3-/4-}$ in 10 mM PBS with CV (A), DPV (B), SWV (C) and EIS (D) with R_{ct} values for a modified Randles' equivalent circuit presented in inset to compare two pretreatment methods.

Two surface treatments were compared : 15 scans at 0.1 V/s in 0.1 M H_2SO_4 and a plasma asher treatment at 0.7 mbar, 50% power for 62 s. Figure A.8 presents a comparison of these two methods. H_2SO_4 CV cycling resulted in better peak resolution and separation for $[Fe(CN)_6]^{3-/4-}$ with cyclic voltammetry (Figure A.8A), higher peak amplitude in DPV and SWV (Figure A.8&C) and a lower R_{ct} value (Figure A.8D). H_2SO_4 CV cycling resulted in a more efficient cleaning and activation protocol and was subsequently used prior testing of actinorhodin solutions.

v. Interdigitated electrodes

Table A.7.2. Gold interdigitated microelectrode specifications.[660]

	Microelectrode width	Microelectrode gap	Number of feet
IDE1	10 μm	10 μm	90
IDE2	10 μm	5 μm	120
IDE3	5 μm	5 μm	180
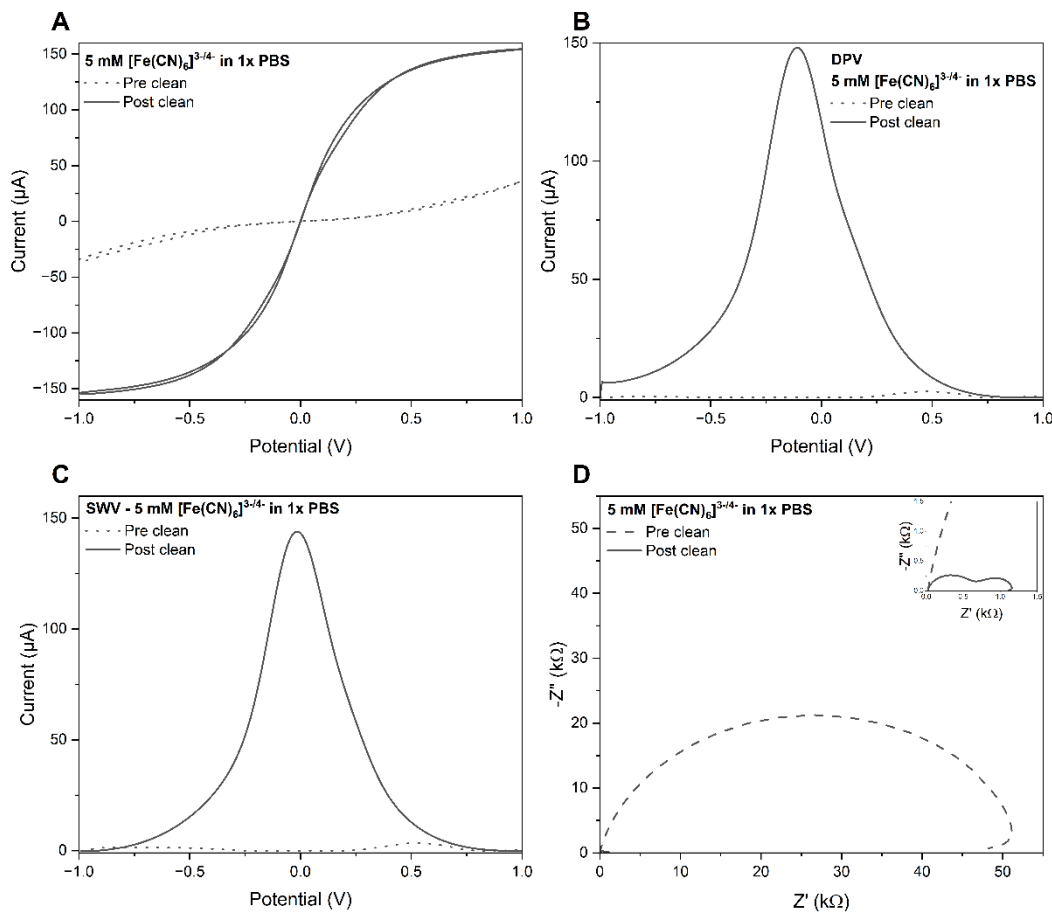
Figure A.9. IDE1 - CV (A), DPV (B), SWV (C) and EIS (D) response in 5 mM of $[Fe(CN)_6]^{3-/4-}$ in 10 mM PBS of a gold interdigitated electrode before and after O_2 plasma cleaning.
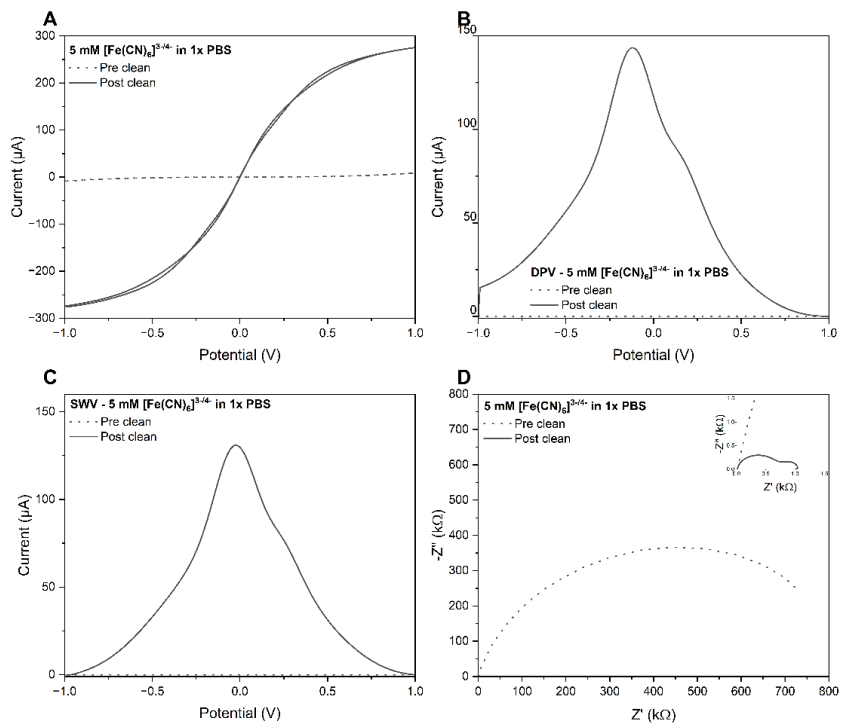
Figure A.10. IDE2 - CV (A), DPV (B), SWV (C) and EIS (D) response in 5 mM of $[Fe(CN)_6]^{3-/4-}$ in 10 mM PBS of a gold interdigitated electrode before and after O_2 plasma cleaning.
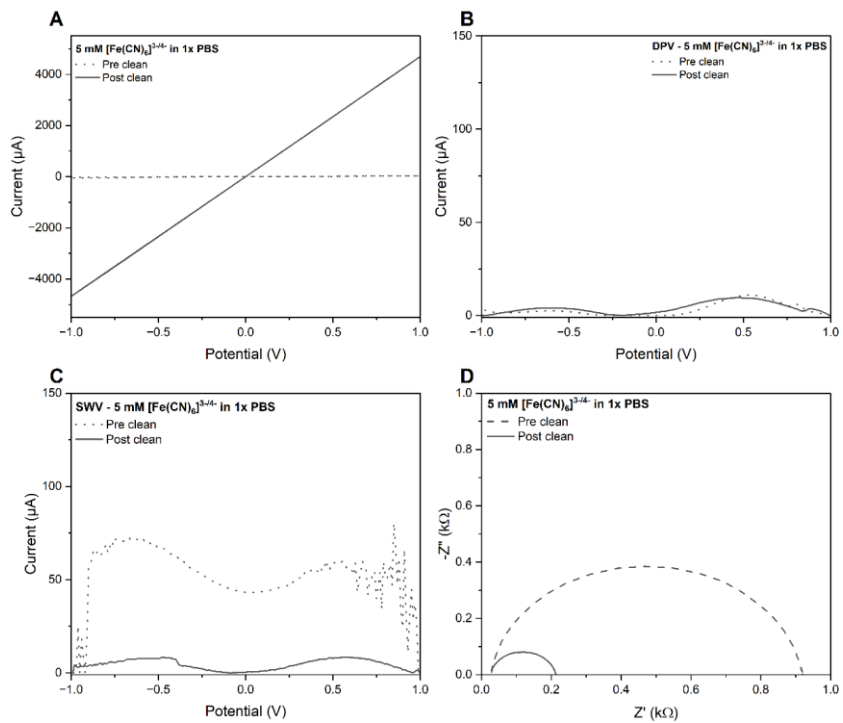
Figure A.11. IDE3 - CV (A), DPV (B), SWV (C) and EIS (D) response in 5 mM of $[Fe(CN)_6]^{3-/4-}$ in 10 mM PBS of a gold interdigitated electrode before and after O_2 plasma cleaning.

vi. Platinum electrodes
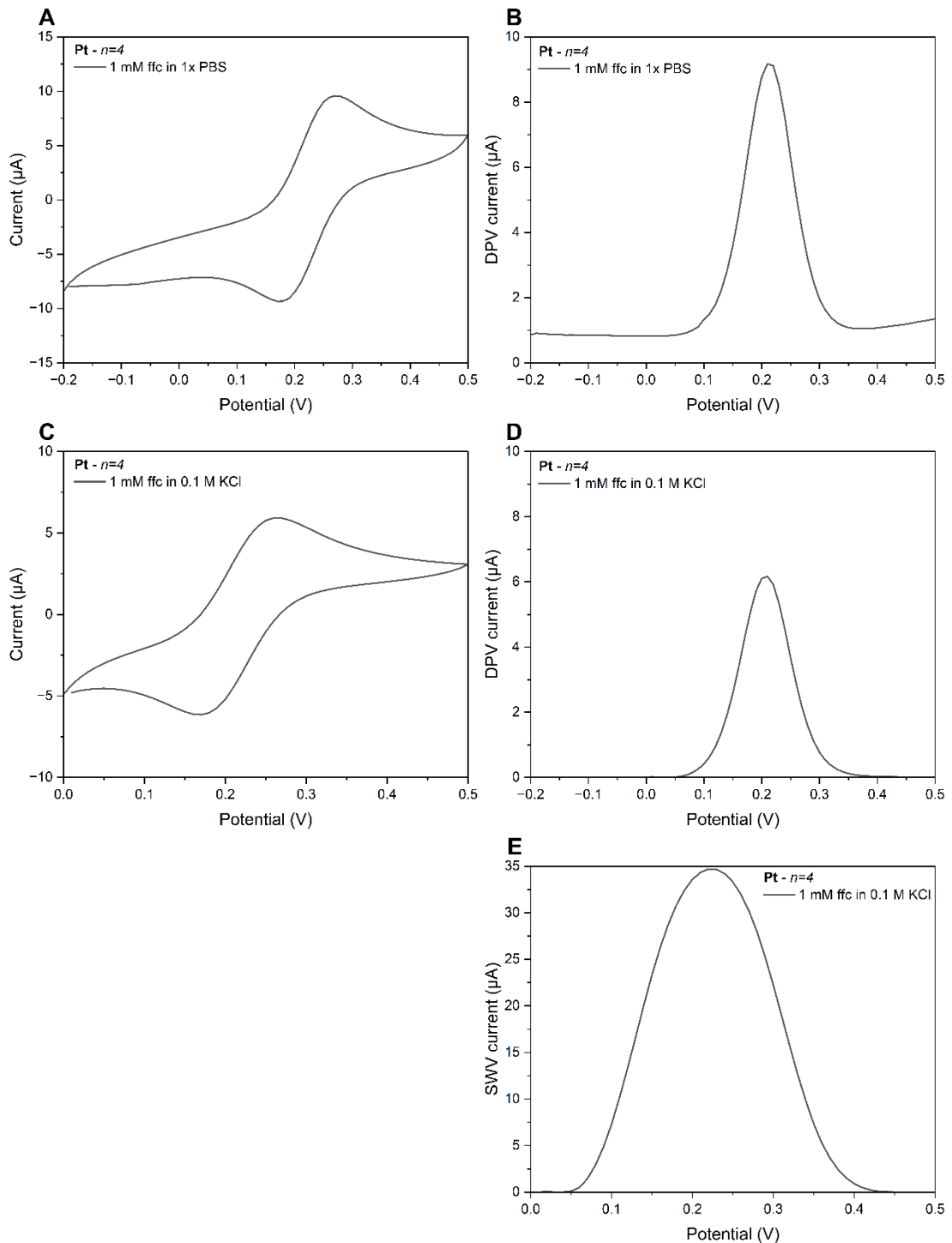
Figure A.12. Platinum (Pt) macroelectrode characterisation with 1 mM $[Fe(CN)_6]^{3-/4-}$ through CV (A) and DPV (B) in PBS and KCl (respectively C&D) along with SWV (E).

IV. Hyperspectral imaging of actinorhodin extracts

Actinorhodin extract dilutions were prepared in 96-well plates and analysed using Headwall VNIR E series and Headwall shortwave-infrared (SWIR) 640 Hyperspectral imaging cameras using the setup from Figure A.13. Images were acquired with 50 ms exposure time at 1.8 mm/s and no binning.
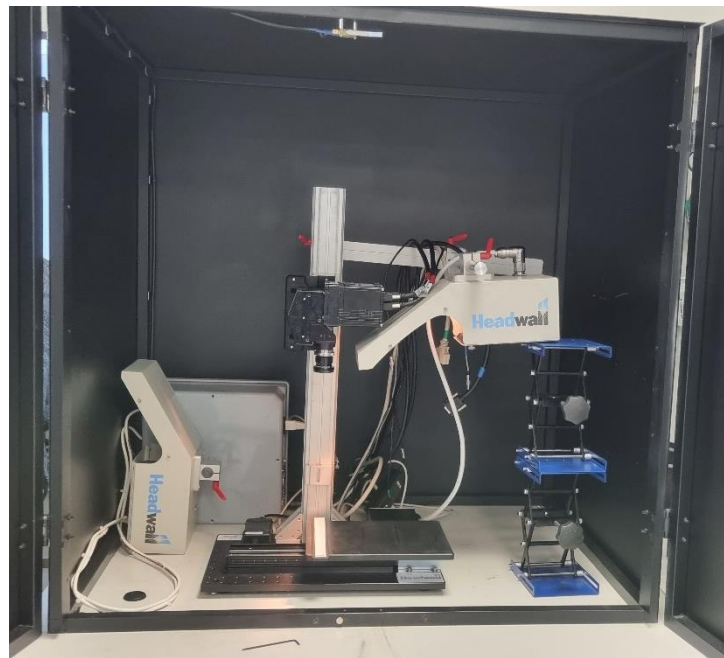
Figure A.13. Hyperspectral imaging set-up with the Headwall VNIR camera.

SWIR results did not yield much difference between samples, however VNIR data provided features of interest. The mean transmittance spectrum was obtained for each well and calibrated. Some wells displayed darker signals due to the shadow from the well itself which would require further data processing but would only affect the spectral properties by a constant scale factor in the VNIR range. Experimental work undertaken from the beginning of IV. until this point was conducted by R. D. Dunphy and P. Lasserre jointly. Absorbance (A) was calculated from the transmittance (T) data obtained as A = 2 − log (T) and the results plotted in Figure A.14. The main absorbance band was located between 550-560 nm and the 970 nm signal was relatable to the culture medium. Eventual features below 400 nm would require a UV

camera - initiated using the HPLC single wavelength UV detector. Any limit of detection through HSI would require further investigations.
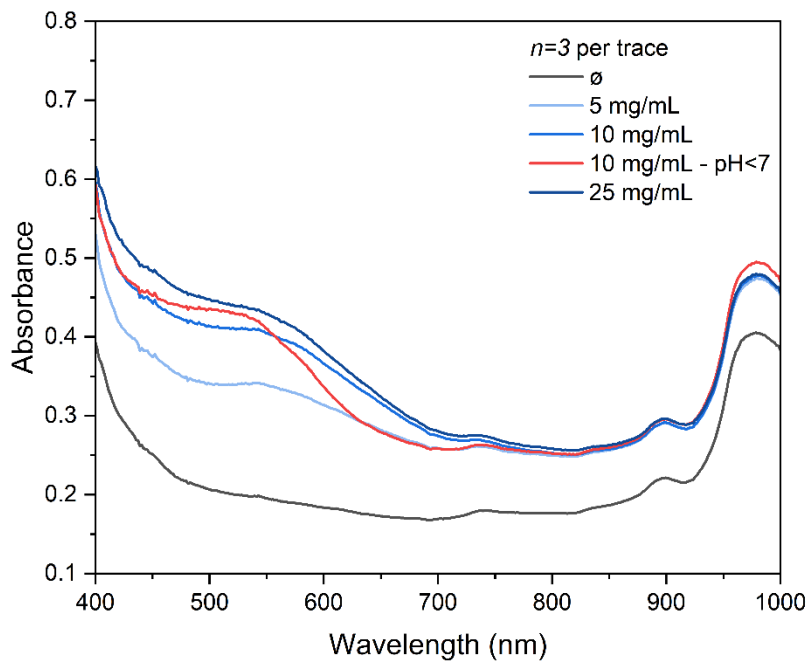
Figure A.14. Absorbance obtained from HSI analysis of actinorhodin samples at different concentrations.
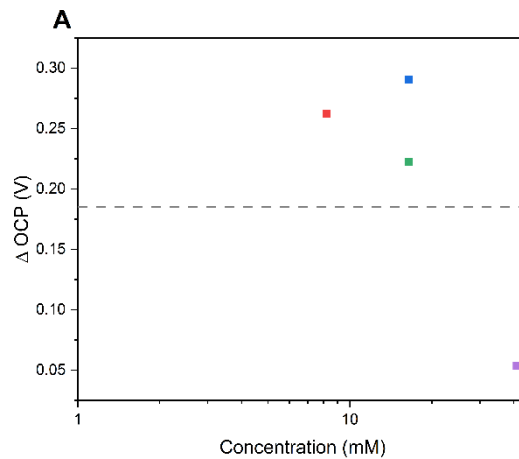
Figure A.15. OCP difference measured prior and post HSI. The blank sample is represented by the dashed line and each data point is the average of 3 replicates. On (A), the blue square is the equivalent concentration diluted.

EIS was also utilised to assess any possible sample alteration from performing HSI. Little changes were observed on the overall impedance from the Nyquist plots, however R_{ct} and Q fits showed some variability between the two stages (Figure A.16).
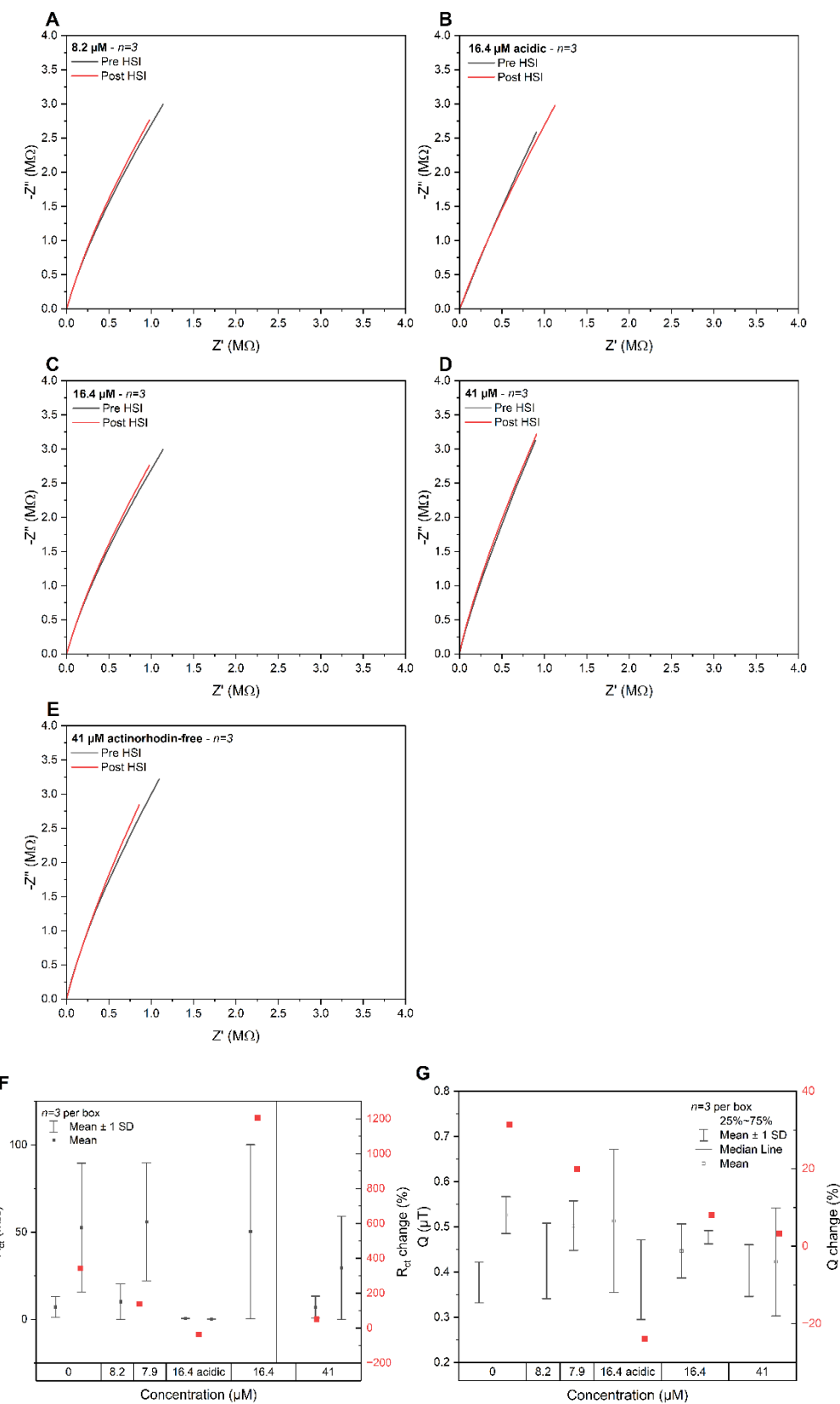
Figure A.16. Nyquist plots of PGE before and after running the HSI measurements in 7.9 (A), 15.8 μM in acidic PBS (B), 15.8 μM (C), 39.4 μM actinorhodin (D) and 39.4 μM actinorhodin-free (E) samples. R_{ct} values and corresponding changes (F) and Q values and associated changes (F) for a modified Randles' circuit fit.

V. Spectrophotometric characterisation in oxidising and reducing environments

i. Material & Methods

Actinorhodin extracts were tested at three pH conditions: 2, 7 and 11. Hydrogen peroxide and iron chloride, as oxidising agents, and TCEP and DTT, as reducing agents were tested, all at a final concentration of 1 mM. Two electrolyte environments were compared: 10 mM of phosphate buffer saline and 0.1 M of potassium chloride. Three actinorhodin extract concentrations were assessed: 520, 208 and 104 mg/L respectively equivalent to 16.4, 6.56 and 3.28 µM. The pH of the electrolyte solution was adjusted at the pH values tested and used to dilute down the actinorhodin at the intended concentrations. Each condition was tested in triplicate in a final volume of 200 µL and results per condition averaged. As reported reduction steps in biosensor functionalisation typically last one hour, spectrophotometric monitoring of the studied reactions were carried out for 60 minutes. An absorbance scan was performed for each well every 15 minutes, in the visible and IR ranges between 400 and 800 nm, with a 10 nm step on a Multiskan Go plate reader (Thermo Scientific).

ii. Results & Discussion

Actinorhodin extracts were tested in acidic, neutral and alkaline conditions. The aim was to decide upon different conditions to enable a distinct differentiation and identification between actinorhodin's forms (Figure 3.9). Since actinorhodin is pH-sensitive[306], which is reflected in its pigmentation, initial spectrophotometric monitoring of on-going reactions was possible. Hydrogen peroxide and iron chloride, as oxidising agents, and TCEP and DTT, as reducing agents were tested, all at an excess concentration compared to the estimated actinorhodin amount. Two electrolytes were compared, based on preliminary observations: phosphate buffer saline and potassium chloride. Initially, low concentrations were tested for comparison with mass spectrometry data, however, too low to record absorbance changes. Three concentrations were assessed, 520, 208 and 104 mg/mL, which are all direct dilutions

of the actinorhodin extract stock solution, along with blank conditions for each electrolyte, pH value and oxidising or reducing agent and represented in Figure A.17. As reported reduction steps in biosensor functionalisation typically last one hour, spectrophotometric monitoring of the studied reactions were carried out for 60 minutes. The order in which reagents were added to the wells ensured actinorhodin was added last for the reactions to begin as close to the monitoring start as possible. However, due to manual pipetting and homogenisation of each well, the time interval between the first and last sample wells being finalised approached 20 minutes. Each plate corresponding to a pH condition was prepared and ran consecutively to avoid supplementary delays. Furthermore, swiftness was also preferred due to actinorhodin's photosensitivity.

Overall trends suggest little changes in absorbance over time (Figure A.17). TCEP in phosphate buffer environment and basic conditions shows the most difference to the other equivalent conditions with pH variation. Most other PBS samples display an overall higher intensity for the basic sample. This peak seems to correspond when using FeCl in a KCl background in basic conditions. Electrochemical assessment of the oxidised/reduced compounds on electrode materials could have helped to differentiate actinorhodin forms, ensuring first the absence of interference from the oxidising/reducing agent if remaining in solution. Moreover, extending the analysis to the UV range could help relate to compound detection and identification with LC-MS.
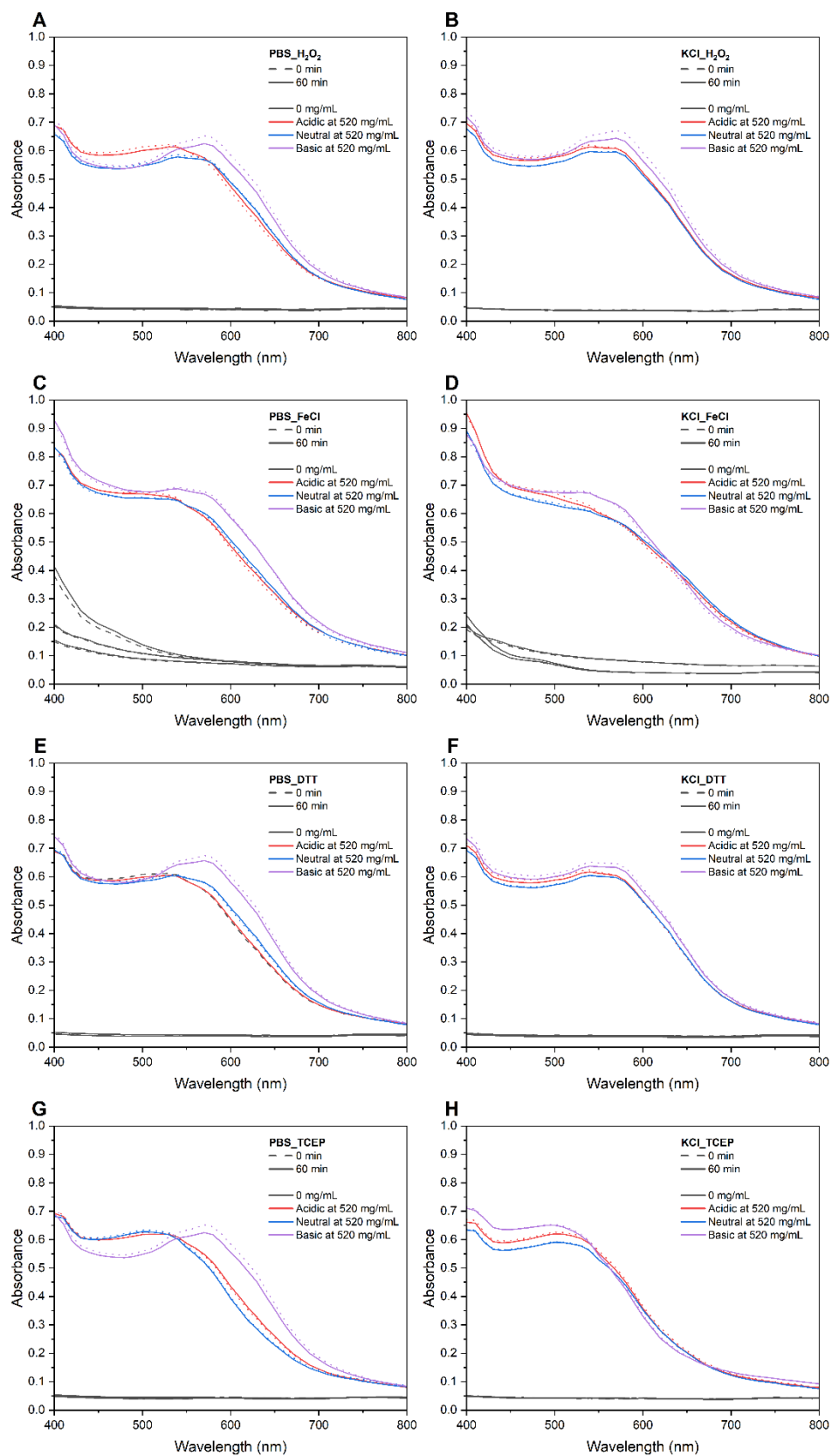
Figure A.17. Spectrophotometric monitoring of actinorhodin samples in acidic, neutral and basic pH conditions with oxidisers (A-D) and reducing agents (E-H) in PBS (left) and KCl (right). Each trace is the average of 3 separate samples.

VI. Mass spectrometry analysis of actinorhodin extracts
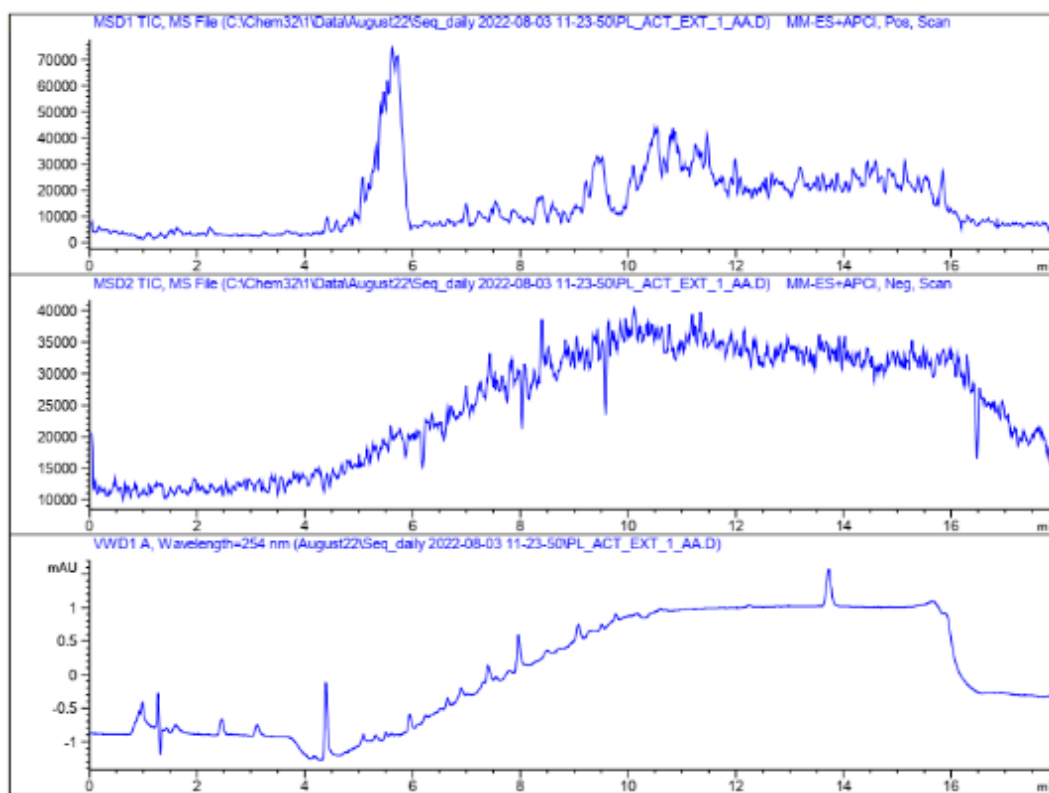
Figure A.18. Total ion count (TIC) chromatogram in positive (top) and negative ionisation modes (middle) of the chloroform extract of the total actinorhodin sample in acidic conditions (respectively top and middle) and UV chromatogram at 254 nm (bottom) with ammonium acetate as a solvent additive.

Comparing the chloroform extract in acidic conditions in Figure A.18 to the whole sample in Figure 3.13, noticeable differences strike in the lower main peak at 9.4 min, more resolved peaks in the gradient region when referring to the UV trace and more evident peaks at 4.5 and 5-6 min.

Table A.7.3. Possible compound identification from the chloroform extract in acidic conditions of the total actinorhodin sample in acidic conditions with ammonium acetate (AA) as a solvent additive.

Rt (min)	Sample	Method	Compound
5.5	EXT1	AA	α-actinorhodin
5.6	EXT1	AA	Actinorhodin
7.0	EXT1	AA	β-actinorhodin
9.5	EXT1	AA	Actinorhodinic acid
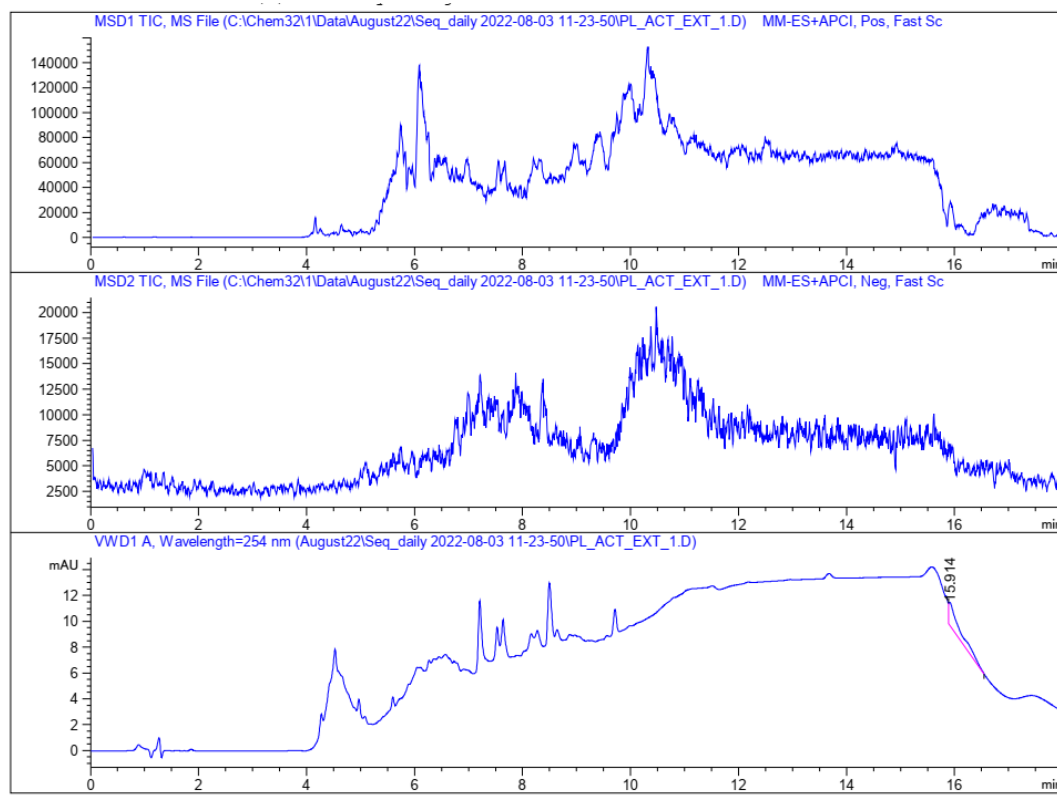
Figure A.19. Total ion count (TIC) chromatogram in positive and negative ionisation modes of the chloroform extract of the total actinorhodin sample in acidic conditions (respectively top and middle) and UV chromatogram at 254 nm (bottom) with formic acid as a solvent additive.

Comparing the chloroform extract obtained in Figure A.19 to the whole sample in Figure A.3, more peaks were recorded in the peak region at 4 minutes and peaks in the gradient region are more resolved but not yet confirmed even if the nature of some compounds was inferred in Table A.7.4.

Table A.7.4. Possible compound identification from the chloroform extract of the total actinorhodin sample in acidic conditions with formic acid (FA) as a solvent additive.

Rt (min)	Sample	Method	Compound
4.2	EXT1	FA	β-actinorhodin
4.655	EXT1	FA	α-actinorhodin
9.4	EXT1	FA	Actinorhodinic acid
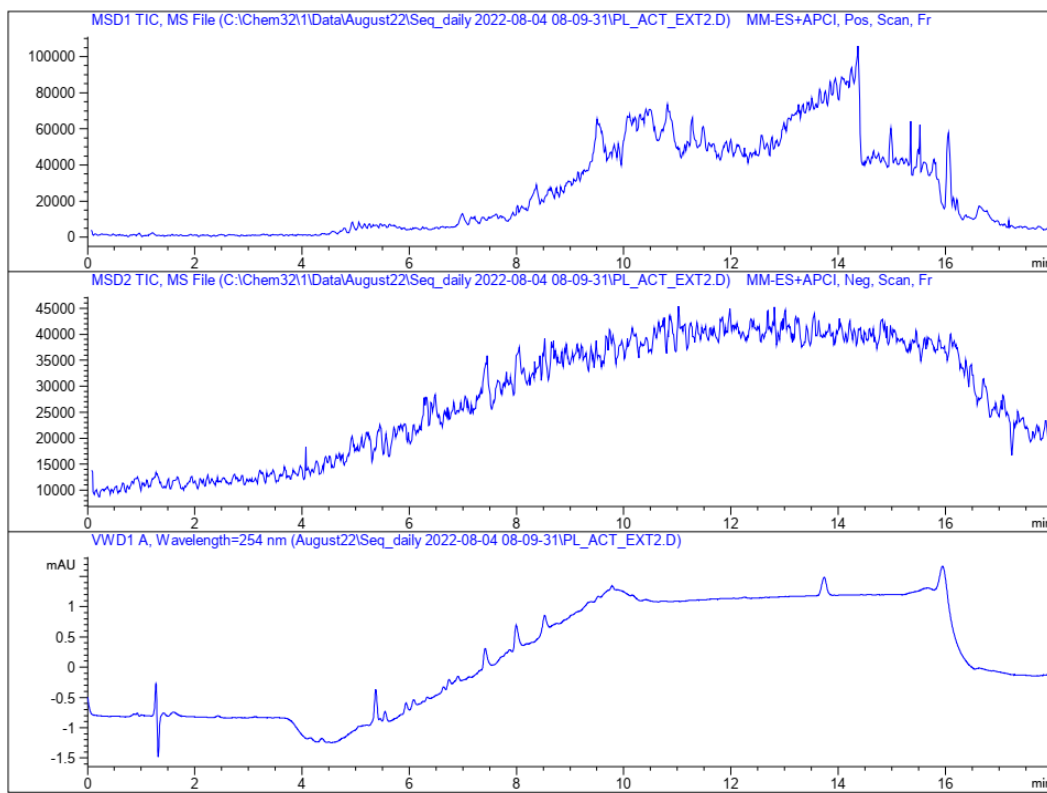
Figure A.20. Total ion count (TIC) chromatogram in positive and negative ionisation modes of the ethyl acetate extract of the total actinorhodin sample in acidic conditions (respectively top and middle) and UV chromatogram at 254 nm (bottom) with ammonium acetate as a solvent additive.

Comparing the ethyl acetate extract obtained in Figure A.20 to the whole sample in Figure 3.13, the main positive ion was absent. Moreover, the number of compounds detected appeared greater in the chloroform extract (Figure A.19) compared to when using ethyl acetate. Inferred compounds from the ethyl acetate extraction process were summarised in Table A.7.5 and Table A.7.6.

Table A.7.5 Possible compound identification from the ethyl acetate extract of the total actinorhodin sample in acidic conditions with ammonium acetate (AA) as a solvent additive.

Rt (min)	Sample	Method	Compound
5.5	EXT2	AA	Actinorhodinic acid
6.9	EXT2	AA	β-actinorhodin
8.3	EXT2	AA	Actinorhodin
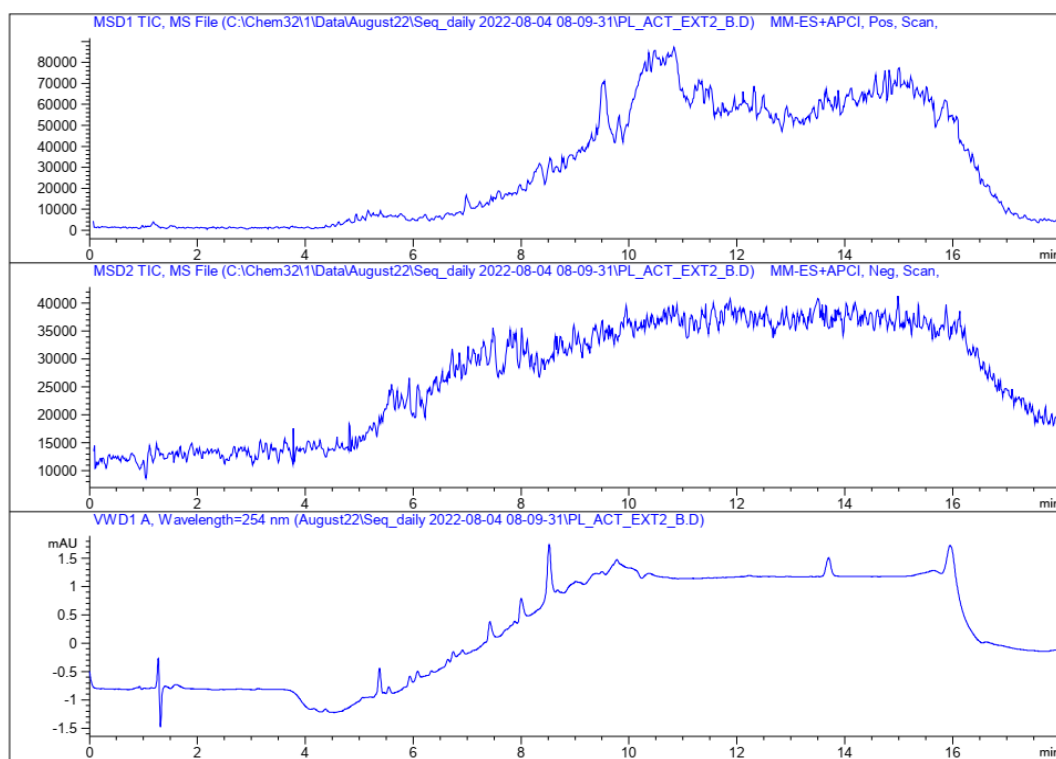
Figure A.21. Total ion count (TIC) chromatogram in positive and negative ionisation modes of the ethyl acetate extract of the total actinorhodin sample (respectively top and middle) and UV chromatogram at 254 nm (bottom) with ammonium acetate as a solvent additive.

Table A.7.6. Compound identification from the ethyl acetate extract of the total actinorhodin sample with ammonium acetate (AA) as a solvent additive.

Rt (min)	Sample	Method	Compound
5.5	EXT2_B	AA	Actinorhodin
6.9	EXT2_B	AA	β-actinorhodin
8.3	EXT2_B	AA	Actinorhodin
9.5	EXT2_B	AA	Actinorhodinic acid

VII. Electrochemical analysis of actinorhodin extracts from an ethyl acetate phase in a PBS environment
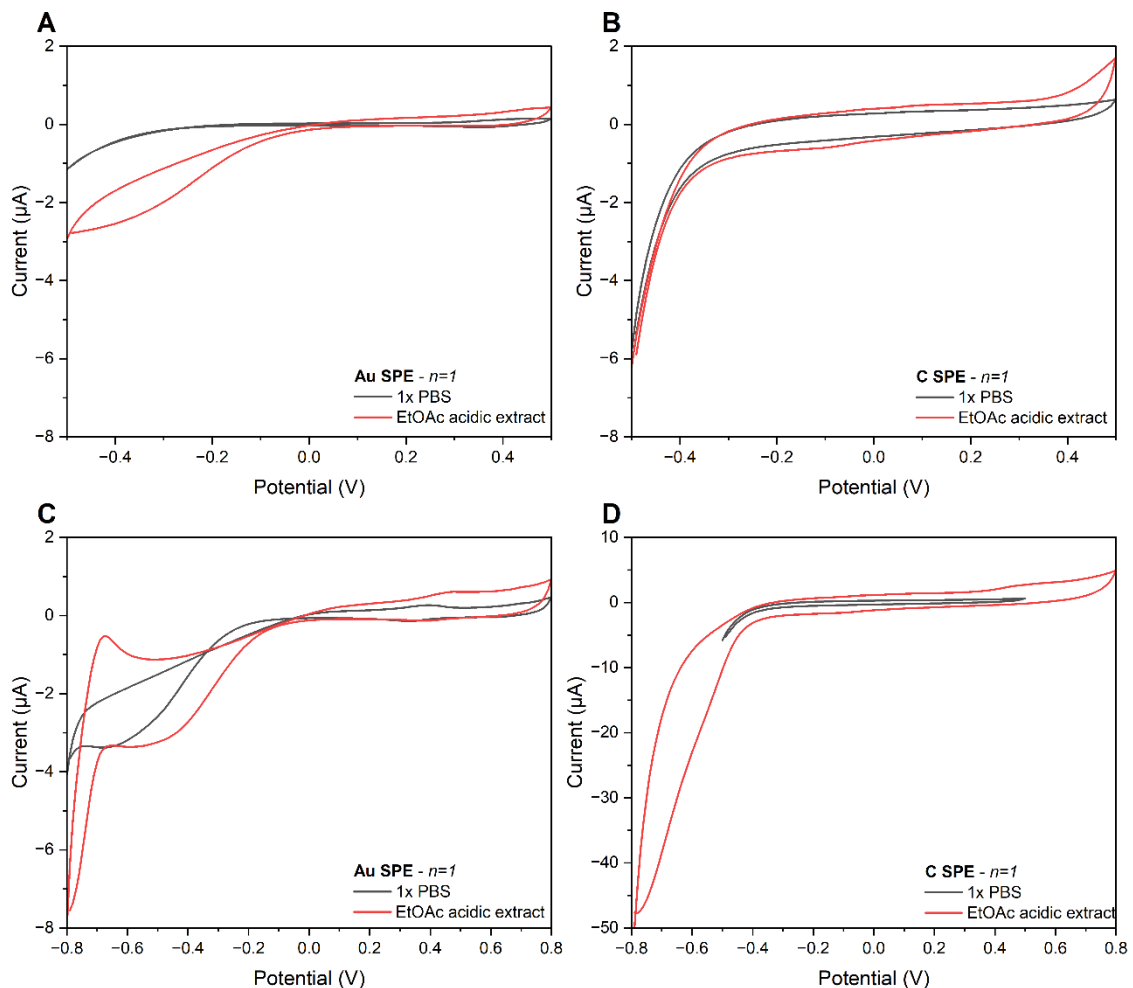
Figure A.22. CV analysis of the acidic ethyl acetate actinorhodin extract in a PBS background on gold (A&C) and carbon (B&D) SPE respectively with [-0.5;0.5] and [-0.8;0.8] voltage windows.

From the ethyl acetate acidic extract, a small oxidation peak could be noticed in the 0.5 V region and a reduction peak in the -0.1 V area on the carbon SPE (Figure A.22B&D). The larger potential window allowed better peak detection on gold, with redox activity recorded in the [-0.7 ;-0.4] and [0.3 ;0.5] regions (Figure A.22C).
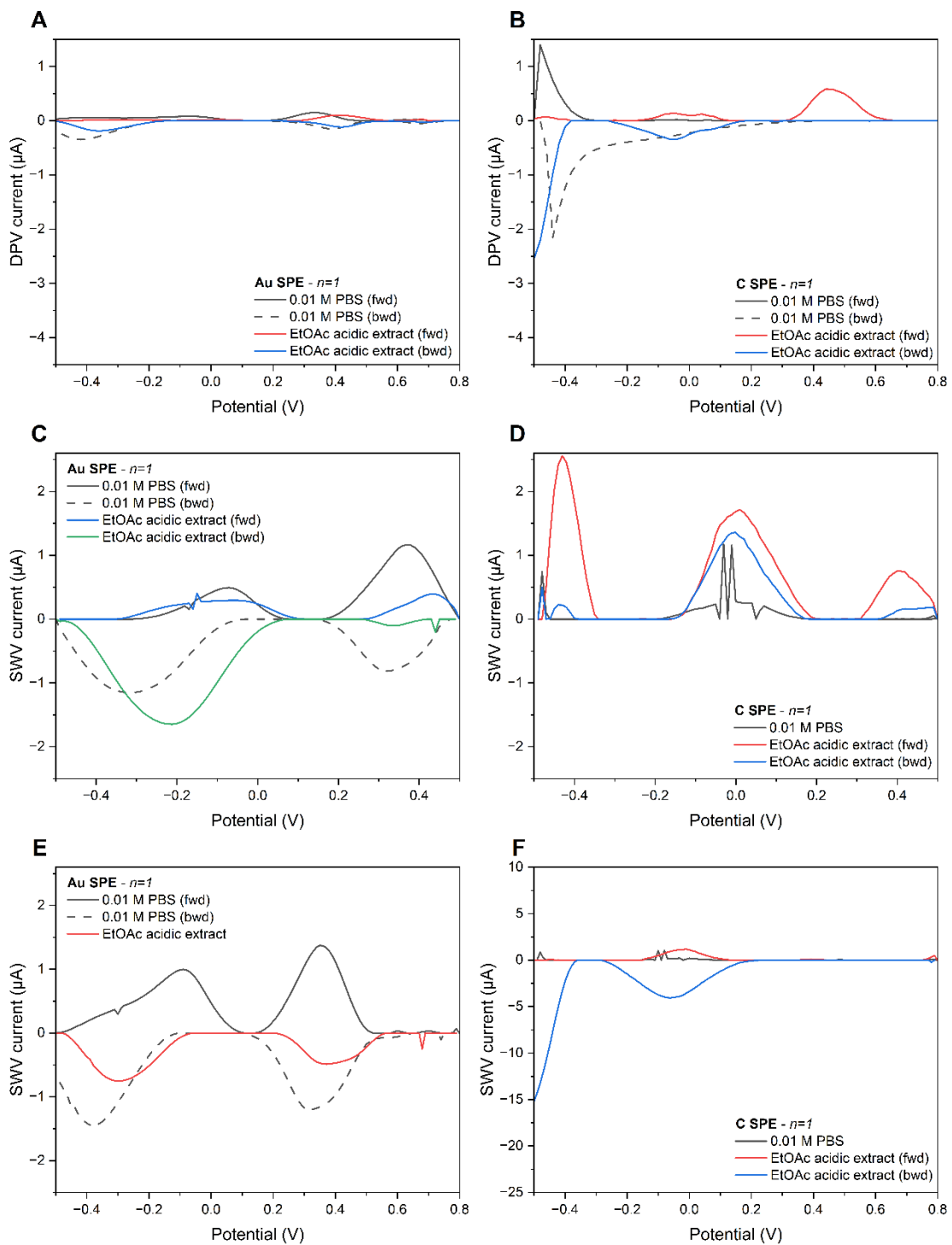
Figure A.23. Pulse voltammetry of an acidic ethyl acetate extract in 10 mM PBS. DPV on gold (A) and carbon (B) SPEs. SWV within [-0.5;0.5] V on gold and carbon SPEs (C&D) and a wider potential window for each electrode material respectively (E&F).

Clear regions around - 0.35 V and two other in the positive regions close to 0.4 and 0.65 V (Figure A.23). DPV on carbon provided a better differentiation between blank and samples. Three regions of redox activity were recorded, namely one around

- 0.5/- 0.4 V, a wide one between -0.1 and 0.1 and a later one around 0.4 V. For SWV on gold, the only peak detected above blank signals was located at - 0.2 V ; similar peak potentials for blank and actinorhodin samples. SWV on carbon yielded higher peak potential than the blank at - 0.4 V, around 0 and 0.4 V (Figure 3.55).

Table A.7.7. Peak detection for acidic actinorhodin extracted samples with ethyl acetate on gold and carbon SPEs in PBS. Peaks included show higher amplitude currents than at least the first electrolyte blank solution tested. Highlights indicate peaks detected on the same electrode material, with the same electrolyte in the whole sample. Fwd = forward scan from negative to positive potentials and bwd = backward scan from positive to negative potentials.

Potential region (V)	Electrode		Measurement			Fig.
	Au	C	CV	DPV	SWV	
-0.6	√		√			Figure A.22
-0.5		√		√ (bwd)	√ (bwd)	Figure A.23
-0.45		√		√ (fwd)		Figure A.23
-0.4		√			√ (bwd)	Figure A.23
-0.35	√			√ (bwd)		Figure A.23
-0.3	√				√ (bwd)	Figure A.23
-0.2	√				√ (bwd)	Figure A.23
-0.05	x	X		X (fwd&bwd)	X (bwd) X (fwd)	Figure A.23
0.05		x		X (fwd)		Figure A.23
0.3	x				X (bwd)	Figure A.23
0.4	X	x		X (fwd&bwd) X (fwd)	X (fwd&bwd) X (fwd)	Figure A.23
0.5	x		X			Figure A.23
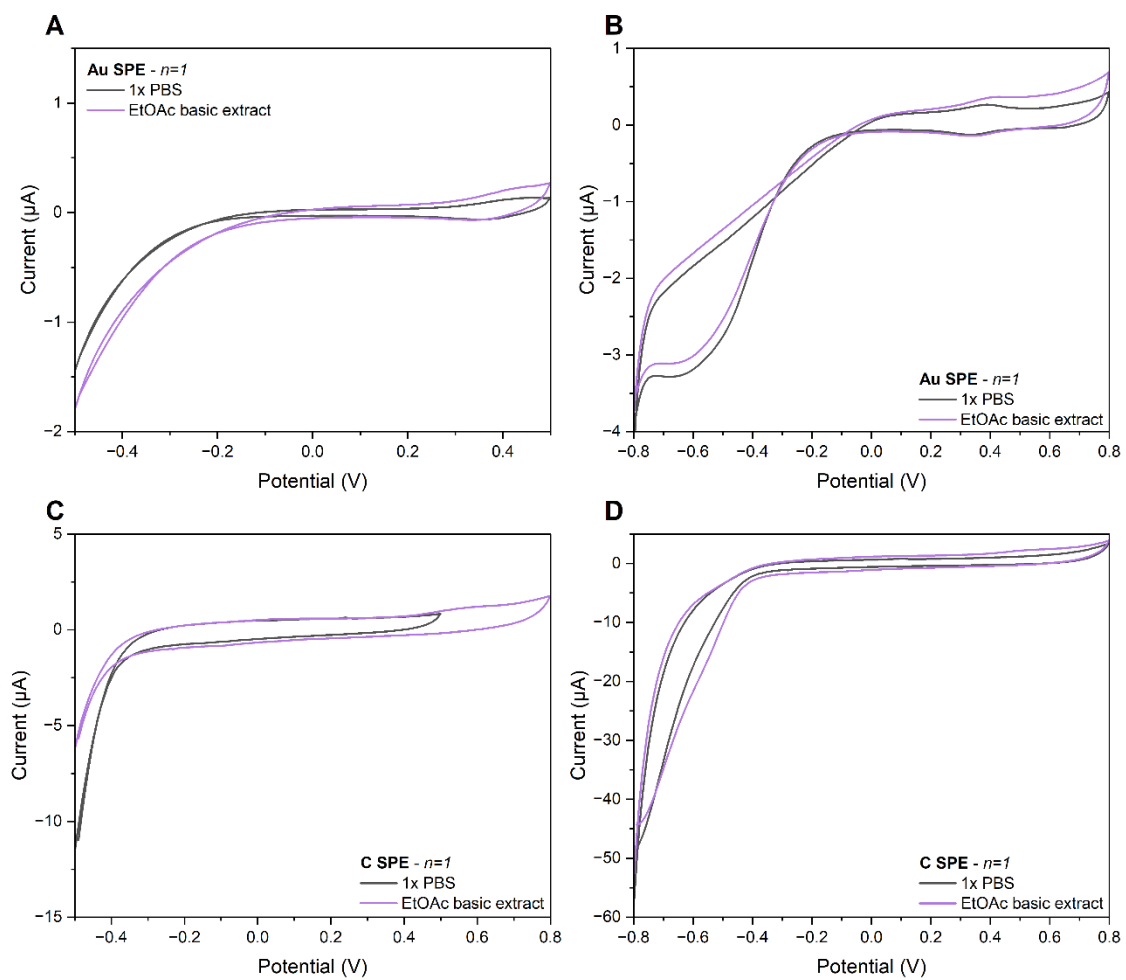
Figure A.24. CV analysis of the ethyl acetate basic actinorhodin extract in a PBS background on gold (A&B) and carbon (C&D) SPE respectively with [-0.5;0.5] and [-0.8;0.8] voltage windows.

On carbon electrodes, a small oxidation peak might was recorded (Figure A.24C&D). On gold electrodes, the absence of peak differing from the blank solution using CV of the basic EtOAc basic extract prompts at examining the pulsed voltammetric response (Figure A.24A&B).
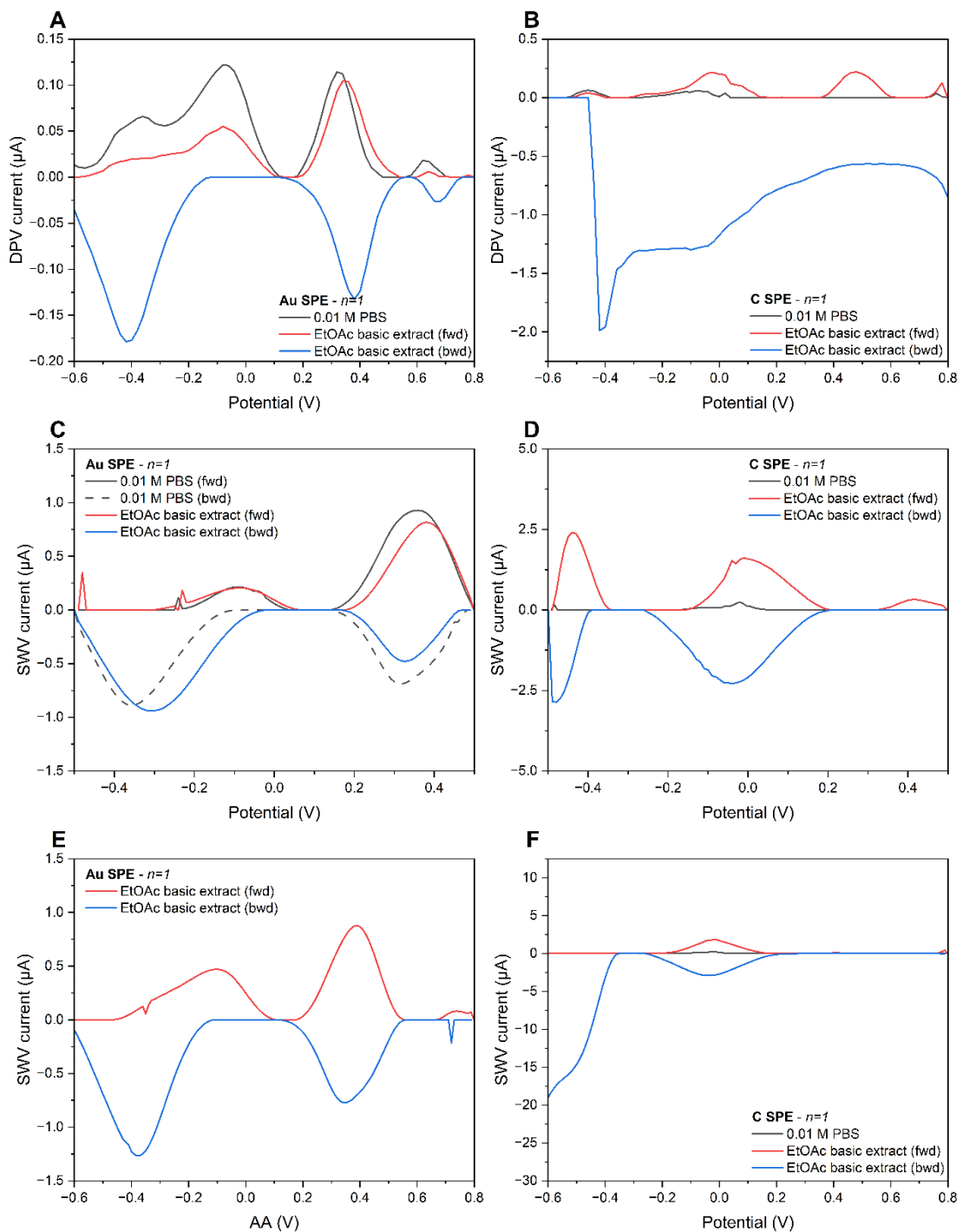
Figure A.25. Pulse voltammetry of an ethyl acetate basic extract in 10 mM PBS. DPV on gold (A) and carbon (B) SPEs. SWV within [-0.5;0.5] V on gold and carbon SPEs (C&D) and a wider potential window for each electrode material respectively (E&F).

Similar behaviour and peaks (with lower amplitudes than blank solutions) were recorded for SWV on gold in the two potential windows. On carbon, the peak at 0.5 V was better recorded in the smaller potential window. Better peak differentiation

was obtained using the DPV compared to SWV. The backward scan was less efficient than the forward one at peak differentiation (Figure A.23).

Table A.7.8. Peak detection for basic actinorhodin extracted samples with ethyl acetate on gold and carbon SPEs in PBS. Peaks included show higher amplitude currents than at least the first electrolyte blank solution tested. Highlights indicate peaks detected on the same electrode material, with the same electrolyte in the whole sample. Fwd = forward scan from negative to positive potentials and bwd = backward scan from positive to negative potentials.

Potential region (V)	Electrode		Measurement			Fig.
	Au	C	CV	DPV	SWV	
-0.5		√			√ (bwd)	Figure A.25
-0.4	√			√ (bwd)	√ (bwd)	Figure A.25
		√		√ (bwd)	√ (fwd)	
-0.3		√			√ (bwd)	Figure A.25
-0.1	√			√ (fwd)	√ (fwd)	Figure A.25
		√		√ (bwd)		
-0.05		√			√ (bwd)	Figure A.25
0.3	√			√ (fwd)	√ (bwd)	Figure A.25
0.35	√				√ (bwd)	Figure A.25
0.4	√		√	√ (bwd)	√ (fwd)	Figure A.24& Figure A.25
		√		√ (bwd)		
0.5		√		√ (fwd)		Figure A.25
0.6	√			√ (fwd)		Figure A.25
0.7	√			√ (bwd)		Figure A.25

CV at the chosen scan rate did not provide an accurate detection method for ethyl acetate extracts. Comparing data obtained for the ethyl acetate extracts at more acidic (Table A.7.7) and more basic pH values (Table A.7.8), overlapping compounds with the total samples are similar as when extracting with chloroform (Table 3.8) with the addition of peaks at - 0.1 V in less acidic samples. Moreover, the abundance of peaks in total actinorhodin samples between - 0.2 and 0.3 V was not reflected in the ethyl acetate extract in PBS, possibly due to poor peak separation. As analyses were only conducted with PBS, assessment of other electrolytes could be help to uncover

compound nature and identification along with an extraction using the same solvent extraction protocol with actinorhodin-free samples. Partitioning between ethyl acetate and water was not as successful as when using chloroform due to closer dipole moments and raised more difficulties in the experimental precision of partitioning phases.

B.

B. Chapter 5 Appendices

I. Quantitative assessment of DNA surface coverage

The challenge in obtaining repeatable trends prompted again a questioning of the aptamer concentration on the electrode surface, which has been partly attributed to the filtration step. Electrochemical evaluation of oligonucleotide surface coverage has therefore been undertaken using the widely reported method from Steel *et al.* (1998)[661] and following Mahajan *et al.* (2008)[662] and Keighley *et al.* (2008)[663] using chronocoulometry and hexaamine ruthenium to quantitatively determine DNA on a gold electrode based upon the electrostatic attraction between a cationic redox marker and the anionic DNA phosphate backbone.

i. Methods

Gold macroelectrodes (*n=6*) were polished with 0.03 µM alumina polish for 2 min, then sonicated for two minutes in water to get rid of the slurry. They were finally rinsed and dried with argon. Polished electrodes were immersed in a piranha bath for 15 minutes, rinsed and dried with argon thereafter. Electrochemical potential cycling was then undertaken from -0.3 to 1.3 V for 20 scans at 0.1 V/s in 0.1 M H_2SO_4.. Once again, electrodes were rinsed with distilled water and dried with argon.

Thiolated oligonucleotide supports were reduced with 1 mM TCEP for an hour, filtered with a NAP-5 column. 1 µM of capture and MCP were then incubated per working electrode overnight at room temperature. 1 mM MCP was then used as a blocking step the following day. Heat-treated methylene blue-labelled aptamers were then hybridised to the support strands for an hour. A solution of 10 mM Tris at pH 7.2 was degassed using N_2 and a chronocoulometry measurement ran following Mahajan *et al.* (2008). 80 µM of hexaamine ruthenium was added to the Tris solution, degassed and another chronocoulometry measurement ran. 10 µM of moxifloxacin was then incubated on sensors for 30 minutes and a final chronocoulometry measurement taken. Rinses after each incubation consisted of 3 times 500 µL of aptamer buffer.

All measurements were taken against a Pt counter and Ag/AgCl reference electrodes in a Faraday cage.

The number of DNA molecules on the surface was estimated thanks to these two equations :

$$Q_{RuHex} - Q_{noRuHex} = nFA\Gamma_0 \text{ and } \Gamma_{dna} = \Gamma_0(z/n_b)N_a$$

where n is the number of electrons exchanged (here one), F= 96485.3321 C/mol, A= 0.03142 cm², z the charge (here 3), n_b the number of bases and N_a = 6.022E+23 mol^{-1}.

ii. Results

Conditions tested included overnight immobilisation of 1 μM of oligonucleotide support in a MCP SAM with and without methylene-blue tagged aptamer and 15 nM of the complex (Figure B.1). As the experimental set-up might have required adjustments, only a few measurements proved successful, meaning that triplicates were not obtained. the number of bases for the aptamer and support are estimated at 42 and 12 bp respectively.[431]

Moreover, the amount of base pairing between the two sequences is also unknown and has been arbitrarily set at 5. Estimations obtained solely for the oligonucleotide support reached 7.5*10^{16} molecules/cm² (Figure B.1A), 1.4-1.5*10^{15} molecules/cm² for 1 μM of the complex on a first trial (Figure B.1B) and 2.0-2.9*10^{16} molecules/cm² (Figure B.1C&D) on the second trial as well as 1.4-2.5*10^{16} molecules/cm² for 15 nM of the complex (Figure B.1E&F), which did not differ much between conditions possibly due to approximations that had to be inferred (Figure B.1). These numbers were above reported values for similar concentrations, which could result from the possible conformation adopted by the aptamer in absence of target and yield closer packing.[518] Moreover, 1 μM of aptamer sequence seemed to saturate the filter, leading to less repeatability in the obtained concentration.
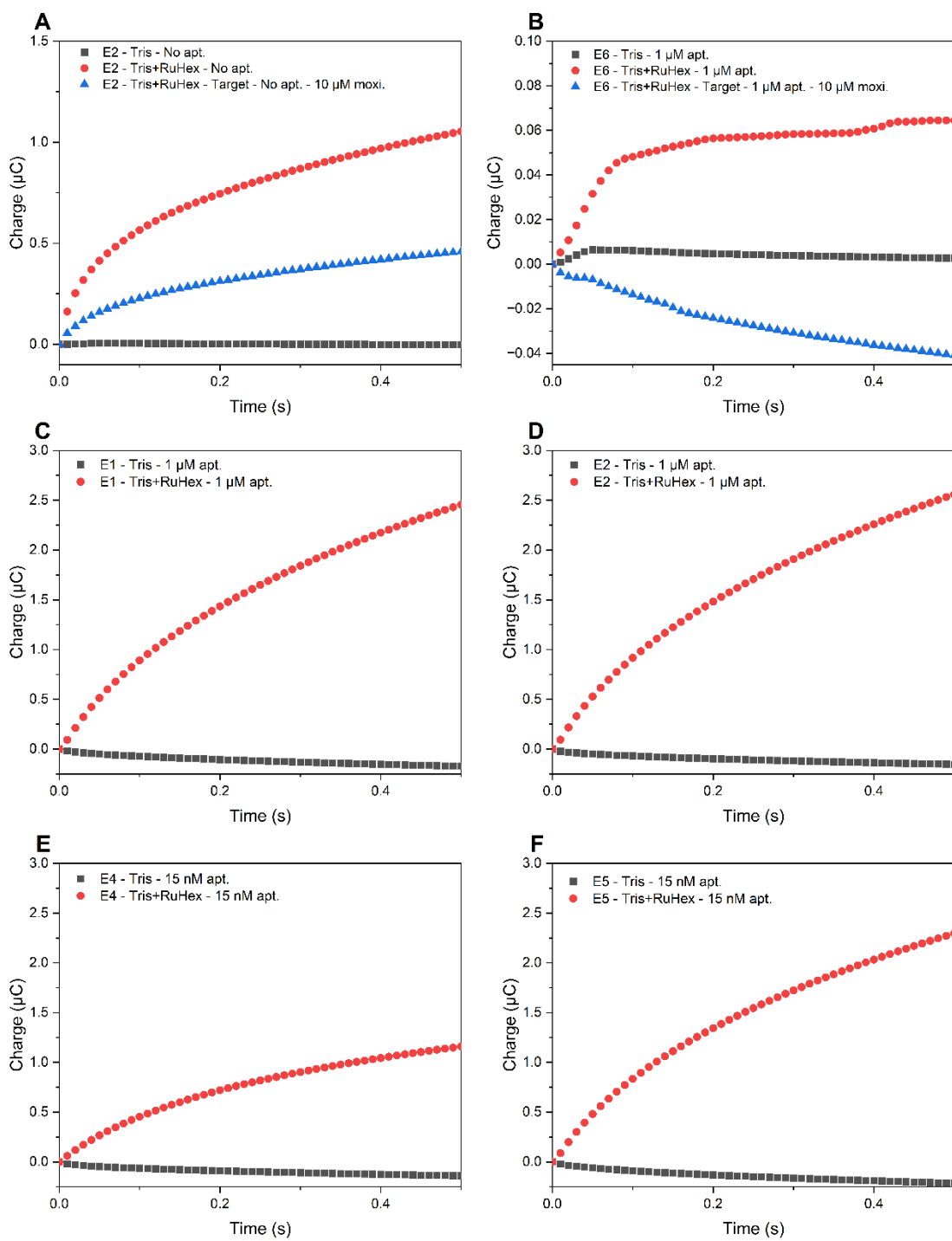
Figure B.1. Chronocoulometry responses for the oligonucleotide support alone (A) compared to the aptamer hybridised to its support (B) and comparison between electrode responses for 1 µM (C&D) vs 15 nM (E&F) hybridisation.

II. MIC assessment of ESKAPE pathogens against moxifloxacin

i. Methods

MIC values were screened for the seven ESKAPE pathogens, namely *Enterobacter faecalis, Staphylococcus aureus, Klebsiella pneumoniae, Acinetobacter baumannii, Pseudomonas aeruginosa, Escherichia coli* to inform the most adequate bacterial target for the Apta-MIP assay. Inocula were grown overnight at 37°C in LB and were tested at a final A_{600} of 0.1 in 200 μL. A moxifloxacin stock was prepared in PBS and filtered through 0.22 μm before use. Plates were incubated for 24 hours at 37°C and under 60 rpm to avoid biofilm formation. Plate absorbance was read at t_0 and t_{24}.

ii. Results

Concentration ranges employed for *B. subtilis, E. coli and S. aureus*, were ten times higher than the four other microorganisms studied and did not reach the MIC in this range (Figure B.2B-C-G). *A. baumannii, E. faecalis* and *P. aeruginosa* reached low absorbance levels for the higher moxifloxacin concentrations tested and were gathered to be compared in the last plot (Figure B.2H). Even if *P. aeruginosa* appeared to be the most sensitive out of the three pathogens tested, its characteristic electrochemical activity is not reflective of other bacterial species behaviour (Figure B.2E). Despite *E. faecalis* apparent MIC at 5 μg/mL, the more linear susceptibility profile of *A. baumannii* to moxifloxacin was picked to develop the assay (Figure B.2A-D).
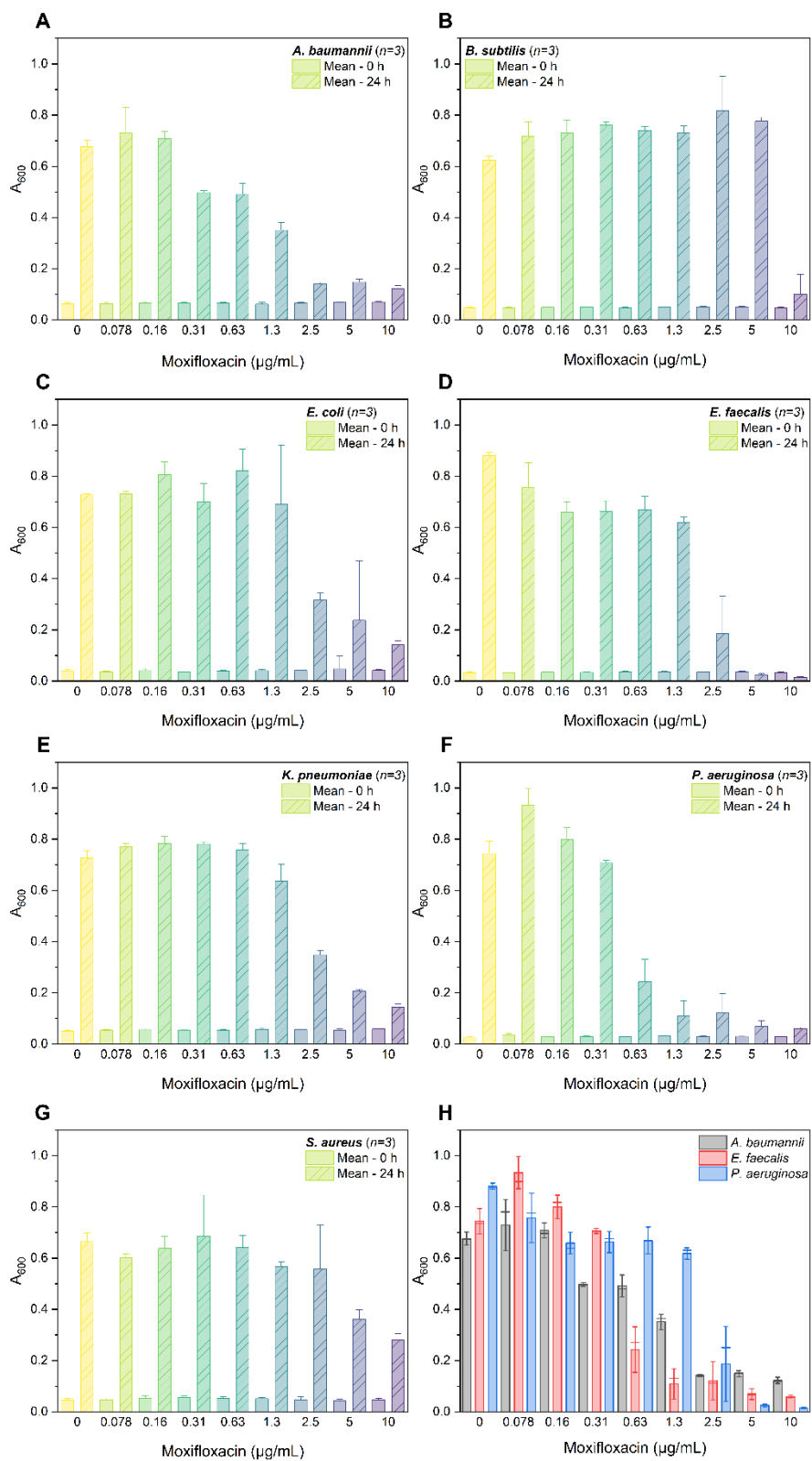
Figure B.2. MIC screening of moxifloxacin for *A. baumannii* (A), *B. subtilis* (B) *E. coli* (C), *E. faecalis* (D), *K. pneumoniae* (E), *P. aeruginosa* (F) and *S. aureus* (G)represented by absorbance values at 600 nm at 0 and 24 hours with background subtraction of LB samples. Comparison at 24 h of the three most susceptible species to moxifloxacin (H). Error bars represent one standard deviation.

III. Curve fits

Table B. 7.9. Fitting equations for DPV monitoring of Apta-MIPs and NanoMIPs with 5, 50 and 500 nM of moxifloxacin on $[Fe(CN)_6]^{3-/4-}$ gel-modified carbon SPEs.

Moxi. (nM)	-	R^2	Apta-MIPs	R^2	NanoMIPs	R^2
			In aptamer buffer			
0	-	-	$y = 13.87241 - 11.71907x + 0.39492x^2$	0.99368	$y = 14.62006 - 11.38211x + 0.53499x^2$	0.99606
5	$y = -1.94247 - 7.71951x$	0.99674	$y = 30.71441 - 12.8153x + 1.57518x^2$	0.99341	$y = 9.85668 - 9.75241x + 0.58943x^2$	0.99538
50	$y = 6.07364 - 9.50816x$	0.98898	$y = 25.69339 - 23.95834x + 2.80192x^2$	0.99345	$y = 11.29653 - 9.62899x + 0.04618x^2$	0.9994
500	$y = 18.927 - 10.0035x$	0.99462	$y = 26.23501 - 30.05039x + 3.86761x^2$	0.99974	$y = 14.90424 - 14.10894x + 1.25373x^2$	0.99964

Table B. 7.10. Fitting equations for DPV monitoring in *A. baumannii* culture at OD_{600} = 0.1 of Apta-MIPs with 100 nM of moxifloxacin on $[Fe(CN)_6]^{3-/4-}$ and $[Ru(NH_3)]^{3+}$ gel-modified carbon SPEs.

Moxi. (nM)	Redox mediator	-	R^2	Apta-MIPs	R^2
		In aptamer buffer			
0	$[Fe(CN)_6]^{3-/4-}$	$y = -27.22237 - 0.7675x + 0.00342x^2$	0.99956		
100	$[Fe(CN)_6]^{3-/4-}$	$y = -27.2115 - 0.77115x + 0.00349x^2$	0.99956		
100	$[Fe(CN)_6]^{3-/4-}$	$y = -27.65294 - 0.50104x + 0.00146x^2$	0.89288	$y = -64.92628 - 0.16883x + 5.13738e^{-4}x^2$	0.69303
	$[Ru(NH_3)_6]^{3+/2+}$	$y = -23.29926 - 0.21452x + 4.59268E - 4x^2$	0.59486	$y = -32.71205 - 0.21338x + 6.07274e^{-4}x^2$	0.89222

393

Table B. 7.11. Fitting equations for R_{ct} monitoring of Apta-MIPs and NanoMIPs with 5, 50 and 500 nM of moxifloxacin on $[Fe(CN)_6]^{3-/4-}$ gel-modified carbon SPEs.

Moxi. (nM)	-	R^2	Apta-MIPs	R^2	NanoMIPs	R^2
			In aptamer buffer			
0			$y = -79.14327 + 3.52169x - 0.3117x^2$	0.21646	$y = -75.53281 - 2.89889x + 0.88676x^2$	0.13157
5	$y = -67.07483 + 28.15072x - 8.215x^2$	0.883	$y = -43.77827 + 94.54236x - 16.4925x^2$	-1.44451	$y = -96.6841 - 1.79511x + 0.38235x^2$	0.81027
50	$y = -72.23009 - 7.43085x + 1.97481x^2$	0.93721	$y = -89.44302 + 40.28427x - 4.45136x^2$	-0.11802	$y = -95.3976 - 2.55296x + 0.54117x^2$	0.8728
500	$y = -67.09271 + 7.88545x - 3.23727x^2$	0.9988	$y = 6.324 - 51.97144x + 10.51528x^2$	0.77531	$y = -90.19801 + 0.46169x + 0.03801x^2$	0.62645

Table B. 7.12. Fitting equations for R_{ct} monitoring in *A. baumannii* culture at OD_{600} = 0.1 of Apta-MIPs with 100 nM of moxifloxacin on $[Fe(CN)_6]^{3-/4-}$ and $[Ru(NH_3)_6]^{3+/2+}$ gel-modified carbon SPEs.

Moxi. (nM)	Redox mediator	-	R^2	Apta-MIPs	R^2
In *A. baumannii* culture at od_{600} = 0.1					
0	$[Fe(CN)_6]^{3-/4-}$	$y = -15.61361 + 1.17504x - 0.00316x^2$	-		
100	$[Fe(CN)_6]^{3-/4-}$	$y = -14.32175 + 1.77849x - 0.00483x^2$	-		
100	$[Fe(CN)_6]^{3-/4-}$	$y = 73.57222 + 3.38769x - 0.00851x^2$	0.99688	$y = 190.45592 + 1.56882x - 0.00412x^2$	0.99517
	$[Ru(NH_3)_6]^{3+/2+}$	$y = -27.8499 + 0.09218x + 2.95389e^{-4}x^2$	0.46564	$y = 11.69435 + 0.78673x - 0.00308x^2$	0.75039

C. Chapter 6 Appendices

I. Combining hyperspectral imaging and electrochemical sensing for the detection of *Pseudomonas aeruginosa* through pyocyanin production
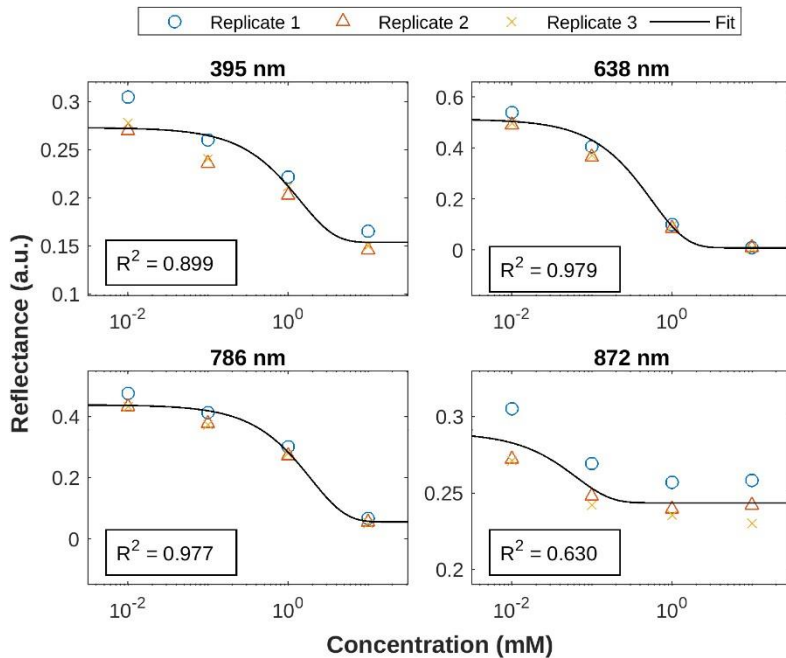
Figure C. 1. Exponential curves fit to additional characteristic wavelength bands. Along with Figure 6.5C, these wavelengths show the highest difference between each concentration. The wavelength of 638 nm, which had the R^2 value closest to 1, was used for pyocyanin estimations.

Table C. 1. Estimated mM of pyocyanin quantity using SWV linear correlation. *n=3* for each condition.

	T = 0	*T* = 24 H	*T* = 48 H
LESB58 OD$_{600}$ 0.5	(0.49)	2.03	1.96
LESB58 OD$_{600}$ 1.0	(0.96)	2.2	1.61
PA14 OD$_{600}$ 0.5	0.16	(0.53)	0.46
PA14 OD$_{600}$ 1.0	(0.49)	(0.52)	0.36

Peak detection was run in the [- 0.35; - 0.15] V region and current amplitudes for each replicate reported. Pyocyanin estimations were calculated for each replicate then averaged. The following equation fits the SWV dose response data with an adjusted R^2 = 0.99892:

SWV peak amplitude = 0.152017 + 2.75069* pyocyanin concentration

Peaks detected for pyocyanin were only recorded if their amplitude was higher than LB in that region and values in parentheses correspond to peak 2, not exactly overlapping the pyocyanin standard potential.
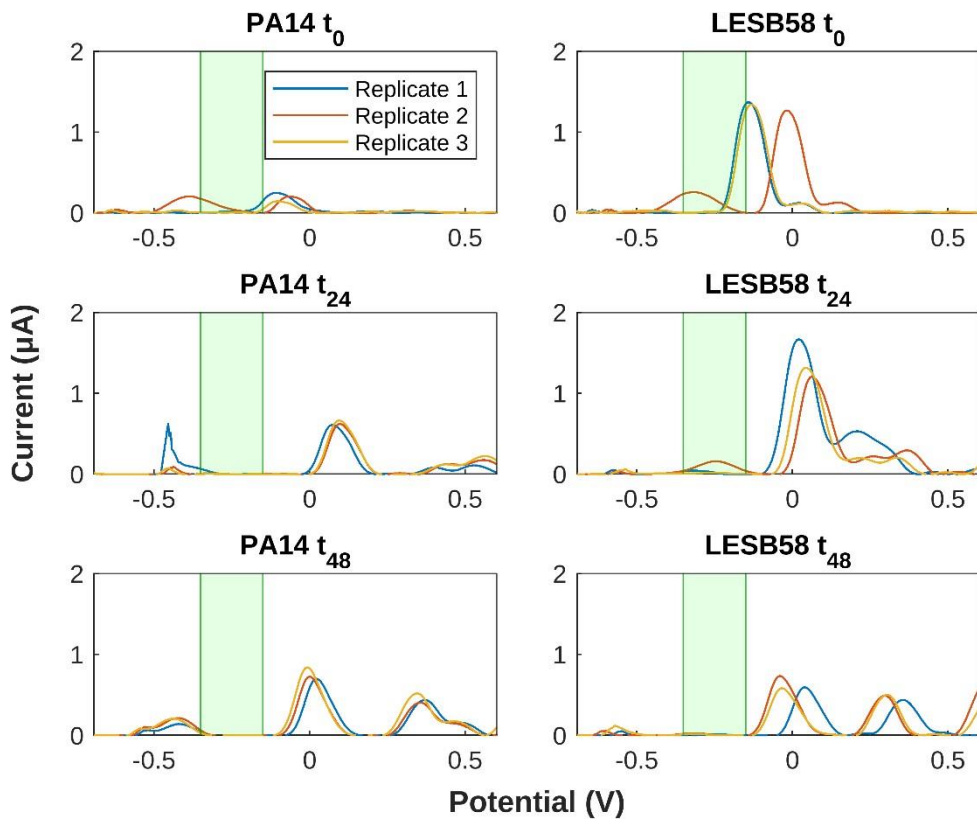
Figure C. 2. Square Wave Voltammograms of PA14 (left) and LESB58 (right) at initial concentrations of OD_{600} = 0.5 grown in the custom-built test cell at 0, 24 and 48 h. The pyocyanin detection area is represented in green. Replicates show slight shifts in response over time and pyocyanin production is not the main metabolic end product as peaks outside of the detection zone display higher current amplitudes.

SWV showed variable sample behaviour regarding pyocyanin production when grown in the sample plate. PA14 replicates showed the likely presence of 5-MCA around - 0.1 V upon inoculation, and of 1-hydroxyphenazine - 0.45 V after 24 and 48 hours, indicating another enzyme was more active than the one leading to pyocyanin production. A series of unidentified peaks between 0.2 and 0.6 V might result from another quorum sensing pathway.[579] For LESB58 samples, replicates behaved differently from one another. Initially, replicate 2 exhibited lower pyocyanin production with a majority of other phenazine precursors and replicates 1 and 2 seem to contain pyocyanin when comparing to the standard behaviour at the same time point. After 24 hours, replicates 2 and 3 have produced small quantities of pyocyanin at - 0.25 V, which is not yet the case for replicate 1. After 48 hours, pyocyanin

production has not varied, except for replicate 1 where a small quantity can be observed. However, compounds outside of pyocyanin detection range have increased in amplitude, suggesting that other metabolic pathways were favoured over pyocyanin production (Figure C. 2).
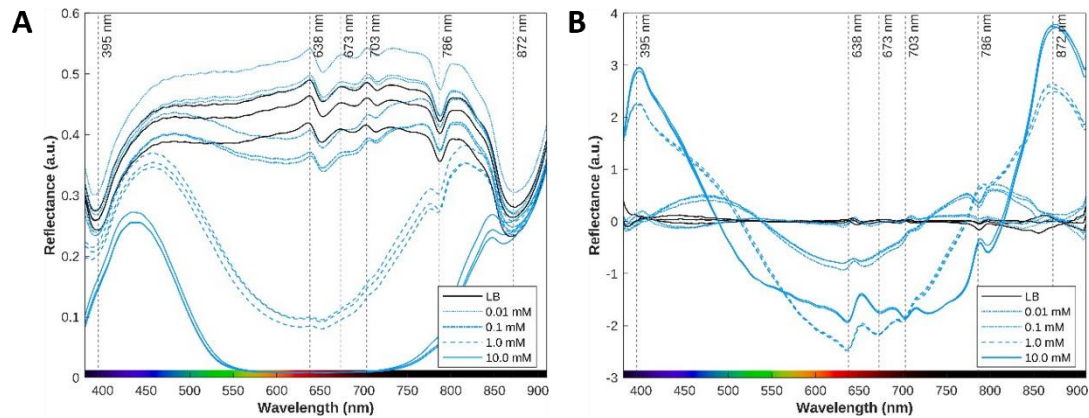
Figure C. 3. Reflectance spectra of pyocyanin in LB at four concentrations (A). Each line represents one of three replicates. The same spectra normalised using SNV and baseline subtraction (B). The normalisation process corrects for constant offsets in the individual spectra that result from slight variations in the imaging conditions and are not indicative spectral properties.
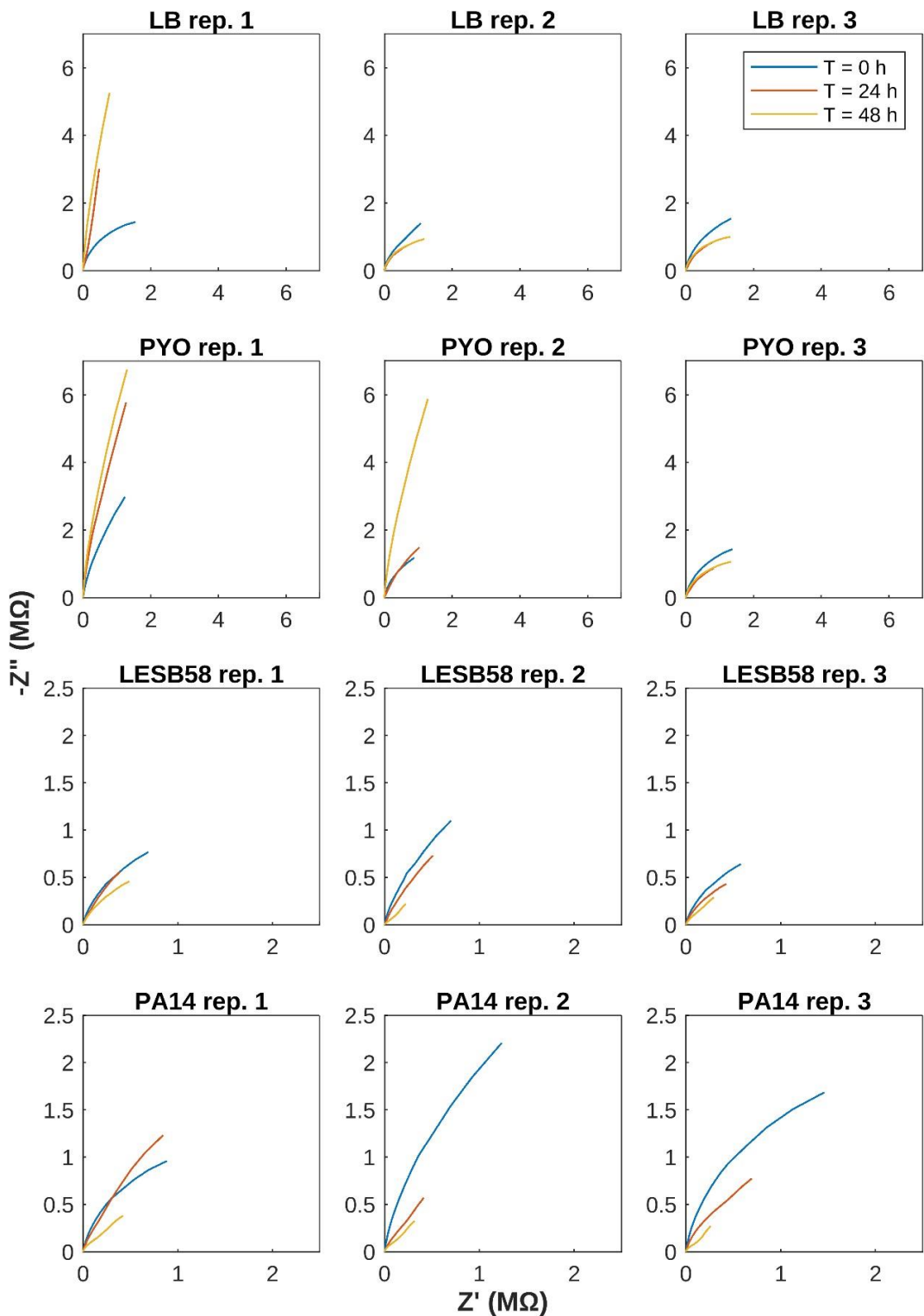
Figure C. 4. Nyquist plots corresponding to data acquired from the test support with the top row corresponding to the medium control, the second row to the pyocyanin standard, the third row to LESB58 inoculated at OD_{600} = 0.5 at t=0 and the bottom row to PA14 inoculated at the same initial concentration.

II. Adapting the electrochemical biofilm sensing strategy for the detection of redox-inactive bacterial species producers using resazurin

LB

0.01% resazurin

$OD_{600} = 0.125 +$ resazurin

$OD_{600} = 0.75 +$ resazurin
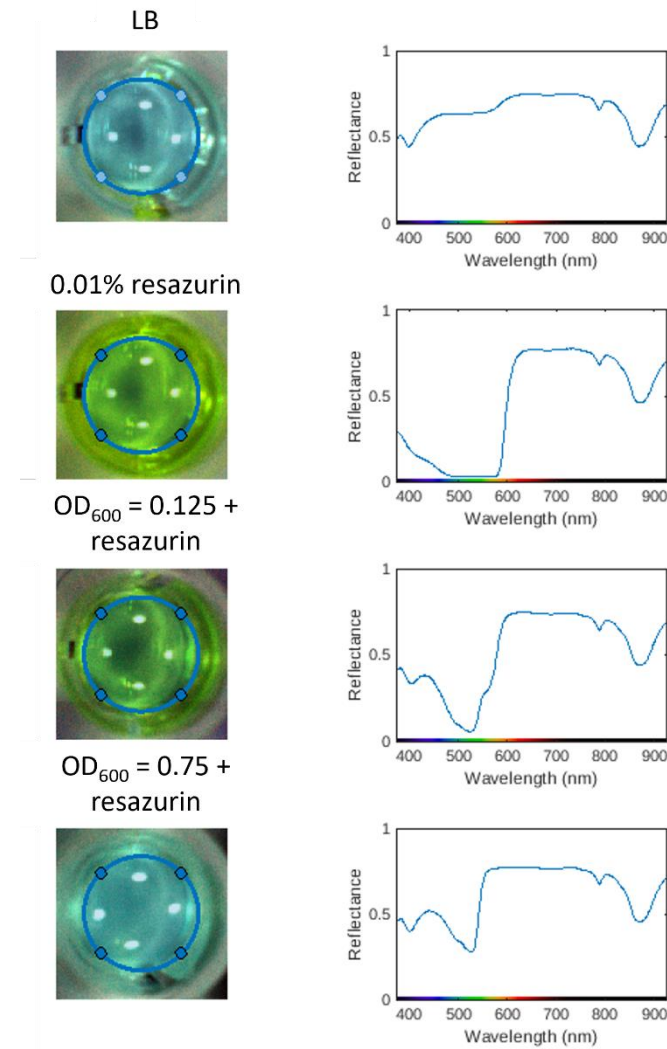
Figure C. 5. Preliminary HSI response of resazurin in bacterial cultures.

The main spectral feature is an absorbance band in the 500-600 nm range, with a colour shift possibly reflected by the absorbance band shifting along the spectrum, rather than its actual magnitude (towards slightly lower wavelength at the higher bacterial concentration compared to the lower one) (Figure C. 5).

Preliminary HSI assessment of *A. baumannii* and *K. pneumoniae*

The main resazurin feature was the absorbance band between 545 nm and 586 nm (Figure C. 6), with a lower band between 400 and 450 nm. LB and resazurin were samples without bacteria, with a noticeable shift between the tow, probably

resulting from the higher concentration of resazurin in the well already containing it. K1 and A1 were the highest bacterial concentrations, decreasing until K4 and A4, being the lowest bacterial concentrations tested. Reflectance data were processed with continuum removal, minimising magnitude shifts, which account for most differences between concentrations at specific timepoints.[664] Results from Figure C. 6 participated in the decision making for strain choice, however they only represent one replicate, requiring further replicates.
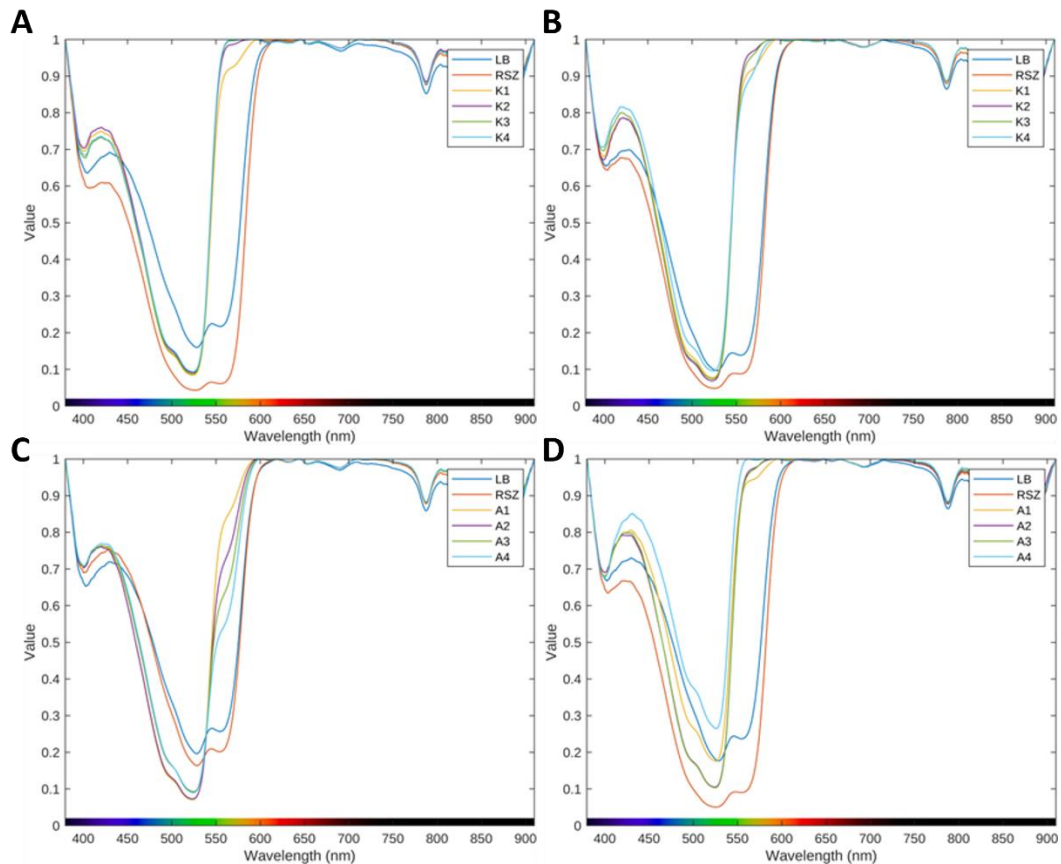
Figure C. 6. Reflectance spectra from an arbitrary region of the centre of the well with continuum removal of *K. pneumoniae* (top row) and *A. baumannii* (bottom row) at 4 and 24 hours (respectively left and right). Each trace represents a single sample.

For *A. baumannii,* a gradient from lowest to highest concentration at the 545-586 nm band was present at 4 hours which disappeared after 24 hours. For *K. pneumoniae*, there was a clear difference between positive and negative conditions, but not a distinct gradient (Figure C. 6).

An index was then calculated using the bands at 528 nm and 555 nm for *A. baumannii*, with higher values corresponding to more resazurin being converted into resorufin in Table C. 2:

$$F = (X_{555}-X_{528})/(X_{555}+X_{528})$$

Table C. 2. *A. baumannii* resazurin conversion based on reflectance data from HSI.

	T = 4 h	T = 24 h
LB	0.14	0.15
Resazurin	0.10	0.28
A1	0.82	0.67
A2	0.79	0.78
A3	0.72	0.78
A4	0.68	0.57

Crystal violet control reproducibility
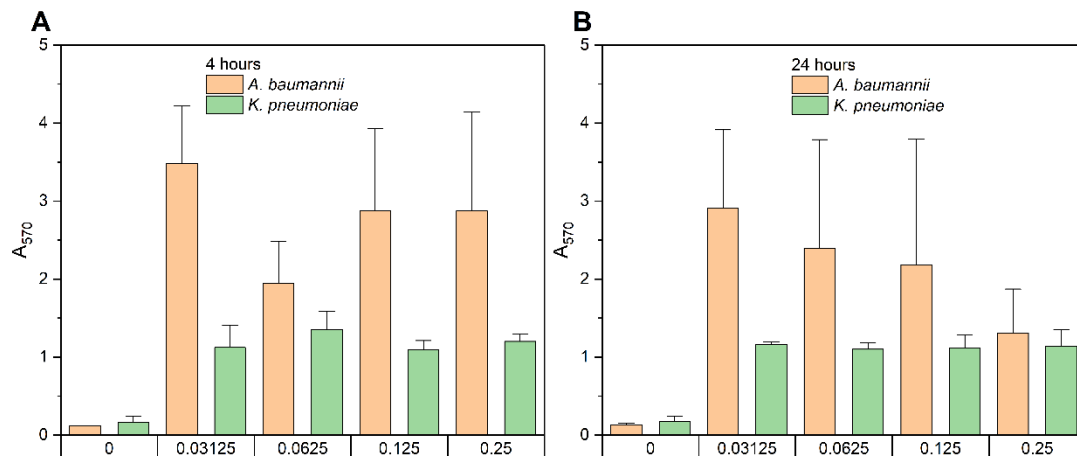
Figure C. 7. Absorbance response at 570 nm after crystal violet assay on *A. baumannii* and *K. pneumoniae* biofilms grown from inoculated OD$_{600}$ values between 0.03125 and 0.25 for 4 (A) and 24 hours (B). Each bar represents an average of 3 samples and the error bars, one standard deviation.

REFERENCES

(1)   Hall, W.; McDonnell, A.; O'Neill, J. *Superbugs: An Arms Race against Bacteria*; Harvard University Press: Cambridge, Massachusetts, 2018.

(2)   Strandell, B. Nobel Lectures. Physiology or Medicine 1942–1962. *Acta Medica Scandinavica* **1964**, *176* (6), 800–800. https://doi.org/10.1111/j.0954-6820.1964.tb00690.x.

(3)   Medicine 1944: 20th Century Seer, Dr. Alexander Fleming: Penicillin. *Time*. October 5, 1983. https://content.time.com/time/subscriber/article/0,33009,952158,00.html (accessed 2023-09-15).

(4)   Europe, R. A. N. D. *How Drug Resistant Infections Are Undermining Modern Medicine*; Wellcome Trust: London, 2021. https://wellcome.org/reports/how-drug-resistant-infections-are-undermining-modern-medicine-and-why-more-research-needed (accessed 2023-09-18).

(5)   World Bank. *Pulling Together to Beat Superbugs: Knowledge and Implementation Gaps in Addressing Antimicrobial Resistance*; World Bank: Washington, DC, 2019.

(6)   Mahoney, A. R.; Safaee, M. M.; Wuest, W. M.; Furst, A. L. The Silent Pandemic: Emergent Antibiotic Resistances Following the Global Response to SARS-CoV-2. *iScience* **2021**, *24* (4), 102304. https://doi.org/10.1016/j.isci.2021.102304.

(7)   Mendelson, M.; Sharland, M.; Mpundu, M. Antibiotic Resistance: Calling Time on the 'Silent Pandemic.' *JAC-Antimicrobial Resistance* **2022**, *4* (2), dlac016. https://doi.org/10.1093/jacamr/dlac016.

(8)   Rayan, R. A. Flare of the Silent Pandemic in the Era of the COVID-19 Pandemic: Obstacles and Opportunities. *World J Clin Cases* **2023**, *11* (6), 1267–1274. https://doi.org/10.12998/wjcc.v11.i6.1267.

(9)   *What would a world without antibiotics be like? - BBC Ideas*. https://www.bbc.co.uk/ideas/videos/what-would-a-world-without-antibiotics-be-like/p0cgmypx?playlist=made-in-partnership-with-the-royal-society (accessed 2024-03-31).

(10)   Ferri, M.; Ranucci, E.; Romagnoli, P.; Giaccone, V. Antimicrobial Resistance: A Global Emerging Threat to Public Health Systems. *Critical Reviews in Food Science and Nutrition* **2017**, *57* (13), 2857–2876. https://doi.org/10.1080/10408398.2015.1077192.

(11)   Antimicrobial Resistance Division, Global Coordination and Partnership. *No Time to Wait: Securing the Future from Drug-Resistant Infections*; World Health Organisation, 2019. https://www.who.int/publications-detail-redirect/no-time-to-wait-securing-the-future-from-drug-resistant-infections (accessed 2023-09-19).

(12)   Hocking, L.; Ali, G.-C.; d'Angelo, C.; Deshpande, A.; Stevenson, C.; Virdee, M. *How Is Modern Medicine Being Affected by Drug-Resistant Infections?*; Wellcome Trust, 2021.

(13)   Murray, C. J. L.; Ikuta, K. S.; Sharara, F.; Swetschinski, L.; Robles Aguilar, G.; Gray, A.; Han, C.; Bisignano, C.; Rao, P.; Wool, E.; Johnson, S. C.; Browne, A. J.;

Chipeta, M. G.; Fell, F.; Hackett, S.; Haines-Woodhouse, G.; Kashef Hamadani, B. H.; Kumaran, E. A. P.; McManigal, B.; Achalapong, S.; Agarwal, R.; Akech, S.; Albertson, S.; Amuasi, J.; Andrews, J.; Aravkin, A.; Ashley, E.; Babin, F.-X.; Bailey, F.; Baker, S.; Basnyat, B.; Bekker, A.; Bender, R.; Berkley, J. A.; Bethou, A.; Bielicki, J.; Boonkasidecha, S.; Bukosia, J.; Carvalheiro, C.; Castañeda-Orjuela, C.; Chansamouth, V.; Chaurasia, S.; Chiurchiù, S.; Chowdhury, F.; Clotaire Donatien, R.; Cook, A. J.; Cooper, B.; Cressey, T. R.; Criollo-Mora, E.; Cunningham, M.; Darboe, S.; Day, N. P. J.; De Luca, M.; Dokova, K.; Dramowski, A.; Dunachie, S. J.; Duong Bich, T.; Eckmanns, T.; Eibach, D.; Emami, A.; Feasey, N.; Fisher-Pearson, N.; Forrest, K.; Garcia, C.; Garrett, D.; Gastmeier, P.; Giref, A. Z.; Greer, R. C.; Gupta, V.; Haller, S.; Haselbeck, A.; Hay, S. I.; Holm, M.; Hopkins, S.; Hsia, Y.; Iregbu, K. C.; Jacobs, J.; Jarovsky, D.; Javanmardi, F.; Jenney, A. W. J.; Khorana, M.; Khusuwan, S.; Kissoon, N.; Kobeissi, E.; Kostyanev, T.; Krapp, F.; Krumkamp, R.; Kumar, A.; Kyu, H. H.; Lim, C.; Lim, K.; Limmathurotsakul, D.; Loftus, M. J.; Lunn, M.; Ma, J.; Manoharan, A.; Marks, F.; May, J.; Mayxay, M.; Mturi, N.; Munera-Huertas, T.; Musicha, P.; Musila, L. A.; Mussi-Pinhata, M. M.; Naidu, R. N.; Nakamura, T.; Nanavati, R.; Nangia, S.; Newton, P.; Ngoun, C.; Novotney, A.; Nwakanma, D.; Obiero, C. W.; Ochoa, T. J.; Olivas-Martinez, A.; Olliaro, P.; Ooko, E.; Ortiz-Brizuela, E.; Ounchanum, P.; Pak, G. D.; Paredes, J. L.; Peleg, A. Y.; Perrone, C.; Phe, T.; Phommasone, K.; Plakkal, N.; Ponce-de-Leon, A.; Raad, M.; Ramdin, T.; Rattanavong, S.; Riddell, A.; Roberts, T.; Robotham, J. V.; Roca, A.; Rosenthal, V. D.; Rudd, K. E.; Russell, N.; Sader, H. S.; Saengchan, W.; Schnall, J.; Scott, J. A. G.; Seekaew, S.; Sharland, M.; Shivamallappa, M.; Sifuentes-Osornio, J.; Simpson, A. J.; Steenkeste, N.; Stewardson, A. J.; Stoeva, T.; Tasak, N.; Thaiprakong, A.; Thwaites, G.; Tigoi, C.; Turner, C.; Turner, P.; Van Doorn, H. R.; Velaphi, S.; Vongpradith, A.; Vongsouvath, M.; Vu, H.; Walsh, T.; Walson, J. L.; Waner, S.; Wangrangsimakul, T.; Wannapinij, P.; Wozniak, T.; Young Sharma, T. E. M. W.; Yu, K. C.; Zheng, P.; Sartorius, B.; Lopez, A. D.; Stergachis, A.; Moore, C.; Dolecek, C.; Naghavi, M. Global Burden of Bacterial Antimicrobial Resistance in 2019: A Systematic Analysis. *The Lancet* **2022**, *399* (10325), 629–655. https://doi.org/10.1016/S0140-6736(21)02724-0.

(14) O'Neill, J. *Tackling Drug-Resistant Infections Globally: Final Report and Recommendations*; Report; Government of the United Kingdom, 2016. https://apo.org.au/node/63983 (accessed 2023-09-15).

(15) Karakonstantis, S.; Kritsotakis, E. I.; Gikas, A. Pandrug-Resistant Gram-Negative Bacteria: A Systematic Review of Current Epidemiology, Prognosis and Treatment Options. *Journal of Antimicrobial Chemotherapy* **2019**, dkz401. https://doi.org/10.1093/jac/dkz401.

(16) De Angelis, G.; Fiori, B.; Menchinelli, G.; D'Inzeo, T.; Liotti, F. M.; Morandotti, G. A.; Sanguinetti, M.; Posteraro, B.; Spanu, T. Incidence and Antimicrobial Resistance Trends in Bloodstream Infections Caused by ESKAPE and *Escherichia Coli* at a Large Teaching Hospital in Rome, a 9-Year Analysis (2007–2015). *Eur J Clin Microbiol Infect Dis* **2018**, *37* (9), 1627–1636. https://doi.org/10.1007/s10096-018-3292-9.

(17) De Socio, G. V.; Rubbioni, P.; Botta, D.; Cenci, E.; Belati, A.; Paggi, R.; Pasticci, M. B.; Mencacci, A. Measurement and Prediction of Antimicrobial Resistance in Bloodstream Infections by ESKAPE Pathogens and *Escherichia Coli*. *Journal of Global Antimicrobial Resistance* **2019**, *19*, 154–160. https://doi.org/10.1016/j.jgar.2019.05.013.

(18) Bogaert, D.; van Belkum, A. Antibiotic Treatment and Stewardship in the Era of Microbiota-Oriented Diagnostics. *Eur J Clin Microbiol Infect Dis* **2018**, *37* (5), 795–798. https://doi.org/10.1007/s10096-018-3198-6.

(19) Robb, A. J.; Vinogradov, S.; Danell, A. S.; Anderson, E.; Blackledge, M. S.; Melander, C.; Hvastkovs, E. G. Electrochemical Detection of Small Molecule Induced *Pseudomonas Aeruginosa* Biofilm Dispersion. *Electrochimica Acta* **2018**, *268*, 276–282. https://doi.org/10.1016/j.electacta.2018.02.113.

(20) Gebreyohannes, G.; Nyerere, A.; Bii, C.; Sbhatu, D. B. Challenges of Intervention, Treatment, and Antibiotic Resistance of Biofilm-Forming Microorganisms. *Heliyon* **2019**, *5* (8), e02192. https://doi.org/10.1016/j.heliyon.2019.e02192.

(21) Haney, E. F.; Trimble, M. J.; Hancock, R. E. W. Microtiter Plate Assays to Assess Antibiofilm Activity against Bacteria. *Nat Protoc* **2021**, *16* (5), 2615–2632. https://doi.org/10.1038/s41596-021-00515-3.

(22) Malone, M.; Goeres, D. M.; Gosbell, I.; Vickery, K.; Jensen, S.; Stoodley, P. Approaches to Biofilm-Associated Infections: The Need for Standardized and Relevant Biofilm Methods for Clinical Applications. *Expert Review of Anti-infective Therapy* **2017**, *15* (2), 147–156. https://doi.org/10.1080/14787210.2017.1262257.

(23) Del Pozo, J. L. Biofilm-Related Disease. *Expert Review of Anti-infective Therapy* **2018**, *16* (1), 51–65. https://doi.org/10.1080/14787210.2018.1417036.

(24) Mountcastle, S. E.; Vyas, N.; Villapun, V. M.; Cox, S. C.; Jabbari, S.; Sammons, R. L.; Shelton, R. M.; Walmsley, A. D.; Kuehne, S. A. Biofilm Viability Checker: An Open-Source Tool for Automated Biofilm Viability Analysis from Confocal Microscopy Images. *npj Biofilms and Microbiomes* **2021**, *7* (1), 44.

(25) Behera, B.; Anil Vishnu, G. K.; Chatterjee, S.; Sitaramgupta V, V. S. N.; Sreekumar, N.; Nagabhushan, A.; Rajendran, N.; Prathik, B. H.; Pandya, H. J. Emerging Technologies for Antibiotic Susceptibility Testing. *Biosensors and Bioelectronics* **2019**, *142*, 111552. https://doi.org/10.1016/j.bios.2019.111552.

(26) Sriram, A.; Kalanxhi, E.; Kapoor, G.; Craig, J.; Balasubramanian, R.; Brar, S.; Criscuolo, N.; Hamilton, A.; Klein, E.; Tseng, K.; Boeckel, T. V.; Laxminarayan, R. *State of the World's Antibiotics 2021: A Global Analysis of Antimicrobial Resistance and Its Drivers*; Center for Disease Dynamics, Economics & Policy: Washington DC, 2021.

(27) Balasegaram, M. Learning from COVID-19 to Tackle Antibiotic Resistance. *ACS Infect. Dis.* **2021**, *7* (4), 693–694. https://doi.org/10.1021/acsinfecdis.1c00079.

(28) Tiseo, K.; Huber, L.; Gilbert, M.; Robinson, T. P.; Van Boeckel, T. P. Global Trends in Antimicrobial Use in Food Animals from 2017 to 2030. *Antibiotics* **2020**, *9* (12), 918. https://doi.org/10.3390/antibiotics9120918.

(29) World Health Organization. *Global Antimicrobial Resistance and Use Surveillance System (GLASS) Report*; World Health Organization: Geneva, 2021.

(30) Lomazzi, M.; Moore, M.; Johnson, A.; Balasegaram, M.; Borisch, B. Antimicrobial Resistance – Moving Forward? *BMC Public Health* **2019**, *19* (1), 858. https://doi.org/10.1186/s12889-019-7173-7.

(31) Roope, L. S. J.; Smith, R. D.; Pouwels, K. B.; Buchanan, J.; Abel, L.; Eibich, P.; Butler, C. C.; Tan, P. S.; Walker, A. S.; Robotham, J. V.; Wordsworth, S. The Challenge of Antimicrobial Resistance: What Economics Can Contribute. *Science* **2019**, *364* (6435), eaau4679. https://doi.org/10.1126/science.aau4679.

(32) The Pew Charitable Trusts. *A Scientific Roadmap for Antibiotic Discovery*; 2016. http://pew.org/28Meh11 (accessed 2023-09-19).

(33) Ventola, C. L. The Antibiotic Resistance Crisis. *P T* **2015**, *40* (4), 277–283.

(34) Theuretzbacher, U.; Outterson, K.; Engel, A.; Karlén, A. The Global Preclinical Antibacterial Pipeline. *Nat Rev Microbiol* **2020**, *18* (5), 275–285. https://doi.org/10.1038/s41579-019-0288-0.

(35) *Economics Behind the Commercialization of an AMR Product - Understanding the Issues and Fixing It*; 2020. https://www.amr-insights.eu/webinar-economics-behind-the-commercialization-of-an-amr-product/ (accessed 2023-09-22).

(36) Wheeler, N. E.; Sánchez-Busó, L.; Argimón, S.; Jeffrey, B. Lean, Mean, Learning Machines. *Nat Rev Microbiol* **2020**, *18* (5), 266–266. https://doi.org/10.1038/s41579-020-0357-4.

(37) Goldman, M. The Innovative Medicines Initiative: A European Response to the Innovation Challenge. *Clin Pharmacol Ther* **2012**, *91* (3), 418–425. https://doi.org/10.1038/clpt.2011.321.

(38) Tommasi, R.; Iyer, R.; Miller, A. A. Antibacterial Drug Discovery: Some Assembly Required. *ACS Infect. Dis.* **2018**, *4* (5), 686–695. https://doi.org/10.1021/acsinfecdis.8b00027.

(39) Global Antibiotic Research & Development Partnership (GARDP). *Annual Report 2022*; 2023.

(40) Combatting Antibiotic-Resistant Bacteria Biopharmaceutical Accelerator (CARB-X). *Annual Report 2021-2022*; 2023.

(41) Shin, D. J.; Andini, N.; Hsieh, K.; Yang, S.; Wang, T.-H. Emerging Analytical Techniques for Rapid Pathogen Identification and Susceptibility Testing. **2019**, *12*, 41–67. https://doi.org/10.1146/annurev-anchem-061318-115529.

(42) Ahmed, A.; Rushworth, J. V.; Hirst, N. A.; Millner, P. A. Biosensors for Whole-Cell Bacterial Detection. *Clin Microbiol Rev* **2014**, *27* (3), 631–646. https://doi.org/10.1128/CMR.00120-13.

(43) Montes-Cebrián, Y.; Álvarez-Carulla, A.; Ruiz-Vega, G.; Colomer-Farrarons, J.; Puig-Vidal, M.; Baldrich, E.; Miribel-Català, P. Ll. Competitive USB-Powered Hand-Held Potentiostat for POC Applications: An HRP Detection Case. *Sensors* **2019**, *19* (24), 5388. https://doi.org/10.3390/s19245388.

(44) Nayak, S.; Blumenfeld, N. R.; Laksanasopin, T.; Sia, S. K. Point-of-Care Diagnostics: Recent Developments in a Connected Age. *Anal. Chem.* **2017**, *89* (1), 102–123. https://doi.org/10.1021/acs.analchem.6b04630.

(45) Mach, K. E.; Wong, P. K.; Liao, J. C. Biosensor Diagnosis of Urinary Tract Infections: A Path to Better Treatment? *Trends in Pharmacological Sciences* **2011**, *32* (6), 330–336. https://doi.org/10.1016/j.tips.2011.03.001.

(46) Cesewski, E.; Johnson, B. N. Electrochemical Biosensors for Pathogen Detection. *Biosens Bioelectron* **2020**, *159*, 112214. https://doi.org/10.1016/j.bios.2020.112214.

(47) Thévenot, D. R.; Toth, K.; Durst, R. A.; Wilson, G. S. Electrochemical Biosensors: Recommended Definitions and Classification. *Analytical Letters* **2001**, *34* (5), 635–659. https://doi.org/10.1081/AL-100103209.

(48) Broughton, J. P.; Deng, X.; Yu, G.; Fasching, C. L.; Servellita, V.; Singh, J.; Miao, X.; Streithorst, J. A.; Granados, A.; Sotomayor-Gonzalez, A.; Zorn, K.; Gopez, A.; Hsu, E.; Gu, W.; Miller, S.; Pan, C.-Y.; Guevara, H.; Wadford, D. A.; Chen, J. S.; Chiu, C. Y. CRISPR–Cas12-Based Detection of SARS-CoV-2. *Nat Biotechnol* **2020**, *38* (7), 870–874. https://doi.org/10.1038/s41587-020-0513-4.

(49) Suea-Ngam, A.; Bezinge, L.; Mateescu, B.; Howes, P. D.; deMello, A. J.; Richards, D. A. Enzyme-Assisted Nucleic Acid Detection for Infectious Disease Diagnostics: Moving toward the Point-of-Care. *ACS Sens.* **2020**, *5* (9), 2701–2723. https://doi.org/10.1021/acssensors.0c01488.

(50) Smyrlaki, I.; Ekman, M.; Lentini, A.; Rufino De Sousa, N.; Papanicolaou, N.; Vondracek, M.; Aarum, J.; Safari, H.; Muradrasoli, S.; Rothfuchs, A. G.; Albert, J.; Högberg, B.; Reinius, B. Massive and Rapid COVID-19 Testing Is Feasible by Extraction-Free SARS-CoV-2 RT-PCR. *Nat Commun* **2020**, *11* (1), 4812. https://doi.org/10.1038/s41467-020-18611-5.

(51) Ventura, B. D.; Cennamo, M.; Minopoli, A.; Campanile, R.; Censi, S. B.; Terracciano, D.; Portella, G.; Velotta, R. Colorimetric Test for Fast Detection of SARS-CoV-2 in Nasal and Throat Swabs. *ACS Sens.* **2020**, *5* (10), 3043–3048. https://doi.org/10.1021/acssensors.0c01742.

(52) Longitude Prize. *AMR Voices Stories from the Frontlines of Antimicrobial Resistance during Covid-19*; 2020.

(53) Benkova, M.; Soukup, O.; Marek, J. Antimicrobial Susceptibility Testing: Currently Used Methods and Devices and the near Future in Clinical Practice. *J. Appl. Microbiol.* **2020**, *129* (4), 806–822. https://doi.org/10.1111/jam.14704.

(54) Berman, J.; Krysan, D. J. Drug Resistance and Tolerance in Fungi. *Nat Rev Microbiol* **2020**, *18* (6), 319–331. https://doi.org/10.1038/s41579-019-0322-2.

(55) Di Martino, P. Antimicrobial Agents and Microbial Ecology. *AIMS Microbiol* **2022**, *8* (1), 1–4. https://doi.org/10.3934/microbiol.2022001.

(56) Ribeiro Da Cunha; Fonseca; Calado. Antibiotic Discovery: Where Have We Come from, Where Do We Go? *Antibiotics* **2019**, *8* (2), 45. https://doi.org/10.3390/antibiotics8020045.

(57) McDonnell, G.; Russell, A. D. Antiseptics and Disinfectants: Activity, Action, and Resistance. *Clin Microbiol Rev* **1999**, *12* (1), 147–179.

(58)   Wainwright, M.; Maisch, T.; Nonell, S.; Plaetzer, K.; Almeida, A.; Tegos, G. P.; Hamblin, M. R. Photoantimicrobials-Are We Afraid of the Light? *Lancet Infect Dis* **2017**, *17* (2), e49–e55. https://doi.org/10.1016/S1473-3099(16)30268-7.

(59)   Wainwright, M. Dyes in the Development of Drugs and Pharmaceuticals. *Dyes and Pigments* **2008**, *76* (3), 582–589. https://doi.org/10.1016/j.dyepig.2007.01.015.

(60)   Baral, B.; Mozafari, M. R. Strategic Moves of "Superbugs" Against Available Chemical Scaffolds: Signaling, Regulation, and Challenges. *ACS Pharmacol. Transl. Sci.* **2020**, *3* (3), 373–400. https://doi.org/10.1021/acsptsci.0c00005.

(61)   Lvovich, V. F. Electrochemical Impedance Spectroscopy (EIS) Applications to Sensors and Diagnostics. In *Encyclopedia of Applied Electrochemistry*; Kreysa, G., Ota, K., Savinell, R. F., Eds.; Springer: New York, NY, 2014; pp 485–507. https://doi.org/10.1007/978-1-4419-6996-5_67.

(62)   Armstrong, T.; Fenn, S. J.; Hardie, K. R. JMM Profile: Carbapenems: A Broad-Spectrum Antibiotic. *J Med Microbiol* **2021**, *70* (12), 001462. https://doi.org/10.1099/jmm.0.001462.

(63)   Butler, M. S.; Hansford, K. A.; Blaskovich, M. A. T.; Halai, R.; Cooper, M. A. Glycopeptide Antibiotics: Back to the Future. *J Antibiot* **2014**, *67* (9), 631–644. https://doi.org/10.1038/ja.2014.111.

(64)   Blaskovich, M. A. T.; Hansford, K. A.; Butler, M. S.; Jia, Z.; Mark, A. E.; Cooper, M. A. Developments in Glycopeptide Antibiotics. *ACS Infect. Dis.* **2018**, *4* (5), 715–735. https://doi.org/10.1021/acsinfecdis.7b00258.

(65)   Webster, C. M.; Shepherd, M. A Mini-Review: Environmental and Metabolic Factors Affecting Aminoglycoside Efficacy. *World J Microbiol Biotechnol* **2022**, *39* (1), 7. https://doi.org/10.1007/s11274-022-03445-8.

(66)   Grossman, T. H. Tetracycline Antibiotics and Resistance. *Cold Spring Harb Perspect Med* **2016**, *6* (4), a025387. https://doi.org/10.1101/cshperspect.a025387.

(67)   Dinos, G. P. The Macrolide Antibiotic Renaissance. *Br J Pharmacol* **2017**, *174* (18), 2967–2983. https://doi.org/10.1111/bph.13936.

(68)   Pham, T. D. M.; Ziora, Z. M.; Blaskovich, M. A. T. Quinolone Antibiotics. *Medchemcomm* **2019**, *10* (10), 1719–1739. https://doi.org/10.1039/c9md00120d.

(69)   Foti, C.; Piperno, A.; Scala, A.; Giuffrè, O. Oxazolidinone Antibiotics: Chemical, Biological and Analytical Aspects. *Molecules* **2021**, *26* (14), 4280. https://doi.org/10.3390/molecules26144280.

(70)   Ovung, A.; Bhattacharyya, J. Sulfonamide Drugs: Structure, Antibacterial Property, Toxicity, and Biophysical Interactions. *Biophys Rev* **2021**, *13* (2), 259–272. https://doi.org/10.1007/s12551-021-00795-9.

(71)   Oong, G. C.; Tadi, P. Chloramphenicol. In *StatPearls*; StatPearls Publishing: Treasure Island (FL), 2023.

(72)   *A Brief Overview of Classes of Antibiotics*. Compound Interest. https://www.compoundchem.com/2014/09/08/antibiotics/ (accessed 2024-05-14).

(73) Ledger, E. V. K.; Sabnis, A.; Edwards, A. M. Polymyxin and Lipopeptide Antibiotics: Membrane-Targeting Drugs of Last Resort. *Microbiology (Reading)* **2022**, *168* (2), 001136. https://doi.org/10.1099/mic.0.001136.

(74) Mohapatra, S. S.; Dwibedy, S. K.; Padhy, I. Polymyxins, the Last-Resort Antibiotics: Mode of Action, Resistance Emergence, and Potential Solutions. *J Biosci* **2021**, *46* (3), 85. https://doi.org/10.1007/s12038-021-00209-8.

(75) Dijkmans, A. C.; Ortiz Zacarías, N. V.; Burggraaf, J.; Mouton, J. W.; Wilms, E. B.; van Nieuwkoop, C.; Touw, D. J.; Stevens, J.; Kamerling, I. M. C. Fosfomycin: Pharmacological, Clinical and Future Perspectives. *Antibiotics (Basel)* **2017**, *6* (4), 24. https://doi.org/10.3390/antibiotics6040024.

(76) Sojo-Dorado, J.; López-Hernández, I.; Rosso-Fernandez, C.; Morales, I. M.; Palacios-Baena, Z. R.; Hernández-Torres, A.; Merino de Lucas, E.; Escolà-Vergé, L.; Bereciartua, E.; García-Vázquez, E.; Pintado, V.; Boix-Palop, L.; Natera-Kindelán, C.; Sorlí, L.; Borrell, N.; Giner-Oncina, L.; Amador-Prous, C.; Shaw, E.; Jover-Saenz, A.; Molina, J.; Martínez-Alvarez, R. M.; Dueñas, C. J.; Calvo-Montes, J.; Silva, J. T.; Cárdenes, M. A.; Lecuona, M.; Pomar, V.; Valiente de Santis, L.; Yagüe-Guirao, G.; Lobo-Acosta, M. A.; Merino-Bohórquez, V.; Pascual, A.; Rodríguez-Baño, J.; REIPI-GEIRAS-FOREST group. Effectiveness of Fosfomycin for the Treatment of Multidrug-Resistant *Escherichia Coli* Bacteremic Urinary Tract Infections: A Randomized Clinical Trial. *JAMA Network Open* **2022**, *5* (1), e2137277. https://doi.org/10.1001/jamanetworkopen.2021.37277.

(77) Mori, T.; Abe, I. Lincosamide Antibiotics: Structure, Activity, and Biosynthesis. *ChemBioChem* **2024**, *25* (6), e202300840. https://doi.org/10.1002/cbic.202300840.

(78) Spížek, J.; Řezanka, T. Lincosamides: Chemical Structure, Biosynthesis, Mechanism of Action, Resistance, and Applications. *Biochemical Pharmacology* **2017**, *133*, 20–28. https://doi.org/10.1016/j.bcp.2016.12.001.

(79) Gao, X.; Ding, J.; Liao, C.; Xu, J.; Liu, X.; Lu, W. Defensins: The Natural Peptide Antibiotic. *Advanced Drug Delivery Reviews* **2021**, *179*, 114008. https://doi.org/10.1016/j.addr.2021.114008.

(80) Hutchings, M. I.; Truman, A. W.; Wilkinson, B. Antibiotics: Past, Present and Future. *Current Opinion in Microbiology* **2019**, *51*, 72–80. https://doi.org/10.1016/j.mib.2019.10.008.

(81) Schramm, V. L.; Meek, T. D. Enhanced Antibiotic Discovery by PROSPECTing. *Biochemistry* **2019**, *58* (33), 3475–3476. https://doi.org/10.1021/acs.biochem.9b00616.

(82) Wong, C. H.; Siah, K. W.; Lo, A. W. Estimation of Clinical Trial Success Rates and Related Parameters. *Biostatistics* **2019**, *20* (2), 273–286. https://doi.org/10.1093/biostatistics/kxx069.

(83) Pelegrin, A. C.; Palmieri, M.; Mirande, C.; Oliver, A.; Moons, P.; Goossens, H.; van Belkum, A. *Pseudomonas Aeruginosa*: A Clinical and Genomics Update. *FEMS Microbiol Rev* **2021**, *45* (6), fuab026. https://doi.org/10.1093/femsre/fuab026.

(84)   *It's time to fix the antibiotic market*. Wellcome. https://wellcome.org/news/its-time-fix-antibiotic-market (accessed 2024-05-15).

(85)   Berthe, Franck Cesar Jean; Wadsworth, Jonathan; Thiebaud, Alessia; Marquez, Patricio V.; Baris, Enis. *Pulling Together to Beat Superbugs: Knowledge and Implementation Gaps in Addressing Antimicrobial Resistance*; 142527; World Bank: Washington DC: World Bank, 2019.

(86)   Wong, F.; Zheng, E. J.; Valeri, J. A.; Donghia, N. M.; Anahtar, M. N.; Omori, S.; Li, A.; Cubillos-Ruiz, A.; Krishnan, A.; Jin, W.; Manson, A. L.; Friedrichs, J.; Helbig, R.; Hajian, B.; Fiejtek, D. K.; Wagner, F. F.; Soutter, H. H.; Earl, A. M.; Stokes, J. M.; Renner, L. D.; Collins, J. J. Discovery of a Structural Class of Antibiotics with Explainable Deep Learning. *Nature* **2023**, 1–9. https://doi.org/10.1038/s41586-023-06887-8.

(87)   Teelucksingh, T.; Thompson, L. K.; Zhu, S.; Kuehfuss, N. M.; Goetz, J. A.; Gilbert, S. E.; MacNair, C. R.; Geddes-McAlister, J.; Brown, E. D.; Cox, G. A Genetic Platform to Investigate the Functions of Bacterial Drug Efflux Pumps. *Nat Chem Biol* **2022**, *18* (12), 1399–1409. https://doi.org/10.1038/s41589-022-01119-y.

(88)   Sharma, K.; Ahmed, F.; Sharma, T.; Grover, A.; Agarwal, M.; Grover, S. Potential Repurposed Drug Candidates for Tuberculosis Treatment: Progress and Update of Drugs Identified in Over a Decade. *ACS Omega* **2023**, *8* (20), 17362–17380. https://doi.org/10.1021/acsomega.2c05511.

(89)   Du, D.; Wang-Kan, X.; Neuberger, A.; van Veen, H. W.; Pos, K. M.; Piddock, L. J. V.; Luisi, B. F. Multidrug Efflux Pumps: Structure, Function and Regulation. *Nat Rev Microbiol* **2018**, *16* (9), 523–539. https://doi.org/10.1038/s41579-018-0048-6.

(90)   Bradford, P. A. Epidemiology of Bacterial Resistance. In *Antimicrobial Resistance in the 21st Century*; Fong, I. W., Shlaes, D., Drlica, K., Eds.; Springer International Publishing: Cham, 2018; pp 299–339. https://doi.org/10.1007/978-3-319-78538-7_10.

(91)   Haider, A.; Ikram, M.; Shahzadi, I.; Asif Raza, M. Antibiotic Drug Resistance. In *Polymeric Nanoparticles for Bovine Mastitis Treatment*; Haider, A., Ikram, M., Shahzadi, I., Asif Raza, M., Eds.; Springer Series in Biomaterials Science and Engineering; Springer Nature Switzerland: Cham, 2023; pp 81–110. https://doi.org/10.1007/978-3-031-39947-3_5.

(92)   Başaran, S. N.; Öksüz, L. The Role of Efflux Pumps in Antibiotic Resistance of Gram Negative Rods. *Arch Microbiol* **2023**, *205* (5), 1–12. https://doi.org/10.1007/s00203-023-03539-3.

(93)   Jacoby, G. A. Transmissible Antibiotic Resistance. In *Antimicrobial Resistance in the 21st Century*; Fong, I. W., Shlaes, D., Drlica, K., Eds.; Springer International Publishing: Cham, 2019; pp C1–C1. https://doi.org/10.1007/978-3-319-78538-7_25.

(94)   Liu, Y.; Tong, Z.; Shi, J.; Jia, Y.; Yang, K.; Wang, Z. Correlation between Exogenous Compounds and the Horizontal Transfer of Plasmid-Borne Antibiotic Resistance Genes. *Microorganisms* **2020**, *8* (8), 1211. https://doi.org/10.3390/microorganisms8081211.

(95) Grande, R.; Puca, V.; Muraro, R. Antibiotic Resistance and Bacterial Biofilm. *Expert Opinion on Therapeutic Patents* **2020**, *30* (12), 897–900. https://doi.org/10.1080/13543776.2020.1830060.

(96) Lomazzi, M.; Moore, M.; Johnson, A.; Balasegaram, M.; Borisch, B. Antimicrobial Resistance – Moving Forward? *BMC Public Health* **2019**, *19* (1), 858. https://doi.org/10.1186/s12889-019-7173-7.

(97) Karakonstantis, S.; Kritsotakis, E. I.; Gikas, A. Pandrug-Resistant Gram-Negative Bacteria: A Systematic Review of Current Epidemiology, Prognosis and Treatment Options. *J Antimicrob Chemother* **2020**, *75* (2), 271–282. https://doi.org/10.1093/jac/dkz401.

(98) Yamashita, M. Auranofin: Past to Present, and Repurposing. *International Immunopharmacology* **2021**, *101*, 108272. https://doi.org/10.1016/j.intimp.2021.108272.

(99) Luo, Y.; Wen, Z.; Xiong, Y.; Chen, X.; Shen, Z.; Li, P.; Peng, Y.; Deng, Q.; Yu, Z.; Zheng, J.; Han, S. The Potential Target of Bithionol against *Staphylococcus Aureus*: Design, Synthesis and Application of Biotinylated Probes Bio-A2. *J Antibiot* **2023**, *76* (7), 406–415. https://doi.org/10.1038/s41429-023-00618-x.

(100) Yang, B.; Mei, Y.; Li, Q.; Zhang, M.; Tang, H.; Liu, T.; Feng, F.; Fu, Q.; Jiang, Y.; Ye, Q. Repurposing Celecoxib Analogues as Leads for Antibiotics. *Future Medicinal Chemistry* **2021**, *13* (11), 959–974. https://doi.org/10.4155/fmc-2021-0030.

(101) Weng, N.; Zhang, Z.; Tan, Y.; Zhang, X.; Wei, X.; Zhu, Q. Repurposing Antifungal Drugs for Cancer Therapy. *J Adv Res* **2022**, *48*, 259–273. https://doi.org/10.1016/j.jare.2022.08.018.

(102) Periyasami, G.; Karuppiah, P.; Karthikeyan, P.; Palaniappan, S. Anti-Infective Efficacy of Duloxetine against Catheter-Associated Urinary Tract Infections Caused by Gram-Positive Bacteria. *ACS Omega* **2023**, *8* (50), 48317–48325. https://doi.org/10.1021/acsomega.3c07676.

(103) An, J.-X.; Ma, Y.; Zhao, W.-B.; Hu, Y.-M.; Wang, Y.-R.; Zhang, Z.-J.; Luo, X.-F.; Zhang, B.-Q.; Ding, Y.-Y.; Liu, Y.-Q. Drug Repurposing Strategy II: From Approved Drugs to Agri-Fungicide Leads. *J Antibiot* **2023**, *76* (3), 131–182. https://doi.org/10.1038/s41429-023-00594-2.

(104) Koh Jing Jie, A.; Hussein, M.; Rao, G. G.; Li, J.; Velkov, T. Drug Repurposing Approaches towards Defeating Multidrug-Resistant Gram-Negative Pathogens: Novel Polymyxin/Non-Antibiotic Combinations. *Pathogens* **2022**, *11* (12), 1420. https://doi.org/10.3390/pathogens11121420.

(105) Khalil, A.; Kamar, A.; Nemer, G. Thalidomide-Revisited: Are COVID-19 Patients Going to Be the Latest Victims of Yet Another Theoretical Drug-Repurposing? *Frontiers in Immunology* **2020**, *11*.

(106) Iskandar, K.; Murugaiyan, J.; Hammoudi Halat, D.; Hage, S. E.; Chibabhai, V.; Adukkadukkam, S.; Roques, C.; Molinier, L.; Salameh, P.; Van Dongen, M. Antibiotic Discovery and Resistance: The Chase and the Race. *Antibiotics* **2022**, *11* (2), 182. https://doi.org/10.3390/antibiotics11020182.

(107) Fernández, L.; Cima-Cabal, M. D.; Duarte, A. C.; Rodriguez, A.; García, P.; García-Suárez, M. D. M. Developing Diagnostic and Therapeutic Approaches to

Bacterial Infections for a New Era: Implications of Globalization. *Antibiotics* **2020**, *9* (12), 916. https://doi.org/10.3390/antibiotics9120916.

(108) Report of a Joint FAO/WHO Expert Consultation. *Evaluation of Health and Nutritional Properties of Probiotics in Food Including Powder Milk with Live Lactic Acid Bacteria*; 2001. http://www.fao.org/tempref/docrep/fao/meeting/009/y6 398e.pdf (accessed 2024-01-13).

(109) Lee, D.-H.; Kim, B. S.; Kang, S.-S. Bacteriocin of *Pediococcus Acidilactici* HW01 Inhibits Biofilm Formation and Virulence Factor Production by *Pseudomonas Aeruginosa*. *Probiotics & Antimicro. Prot.* **2020**, *12* (1), 73–81. https://doi.org/10.1007/s12602-019-09623-9.

(110) Mageswary, M. U.; Ang, X.-Y.; Lee, B.-K.; Chung, Y.-L. F.; Azhar, S. N. A.; Hamid, I. J. A.; Bakar, H. A.; Roslan, N. S.; Liu, X.; Kang, X.; Dai, L.; Sreenivasan, S.; Taib, F.; Zhang, H.; Liong, M.-T. Probiotic *Bifidobacterium Lactis* Probio-M8 Treated and Prevented Acute RTI, Reduced Antibiotic Use and Hospital Stay in Hospitalized Young Children: A Randomized, Double-Blind, Placebo-Controlled Study. *Eur J Nutr* **2022**, *61* (3), 1679–1691. https://doi.org/10.1007/s00394-021-02689-8.

(111) Piewngam, P.; Khongthong, S.; Roekngam, N.; Theapparat, Y.; Sunpaweravong, S.; Faroongsarng, D.; Otto, M. Probiotic for Pathogen-Specific *Staphylococcus Aureus* Decolonisation in Thailand: A Phase 2, Double-Blind, Randomised, Placebo-Controlled Trial. *The Lancet Microbe* **2023**, *4* (2), e75–e83. https://doi.org/10.1016/S2666-5247(22)00322-6.

(112) Wang, L. M.; Mandell, I. B.; Bohrer, B. M. Effects of Feeding Essential Oils and Benzoic Acid to Replace Antibiotics on Finishing Beef Cattle Growth, Carcass Characteristics, and Sensory Attributes. *Applied Animal Science* **2020**, *36* (2), 145–156. https://doi.org/10.15232/aas.2019-01908.

(113) Andrés, S.; Gini, C.; Ceciliani, F.; Gutiérrez-Expósito, D.; Arteche-Villasol, N.; Martín, A.; Cremonesi, P.; Faré, F.; Ghaffari, M. H.; Giráldez, F. J.; Abdennebi-Najar, L. Essential Oil Supplementation in Milk Replacers: Short- and Long-Term Impacts on Feed Efficiency, the Faecal Microbiota and the Plasma Metabolome in Dairy Calves. *Journal of Developmental Origins of Health and Disease* **2024**, *15*, e5. https://doi.org/10.1017/S2040174424000084.

(114) Li, M.; Liu, Y.; Gong, Y.; Yan, X.; Wang, L.; Zheng, W.; Ai, H.; Zhao, Y. Recent Advances in Nanoantibiotics against Multidrug-Resistant Bacteria. *Nanoscale Adv.* **2023**, *5* (23), 6278–6317. https://doi.org/10.1039/D3NA00530E.

(115) Rosini, R.; Nicchi, S.; Pizza, M.; Rappuoli, R. Vaccines Against Antimicrobial Resistance. *Front. Immunol.* **2020**, *11*, 1048. https://doi.org/10.3389/fimmu.2020.01048.

(116) Umair, M.; Hassan, B.; Farzana, R.; Ali, Q.; Sands, K.; Mathias, J.; Afegbua, S.; Haque, M. N.; Walsh, T. R.; Mohsin, M. International Manufacturing and Trade in Colistin, Its Implications in Colistin Resistance and One Health Global Policies: A Microbiological, Economic, and Anthropological Study. *The Lancet Microbe* **2023**, *4* (4), e264–e276. https://doi.org/10.1016/S2666-5247(22)00387-1.

(117) Van Belkum, A.; Burnham, C.-A. D.; Rossen, J. W. A.; Mallard, F.; Rochas, O.; Dunne, W. M. Innovative and Rapid Antimicrobial Susceptibility Testing Systems. *Nat Rev Microbiol* **2020**, *18* (5), 299–311. https://doi.org/10.1038/s41579-020-0327-x.

(118) Benkova, M.; Soukup, O.; Marek, J. Antimicrobial Susceptibility Testing: Currently Used Methods and Devices and the near Future in Clinical Practice. *J. Appl. Microbiol.* **2020**, *129* (4), 806–822. https://doi.org/10.1111/jam.14704.

(119) Leonard, H.; Colodner, R.; Halachmi, S.; Segal, E. Recent Advances in the Race to Design a Rapid Diagnostic Test for Antimicrobial Resistance. *ACS Sens.* **2018**, *3* (11), 2202–2217. https://doi.org/10.1021/acssensors.8b00900.

(120) Giuliano, C.; Patel, C. R.; Kale-Pradhan, P. B. A Guide to Bacterial Culture Identification And Results Interpretation. *P T* **2019**, *44* (4), 192–200.

(121) Kaprou, G. D.; Bergšpica, I.; Alexa, E. A.; Alvarez-Ordóñez, A.; Prieto, M. Rapid Methods for Antimicrobial Resistance Diagnostics. *Antibiotics (Basel)* **2021**, *10* (2), 209. https://doi.org/10.3390/antibiotics10020209.

(122) Ericsson, H. M.; Sherris, J. C. Antibiotic Sensitivity Testing. Report of an International Collaborative Study. *Acta Pathol Microbiol Scand B Microbiol Immunol* **1971**, *217*, Suppl 217:1+.

(123) Idelevich, E. A.; Becker, K. How to Accelerate Antimicrobial Susceptibility Testing. *Clinical Microbiology and Infection* **2019**, *25* (11), 1347–1355. https://doi.org/10.1016/j.cmi.2019.04.025.

(124) Mulet Bayona, J. V.; Salvador García, C.; Tormo Palop, N.; Valentín Martín, A.; González Padrón, C.; Colomina Rodríguez, J.; Pemán, J.; Gimeno Cardona, C. Novel Chromogenic Medium CHROMagarTM Candida Plus for Detection of *Candida Auris* and Other Candida Species from Surveillance and Environmental Samples: A Multicenter Study. *Journal of Fungi* **2022**, *8* (3), 281. https://doi.org/10.3390/jof8030281.

(125) Bouslah, Z.; Mahjoub, R.; Allagui, Z.; Dabboussi, M.; Zouaoui, M.; Bibi, A. Apport Des Milieux Chromogènes Uriselect4® et CPS ID3® Dans l'isolement et l'identification Des Germes Responsables d'infections Urinaires. *Annales de Biologie Clinique* **2020**, *78* (1), 47–53. https://doi.org/10.1684/abc.2019.1512.

(126) Złoch, M.; Maślak, E.; Kupczyk, W.; Jackowski, M.; Pomastowski, P.; Buszewski, B. Culturomics Approach to Identify Diabetic Foot Infection Bacteria. *International Journal of Molecular Sciences* **2021**, *22* (17), 9574. https://doi.org/10.3390/ijms22179574.

(127) Wootton, M.; MacGowan, A. P.; Howe, R. A. Towards Better Antimicrobial Susceptibility Testing: Impact of the *Journal of Antimicrobial Chemotherapy*. *J. Antimicrob. Chemother.* **2017**, *72* (2), 323–329. https://doi.org/10.1093/jac/dkw494.

(128) Truswell, A.; Abraham, R.; O'Dea, M.; Lee, Z. Z.; Lee, T.; Laird, T.; Blinco, J.; Kaplan, S.; Turnidge, J.; Trott, D. J.; Jordan, D.; Abraham, S. Robotic Antimicrobial Susceptibility Platform (RASP): A next-Generation Approach to One Health Surveillance of Antimicrobial Resistance. *Journal of Antimicrobial Chemotherapy* **2021**, *76* (7), 1800–1807. https://doi.org/10.1093/jac/dkab107.

(129) Kim, J.-H.; Kim, T. S.; Jung, H. gul; Kang, C. K.; Jun, K.-I.; Han, S.; Kim, D. Y.; Kwon, S.; Song, K.-H.; Choe, P. G.; Bang, J. H.; Kim, E. S.; Park, S. W.; Kim, H. B.; Kim, N. J.; Park, W. B.; Oh, M. Prospective Evaluation of a Rapid Antimicrobial Susceptibility Test (QMAC-dRAST) for Selecting Optimal Targeted Antibiotics in Positive Blood Culture. *Journal of Antimicrobial Chemotherapy* **2019**, *74* (8), 2255–2260. https://doi.org/10.1093/jac/dkz168.

(130) Jiang, L.; Boitard, L.; Broyer, P.; Chareire, A.-C.; Bourne-Branchu, P.; Mahé, P.; Tournoud, M.; Franceschi, C.; Zambardi, G.; Baudry, J.; Bibette, J. Digital Antimicrobial Susceptibility Testing Using the MilliDrop Technology. *Eur J Clin Microbiol Infect Dis* **2016**, *35* (3), 415–422. https://doi.org/10.1007/s10096-015-2554-z.

(131) Avesar, J.; Rosenfeld, D.; Truman-Rosentsvit, M.; Ben-Arye, T.; Geffen, Y.; Bercovici, M.; Levenberg, S. Rapid Phenotypic Antimicrobial Susceptibility Testing Using Nanoliter Arrays. *Proceedings of the National Academy of Sciences* **2017**, *114* (29), E5787–E5795. https://doi.org/10.1073/pnas.1703736114.

(132) Wheat, P. F. History and Development of Antimicrobial Susceptibility Testing Methodology. *J Antimicrob Chemother* **2001**, *48 Suppl 1*, 1–4. https://doi.org/10.1093/jac/48.suppl_1.1.

(133) Van Belkum, A.; Dunne, W. M. Next-Generation Antimicrobial Susceptibility Testing. *J Clin Microbiol* **2013**, *51* (7), 2018–2024. https://doi.org/10.1128/JCM.00313-13.

(134) Fleming, A. On the Antibacterial Action of Cultures of a Penicillium, with Special Reference to Their Use in the Isolation of *B. Influenzæ*. *Br J Exp Pathol* **1929**, *10* (3), 226–236.

(135) Wilkins, T. D.; Holdeman, L. V.; Abramson, I. J.; Moore, W. E. C. Standardized Single-Disc Method for Antibiotic Susceptibility Testing of Anaerobic Bacteria. *Antimicrob Agents Chemother* **1972**, *1* (6), 451–459. https://doi.org/10.1128/AAC.1.6.451.

(136) Zinner, S. H.; Dudley, M.; Blaser, J. In Vitro Models for the Study of Combination Antibiotic Therapy in Neutropenic Patients. *Am J Med* **1986**, *80* (6B), 156–160. https://doi.org/10.1016/0002-9343(86)90494-8.

(137) Donay, J.-L.; Mathieu, D.; Fernandes, P.; Prégermain, C.; Bruel, P.; Wargnier, A.; Casin, I.; Weill, F. X.; Lagrange, P. H.; Herrmann, J. L. Evaluation of the Automated Phoenix System for Potential Routine Use in the Clinical Microbiology Laboratory. *J Clin Microbiol* **2004**, *42* (4), 1542–1546. https://doi.org/10.1128/JCM.42.4.1542-1546.2004.

(138) Giske, C. G.; Kahlmeter, G. Colistin Antimicrobial Susceptibility Testing - Can the Slow and Challenging Be Replaced by the Rapid and Convenient? *Clinical Microbiology and Infection* **2018**, *24* (2), 93–94. https://doi.org/10.1016/j.cmi.2017.10.007.

(139) Sellenriek, P.; Holmes, J.; Ferrett, R.; Drury, R.; Storch, G. A. Comparison of MicroScan Walk-Away®, Phoenix™ and VITEK-TWO® Microbiology Systems Used in the Identification and Susceptibility Testing of Bacteria, 2005.

https://journals.asm.org/doi/10.1128/jcm.33.11.3044-3046.1995   (accessed 2024-05-18).

(140) Richter, S. S.; Howard, W. J.; Weinstein, M. P.; Bruckner, D. A.; Hindler, J. F.; Saubolle, M.; Doern, G. V. Multicenter Evaluation of the BD Phoenix Automated Microbiology System for Antimicrobial Susceptibility Testing of *Streptococcus* Species. *J Clin Microbiol* **2007**, *45* (9), 2863–2871. https://doi.org/10.1128/JCM.00981-07.

(141) Delost, M. D. *Introduction to Diagnostic Microbiology for the Laboratory Sciences*, Second edition.; Jones & Bartlett Learning: Burlington, MA, 2022.

(142) Jorgensen, J. H.; Ferraro, M. J. Antimicrobial Susceptibility Testing: A Review of General Principles and Contemporary Practices. *CLIN INFECT DIS* **2009**, *49* (11), 1749–1755. https://doi.org/10.1086/647952.

(143) Pancholi, P.; Carroll, K. C.; Buchan, B. W.; Chan, R. C.; Dhiman, N.; Ford, B.; Granato, P. A.; Harrington, A. T.; Hernandez, D. R.; Humphries, R. M.; Jindra, M. R.; Ledeboer, N. A.; Miller, S. A.; Mochon, A. B.; Morgan, M. A.; Patel, R.; Schreckenberger, P. C.; Stamper, P. D.; Simner, P. J.; Tucci, N. E.; Zimmerman, C.; Wolk, D. M. Multicenter Evaluation of the Accelerate PhenoTest BC Kit for Rapid Identification and Phenotypic Antimicrobial Susceptibility Testing Using Morphokinetic Cellular Analysis. *J Clin Microbiol* **2018**, *56* (4), e01329-17. https://doi.org/10.1128/JCM.01329-17.

(144) Choi, J.; Jeong, H. Y.; Lee, G. Y.; Han, S.; Han, S.; Jin, B.; Lim, T.; Kim, S.; Kim, D. Y.; Kim, H. C.; Kim, E.-C.; Song, S. H.; Kim, T. S.; Kwon, S. Direct, Rapid Antimicrobial Susceptibility Test from Positive Blood Cultures Based on Microscopic Imaging Analysis. *Sci Rep* **2017**, *7* (1), 1148. https://doi.org/10.1038/s41598-017-01278-2.

(145) Braga, P. C.; Bovio, C.; Culici, M.; Dal Sasso, M. Flow Cytometric Assessment of Susceptibilities of *Streptococcus Pyogenes* to Erythromycin and Rokitamycin. *Antimicrob Agents Chemother* **2003**, *47* (1), 408–412. https://doi.org/10.1128/AAC.47.1.408-412.2003.

(146) Angeletti, S. Matrix Assisted Laser Desorption Time of Flight Mass Spectrometry (MALDI-TOF MS) in Clinical Microbiology. *Journal of Microbiological Methods* **2017**, *138*, 20–29. https://doi.org/10.1016/j.mimet.2016.09.003.

(147) Belkum, A. V.; Welker, M.; Pincus, D.; Charrier, J.-P.; Girard, V. Matrix-Assisted Laser Desorption Ionization Time-of-Flight Mass Spectrometry in Clinical Microbiology: What Are the Current Issues? *Ann Lab Med* **2017**, *37* (6), 475–483. https://doi.org/10.3343/alm.2017.37.6.475.

(148) Gitman, M. R.; McTaggart, L.; Spinato, J.; Poopalarajah, R.; Lister, E.; Husain, S.; Kus, J. V. Antifungal Susceptibility Testing of Aspergillus Spp. by Using a Composite Correlation Index (CCI)-Based Matrix-Assisted Laser Desorption Ionization–Time of Flight Mass Spectrometry Method Appears To Not Offer Benefit over Traditional Broth Microdilution Testing. *J Clin Microbiol* **2017**, *55* (7), 2030–2034. https://doi.org/10.1128/JCM.00254-17.

(149) Vella, A.; De Carolis, E.; Mello, E.; Perlin, D. S.; Sanglard, D.; Sanguinetti, M.; Posteraro, B. Potential Use of MALDI-ToF Mass Spectrometry for Rapid

Detection of Antifungal Resistance in the Human Pathogen *Candida Glabrata*. *Sci Rep* **2017**, *7* (1), 9099. https://doi.org/10.1038/s41598-017-09329-4.

(150) Fredborg, M.; Rosenvinge, F. S.; Spillum, E.; Kroghsbo, S.; Wang, M.; Sondergaard, T. E. Rapid Antimicrobial Susceptibility Testing of Clinical Isolates by Digital Time-Lapse Microscopy. *Eur J Clin Microbiol Infect Dis* **2015**, *34* (12), 2385–2394. https://doi.org/10.1007/s10096-015-2492-9.

(151) Fredborg, M.; Andersen, K. R.; Jørgensen, E.; Droce, A.; Olesen, T.; Jensen, B. B.; Rosenvinge, F. S.; Sondergaard, T. E. Real-Time Optical Antimicrobial Susceptibility Testing. *J Clin Microbiol* **2013**, *51* (7), 2047–2053. https://doi.org/10.1128/JCM.00440-13.

(152) Laugier, J. The "Comfort Timing" Strategy: A Potential Pathway for the Cultivation of Uncultured Microorganisms and a Possible Adaptation for Environmental Colonisation. *FEMS Microbiology Ecology* **2023**, *99* (4), fiad026. https://doi.org/10.1093/femsec/fiad026.

(153) Yoon, E.-J.; Jeong, S. H. MALDI-TOF Mass Spectrometry Technology as a Tool for the Rapid Diagnosis of Antimicrobial Resistance in Bacteria. *Antibiotics* **2021**, *10* (8), 982. https://doi.org/10.3390/antibiotics10080982.

(154) Wilcox, M. Assuring the Quality of Diagnostic Tests. *BMJ* **2013**, *346* (feb12 4), f836–f836. https://doi.org/10.1136/bmj.f836.

(155) Goff, D. A.; Jankowski, C.; Tenover, F. C. Using Rapid Diagnostic Tests to Optimize Antimicrobial Selection in Antimicrobial Stewardship Programs. *Pharmacotherapy* **2012**, *32* (8), 677–687. https://doi.org/10.1002/j.1875-9114.2012.01137.x.

(156) Ersoy, S. C.; Heithoff, D. M.; Barnes, L.; Tripp, G. K.; House, J. K.; Marth, J. D.; Smith, J. W.; Mahan, M. J. Correcting a Fundamental Flaw in the Paradigm for Antimicrobial Susceptibility Testing. *EBioMedicine* **2017**, *20*, 173–181. https://doi.org/10.1016/j.ebiom.2017.05.026.

(157) Brown, D. F. J.; Kothari, D. Antimicrobial-Susceptibility Testing of Rapidly Growing Pathogenic Bacteria: I. A Comparison of Disc-Diffusion Methods in One Laboratory. *Journal of Antimicrobial Chemotherapy* **1978**, *4* (1), 19–26. https://doi.org/10.1093/jac/4.1.19.

(158) van Belkum, A.; Bachmann, T. T.; Lüdke, G.; Lisby, J. G.; Kahlmeter, G.; Mohess, A.; Becker, K.; Hays, J. P.; Woodford, N.; Mitsakakis, K.; Moran-Gilad, J.; Vila, J.; Peter, H.; Rex, J. H.; Dunne, W. M. Developmental Roadmap for Antimicrobial Susceptibility Testing Systems. *Nat Rev Microbiol* **2019**, *17* (1), 51–62. https://doi.org/10.1038/s41579-018-0098-9.

(159) Valentin, T.; Koenig, E.; Prattes, J.; Wunsch, S.; Loizenbaur, T.; Krause, R.; Zollner-Schwetz, I. Implementation of Rapid Antimicrobial Susceptibility Testing Combined with Routine Infectious Disease Bedside Consultation in Clinical Practice (RAST-ID): A Prospective Single-Centre Study. *Journal of Antimicrobial Chemotherapy* **2021**, *76* (1), 233–238. https://doi.org/10.1093/jac/dkaa380.

(160) Berinson, B.; Olearo, F.; Both, A.; Brossmann, N.; Christner, M.; Aepfelbacher, M.; Rohde, H. EUCAST Rapid Antimicrobial Susceptibility Testing (RAST): Analytical Performance and Impact on Patient Management. *Journal of*

Antimicrobial Chemotherapy **2021**, *76* (5), 1332–1338. https://doi.org/10.1093/jac/dkab026.

(161) Dubreuil, L.; Jehl, F.; Cattoen, C.; Bonnet, R.; Bru, J. P.; Caron, F.; Cattoir, V.; Courvalin, P.; Jarlier, V.; Lina, G.; Merens, A.; Plesiat, P.; Marie-Cécile, P. L. O. Y.; Soussy, C.-J.; Varon, E.; Weber, P. Improvement of a Disk Diffusion Method for Antibiotic Susceptibility Testing of Anaerobic Bacteria. French Recommendations Revisited for 2020. *Anaerobe* **2020**, *64*, 102213. https://doi.org/10.1016/j.anaerobe.2020.102213.

(162) Jonasson, E.; Matuschek, E.; Kahlmeter, G. The EUCAST Rapid Disc Diffusion Method for Antimicrobial Susceptibility Testing Directly from Positive Blood Culture Bottles. *Journal of Antimicrobial Chemotherapy* **2020**, *75* (4), 968–978. https://doi.org/10.1093/jac/dkz548.

(163) Ombelet, S.; Ronat, J.-B.; Walsh, T.; Yansouni, C. P.; Cox, J.; Vlieghe, E.; Martiny, D.; Semret, M.; Vandenberg, O.; Jacobs, J.; Lunguya, O.; Phoba, M.-F.; Lompo, P.; Phe, T.; Kariuki, S.; Newton, P. N.; Dance, D. A. B.; Muvunyi, C.; El Safi, S.; Barbe, B.; Falay, D.; Affolabi, D.; Page, M.; Langendorf, C.; Gille, Y.; Leenstra, T.; Stelling, J.; Naas, T.; Kesteman, T.; Seifu, D.; Delarocque-Astagneau, E.; Schultsz, C.; Schutt-Gerowitt, H.; Letchford, J.; Wertheim, H.; Kahlmeter, G.; Aidara Kane, A. Clinical Bacteriology in Low-Resource Settings: Today's Solutions. *The Lancet Infectious Diseases* **2018**, *18* (8), e248–e258. https://doi.org/10.1016/S1473-3099(18)30093-8.

(164) Lam, T. T.; Dang, D. A.; Tran, H. H.; Do, D. V.; Le, H.; Negin, J.; Jan, S.; Marks, G. B.; Nguyen, T. A.; Fox, G. J.; Beardsley, J. What Are the Most Effective Community-Based Antimicrobial Stewardship Interventions in Low- and Middle-Income Countries? A Narrative Review. *Journal of Antimicrobial Chemotherapy* **2021**, *76* (5), 1117–1129. https://doi.org/10.1093/jac/dkaa556.

(165) Chen, C.; Hong, W. Recent Development of Rapid Antimicrobial Susceptibility Testing Methods through Metabolic Profiling of Bacteria. *Antibiotics* **2021**, *10* (3), 311. https://doi.org/10.3390/antibiotics10030311.

(166) Bhattacharyya, R. P.; Bandyopadhyay, N.; Ma, P.; Son, S. S.; Liu, J.; He, L. L.; Wu, L.; Khafizov, R.; Boykin, R.; Cerqueira, G. C.; Pironti, A.; Rudy, R. F.; Patel, M. M.; Yang, R.; Skerry, J.; Nazarian, E.; Musser, K. A.; Taylor, J.; Pierce, V. M.; Earl, A. M.; Cosimi, L. A.; Shoresh, N.; Beechem, J.; Livny, J.; Hung, D. T. Simultaneous Detection of Genotype and Phenotype Enables Rapid and Accurate Antibiotic Susceptibility Determination. *Nat Med* **2019**, *25* (12), 1858–1864. https://doi.org/10.1038/s41591-019-0650-9.

(167) Leshchiner, D.; Rosconi, F.; Sundaresh, B.; Rudmann, E.; Ramirez, L. M. N.; Nishimoto, A. T.; Wood, S. J.; Jana, B.; Buján, N.; Li, K.; Gao, J.; Frank, M.; Reeve, S. M.; Lee, R. E.; Rock, C. O.; Rosch, J. W.; Van Opijnen, T. A Genome-Wide Atlas of Antibiotic Susceptibility Targets and Pathways to Tolerance. *Nat Commun* **2022**, *13* (1), 3165. https://doi.org/10.1038/s41467-022-30967-4.

(168) Ramzan, M.; Raza, A.; Nisa, Z. U.; Abdel-Massih, R. M.; Al Bakain, R.; Cabrerizo, F. M.; Dela Cruz, T. E.; Aziz, R. K.; Musharraf, S. G. Detection of Antimicrobial Resistance (AMR) and Antimicrobial Susceptibility Testing (AST) Using

Advanced Spectroscopic Techniques: A Review. *TrAC Trends in Analytical Chemistry* **2024**, *172*, 117562. https://doi.org/10.1016/j.trac.2024.117562.

(169) Jang, K.-S.; Kim, Y. H. Rapid and Robust MALDI-TOF MS Techniques for Microbial Identification: A Brief Overview of Their Diverse Applications. *J Microbiol.* **2018**, *56* (4), 209–216. https://doi.org/10.1007/s12275-018-7457-0.

(170) Rath, C. M.; Benton, B. M.; de Vicente, J.; Drumm, J. E.; Geng, M.; Li, C.; Moreau, R. J.; Shen, X.; Skepper, C. K.; Steffek, M.; Takeoka, K.; Wang, L.; Wei, J.-R.; Xu, W.; Zhang, Q.; Feng, B. Y. Optimization of CoaD Inhibitors against Gram-Negative Organisms through Targeted Metabolomics. *ACS Infect. Dis.* **2018**, *4* (3), 391–402. https://doi.org/10.1021/acsinfecdis.7b00214.

(171) Davis, T. D.; Gerry, C. J.; Tan, D. S. General Platform for Systematic Quantitative Evaluation of Small-Molecule Permeability in Bacteria. *ACS Chem Biol* **2014**, *9* (11), 2535–2544. https://doi.org/10.1021/cb5003015.

(172) Maelegheer, K.; Nulens, E. Same-Day Identification and Antibiotic Susceptibility Testing on Positive Blood Cultures: A Simple and Inexpensive Procedure. *Eur J Clin Microbiol Infect Dis* **2017**, *36* (4), 681–687. https://doi.org/10.1007/s10096-016-2849-8.

(173) Kyriazopoulou, E.; Giamarellos-Bourboulis, E. J. Antimicrobial Stewardship Using Biomarkers: Accumulating Evidence for the Critically Ill. *Antibiotics* **2022**, *11* (3), 367. https://doi.org/10.3390/antibiotics11030367.

(174) Novikov, A.; Sayfutdinova, A.; Botchkova, E.; Kopitsyn, D.; Fakhrullin, R. Antibiotic Susceptibility Testing with Raman Biosensing. *Antibiotics (Basel)* **2022**, *11* (12), 1812. https://doi.org/10.3390/antibiotics11121812.

(175) Dina, N. E.; Tahir, M. A.; Bajwa, S. Z.; Amin, I.; Valev, V. K.; Zhang, L. SERS-Based Antibiotic Susceptibility Testing: Towards Point-of-Care Clinical Diagnosis. *Biosensors and Bioelectronics* **2023**, *219*, 114843. https://doi.org/10.1016/j.bios.2022.114843.

(176) Zhang, X.; Jiang, X.; Hao, Z.; Qu, K. Advances in Online Methods for Monitoring Microbial Growth. *Biosensors and Bioelectronics* **2019**, *126*, 433–447. https://doi.org/10.1016/j.bios.2018.10.035.

(177) Jung, J. H.; Lee, J. E. Real-Time Bacterial Microcolony Counting Using on-Chip Microscopy. *Sci Rep* **2016**, *6* (1), 21473. https://doi.org/10.1038/srep21473.

(178) Chantell, C. Multiplexed Automated Digital Microscopy for Rapid Identification and Antimicrobial Susceptibility Testing of Bacteria and Yeast Directly from Clinical Samples. *Clinical Microbiology Newsletter* **2015**, *37* (20), 161–167. https://doi.org/10.1016/j.clinmicnews.2015.10.001.

(179) Choi, J.; Yoo, J.; Lee, M.; Kim, E.-G.; Lee, J. S.; Lee, S.; Joo, S.; Song, S. H.; Kim, E.-C.; Lee, J. C.; Kim, H. C.; Jung, Y.-G.; Kwon, S. A Rapid Antimicrobial Susceptibility Test Based on Single-Cell Morphological Analysis. *Sci Transl Med* **2014**, *6* (267), 267ra174. https://doi.org/10.1126/scitranslmed.3009650.

(180) Syal, K.; Mo, M.; Yu, H.; Iriya, R.; Jing, W.; Guodong, S.; Wang, S.; Grys, T. E.; Haydel, S. E.; Tao, N. Current and Emerging Techniques for Antibiotic Susceptibility Tests. *Theranostics* **2017**, *7* (7), 1795–1805. https://doi.org/10.7150/thno.19217.

(181) Hayden, R. T.; Clinton, L. K.; Hewitt, C.; Koyamatsu, T.; Sun, Y.; Jamison, G.; Perkins, R.; Tang, L.; Pounds, S.; Bankowski, M. J. Rapid Antimicrobial Susceptibility Testing Using Forward Laser Light Scatter Technology. *J Clin Microbiol* **2016**, *54* (11), 2701–2706. https://doi.org/10.1128/JCM.01475-16.

(182) Metkar, S. K.; Girigoswami, K. Diagnostic Biosensors in Medicine – A Review. *Biocatalysis and Agricultural Biotechnology* **2019**, *17*, 271–283. https://doi.org/10.1016/j.bcab.2018.11.029.

(183) Ma, T.-F.; Chen, Y.-P.; Guo, J.-S.; Wang, W.; Fang, F. Cellular Analysis and Detection Using Surface Plasmon Resonance Imaging. *TrAC Trends in Analytical Chemistry* **2018**, *103*, 102–109. https://doi.org/10.1016/j.trac.2018.03.010.

(184) Heller, A. A.; Spence, D. M. A Rapid Method for Post-Antibiotic Bacterial Susceptibility Testing. *PLoS ONE* **2019**, *14* (1), e0210534. https://doi.org/10.1371/journal.pone.0210534.

(185) Fatima, T.; Bansal, S.; Husain, S.; Khanuja, M. Biosensors. In *Electrochemical Sensors*; Elsevier, 2022; pp 1–30. https://doi.org/10.1016/B978-0-12-823148-7.00001-5.

(186) Ahmed, A.; Rushworth, J. V.; Hirst, N. A.; Millner, P. A. Biosensors for Whole-Cell Bacterial Detection. *Clin Microbiol Rev* **2014**, *27* (3), 631–646. https://doi.org/10.1128/CMR.00120-13.

(187) Needs, S. H.; Pivetal, J.; Hayward, J.; Kidd, S. P.; Lam, H.; Diep, T.; Gill, K.; Woodward, M.; Reis, N. M.; Edwards, A. D. Moving Microcapillary Antibiotic Susceptibility Testing (mcAST) towards the Clinic: Unravelling Kinetics of Detection of Uropathogenic *E. Coli*, Mass-Manufacturing and Usability for Detection of Urinary Tract Infections in Human Urine. *Sens. Diagn.* **2023**, *2* (3), 736–750. https://doi.org/10.1039/D2SD00138A.

(188) Hernández-Rodríguez, J. F.; Rojas, D.; Escarpa, A. Electrochemical Sensing Directions for Next-Generation Healthcare: Trends, Challenges, and Frontiers. *Anal Chem* **2021**, *93* (1), 167–183. https://doi.org/10.1021/acs.analchem.0c04378.

(189) Dhesi, Z.; Enne, V. I.; O'Grady, J.; Gant, V.; Livermore, D. M. Rapid and Point-of-Care Testing in Respiratory Tract Infections: An Antibiotic Guardian? *ACS Pharmacol. Transl. Sci.* **2020**, *3* (3), 401–417. https://doi.org/10.1021/acsptsci.0c00027.

(190) Hays, J. P.; Mitsakakis, K.; Luz, S.; Van Belkum, A.; Becker, K.; Van Den Bruel, A.; Harbarth, S.; Rex, J. H.; Simonsen, G. S.; Werner, G.; Di Gregori, V.; Lüdke, G.; Van Staa, T.; Moran-Gilad, J.; Bachmann, T. T. The Successful Uptake and Sustainability of Rapid Infectious Disease and Antimicrobial Resistance Point-of-Care Testing Requires a Complex 'Mix-and-Match' Implementation Package. *Eur J Clin Microbiol Infect Dis* **2019**, *38* (6), 1015–1022. https://doi.org/10.1007/s10096-019-03492-4.

(191) Li, L. X.; Szymczak, J. E.; Keller, S. C. Antibiotic Stewardship in Direct-to-Consumer Telemedicine: Translating Interventions into the Virtual Realm. *Journal of Antimicrobial Chemotherapy* **2021**, *77* (1), 13–15. https://doi.org/10.1093/jac/dkab371.

(192) Hand, K. S.; Clancy, B.; Allen, M.; Mayes, A.; Patel, Y.; Latter, S. M. 'It Makes Life so Much Easier'—Experiences of Users of the MicroGuide™ Smartphone App for Improving Antibiotic Prescribing Behaviour in UK Hospitals: An Interview Study. *JAC-Antimicrobial Resistance* **2021**, *3* (3), dlab111. https://doi.org/10.1093/jacamr/dlab111.

(193) Nowakowska, M.; Van Staa, T.; Mölter, A.; Ashcroft, D. M.; Tsang, J. Y.; White, A.; Welfare, W.; Palin, V. Antibiotic Choice in UK General Practice: Rates and Drivers of Potentially Inappropriate Antibiotic Prescribing. *Journal of Antimicrobial Chemotherapy* **2019**, *74* (11), 3371–3378. https://doi.org/10.1093/jac/dkz345.

(194) Wu, J.; Liu, H.; Chen, W.; Ma, B.; Ju, H. Device Integration of Electrochemical Biosensors. *Nat Rev Bioeng* **2023**, *1* (5), 346–360. https://doi.org/10.1038/s44222-023-00032-w.

(195) Blanco-López, M. C.; Lobo-Castañón, M. J.; Fernández Abedul, M. T. Chapter 17 - Bienzymatic Amperometric Glucose Biosensor. In *Laboratory Methods in Dynamic Electroanalysis*; Fernandez Abedul, M. T., Ed.; Elsevier, 2020; pp 173–181. https://doi.org/10.1016/B978-0-12-815932-3.00017-6.

(196) Morales, M. A.; Halpern, J. M. Guide to Selecting a Biorecognition Element for Biosensors. *Bioconjugate Chem.* **2018**, *29* (10), 3231–3239. https://doi.org/10.1021/acs.bioconjchem.8b00592.

(197) Das, S. K.; Nayak, K. K.; Krishnaswamy, P. R.; Kumar, V.; Bhat, N. Review - Electrochemistry and Other Emerging Technologies for Continuous Glucose Monitoring Devices. *ECS Sens. Plus* **2022**, *1* (3), 031601. https://doi.org/10.1149/2754-2726/ac7abb.

(198) Dhar, D.; Roy, S.; Nigam, V. K. Chapter 10 - Advances in Protein/Enzyme-Based Biosensors for the Detection of Pharmaceutical Contaminants in the Environment. In *Tools, Techniques and Protocols for Monitoring Environmental Contaminants*; Kaur Brar, S., Hegde, K., Pachapur, V. L., Eds.; Elsevier, 2019; pp 207–229. https://doi.org/10.1016/B978-0-12-814679-8.00010-8.

(199) Jia, Z.; Müller, M.; Le Gall, T.; Riool, M.; Müller, M.; Zaat, S. A. J.; Montier, T.; Schönherr, H. Multiplexed Detection and Differentiation of Bacterial Enzymes and Bacteria by Color-Encoded Sensor Hydrogels. *Bioactive Materials* **2021**, *6* (12), 4286–4300. https://doi.org/10.1016/j.bioactmat.2021.04.022.

(200) Gunasekaran, D.; Rostovsky, I.; Taussig, D.; Bar-Am, T.; Wine, Y.; Sal-Man, N.; Vernick, S. A Dual-Channel Electrochemical Biosensor Enables Concurrent Detection of Pathogens and Antibiotic Resistance. *Biosensors and Bioelectronics* **2024**, *257*, 116314. https://doi.org/10.1016/j.bios.2024.116314.

(201) Poschenrieder, A.; Thaler, M.; Junker, R.; Luppa, P. B. Recent Advances in Immunodiagnostics Based on Biosensor Technologies - from Central Laboratory to the Point of Care. *Anal Bioanal Chem* **2019**, *411* (29), 7607–7621. https://doi.org/10.1007/s00216-019-01915-x.

(202) Pollap, A.; Kochana, J. Electrochemical Immunosensors for Antibiotic Detection. *Biosensors (Basel)* **2019**, *9* (2), 61. https://doi.org/10.3390/bios9020061.

(203) Leva-Bueno, J.; Peyman, S. A.; Millner, P. A. A Review on Impedimetric Immunosensors for Pathogen and Biomarker Detection. *Med Microbiol Immunol* **2020**, *209* (3), 343–362. https://doi.org/10.1007/s00430-020-00668-0.

(204) Cui, F.; Yue, Y.; Zhang, Y.; Zhang, Z.; Zhou, H. S. Advancing Biosensors with Machine Learning. *ACS Sens.* **2020**, *5* (11), 3346–3364. https://doi.org/10.1021/acssensors.0c01424.

(205) Bertok, T.; Lorencova, L.; Chocholova, E.; Jane, E.; Vikartovska, A.; Kasak, P.; Tkac, J. Electrochemical Impedance Spectroscopy Based Biosensors: Mechanistic Principles, Analytical Examples and Challenges towards Commercialization for Assays of Protein Cancer Biomarkers. *ChemElectroChem* **2019**, *6* (4), 989–1003. https://doi.org/10.1002/celc.201800848.

(206) Farzadfard, A.; Shayeh, J. S.; Habibi-Rezaei, M.; Omidi, M. Modification of Reduced Graphene/Au-Aptamer to Develop an Electrochemical Based Aptasensor for Measurement of Glycated Albumin. *Talanta* **2020**, *211*, 120722. https://doi.org/10.1016/j.talanta.2020.120722.

(207) Liang, G.; Song, L.; Gao, Y.; Wu, K.; Guo, R.; Chen, R.; Zhen, J.; Pan, L. Aptamer Sensors for the Detection of Antibiotic Residues - A Mini-Review. *Toxics* **2023**, *11* (6), 513. https://doi.org/10.3390/toxics11060513.

(208) Mehlhorn, A.; Rahimi, P.; Joseph, Y. Aptamer-Based Biosensors for Antibiotic Detection: A Review. *Biosensors (Basel)* **2018**, *8* (2), 54. https://doi.org/10.3390/bios8020054.

(209) Kizilkurtlu, A. A.; Demirbas, E.; Agel, H. E. Electrochemical Aptasensors for Pathogenic Detection toward Point-of-care Diagnostics. *Biotech and App Biochem* **2023**, *70* (4), 1460–1479. https://doi.org/10.1002/bab.2485.

(210) Ayankojo, A. G.; Reut, J.; Nguyen, V. B. C.; Boroznjak, R.; Syritski, V. Advances in Detection of Antibiotic Pollutants in Aqueous Media Using Molecular Imprinting Technique - A Review. *Biosensors* **2022**, *12* (7), 441. https://doi.org/10.3390/bios12070441.

(211) Pilvenyte, G.; Ratautaite, V.; Boguzaite, R.; Ramanavicius, S.; Chen, C.-F.; Viter, R.; Ramanavicius, A. Molecularly Imprinted Polymer-Based Electrochemical Sensors for the Diagnosis of Infectious Diseases. *Biosensors* **2023**, *13* (6), 620. https://doi.org/10.3390/bios13060620.

(212) Strong, M. E.; Richards, J. R.; Torres, M.; Beck, C. M.; La Belle, J. T. Faradaic Electrochemical Impedance Spectroscopy for Enhanced Analyte Detection in Diagnostics. *Biosensors and Bioelectronics* **2021**, *177*, 112949. https://doi.org/10.1016/j.bios.2020.112949.

(213) Munteanu, F.-D.; Titoiu, A. M.; Marty, J.-L.; Vasilescu, A. Detection of Antibiotics and Evaluation of Antibacterial Activity with Screen-Printed Electrodes. *Sensors* **2018**, *18* (3), 901. https://doi.org/10.3390/s18030901.

(214) Mullard, A. Drug Sales to Reach $1.9 Trillion within 5 Years? *Nat Rev Drug Discov* **2023**, *22* (3), 172–172. https://doi.org/10.1038/d41573-023-00026-8.

(215) Contrive Datum Insights Pvt Ltd. *The Biosensors Market Is Projected To Reach USD 70.18 Billion By 2030, From USD 28.6 Billion in 2022, Registering a CAGR Of 7.90% During The Forecast Period 2023-2030*; 2023.

https://www.globenewswire.com/en/news-release/2023/05/10/2666119/0/en/The-Biosensors-Market-is-Projected-To-Reach-USD-70-18-billion-By-2030-From-USD-28-6-billion-in-2022-Registering-a-CAGR-Of-7-90-During-The-Forecast-Period-2023-2030-Data-By-Contrive.html (accessed 2023-09-21).

(216) DataHorizzon Research. *Biosensors Market Size, Share, Growth, Statistics Analysis Report, By Type (Sensor Patch, Embedded Device), By Technology (Electrochemical, Optical, Piezoelectric, Thermal, Nanomechanical), By Application (POC, Home Diagnostics, Research Labs, Others), By Region And Segment Forecasts, 2023-2032.*; 2023. https://datahorizzonresearch.com/biosensors-market-2409 (accessed 2023-09-21).

(217) Global Market Insights. *Biosensors Market - By Type (Wearable, Non-Wearable), By Technology (Electrochemical, Optical, Thermal, Piezoelectric), By Medical Application (Blood Glucose Testing, Cholesterol Testing, Blood Gas Analysis, Pregnancy Testing), By End-Use & Forecast, 2023-2032*; 2022. https://www.gminsights.com/industry-analysis/biosensors-market (accessed 2023-09-21).

(218) Magar, H. S.; Hassan, R. Y. A.; Mulchandani, A. Electrochemical Impedance Spectroscopy (EIS): Principles, Construction, and Biosensing Applications. *Sensors* **2021**, *21* (19), 6578. https://doi.org/10.3390/s21196578.

(219) Wang, J. *Analytical Electrochemistry*, 1st ed.; Wiley, 2006. https://doi.org/10.1002/0471790303.

(220) Damiati, S.; Haslam, C.; Søpstad, S.; Peacock, M.; Whitley, T.; Davey, P.; Awan, S. A. Sensitivity Comparison of Macro- and Micro-Electrochemical Biosensors for Human Chorionic Gonadotropin (hCG) Biomarker Detection. *IEEE Access* **2019**, *7*, 94048–94058. https://doi.org/10.1109/ACCESS.2019.2928132.

(221) Blair, E. O.; Hannah, S.; Vezza, V.; Avcı, H.; Kocagoz, T.; Hoskisson, P. A.; Güzel, F. D.; Corrigan, D. K. Biologically Modified Microelectrode Sensors Provide Enhanced Sensitivity for Detection of Nucleic Acid Sequences from *Mycobacterium Tuberculosis*. *Sensors and Actuators Reports* **2020**, *2* (1), 100008. https://doi.org/10.1016/j.snr.2020.100008.

(222) Nirmaier, H.-P.; Henze, G. Characteristic Behavior of Macro-, Semimicro- and Microelectrodes in Voltammetric and Chronoamperometric Measurements. *Electroanalysis* **1997**, *9* (8), 619–624. https://doi.org/10.1002/elan.1140090808.

(223) Kahlert, H. Reference Electrodes. In *Electroanalytical Methods: Guide to Experiments and Applications*; Scholz, F., Bond, A. M., Compton, R. G., Fiedler, D. A., Inzelt, G., Kahlert, H., Komorsky-Lovrić, Š., Lohse, H., Lovrić, M., Marken, F., Neudeck, A., Retter, U., Scholz, F., Stojek, Z., Eds.; Springer: Berlin, Heidelberg, 2010; pp 291–308. https://doi.org/10.1007/978-3-642-02915-8_15.

(224) *Laboratory Techniques in Electroanalytical Chemistry, Revised and Expanded*, 2nd ed.; Kissinger, P., Heineman, W. R., Eds.; CRC Press: Boca Raton, 2018. https://doi.org/10.1201/9781315274263.

(225) Scholz, F. Voltammetric Techniques of Analysis: The Essentials. *ChemTexts* **2015**, *1* (4), 1–24. https://doi.org/10.1007/s40828-015-0016-y.

(226) Khan, N. I.; Song, E. Lab-on-a-Chip Systems for Aptamer-Based Biosensing. *Micromachines* **2020**, *11* (2), 220. https://doi.org/10.3390/mi11020220.

(227) Corrigan, D. K. 10 - Impedance Biosensors. In *Fundamentals of Sensor Technology*; Woodhead Publishing Series in Electronic and Optical Materials; Elsevier, 2023; pp 239–264. https://doi.org/10.1016/C2020-0-03445-6.

(228) Steinmetz, C. P. Complex Quantities and Their Use in Electrical Engineering; 1893; pp 33–74.

(229) Magar, H. S.; Hassan, R. Y. A.; Mulchandani, A. Electrochemical Impedance Spectroscopy (EIS): Principles, Construction, and Biosensing Applications. *Sensors* **2021**, *21* (19), 6578. https://doi.org/10.3390/s21196578.

(230) Strong, M. E.; Richards, J. R.; Torres, M.; Beck, C. M.; La Belle, J. T. Faradaic Electrochemical Impedance Spectroscopy for Enhanced Analyte Detection in Diagnostics. *Biosens Bioelectron* **2021**, *177*, 112949. https://doi.org/10.1016/j.bios.2020.112949.

(231) Spencer, D. C.; Paton, T. F.; Mulroney, K. T.; Inglis, T. J. J.; Sutton, J. M.; Morgan, H. A Fast Impedance-Based Antimicrobial Susceptibility Test. *Nat Commun* **2020**, *11* (1), 5328. https://doi.org/10.1038/s41467-020-18902-x.

(232) Sypabekova, M.; Jolly, P.; Estrela, P.; Kanayeva, D. Electrochemical Aptasensor Using Optimized Surface Chemistry for the Detection of *Mycobacterium Tuberculosis* Secreted Protein MPT64 in Human Serum. *Biosensors and Bioelectronics* **2019**, *123*, 141–151. https://doi.org/10.1016/j.bios.2018.07.053.

(233) Zhang, X.; Jiang, X.; Yang, Q.; Wang, X.; Zhang, Y.; Zhao, J.; Qu, K.; Zhao, C. Online Monitoring of Bacterial Growth with an Electrical Sensor. *Anal. Chem.* **2018**, *90* (10), 6006–6011. https://doi.org/10.1021/acs.analchem.8b01214.

(234) Nemr, C. R.; Smith, S. J.; Liu, W.; Mepham, A. H.; Mohamadi, R. M.; Labib, M.; Kelley, S. O. Nanoparticle-Mediated Capture and Electrochemical Detection of Methicillin-Resistant *Staphylococcus Aureus*. *Anal. Chem.* **2019**, *91* (4), 2847–2853. https://doi.org/10.1021/acs.analchem.8b04792.

(235) Shi, X.; Kadiyala, U.; VanEpps, J. S.; Yau, S.-T. Culture-Free Bacterial Detection and Identification from Blood with Rapid, Phenotypic, Antibiotic Susceptibility Testing. *Sci Rep* **2018**, *8* (1), 3416. https://doi.org/10.1038/s41598-018-21520-9.

(236) Ibarlucea, B.; Rim, T.; Baek, C. K.; De Visser, J. A. G. M.; Baraban, L.; Cuniberti, G. Nanowire Sensors Monitor Bacterial Growth Kinetics and Response to Antibiotics. *Lab Chip* **2017**, *17* (24), 4283–4293. https://doi.org/10.1039/C7LC00807D.

(237) Rueda, D.; Furukawa, R.; Fuentes, P.; Comina, G.; Rey De Castro, N.; Requena, D.; Gilman, R.; Sheen, P.; Zimic, M. A Novel Inexpensive Electrochemical Sensor for Pyrazinoic Acid as a Potential Tool for the Identification of Pyrazinamide-Resistant *Mycobacterium Tuberculosis*. *Int J Mycobacteriol* **2018**, *7* (3), 275. https://doi.org/10.4103/ijmy.ijmy_63_18.

(238) Kumar, N.; Wang, W.; Ortiz-Marquez, J. C.; Catalano, M.; Gray, M.; Biglari, N.; Hikari, K.; Ling, X.; Gao, J.; Van Opijnen, T.; Burch, K. S. Dielectrophoresis Assisted Rapid, Selective and Single Cell Detection of Antibiotic Resistant Bacteria with G-FETs. *Biosensors and Bioelectronics* **2020**, *156*, 112123. https://doi.org/10.1016/j.bios.2020.112123.

(239) Rao R, P.; Sharma, S.; Mehrotra, T.; Das, R.; Kumar, R.; Singh, R.; Roy, I.; Basu, T. Rapid Electrochemical Monitoring of Bacterial Respiration for Gram-Positive and Gram-Negative Microbes: Potential Application in Antimicrobial Susceptibility Testing. *Anal. Chem.* **2020**, *92* (6), 4266–4274. https://doi.org/10.1021/acs.analchem.9b04810.

(240) Xu, Y.; Ren, D. A Novel Inductively Coupled Capacitor Wireless Sensor System for Rapid Antibiotic Susceptibility Testing. *J Biol Eng* **2023**, *17* (1), 54. https://doi.org/10.1186/s13036-023-00373-5.

(241) Gill, A. A. S.; Singh, S.; Nate, Z.; Chauhan, R.; Thapliyal, N. B.; Karpoormath, R.; Maru, S. M.; Reddy, T. M. A Novel Copper-Based 3D Porous Nanocomposite for Electrochemical Detection and Inactivation of Pathogenic Bacteria. *Sensors and Actuators B: Chemical* **2020**, *321*, 128449. https://doi.org/10.1016/j.snb.2020.128449.

(242) Swami, P.; Verma, G.; Holani, A.; Kamaraju, S.; Manchanda, V.; Sritharan, V.; Gupta, S. Rapid Antimicrobial Susceptibility Profiling Using Impedance Spectroscopy. *Biosensors and Bioelectronics* **2022**, *200*, 113876. https://doi.org/10.1016/j.bios.2021.113876.

(243) Pitruzzello, G.; Johnson, S.; Krauss, T. F. Exploring the Fundamental Limit of Antimicrobial Susceptibility by Near-Single-Cell Electrical Impedance Spectroscopy. *Biosensors and Bioelectronics* **2023**, *224*, 115056. https://doi.org/10.1016/j.bios.2022.115056.

(244) Hannah, S.; Addington, E.; Alcorn, D.; Shu, W.; Hoskisson, P. A.; Corrigan, D. K. Rapid Antibiotic Susceptibility Testing Using Low-Cost, Commercially Available Screen-Printed Electrodes. *Biosensors and Bioelectronics* **2019**, *145*, 111696. https://doi.org/10.1016/j.bios.2019.111696.

(245) Mishra, P.; Singh, D.; Mishra, K. P.; Kaur, G.; Dhull, N.; Tomar, M.; Gupta, V.; Kumar, B.; Ganju, L. Rapid Antibiotic Susceptibility Testing by Resazurin Using Thin Film Platinum as a Bio-Electrode. *Journal of Microbiological Methods* **2019**, *162*, 69–76. https://doi.org/10.1016/j.mimet.2019.05.009.

(246) Bolotsky, A.; Muralidharan, R.; Butler, D.; Root, K.; Murray, W.; Liu, Z.; Ebrahimi, A. Organic Redox-Active Crystalline Layers for Reagent-Free Electrochemical Antibiotic Susceptibility Testing (ORACLE-AST). *Biosensors and Bioelectronics* **2021**, *172*, 112615. https://doi.org/10.1016/j.bios.2020.112615.

(247) Besant, J. D.; Sargent, E. H.; Kelley, S. O. Rapid Electrochemical Phenotypic Profiling of Antibiotic-Resistant Bacteria. *Lab Chip* **2015**, *15* (13), 2799–2807. https://doi.org/10.1039/C5LC00375J.

(248) Swami, P.; Sharma, A.; Anand, S.; Gupta, S. DEPIS: A Combined Dielectrophoresis and Impedance Spectroscopy Platform for Rapid Cell Viability and Antimicrobial Susceptibility Analysis. *Biosensors and*

Bioelectronics **2021**, *182*, 113190. https://doi.org/10.1016/j.bios.2021.113190.

(249) Spencer, D.; Li, Y.; Zhu, Y.; Sutton, J. M.; Morgan, H. Electrical Broth Micro-Dilution for Rapid Antibiotic Resistance Testing. *ACS Sens.* **2023**, *8* (3), 1101–1108. https://doi.org/10.1021/acssensors.2c02166.

(250) Settu, K.; Chen, C.-J.; Liu, J.-T.; Chen, C.-L.; Tsai, J.-Z. Impedimetric Method for Measuring Ultra-Low *E. Coli* Concentrations in Human Urine. *Biosensors and Bioelectronics* **2015**, *66*, 244–250. https://doi.org/10.1016/j.bios.2014.11.027.

(251) Safavieh, M.; Pandya, H. J.; Venkataraman, M.; Thirumalaraju, P.; Kanakasabapathy, M. K.; Singh, A.; Prabhakar, D.; Chug, M. K.; Shafiee, H. Rapid Real-Time Antimicrobial Susceptibility Testing with Electrical Sensing on Plastic Microchips with Printed Electrodes. *ACS Appl. Mater. Interfaces* **2017**, *9* (14), 12832–12840. https://doi.org/10.1021/acsami.6b16571.

(252) Crane, B.; Hughes, J. P.; Rowley Neale, S. J.; Rashid, M.; Linton, P. E.; Banks, C. E.; Shaw, K. J. Rapid Antibiotic Susceptibility Testing Using Resazurin Bulk Modified Screen-Printed Electrochemical Sensing Platforms. *Analyst* **2021**, *146* (18), 5574–5583. https://doi.org/10.1039/D1AN00850A.

(253) Domingo-Roca, R.; Lasserre, P.; Riordan, L.; Macdonald, A. R.; Dobrea, A.; Duncan, K. R.; Hannah, S.; Murphy, M.; Hoskisson, P. A.; Corrigan, D. K. Rapid Assessment of Antibiotic Susceptibility Using a Fully 3D-Printed Impedance-Based Biosensor. *Biosensors and Bioelectronics: X* **2023**, *13*, 100308. https://doi.org/10.1016/j.biosx.2023.100308.

(254) Tibbits, G.; Mohamed, A.; Call, D. R.; Beyenal, H. Rapid Differentiation of Antibiotic-Susceptible and -Resistant Bacteria through Mediated Extracellular Electron Transfer. *Biosensors and Bioelectronics* **2022**, *197*, 113754. https://doi.org/10.1016/j.bios.2021.113754.

(255) Brosel-Oliu, S.; Mergel, O.; Uria, N.; Abramova, N.; Van Rijn, P.; Bratov, A. 3D Impedimetric Sensors as a Tool for Monitoring Bacterial Response to Antibiotics. *Lab Chip* **2019**, *19* (8), 1436–1447. https://doi.org/10.1039/C8LC01220B.

(256) Menon, S.; Vishnu, N.; Panchapakesan, S. S. S.; Kumar, A. S.; Sankaran, K.; Unrau, P.; Parameswaran, M. A. Electrochemical Sensing Methodology for Antibiogram Assays. *J. Electrochem. Soc.* **2014**, *161* (2), B3061–B3063. https://doi.org/10.1149/2.011402jes.

(257) Abeyrathne, C. D.; Huynh, D. H.; Mcintire, T. W.; Nguyen, T. C.; Nasr, B.; Zantomio, D.; Chana, G.; Abbott, I.; Choong, P.; Catton, M.; Skafidas, E. Lab on a Chip Sensor for Rapid Detection and Antibiotic Resistance Determination of *Staphylococcus Aureus* . *Analyst* **2016**, *141* (6), 1922–1929. https://doi.org/10.1039/C5AN02301G.

(258) Yang, Y.; Gupta, K.; Ekinci, K. L. All-Electrical Monitoring of Bacterial Antibiotic Susceptibility in a Microfluidic Device. *Proc. Natl. Acad. Sci. U.S.A.* **2020**, *117* (20), 10639–10644. https://doi.org/10.1073/pnas.1922172117.

(47) Hannah, S.; Dobrea, A.; Lasserre, P.; Blair, E. O.; Alcorn, D.; Hoskisson, P. A.; Corrigan, D. K. Development of a Rapid, Antimicrobial Susceptibility Test for *E.*

coli Based on Low-Cost, Screen-Printed Electrodes. *Biosensors* **2020**, *10* (11), 153. https://doi.org/10.3390/bios10110153.

(260) Niyomdecha, S.; Limbut, W.; Numnuam, A.; Asawatreratanakul, P.; Kanatharana, P.; Thavarungkul, P. Capacitive Antibacterial Susceptibility Screening Test with a Simple Renewable Sensing Surface. *Biosens Bioelectron* **2017**, *96*, 84–88. https://doi.org/10.1016/j.bios.2017.04.042.

(261) Putney, S.; Theiss, A. H.; Rajan, N. K.; Deak, E.; Buie, C.; Ngo, Y.; Shah, H.; Yuan, V.; Botbol-Ponte, E.; Hoyos-Urias, A.; Knopfmacher, O.; Hogan, C. A.; Banaei, N.; Herget, M. S. Novel Electronic Biosensor for Automated Inoculum Preparation to Accelerate Antimicrobial Susceptibility Testing. *Sci Rep* **2021**, *11* (1), 11360. https://doi.org/10.1038/s41598-021-90830-2.

(262) Buppasirakul, K.; Suginta, W.; Schulte, A. Rapid and Directly Interpretable Antimicrobial Susceptibility Profiling by Continuous Microvolume-Electroanalysis of Ferricyanide-Mediated Bacterial Respiration. *Chem. Commun.* **2024**, *60* (3), 308–311. https://doi.org/10.1039/D3CC04683D.

(263) Altobelli, E.; Mohan, R.; Mach, K. E.; Sin, M. L. Y.; Anikst, V.; Buscarini, M.; Wong, P. K.; Gau, V.; Banaei, N.; Liao, J. C. Integrated Biosensor Assay for Rapid Uropathogen Identification and Phenotypic Antimicrobial Susceptibility Testing. *European Urology Focus* **2017**, *3* (2–3), 293–299. https://doi.org/10.1016/j.euf.2015.12.010.

(264) Tang, T.; Liu, X.; Yuan, Y.; Kiya, R.; Zhang, T.; Yang, Y.; Suetsugu, S.; Yamazaki, Y.; Ota, N.; Yamamoto, K.; Kamikubo, H.; Tanaka, Y.; Li, M.; Hosokawa, Y.; Yalikun, Y. Machine Learning-Based Impedance System for Real-Time Recognition of Antibiotic-Susceptible Bacteria with Parallel Cytometry. *Sensors and Actuators B: Chemical* **2023**, *374*, 132698. https://doi.org/10.1016/j.snb.2022.132698.

(265) Ibarlucea, B.; Rim, T.; Baek, C. K.; Visser, J. A. G. M. de; Baraban, L.; Cuniberti, G. Nanowire Sensors Monitor Bacterial Growth Kinetics and Response to Antibiotics. *Lab Chip* **2017**, *17* (24), 4283–4293. https://doi.org/10.1039/C7LC00807D.

(266) Lee, K.-S.; Lee, S.-M.; Oh, J.; Park, I. H.; Song, J. H.; Han, M.; Yong, D.; Lim, K. J.; Shin, J.-S.; Yoo, K.-H. Electrical Antimicrobial Susceptibility Testing Based on Aptamer-Functionalized Capacitance Sensor Array for Clinical Isolates. *Sci Rep* **2020**, *10* (1), 13709. https://doi.org/10.1038/s41598-020-70459-3.

(267) Jo, N.; Kim, B.; Lee, S.-M.; Oh, J.; Park, I. H.; Jin Lim, K.; Shin, J.-S.; Yoo, K.-H. Aptamer-Functionalized Capacitance Sensors for Real-Time Monitoring of Bacterial Growth and Antibiotic Susceptibility. *Biosensors and Bioelectronics* **2018**, *102*, 164–170. https://doi.org/10.1016/j.bios.2017.11.010.

(268) Rashid, J. I. A.; Kannan, V.; Ahmad, M. H.; Mon, A. A.; Taufik, S.; Miskon, A.; Ong, K. K.; Yusof, N. A. An Electrochemical Sensor Based on Gold Nanoparticles-Functionalized Reduced Graphene Oxide Screen Printed Electrode for the Detection of Pyocyanin Biomarker in *Pseudomonas Aeruginosa* Infection. *Materials Science and Engineering: C* **2021**, *120*, 111625. https://doi.org/10.1016/j.msec.2020.111625.

(269) Butler, D.; Kammarchedu, V.; Zhou, K.; Peeke, L.; Lyle, L.; Snyder, D. W.; Ebrahimi, A. Cellulose-Based Laser-Induced Graphene Devices for Electrochemical Monitoring of Bacterial Phenazine Production and Viability. *Sensors and Actuators B: Chemical* **2023**, *378*, 133090. https://doi.org/10.1016/j.snb.2022.133090.

(270) Poma, N.; Vivaldi, F.; Bonini, A.; Salvo, P.; Kirchhain, A.; Melai, B.; Bottai, D.; Tavanti, A.; Di Francesco, F. A Graphenic and Potentiometric Sensor for Monitoring the Growth of Bacterial Biofilms. *Sensors and Actuators B: Chemical* **2020**, *323*, 128662. https://doi.org/10.1016/j.snb.2020.128662.

(271) Ferrer, M. D.; Rodriguez, J. C.; Álvarez, L.; Artacho, A.; Royo, G.; Mira, A. Effect of Antibiotics on Biofilm Inhibition and Induction Measured by Real-Time Cell Analysis. *J Appl Microbiol* **2017**, *122* (3), 640–650. https://doi.org/10.1111/jam.13368.

(272) van Duuren, J. B. J. H.; Müsken, M.; Karge, B.; Tomasch, J.; Wittmann, C.; Häussler, S.; Brönstrup, M. Use of Single-Frequency Impedance Spectroscopy to Characterize the Growth Dynamics of Biofilm Formation in *Pseudomonas Aeruginosa*. *Sci Rep* **2017**, *7*. https://doi.org/10.1038/s41598-017-05273-5.

(273) Bhattarai, K.; Bastola, R.; Baral, B. Antibiotic Drug Discovery: Challenges and Perspectives in the Light of Emerging Antibiotic Resistance. In *Advances in Genetics*; Elsevier, 2020; Vol. 105, pp 229–292. https://doi.org/10.1016/bs.adgen.2019.12.002.

(274) Keulen, G. van; Dyson, P. Production of Specialized Metabolites by *Streptomyces Coelicolor A3(2)*. *Advances in applied microbiology* **2014**. https://doi.org/10.1016/B978-0-12-800259-9.00006-8.

(275) Laskaris, P.; Karagouni, A. D. Streptomyces, Greek Habitats and Novel Pharmaceuticals: A Promising Challenge. *Microbiology Research* **2021**, *12* (4), 840–846. https://doi.org/10.3390/microbiolres12040061.

(276) Xia, H.; Li, X.; Li, Z.; Zhan, X.; Mao, X.; Li, Y. The Application of Regulatory Cascades in Streptomyces: Yield Enhancement and Metabolite Mining. *Front. Microbiol.* **2020**, *11*, 406. https://doi.org/10.3389/fmicb.2020.00406.

(277) Tong, Y.; Deng, Z. An Aurora of Natural Products-Based Drug Discovery Is Coming. *Synthetic and Systems Biotechnology* **2020**, *5* (2), 92–96. https://doi.org/10.1016/j.synbio.2020.05.003.

(278) Waksman, S. A. On the Classification of Actinomycetes. *J Bacteriol* **1940**, *39* (5), 549–558. https://doi.org/10.1128/jb.39.5.549-558.1940.

(279) Lee, N.; Hwang, S.; Kim, W.; Lee, Y.; Kim, J. H.; Cho, S.; Kim, H. U.; Yoon, Y. J.; Oh, M.-K.; Palsson, B. O.; Cho, B.-K. Systems and Synthetic Biology to Elucidate Secondary Metabolite Biosynthetic Gene Clusters Encoded in *Streptomyces* Genomes. *Nat. Prod. Rep.* **2021**, *38* (7), 1330–1361. https://doi.org/10.1039/D0NP00071J.

(280) Hopwood, D. A. *Streptomyces in Nature and Medicine: The Antibiotic Makers*; Oxford University Press, 2007.

(281) Manteca, Á.; Yagüe, P. Streptomyces Differentiation in Liquid Cultures as a Trigger of Secondary Metabolism. *Antibiotics* **2018**, *7* (2), 41. https://doi.org/10.3390/antibiotics7020041.

(282) Quinn, G. A.; Banat, A. M.; Abdelhameed, A. M.; Banat, I. M. Streptomyces from Traditional Medicine: Sources of New Innovations in Antibiotic Discovery. *Journal of Medical Microbiology* **2020**, *69* (8), 1040–1048. https://doi.org/10.1099/jmm.0.001232.

(283) Hiltner, J. K.; Hunter, I. S.; Hoskisson, P. A. Tailoring Specialized Metabolite Production in Streptomyces. In *Advances in Applied Microbiology*; Elsevier, 2015; Vol. 91, pp 237–255. https://doi.org/10.1016/bs.aambs.2015.02.002.

(284) Rokem, J. S.; Lantz, A. E.; Nielsen, J. Systems Biology of Antibiotic Production by Microorganisms. *Nat. Prod. Rep.* **2007**, *24* (6), 1262. https://doi.org/10.1039/b617765b.

(285) Breitling, R.; Takano, E. Synthetic Biology of Natural Products. *Cold Spring Harb Perspect Biol* **2016**, a023994. https://doi.org/10.1101/cshperspect.a023994.

(286) Traxler, M. F.; Kolter, R. Natural Products in Soil Microbe Interactions and Evolution. *Nat. Prod. Rep.* **2015**, *32* (7), 956–970. https://doi.org/10.1039/C5NP00013K.

(287) van der Heul, H. U.; Bilyk, B. L.; McDowall, K. J.; Seipke, R. F.; van Wezel, G. P. Regulation of Antibiotic Production in Actinobacteria: New Perspectives from the Post-Genomic Era. *Nat. Prod. Rep.* **2018**, *35* (6), 575–604. https://doi.org/10.1039/C8NP00012C.

(288) Baral, B.; Akhgari, A.; Metsä-Ketelä, M. Activation of Microbial Secondary Metabolic Pathways: Avenues and Challenges. *Synthetic and Systems Biotechnology* **2018**, *3* (3), 163–178. https://doi.org/10.1016/j.synbio.2018.09.001.

(289) Liu, G.; Catacutan, D. B.; Rathod, K.; Swanson, K.; Jin, W.; Mohammed, J. C.; Chiappino-Pepe, A.; Syed, S. A.; Fragis, M.; Rachwalski, K.; Magolan, J.; Surette, M. G.; Coombes, B. K.; Jaakkola, T.; Barzilay, R.; Collins, J. J.; Stokes, J. M. Deep Learning-Guided Discovery of an Antibiotic Targeting *Acinetobacter Baumannii*. *Nat Chem Biol* **2023**, *19* (11), 1342–1350. https://doi.org/10.1038/s41589-023-01349-8.

(290) Stokes, J. M.; Yang, K.; Swanson, K.; Jin, W.; Cubillos-Ruiz, A.; Donghia, N. M.; MacNair, C. R.; French, S.; Carfrae, L. A.; Bloom-Ackermann, Z.; Tran, V. M.; Chiappino-Pepe, A.; Badran, A. H.; Andrews, I. W.; Chory, E. J.; Church, G. M.; Brown, E. D.; Jaakkola, T. S.; Barzilay, R.; Collins, J. J. A Deep Learning Approach to Antibiotic Discovery. *Cell* **2020**, *180* (4), 688-702.e13. https://doi.org/10.1016/j.cell.2020.01.021.

(291) Wong, F.; Zheng, E. J.; Valeri, J. A.; Donghia, N. M.; Anahtar, M. N.; Omori, S.; Li, A.; Cubillos-Ruiz, A.; Krishnan, A.; Jin, W.; Manson, A. L.; Friedrichs, J.; Helbig, R.; Hajian, B.; Fiejtek, D. K.; Wagner, F. F.; Soutter, H. H.; Earl, A. M.; Stokes, J. M.; Renner, L. D.; Collins, J. J. Discovery of a Structural Class of Antibiotics with Explainable Deep Learning. *Nature* **2024**, *626* (7997), 177–185. https://doi.org/10.1038/s41586-023-06887-8.

(292) Swanson, K.; Liu, G.; Catacutan, D. B.; Arnold, A.; Zou, J.; Stokes, J. M. Generative AI for Designing and Validating Easily Synthesizable and Structurally Novel Antibiotics. *Nat Mach Intell* **2024**, *6* (3), 338–353. https://doi.org/10.1038/s42256-024-00809-7.

(293) Bentley, S. D.; Chater, K. F.; Cerdeño-Tárraga, A.-M.; Challis, G. L.; Thomson, N. R.; James, K. D.; Harris, D. E.; Quail, M. A.; Kieser, H.; Harper, D.; Bateman, A.; Brown, S.; Chandra, G.; Chen, C. W.; Collins, M.; Cronin, A.; Fraser, A.; Goble, A.; Hidalgo, J.; Hornsby, T.; Howarth, S.; Huang, C.-H.; Kieser, T.; Larke, L.; Murphy, L.; Oliver, K.; O'Neil, S.; Rabbinowitsch, E.; Rajandream, M.-A.; Rutherford, K.; Rutter, S.; Seeger, K.; Saunders, D.; Sharp, S.; Squares, R.; Squares, S.; Taylor, K.; Warren, T.; Wietzorrek, A.; Woodward, J.; Barrell, B. G.; Parkhill, J.; Hopwood, D. A. Complete Genome Sequence of the Model Actinomycete *Streptomyces Coelicolor A3(2)*. *Nature* **2002**, *417* (6885), 141–147. https://doi.org/10.1038/417141a.

(294) Faddetta, T.; Renzone, G.; Vassallo, A.; Rimini, E.; Nasillo, G.; Buscarino, G.; Agnello, S.; Licciardi, M.; Botta, L.; Scaloni, A.; Palumbo Piccionello, A.; Puglia, A. M.; Gallo, G. *Streptomyces Coelicolor* Vesicles: Many Molecules To Be Delivered. *Appl Environ Microbiol* **2022**, *88* (1), e01881-21. https://doi.org/10.1128/AEM.01881-21.

(295) Vaidyanathan, S.; Fletcher, J. S.; Goodacre, R.; Lockyer, N. P.; Micklefield, J.; Vickerman, J. C. Subsurface Biomolecular Imaging of *Streptomyces Coelicolor* Using Secondary Ion Mass Spectrometry. *Anal. Chem.* **2008**, *80* (6), 1942–1951. https://doi.org/10.1021/ac701921e.

(296) Rudd, B. A. M.; Hopwood, D. A. Genetics of Actinorhodin Biosynthesis by *Streptomyces Coelicolor A3(2)*. *Journal of General Microbiology* **1979**, *114* (1), 35–43. https://doi.org/10.1099/00221287-114-1-35.

(297) Musiol-Kroll, E. M.; Tocchetti, A.; Sosio, M.; Stegmann, E. Challenges and Advances in Genetic Manipulation of Filamentous Actinomycetes – the Remarkable Producers of Specialized Metabolites. *Nat. Prod. Rep.* **2019**, *36* (9), 1351–1369. https://doi.org/10.1039/C9NP00029A.

(298) van Keulen, G.; Dyson, P. J. Production of Specialized Metabolites by *Streptomyces Coelicolor A3(2)*. In *Advances in Applied Microbiology*; Elsevier, 2014; Vol. 89, pp 217–266. https://doi.org/10.1016/B978-0-12-800259-9.00006-8.

(299) Manteca, A.; Jung, H. R.; Schwämmle, V.; Jensen, O. N.; Sanchez, J. Quantitative Proteome Analysis of *Streptomyces Coelicolor* Nonsporulating Liquid Cultures Demonstrates a Complex Differentiation Process Comparable to That Occurring in Sporulating Solid Cultures. *J Proteome Res* **2010**, *9* (9), 4801–4811. https://doi.org/10.1021/pr100513p.

(300) Sevcikova, B.; Kormanec, J. Differential Production of Two Antibiotics of *Streptomyces Coelicolor A3(2)*, Actinorhodin and Undecylprodigiosin, upon Salt Stress Conditions. *Archives of Microbiology* **2004**, *181* (5), 384–389. https://doi.org/10.1007/s00203-004-0669-1.

(301) Doull, J. L.; Vining, L. C. Nutritional Control of Actinorhodin Production by *Streptomyces Coelicolor A3(2)*: Suppressive Effects of Nitrogen and Phosphate. *Appl Microbiol Biotechnol* **1990**, *32* (4), 449–454. https://doi.org/10.1007/BF00903781.

(302) Elibol, M. Optimization of Medium Composition for Actinorhodin Production by *Streptomyces Coelicolor A3(2)* with Response Surface Methodology. *Process*

Biochemistry **2004**, *39* (9), 1057–1062. https://doi.org/10.1016/S0032-9592(03)00232-2.

(303) Myronovskyi, M.; Luzhetskyy, A. Heterologous Production of Small Molecules in the Optimized *Streptomyces* Hosts. *Nat. Prod. Rep.* **2019**, *36* (9), 1281–1294. https://doi.org/10.1039/C9NP00023B.

(304) Olano, C.; Méndez, C.; Salas, J. A. Post-PKS Tailoring Steps in Natural Product-Producing Actinomycetes from the Perspective of Combinatorial Biosynthesis. *Nat. Prod. Rep.* **2010**, *27* (4), 571. https://doi.org/10.1039/b911956f.

(305) Nass, N. M.; Farooque, S.; Hind, C.; Wand, M. E.; Randall, C. P.; Sutton, J. M.; Seipke, R. F.; Rayner, C. M.; O'Neill, A. J. Revisiting Unexploited Antibiotics in Search of New Antibacterial Drug Candidates: The Case of γ-Actinorhodin. *Sci Rep* **2017**, *7* (1), 17419. https://doi.org/10.1038/s41598-017-17232-1.

(306) Mulay, S. V.; Fernandes, R. A. Synthetic Studies on Actinorhodin and γ-Actinorhodin: Synthesis of Deoxyactinorhodin and Deoxy-γ-Actinorhodin/Crisamicin A Isomer. *Chem. Eur. J.* **2015**, *21* (12), 4842–4852. https://doi.org/10.1002/chem.201406431.

(307) Finger, M.; Sentek, F.; Hartmann, L.; Palacio-Barrera, A. M.; Schlembach, I.; Rosenbaum, M. A.; Büchs, J. Insights into *Streptomyces Coelicolor A3(2)* Growth and Pigment Formation with High-throughput Online Monitoring. *Engineering in Life Sciences* **2022**, elsc.202100151. https://doi.org/10.1002/elsc.202100151.

(308) Galet, J.; Deveau, A.; Hôtel, L.; Leblond, P.; Frey-Klett, P.; Aigle, B. Gluconic Acid-Producing Pseudomonas Sp. Prevent γ-Actinorhodin Biosynthesis by *Streptomyces Coelicolor A3(2)*. *Arch Microbiol* **2014**, *196* (9), 619–627. https://doi.org/10.1007/s00203-014-1000-4.

(309) Yang, Y.-L.; Xu, Y.; Straight, P.; Dorrestein, P. C. Translating Metabolic Exchange with Imaging Mass Spectrometry. *Nat Chem Biol* **2009**, *5* (12), 885–887. https://doi.org/10.1038/nchembio.252.

(310) Pérez, J.; Muñoz-Dorado, J.; Braña, A. F.; Shimkets, L. J.; Sevillano, L.; Santamaría, R. I. *Myxococcus Xanthus* Induces Actinorhodin Overproduction and Aerial Mycelium Formation by *Streptomyces Coelicolor*. *Microbial Biotechnology* **2011**, *4* (2), 175–183. https://doi.org/10.1111/j.1751-7915.2010.00208.x.

(311) Traxler, M. F.; Watrous, J. D.; Alexandrov, T.; Dorrestein, P. C.; Kolter, R. Interspecies Interactions Stimulate Diversification of the *Streptomyces Coelicolor* Secreted Metabolome. *mBio* **2013**, *4* (4), 10.1128/mbio.00459-13. https://doi.org/10.1128/mbio.00459-13.

(312) Brockmann, H.; Pini, H. Actinorhodin, ein roter Farbstoff aus Actinomyceten. *Naturwissenschaften* **1947**, *34* (6), 190–190. https://doi.org/10.1007/BF00602581.

(313) Ninomiya, M.; Ando, Y.; Kudo, F.; Ohmori, K.; Suzuki, K. Total Synthesis of Actinorhodin. *Angew. Chem. Int. Ed.* **2019**, *58* (13), 4264–4270. https://doi.org/10.1002/anie.201814172.

(314) Wright, L. F.; Hopwood, D. A. Actinorhodin Is a Chromosomally-Determined Antibiotic in *Streptomyces Coelicolor A3(2)*. *Journal of General Microbiology* **1976**, *96* (2), 289–297. https://doi.org/10.1099/00221287-96-2-289.

(315) Mak, S.; Nodwell, J. R. Actinorhodin Is a Redox-Active Antibiotic with a Complex Mode of Action against Gram-Positive Cells: Molecular Action of Actinorhodin. *Molecular Microbiology* **2017**, *106* (4), 597–613. https://doi.org/10.1111/mmi.13837.

(316) Nass, N. M.; Farooque, S.; Hind, C.; Wand, M. E.; Randall, C. P.; Sutton, J. M.; Seipke, R. F.; Rayner, C. M.; O'Neill, A. J. Revisiting Unexploited Antibiotics in Search of New Antibacterial Drug Candidates: The Case of γ-Actinorhodin. *Sci Rep* **2017**, *7* (1), 17419. https://doi.org/10.1038/s41598-017-17232-1.

(317) Nishiyama, T.; Hashimoto, Y.; Kusakabe, H.; Kumano, T.; Kobayashi, M. Natural Low-Molecular Mass Organic Compounds with Oxidase Activity as Organocatalysts. Proceedings of the National Academy of Sciences December 2, 2014, pp 17152–17157.

(318) Abbas, A. S.; Edwards, C. Effects of Metals on *Streptomyces Coelicolor* Growth and Actinorhodin Production. *Appl Environ Microbiol* **1990**, *56* (3), 675–680.

(319) Elibol, M.; Mavituna, F. A Kinetic Model for Actinorhodin Production by *Streptomyces Coelicolor A3(2)*. *Process Biochemistry* **1999**, *34* (6), 625–631. https://doi.org/10.1016/S0032-9592(98)00136-8.

(320) Xu, Y.; Willems, A.; Au-yeung, C.; Tahlan, K.; Nodwell, J. R. A Two-Step Mechanism for the Activation of Actinorhodin Export and Resistance in *Streptomyces Coelicolor*. *mBio* **2012**, *3* (5), e00191-12. https://doi.org/10.1128/mBio.00191-12.

(321) Bystrykh, L. V.; Fernández-Moreno, M. A.; Herrema, J. K.; Malpartida, F.; Hopwood, D. A.; Dijkhuizen, L. Production of Actinorhodin-Related "Blue Pigments" by *Streptomyces Coelicolor A3(2)*. *J Bacteriol* **1996**, *178* (8), 2238–2244. https://doi.org/10.1128/jb.178.8.2238-2244.1996.

(322) Brockmann, H.; Pini, H.; v. Plotho, O. Über Actinomycetenfarbstoffe, I. Mitteil.: Actinorhodin, ein roter, antibiotisch wirksamer Farbstoff aus Actinomyceten. *Chemische Berichte* **1950**, *83* (2), 161–167. https://doi.org/10.1002/cber.19500830209.

(323) Brockmann, H.; Zeeck, A.; Merwe, K. V. D.; Müller, W. Über Actinomycetenfarbstoffe, VIII. Die Konstitution des Actinorhodins. *Justus Liebigs Annalen der Chemie* **1966**, *698* (1), 209–229. https://doi.org/10.1002/jlac.19666980125.

(324) Zeeck, A.; Christiansen, P. Über Actinomycetenfarbstoffe, IX1) Konformation und absolute Konfiguration des Actinorhodins. *Justus Liebigs Annalen der Chemie* **1969**, *724* (1), 172–182. https://doi.org/10.1002/jlac.19697240122.

(325) van Dissel, D.; van Wezel, G. P. Morphology-Driven Downscaling of *Streptomyces Lividans* to Micro-Cultivation. *Antonie Van Leeuwenhoek* **2018**, *111* (3), 457–469. https://doi.org/10.1007/s10482-017-0967-7.

(326) van Wezel, G. P.; Krabben, P.; Traag, B. A.; Keijser, B. J. F.; Kerste, R.; Vijgenboom, E.; Heijnen, J. J.; Kraal, B. Unlocking Streptomyces Spp. for Use as Sustainable Industrial Production Platforms by Morphological Engineering.

Appl Environ Microbiol **2006**, *72* (8), 5283–5288. https://doi.org/10.1128/AEM.00808-06.

(327) Zhang, H.; Zhan, J.; Su, K.; Zhang, Y. A Kind of Potential Food Additive Produced by *Streptomyces Coelicolor*: Characteristics of Blue Pigment and Identification of a Novel Compound, λ-Actinorhodin. *Food Chemistry* **2006**, *95* (2), 186–192. https://doi.org/10.1016/j.foodchem.2004.12.028.

(328) Strauch, E.; Takano, E.; Baylts, H. A.; Bibb, M. J. The Stringent Response in *Streptomyces Coelicolor* A3(2). *Molecular Microbiology* **1991**, *5* (2), 289–298. https://doi.org/10.1111/j.1365-2958.1991.tb02109.x.

(329) Gramajo, H. C.; Takano, E.; Bibb, M. J. Stationary-phase Production of the Antibiotic Actinorhodin in *Streptomyces Coelicolor A3(2)* Is Transcriptionally Regulated. *Molecular Microbiology* **1993**, *7* (6), 837–845. https://doi.org/10.1111/j.1365-2958.1993.tb01174.x.

(330) Hobbs, G.; Frazer, C. M.; Gardner, D. C. J.; Flett, F.; Oliver, S. G. Pigmented Antibiotic Production by *Streptomyces Coelicolor A3(2)*: Kinetics and the Influence of Nutrients. *Microbiology* **1990**, *136* (11), 2291–2296. https://doi.org/10.1099/00221287-136-11-2291.

(331) Hu, H.; Ochi, K. Novel Approach for Improving the Productivity of Antibiotic-Producing Strains by Inducing Combined Resistant Mutations. *Appl Environ Microbiol* **2001**, *67* (4), 1885–1892. https://doi.org/10.1128/AEM.67.4.1885-1892.2001.

(332) Kang, S. G.; Jin, W.; Bibb, M.; Lee, K. J. Actinorhodin and Undecylprodigiosin Production in Wild-Type and *relA* Mutant Strains of *Streptomyces Coelicolor A3(2)* Grown in Continuous Culture. *FEMS Microbiology Letters* **1998**, *168* (2), 221–226. https://doi.org/10.1111/j.1574-6968.1998.tb13277.x.

(333) Ryu, Y.-G.; Butler, M. J.; Chater, K. F.; Lee, K. J. Engineering of Primary Carbohydrate Metabolism for Increased Production of Actinorhodin in *Streptomyces Coelicolor*. *Appl Environ Microbiol* **2006**, *72* (11), 7132–7139. https://doi.org/10.1128/AEM.01308-06.

(334) Hiltner, J. K.; Hunter, I. S.; Hoskisson, P. A. Tailoring Specialized Metabolite Production in Streptomyces. In *Advances in Applied Microbiology*; Elsevier, 2015; Vol. 91, pp 237–255. https://doi.org/10.1016/bs.aambs.2015.02.002.

(335) Kieser, T.; Bibb, M. J.; Buttner, M. J.; Chater, K. F.; Hopwood, D. A. *Practical Streptomyces Genetics*; John Innes Foundation, 2000.

(336) Wang, G.; Hosaka, T.; Ochi, K. Dramatic Activation of Antibiotic Production in *Streptomyces Coelicolor* by Cumulative Drug Resistance Mutations. *Appl Environ Microbiol* **2008**, *74* (9), 2834–2840. https://doi.org/10.1128/AEM.02800-07.

(337) Vaidyanathan, S.; Fletcher, J. S.; Goodacre, R.; Lockyer, N. P.; Micklefield, J.; Vickerman, J. C. Subsurface Biomolecular Imaging of *Streptomyces Coelicolor* Using Secondary Ion Mass Spectrometry. *Anal. Chem.* **2008**, *80* (6), 1942–1951. https://doi.org/10.1021/ac701921e.

(338) Elibol, M.; Mavituna, F. A Kinetic Model for Actinorhodin Production by *Streptomyces Coelicolor A3(2)*. *Process Biochemistry* **1999**, *34* (6–7), 625–631. https://doi.org/10.1016/S0032-9592(98)00136-8.

(339) García Cancela, P.; González Quiñónez, N.; Corte-Rodríguez, M.; Bettmer, J.; Manteca, A.; Montes-Bayón, M. Evaluation of Copper Uptake in Individual Spores of *Streptomyces Coelicolor* and Endogenic Nanoparticles Formation to Modulate the Secondary Metabolism. *Metallomics* **2022**, *14* (3), mfac015. https://doi.org/10.1093/mtomcs/mfac015.

(340) Doull, J. L.; Vining, L. C. Nutritional Control of Actinorhodin Production by *Streptomyces Coelicolor A3(2)*: Suppressive Effects of Nitrogen and Phosphate. *Appl Microbiol Biotechnol* **1990**, *32* (4), 449–454. https://doi.org/10.1007/BF00903781.

(341) Sohoni, S. V.; Bapat, P. M.; Lantz, A. E. Robust, Small-Scale Cultivation Platform for *Streptomyces Coelicolor*. *Microb Cell Fact* **2012**, *11* (1), 9. https://doi.org/10.1186/1475-2859-11-9.

(342) Bystrykh, L. V.; Fernández-Moreno, M. A.; Herrema, J. K.; Malpartida, F.; Hopwood, D. A.; Dijkhuizen, L. Production of Actinorhodin-Related "Blue Pigments" by *Streptomyces Coelicolor* A3(2). *J Bacteriol* **1996**, *178* (8), 2238–2244. https://doi.org/10.1128/jb.178.8.2238-2244.1996.

(343) Xu, Y.; Willems, A.; Au-yeung, C.; Tahlan, K.; Nodwell, J. R. A Two-Step Mechanism for the Activation of Actinorhodin Export and Resistance in *Streptomyces Coelicolor*. *mBio* **2012**, *3* (5), e00191-12. https://doi.org/10.1128/mBio.00191-12.

(344) Kumar, K.; Bruheim, P. Nutrient-Depended Metabolic Switching during Batch Cultivation of *Streptomyces Coelicolor* Explored with Absolute Quantitative Mass Spectrometry-Based Metabolite Profiling. *3 Biotech* **2022**, *12* (3), 80. https://doi.org/10.1007/s13205-022-03146-x.

(345) Ninomiya, M.; Ando, Y.; Kudo, F.; Ohmori, K.; Suzuki, K. Total Synthesis of Actinorhodin. *Angew. Chem.* **2019**, *131* (13), 4308–4314. https://doi.org/10.1002/ange.201814172.

(346) Brockmann, H.; Müller, W.; van der Merve, K. Die Konstitution des Actinorhodins. *Naturwissenschaften* **1962**, *49* (6), 131–131. https://doi.org/10.1007/BF00621127.

(347) Faddetta, T.; Renzone, G.; Vassallo, A.; Rimini, E.; Nasillo, G.; Buscarino, G.; Agnello, S.; Licciardi, M.; Botta, L.; Scaloni, A.; Palumbo Piccionello, A.; Puglia, A. M.; Gallo, G. *Streptomyces Coelicolor* Vesicles: Many Molecules To Be Delivered. *Appl Environ Microbiol* **2022**, *88* (1), e01881-21. https://doi.org/10.1128/AEM.01881-21.

(348) Mak, S. H. C. The Molecular Action of Actinorhodin, an Antibiotic Produced by *Streptomyces Coelicolor*. Ph.D., University of Toronto (Canada), Canada -- Ontario, CA, 2017. https://www.proquest.com/dissertations-theses/molecular-action-actinorhodin-antibiotic-produced/docview/2011025565/se-2?accountid=14116.

(349) Sun, Y.-Q.; Busche, T.; Rückert, C.; Paulus, C.; Rebets, Y.; Novakova, R.; Kalinowski, J.; Luzhetskyy, A.; Kormanec, J.; Sekurova, O. N.; Zotchev, S. B. Development of a Biosensor Concept to Detect the Production of Cluster-Specific Secondary Metabolites. *ACS Synth Biol* **2017**, *6* (6), 1026–1033. https://doi.org/10.1021/acssynbio.6b00353.

(350) Kendrew, S. G.; Harding, S. E.; Hopwood, D. A.; Marsh, E. N. Identification of a Flavin:NADH Oxidoreductase Involved in the Biosynthesis of Actinorhodin. Purification and Characterization of the Recombinant Enzyme. *J Biol Chem* **1995**, *270* (29), 17339–17343. https://doi.org/10.1074/jbc.270.29.17339.

(351) Krayz, G. T.; Bittner, S.; Dhiman, A.; Becker, J. Y. Electrochemistry of Quinones with Respect to Their Role in Biomedical Chemistry. *The Chemical Record* **2021**, *21* (9), 2332–2343. https://doi.org/10.1002/tcr.202100069.

(352) Marshall, A. P.; Carlson, E. E. Metabolomics Reveals a "Trimeric" γ-Actinorhodin from *Streptomyces Coelicolor* M145. *ChemBioChem* **2023**, *24* (7), e202200757. https://doi.org/10.1002/cbic.202200757.

(353) Kieser, T.; Bibb, M. J.; Buttner, M. J.; Chater, K. F.; Hopwood, D. A. *Practical Streptomyces Genetics*; John Innes Foundation Norwich, 2000; Vol. 291.

(354) van Dissel, D.; van Wezel, G. P. Morphology-Driven Downscaling of *Streptomyces Lividans* to Micro-Cultivation. *Antonie van Leeuwenhoek* **2018**, *111* (3), 457–469. https://doi.org/10.1007/s10482-017-0967-7.

(355) Čihák, M.; Kameník, Z.; Šmídová, K.; Bergman, N.; Benada, O.; Kofroňová, O.; Petříčková, K.; Bobek, J. Secondary Metabolites Produced during the Germination of *Streptomyces Coelicolor*. *Front. Microbiol.* **2017**, *8*, 2495. https://doi.org/10.3389/fmicb.2017.02495.

(356) Kang, S. G.; Jin, W.; Bibb, M.; Lee, K. J. Actinorhodin and Undecylprodigiosin Production in Wild-Type and relA Mutant Strains of *Streptomyces Coelicolor A3(2)* Grown in Continuous Culture. *FEMS Microbiology Letters* **1998**, *168* (2), 221–226. https://doi.org/10.1111/j.1574-6968.1998.tb13277.x.

(357) Zhang, H.; Zhan, J.; Su, K.; Zhang, Y. A Kind of Potential Food Additive Produced by *Streptomyces Coelicolor*: Characteristics of Blue Pigment and Identification of a Novel Compound, λ-Actinorhodin. *Food Chemistry* **2006**, *95* (2), 186–192. https://doi.org/10.1016/j.foodchem.2004.12.028.

(358) Heinisch, S.; D'Attoma, A.; Grivel, C. Effect of pH Additive and Column Temperature on Kinetic Performance of Two Different Sub-2μm Stationary Phases for Ultrafast Separation of Charged Analytes. *Journal of Chromatography A* **2012**, *1228*, 135–147. https://doi.org/10.1016/j.chroma.2011.08.041.

(359) Bellin, D. L.; Sakhtah, H.; Rosenstein, J. K.; Levine, P. M.; Thimot, J.; Emmett, K.; Dietrich, L. E. P.; Shepard, K. L. Integrated Circuit-Based Electrochemical Sensor for Spatially Resolved Detection of Redox-Active Metabolites in Biofilms. *Nat Commun* **2014**, *5* (1), 3256. https://doi.org/10.1038/ncomms4256.

(360) Mazur, B.; Haroon, Y. Redox Mode Electrochemical Detection Approach with Chemically Modified Electrodes for the Measurement of Frenolicin B (Antibiotic) and Related Compounds in Poultry Feed. *J. Agric. Food Chem.* **1995**, *43* (12), 3042–3045. https://doi.org/10.1021/jf00060a010.

(361) Dreyer, D. R.; Miller, D. J.; Freeman, B. D.; Paul, D. R.; Bielawski, C. W. Elucidating the Structure of Poly(Dopamine). *Langmuir* **2012**, *28* (15), 6428–6435. https://doi.org/10.1021/la204831b.

(362) Longatte, G.; Buriez, O.; Labbé, E.; Guille-Collignon, M.; Lemaître, F. Electrochemical Behavior of Quinones Classically Used for Bioenergetical

Applications: Considerations and Insights about the Anodic Side. *ChemElectroChem* **2024**, e202300542. https://doi.org/10.1002/celc.202300542.

(363) Silva, T. L.; De Azevedo, M. D. L. S. G.; Ferreira, F. R.; Santos, D. C.; Amatore, C.; Goulart, M. O. F. Quinone-Based Molecular Electrochemistry and Their Contributions to Medicinal Chemistry: A Look at the Present and Future. *Current Opinion in Electrochemistry* **2020**, *24*, 79–87. https://doi.org/10.1016/j.coelec.2020.06.011.

(364) Frontana, C.; González, I. Revisiting the Effects of the Molecular Structure in the Kinetics of Electron Transfer of Quinones: Kinetic Differences in Structural Isomers. *Journal of the Mexican Chemical Society* **2008**, *52* (1), 11–18.

(365) Prince, R. C.; Dutton, P. L.; Gunner, M. R. The Aprotic Electrochemistry of Quinones. *Biochimica et Biophysica Acta (BBA) - Bioenergetics* **2022**, *1863* (6), 148558. https://doi.org/10.1016/j.bbabio.2022.148558.

(366) Hubig, S. M.; Rathore, R.; Kochi, J. K. Steric Control of Electron Transfer. Changeover from Outer-Sphere to Inner-Sphere Mechanisms in Arene/Quinone Redox Pairs. *J. Am. Chem. Soc.* **1999**, *121* (4), 617–626. https://doi.org/10.1021/ja9831002.

(367) Yang, X.; Wang, Y.; Zhang, C.; Fang, T.; Zhou, L.; Zhang, W.; Xu, J. Steric Effects of Substituents of Quinones on the Oxygenation of Ethylbenzene Catalyzed by NHPI/Quinone and the Catalytic Oxidation of Ascorbate. *J of Physical Organic Chem* **2011**, *24* (8), 693–697. https://doi.org/10.1002/poc.1810.

(368) Bui, A. T.; Hartley, N. A.; Thom, A. J. W.; Forse, A. C. Trade-Off between Redox Potential and the Strength of Electrochemical CO_2 Capture in Quinones. *J. Phys. Chem. C* **2022**, *126* (33), 14163–14172. https://doi.org/10.1021/acs.jpcc.2c03752.

(369) Merck. *LC-MS Contaminants*; Technical Bulletin TP6453ENEU Ver. 2.0 2016-00149; 2017.

(370) Abbas, A. S.; Edwards, C. Effects of Metals on *Streptomyces Coelicolor* Growth and Actinorhodin Production. *Appl Environ Microbiol* **1990**, *56* (3), 675–680. https://doi.org/10.1128/aem.56.3.675-680.1990.

(371) Wang, G.; Inaoka, T.; Okamoto, S.; Ochi, K. A Novel Insertion Mutation in *Streptomyces Coelicolor* Ribosomal S12 Protein Results in Paromomycin Resistance and Antibiotic Overproduction. *Antimicrob Agents Chemother* **2009**, *53* (3), 1019–1026. https://doi.org/10.1128/AAC.00388-08.

(372) Nass, N. M.; Farooque, S.; Hind, C.; Wand, M. E.; Randall, C. P.; Sutton, J. M.; Seipke, R. F.; Rayner, C. M.; O'Neill, A. J. Revisiting Unexploited Antibiotics in Search of New Antibacterial Drug Candidates: The Case of γ-Actinorhodin. *Sci Rep* **2017**, *7* (1), 17419. https://doi.org/10.1038/s41598-017-17232-1.

(373) Butler, M. J.; Bruheim, P.; Jovetic, S.; Marinelli, F.; Postma, P. W.; Bibb, M. J. Engineering of Primary Carbon Metabolism for Improved Antibiotic Production in *Streptomyces Lividans*. *Appl Environ Microbiol* **2002**, *68* (10), 4731–4739. https://doi.org/10.1128/AEM.68.10.4731-4739.2002.

(374) Snyder, L. R. Classification of the Solvent Properties of Common Liquids. *Journal of Chromatography A* **1974**, *92* (2), 223–230. https://doi.org/10.1016/S0021-9673(00)85732-5.

(375) Sandford, C.; A. Edwards, M.; J. Klunder, K.; P. Hickey, D.; Li, M.; Barman, K.; S. Sigman, M.; S. White, H.; D. Minteer, S. A Synthetic Chemist's Guide to Electroanalytical Tools for Studying Reaction Mechanisms. *Chemical Science* **2019**, *10* (26), 6404–6422. https://doi.org/10.1039/C9SC01545K.

(376) Hannah, S.; Dobrea, A.; Lasserre, P.; Blair, E. O.; Alcorn, D.; Hoskisson, P. A.; Corrigan, D. K. Development of a Rapid, Antimicrobial Susceptibility Test for *E. Coli* Based on Low-Cost, Screen-Printed Electrodes. *Biosensors* **2020**, *10* (11), 153. https://doi.org/10.3390/bios10110153.

(377) David Dunphy, R.; Lasserre, P.; Riordan, L.; R. Duncan, K.; McCormick, C.; Murray, P.; K. Corrigan, D. Combining Hyperspectral Imaging and Electrochemical Sensing for Detection of *Pseudomonas Aeruginosa* through Pyocyanin Production. *Sensors & Diagnostics* **2022**, *1* (4), 841–850. https://doi.org/10.1039/D2SD00044J.

(378) Raykova, M. R.; McGuire, K.; Peveler, W. J.; Corrigan, D. K.; Henriquez, F. L.; Ward, A. C. Towards Direct Detection of Tetracycline Residues in Milk with a Gold Nanostructured Electrode. *PLOS ONE* **2023**, *18* (6), e0287824. https://doi.org/10.1371/journal.pone.0287824.

(379) Trujillo-Rodríguez, M. J.; Nan, H.; Varona, M.; Emaus, M. N.; Souza, I. D.; Anderson, J. L. Advances of Ionic Liquids in Analytical Chemistry. *Anal. Chem.* **2019**, *91* (1), 505–531. https://doi.org/10.1021/acs.analchem.8b04710.

(380) Oziat, J.; Babin, T.; Gougis, M.; Malliaras, G. G.; Mailley, P. Electrochemical Detection of Redox Molecules Secreted by *Pseudomonas Aeruginosa* – Part 2: Enhanced Detection Owing to PEDOT:PSS Electrode Structuration. *Bioelectrochemistry* **2023**, *154*, 108538. https://doi.org/10.1016/j.bioelechem.2023.108538.

(381) Oziat, J.; Cohu, T.; Elsen, S.; Gougis, M.; Malliaras, G. G.; Mailley, P. Electrochemical Detection of Redox Molecules Secreted by *Pseudomonas Aeruginosa* – Part 1: Electrochemical Signatures of Different Strains. *Bioelectrochemistry* **2021**, *140*, 107747. https://doi.org/10.1016/j.bioelechem.2021.107747.

(382) Schneider, S.; Ettenauer, J.; Pap, I.-J.; Aspöck, C.; Walochnik, J.; Brandl, M. Main Metabolites of *Pseudomonas Aeruginosa*: A Study of Electrochemical Properties. *Sensors* **2022**, *22* (13), 4694. https://doi.org/10.3390/s22134694.

(383) Joosten, F.; Parrilla, M.; van Nuijs, A. L. N.; Ozoemena, K. I.; De Wael, K. Electrochemical Detection of Illicit Drugs in Oral Fluid: Potential for Forensic Drug Testing. *Electrochimica Acta* **2022**, *436*, 141309. https://doi.org/10.1016/j.electacta.2022.141309.

(384) Lee, I.; Probst, D.; Klonoff, D.; Sode, K. Continuous Glucose Monitoring Systems - Current Status and Future Perspectives of the Flagship Technologies in Biosensor Research. *Biosensors and Bioelectronics* **2021**, *181*, 113054. https://doi.org/10.1016/j.bios.2021.113054.

(385) Kumar, N.; Shetti, N. P.; Jagannath, S.; Aminabhavi, T. M. Electrochemical Sensors for the Detection of SARS-CoV-2 Virus. *Chemical Engineering Journal* **2022**, *430*, 132966. https://doi.org/10.1016/j.cej.2021.132966.

(386) Hug, J. J.; Bader, C. D.; Remškar, M.; Cirnski, K.; Müller, R. Concepts and Methods to Access Novel Antibiotics from Actinomycetes. *Antibiotics* **2018**, *7* (2), 44. https://doi.org/10.3390/antibiotics7020044.

(387) Hopwood, D. A. Genetics of Antibiotic Production by Actinomycetes. *Journal of Natural Products* **1979**, *42* (6), 596–602.

(388) Wilkinson, J. L.; Boxall, A. B. A.; Kolpin, D. W.; Leung, K. M. Y.; Lai, R. W. S.; Galbán-Malagón, C.; Adell, A. D.; Mondon, J.; Metian, M.; Marchant, R. A.; Bouzas-Monroy, A.; Cuni-Sanchez, A.; Coors, A.; Carriquiriborde, P.; Rojo, M.; Gordon, C.; Cara, M.; Moermond, M.; Luarte, T.; Petrosyan, V.; Perikhanyan, Y.; Mahon, C. S.; McGurk, C. J.; Hofmann, T.; Kormoker, T.; Iniguez, V.; Guzman-Otazo, J.; Tavares, J. L.; Gildasio De Figueiredo, F.; Razzolini, M. T. P.; Dougnon, V.; Gbaguidi, G.; Traoré, O.; Blais, J. M.; Kimpe, L. E.; Wong, M.; Wong, D.; Ntchantcho, R.; Pizarro, J.; Ying, G.-G.; Chen, C.-E.; Páez, M.; Martínez-Lara, J.; Otamonga, J.-P.; Poté, J.; Ifo, S. A.; Wilson, P.; Echeverría-Sáenz, S.; Udikovic-Kolic, N.; Milakovic, M.; Fatta-Kassinos, D.; Ioannou-Ttofa, L.; Belušová, V.; Vymazal, J.; Cárdenas-Bustamante, M.; Kassa, B. A.; Garric, J.; Chaumot, A.; Gibba, P.; Kunchulia, I.; Seidensticker, S.; Lyberatos, G.; Halldórsson, H. P.; Melling, M.; Shashidhar, T.; Lamba, M.; Nastiti, A.; Supriatin, A.; Pourang, N.; Abedini, A.; Abdullah, O.; Gharbia, S. S.; Pilla, F.; Chefetz, B.; Topaz, T.; Yao, K. M.; Aubakirova, B.; Beisenova, R.; Olaka, L.; Mulu, J. K.; Chatanga, P.; Ntuli, V.; Blama, N. T.; Sherif, S.; Aris, A. Z.; Looi, L. J.; Niang, M.; Traore, S. T.; Oldenkamp, R.; Ogunbanwo, O.; Ashfaq, M.; Iqbal, M.; Abdeen, Z.; O'Dea, A.; Morales-Saldaña, J. M.; Custodio, M.; De La Cruz, H.; Navarrete, I.; Carvalho, F.; Gogra, A. B.; Koroma, B. M.; Cerkvenik-Flajs, V.; Gombač, M.; Thwala, M.; Choi, K.; Kang, H.; Ladu, J. L. C.; Rico, A.; Amerasinghe, P.; Sobek, A.; Horlitz, G.; Zenker, A. K.; King, A. C.; Jiang, J.-J.; Kariuki, R.; Tumbo, M.; Tezel, U.; Onay, T. T.; Lejju, J. B.; Vystavna, Y.; Vergeles, Y.; Heinzen, H.; Pérez-Parada, A.; Sims, D. B.; Figy, M.; Good, D.; Teta, C. Pharmaceutical Pollution of the World's Rivers. *Proc. Natl. Acad. Sci. U.S.A.* **2022**, *119* (8), e2113947119. https://doi.org/10.1073/pnas.2113947119.

(389) Murray, A. K.; Stanton, I. C.; Wright, J.; Zhang, L.; Snape, J.; Gaze, W. H. The 'SELection End Points in Communities of bacTeria' (SELECT) Method: A Novel Experimental Assay to Facilitate Risk Assessment of Selection for Antimicrobial Resistance in the Environment. *Environmental Health Perspectives 128* (10), 107007. https://doi.org/10.1289/EHP6635.

(390) Daprà, J.; Lauridsen, L. H.; Nielsen, A. T.; Rozlosnik, N. Comparative Study on Aptamers as Recognition Elements for Antibiotics in a Label-Free All-Polymer Biosensor. *Biosensors and Bioelectronics* **2013**, *43*, 315–320. https://doi.org/10.1016/j.bios.2012.12.058.

(391) Grillon, A.; Schramm, F.; Kleinberg, M.; Jehl, F. Comparative Activity of Ciprofloxacin, Levofloxacin and Moxifloxacin against *Klebsiella Pneumoniae*, *Pseudomonas Aeruginosa* and *Stenotrophomonas Maltophilia* Assessed by

Minimum Inhibitory Concentrations and Time-Kill Studies. *PLoS ONE* **2016**, *11* (6), e0156690. https://doi.org/10.1371/journal.pone.0156690.

(392) Rudnicki, K.; Sipa, K.; Brycht, M.; Borgul, P.; Skrzypek, S.; Poltorak, L. Electrochemical Sensing of Fluoroquinolone Antibiotics. *TrAC Trends in Analytical Chemistry* **2020**, *128*, 115907. https://doi.org/10.1016/j.trac.2020.115907.

(393) Li, J.; Xue, Q.; Chen, T.; Liu, F.; Wang, Q.; Chang, C.; Lu, X.; Zhou, T.; Niwa, O. The Influence Mechanism of the Molecular Structure on the Peak Current and Peak Potential in Electrochemical Detection of Typical Quinolone Antibiotics. *Phys. Chem. Chem. Phys.* **2021**, *23* (25), 13873–13877. https://doi.org/10.1039/D1CP01358K.

(394) Majdinasab, M.; Mitsubayashi, K.; Marty, J. L. Optical and Electrochemical Sensors and Biosensors for the Detection of Quinolones. *Trends in Biotechnology* **2019**, *37* (8), 898–915. https://doi.org/10.1016/j.tibtech.2019.01.004.

(395) *Moxifloxacin*. https://go.drugbank.com/drugs/DB00218 (accessed 2023-08-28).

(396) World Health Organisation. *Global Tuberculosis Report 2020*; Geneva: World Health Organization, 2020.

(397) WHO Expert Committee on the Selection and Use of Essential Medicines. *World Health Organization Model List of Essential Medicines – 23rd List, 2023.*; World Health Organization: Geneva, 2023.

(398) Vanino, E.; Granozzi, B.; Akkerman, O. W.; Munoz-Torrico, M.; Palmieri, F.; Seaworth, B.; Tiberi, S.; Tadolini, M. Update of Drug-Resistant Tuberculosis Treatment Guidelines: A Turning Point. *International Journal of Infectious Diseases* **2023**, *130*, S12–S15. https://doi.org/10.1016/j.ijid.2023.03.013.

(399) Baraldi, E.; Ciabuschi, F.; Fratocchi, L. The Pros and Cons of Reshoring to Address the Problems of Shortages in Global Pharmaceutical Value Chains: The Case of Antibiotics. *JGOSS* **2023**, *16* (3), 618–640. https://doi.org/10.1108/JGOSS-11-2021-0092.

(400) Guerin, P. J.; Singh-Phulgenda, S.; Strub-Wourgaft, N. The Consequence of COVID-19 on the Global Supply of Medical Products: Why Indian Generics Matter for the World? *F1000Res* **2020**, *9*, 225. https://doi.org/10.12688/f1000research.23057.1.

(401) *International Instruments on the Use of Antimicrobials across the Human, Animal and Plant Sectors*; World Health Organization, Food and Agriculture Organization, World Organisation for Animal Health, 2020. https://www.who.int/publications-detail-redirect/9789240013964 (accessed 2023-07-20).

(402) Kudłak, B.; Wieczerzak, M. Aptamer Based Tools for Environmental and Therapeutic Monitoring: A Review of Developments, Applications, Future Perspectives. *Critical Reviews in Environmental Science and Technology* **2020**, *50* (8), 816–867. https://doi.org/10.1080/10643389.2019.1634457.

(403) Mehlhorn, A.; Rahimi, P.; Joseph, Y. Aptamer-Based Biosensors for Antibiotic Detection: A Review. *Biosensors* **2018**, *8* (2), 54. https://doi.org/10.3390/bios8020054.

(404) Shehata, M.; Fekry, A. M.; Walcarius, A. Moxifloxacin Hydrochloride Electrochemical Detection at Gold Nanoparticles Modified Screen-Printed Electrode. *Sensors* **2020**, *20* (10), 2797. https://doi.org/10.3390/s20102797.

(405) Gavrilaș, S.; Ursachi, C. Ștefan; Perța-Crișan, S.; Munteanu, F.-D. Recent Trends in Biosensors for Environmental Quality Monitoring. *Sensors* **2022**, *22* (4), 1513. https://doi.org/10.3390/s22041513.

(406) Evtugyn, G.; Porfireva, A.; Tsekenis, G.; Oravczova, V.; Hianik, T. Electrochemical Aptasensors for Antibiotics Detection: Recent Achievements and Applications for Monitoring Food Safety. *Sensors* **2022**, *22* (10), 3684. https://doi.org/10.3390/s22103684.

(407) Zhang, S.; Hu, X.; Yang, X.; Sun, Q.; Xu, X.; Liu, X.; Shen, G.; Lu, J.; Shen, G.; Yu, R. Background Eliminated Signal-on Electrochemical Aptasensing Platform for Highly Sensitive Detection of Protein. *Biosensors and Bioelectronics* **2015**, *66*, 363–369. https://doi.org/10.1016/j.bios.2014.11.044.

(408) John Ho, L. S.; Fogel, R.; Limson, J. L. Generation and Screening of Histamine-Specific Aptamers for Application in a Novel Impedimetric Aptamer-Based Sensor. *Talanta* **2020**, *208*, 120474. https://doi.org/10.1016/j.talanta.2019.120474.

(409) Oberhaus, F. V.; Frense, D.; Beckmann, D. Immobilization Techniques for Aptamers on Gold Electrodes for the Electrochemical Detection of Proteins: A Review. *Biosensors* **2020**, *10* (5), 45. https://doi.org/10.3390/bios10050045.

(410) Strong, M. E.; Richards, J. R.; Torres, M.; Beck, C. M.; La Belle, J. T. Faradaic Electrochemical Impedance Spectroscopy for Enhanced Analyte Detection in Diagnostics. *Biosensors and Bioelectronics* **2021**, *177*, 112949. https://doi.org/10.1016/j.bios.2020.112949.

(411) Niegowska, M.; Sanseverino, I.; Navarro, A.; Lettieri, T. Knowledge Gaps in the Assessment of Antimicrobial Resistance in Surface Waters. *FEMS Microbiology Ecology* **2021**, *97* (11), fiab140. https://doi.org/10.1093/femsec/fiab140.

(412) Grabowska, I.; Hepel, M.; Kurzątkowska-Adaszyńska, K. Advances in Design Strategies of Multiplex Electrochemical Aptasensors. *Sensors* **2021**, *22* (1), 161. https://doi.org/10.3390/s22010161.

(413) Ellington, A. D.; Szostak, J. W. *In Vitro* Selection of RNA Molecules That Bind Specific Ligands. *Nature* **1990**, *346* (6287), 818–822. https://doi.org/10.1038/346818a0.

(414) Ellington, A. D.; Szostak, J. W. Selection *in Vitro* of Single-Stranded DNA Molecules That Fold into Specific Ligand-Binding Structures. *Nature* **1992**, *355* (6363), 850–852. https://doi.org/10.1038/355850a0.

(415) Ziółkowski, R.; Jarczewska, M.; Górski, Ł.; Malinowska, E. From Small Molecules toward Whole Cells Detection: Application of Electrochemical Aptasensors in Modern Medical Diagnostics. *Sensors* **2021**, *21* (3), 724. https://doi.org/10.3390/s21030724.

(416) Yang, S.; Li, H.; Xu, L.; Deng, Z.; Han, W.; Liu, Y.; Jiang, W.; Zu, Y. Oligonucleotide Aptamer-Mediated Precision Therapy of Hematological Malignancies. *Molecular Therapy - Nucleic Acids* **2018**, *13*, 164–175. https://doi.org/10.1016/j.omtn.2018.08.023.

(417) Amor-Gutiérrez, O.; Selvolini, G.; Fernández-Abedul, M. T.; de la Escosura-Muñiz, A.; Marrazza, G. Folding-Based Electrochemical Aptasensor for the Determination of β-Lactoglobulin on Poly-L-Lysine Modified Graphite Electrodes. *Sensors* **2020**, *20* (8), 2349. https://doi.org/10.3390/s20082349.

(418) Hasegawa, H.; Savory, N.; Abe, K.; Ikebukuro, K. Methods for Improving Aptamer Binding Affinity. *Molecules* **2016**, *21* (4), 421. https://doi.org/10.3390/molecules21040421.

(419) Xu, R.; Cheng, Y.; Li, X.; Zhang, Z.; Zhu, M.; Qi, X.; Chen, L.; Han, L. Aptamer-Based Signal Amplification Strategies Coupled with Microchips for High-Sensitivity Bioanalytical Applications: A Review. *Analytica Chimica Acta* **2022**, *1209*, 339893. https://doi.org/10.1016/j.aca.2022.339893.

(420) Miodek, A.; Regan, E.; Bhalla, N.; Hopkins, N.; Goodchild, S.; Estrela, P. Optimisation and Characterisation of Anti-Fouling Ternary SAM Layers for Impedance-Based Aptasensors. *Sensors* **2015**, *15* (10), 25015–25032. https://doi.org/10.3390/s151025015.

(421) Fang, L.; Liao, X.; Jia, B.; Shi, L.; Kang, L.; Zhou, L.; Kong, W. Recent Progress in Immunosensors for Pesticides. *Biosensors and Bioelectronics* **2020**, *164*, 112255. https://doi.org/10.1016/j.bios.2020.112255.

(422) Li, L.; Xu, S.; Yan, H.; Li, X.; Yazd, H. S.; Li, X.; Huang, T.; Cui, C.; Jiang, J.; Tan, W. Nucleic Acid Aptamers for Molecular Diagnostics and Therapeutics: Advances and Perspectives. *Angew. Chem. Int. Ed.* **2021**, *60* (5), 2221–2231. https://doi.org/10.1002/anie.202003563.

(423) Su, C.-H.; Tsai, M.-H.; Lin, C.-Y.; Ma, Y.-D.; Wang, C.-H.; Chung, Y.-D.; Lee, G.-B. Dual Aptamer Assay for Detection of *Acinetobacter Baumannii* on an Electromagnetically-Driven Microfluidic Platform. *Biosensors and Bioelectronics* **2020**, *159*, 112148. https://doi.org/10.1016/j.bios.2020.112148.

(424) Szeitner, Z.; András, J.; Gyurcsányi, R. E.; Mészáros, T. Is Less More? Lessons from Aptamer Selection Strategies. *Journal of Pharmaceutical and Biomedical Analysis* **2014**, *101*, 58–65. https://doi.org/10.1016/j.jpba.2014.04.018.

(425) Odeh, F.; Nsairat, H.; Alshaer, W.; Ismail, M. A.; Esawi, E.; Qaqish, B.; Bawab, A. A.; Ismail, S. I. Aptamers Chemistry: Chemical Modifications and Conjugation Strategies. *Molecules* **2019**, *25* (1), 3. https://doi.org/10.3390/molecules25010003.

(426) Agnello, L.; Camorani, S.; Fedele, M.; Cerchia, L. Aptamers and Antibodies: Rivals or Allies in Cancer Targeted Therapy? *Exploration of Targeted Anti-tumor Therapy* **2021**. https://doi.org/10.37349/etat.2021.00035.

(427) Li, L.; Xu, S.; Yan, H.; Li, X.; Yazd, H. S.; Li, X.; Huang, T.; Cui, C.; Jiang, J.; Tan, W. Nucleic Acid Aptamers for Molecular Diagnostics and Therapeutics: Advances and Perspectives. *Angewandte Chemie International Edition* **2021**, *60* (5), 2221–2231. https://doi.org/10.1002/anie.202003563.

(428) Sullivan, M. V.; Allabush, F.; Bunka, D.; Tolley, A.; Mendes, P. M.; Tucker, J. H. R.; Turner, N. W. Hybrid Aptamer-Molecularly Imprinted Polymer (AptaMIP) Nanoparticles Selective for the Antibiotic Moxifloxacin. *Polym. Chem.* **2021**, *12* (30), 4394–4405. https://doi.org/10.1039/D1PY00607J.

(429) Lasserre, P.; Balansethupathy, B.; Vezza, V. J.; Butterworth, A.; Macdonald, A.; Blair, E. O.; McAteer, L.; Hannah, S.; Ward, A. C.; Hoskisson, P. A.; Longmuir, A.; Setford, S.; Farmer, E. C. W.; Murphy, M. E.; Flynn, H.; Corrigan, D. K. SARS-CoV-2 Aptasensors Based on Electrochemical Impedance Spectroscopy and Low-Cost Gold Electrode Substrates. *Anal Chem* **2022**, *94* (4), 2126–2133. https://doi.org/10.1021/acs.analchem.1c04456.

(430) Fischer, L. M.; Tenje, M.; Heiskanen, A. R.; Masuda, N.; Castillo, J.; Bentien, A.; Émneus, J.; Jakobsen, M. H.; Boisen, A. Gold Cleaning Methods for Electrochemical Detection Applications. *Microelectronic Engineering* **2009**, *86* (4–6), 1282–1285. https://doi.org/10.1016/j.mee.2008.11.045.

(431) Maugi, R.; Gamble, B.; Bunka, D.; Platt, M. A Simple Displacement Aptamer Assay on Resistive Pulse Sensor for Small Molecule Detection. *Talanta* **2021**, *225*, 122068. https://doi.org/10.1016/j.talanta.2020.122068.

(432) Xu, X.; Makaraviciute, A.; Kumar, S.; Wen, C.; Sjödin, M.; Abdurakhmanov, E.; Danielson, U. H.; Nyholm, L.; Zhang, Z. Structural Changes of Mercaptohexanol Self-Assembled Monolayers on Gold and Their Influence on Impedimetric Aptamer Sensors. *Anal. Chem.* **2019**, *91* (22), 14697–14704. https://doi.org/10.1021/acs.analchem.9b03946.

(433) Nakatsuka, N.; Yang, K.-A.; Abendroth, J. M.; Cheung, K. M.; Xu, X.; Yang, H.; Zhao, C.; Zhu, B.; Rim, Y. S.; Yang, Y.; Weiss, P. S.; Stojanović, M. N.; Andrews, A. M. Aptamer–Field-Effect Transistors Overcome Debye Length Limitations for Small-Molecule Sensing. *Science* **2018**, *362* (6412), 319–324. https://doi.org/10.1126/science.aao6750.

(434) Dalirirad, S.; Steckl, A. J. Lateral Flow Assay Using Aptamer-Based Sensing for on-Site Detection of Dopamine in Urine. *Analytical Biochemistry* **2020**, *596*, 113637. https://doi.org/10.1016/j.ab.2020.113637.

(435) Dalirirad, S.; Han, D.; Steckl, A. J. Aptamer-Based Lateral Flow Biosensor for Rapid Detection of Salivary Cortisol. *ACS Omega* **2020**, *5* (51), 32890–32898. https://doi.org/10.1021/acsomega.0c03223.

(436) Yang, K.-A.; Chun, H.; Zhang, Y.; Pecic, S.; Nakatsuka, N.; Andrews, A. M.; Worgall, T. S.; Stojanovic, M. N. High-Affinity Nucleic-Acid-Based Receptors for Steroids. *ACS Chem. Biol.* **2017**, *12* (12), 3103–3112. https://doi.org/10.1021/acschembio.7b00634.

(437) Huang, Y.; Yan, X.; Zhao, L.; Qi, X.; Wang, S.; Liang, X. An Aptamer Cocktail-Based Electrochemical Aptasensor for Direct Capture and Rapid Detection of Tetracycline in Honey. *Microchemical Journal* **2019**, *150*, 104179. https://doi.org/10.1016/j.microc.2019.104179.

(438) Shaha, C. K.; Saha, S.; Karmaker, S.; Saha, T. K. Efficient Removal of Moxifloxacin from Aqueous Solutions Using Sulfonated Graphene Oxide: Adsorption Mechanisms, Thermodynamics, and Reusability. *Journal of Water Process Engineering* **2024**, *67*, 106187. https://doi.org/10.1016/j.jwpe.2024.106187.

(439) Jia, A.; Wan, Y.; Xiao, Y.; Hu, J. Occurrence and Fate of Quinolone and Fluoroquinolone Antibiotics in a Municipal Sewage Treatment Plant. *Water Research* **2012**, *46* (2), 387–394. https://doi.org/10.1016/j.watres.2011.10.055.

(440) Antler, M. Gold in Electrical Contacts. *Gold Bull* **1971**, *4* (3), 42–46. https://doi.org/10.1007/BF03215140.

(441) Nano, A.; Furst, A. L.; Hill, M. G.; Barton, J. K. DNA Electrochemistry: Charge-Transport Pathways through DNA Films on Gold. *J. Am. Chem. Soc.* **2021**, *143* (30), 11631–11640. https://doi.org/10.1021/jacs.1c04713.

(442) Schoukroun-Barnes, L. R.; Wagan, S.; White, R. J. Enhancing the Analytical Performance of Electrochemical RNA Aptamer-Based Sensors for Sensitive Detection of Aminoglycoside Antibiotics. *Anal. Chem.* **2014**, *86* (2), 1131–1137. https://doi.org/10.1021/ac4029054.

(443) Sharma, H.; Mutharasan, R. Half Antibody Fragments Improve Biosensor Sensitivity without Loss of Selectivity. *Anal. Chem.* **2013**, *85* (4), 2472–2477. https://doi.org/10.1021/ac3035426.

(444) Liu, Y.; Canoura, J.; Alkhamis, O.; Xiao, Y. Immobilization Strategies for Enhancing Sensitivity of Electrochemical Aptamer-Based Sensors. *ACS Appl. Mater. Interfaces* **2021**, *13* (8), 9491–9499. https://doi.org/10.1021/acsami.0c20707.

(445) Butterworth, A.; Blues, E.; Williamson, P.; Cardona, M.; Gray, L.; Corrigan, D. K. SAM Composition and Electrode Roughness Affect Performance of a DNA Biosensor for Antibiotic Resistance. *Biosensors* **2019**, *9* (1), 22. https://doi.org/10.3390/bios9010022.

(446) Williamson, P.; Piskunen, P.; Ijäs, H.; Butterworth, A.; Linko, V.; Corrigan, D. K. Signal Amplification in Electrochemical DNA Biosensors Using Target-Capturing DNA Origami Tiles. *ACS Sens.* **2023**, *8* (4), 1471–1480. https://doi.org/10.1021/acssensors.2c02469.

(447) Keighley, S. D.; Li, P.; Estrela, P.; Migliorato, P. Optimization of DNA Immobilization on Gold Electrodes for Label-Free Detection by Electrochemical Impedance Spectroscopy. *Biosensors and Bioelectronics* **2008**, *23* (8), 1291–1297. https://doi.org/10.1016/j.bios.2007.11.012.

(448) Leung, K. K.; Downs, A. M.; Ortega, G.; Kurnik, M.; Plaxco, K. W. Elucidating the Mechanisms Underlying the Signal Drift of Electrochemical Aptamer-Based Sensors in Whole Blood. *ACS Sens.* **2021**, *6* (9), 3340–3347. https://doi.org/10.1021/acssensors.1c01183.

(449) Clark, V.; Pellitero, M. A.; Arroyo-Currás, N. Explaining the Decay of Nucleic Acid-Based Sensors under Continuous Voltammetric Interrogation. *Anal. Chem.* **2023**, *95* (11), 4974–4983. https://doi.org/10.1021/acs.analchem.2c05158.

(450) Shaver, A.; Curtis, S. D.; Arroyo-Currás, N. Alkanethiol Monolayer End Groups Affect the Long-Term Operational Stability and Signaling of Electrochemical, Aptamer-Based Sensors in Biological Fluids. *ACS Appl. Mater. Interfaces* **2020**, *12* (9), 11214–11223. https://doi.org/10.1021/acsami.9b22385.

(451) Vogiazi, V.; De La Cruz, A.; Heineman, W. R.; White, R. J.; Dionysiou, D. D. Effects of Experimental Conditions on the Signaling Fidelity of Impedance-Based Nucleic Acid Sensors. *Anal. Chem.* **2021**, *93* (2), 812–819. https://doi.org/10.1021/acs.analchem.0c03269.

(452) Ciani, I.; Schulze, H.; Corrigan, D. K.; Henihan, G.; Giraud, G.; Terry, J. G.; Walton, A. J.; Pethig, R.; Ghazal, P.; Crain, J.; Campbell, C. J.; Bachmann, T. T.; Mount, A. R. Development of Immunosensors for Direct Detection of Three Wound Infection Biomarkers at Point of Care Using Electrochemical Impedance Spectroscopy. *Biosensors and Bioelectronics* **2012**, *31* (1), 413–418. https://doi.org/10.1016/j.bios.2011.11.004.

(453) Vezza, V. J.; Butterworth, A.; Lasserre, P.; Blair, E. O.; MacDonald, A.; Hannah, S.; Rinaldi, C.; Hoskisson, P. A.; Ward, A. C.; Longmuir, A.; Setford, S.; Farmer, E. C. W.; Murphy, M. E.; Corrigan, D. K. An Electrochemical SARS-CoV-2 Biosensor Inspired by Glucose Test Strip Manufacturing Processes. *Chem. Commun.* **2021**, *57* (30), 3704–3707. https://doi.org/10.1039/D1CC00936B.

(454) Cecchet, F.; Marcaccio, M.; Margotti, M.; Paolucci, F.; Rapino, S.; Rudolf, P. Redox Mediation at 11-Mercaptoundecanoic Acid Self-Assembled Monolayers on Gold. *J. Phys. Chem. B* **2006**, *110* (5), 2241–2248. https://doi.org/10.1021/jp054290n.

(455) Dauphin-Ducharme, P.; Plaxco, K. W. Maximizing the Signal Gain of Electrochemical-DNA Sensors. *Anal. Chem.* **2016**, *88* (23), 11654–11662. https://doi.org/10.1021/acs.analchem.6b03227.

(456) Jolly, P.; Zhurauski, P.; Hammond, J. L.; Miodek, A.; Liébana, S.; Bertok, T.; Tkáč, J.; Estrela, P. Self-Assembled Gold Nanoparticles for Impedimetric and Amperometric Detection of a Prostate Cancer Biomarker. *Sensors and Actuators B: Chemical* **2017**, *251*, 637–643. https://doi.org/10.1016/j.snb.2017.05.040.

(457) Díaz-Fernández, A.; Miranda-Castro, R.; de-los-Santos-Álvarez, N.; Lobo-Castañón, M. J.; Estrela, P. Impedimetric Aptamer-Based Glycan PSA Score for Discrimination of Prostate Cancer from Other Prostate Diseases. *Biosensors and Bioelectronics* **2021**, *175*, 112872. https://doi.org/10.1016/j.bios.2020.112872.

(458) Ansah, F.; Krampa, F.; Donkor, J. K.; Owusu-Appiah, C.; Ashitei, S.; Kornu, V. E.; Danku, R. K.; Chirawurah, J. D.; Awandare, G. A.; Aniweh, Y.; Kanyong, P. Ultrasensitive Electrochemical Genosensors for Species-Specific Diagnosis of Malaria. *Electrochimica Acta* **2022**, *429*, 140988. https://doi.org/10.1016/j.electacta.2022.140988.

(459) Santarino, I. B.; Oliveira, S. C. B.; Oliveira-Brett, A. M. Protein Reducing Agents Dithiothreitol and Tris(2-Carboxyethyl)Phosphine Anodic Oxidation. *Electrochemistry Communications* **2012**, *23*, 114–117. https://doi.org/10.1016/j.elecom.2012.06.027.

(460) Vasilescu, A.; Nunes, G.; Hayat, A.; Latif, U.; Marty, J.-L. Electrochemical Affinity Biosensors Based on Disposable Screen-Printed Electrodes for Detection of Food Allergens. *Sensors* **2016**, *16* (11), 1863. https://doi.org/10.3390/s16111863.

(461) Rozenblum; Pollitzer; Radrizzani. Challenges in Electrochemical Aptasensors and Current Sensing Architectures Using Flat Gold Surfaces. *Chemosensors* **2019**, *7* (4), 57. https://doi.org/10.3390/chemosensors7040057.

(462) Sánchez-Salcedo, R.; Miranda-Castro, R.; de-los-Santos-Álvarez, N.; Lobo-Castañón, M. J.; Corrigan, D. K. Comparing Nanobody and Aptamer-Based Capacitive Sensing for Detection of Interleukin-6 (IL-6) at Physiologically Relevant Levels. *Anal Bioanal Chem* **2023**. https://doi.org/10.1007/s00216-023-04973-4.

(463) Garrote, B. L.; Santos, A.; Bueno, P. R. Perspectives on and Precautions for the Uses of Electric Spectroscopic Methods in Label-Free Biosensing Applications. *ACS Sens.* **2019**, *4* (9), 2216–2227. https://doi.org/10.1021/acssensors.9b01177.

(464) Savory, N.; Abe, K.; Sode, K.; Ikebukuro, K. Selection of DNA Aptamer against Prostate Specific Antigen Using a Genetic Algorithm and Application to Sensing. *Biosensors and Bioelectronics* **2010**, *26* (4), 1386–1391. https://doi.org/10.1016/j.bios.2010.07.057.

(465) Jolly, P.; Tamboli, V.; Harniman, R. L.; Estrela, P.; Allender, C. J.; Bowen, J. L. Aptamer–MIP Hybrid Receptor for Highly Sensitive Electrochemical Detection of Prostate Specific Antigen. *Biosensors and Bioelectronics* **2016**, *75*, 188–195. https://doi.org/10.1016/j.bios.2015.08.043.

(466) White, R. J.; Phares, N.; Lubin, A. A.; Xiao, Y.; Plaxco, K. W. Optimization of Electrochemical Aptamer-Based Sensors via Optimization of Probe Packing Density and Surface Chemistry. *Langmuir* **2008**, *24* (18), 10513–10518. https://doi.org/10.1021/la800801v.

(467) Ricci, F.; Lai, R. Y.; Heeger, A. J.; Plaxco, K. W.; Sumner, J. J. Effect of Molecular Crowding on the Response of an Electrochemical DNA Sensor. *Langmuir* **2007**, *23* (12), 6827–6834. https://doi.org/10.1021/la700328r.

(468) Slowey, A. J.; Marvin-DiPasquale, M. How to Overcome Inter-Electrode Variability and Instability to Quantify Dissolved Oxygen, Fe(II), Mn(II), and S(−II) in Undisturbed Soils and Sediments Using Voltammetry. *Geochem Trans* **2012**, *13* (1), 6. https://doi.org/10.1186/1467-4866-13-6.

(469) Ikebukuro, K.; Kiyohara, C.; Sode, K. Novel Electrochemical Sensor System for Protein Using the Aptamers in Sandwich Manner. *Biosensors and Bioelectronics* **2005**, *20* (10), 2168–2172. https://doi.org/10.1016/j.bios.2004.09.002.

(470) Radi, A.-E.; Acero Sánchez, J. L.; Baldrich, E.; O'Sullivan, C. K. Reusable Impedimetric Aptasensor. *Anal. Chem.* **2005**, *77* (19), 6320–6323. https://doi.org/10.1021/ac0505775.

(471) Wink, Th.; Van Zuilen, S. J.; Bult, A.; Van Bennekom, W. P. Self-Assembled Monolayers for Biosensors. *Analyst* **1997**, *122* (4), 43R-50R. https://doi.org/10.1039/a606964i.

(472) Brett, C. M. A. Perspectives and Challenges for Self-Assembled Layer-by-Layer Biosensor and Biomaterial Architectures. *Current Opinion in Electrochemistry* **2018**, *12*, 21–26. https://doi.org/10.1016/j.coelec.2018.11.004.

(473) Yan, X.; Tang, J.; Tanner, D.; Ulstrup, J.; Xiao, X. Direct Electrochemical Enzyme Electron Transfer on Electrodes Modified by Self-Assembled Molecular Monolayers. *Catalysts* **2020**, *10* (12), 1458. https://doi.org/10.3390/catal10121458.

(474) Tan, D. Antifouling Self-Assembled Monolayers for Designing of Electrochemical Biosensors. *Int. J. Electrochem. Sci.* **2020**, 9446–9458. https://doi.org/10.20964/2020.09.56.

(475) Arroyo-Currás, N.; Dauphin-Ducharme, P.; Scida, K.; Chávez, J. L. From the Beaker to the Body: Translational Challenges for Electrochemical, Aptamer-Based Sensors. *Anal. Methods* **2020**, *12* (10), 1288–1310. https://doi.org/10.1039/D0AY00026D.

(476) Inkpen, M. S.; Liu, Z.-F.; Li, H.; Campos, L. M.; Neaton, J. B.; Venkataraman, L. Non-Chemisorbed Gold–Sulfur Binding Prevails in Self-Assembled Monolayers. *Nat. Chem.* **2019**, *11* (4), 351–358. https://doi.org/10.1038/s41557-019-0216-y.

(477) Corrigan, D.; Vezza, V.; Schulze, H.; Bachmann, T.; Mount, A.; Walton, A.; Terry, J. A Microelectrode Array with Reproducible Performance Shows Loss of Consistency Following Functionalization with a Self-Assembled 6-Mercapto-1-Hexanol Layer. *Sensors* **2018**, *18* (6), 1891. https://doi.org/10.3390/s18061891.

(478) Rowe, A. A.; Chuh, K. N.; Lubin, A. A.; Miller, E. A.; Cook, B.; Hollis, D.; Plaxco, K. W. Electrochemical Biosensors Employing an Internal Electrode Attachment Site and Achieving Reversible, High Gain Detection of Specific Nucleic Acid Sequences. *Anal. Chem.* **2011**, *83* (24), 9462–9466. https://doi.org/10.1021/ac202171x.

(479) Bennett, H.-A.; Li, Y.; Yan, H. Thermal Treatment Affects Aptamers' Structural Profiles. *Bioorganic & Medicinal Chemistry Letters* **2023**, *82*, 129150. https://doi.org/10.1016/j.bmcl.2023.129150.

(480) Shaver, A.; Arroyo-Currás, N. The Challenge of Long-Term Stability for Nucleic Acid-Based Electrochemical Sensors. *Current Opinion in Electrochemistry* **2022**, *32*, 100902. https://doi.org/10.1016/j.coelec.2021.100902.

(481) Ruscito, A.; DeRosa, M. C. Small-Molecule Binding Aptamers: Selection Strategies, Characterization, and Applications. *Front. Chem.* **2016**, *4*. https://doi.org/10.3389/fchem.2016.00014.

(482) Zhao, Y.; Yavari, K.; Liu, J. Critical Evaluation of Aptamer Binding for Biosensor Designs. *TrAC Trends in Analytical Chemistry* **2022**, *146*, 116480. https://doi.org/10.1016/j.trac.2021.116480.

(483) Villalonga, A.; Pérez-Calabuig, A. M.; Villalonga, R. Electrochemical Biosensors Based on Nucleic Acid Aptamers. *Anal Bioanal Chem* **2020**, *412* (1), 55–72. https://doi.org/10.1007/s00216-019-02226-x.

(484) Mohammad Danesh, N.; Ramezani, M.; Sarreshtehdar Emrani, A.; Abnous, K.; Taghdisi, S. M. A Novel Electrochemical Aptasensor Based on Arch-Shape Structure of Aptamer-Complimentary Strand Conjugate and Exonuclease I for Sensitive Detection of Streptomycin. *Biosensors and Bioelectronics* **2016**, *75*, 123–128. https://doi.org/10.1016/j.bios.2015.08.017.

(485) Zhou, N.; Luo, J.; Zhang, J.; You, Y.; Tian, Y. A Label-Free Electrochemical Aptasensor for the Detection of Kanamycin in Milk. *Analytical Methods* **2015**, *7* (5), 1991–1996. https://doi.org/10.1039/C4AY02710H.

(486) Hu, X.; Goud, K. Y.; Kumar, V. S.; Catanante, G.; Li, Z.; Zhu, Z.; Marty, J. L. Disposable Electrochemical Aptasensor Based on Carbon Nanotubes- V2O5-Chitosan Nanocomposite for Detection of Ciprofloxacin. *Sensors and Actuators B: Chemical* **2018**, *268*, 278–286. https://doi.org/10.1016/j.snb.2018.03.155.

(487) Zhu, C.; Feng, Z.; Qin, H.; Chen, L.; Yan, M.; Li, L.; Qu, F. Recent Progress of SELEX Methods for Screening Nucleic Acid Aptamers. *Talanta* **2024**, *266*, 124998. https://doi.org/10.1016/j.talanta.2023.124998.

(488) Oberhaus, F. V.; Frense, D.; Beckmann, D. Immobilization Techniques for Aptamers on Gold Electrodes for the Electrochemical Detection of Proteins: A Review. *Biosensors* **2020**, *10* (5), 45. https://doi.org/10.3390/bios10050045.

(489) Manea, F.; Houillon, F. B.; Pasquato, L.; Scrimin, P. Nanozymes: Gold-Nanoparticle-Based Transphosphorylation Catalysts. *Angewandte Chemie International Edition* **2004**, *43* (45), 6165–6169. https://doi.org/10.1002/anie.200460649.

(490) Grieshaber, D.; MacKenzie, R.; Vörös, J.; Reimhult, E. Electrochemical Biosensors - Sensor Principles and Architectures. *Sensors* **2008**, *8* (3), 1400–1458. https://doi.org/10.3390/s80314000.

(491) Zhou, L.; Li, D.-J.; Gai, L.; Wang, J.-P.; Li, Y.-B. Electrochemical Aptasensor for the Detection of Tetracycline with Multi-Walled Carbon Nanotubes Amplification. *Sensors and Actuators B: Chemical* **2012**, *162* (1), 201–208. https://doi.org/10.1016/j.snb.2011.12.067.

(6) Dong, Y.; Zhang, T.; Lin, X.; Feng, J.; Luo, F.; Gao, H.; Wu, Y.; Deng, R.; He, Q. Graphene/Aptamer Probes for Small Molecule Detection: From *in Vitro* Test to in Situ Imaging. *Microchim Acta* **2020**, *187* (3), 179. https://doi.org/10.1007/s00604-020-4128-8.

(493) Wang, L.; Wu, A.; Wei, G. Graphene-Based Aptasensors: From Molecule–Interface Interactions to Sensor Design and Biomedical Diagnostics. *Analyst* **2018**, *143* (7), 1526–1543. https://doi.org/10.1039/C8AN00081F.

(494) Romanholo, P. V. V.; Razzino, C. A.; Raymundo-Pereira, P. A.; Prado, T. M.; Machado, S. A. S.; Sgobbi, L. F. Biomimetic Electrochemical Sensors: New Horizons and Challenges in Biosensing Applications. *Biosensors and Bioelectronics* **2021**, *185*, 113242. https://doi.org/10.1016/j.bios.2021.113242.

(495) Rozenblum; Pollitzer; Radrizzani. Challenges in Electrochemical Aptasensors and Current Sensing Architectures Using Flat Gold Surfaces. *Chemosensors* **2019**, *7* (4), 57. https://doi.org/10.3390/chemosensors7040057.

(496) Evtugyn, G.; Porfireva, A.; Tsekenis, G.; Oravczova, V.; Hianik, T. Electrochemical Aptasensors for Antibiotics Detection: Recent Achievements and Applications for Monitoring Food Safety. *Sensors* **2022**, *22* (10), 3684. https://doi.org/10.3390/s22103684.

(497) Arroyo-Currás, N.; Dauphin-Ducharme, P.; Scida, K.; Chávez, J. L. From the Beaker to the Body: Translational Challenges for Electrochemical, Aptamer-

Based Sensors. *Anal. Methods* **2020**, *12* (10), 1288–1310. https://doi.org/10.1039/D0AY00026D.

(498) Munteanu, F.-D.; Titoiu, A.; Marty, J.-L.; Vasilescu, A. Detection of Antibiotics and Evaluation of Antibacterial Activity with Screen-Printed Electrodes. *Sensors* **2018**, *18* (3), 901. https://doi.org/10.3390/s18030901.

(499) Shreffler, J.; Huecker, M. R. Diagnostic Testing Accuracy: Sensitivity, Specificity, Predictive Values and Likelihood Ratios. In *StatPearls*; StatPearls Publishing: Treasure Island (FL), 2024.

(500) Vessman, J.; Stefan, R. I.; Staden, J. F. van; Danzer, K.; Lindner, W.; Burns, D. T.; Fajgelj, A.; Müller, H. Selectivity in Analytical Chemistry (IUPAC Recommendations 2001). *Pure and Applied Chemistry* **2001**, *73* (8), 1381–1386. https://doi.org/10.1351/pac200173081381.

(501) Crapnell, R.; Hudson, A.; Foster, C.; Eersels, K.; Grinsven, B.; Cleij, T.; Banks, C.; Peeters, M. Recent Advances in Electrosynthesized Molecularly Imprinted Polymer Sensing Platforms for Bioanalyte Detection. *Sensors* **2019**, *19* (5), 1204. https://doi.org/10.3390/s19051204.

(502) Ali, G. K.; Omer, K. M. Molecular Imprinted Polymer Combined with Aptamer (MIP-Aptamer) as a Hybrid Dual Recognition Element for Bio(Chemical) Sensing Applications. Review. *Talanta* **2022**, *236*, 122878. https://doi.org/10.1016/j.talanta.2021.122878.

(503) Jolly, P.; Tamboli, V.; Harniman, R. L.; Estrela, P.; Allender, C. J.; Bowen, J. L. Aptamer–MIP Hybrid Receptor for Highly Sensitive Electrochemical Detection of Prostate Specific Antigen. *Biosensors and Bioelectronics* **2016**, *75*, 188–195. https://doi.org/10.1016/j.bios.2015.08.043.

(504) Tamboli, V. K.; Bhalla, N.; Jolly, P.; Bowen, C. R.; Taylor, J. T.; Bowen, J. L.; Allender, C. J.; Estrela, P. Hybrid Synthetic Receptors on MOSFET Devices for Detection of Prostate Specific Antigen in Human Plasma. *Anal. Chem.* **2016**, *88* (23), 11486–11490. https://doi.org/10.1021/acs.analchem.6b02619.

(505) Li, S.; Liu, C.; Yin, G.; Zhang, Q.; Luo, J.; Wu, N. Aptamer-Molecularly Imprinted Sensor Base on Electrogenerated Chemiluminescence Energy Transfer for Detection of Lincomycin. *Biosensors and Bioelectronics* **2017**, *91*, 687–691. https://doi.org/10.1016/j.bios.2017.01.038.

(506) Shahdost-fard, F.; Roushani, M. Impedimetric Detection of Trinitrotoluene by Using a Glassy Carbon Electrode Modified with a Gold Nanoparticle@fullerene Composite and an Aptamer-Imprinted Polydopamine. *Microchim Acta* **2017**, *184* (10), 3997–4006. https://doi.org/10.1007/s00604-017-2424-8.

(507) Li, S.; Li, J.; Luo, J.; Xu, Z.; Ma, X. A Microfluidic Chip Containing a Molecularly Imprinted Polymer and a DNA Aptamer for Voltammetric Determination of Carbofuran. *Microchim Acta* **2018**, *185* (6), 295. https://doi.org/10.1007/s00604-018-2835-1.

(508) Rad, A. O.; Azadbakht, A. An Aptamer Embedded in a Molecularly Imprinted Polymer for Impedimetric Determination of Tetracycline. *Microchim Acta* **2019**, *186* (2), 56. https://doi.org/10.1007/s00604-018-3123-9.

(509) Ghanbari, K.; Roushani, M. A Nanohybrid Probe Based on Double Recognition of an Aptamer MIP Grafted onto a MWCNTs-Chit Nanocomposite for Sensing

Hepatitis C Virus Core Antigen. *Sensors and Actuators B: Chemical* **2018**, *258*, 1066–1071. https://doi.org/10.1016/j.snb.2017.11.145.

(510) Roushani, M.; Rahmati, Z.; Hoseini, S. J.; Hashemi Fath, R. Impedimetric Ultrasensitive Detection of Chloramphenicol Based on Aptamer MIP Using a Glassy Carbon Electrode Modified by 3-Ampy-RGO and Silver Nanoparticle. *Colloids and Surfaces B: Biointerfaces* **2019**, *183*, 110451. https://doi.org/10.1016/j.colsurfb.2019.110451.

(511) Yang, S.; Teng, Y.; Cao, Q.; Bai, C.; Fang, Z.; Xu, W. Electrochemical Sensor Based on Molecularly Imprinted Polymer-Aptamer Hybrid Receptor for Voltammetric Detection of Thrombin. *J. Electrochem. Soc.* **2019**, *166* (2), B23–B28. https://doi.org/10.1149/2.0131902jes.

(512) Yarahmadi, S.; Azadbakht, A.; Derikvand, R. M. Hybrid Synthetic Receptor Composed of Molecularly Imprinted Polydopamine and Aptamers for Impedimetric Biosensing of Urea. *Microchim Acta* **2019**, *186* (2), 71. https://doi.org/10.1007/s00604-018-3180-0.

(513) Shen, M.; Kan, X. Aptamer and Molecularly Imprinted Polymer: Synergistic Recognition and Sensing of Dopamine. *Electrochimica Acta* **2021**, *367*, 137433. https://doi.org/10.1016/j.electacta.2020.137433.

(514) Mahmoud, A. M.; Alkahtani, S. A.; Alyami, B. A.; El-Wekil, M. M. Dual-Recognition Molecularly Imprinted Aptasensor Based on Gold Nanoparticles Decorated Carboxylated Carbon Nanotubes for Highly Selective and Sensitive Determination of Histamine in Different Matrices. *Analytica Chimica Acta* **2020**, *1133*, 58–65. https://doi.org/10.1016/j.aca.2020.08.001.

(515) You, M.; Yang, S.; An, Y.; Zhang, F.; He, P. A Novel Electrochemical Biosensor with Molecularly Imprinted Polymers and Aptamer-Based Sandwich Assay for Determining Amyloid-β Oligomer. *Journal of Electroanalytical Chemistry* **2020**, *862*, 114017. https://doi.org/10.1016/j.jelechem.2020.114017.

(516) Downs, A. M.; Gerson, J.; Leung, K. K.; Honeywell, K. M.; Kippin, T.; Plaxco, K. W. Improved Calibration of Electrochemical Aptamer-Based Sensors. *Sci Rep* **2022**, *12* (1), 5535. https://doi.org/10.1038/s41598-022-09070-7.

(517) Santos-Cancel, M.; Lazenby, R. A.; White, R. J. Rapid Two-Millisecond Interrogation of Electrochemical, Aptamer-Based Sensor Response Using Intermittent Pulse Amperometry. *ACS Sens.* **2018**, *3* (6), 1203–1209. https://doi.org/10.1021/acssensors.8b00278.

(518) White, R. J.; Phares, N.; Lubin, A. A.; Xiao, Y.; Plaxco, K. W. Optimization of Electrochemical Aptamer-Based Sensors via Optimization of Probe Packing Density and Surface Chemistry. *Langmuir* **2008**, *24* (18), 10513–10518. https://doi.org/10.1021/la800801v.

(519) Arroyo-Currás, N.; Dauphin-Ducharme, P.; Ortega, G.; Ploense, K. L.; Kippin, T. E.; Plaxco, K. W. Subsecond-Resolved Molecular Measurements in the Living Body Using Chronoamperometrically Interrogated Aptamer-Based Sensors. *ACS Sens.* **2018**, *3* (2), 360–366. https://doi.org/10.1021/acssensors.7b00787.

(520) Li, S.; Lin, L.; Chang, X.; Si, Z.; Plaxco, K. W.; Khine, M.; Li, H.; Xia, F. A Wrinkled Structure of Gold Film Greatly Improves the Signaling of Electrochemical

Aptamer-Based Biosensors. *RSC Adv.* **2021**, *11* (2), 671–677. https://doi.org/10.1039/D0RA09174J.

(521) Pellitero, M. A.; Arroyo-Currás, N. Study of Surface Modification Strategies to Create Glassy Carbon-Supported, Aptamer-Based Sensors for Continuous Molecular Monitoring. *Anal Bioanal Chem* **2022**, *414* (18), 5627–5641. https://doi.org/10.1007/s00216-022-04015-5.

(522) White, R. J.; Kallewaard, H. M.; Hsieh, W.; Patterson, A. S.; Kasehagen, J. B.; Cash, K. J.; Uzawa, T.; Soh, H. T.; Plaxco, K. W. Wash-Free, Electrochemical Platform for the Quantitative, Multiplexed Detection of Specific Antibodies. *Anal. Chem.* **2012**, *84* (2), 1098–1103. https://doi.org/10.1021/ac202757c.

(523) Poma, A.; Brahmbhatt, H.; Pendergraff, H. M.; Watts, J. K.; Turner, N. W. Generation of Novel Hybrid Aptamer–Molecularly Imprinted Polymeric Nanoparticles. *Advanced Materials* **2015**, *27* (4), 750–758. https://doi.org/10.1002/adma.201404235.

(524) Shin, B.; Park, C.; Park, W. Stress Responses Linked to Antimicrobial Resistance in *Acinetobacter* Species. *Appl Microbiol Biotechnol* **2020**, *104* (4), 1423–1435. https://doi.org/10.1007/s00253-019-10317-z.

(42) Kon, H.; Schwartz, D.; Temkin, E.; Carmeli, Y.; Lellouche, J. Rapid Identification of Capsulated *Acinetobacter Baumannii* Using a Density-Dependent Gradient Test. *BMC Microbiology* **2020**, *20* (1), 285. https://doi.org/10.1186/s12866-020-01971-9.

(43) Selvaraj, A.; Valliammai, A.; Sivasankar, C.; Suba, M.; Sakthivel, G.; Pandian, S. K. Antibiofilm and Antivirulence Efficacy of Myrtenol Enhances the Antibiotic Susceptibility of *Acinetobacter baumannii*. *Sci Rep* **2020**, *10* (1), 21975. https://doi.org/10.1038/s41598-020-79128-x.

(44) Yang, Q.; Olaifa, K.; Andrew, F. P.; Ajibade, P. A.; Ajunwa, O. M.; Marsili, E. Assessment of Physiological and Electrochemical Effects of a Repurposed Zinc Dithiocarbamate Complex on *Acinetobacter baumannii* Biofilms. *Sci Rep* **2022**, *12* (1), 11701. https://doi.org/10.1038/s41598-022-16047-z.

(45) Roy, S.; Chatterjee, S.; Bhattacharjee, A.; Chattopadhyay, P.; Saha, B.; Dutta, S.; Basu, S. Overexpression of Efflux Pumps, Mutations in the Pumps' Regulators, Chromosomal Mutations, and AAC(6')-Ib-Cr Are Associated With Fluoroquinolone Resistance in Diverse Sequence Types of Neonatal Septicaemic *Acinetobacter baumannii*: A 7-Year Single Center Study. *Frontiers in Microbiology* **2021**, *12*.

(529) Domingo-Roca, R.; Lasserre, P.; Riordan, L.; Macdonald, A. R.; Dobrea, A.; Duncan, K. R.; Hannah, S.; Murphy, M.; Hoskisson, P. A.; Corrigan, D. K. Rapid Assessment of Antibiotic Susceptibility Using a Fully 3D-Printed Impedance-Based Biosensor. *Biosensors and Bioelectronics: X* **2023**, *13*, 100308. https://doi.org/10.1016/j.biosx.2023.100308.

(49) Dahdouh, E.; Gómez-Gil, R.; Pacho, S.; Mingorance, J.; Daoud, Z.; Suárez, M. Clonality, Virulence Determinants, and Profiles of Resistance of Clinical *Acinetobacter baumannii* Isolates Obtained from a Spanish Hospital. *PLOS ONE* **2017**, *12* (4), e0176824. https://doi.org/10.1371/journal.pone.0176824.

(531) Wei, H.; Sun, J.-J.; Xie, Y.; Lin, C.-G.; Wang, Y.-M.; Yin, W.-H.; Chen, G.-N. Enhanced Electrochemical Performance at Screen-Printed Carbon Electrodes by a New Pretreating Procedure. *Analytica Chimica Acta* **2007**, *588* (2), 297–303. https://doi.org/10.1016/j.aca.2007.02.006.

(532) Yadav, A. K.; Verma, D.; Dalal, N.; Kumar, A.; Solanki, P. R. Molecularly Imprinted Polymer-Based Nanodiagnostics for Clinically Pertinent Bacteria and Virus Detection for Future Pandemics. *Biosensors and Bioelectronics: X* **2022**, *12*, 100257. https://doi.org/10.1016/j.biosx.2022.100257.

(533) Costerton, J. W.; Lewandowski, Z.; Caldwell, D. E.; Korber, D. R.; Lappin-Scott, H. M. MICROBIAL BIOFILMS. *Annu. Rev. Microbiol.* **1995**, *49* (1), 711–745. https://doi.org/10.1146/annurev.mi.49.100195.003431.

(534) National Biofilms Innovation Centre. *International Biofilm Markets and Infographics*. https://www.biofilms.ac.uk/international-biofilm-markets/ (accessed 2021-11-17).

(535) Subramanian, S.; Huiszoon, R. C.; Chu, S.; Bentley, W. E.; Ghodssi, R. Microsystems for Biofilm Characterization and Sensing – A Review. *Biofilm* **2020**, *2*, 100015. https://doi.org/10.1016/j.bioflm.2019.100015.

(536) Khatoon, Z.; McTiernan, C. D.; Suuronen, E. J.; Mah, T.-F.; Alarcon, E. I. Bacterial Biofilm Formation on Implantable Devices and Approaches to Its Treatment and Prevention. *Heliyon* **2018**, *4* (12), e01067. https://doi.org/10.1016/j.heliyon.2018.e01067.

(537) Yadav, M. K.; Vidal, J. E.; Song, J.-J. Chapter 2 - Microbial Biofilms on Medical Indwelling Devices. In *New and Future Developments in Microbial Biotechnology and Bioengineering: Microbial Biofilms*; Yadav, M. K., Singh, B. P., Eds.; Elsevier, 2020; pp 15–28. https://doi.org/10.1016/B978-0-444-64279-0.00002-5.

(538) Kour, D.; Kaur, T.; Fahliyani, S. A.; Rastegari, A. A.; Yadav, N.; Yadav, A. N. Microbial Biofilms in the Human: Diversity and Potential Significances in Health and Disease. In *New and Future Developments in Microbial Biotechnology and Bioengineering*; Elsevier, 2020; pp 89–124.

(539) Gedefie, A.; Demsiss, W.; Belete, M. A.; Kassa, Y.; Tesfaye, M.; Tilahun, M.; Bisetegn, H.; Sahle, Z. *Acinetobacter Baumannii* Biofilm Formation and Its Role in Disease Pathogenesis: A Review. *IDR* **2021**, *Volume 14*, 3711–3719. https://doi.org/10.2147/IDR.S332051.

(540) Behzadi, P.; Baráth, Z.; Gajdács, M. It's Not Easy Being Green: A Narrative Review on the Microbiology, Virulence and Therapeutic Prospects of Multidrug-Resistant *Pseudomonas Aeruginosa*. *Antibiotics* **2021**, *10* (1), 42. https://doi.org/10.3390/antibiotics10010042.

(541) Shetti, N. P.; Malode, S. J.; Roy, S.; Chandra, P.; Reddy, K. R.; Chatterjee, S. Electroanalytical Techniques for Investigating Biofilms: Applications in Biosensing and Biomolecular Interfacing. In *Nanomaterials in Diagnostic Tools and Devices*; Elsevier, 2020; pp 293–329. https://doi.org/10.1016/B978-0-12-817923-9.00011-0.

(542) Seneviratne, C. J.; Suriyanarayanan, T.; Widyarman, A. S.; Lee, L. S.; Lau, M.; Ching, J.; Delaney, C.; Ramage, G. Multi-Omics Tools for Studying Microbial

Biofilms: Current Perspectives and Future Directions. *Critical Reviews in Microbiology* **2020**, *46* (6), 759–778. https://doi.org/10.1080/1040841X.2020.1828817.

(543) Gędas, A.; Olszewska, M. A. Chapter 1 - Biofilm Formation and Resistance. In *Recent Trends in Biofilm Science and Technology*; Simoes, M., Borges, A., Chaves Simoes, L., Eds.; Academic Press, 2020; pp 1–21. https://doi.org/10.1016/B978-0-12-819497-3.00001-5.

(544) Hu, Y.; Han, X.; Shi, L.; Cao, B. Electrochemically Active Biofilm-Enabled Biosensors: Current Status and Opportunities for Biofilm Engineering. *Electrochimica Acta* **2022**, 140917.

(545) Cai, T.; Zhang, Y.; Wang, N.; Zhang, Z.; Lu, X.; Zhen, G. Electrochemically Active Microorganisms Sense Charge Transfer Resistance for Regulating Biofilm Electroactivity, Spatio-Temporal Distribution, and Catabolic Pathway. *Chemical Engineering Journal* **2022**, *442*, 136248.

(546) Li, S.-W.; Sheng, G.-P.; Cheng, Y.-Y.; Yu, H.-Q. Redox Properties of Extracellular Polymeric Substances (EPS) from Electroactive Bacteria. *Sci Rep* **2016**, *6* (1), 39098. https://doi.org/10.1038/srep39098.

(547) Paquete, C. M.; Rosenbaum, M. A.; Bañeras, L.; Rotaru, A.-E.; Puig, S. Leťs Chat: Communication between Electroactive Microorganisms. *Bioresource Technology* **2022**, 126705.

(548) Béchon, N.; Ghigo, J.-M. Gut Biofilms: *Bacteroides* as Model Symbionts to Study Biofilm Formation by Intestinal Anaerobes. *FEMS Microbiology Reviews* **2022**, *46* (2), fuab054. https://doi.org/10.1093/femsre/fuab054.

(549) Tumbarello, M.; Posteraro, B.; Trecarichi, E. M.; Fiori, B.; Rossi, M.; Porta, R.; De Gaetano Donati, K.; La Sorda, M.; Spanu, T.; Fadda, G.; Cauda, R.; Sanguinetti, M. Biofilm Production by *Candida* Species and Inadequate Antifungal Therapy as Predictors of Mortality for Patients with Candidemia. *J Clin Microbiol* **2007**, *45* (6), 1843–1850. https://doi.org/10.1128/JCM.00131-07.

(550) Uppuluri, P.; Srinivasan, A.; Ramasubramanian, A.; Lopez-Ribot, J. L. Effects of Fluconazole, Amphotericin B, and Caspofungin on *Candida Albicans* Biofilms under Conditions of Flow and on Biofilm Dispersion. *Antimicrob Agents Chemother* **2011**, *55* (7), 3591–3593. https://doi.org/10.1128/AAC.01701-10.

(551) Wong, G. C. L.; Antani, J. D.; Lele, P. P.; Chen, J.; Nan, B.; Kühn, M. J.; Persat, A.; Bru, J.-L.; Høyland-Kroghsbo, N. M.; Siryaporn, A.; Conrad, J. C.; Carrara, F.; Yawata, Y.; Stocker, R.; V Brun, Y.; Whitfield, G. B.; Lee, C. K.; de Anda, J.; Schmidt, W. C.; Golestanian, R.; O'Toole, G. A.; Floyd, K. A.; Yildiz, F. H.; Yang, S.; Jin, F.; Toyofuku, M.; Eberl, L.; Nomura, N.; Zacharoff, L. A.; El-Naggar, M. Y.; Yalcin, S. E.; Malvankar, N. S.; Rojas-Andrade, M. D.; Hochbaum, A. I.; Yan, J.; Stone, H. A.; Wingreen, N. S.; Bassler, B. L.; Wu, Y.; Xu, H.; Drescher, K.; Dunkel, J. Roadmap on Emerging Concepts in the Physical Biology of Bacterial Biofilms: From Surface Sensing to Community Formation. *Phys. Biol.* **2021**, *18* (5), 051501. https://doi.org/10.1088/1478-3975/abdc0e.

(552) Da Silva, R. A. G.; Afonina, I.; Kline, K. A. Eradicating Biofilm Infections: An Update on Current and Prospective Approaches. *Current Opinion in Microbiology* **2021**, *63*, 117–125. https://doi.org/10.1016/j.mib.2021.07.001.

(553) Li, P.; Yin, R.; Cheng, J.; Lin, J. Bacterial Biofilm Formation on Biomaterials and Approaches to Its Treatment and Prevention. *IJMS* **2023**, *24* (14), 11680. https://doi.org/10.3390/ijms241411680.

(554) Achinas, S.; Yska, S. K.; Charalampogiannis, N.; Krooneman, J.; Euverink, G. J. W. A Technological Understanding of Biofilm Detection Techniques: A Review. *Materials* **2020**, *13* (14), 3147. https://doi.org/10.3390/ma13143147.

(555) Olivares, E.; Badel-Berchoux, S.; Provot, C.; Jaulhac, B.; Prévost, G.; Bernardi, T.; Jehl, F. The BioFilm Ring Test: A Rapid Method for Routine Analysis of Pseudomonas Aeruginosa Biofilm Formation Kinetics. *J Clin Microbiol* **2016**, *54* (3), 657–661. https://doi.org/10.1128/JCM.02938-15.

(556) Magana, M.; Sereti, C.; Ioannidis, A.; Mitchell, C. A.; Ball, A. R.; Magiorkinis, E.; Chatzipanagiotou, S.; Hamblin, M. R.; Hadjifrangiskou, M.; Tegos, G. P. Options and Limitations in Clinical Investigation of Bacterial Biofilms. *Clin Microbiol Rev* **2018**, *31* (3), e00084-16. https://doi.org/10.1128/CMR.00084-16.

(557) Ceri, H.; Olson, M. E.; Stremick, C.; Read, R. R.; Morck, D.; Buret, A. The Calgary Biofilm Device: New Technology for Rapid Determination of Antibiotic Susceptibilities of Bacterial Biofilms. *J Clin Microbiol* **1999**, *37* (6), 1771–1776. https://doi.org/10.1128/JCM.37.6.1771-1776.1999.

(558) Stockert, J. C.; Horobin, R. W.; Colombo, L. L.; Blázquez-Castro, A. Tetrazolium Salts and Formazan Products in Cell Biology: Viability Assessment, Fluorescence Imaging, and Labeling Perspectives. *Acta Histochemica* **2018**, *120* (3), 159–167. https://doi.org/10.1016/j.acthis.2018.02.005.

(559) Yadav, M. K.; Song, J.-J.; Singh, B. P.; Vidal, J. E. Chapter 1 - Microbial Biofilms and Human Disease: A Concise Review. In *New and Future Developments in Microbial Biotechnology and Bioengineering: Microbial Biofilms*; Yadav, M. K., Singh, B. P., Eds.; Elsevier, 2020; pp 1–13. https://doi.org/10.1016/B978-0-444-64279-0.00001-3.

(560) Høiby, N.; Bjarnsholt, T.; Moser, C.; Bassi, G. L.; Coenye, T.; Donelli, G.; Hall-Stoodley, L.; Holá, V.; Imbert, C.; Kirketerp-Møller, K.; Lebeaux, D.; Oliver, A.; Ullmann, A. J.; Williams, C. ESCMID Guideline for the Diagnosis and Treatment of Biofilm Infections 2014. *Clinical Microbiology and Infection* **2015**, *21*, S1–S25. https://doi.org/10.1016/j.cmi.2014.10.024.

(561) Prinz, J.; Wink, M.; Neuhaus, S.; Grob, M. C.; Walt, H.; Bosshard, P. P.; Achermann, Y. Effective Biofilm Eradication on Orthopedic Implants with Methylene Blue Based Antimicrobial Photodynamic Therapy *in Vitro*. *Antibiotics* **2023**, *12* (1), 118. https://doi.org/10.3390/antibiotics12010118.

(562) Roberts, A. E. L.; Kragh, K. N.; Bjarnsholt, T.; Diggle, S. P. The Limitations of *in Vitro* Experimentation in Understanding Biofilms and Chronic Infection. *Journal of Molecular Biology* **2015**, *427* (23), 3646–3661. https://doi.org/10.1016/j.jmb.2015.09.002.

(563) Sauer, K.; Stoodley, P.; Goeres, D. M.; Hall-Stoodley, L.; Burmølle, M.; Stewart, P. S.; Bjarnsholt, T. The Biofilm Life Cycle: Expanding the Conceptual Model of

Biofilm Formation. *Nat Rev Microbiol* **2022**, *20* (10), 608–620. https://doi.org/10.1038/s41579-022-00767-0.

(564) World Health Organization. *Prioritization of Pathogens to Guide Discovery, Research and Development of New Antibiotics for Drug-Resistant Bacterial Infections, Including Tuberculosis.*; World Health Organization, 2017.

(565) Gandouzi, I.; Tertis, M.; Cernat, A.; Saidane-Mosbahi, D.; Ilea, A.; Cristea, C. A Nanocomposite Based on Reduced Graphene and Gold Nanoparticles for Highly Sensitive Electrochemical Detection of *Pseudomonas Aeruginosa* through Its Virulence Factors. *Materials* **2019**, *12* (7), 1180. https://doi.org/10.3390/ma12071180.

(566) Lee, K.; Yoon, S. S. *Pseudomonas Aeruginosa* Biofilm, a Programmed Bacterial Life for Fitness. *J Microbiol Biotechnol* **2017**, *27* (6), 1053–1064. https://doi.org/10.4014/jmb.1611.11056.

(567) Karami, P.; Khaledi, A.; Mashoof, R. Y.; Yaghoobi, M. H.; Karami, M.; Dastan, D.; Alikhani, M. Y. The Correlation between Biofilm Formation Capability and Antibiotic Resistance Pattern in *Pseudomonas Aeruginosa*. *Gene Reports* **2020**, *18*, 100561. https://doi.org/10.1016/j.genrep.2019.100561.

(568) Zhang, K.; Li, X.; Yu, C.; Wang, Y. Promising Therapeutic Strategies Against Microbial Biofilm Challenges. *Front Cell Infect Mi* **2020**, *10*, 359. https://doi.org/10.3389/fcimb.2020.00359.

(569) Robb, A. J.; Vinogradov, S.; Danell, A. S.; Anderson, E.; Blackledge, M. S.; Melander, C.; Hvastkovs, E. G. Electrochemical Detection of Small Molecule Induced *Pseudomonas Aeruginosa* Biofilm Dispersion. *Electrochim Acta* **2018**, *268*, 276–282. https://doi.org/10.1016/j.electacta.2018.02.113.

(570) Alatraktchi, F. A.; Noori, J. S.; Tanev, G. P.; Mortensen, J.; Dimaki, M.; Johansen, H. K.; Madsen, J.; Molin, S.; Svendsen, W. E. Paper-Based Sensors for Rapid Detection of Virulence Factor Produced by *Pseudomonas Aeruginosa*. *PLOS ONE* **2018**, *13* (3), e0194157. https://doi.org/10.1371/journal.pone.0194157.

(571) Alatraktchi, F. A.; Svendsen, W. E.; Molin, S. Electrochemical Detection of Pyocyanin as a Biomarker for *Pseudomonas Aeruginosa*: A Focused Review. *Sensors* **2020**, *20* (18), 5218. https://doi.org/10.3390/s20185218.

(572) McEachern, F.; Harvey, E.; Merle, G. Emerging Technologies for the Electrochemical Detection of Bacteria. *Biotechnol J* **2020**, *15* (9), 2000140. https://doi.org/10.1002/biot.202000140.

(573) Rajamani, S.; Sandy, R.; Kota, K.; Lundh, L.; Gomba, G.; Recabo, K.; Duplantier, A.; Panchal, R. G. Robust Biofilm Assay for Quantification and High Throughput Screening Applications. *J Microbiol Meth* **2019**, *159*, 179–185. https://doi.org/10.1016/j.mimet.2019.02.018.

(574) Jun, W.; Kim, M. S.; Lee, K.; Millner, P.; Chao, K. Assessment of Bacterial Biofilm on Stainless Steel by Hyperspectral Fluorescence Imaging. *Sens. & Instrumen. Food Qual.* **2009**, *3* (1), 41–48. https://doi.org/10.1007/s11694-009-9069-1.

(575) Wang, Y.; Reardon, C. P.; Read, N.; Thorpe, S.; Evans, A.; Todd, N.; Van Der Woude, M.; Krauss, T. F. Attachment and Antibiotic Response of Early-Stage Biofilms Studied Using Resonant Hyperspectral Imaging. *NPJ Biofilms Microbiomes* **2020**, *6* (1), 57. https://doi.org/10.1038/s41522-020-00169-1.

(576) Czerwińska-Główka, D.; Krukiewicz, K. A Journey in the Complex Interactions between Electrochemistry and Bacteriology: From Electroactivity to Electromodulation of Bacterial Biofilms. *Bioelectrochemistry* **2020**, *131*, 107401. https://doi.org/10.1016/j.bioelechem.2019.107401.

(577) Windham, W. R.; Yoon, S.-C.; Ladely, S. R.; Haley, J. A.; Heitschmidt, J. W.; Lawrence, K. C.; Park, B.; Narrang, N.; Cray, W. C. Detection by Hyperspectral Imaging of Shiga Toxin–Producing *Escherichia Coli* Serogroups O26, O45, O103, O111, O121, and O145 on Rainbow Agar. *J Food Protect* **2013**, *76* (7), 1129–1136. https://doi.org/10.4315/0362-028X.JFP-12-497.

(578) Elliott, J.; Simoska, O.; Karasik, S.; Shear, J. B.; Stevenson, K. J. Transparent Carbon Ultramicroelectrode Arrays for the Electrochemical Detection of a Bacterial Warfare Toxin, Pyocyanin. *Anal Chem* **2017**, *89* (12), 6285–6289. https://doi.org/10.1021/acs.analchem.7b00876.

(579) Oziat, J.; Gougis, M.; Malliaras, G. G.; Mailley, P. Electrochemical Characterizations of Four Main Redox-Metabolites of *Pseudomonas Aeruginosa*. *Electroanal* **2017**, *29* (5), 1332–1340. https://doi.org/10.1002/elan.201600799.

(580) Glasser, N. R.; Saunders, S. H.; Newman, D. K. The Colorful World of Extracellular Electron Shuttles. *Annu Rev Microbiol* **2017**, *71* (1), 731–751. https://doi.org/10.1146/annurev-micro-090816-093913.

(581) Mandakhalikar, K. D.; Rahmat, J. N.; Chiong, E.; Neoh, K. G.; Shen, L.; Tambyah, P. A. Extraction and Quantification of Biofilm Bacteria: Method Optimized for Urinary Catheters. *Sci Rep-UK* **2018**, *8* (1), 8069. https://doi.org/10.1038/s41598-018-26342-3.

(582) Alatraktchi, F. A.; Johansen, H. K.; Molin, S.; Svendsen, W. E. Electrochemical Sensing of Biomarker for Diagnostics of Bacteria-Specific Infections. *Nanomedicine-UK* **2016**, *11* (16), 2185–2195. https://doi.org/10.2217/nnm-2016-0155.

(583) Santiveri, C. R.; Sismaet, H. J.; Kimani, M.; Goluch, E. D. Electrochemical Detection of *Pseudomonas Aeruginosa* in Polymicrobial Environments. *ChemistrySelect* **2018**, *3* (11), 2926–2930. https://doi.org/10.1002/slct.201800569.

(584) Sismaet, H. J.; Pinto, A. J.; Goluch, E. D. Electrochemical Sensors for Identifying Pyocyanin Production in Clinical *Pseudomonas Aeruginosa* Isolates. *Biosens Bioelectron* **2017**, *97*, 65–69. https://doi.org/10.1016/j.bios.2017.05.042.

(585) Webster, T. A.; Sismaet, H. J.; Chan, I. -ping J.; Goluch, E. D. Electrochemically Monitoring the Antibiotic Susceptibility of *Pseudomonas Aeruginosa* Biofilms. *Analyst* **2015**, *140* (21), 7195–7201. https://doi.org/10.1039/C5AN01358E.

(586) Bouguer, P. *Essai d'optique Sur La Gradation de La Lumière*; Claude Jombert, 1729.

(587) Kragh, K. N.; Alhede, M.; Kvich, L.; Bjarnsholt, T. Into the Well—A Close Look at the Complex Structures of a Microtiter Biofilm and the Crystal Violet Assay. *Biofilm* **2019**, *1*, 100006. https://doi.org/10.1016/j.bioflm.2019.100006.

(588) El-Shaded, M. M. S.; Mahmoud, D. E.; Soliman, N. S.; ElMahdy, Y. A.; Mohamed, S. H. Characterization of Biofilm Formation, Pyocyanin Production, and

Antibiotic Resistance Mechanisms in Drug-Resistant *Pseudomonas Aeruginosa* Isolated from Children in Egypt. *J Appl Pharm Sci* **2020**. https://doi.org/10.7324/JAPS.2020.101110.

(589) Dey, P.; Parai, D.; Banerjee, M.; Hossain, S. T.; Mukherjee, S. K. Naringin Sensitizes the Antibiofilm Effect of Ciprofloxacin and Tetracycline against *Pseudomonas Aeruginosa* Biofilm. *Int J Med Microbiol* **2020**, *310* (3), 151410. https://doi.org/10.1016/j.ijmm.2020.151410.

(590) Ward, A. C.; Connolly, P.; Tucker, N. P. *Pseudomonas Aeruginosa* Can Be Detected in a Polymicrobial Competition Model Using Impedance Spectroscopy with a Novel Biosensor. *PLOS ONE* **2014**, *9* (3), e91732. https://doi.org/10.1371/journal.pone.0091732.

(591) Flanagan, L.; Steen, R. R.; Saxby, K.; Klatter, M.; Aucott, B. J.; Winstanley, C.; Fairlamb, I. J. S.; Lynam, J. M.; Parkin, A.; Friman, V.-P. The Antimicrobial Activity of a Carbon Monoxide Releasing Molecule (EBOR-CORM-1) Is Shaped by Intraspecific Variation within *Pseudomonas Aeruginosa* Populations. *Front Microbiol* **2018**, *9*, 195. https://doi.org/10.3389/fmicb.2018.00195.

(592) Das, T.; Manos, J. *Pseudomonas Aeruginosa* Extracellular Secreted Molecules Have a Dominant Role in Biofilm Development and Bacterial Virulence in Cystic Fibrosis Lung Infections. In *Progress in Understanding Cystic Fibrosis*; Sriramulu, D., Ed.; InTech, 2017. https://doi.org/10.5772/66308.

(593) Abdelaziz, A. A.; Kamer, A. M. A.; Al-Monofy, K. B.; Al-Madboly, L. A. *Pseudomonas Aeruginosa*'s Greenish-Blue Pigment Pyocyanin: Its Production and Biological Activities. *Microbial Cell Factories* **2023**, *22* (1), 110. https://doi.org/10.1186/s12934-023-02122-1.

(594) Reszka, K. J.; O'Malley, Y.; McCormick, M. L.; Denning, G. M.; Britigan, B. E. Oxidation of Pyocyanin, a Cytotoxic Product from *Pseudomonas Aeruginosa,* by Microperoxidase 11 and Hydrogen Peroxide. *Free Radical Biology and Medicine* **2004**, *36* (11), 1448–1459. https://doi.org/10.1016/j.freeradbiomed.2004.03.011.

(595) Bellin, D. L.; Sakhtah, H.; Zhang, Y.; Price-Whelan, A.; Dietrich, L. E. P.; Shepard, K. L. Electrochemical Camera Chip for Simultaneous Imaging of Multiple Metabolites in Biofilms. *Nat Commun* **2016**, *7* (1), 10535. https://doi.org/10.1038/ncomms10535.

(596) Rodriguez-Urretavizcaya, B.; Pascual, N.; Pastells, C.; Martin-Gomez, M. T.; Vilaplana, L.; Marco, M.-P. Diagnosis and Stratification of *Pseudomonas Aeruginosa* Infected Patients by Immunochemical Quantitative Determination of Pyocyanin From Clinical Bacterial Isolates. *Front Cell Infect Microbiol* **2021**, *11*, 786929. https://doi.org/10.3389/fcimb.2021.786929.

(597) Simoska, O.; Sans, M.; Fitzpatrick, M. D.; Crittenden, C. M.; Eberlin, L. S.; Shear, J. B.; Stevenson, K. J. Real-Time Electrochemical Detection of *Pseudomonas Aeruginosa* Phenazine Metabolites Using Transparent Carbon Ultramicroelectrode Arrays. *ACS Sens.* **2019**, *4* (1), 170–179. https://doi.org/10.1021/acssensors.8b01152.

(598) The International Union of Pure and Applied. *Glossary of Terms Used in Bioinorganic Chemistry*; 1997. https://doi.org/10.1351/goldbook.ST06784.

(599) Fu, J.; Hall, S.; Boon, E. M. Recent Evidence for Multifactorial Biofilm Regulation by Heme Sensor Proteins NosP and H-NOX. *Chemistry letters* **2021**, *50* (5), 1095. https://doi.org/10.1246/cl.200945.

(600) Islam, Md. S.; Alatishe, A.; Lee-Lopez, C. C.; Serrano, F.; Yukl, E. T. H-NOX Influences Biofilm Formation, Central Metabolism, and Quorum Sensing in *Paracoccus Denitrificans*. *J. Proteome Res.* **2024**, *23* (11), 4988–5000. https://doi.org/10.1021/acs.jproteome.4c00466.

(601) Kretzschmar, J.; Harnisch, F. Electrochemical Impedance Spectroscopy on Biofilm Electrodes – Conclusive or Euphonious? *Curr Opin Electrochem* **2021**, *29*, 100757. https://doi.org/10.1016/j.coelec.2021.100757.

(602) Price-Whelan, A.; Dietrich, L. E. P.; Newman, D. K. Pyocyanin Alters Redox Homeostasis and Carbon Flux through Central Metabolic Pathways in *Pseudomonas Aeruginosa* PA14. *J Bacteriol* **2007**, *189* (17), 6372–6381. https://doi.org/10.1128/JB.00505-07.

(603) Price-Whelan, A.; Dietrich, L. E. P.; Newman, D. K. Rethinking "secondary" Metabolism: Physiological Roles for Phenazine Antibiotics. *Nat Chem Biol* **2006**, *2* (2), 71–78. https://doi.org/10.1038/nchembio764.

(604) Gajdács, M.; Baráth, Z.; Kárpáti, K.; Szabó, D.; Usai, D.; Zanetti, S.; Donadu, M. G. No Correlation between Biofilm Formation, Virulence Factors, and Antibiotic Resistance in *Pseudomonas Aeruginosa*: Results from a Laboratory-Based In Vitro Study. *Antibiotics* **2021**, *10* (9), 1134. https://doi.org/10.3390/antibiotics10091134.

(605) Buzid, A.; Shang, F.; Reen, F. J.; Muimhneacháin, E. Ó.; Clarke, S. L.; Zhou, L.; Luong, J. H. T.; O'Gara, F.; McGlacken, G. P.; Glennon, J. D. Molecular Signature of *Pseudomonas Aeruginosa* with Simultaneous Nanomolar Detection of Quorum Sensing Signaling Molecules at a Boron-Doped Diamond Electrode. *Sci Rep-UK* **2016**, *6* (1), 30001. https://doi.org/10.1038/srep30001.

(606) Tan, X.; Huang, Y.; Rana, A.; Singh, N.; Abbey, T. C.; Chen, H.; Toth, P. T.; Bulman, Z. P. Optimization of an in Vitro Pseudomonas Aeruginosa Biofilm Model to Examine Antibiotic Pharmacodynamics at the Air-Liquid Interface. *npj Biofilms Microbiomes* **2024**, *10* (1), 1–12. https://doi.org/10.1038/s41522-024-00483-y.

(607) Behere, M. J.; Shinde, A. H.; Haldar, S. Determination of Antibiotic Resistance Profile of Bacterial Community from Environmental Water Using Antibiotic-Resistant Bacterial Contamination Detection (ABCD) Kit. *Biosensors and Bioelectronics* **2023**, *221*, 114943. https://doi.org/10.1016/j.bios.2022.114943.

(608) Coenye, T.; Kjellerup, B.; Stoodley, P.; Bjarnsholt, T. The Future of Biofilm Research – Report on the '2019 Biofilm Bash.' *Biofilm* **2020**, *2*, 100012. https://doi.org/10.1016/j.bioflm.2019.100012.

(609) Oziat, J.; Cohu, T.; Elsen, S.; Gougis, M.; Malliaras, G. G.; Mailley, P. Electrochemical Detection of Redox Molecules Secreted by *Pseudomonas Aeruginosa* – Part 1: Electrochemical Signatures of Different Strains. *Bioelectrochemistry* **2021**, *140*, 107747. https://doi.org/10.1016/j.bioelechem.2021.107747.

(610) Fu, L.; Zheng, Y.; Zhang, P.; Zhang, H.; Xu, Y.; Zhou, J.; Zhang, H.; Karimi-Maleh, H.; Lai, G.; Zhao, S.; Su, W.; Yu, J.; Lin, C.-T. Development of an Electrochemical Biosensor for Phylogenetic Analysis of Amaryllidaceae Based on the Enhanced Electrochemical Fingerprint Recorded from Plant Tissue. *Biosens Bioelectron* **2020**, *159*, 112212. https://doi.org/10.1016/j.bios.2020.112212.

(611) Van den Driessche, F.; Rigole, P.; Brackman, G.; Coenye, T. Optimization of Resazurin-Based Viability Staining for Quantification of Microbial Biofilms. *Journal of microbiological methods* **2014**, *98*, 31–34.

(612) Fan, Y.; Hao, R.; Han, C.; Zhang, B. Counting Single Redox Molecules in a Nanoscale Electrochemical Cell. *Anal. Chem.* **2018**, *90* (23), 13837–13841. https://doi.org/10.1021/acs.analchem.8b04659.

(613) Roy, S.; Chowdhury, G.; Mukhopadhyay, A. K.; Dutta, S.; Basu, S. Convergence of Biofilm Formation and Antibiotic Resistance in *Acinetobacter Baumannii* Infection. *Front. Med.* **2022**, *9*, 793615. https://doi.org/10.3389/fmed.2022.793615.

(614) Semenec, L.; Cain, A. K.; Dawson, C. J.; Liu, Q.; Dinh, H.; Lott, H.; Penesyan, A.; Maharjan, R.; Short, F. L.; Hassan, K. A.; Paulsen, I. T. Cross-Protection and Cross-Feeding between *Klebsiella Pneumoniae* and *Acinetobacter Baumannii* Promotes Their Co-Existence. *Nat Commun* **2023**, *14* (1), 702. https://doi.org/10.1038/s41467-023-36252-2.

(615) Monteiro, M. C.; De La Cruz, M.; Cantizani, J.; Moreno, C.; Tormo, J. R.; Mellado, E.; De Lucas, J. R.; Asensio, F.; Valiante, V.; Brakhage, A. A.; Latgé, J.-P.; Genilloud, O.; Vicente, F. A New Approach to Drug Discovery: High-Throughput Screening of Microbial Natural Extracts against *Aspergillus Fumigatus* Using Resazurin. *SLAS Discovery* **2012**, *17* (4), 542–549. https://doi.org/10.1177/1087057111433459.

(616) Mishra, P.; Singh, D.; Mishra, K. P.; Kaur, G.; Dhull, N.; Tomar, M.; Gupta, V.; Kumar, B.; Ganju, L. Rapid Antibiotic Susceptibility Testing by Resazurin Using Thin Film Platinum as a Bio-Electrode. *Journal of Microbiological Methods* **2019**, *162*, 69–76. https://doi.org/10.1016/j.mimet.2019.05.009.

(617) Çakir, S.; Arslan, E. Voltammetry of Resazurin at a Mercury Electrode. *Chemical Papers* **2010**, *64* (3). https://doi.org/10.2478/s11696-010-0007-9.

(618) Besant, J. D.; Sargent, E. H.; Kelley, S. O. Rapid Electrochemical Phenotypic Profiling of Antibiotic-Resistant Bacteria. *Lab Chip* **2015**, *15* (13), 2799–2807. https://doi.org/10.1039/C5LC00375J.

(619) Crane, B.; Hughes, J. P.; Rowley Neale, S. J.; Rashid, M.; Linton, P. E.; Banks, C. E.; Shaw, K. J. Rapid Antibiotic Susceptibility Testing Using Resazurin Bulk Modified Screen-Printed Electrochemical Sensing Platforms. *Analyst* **2021**, *146* (18), 5574–5583. https://doi.org/10.1039/D1AN00850A.

(620) Annang, F. B.; Pérez-Moreno, G.; Bosch-Navarrete, C.; González-Menéndez, V.; Martín, J.; Mackenzie, T. A.; Ramos, M. C.; Ruiz-Pérez, L. M.; Genilloud, O.; González-Pacanowska, D.; Vicente, F.; Reyes, F. Antiparasitic Meroterpenoids Isolated from *Memnoniella Dichroa* CF-080171. *Pharmaceutics* **2023**, *15* (2), 492. https://doi.org/10.3390/pharmaceutics15020492.

(621) Varçin, M.; Şener, B. B.; Bayraç, C. Adsorption of Resazurin by Poly(Acrylic Acid) Hydrogels and Evaluation of Its Use in Reduction Assay for Quantification of Cell Viability. *Dyes and Pigments* **2021**, *186*, 109038. https://doi.org/10.1016/j.dyepig.2020.109038.

(622) Almasaudi, S. B. *Acinetobacter* Spp. as Nosocomial Pathogens: Epidemiology and Resistance Features. *Saudi Journal of Biological Sciences* **2018**, *25* (3), 586–596. https://doi.org/10.1016/j.sjbs.2016.02.009.

(623) Samanta, I.; Bandyopadhyay, S. Chapter 14 - Klebsiella. In *Antimicrobial Resistance in Agriculture*; Samanta, I., Bandyopadhyay, S., Eds.; Academic Press, 2020; pp 153–169. https://doi.org/10.1016/B978-0-12-815770-1.00014-6.

(624) Skogman, M. E.; Vuorela, P. M.; Fallarero, A. Combining Biofilm Matrix Measurements with Biomass and Viability Assays in Susceptibility Assessments of Antimicrobials against *Staphylococcus Aureus* Biofilms. *J Antibiot* **2012**, *65* (9), 453–459. https://doi.org/10.1038/ja.2012.49.

(625) Lu, Y.; Hu, X.; Nie, T.; Yang, X.; Li, C.; You, X. Strategies for Rapid Identification of *Acinetobacter Baumannii* Membrane Proteins and Polymyxin B's Effects. *Front. Cell. Infect. Microbiol.* **2021**, *11*, 734578. https://doi.org/10.3389/fcimb.2021.734578.

(626) *Standard Microplates - 96-,384-, and 1536-well format*. WellPlate.com. https://www.wellplate.com/standard-microplates/ (accessed 2023-09-27).

(627) The European Committee on Antimicrobial Susceptibility Testing. *Breakpoint Tables for Interpretation of MICs and Zone Diameters.*; Version 12.0; 2022. http://www.eucast.org.

(628) Muñoz-Berbel, X.; García-Aljaro, C.; Muñoz, F. J. Impedimetric Approach for Monitoring the Formation of Biofilms on Metallic Surfaces and the Subsequent Application to the Detection of Bacteriophages. *Electrochimica Acta* **2008**, *53* (19), 5739–5744. https://doi.org/10.1016/j.electacta.2008.03.050.

(629) Poma, N.; Vivaldi, F.; Bonini, A.; Salvo, P.; Kirchhain, A.; Ates, Z.; Melai, B.; Bottai, D.; Tavanti, A.; Di Francesco, F. Microbial Biofilm Monitoring by Electrochemical Transduction Methods. *TrAC Trends in Analytical Chemistry* **2021**, *134*, 116134. https://doi.org/10.1016/j.trac.2020.116134.

(630) Muñoz-Berbel, X.; Muñoz, F. J.; Vigués, N.; Mas, J. On-Chip Impedance Measurements to Monitor Biofilm Formation in the Drinking Water Distribution Network. *Sensors and Actuators B: Chemical* **2006**, *118* (1–2), 129–134. https://doi.org/10.1016/j.snb.2006.04.070.

(631) Pires, L.; Sachsenheimer, K.; Kleintschek, T.; Waldbaur, A.; Schwartz, T.; Rapp, B. E. Online Monitoring of Biofilm Growth and Activity Using a Combined Multi-Channel Impedimetric and Amperometric Sensor. *Biosensors and Bioelectronics* **2013**, *47*, 157–163. https://doi.org/10.1016/j.bios.2013.03.015.

(632) Lee, A.; Seo, Y.; Lim, J.; Park, S.; Yoo, J.; Kim, B.; Kim, G. Detection of *E. Coli* Biofilms with Hyperspectral Imaging and Machine Learning Techniques. 농업과학연구 **2020**, *47* (3), 645–655. https://doi.org/10.7744/KJOAS.20200052.

(633) Wilt, I. K.; Hari, T. P. A.; Wuest, W. M. Hijacking the Bacterial Circuitry of Biofilm Processes via Chemical "Hot-Wiring": An Under-Explored Avenue for Therapeutic Development. *ACS Infect. Dis.* **2019**, *5* (6), 789–795. https://doi.org/10.1021/acsinfecdis.9b00104.

(634) Ren, Y.; Ji, J.; Sun, J.; Pi, F.; Zhang, Y.; Sun, X. Rapid Detection of Antibiotic Resistance in Salmonella with Screen Printed Carbon Electrodes. *J Solid State Electrochem* **2020**, *24* (7), 1539–1549. https://doi.org/10.1007/s10008-020-04645-8.

(635) Laugier, J. The "Comfort Timing" Strategy: A Potential Pathway for the Cultivation of Uncultured Microorganisms and a Possible Adaptation for Environmental Colonisation. *FEMS Microbiology Ecology* **2023**, *99* (4), fiad026. https://doi.org/10.1093/femsec/fiad026.

(636) Costerton, J. W.; Stewart, P. S.; Greenberg, E. P. Bacterial Biofilms: A Common Cause of Persistent Infections. *science* **1999**, *284* (5418), 1318–1322.

(637) Baral, B.; Mozafari, M. R. Strategic Moves of "Superbugs" Against Available Chemical Scaffolds: Signaling, Regulation, and Challenges. *ACS Pharmacol. Transl. Sci.* **2020**, *3* (3), 373–400. https://doi.org/10.1021/acsptsci.0c00005.

(638) Nass, N. M.; Farooque, S.; Hind, C.; Wand, M. E.; Randall, C. P.; Sutton, J. M.; Seipke, R. F.; Rayner, C. M.; O'Neill, A. J. Revisiting Unexploited Antibiotics in Search of New Antibacterial Drug Candidates: The Case of γ-Actinorhodin. *Sci Rep* **2017**, *7* (1), 17419. https://doi.org/10.1038/s41598-017-17232-1.

(639) Corrigan, D. K. 10 - Impedance Biosensors. In *Fundamentals of Sensor Technology*; Barhoum, A., Altintas, Z., Eds.; Woodhead Publishing Series in Electronic and Optical Materials; Woodhead Publishing, 2023; pp 239–264. https://doi.org/10.1016/B978-0-323-88431-0.00004-1.

(640) Keighley, S. D.; Estrela, P.; Li, P.; Migliorato, P. Optimization of Label-Free DNA Detection with Electrochemical Impedance Spectroscopy Using PNA Probes. *Biosensors and Bioelectronics* **2008**, *24* (4), 906–911. https://doi.org/10.1016/j.bios.2008.07.041.

(641) Xiao, Y.; Lubin, A. A.; Baker, B. R.; Plaxco, K. W.; Heeger, A. J. Single-Step Electronic Detection of Femtomolar DNA by Target-Induced Strand Displacement in an Electrode-Bound Duplex. *Proc. Natl. Acad. Sci. U.S.A.* **2006**, *103* (45), 16677–16680. https://doi.org/10.1073/pnas.0607693103.

(642) Zhang, Z.; Tao, C.; Yin, J.; Wang, Y.; Li, Y. Enhancing the Response Rate of Strand Displacement-Based Electrochemical Aptamer Sensors Using Bivalent Binding Aptamer-cDNA Probes. *Biosensors and Bioelectronics* **2018**, *103*, 39–44. https://doi.org/10.1016/j.bios.2017.12.027.

(643) Liu, R.; Yang, Z.; Guo, Q.; Zhao, J.; Ma, J.; Kang, Q.; Tang, Y.; Xue, Y.; Lou, X.; He, M. Signaling-Probe Displacement Electrochemical Aptamer-Based Sensor (SD-EAB) for Detection of Nanomolar Kanamycin A. *Electrochimica Acta* **2015**, *182*, 516–523. https://doi.org/10.1016/j.electacta.2015.09.140.

(644) Ziółkowski, R.; Jarczewska, M.; Górski, Ł.; Malinowska, E. From Small Molecules toward Whole Cells Detection: Application of Electrochemical Aptasensors in Modern Medical Diagnostics. *Sensors* **2021**, *21* (3), 724. https://doi.org/10.3390/s21030724.

(645) Zhao, Y.; Yavari, K.; Liu, J. Critical Evaluation of Aptamer Binding for Biosensor Designs. *TrAC Trends in Analytical Chemistry* **2022**, *146*, 116480. https://doi.org/10.1016/j.trac.2021.116480.

(646) Toma, L.; Mattarozzi, M.; Ronda, L.; Marassi, V.; Zattoni, A.; Fortunati, S.; Giannetto, M.; Careri, M. Are Aptamers Really Promising as Receptors for Analytical Purposes? Insights into Anti-Lysozyme DNA Aptamers through a Multitechnique Study. *Anal. Chem.* **2024**, *96* (6), 2719–2726. https://doi.org/10.1021/acs.analchem.3c05883.

(647) Fletcher, M. The Effects of Culture Concentration and Age, Time, and Temperature on Bacterial Attachment to Polystyrene. *Can. J. Microbiol.* **1977**, *23* (1), 1–6. https://doi.org/10.1139/m77-001.

(648) Wang, Y.; Reardon, C. P.; Read, N.; Thorpe, S.; Evans, A.; Todd, N.; Van Der Woude, M.; Krauss, T. F. Attachment and Antibiotic Response of Early-Stage Biofilms Studied Using Resonant Hyperspectral Imaging. *npj Biofilms Microbiomes* **2020**, *6* (1), 1–7. https://doi.org/10.1038/s41522-020-00169-1.

(649) Lee, A.; Park, S.; Yoo, J.; Kang, J.; Lim, J.; Seo, Y.; Kim, B.; Kim, G. Detecting Bacterial Biofilms Using Fluorescence Hyperspectral Imaging and Various Discriminant Analyses. *Sensors* **2021**, *21* (6), 2213. https://doi.org/10.3390/s21062213.

(650) Le, H. N. D.; Hitchins, V. M.; Ilev, I. K.; Kim, D.-H. Monitoring Biofilm Attachment on Medical Devices Surfaces Using Hyperspectral Imaging. In *Optical Fibers and Sensors for Medical Diagnostics and Treatment Applications XIV*; SPIE, 2014; Vol. 8938, pp 46–55. https://doi.org/10.1117/12.2047867.

(651) Glover, R.; Al-Haboubi, M.; Petticrew, M.; Peacock, S. Reviewing the Use of Turnaround Time in Rapid Identification and Antibiotic Susceptibility Testing. *European Journal of Public Health* **2018**, *28* (suppl_4), cky214.121. https://doi.org/10.1093/eurpub/cky214.121.

(652) Villalonga, A.; Pérez-Calabuig, A. M.; Villalonga, R. Electrochemical Biosensors Based on Nucleic Acid Aptamers. *Anal Bioanal Chem* **2020**, *412* (1), 55–72. https://doi.org/10.1007/s00216-019-02226-x.

(653) Colson, A. R.; Morton, A.; Årdal, C.; Chalkidou, K.; Davies, S. C.; Garrison, L. P.; Jit, M.; Laxminarayan, R.; Megiddo, I.; Morel, C.; Nonvignon, J.; Outterson, K.; Rex, J. H.; Sarker, A. R.; Sculpher, M.; Woods, B.; Xiao, Y. Antimicrobial Resistance: Is Health Technology Assessment Part of the Solution or Part of the Problem? *Value Health* **2021**, *24* (12), 1828–1834. https://doi.org/10.1016/j.jval.2021.06.002.

(654) Chang, H.-J. *Edible Economics: The World in 17 Dishes*, 1st edition.; Penguin, 2023.

(655) Nielsen, J. Cell Factory Engineering for Improved Production of Natural Products. *Natural Product Reports* **2019**, *36* (9), 1233–1236. https://doi.org/10.1039/C9NP00005D.

(656) Rohr, J.; Hertweck, C. 1.07 - Type II PKS. In *Comprehensive Natural Products II*; Liu, H.-W. (Ben), Mander, L., Eds.; Elsevier: Oxford, 2010; pp 227–303. https://doi.org/10.1016/B978-008045382-8.00703-6.

(657) Das, A.; Khosla, C. Biosynthesis of Aromatic Polyketides in Bacteria. *Acc Chem Res* **2009**, *42* (5), 631–639. https://doi.org/10.1021/ar8002249.

(658) Korman, T. P.; Ames, B.; (Sheryl) Tsai, S.-C. Structural Enzymology of Polyketide Synthase: The Structure–Sequence–Function Correlation. In *Comprehensive Natural Products II*; Elsevier, 2010; pp 305–345. https://doi.org/10.1016/B978-008045382-8.00020-4.

(659) Hannah, S.; Al-Hatmi, M.; Gray, L.; Corrigan, D. K. Low-Cost, Thin-Film, Mass-Manufacturable Carbon Electrodes for Detection of the Neurotransmitter Dopamine. *Bioelectrochemistry* **2020**, *133*, 107480. https://doi.org/10.1016/j.bioelechem.2020.107480.

(660) MicruX. *Thin-Film InterDigitated Electrodes*. https://www.micruxfluidic.com/en/electrochemical-solutions/thin-film-electrochemical-sensors/interdigitated-electrodes-ide/ (accessed 2024-05-11).

(661) Steel, A. B.; Herne, T. M.; Tarlov, M. J. Electrochemical Quantitation of DNA Immobilized on Gold. *Anal. Chem.* **1998**, *70* (22), 4670–4677. https://doi.org/10.1021/ac980037q.

(662) Mahajan, S.; Richardson, J.; Brown, T.; Bartlett, P. N. SERS-Melting: A New Method for Discriminating Mutations in DNA Sequences. *J. Am. Chem. Soc.* **2008**, *130* (46), 15589–15601. https://doi.org/10.1021/ja805517q.

(663) Keighley, S. D.; Estrela, P.; Li, P.; Migliorato, P. Optimization of Label-Free DNA Detection with Electrochemical Impedance Spectroscopy Using PNA Probes. *Biosensors and Bioelectronics* **2008**, *24* (4), 906–911. https://doi.org/10.1016/j.bios.2008.07.041.

(664) Yoon, S. C.; Lawrence, K. C.; Line, J. E.; Siragusa, G. R.; Feldner, P. W.; Park, B.; Windham, W. R. Detection of Campylobacter Colonies Using Hyperspectral Imaging. *Sens. & Instrumen. Food Qual.* **2010**, *4* (1), 35–49. https://doi.org/10.1007/s11694-010-9094-0.